Molecular Characterisation of *Flavivirus* Interactions with the Host Innate Immune Response

Rosa Coldbeck-Shackley, B.Sc.

Discipline of Molecular and Cellular Biology

School of Biological Sciences

The University of Adelaide

A dissertation submitted to The University of Adelaide

in candidature for the degree of

Doctor of Philosophy in the Faculty of Sciences

February 2021

Table of Contents

LIST OF FIGURES ..... **x**

LIST OF TABLES ..... **xiv**

ABSTRACT ..... **xv**

DECLARATION ..... **xviii**

ACKNOWLEDGEMENTS ..... **xix**

PRESENTATIONS, PUBLICATIONS AND AWARDS ARISING FROM THIS PHD ..... **xx**

MATERIALS PROVIDERS ..... **xxii**

ABBREVIATIONS USED ..... **xxiii**

CHAPTER 1 ..... **1**

1 INTRODUCTION **1**

1.1 Zika virus and dengue virus 1

1.1.1 ZIKV and DENV epidemiology 1

1.1.2 Transmission of ZIKV and DENV 4

1.1.2.1 Mosquito borne transmission 4

1.1.2.2 Alternative transmission modes 6

1.1.2.2.1 Sexual transmission 6

1.1.2.2.2 Vertical transmission 7

1.1.3 Clinical presentation and pathogenesis of ZIKV and DENV infections 8

1.1.3.1 ZIKV clinical manifestations 10

1.1.3.2 ZIKV pathogenesis 10

1.1.3.3 DENV clinical manifestations 11

1.1.3.4 DENV pathogenesis 12

1.1.4 Current control measures 13

1.1.5 Molecular virology of ZIKV and DENV 13

1.1.5.1 ZIKV and DENV phylogeny and genetic diversity 13

1.1.5.2 ZIKV and DENV Genome and Proteins 14

1.1.5.2.1 Genome structure 15

1.1.5.2.2 Virion structure 17

1.1.5.2.3 Viral proteins 17
1.1.5.2.3.1 Structural proteins 18
1.1.5.2.3.2 Non-structural proteins 19
1.1.5.3 Lifecycle 21
1.2 The innate immune response to viral infection overview 25
1.2.1 Recognition of flaviviruses by innate immune pattern recognition receptors 25
1.2.2 The Interferons 29
1.2.2.1 Type-I Interferons 29
1.2.2.1.1 Signalling from the type-I IFN receptor 29
1.2.2.1.2 Switching off the type-I IFN response 30
1.2.2.1.3 Differential type-I IFN signalling 33
1.2.2.2 IFN-epsilon overview 34
1.2.2.2.1 Discovery of IFNε 34
1.2.2.2.2 Expression of IFNε 35
1.2.2.2.3 Properties of recombinant human and mouse IFNε protein 37
1.2.2.2.4 IFNε antiviral activity 38
1.2.2.3 Similarities and differences between Type-I and Type-III IFN signalling 40
1.2.2.3.1 Production of type-III IFN 41
1.2.2.3.2 Type-III receptor localization 41
1.2.2.3.3 Switching off the type-III IFN response 41
1.2.2.3.4 Physiological outcomes of type-I and III IFN signalling 42
1.2.3 Inhibition of ZIKV and DENV infection by Interferon 43
1.2.3.1 Interferon stimulated genes that inhibit ZIKV and DENV 43
1.3 DENV and ZIKV mediated evasion of the IFN response 46
1.3.1 Common strategies between flaviviruses 47
1.3.2 ZIKV specific mechanisms to evade IFN responses 48
1.3.3 DENV specific mechanisms to evade the IFN response 49
1.4 Experimental model systems used in this thesis 51
1.4.1 Reverse genetics systems as tools for mutational profiling of viral genomes 51
1.4.2 Transposon mutagenesis as a method for high-throughput genome wide mutational profiling 54

1.4.2.1 Applications of Mu A transposon mutagenesis for high-throughput mutational studies of infectious clones 56
1.4.3 Mouse models of ZIKV sexual transmission 58
1.5 Experimental rationale, hypotheses and aims 62

CHAPTER 2 63
2 MATERIALS AND METHODS 63
2.1 General laboratory methods 63
2.1.1 Bacterial transformation methods 63
2.1.1.1 Chemically competent cells 63
2.1.1.2 Electro-competent cells 64
2.1.2 DNA purification methods 64
2.1.2.1 Small-scale plasmid DNA extraction (mini-preparation) 64
2.1.2.2 Large-scale plasmid DNA extraction (maxi-preparation) 65
2.1.2.3 Gel extraction 66
2.1.2.4 Column purification reaction clean-up 66
2.1.2.5 Ethanol DNA precipitation reaction clean-up 67
2.1.3 Recombinant DNA cloning methods 67
2.1.3.1 Restriction enzyme digestion 67
2.1.3.2 Primer design 67
2.1.3.3 Q5 High-fidelity Polymerase Chain Reaction (PCR) 68
2.1.3.4 Agarose gel electrophoresis 68
2.1.3.5 DNA ligation 68
2.1.3.6 Gibson assembly 69
2.1.3.7 Plasmid DNA Sanger Sequencing 69
2.1.4 Total RNA extraction 69
2.1.4.1 TRIsure (Bioline) 69
2.1.4.2 NucleoZOL (Macherey Nagel) 70
2.1.4.3 RNeasy Mini Kit (Qiagen) with or without DNase treatment 71
2.1.5 Nucleic acid quantification 72
2.1.6 cDNA synthesis 72
2.1.6.1 M-MLV reverse transcriptase cDNA preparation (Promega) 72

2.1.6.2 SuperScript™ III first-strand synthesis (Invitrogen) 73
2.1.7 Real-Time Quantitative PCR (qRT-PCR) 73
2.1.7.1 FastStart Universal SYBR Green Master (Rox) (Roche) 73
2.1.7.2 Luna® Universal One-Step qRT-PCR (NEB) 74
2.1.8 SDS-PAGE Western Blot assay 74
2.1.9 Dual luciferase assay (Promega) 75
2.1.10 Immunofluorescence staining 75
2.2 Tissue culture methods 76
2.2.1 Tissue culture medium, cell culture reagents and recombinant interferons 76
2.2.2 Cell maintenance 77
2.2.3 Enumeration of cells - trypan blue exclusion 77
2.2.4 Cryopreservation of cells 78
2.2.5 Resuscitating cells from cryopreservation 78
2.2.6 Transient transfection of plasmid DNA or poly I:C (Lipofectamine 2000, Invitrogen) 78
2.2.7 Transient siRNA transfection (RNAiMAX, Invitrogen) 79
2.2.8 Concentration of protein in cell-culture supernatant 79
2.2.9 Amplification of viral seed stocks 80
2.2.10 Plaque assay 80
2.2.11 Focus forming assay 81
2.3 Specific protocols for mutagenesis and mutant screening (Chapters 3 and 4) 81
2.3.1 Generation of viral seed stocks from DNA transfection of ZIKV infectious clones 81
2.3.2 Half maximal inhibitory concentration (IC_{50}) assay for IFNα treatment 81
2.3.3 Cloning the ZIKV MuA transposon insertion mutant library (Mutation Generation System Kit, Thermo Scientific) 82
2.3.4 DENV mutant screening 84
2.3.4.1 Recovery of library from frozen stock 84
2.3.4.2 Passaging of the recovered mutant library 84
2.3.4.3 Genome sample preparation and NGS sequencing 85
2.3.5 Preparation of DENV infectious clone plasmids and in vitro synthesis of viral RNA (mMESSAGE mMACHINE® SP6, Invitrogen) 85

2.3.6 Transfection of in vitro transcribed RNA for viral production kinetics assays and the propagation of DENV infectious virus stocks (DMRIE-C, Invitrogen) 86
2.3.7 IFN sensitivity assay 87
2.4 Cultured Cell lines 87
2.4.1 Ect1 87
2.4.2 HeLa 87
2.4.3 Huh-7 87
2.4.4 Huh-7.5 87
2.4.5 HTR8 88
2.4.6 HEK 293T 88
2.4.7 Ishikawa 88
2.4.8 Vero E6 88
2.4.9 VK2 88

CHAPTER 3 89
3 CONSTRUCTION OF A ZIKV TRANSPOSON MUTANT LIBRARY 89
3.1 Introduction 89
3.2 Results 90
3.2.1 Testing ZIKV reverse genetics systems 90
3.2.2 Optimisation of screening conditions 94
3.2.3 Generation of the ZIKV MuA transposon mutant library 98
3.2.4 Testing the ZIKV MuA transposon mutant library for viability 104
3.3 Discussion 106
3.4 Conclusions 108

CHAPTER 4 109
4 SCREENING A DENV TRANSPOSON MUTANT LIBRARY TO IDENTIFY MUTATIONS THAT CONFER IFN SENSITIVITY 109
4.1 Introduction 109
4.2 Results 111
4.2.1 Optimisation of screening conditions 111
4.2.2 Recovery of the DENV2 insertion library 113

4.2.3 Sample preparation and NGS analysis 118
4.2.4 Identification of mutations that are likely to enhance DENV IFN sensitivity 122
4.2.5 Cloning individual mutations into the full-length DENV genome 122
4.2.6 Testing the replication kinetics of the individual DENV mutants 126
4.2.7 Testing the IFN sensitivity of the individual DENV mutants 133
4.3 Discussion 137
4.4 Conclusions 146

CHAPTER 5 147
5 (Manuscript in preparation) IFN-epsilon (IFNε) is a distinct constitutively expressed type-I IFN in the female reproductive tract that protects against ZIKV infection 147
5.1 Abstract 148
5.2 Introduction 148
5.3 Results 149
5.3.1 ZIKV replication is inhibited by endogenous IFNε in a mouse model of vaginal transmission 149
5.3.2 Antiviral effect of IFNε on cells of vaginal and cervical origin 151
5.3.3 Treatment of cells with IFNε prior to infection precedes ZIKV evasion of type-I and type-III IFN signalling pathways 152
5.3.4 IFNε constitutive expression is not inhibited by ZIKV infection or NS proteins 154
5.4 Discussion 155
5.5 Conclusion 159
5.6 Materials and Methods 159
5.6.1 Virus 159
5.6.2 Cell lines, reagents and recombinant IFNs 159
5.6.3 Mice 159
5.6.4 Intravaginal infection and treatments of mice 159
5.6.5 Plaque assay – detection of infectious virus and collection of vaginal wash samples 160
5.6.6 Tissue RNA extractions and cDNA preparation and qRT-PCR 160
5.6.7 Quantification and analysis of viral RNA (vRNA) genome copies per µg RNA determination of lower LOD for uninfected tissues 161

5.6.8 Viral RNA *In Situ* Hybridization 161
5.6.9 RNAseq sample preparation and analysis 161
5.6.10 Focus forming assay – detection of infectious virus 162
5.6.11 Plasmids and transfections 162
5.6.12 Dual luciferase assay 163
5.6.13 Immunofluorescence microscopy 163
5.6.14 Western blot for STAT1/STAT2 phosphorylation 163
5.6.15 Statistical analyses 164
5.6.16 Acknowledgements 164
5.6.17 Funding 164
5.7 Figures 165
5.8 Supplementary Figures 174

CHAPTER 6 182
6 CHARACTERISING THE REGULATION AND INTRINSIC PROPERTIES OF IFNε *IN VITRO*.. 182
6.1 Introduction 182
6.2 Results 184
6.2.1 Cell lines of FRT origin express high levels of IFNε RNA 184
6.2.2 Primary transformed FRT cell lines express high basal levels of ISGs 186
6.2.3 Huh7 cells upregulate expression of ISGs in response to Ect1 culture supernatant...189
6.2.4 Transfection of siRNA targeting endogenous IFNε does not alter the levels of IFNε RNA, ISG RNA expression or ZIKV infection in Ect1 cells 192
6.2.5 IFNε RNA is regulated by progesterone *in vitro* 195
6.2.6 The constitutive expression of IFNε RNA is not altered by PRR activation or ZIKV infection compared to other type-I and III IFNs 198
6.2.7 Human recombinant IFNε is resistant to long-term receptor desensitization compared to IFNα *in vitro* 200
6.3 Discussion 204
6.4 Conclusion 208

CHAPTER 7 210
7 CONCLUSIONS AND FUTURE DIRECTIONS 210

APPENDICES…… 223
Appendix I: Primer sequences used in this study …….. 223
Appendix II: General solutions and buffers …… 227
Appendix III: Antibodies …….. 229
Appendix IV: ZIKV infectious clone plasmid maps …….. 231
Appendix V: DENV infectious clone and intermediate cloning vector plasmid maps, specific mutation sequences changes and 1 % agarose gel images for *in vitro* RNA…… 233
Appendix VI: Mammalian expression plasmids for ZIKV non-structural (NS) proteins ……. 238
Appendix VII: Mammalian expression plasmid for the human IFNε-FLAG protein …….. 242
Appendix VIII: Published first author manuscript “The molecular interactions of DENV and ZIKV with the type-I IFN response” (21 page PDF)…….. 243

BIBLIOGRAPHIC REFERENCES …… 265

List of Figures

Figure 1.1: The geographic distribution of ZIKV and DENV ……2

Figure 1.2: Mosquito transmission cycles of ZIKV and DENV ……5

Figure 1.3: Alternative transmission modes of ZIKV ……5

Figure 1.4: Symptoms caused by ZIKV and DENV infection ……9

Figure 1.5: The *Flavivirus* genome ……16

Figure 1.6: Interior and exterior views of the mature *Flavivirus* virion ……16

Figure 1.7: Stages of the *Flavivirus* lifecycle ……22

Figure 1.8: Recognition of RNA viruses by host pattern recognition receptors ……27

Figure 1.9: Type-I and type-III IFN signalling pathways ……31

Figure 1.10: Hormonal regulation of IFNε in mice and humans ……36

Figure 1.11: Binding kinetics of the IFNs with the type-I IFN receptor ……39

Figure 1.12: Uses of reverse genetics systems for *de novo* generation of infectious virus ……52

Figure 1.13: MuA transposon mutagenesis ……55

Figure 3.1: Schematic representation of the ZIKV infectious clones pZIKV-ICD and pZIKV-MR766-WT ……91

Figure 3.2: Transfection of the infectious clone pZIKV-ICD or pZIKV-MR766-WT into permissive cells initiates the complete ZIKV lifecycle ……93

Figure 3.3: The spread of infection following pZIKV-ICD transfection and the permissiveness of cells to ZIKV infection varies between cell lines ……95

Figure 3.4: The kinetics of infectious virus production following transfection with the pZIKV-ICD infectious clone in various cell lines ……97

Figure 3.5: Determination of the IC_{50} concentration of IFNα for inhibition of ZIKV replication ……99

Figure 3.6: The MuA reaction transformation efficiency and diagnostic digest of the pooled intermediate pZIKV-ICD mutant library ……101

Figure 3.7: Diagnostic restriction digest to detect recombination in the final pooled pZIKV-ICD mutant library ……103

Figure 3.8: Transfection efficiency and infectious virus production are impaired following transfection of the final pooled pZIKV-ICD mutant library ……105

Figure 4.1: Determination of the IC50 concentration of IFNα treatment against DENV infection ……112
Figure 4.2: Re-purposing the DENV2 MuA mutant library to identify mutations that alter DENV IFN evasion ……114
Figure 4.3: IFN selection of the DENV mutant library ……116
Figure 4.4: Next generation sequencing of the selected DENV mutant library ……119
Figure 4.5: Zoomed insets of specific regions of interest from passage 2 ……121
Figure 4.6: Statistical analysis of the top hits for IFN hypersensitive mutations as determined by NGS ……123
Figure 4.7: 1% Agarose gel-electrophoresis for visualisation of diagnostic restriction digests performed for each final preparation of pFK-DVs parent, Wildtype synthetic mutation (WT-s.m) or insertion mutant plasmid ……127
Figure 4.8: Replication kinetics of individual mutant viruses containing transposon insertions at nucleotide positions 1610, 1760, 2941 and 4884 within the DENV2 genome ……129
Figure 4.9: Replication kinetics of individual mutant viruses containing transposon insertions at nucleotide positions 8069, 8077 and 8086 within the DENV2 genome including the corresponding parental WT clone with synthetic mutations ……130
Figure 4.10: Replication kinetics of individual mutant viruses containing transposon insertions at nucleotide positions 9795, 10297 and 10388 within the DENV2 genome including the corresponding parental WT clone with synthetic mutations ……131
Figure 4.11: IFN sensitivity assay of mutant viruses containing transposon insertions at nucleotide positions 1610, 1760, 2941 and 4884 within the DENV2 genome ……134
Figure 4.12: IFN sensitivity assay of mutant viruses containing a transposon insertion mutation at nucleotide position 8086 within the DENV2 genome and including the synthetic mutation (WT) counterpart ……135
Figure 4.13: IFN sensitivity assay of mutant viruses containing transposon insertions at nucleotide positions 9795, 10297 and 10388 within the DENV2 genome including the corresponding WT clone with synthetic mutations ……136
Figure 5.1: ZIKV replication is inhibited by IFNε in a mouse model of vaginal transmission …165
Figure 5.2: Ectocervical and Vaginal cell lines are permissive to ZIKV infection and treatment with IFNε is antiviral ……167

Figure 5.3: IFNε displays typical type-I IFN kinetics but induces an antiviral gene signature like IFNλ-3 at early time points in ectocervical and vaginal cells ……168
Figure 5.4: ZIKV evades type-I and III IFN antiviral activity post-infection ……170
Figure 5.5: Antiviral protection mediated by IFNε and other type-I IFNs is potently inhibited due to ZIKV inhibition of STAT1/2 signalling ……171
Figure 5.6: Evasion of IFNε antiviral activity is mediated by ZIKV NS5 degradation of STAT2……172
Figure 5.7: IFNε RNA expression is not reduced by ZIKV infection or NS protein expression ……173
Supplementary Figure 5.1: ZIKV replication is inhibited by IFNε in a mouse model of vaginal transmission……174
Supplementary Figure 5.2: IFNε is highly expressed by tissues of the FRT and in the brain of WT mice ……175
Supplementary Figure 5.3: RNAscope in-situ hybridisation (ISH) of ZIKV RNA in FRT tissues at 5 dpi ……176
Supplementary Figure 5.4: ISG induction in the uterus and ovary in DMPA treated uninfected IFNε-/- mice ……177
Supplementary Figure 5.5: iVag treatment of wildtype mice with IFNε neutralising antibody enhances ZIKV infection in the vagina but not in other tissues desensitization ……178
Supplementary Figure 5.6: Ect1 and VK2 cells were treated with IFNε, IFNα-2a or IFNλ-3 (100 ng/mL) or left untreated (n = 4) for 6hr prior to RNASeq analysis ……179
Supplementary Figure 5.7: Protein expression for ZIKV NS-FLAG expression constructs as indicated by immunofluorescence staining of FLAG protein ……180
Supplementary Figure 5.8: Murine IFNε stimulate the ISG expression in human cell lines via ISRE driven JAK/STAT pathway activation ……181
Figure 6.1: Cell lines of female reproductive tract origin express high levels of IFNε RNA …185
Figure 6.2: Primary transformed female reproductive tract cell lines express high basal levels of ISGs ……187
Figure 6.3: Primary transformed female reproductive tract cell lines are naturally resistant to ZIKV infection ……188
Figure 6.4: Huh7 cells upregulate expression of ISGs in response to supernatant from primary transformed female reproductive tract cell lines ……190

Figure 6.5: Treatment of Huh7 cells with Ect1 supernatant increases ISRE promoter activity……191
Figure 6.6: Transfection of IFNε siRNA reduces the levels of overexpressed IFNε-FLAG protein ……193
Figure 6.7: Transfection of siRNA targeting endogenous IFNε does not alter the levels of IFNε RNA, ISG RNA expression in Ect1 cells ……194
Figure 6.8: Transfection of siRNA targeting endogenous IFNε does not alter the levels of ZIKV infection in Ect1 cells ……196
Figure 6.9: IFNε RNA is regulated by progesterone in vitro ……197
Figure 6.10: The constitutive expression of IFNε RNA in primary transformed FRT cell lines is not altered by ZIKV infection like other type-I and III IFNs ……199
Figure 6.11: IFNα but not IFNβ signal transduction is regulated by long-term, IFN-induced receptor desensitization……201
Figure 6.12: Human recombinant IFNε is resistant to long-term, IFN-induced receptor desensitization compared to IFNα *in vitro*……203
Figure 7.1: Working model of IFNε-mediated protection of the FRT from ZIKV infection, compared to canonical type-I IFN(α/β) ……221

List of Tables

Table 3.1: Summary of the initial and optimised reaction conditions for bacterial transformations of the ZIKV-ICD MuA transposase reaction ……101

Table 3.2: Summary of the initial and optimised reaction conditions for bacterial transformations of the final ligation reaction of the pZIKV-ICD mutant library ……103

Table 4.1: Summary of methods used to subclone insertion mutations with synthetic restriction sites into the respective pUC57 intermediate vectors ……125

Table 4.2: Summary of methods used to subclone insertion mutations (either directly from a synthetic dsDNA fragment or from the pUC57 intermediate vector) into the pFK-DVs destination vector ……125

Abstract

The emergence of zoonotic viruses is an inherent risk to our global civilisation as we encroach on new environments and increase our reliance on high-intensity farming to feed a growing population. Aside from the current SARS-CoV-2 pandemic, zoonotic flaviviruses like dengue virus (DENV) and Zika virus (ZIKV) are significant human pathogens and are rapidly expanding their geographic range. Outbreaks caused by these viruses result in death and disease especially in young children and the developing foetus. Moreover, these viruses place a significant economic burden on the worlds most under-developed nations. As a society we are now left grappling with the question of how we will manage future viral outbreaks and how we will protect ourselves when they occur. Type-I Interferons (IFN) are expressed by the host in response to viral infection. The IFNs act to clear viral infection by inducing the expression of hundreds of interferon stimulated genes (ISGs) that have direct antiviral or immune regulatory functions. However, viruses have evolved mechanisms to counteract the IFN response allowing them to replicate, spread and cause disease. Furthermore, our understanding of the antiviral action of IFNs in specific anatomical niches is rudimentary. In this thesis we explore the virus dependent mechanisms that abrogate the type-I IFN response and characterise the role of novel IFNε in preventing ZIKV infection of the female reproductive tract (FRT).

Viral evasion of the innate immune system relies on interaction between viral and cellular proteins. These interactions are often not recapitulated by expression of individual viral genetic elements. While some of these evasion mechanisms are known for both viruses, the lack of whole genome mutational studies means that our knowledge of these interactions is incomplete. To overcome this limitation, this thesis aimed to apply a genome-wide high-throughput mutagenesis approach coupled to Next Generation Sequencing (NGS) to screen for regions of the ZIKV and DENV genome that confer IFN evasion. Initial attempts to introduce genome-wide mutations into ZIKV were hampered by reaction efficiency and recombination of the infectious clone. Within the field this is recognised as a commonly occurring issue and is often reliant on subtle nuances within the viral genome sequence. As a

result, a DENV mutant library was used to screen viruses based on their ability to complete the full virus lifecycle under low level IFN stimulation (IFNα, IC_{50} 1 U/mL). This led to the generation of a functional map, highlighting regions of the DENV genome likely to be involved with IFN evasion including a specific region within NS5 as a known mediator of DENV evasion. Specific mutations highlighted as most likely to render DENV hypersensitive to IFN were systematically re-introduced into the wildtype DENV genome. However, none of these mutations were able to confer IFN hypersensitivity likely because of accumulation of linked mutations in the library. Several important recommendations to improve future genome-wide high-throughput mutagenesis screens have arisen from this thesis. These include reducing the rate of co-infection, increasing selection pressure and utilising new long-read sequencing technology to detect linked mutations. Collectively this would reduce the accumulation of unintended mutations in similar screens and provide the means to detect them when they occur.

As mentioned above, the classical type-I IFN response is reactionary, and this delay is exploited by viruses to gain a foothold and cause disease. In contrast, the newly discovered IFNε, is constitutively expressed predominantly in the FRT. The FRT is highly permissive to ZIKV infection via sexual transmission and in some cases infection of the developing foetus during pregnancy. Currently, IFNε is known to protect against Herpes Simplex Virus (HSV) in the FRT and Human Immunodeficiency Virus (HIV) in cell culture but its potential to protect against sexually acquired ZIKV is unknown. To address this a multifaceted approach using *in vivo* and *in vitro* modelling of ZIKV infection in the FRT was applied. The results of this thesis show that IFNε is unequivocally important to protect the FRT from viral infection. Using a mouse model of intravaginal ZIKV transmission we showed IFNε knockout mice were more susceptible to ZIKV infection compared to wildtype mice. Our transcriptomic analysis revealed IFNε mediated the induction of a protective anti-ZIKV gene profile involving multiple ISGs in FRT cells but with minimal induction of pro-inflammatory genes. This discovery is significant to the field as inflammation disrupts FRT barrier integrity and may promote infection of deeper tissues. Although the antiviral activity of IFNε was susceptible to ZIKV NS5 mediated evasion after infection was established, the prophylactic expression of IFNε was not inhibited by ZIKV meaning it can circumvent this evasion. The potential of IFNε as a prophylactic treatment was proven by intravaginal administration of exogenous IFNε that rescued antiviral protection in IFNε knockout mice challenged with ZIKV. Collectively this data

highlights the prophylactic potential of naturally expressed and exogenous IFNε in protecting the FRT from ZIKV sexual transmission. Importantly, this shifts our understanding of innate immunity in the FRT from its reliance on reactionary responses to pre-emptive protection against viral infections.

In conclusion, genome-wide mutational studies are a valuable tool to provide insight into the molecular aspects of viral evasion. Despite not finding novel ZIKV or DENV evasion mechanisms by this method, the screening and NGS approach used here could be modified for future endeavours. Additionally, to protect environments with high exposure risk to viral pathogens the host has evolved niche specific immunity. One example of this is IFNε in the FRT. Here we have shown constitutively expressed IFNε prophylactically protects the FRT from ZIKV infection. This finding has shifted the paradigm of antiviral protection of the FRT, demonstrating constitutive protection rather than reactionary IFN responses can effectively protect against ZIKV sexual transmission. Collectively, this thesis has made significant headway in characterizing the molecular interactions between the host innate immune response and globally significant flaviviruses on both sides of the evolutionary arms race.

Declaration

I certify that this work contains no material which has been accepted for the award of any other degree or diploma in my name, in any university or other tertiary institution and, to the best of my knowledge and belief, contains no material previously published or written by another person, except where due reference has been made in the text. In addition, I certify that no part of this work will, in the future, be used in a submission in my name, for any other degree or diploma in any university or other tertiary institution without the prior approval of the University of Adelaide and where applicable, any partner institution responsible for the joint-award of this degree. I acknowledge that copyright of published works contained within this thesis resides with the copyright holder(s) of those works. I also give permission for the digital version of my thesis to be made available on the web, via the University's digital research repository, the Library Search and also through web search engines, unless permission has been granted by the University to restrict access for a period of time. I acknowledge the support I have received for my research through the provision of an Australian Government Research Training Program Scholarship.

Rosa Coldbeck-Shackley

Date: 22/02/2021

Acknowledgements

To my amazing partner Olexij. Thank-you for your patience and support. You have seen me through the rollercoaster ride of secondary, tertiary, and now doctoral qualifications. Now that I am finally finishing my formal education, I look forward to sharing the profits with you into the future.

A special thank-you to my mother and father, Sue and Adrian. I have been very privileged to grow-up in an environment so encouraging in the pursuit of knowledge. Without your example and support I would not have been set on this life path.

Thank-you to my supervisor, Professor Michael Beard, for the opportunity to complete my PhD in your lab, for your guidance, and for the knowledge that you have given to me as your student.

I would also like to thank my co-supervisor, Doctor Nicholas Eyre. Your experience, patience and troubleshooting skills have been vital to completion of my PhD. I look forward to working with you into the future.

Thank-you to all the members of the Viral Pathogenesis and Molecular Virology Group Laboratories. I have made some great friendships with all of you. Thanks for being there to support me and for helping me to blow-off some steam after a hard week's work.

Thankyou also to all our interstate collaborators at the Hudson Institute of Medical Research, especially Professor Paul Hertzog and Associate Professor Michelle Tate. The opportunity to meet, collaborate and share good wine with such excellent scientists has vastly improved my experience of research. I hope to continue to work with you both into the future.

Presentations, Publications and Awards Arising from this PhD

Presentations:

Rosa Coldbeck-Shackley, Michelle Tate, Sarah Rosli, Jamie Gearing, Jodee Gould, San Lim, Kylie Van der Hoek, Nicholas Eyre, Sarah Robertson, Sonja Best, Paul Hertzog and Michael Beard. The unique type-I Interferon-epsilon (IFNε) constitutively protects the female reproductive tract from Zika Virus infection. E-poster. Lorne Infection & Immunity Conference 2021 meeting, Hosted online

Rosa Coldbeck-Shackley, Michelle Tate, Sarah Rosli, Jamie Gearing, Jodee Gould, San Lim, Kylie Van der Hoek, Nicholas Eyre, Sarah Robertson, Sonja Best, Paul Hertzog and Michael Beard. The unique type-I Interferon-epsilon (IFNε) constitutively protects the female reproductive tract from Zika Virus infection. Oral presentation. International Cytokine & Interferon Society Cytokines 2020 meeting, Hosted online

Rosa Coldbeck-Shackley, Michelle Tate, Sarah Rosli, Jamie Gearing, Jodee Gould, San Lim, Kylie Van der Hoek, Nicholas Eyre, Sarah Robertson, Sonja Best, Paul Hertzog and Michael Beard. Interferons, Zika Virus and their Host Pathogen Interaction in the Female Reproductive Tract. Oral presentation. Guest student speaker with the Department of Immunology, University of Toronto hosted by the Hudson Institute of Medical Research, Victoria, Australia, 2020

Rosa Coldbeck-Shackley, Michelle Tate, Sarah Rosli, Jamie Gearing, Jodee Gould, San Lim, Kylie Van der Hoek, Nicholas Eyre, Sarah Robertson, Sonja Best, Paul Hertzog and Michael Beard. INTERFERON-EPSILON IS A UNIQUE TYPE-I IFN EXPRESSED IN THE FEMALE REPRODUCTIVE TRACT THAT SUPRESSES ZIKV REPLICATION AND INTRAVAGINAL TRANSMISSION. Poster presentation. International Cytokine & Interferon Society Cytokines 2019 meeting, Vienna, Austria, 2019

Rosa Coldbeck-Shackley, Michelle Tate, Sarah Rosli, Jamie Gearing, Jodee Gould, San Lim, Kylie Van der Hoek, Nicholas Eyre, Sarah Robertson, Sonja Best, Paul Hertzog and Michael Beard. SEXUAL HEALING: IFNε a Type-I Interferon in the female reproductive tract protects

against ZIKV replication in vitro and in a mouse model of intra-vaginal transmission. Oral presentation. Lorne Infection & Immunity Conference, Victoria, Australia, 2019

Publications:

Rosa Coldbeck-Shackley, Michelle Tate, Sarah Rosli, Jamie Gearing, Jodee Gould, San Lim, Kylie Van der Hoek, Nicholas Eyre, Sarah Robertson, Sonja Best, Paul Hertzog and Michael Beard. IFNε is a novel type-I IFN in the female reproductive tract that protects against ZIKV replication in vitro and in a mouse model of intra-vaginal transmission. (manuscript in preparation)

Rosa Coldbeck-Shackley, Nicholas Eyre and Michael Beard. The molecular interactions of DENV and ZIKV with the type-I IFN response (review), Vaccines, Issue 8, 2020 (published manuscript), see Appendix VIII for full version.

Awards:

2020 Milstein Abstract Award – 8th Annual Meeting of the International Cytokine and Interferon Society - Cytokines 2020 (held online), $500 AUD.

2020 DMM Conference Travel Grant for International Travel (cancelled due to COVID19), 1,000 AUD.

2019 University of Adelaide Research Travel Scholarship for International Travel, $ 1,000 AUD.

2018 Faculty of Sciences 9th Annual Postgraduate Symposium Poster Award, $ 200 AUD.

2017 Australian Government Research Training Program Scholarship for Doctor of Philosophy program, $28,092 AUD per annum.

2017 Scholarship award for Master of Philosophy by Research program, $22,500 AUD per annum.

Materials Providers

Abcam	Cambridge, UK
Applied Biosystems	Massachusetts, USA
Beckman Coulter	Miami, FL, USA
Bioline	Sydney, Australia
BioRad Laboratories	California, USA
Cell Signaling	Massachusetts, USA
Corning	New York, USA
Dharmacon	Lafayette, USA
Eppendorf	Hamburg, Germany
GeneWorks	Adelaide, SA, Australia
iNtRON Biotechnology	Seoul, South Korea
Invitrogen	California, USA
Kimble-Chase Life Science	Tennessee, USA
Lucigen	Wisconsin, USA
Macherey Nagel	Düren, Germany
Merck Serono	Darmstadt, Germany
New England Biolabs	Massachusetts, USA
Nikon	Tokyo, Japan
Olympus	Tokyo, Japan
PeproTech	New Jersey, USA
Promega	Wisconsin, USA
QIAgen	Hilden, Germany
R&D systems	Minneapolis, USA
Roche	Indiana, USA
Sartorius Stedim	Göttingen, Germany
Sigma Aldrich	Missouri, USA
Strategene	California, USA

Abbreviations

Abbreviation or symbol	Term
^{o}C	Degree(s) Celsius
µg	Microgram(s)
µl	Microliter(s)
µm	Micrometre(s)
A	Adenine, Alanine
ADE	Antibody dependent enhancement
AmpR	Ampicillin resistance
ATP	Adenosine triphosphate
bp	Base pair(s)
BSA	Bovine serum albumin
C	Cytosine
CARD	Caspase recruitment and activation domain
CDC	Centre for disease control
cDNA	Complementary deoxyribonucleic acid
cGAS	Cyclic GMP-AMP synthase
CMV	Cytomegalovirus
DAPI	4', 6-Diamidino-2-pheylinodole
dATP	Deoxyadenosine triphosphate
DB	Dumbbell
dCTP	Deoxy cytosine triphosphate
DENV	Dengue Virus
DF	Dengue fever
dGTP	Deoxy guanosine triphosphate
dH2O	Deionised water
DHF	Dengue haemorrhagic fever
DMEM	Dulbecco's Modified Eagle Medium with HEPES
DMPA	Depot medroxyprogesterone acetate

DMSO	Dimethyl sulfoxide
DNA	Deoxyribonucleic acid
dNTP	Deoxynucleotide triphosphate
dsRNA	Double stranded RNA
DSS	Dengue shock syndrome
dTTP	Deoxythymidine triphosphate
E2	Estrogen
E. coli	Escherichia coli
EDTA	Ethylenediamine tetra acetic acid
ER	Endoplasmic reticulum
ERα	Estrogen receptor alpha
ERβ	Estrogen receptor beta
FCS	Foetal calf serum
FFU	Focus forming units
FRT	Female reproductive tract
G	Guanosine
g	Gram(s) or *acceleration gravity*
GAG	Glycosaminoglycan
GBS	Guillain-Barre syndrome
GFP	Green fluorescent protein
h	hours
HCV	Hepatitis C virus
HIV	Human immunodeficiency virus
hpi	Hours post infection
hpt	Hours post transfection
HRP	Horse radish peroxidase
Huh	Human hepatoma
HSV	Herpes Simplex Virus
IAV	Influenza A virus
IC_{50}	Half maximal inhibitory concentration
IFNα	Interferon alpha
IFNAR1/2	Interferon alpha receptor subunit 1 / 2
IFNβ	Interferon beta
IFNε	Interferon epsilon

IFNλ	Interferon lambda
IFNL1R	Interferon lambda receptor subunit 1
Ig	Immunoglobulin(s)
IKKε	IκB kinase-ε
IP	Intraperitoneal
IRF	Interferon response factor
ISG(s)	Interferon stimulated gene(s)
ISGF3	Interferon stimulated gene transcription factor 3
ISRE	Interferon stimulated response element
IV	Intravenous
iVag	Intravaginal
JAK	Janus kinase
JEV	Japanese Encephalitis Virus
KanR	Kanamycin resistance
kb	Kilo-base(s)
kDa	Kilodalton(s)
kg(s)	Kilogram(s)
KO	Knock out
LB-Agar	LB + agar
LB	Luria Bertani broth
LFRT	Lower female reproductive tract
LPS	Lipopolysaccharide
Luc	Luciferase
M	Mole
mA	Milliampere(s)
mAb	Monoclonal antibody
MAVS	Mitochondrial antiviral-signalling protein
MDA5	Melanoma differentiation-associated gene 5
mg	Milligram(s)
min	Minute(s)
mL	Millilitre(s)
mM	Millimolar(s)
MOI	Multiplicity of infection

mRNA	Messenger ribonucleic acid
MuA	MuA transposase enzyme
MTase	Methyltransferase
MW	Molecular weight
N/A	Not applicable
N/D	None detected
NF	Nuclease free
ng	Nanogram(s)
NGS	Next generation sequencing
NK	Natural killer
nM	Nanomolar
NS	Non-structural
nt (s)	Nucleotide (s)
NTP(s)	Nucleotide triphosphate(s)
ORF	Open reading frame
P4	Progesterone
PAMP	Pathogen associated molecular pattern
PBS	Phosphate buffered saline
PCR	Polymerase chain reaction
PFU	Plaque forming unit
pg	Picograms
pH	Negative logarithm of hydrogen ion activity
pM	Picomolar
PRA	Progesterone receptor isoform A
PRB	Progesterone receptor isoform B
PRR	Pattern recognition receptor
qRT-PCR	Quantitative reverse transcribed polymerase chain reaction
RC	Replication complex
RdRp	RNA-dependent RNA polymerase
RIG-I	Retinoic acid-inducible gene I
RIG-I-N	Retinoic acid-inducible gene I N-terminal mutant construct
RNA	Ribonucleic acid

RNase	Ribonuclease
rpm	Revolutions per minute
RT	Room temperature
SC	Subcutaneous
sd	Standard deviation
SDS	Sodium dodecyl sulphate
SDS-PAGE	Sodium dodecyl sulphate polyacrylamide gel electrophoresis
sfRNA(s)	Sub-genomic *Flavivirus* RNA(s)
sec	Second(s)
SL	Stem-loop
SOC	Super optimal broth with catabolite repression
SOCS	Suppressor of cytokine signalling
ss	Single stranded
ssRNA	Single stranded RNA
STAT	Signal transducer and activator of transcription
STING	Stimulator of Interferon Genes
T	Thymidine
TAE	Tris, acetic acid, EDTA (TAE) buffer
TLR	Toll-like receptor
TORCH pathogens	Toxoplasma gondii, others, rubella virus, cytomegalovirus (CMV), and herpes simplex virus (HSV) – pathogens are a high risk in pregnancy
TYK2	Tyrosine kinase 2
UFRT	Upper female reproductive tract
U/mL	International unit(s) of IFN per microliter
USP18	Ubiquitin specific peptidase 18
UTR	Untranslated region
uv	Ultraviolet
V	Volt(s)
vRNA	Viral RNA

v/v	Volume per unit volume
w/v	Weight per volume
WHO	World Health Organization
WNV	West Nile Virus
WT	Wildtype
ZIKV	Zika Virus
ZVCS	Zika Virus congenital syndrome

Chapter 1

Introduction

1.1 Zika virus and dengue virus

1.1.1 ZIKV and DENV epidemiology

Flaviviruses that cause human disease exist on every inhabited continent and combined cause a significant health and economic burden [23]. The global distribution and geographic range of these viruses are largely determined by their corresponding arthropod vector [118]. In general, these are either tick-borne viruses or they are transmitted by mosquitoes [23]. Specifically, this thesis will focus on Zika Virus (ZIKV) and Dengue Virus (DENV) that are primarily transmitted by mosquitoes of the *Aedes* species (*aegypti* and *albopictus*) and as a result have a broad geographic range as shown in Figure 1.1 [337]. Mosquitoes that transmit ZIKV and DENV are endemic in tropical and subtropical regions of the Americas, Africa, Europe, Asia and the South Pacific region including Australia [199].

ZIKV is an emerging *Flavivirus* that has rapidly expanded its epidemiological niche due to a series of outbreaks occurring since the early 2000's. ZIKV was first discovered in Uganda, Africa in 1947 and for the following 60 years its geographic range was confined to equatorial regions of Africa and Asia [240, 329]. In the years following its discovery ZIKV was not heavily studied because at the time it was thought to only cause mild symptoms in humans. In 2007 ZIKV caused the first outbreak outside of Africa or Asia on Yap Island in the Pacific region. Introduction of ZIKV into a naive population resulted in approximately 73% of the Islands 7000 inhabitants becoming infected, with the majority showing no clinical symptoms (see section 1.1.3 for a list of symptoms) [86]. Following this initial outbreak, ZIKV spread to new regions causing a series of outbreaks incrementally increasing in size. First in French Polynesia during 2013–2014 [39], then Latin America in 2015 [390] and finally disseminating into North America during 2016 [144]. The 2015-2016 outbreak in the Americas was the event that brought ZIKV onto the world stage. Transmission was first detected in Brazil early 2015 [390] and by the years end between 440,000 and 1,300,000 suspected ZIKV cases were recorded in Brazil alone [38]. As the outbreak unfolded, scientists and clinicians began to realize that ZIKV infection was associated with more severe symptoms that had been previously undetected in

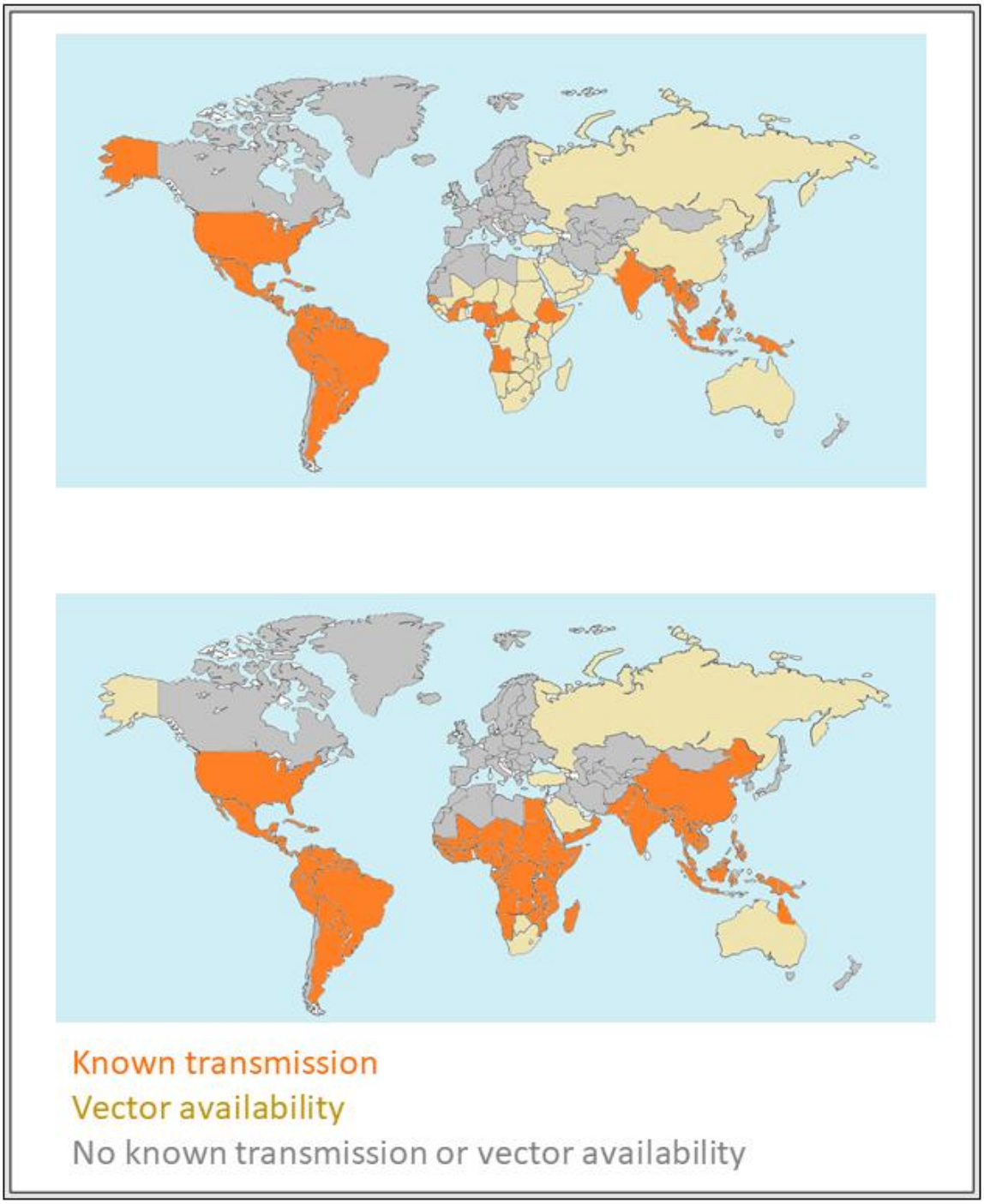

Figure 1.1: The geographic distribution of Zika Virus (A) and Dengue Virus (B). Graphs display global regions with known transmission (orange), mosquito vector (*Aedes aegypti* and *albopictus*) availability (brown). Adapted from sources: [400], [401].

smaller population sizes. These symptoms included neurological complications such as Guillain-Barre Syndrome (GBS) in adults and microcephaly in new-borns. Retrospective analyses have now confirmed that these symptoms were also a feature of prior outbreaks [40]. Because of its large scale and the developing knowledge of ZIKV pathology the World Health Organization (WHO) declared the 2015-2016 outbreak a public health emergency of international concern [363]. In the wake of the 2015-16 outbreak ZIKV has spread to more than 87 countries globally including a small number of transported cases to Europe. Most recently in October 2019 three vector-borne autochthonous cases of ZIKV were detected in Hyeres, France indicating ZIKV is circulating in this region [112]. Several hypotheses have been proposed to explain the explosive scale of the Americas outbreak. Factors such as geo-climactic conditions, socio-economic circumstances, increased travel into affected areas, introduction into a naïve population and viral adaptation all likely played a role [267]. The rapid spread of ZIKV across the globe serves as a warning against future outbreaks of emerging zoonotic virus infections.

In contrast to the historically obscure ZIKV, the disease caused by DENV infection has been recorded in historical texts for centuries. The earliest record of symptoms compatible with DENV infection were published in a Chinese medical encyclopaedia in 992 AD [239]. However, the virus that is the causative agent of Dengue fever was not isolated until 1943 during an epidemic outbreak in Nagasaki, Japan [337]. DENV like ZIKV likely originated in Africa or Asia. However, by the 1800's it had spread across the globe as a result of the increasing global shipping and trade [239]. DENV causes the greatest disease burden of all flaviviruses. Alone it is estimated to cause 390 million cases resulting in approximately 21,000 deaths annually. DENV is endemic in over 100 tropical and sub-tropical countries in Southeast Asia, the Pacific and the Americas [126, 127]. Its wide-spread distribution means that approximately 3.6 billion people are living in areas with a risk of DENV infection [23]. In Australia DENV is a nationally notifiable disease with seasonal cases reported each year. Between 2010-2015 there was 1,773 total cases and of these 632 resulted from autochthonous transmission with the remaining 1,141 cases being acquired overseas [8]. Alarmingly, DENV incidence has increased 30-fold in the last 50 years and has spread to new geographic regions [362]. Increasing incidence of DENV infection is caused by factors including population growth in endemic regions, global warming impacting mosquito population distribution, unplanned urbanization, inefficient mosquito control and increasing travel into DENV endemic regions

[119, 136]. In addition to the deaths caused by DENV, the scale of this disease has serious economic burden owing to the roughly 2 million cases of the severe disease requiring hospitalization annually [125].

1.1.2 Transmission of ZIKV and DENV

Human pathogenic flaviviruses are generally arthropod borne viruses (arboviruses) and are carried by two types of vectors, ticks and mosquitoes. Tick-borne viruses circulate in regional Europe and Asia and are transmitted from rodents and small animals to humans [119]. As a result of this transmission cycle these viruses tend to have a limited geographic range and reduced epidemic potential [118]. Conversely mosquito borne flaviviruses such as DENV and ZIKV have an ability to rapidly expand their geographic range upon introduction into new populations due to the widespread and increasing dispersal of their vectors [199].

1.1.2.1 Mosquito-borne transmission

Both ZIKV and DENV are transmitted by mosquitoes of the *Aedes* species, mainly *Ae. albopictus* and *Ae. aegypti*. As a result of their shared vector transmission these viruses have a similar geographic distribution and mode of transmission. These viruses are circulated in two overlapping transmission cycles as depicted in Figure 1.2 [329]. The first transmission cycle is the sylvatic cycle, where these viruses circulate between non-human primates and tree-dwelling mosquitoes maintaining a zoonotic reservoir in forested areas. The second urban cycle occurs between humans and mosquitoes adapted to living in towns and cities and is the cause of epidemic outbreaks in human populations. Generally, the level of host viremia is the most important determinant for the duration of vector borne transmission [90]. Median viremia lasts 3.5 days for ZIKV and 5 days for primary DENV infections [246, 355]. Generally, ZIKV infections have lower levels of viremia compared to DENV [357]. For ZIKV, the level of viremia directly correlates to the rate of infection and transmission in mosquitoes [345]. This is more complicated in DENV infections where asymptomatic or pre-symptomatic cases at any level of viremia are more infectious than symptomatic DENV as a result of exacerbated host immune responses interacting with the mosquito vector [90]. For ZIKV, the level of viremia has no correlation to the severity of clinical symptoms, facilitating a-symptomatic transmissions [246]. Together this information demonstrates the complicated nature of

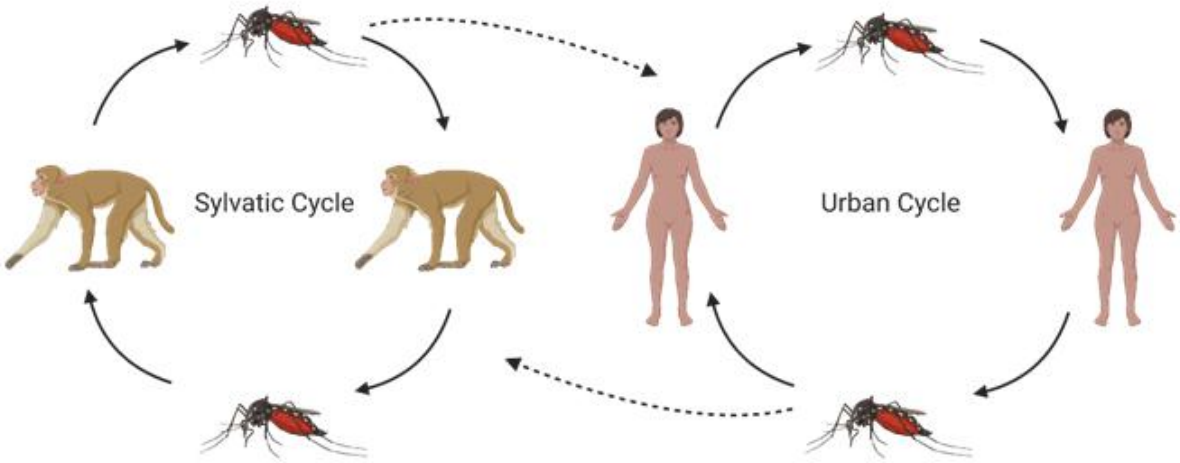

Figure 1.2: Mosquito transmission cycles of ZIKV and DENV. ZIKV and DENV are transmitted by mosquitoes of the Aedes species in two overlapping cycles. The Sylvatic cycle occurs between arboreal mosquitoes and non-human primates in forested areas. Alternatively the urban cycle occurs when the virus is transferred to towns and cities, cycling between humans and urban mosquito populations.

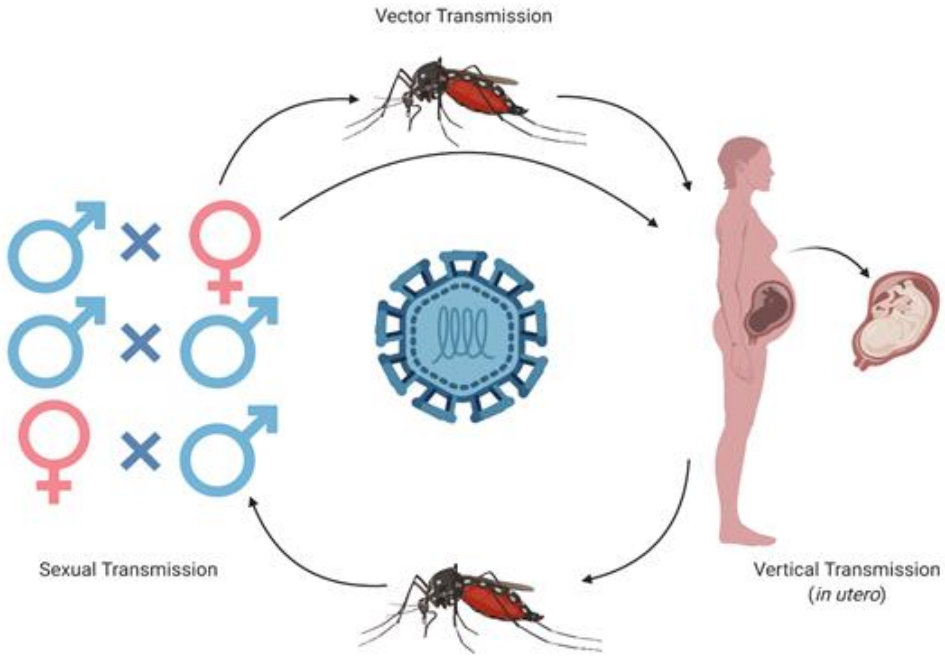

Figure 1.3: Alternative transmission modes of ZIKV. In addition to mosquito vector transmission, ZIKV has several alternative transmission routes that are caused by infection of the male and female reproductive tracts. These include sexual transmission, and vertically from mother to foetus *in utero*.

vector borne transmission even for closely related flaviviruses and highlights the importance of detailed demographic studies to predict and manage future outbreaks.

1.1.2.2 Alternative transmission modes

In addition to vector-borne transmission ZIKV is unique amongst flaviviruses because it can also be transmitted sexually and vertically from mother to foetus *in utero* as summarized in Figure 1.3 [329]. These a-typical transmission routes are facilitated by ZIKVs tropism for a wide variety of cell types in the male and female reproductive tracts [223]. Both sexual and vertical transmission can occur without presentation of clinical symptoms [33, 258].

1.1.2.2.1 Sexual transmission

Cases of ZIKV sexual transmission occur mainly between male to female partners (92.5%), but cases of both female to male and male to male transmission have been reported [228]. Sexual transmission was responsible for several transported cases outside of ZIKV endemic areas and likely complicates existing control measures within endemic areas [124]. In addition to aiding spread of the virus, animal models show sexual transmission increases the risk of foetal infection during pregnancy [88]. Unlike vector transmission that is dependent on the duration of viremia and is relatively short-lived, sexual transmission can occur months after the virus in cleared from the blood. In women, detection of ZIKV RNA persists in cervical mucous for up to 3 months post-symptom onset [272], which is far longer than its persistence in blood or urine [271]. In men, viral RNA has been recovered at a median of 25 days post symptom onset but the longest recorded detection was a staggering 370 days [20]. More importantly, infectious virus can be recovered from semen up to 69 days post-symptom onset [261]. This extended period of virus shedding in semen led the Centre for Disease Control's (CDC) to recommend a preconception waiting period for male travellers of at least 3 months post-exposure to ZIKV [48].

Sexual transmission relies on ZIKVs tropism for cells and tissues in both the male and female reproductive tract. In men, the long duration of sexual transmission correlates with viral persistence in the testes as an immune privileged site [334]. Studies in humans show ZIKV can infect spermatozoa [204]. Additionally, in non-human primate models, ZIKV infects both sperm progenitor and macrophage cells inside the seminiferous tubules and can persist up to 41 days post infection in semen [263]. Moreover, *in vitro* studies have demonstrated ZIKV

infection in prostate mesenchymal cells [331] and Sertoli cell culture persists for more than a month [177]. Currently there are fewer studies investigating ZIKV infection in the non-pregnant female reproductive tract. However, one study demonstrated that that ZIKV can be detected in both the vagina and uterus of vaginally inoculated non-pregnant rhesus macaques [41]. Furthermore, this detection persisted in the uterus after clearance of ZIKV RNA in plasma suggesting ZIKV preferentially replicates in these tissues when challenged intravaginally compared to subcutaneous inoculation.

The longevity of transmission risk, localised introduction into the female reproductive tract and the increased risk of infection during early pregnancy makes ZIKV sexual transmission an important consideration when preparing for future outbreaks and understanding ZIKV pathology. Interestingly one case of DENV sexual transmission has recently been reported by the European Centre for Disease Prevention and Control, perhaps suggesting this is an overlooked or evolving mode of DENV transmission [55].

1.1.2.2.2 Vertical transmission

In addition to sexual transmission ZIKV also infects the placenta and the developing foetus *in utero*. Vertical transmission resulting in foetal infection underpins ZIKVs most severe pathologies in neonates [153].

The placenta is an organ that transiently develops during pregnancy. It is derived from cells of foetal origin that embed into the maternal decidua, forming an interface between maternal and foetal circulation [201]. Its primary role is to facilitate the exchange of gases, nutrients, waste products, and hormones to support the growing foetus [227]. Additionally, the placenta functions as a physical and immunological barrier between maternal and foetal circulation [227]. The placenta contributes to the dynamic immunology of pregnancy, balancing roles in supporting the growth of a semi-allogenic foetus while protecting against viral and bacterial infections [72].

Like the male testes, ZIKV infection persists for longer in the placenta than it does in other tissues [25]. ZIKV persistence in the placenta likely exploits the unique immune environment of this tissue that balances between inflammatory processes during implantation and a tolerogenic response later in pregnancy to promote foetal growth [227]. In pregnant women infected during their first trimester, ZIKV RNA can be detected in the placenta up to 210 days (mean 81 days) after symptom onset with continued detection in the foetal brain and

placenta after clearance from maternal circulation [25]. In addition, studies show that placental infection is correlated with prolonged viremia in maternal circulation [338]. In some recorded cases ZIKV RNA persisted in blood until delivery [20]. Together this data implicates the placenta as a reservoir for both maternal and foetal ZIKV infections.

The mechanisms used by ZIKV to cross this barrier and infect the foetus are currently the subject of considerable active research. It is now known ZIKV can infect a wide range of cells and tissues of the maternal-foetal interface including maternally derived endometrial cells and decidua resident macrophages [92, 257, 359], as well as foetal derived cells of the placenta such as extra villous trophoblasts, Hofbauer cells, umbilical cord endothelial cells and the amniochorionic membranes [92, 340].

Together, these tropisms of the male and female reproductive tracts aid ZIKVs sexual and vertical transmission while also hindering its clearance by the immune system due to persistence in immune privileged sites.

1.1.3 Clinical presentation and pathogenesis of ZIKV and DENV infections

Broadly, there are two major categories of clinical presentation for *Flavivirus* infections dependent on disease pathogenesis and tissue or cell tropism of the virus. The first is primarily a neurological disease, such as for ZIKV infection, and is caused by direct infection of neurons leading to neuronal death or damage as a result of inflammation [23]. The second is a systemic disease characterized by vascular leakage and may include haemorrhagic symptoms. These symptoms are characteristic of DENV infections and arise due to systemic inflammation impacting upon immune cell function and endothelial cell permeability [118]. However, these manifestations are not always mutually exclusive. DENV, although not considered a classical neurotropic *Flavivirus*, can cause neurological and ocular complications as a result of infection [323]. In addition to these specific clinical manifestations ZIKV and DENV also cause a range of non-specific symptoms such as fever, rash, muscle pain and tiredness. These non-specific symptoms vary in severity and are largely caused by the innate immune response to infection. Figure 1.4 summarizes the symptoms for both ZIKV and DENV.

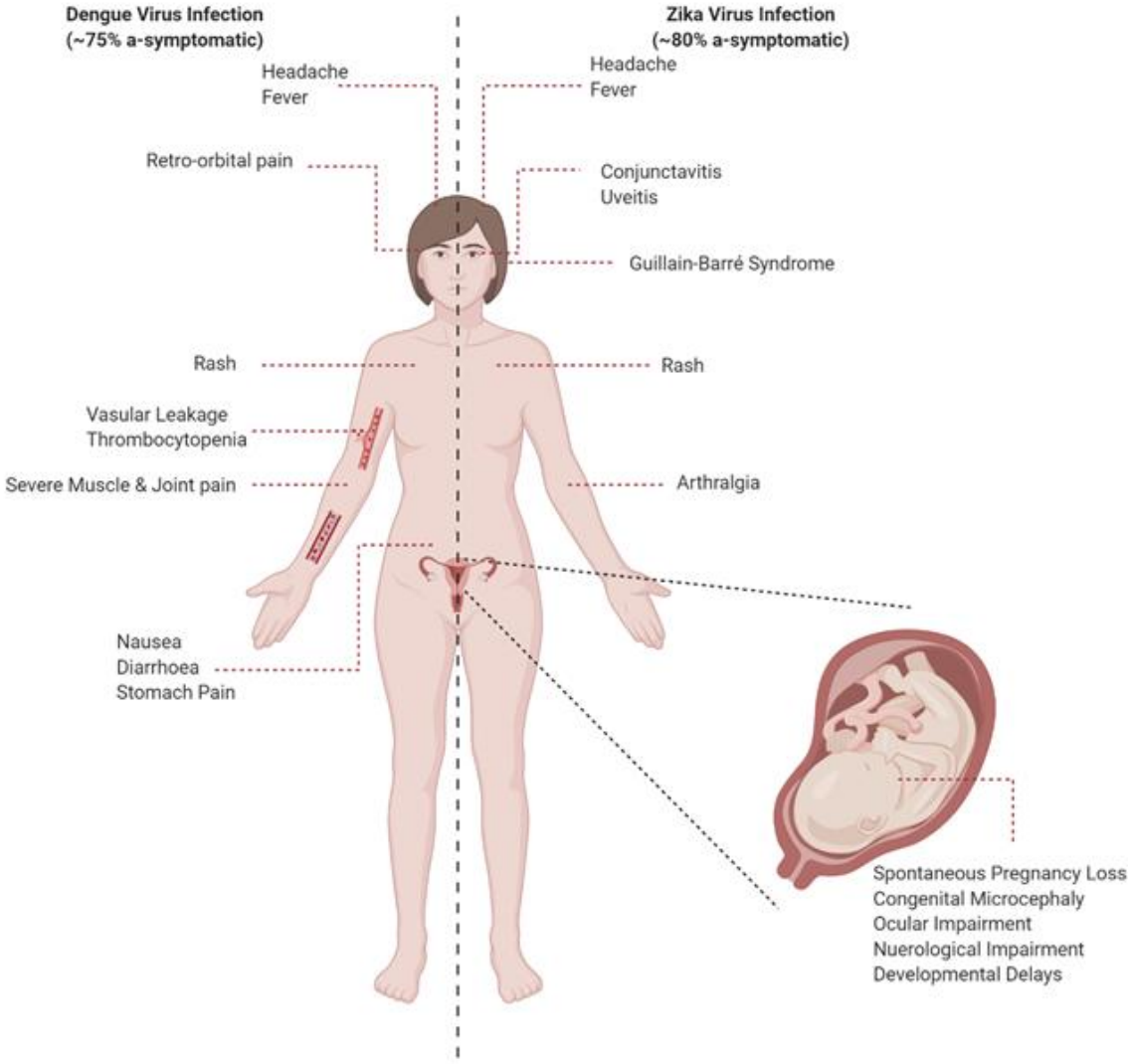

Figure 1.4: Symptoms caused by ZIKV and DENV infection. ZIKV and DENV have shared and distinct clinical presentations. Both viruses share similar rates of a-symptomatic infection and non-specific symptoms including headache, fever and rash. In addition, ZIKV infection can cause Guillain-Barre syndrome in adults and congenital abnormalities during pregnancy. DENV infections can also cause severe muscle and joint pain and haemorrhagic complications.

1.1.3.1 ZIKV clinical manifestations

ZIKV is now recognized as a neurotropic *Flavivirus* but historically these infections were considered relatively benign. This is because in healthy adults approximately 80% of cases are asymptomatic [329]. The remaining 20% of cases mostly result in a mild, self-limiting febrile illness and includes symptoms such as fever, rash, arthralgia, and conjunctivitis [329, 388]. However, recent largescale outbreaks have highlighted previously undetected pathologies of ZIKV infection such as ocular symptoms, neurological disease, and adverse pregnancy outcomes. These include uveitis, meningoencephalitis, rare (24 per 100,000) cases of GBS in adults and Zika Virus Congenital Syndrome (ZVCS) [40, 294, 308]. ZVCS encompasses a spectrum of neurological or developmental symptoms that vary in severity and occur during pregnancy or are present in neonates born to infected mothers. These include spontaneous pregnancy loss, inter-uterine growth restriction, ocular abnormalities and hearing impairment, developmental and neurological impairment and microcephaly [53]. Alarmingly, reported rates of microcephaly increased 20-fold in affected regions during the 2015/16 outbreak [54]. The incidence and severity of ZVCS increases when infection occurs during early pregnancy and it is estimated roughly one third of children born to ZIKV infected mothers display some degree of developmental delay or neurological impairment [251]. Alarmingly, ZVCS can arise even in the absence of clinical symptoms in the mother [258]. The correlation with neurological disease was confirmed retrospectively for the 2013 -2014 French Polynesia outbreak [159, 223, 279, 329] and is now widely acknowledged to be causative due to patient studies, *in vitro* and *in vivo* modelling [37, 60, 80, 181].

1.1.3.2 ZIKV pathogenesis

The clinical manifestations and pathogenesis of ZIKV infection are a result of the tissue tropism of the virus. ZIKV can cause direct cytotoxic effects on target cells, but infection can also result in inflammation that drives ZIKV pathology. From work in patient studies and mouse models ZIKV infects a wide variety of cells and tissues.

<u>Ocular symptom pathogenesis:</u>

ZIKV infections are associated with varying degrees of ocular pathologies such as conjunctivitis and uveitis in adult patients [173], and or ocular abnormalities in new-borns including focal pigment mottling and chorioretinal atrophy [69]. One study by Miner *et al*.

found in a mouse model using subcutaneous inoculation that ZIKV infected various tissues of the eye including the cornea, iris, optic nerve, and the ganglion and bipolar cells in the retina [222]. Infection of the eye in this model caused conjunctivitis and uveitis like the symptoms observed in humans. Correspondingly, *in vitro* modelling in induced pluripotent stem cell derived retinal pigment epithelial cells (cells lining the retinal-blood barrier) demonstrated that these cells were highly permissive to ZIKV infection [324]. Furthermore, ZIKV infection triggered antiviral and inflammatory responses that correlated with impairment of membrane dynamics and retinal pigment epithelial cell homeostasis that could contribute to the ocular lesions observed in new-borns.

Neurological symptom pathogenesis:

ZIKV is now known to be highly neurotropic. ZIKV can infect multiple cell types in the human brain, including neural progenitor cells [193], developed neurons, and glial cells within the cerebral cortex [25]. Infection of these cell types has been shown in an immune competent mouse model of intracranial injection to result in direct cytopathic effect on neuronal cells [153]. Additionally, in a similar model the contribution of ZIKV induced innate immune signalling was linked to encephalitis [138]. Furthermore, adaptive immune responses that generated anti-ganglioside antibodies in response to ZIKV infection are linked to the development of GBS in patient studies [287].

Adverse pregnancy outcomes:

ZVCS is caused by infections of the placenta and developing foetus, disrupting the immune balance required to maintain healthy pregnancy as well as having direct cytopathic effects [226]. ZIKV has been shown in mouse models and organoid culture to have a striking affinity for the foetal brain and eye explaining neurologic and ocular manifestations. ZIKV infection in developing neurons causes cell death and neural inflammation [181, 353, 360]. Additionally, ZIKV directly infects the placenta resulting in activation of innate immune responses, abnormal placental development and intrauterine growth restriction that can result in spontaneous pregnancy loss or developmental impairment due to disrupted nutrient and gas exchange [382, 383].

1.1.3.3 DENV clinical manifestations

Like ZIKV, most (75%) of DENV cases are asymptomatic and patients that do present symptoms mainly have a self-limiting febrile illness known as dengue fever (DF). DF or the

aptly named “break-bone” fever, normally lasts between 7-10 days and is characterised by severe muscle and joint pain, rash and headache [76]. A small proportion (<1%) of symptomatic infections progress to potentially lethal forms of severe disease [75]. This includes dengue haemorrhagic fever (DHF) or dengue shock syndrome (DSS). These severe forms of disease are characterized by the sudden onset of vascular leakage, thrombocytopenia, haemorrhagic manifestations and moderate liver damage [297].

1.1.3.4 DENV pathogenesis

DHF and DSS symptoms are caused by DENV’s tropism for, or pathological effect on cells of the immune system, the liver and endothelial cells lining blood vessels [208]. Several studies have used immunohistochemical analysis or *in-situ* hybridisation to detect DENV RNA or protein in tissues taken from patient autopsies. These show the presence of DENV in cells of the skin, liver, spleen, lymph node, kidney, lung, thymus and brain [24, 168, 219]. Generally, severe DENV infections lead to elevated levels of pro-inflammatory and vasoactive cytokines released from infected cells that impact upon blood vessel permeability causing fluid loss either externally or into the tissue space that if left untreated leads to mortality [128, 291]. This wide array of DENV’s clinical manifestations and risk factors for severe dengue are dependent on the infecting serotype, pre-exposure to heterotypic strains of DENV, age, gender, nutritional and immunological status of the infected host [130, 314, 330, 347]. The main risk factor for severe dengue across all demographic groups is pre-exposure to a heterotypic strain of DENV. Recovery from infection provides life-long immunity against DENV strains of the same serotype [367]. However, antibodies generated against one serotype provide incomplete protection against heterotypic serotypes as the antibody titers wane over time. This leads to antibody dependent enhancement (ADE) of infection. ADE occurs when the Fc portion of heterotypic non-neutralizing antibodies facilitate DENV entry into target cells that express Fc receptors on their cell surface such as dendritic cells and macrophages [291]. DENV infection in these immune cell subtypes exacerbates inflammation and cytokine release and leads to increasingly severe symptoms [332]. Importantly, severe dengue is a leading cause of morbidity and mortality in young children in parts of Asia and Latin America [367]. Particularly young children and infants have an increased risk of DSS and DHF likely due to their increased microvascular fragility compared to adults. Additionally, young children also have a greater risk of exposure to DENV infections due to lifestyle factors [197].

1.1.4 Current control measures

The main control measures for both ZIKV and DENV infections are vector control strategies and prevention of mosquito bites. For ZIKV these basic control measures include safe-sex practices for a minimum of 3 months after potential exposure for men and 2 months for women [366]. There are no approved vaccines or antivirals for ZIKV, but several vaccine candidates are currently being investigated. As of late 2019, the WHO listed 15 vaccine candidates in phase I/II clinical trials [365]. These include DNA, RNA, recombinant protein, recombinant viral vector, and inactivated whole virus vaccines. As for DENV, there are also no approved antivirals but there is an approved vaccine (Dengvaxia®) developed by Sanofi Pasteur. However, this vaccine is not recommended for children under 9 years of age and has been plagued by controversy because it can increase the risk of severe DENV developing in people who are seronegative when receiving vaccination [364].

The development of specific, effective, and safe treatments and vaccines for the prevention of both ZIKV and DENV requires understanding of their fundamental biology, pathogenesis, and interactions with host immune responses.

1.1.5 Molecular virology of ZIKV and DENV

1.1.5.1 ZIKV and DENV phylogeny and genetic diversity

Flavivirus are a genus of primarily arthropod borne, enveloped, positive-sense single stranded RNA (+ssRNA) viruses that include several major human pathogens including DENV and ZIKV, and other such as Yellow Fever Virus (YFV), Japanese Encephalitis virus (JEV), and West Nile Virus (WNV). Amongst flaviviruses DENV and ZIKV are closely related, sharing on average 55% amino acid identity [45].

ZIKV is classified as a single serotype but has two genetically distinct lineages; African and Asian, pertaining to their region of first isolation. Interestingly, all significant outbreaks have been attributed to the Asian lineage [329]. For this reason, considerable attention has been given to strain specific nucleotide substitutions occurring in both regulatory or protein coding regions and their potential contribution to altered pathogenicity and enhanced transmissibility of the Asian strains [267, 380]. Incidentally, a recent study found that an envelope protein V473M substitution mutation that occurred within the Asian strain prior to its introduction into the Americas conferred enhanced neurovirulence, maternal-to-fetal transmission, and increased viremia to facilitate mosquito borne transmission [315].

Moreover, a single nucleotide polymorphism resulting in an Alanine to Valine switch within the NS1 dimerization domain of recent outbreak strains of ZIKV has been shown to enhance infectivity in mosquito vectors, likely contributing to enhanced transmissibility [195].

Additionally, there are strain specific differences in innate immune evasion between African, early Asian and the most recent South American clades. For example, a recent South American ZIKV strain demonstrated weaker and delayed interferon responses compared to the MR766 strain that was originally isolated in Africa in 1947 and this likely contributes to strain specific differences in pathogenesis [93]. These findings support a possible evolutionary shift enhancing the severity of recent outbreaks and raise concern over future adaptation of the virus when introduced to naive populations.

In contrast to ZIKV, DENV has 4 distinct serotypes with a 5th emerging (DENV1-5), these have approximately 30% difference in their overall amino acid sequences [150, 191]. Importantly, neutralizing antibodies generated against one serotype offer little to no protection against heterotypic strains of DENV. This complicates vaccine design and contributes to ADE and DENV pathogenesis. Between the different serotypes there are clinically relevant differences in the outcome of both primary and secondary infections. One study found that the DENV3 serotype from Southeast Asia (SEA) caused the greatest incidence of severe dengue during primary infections. In contrast, DENV2 caused the greatest incidence of severe infection upon secondary exposure to a heterotypic subtype in strains isolated from both SEA and non-SEA regions [330].

The elements that contribute to DENV and ZIKV pathogenesis and immune evasion are still poorly understood. To improve therapeutics and vaccines that can combat these viruses will require continued study into their genetics and specific functions of their encoded proteins.

1.1.5.2 ZIKV and DENV genome and proteins

Typical to flaviviruses, both DENV and ZIKV have an approximately 11 kb linear single-stranded positive-sense RNA genome. The genome contains a single open reading frame (ORF) encoding the viral polyprotein. The central ORF is flanked by 5’ and 3’ untranslated regions (UTRs) and the 5’ end of the genome is capped. Both the 5’ and 3’ UTR contain conserved secondary structures that are involved in long range RNA:RNA interactions that promote viral RNA replication [247]. The overall structure and arrangement of the *Flavivirus*

genome is shown in Figure 1.5 (from source [29]) and its individual elements are described below in more detail.

1.1.5.2.1 Genome structure

5'UTR

The *Flavivirus* 5' UTR is an approximately 100 nucleotide (*nt*) sequence directly upstream of the capsid protein. It contains a 5' type-I cap that resembles host mRNA. This cap is important for recruitment of host translational machinery, preventing genome degradation by host exonucleases and evading innate immune recognition [247]. The 5' UTR also contains two conserved stem-loop structures, stem-loop A and B (SLA, SLB). SLA is approximately a 70 nt length and is required for viral replication by recruiting the NS5 RNA dependent RNA polymerase (RdRp) protein [196]. The SLB is approximately 16 nt in length and contains a conserved AUG sequence that is complementary to the cyclization sequence in the 3' UTR. Complementary binding of these 5' and 3' UTR regions promotes genome cyclisation and NS5 recruitment [31].

Open reading frame encoding the viral polyprotein

The *Flavivirus* ORF encodes a polyprotein that is roughly 3400 amino acids in length. From 5' to 3' it encodes the structural Capsid (C), pre-Membrane (prM), Envelope (E) protein, and non-structural (NS) proteins NS1, NS2A, NS2B, NS3, NS4A-2k-NS4B and NS5. The polyprotein is synthesized by host translational machinery as a multi-pass transmembrane protein inserted into the endoplasmic reticulum (ER) membrane [248]. This polyprotein is then co-translationally cleaved by host or by the viral proteases into its individual proteins (see Figure 1.5) [234].

3' UTR

The 3' UTR is positioned immediately after the viral ORF and for ZIKV and DENV is roughly 450 *nt* in length. The 3' UTR of DENV contains two stem-loop structures (SL1 and SL2), two dumbbell structures (DB1 and DB2), a small hairpin (sHP) and an evolutionarily conserved 3' stem loop (3'SL) common to all flaviviruses [247]. The ZIKV 3' UTR is similar to DENV except it has a single functional DB1 structure and a pseudo-DB structure in place of DB2 [114]. These SL and DB structures are required to maintain RNA genome structure and are involved with

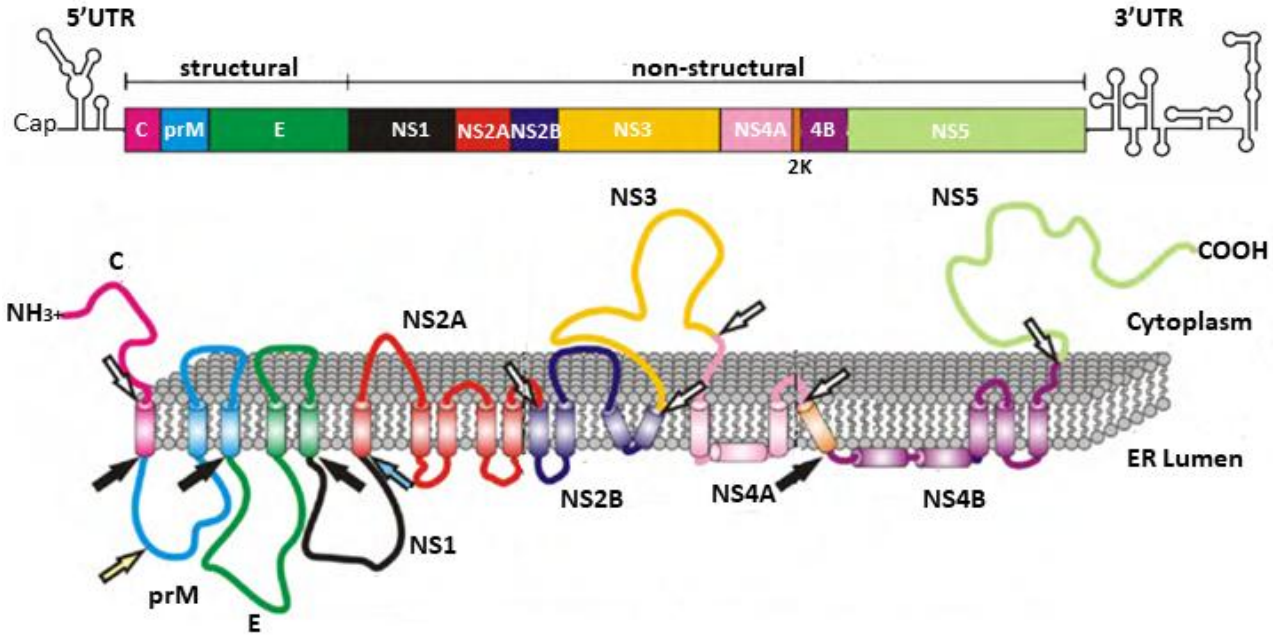

Figure 1.5: The *Flavivirus* genome. A schematic representation of the *Flavivirus* genome and translated polyprotein. The genome is a +ssRNA roughly 11 kb in size, capped at the 5' terminus and flanked by 5' and 3' UTRs. The central open reading frame encodes a polyprotein that is cleaved into individual structural and non-structural viral proteins. Arrows represent viral or host protease cleavage sites that separate the individual viral proteins. White arrows indicate NS3 viral protease cleavage sites, black arrows indicate host signal peptidase cleavage sites, the yellow arrow indicates a host Furin cleavage site and the blue arrow represents an unknown host protease cleavage site [29].

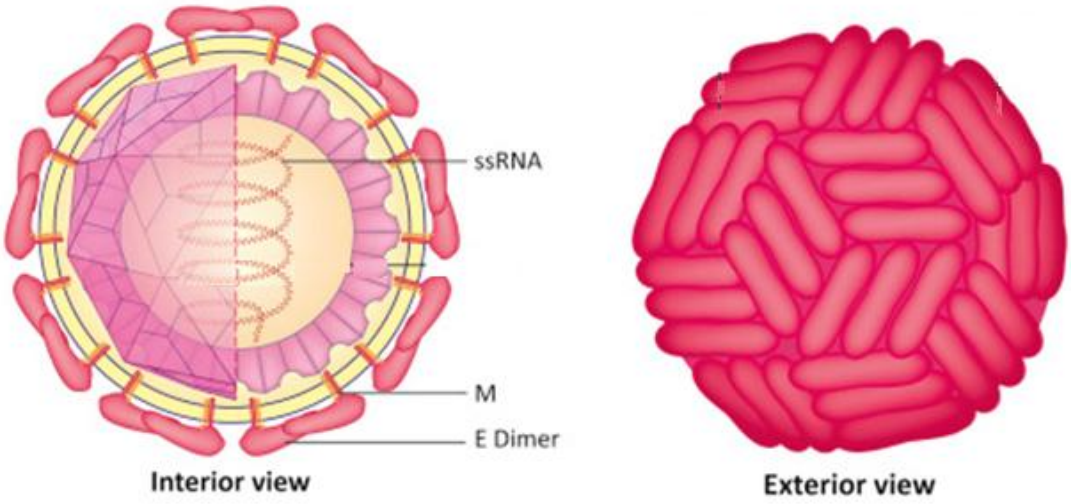

Figure 1.6: Interior and exterior views of the mature *Flavivirus* virion. The virion in comprised of a single copy of the +ssRNA genome associated with multiple copies of the capsid protein. The nucleocapsid is enclosed within the viral lipid envelope imbedded with membrane (M) and envelope (E) protein dimers [260].

immune evasion through the generation of short sub-genomic *Flavivirus* RNAs (sfRNAs) [82, 247]. The generation and function of these sfRNAs is discussed further in section 1.3 of the Introduction. The evolutionarily conserved 3'SL is essential for complementary long range RNA:RNA with the 5' UTR resulting in genome cyclisation. This 3'SL structure also contains the NS5 binding recognition sequences required to initiate RNA replication [31].

1.1.5.2.2 Virion structure

Together the structural proteins are involved with the formation of new infectious virus particles (virions) shown in Figure 1.6 [260]. The mature *Flavivirus* virion is approximately 50 nm in diameter consisting of an outer envelope and an internal nucleocapsid encasing a single copy of the +ssRNA genome. The viral envelope is a lipid bilayer derived from host cell membranes formed upon budding into the ER lumen. Embedded in the lipid bilayer is 180 copies of each the E and M proteins [265]. The E protein dimerizes to form 90 homodimers that lie flat against the lipid surface forming a smooth outer coat. The M protein is positioned underneath this smooth coat and is embedded into the lipid bilayer. For both ZIKV and DENV these dimers are arranged in a characteristic herringbone structure in the mature virion [328]. The envelope surrounds the viral nucleoprotein. The nucleoprotein comprises multiple copies of the C protein associated with the viral RNA in a relatively unordered structure [256].

1.1.5.2.3 Viral proteins

The viral genome encodes for a single, multi-pass trans-membrane polyprotein that is expressed embedded into the ER membrane. This polyprotein is cleaved by the viral protease (NS3) on the cytoplasmic side, and by host peptidases (ER resident signal peptidases or Golgi resident Furin protease) on the luminal side of the ER membrane or during virion maturation [234]. Following polyprotein cleavage, the individual viral proteins are released. These proteins either remain associated with the ER membrane, are released into the cytosol or into the ER lumen depending on their topology in the polyprotein transmembrane domain architecture (see Figure 1.5) [29, 234]. In general, the structural proteins have roles in generation of new infectious virus particles and the non-structural proteins are involved with viral RNA replication.

1.1.5.2.3.1 Structural proteins

Capsid

The immature C protein is formed by 114 amino acids that are cleaved by the NS3 viral protease into a final 100 amino acid mature form [256]. Structurally two copies of the C protein form dimers that organize symmetrically, with each monomer containing four α-helices and an unstructured N terminal region [256]. Helix 4 contains multiple arginine residues that are positively changed at physiological pH and are predicted to facilitate RNA binding [256]. Once cleaved from the viral polyprotein multiple copies of the mature C protein interact on the cytoplasmic side of the ER membrane with a single copy of the RNA genome thereby forming the unstructured nucleocapsid [234].

Envelope

The E protein is the major surface glycoprotein and is 504 amino acids in length. In the mature virion 180 copies of the E protein dimerize to form a smooth outer coat [265]. In its dimeric form each E protein monomer is made up of three distinct domains (EDI, II and III) interconnected by flexible linkers and contains a helical anchor domain that is imbedded into the lipid bilayer [234]. The N-terminal EDI plays a structural role at the centre of the dimer complex. EDII is a dimerization domain and contains the fusion peptide loop. EDIII is an immunoglobulin-like domain and is thought to contain receptor binding sites [234]. Typically, the *Flavivirus* E protein contains one or more N-glycosylation sites that are thought to play roles in receptor specificity. For DENV, the mature E protein is glycosylated at positions N67 and N153 [97]. Interestingly, there are lineage specific differences in ZIKV E protein glycosylation leading to differences in strain virulence. Historical strains of ZIKV such as the African MR766 or the Malaysian P6-740 lack the conserved N-X-T/S glycosylation motif at position N154 that is present in contemporary epidemic strains [97]. Mutation of the N154 glycosylation site in contemporary stains causes attenuation of ZIKV virulence in mouse models [97].

Membrane

The mature M protein is anchored into the lipid bilayer and lies underneath the external E protein coat of the mature virion. Its domain structure consists of the soluble M-loop at the N-terminus, a single α-helical stem region and a double α-helical transmembrane region

[328]. The M protein is first synthesized in a pre-protein form (prM). During virion egress the low pH environment of the trans-Golgi network leads to a conformational change in prM, exposing a Furin cleavage site (Figure 1.5, yellow arrow) [234]. Furin then cleaves prM to the mature M protein. Cleavage of prM to M leads to virion maturation by causing disassociation of the immature 60 prM-E trimers and formation of the 90 E homodimers present in the mature virion [234].

1.1.5.2.3.2 Non-structural proteins

The 7 non-structural proteins (NS1, NS2A, NS2B, NS3, NS4A, NS4B and NS5) play multiple roles in the virus lifecycle during viral replication, virion packaging and immune modulation. Historically, more is known about the specific functions of DENV NS proteins than ZIKV as this field of research is still under development. However, due to their close evolutionary relationship it is likely the essential functions of NS proteins are conserved between DENV and ZIKV. The specific immune modulatory functions of both DENV and ZIKV NS proteins are discussed in depth in section 1.3.

<u>NS1</u>

NS1 is a 45 kDa protein that is released into the ER lumen upon polyprotein processing and plays different roles in the virus lifecycle depending on whether it is cell associated or secreted [265]. In solution NS1 is present as stable oligomers (dimers or hexamers) [6]. Cell associated NS1 is important for viral replication, and secreted NS1 plays other roles in DENV pathogenesis [148]. Cell associated NS1 interacts with multiple host factors assisting in virus replication, translation of the viral polyprotein and virion production. Specifically, NS1 interacts with and recruits multiple ribosomal proteins to the replication complex [280]. In DENV infection secreted NS1 activates the pattern recognition receptor TLR4 expressed on peripheral blood mononuclear cells, leading to upregulation of proinflammatory cytokines that contribute to DENV pathogenesis and symptoms severity [225].

<u>NS2A</u>

NS2A is 22 kDa multi-pass transmembrane protein associated with the viral replication complex [265]. DENV NS2A has been shown to be essential for RNA replication, virus assembly and secretion [372].

NS2B

NS2B is a 130 amino acid protein that acts as a co-factor for the NS3 protease. It associates with NS3 by wrapping around the protease domain, forming part of the active site [265]. Structurally the N-terminal domain of NS2B forms a β-strand that interacts with the NS3 β-barrel, stabilizing NS3 conformation [396]. In DENV and WNV the C-terminal portion of the protein makes up part of the active site and likely contributes to fine sequence specificity of the protease [396]. The flanking transmembrane regions are predicted to embed NS2B in the ER membrane [265].

NS3

NS3 is the second largest protein encoded in the *Flavivirus* genome. It is a 618 amino acid protein that performs multiple enzymatic functions in the *Flavivirus* lifecycle [265]. The N-terminal protease domain in conjunction with its associated cofactor (NS2B) is responsible for cleaving multiple sites of the viral polyprotein (see Figure 1.5 white arrows). The C-terminal domain is made up of three distinct sub domains and possesses RNA helicase, nucleotide triphosphatase and ribonucleotide triphosphatase activities [339]. The NS3 helicase is responsible for unwinding the dsRNA replication intermediate, releasing functional +ssRNA allowing for genome capping and methylation by the coordinated actions of NS3 and NS5 protein [376].

NS4A

NS4A is a 16 kDa integral membrane protein [265]. DENV NS4A induces membrane remodelling to assist with replication complex formation. This activity is dependent on the proteolytic cleavage of the 2K fragment separating NS4A and NS4B [220] and likely involves other protein-protein or protein-lipid interactions [234].

NS4B

Like NS4A, NS4B is a 27 kDa integral membrane protein embedded in the ER membrane [265]. NS4B is known to localize to the site of viral replication and interact with several host and viral proteins to promote formation of the replication complex [398].

NS5

NS5 is a 104 kDa, 900 residue protein and is the most highly conserved *Flavivirus* protein [265]. It is arranged into two distinct domains, the N-terminal Methyltransferase (MTase) domain and the C-terminal RNA dependent RNA polymerase (RdRp) domain. The MTase is structured in an α/β/α sandwich formation that generates the conserved 4 amino acid catalytic site at the centre of the domain. The RdRp domain is formed in a right-hand structure made up of three subdomains the finger, palm, and thumb. This domain is shaped to generate three channels that individually bind the template RNA, allow the entry of new NTPs and allow the exit of the newly synthesized RNA [391]. NS5 performs essential functions in replicating the RNA genome and 5' genome capping through its methyl transferase domain [289].

1.1.5.3 Lifecycle

As closely related flaviviruses, ZIKV and DENV share many similarities in their lifecycle within host cells. In overview, the *Flavivirus* lifecycle is carried out in several stages as shown in Figure 1.7. The lifecycle begins when a virion binds to its receptor expressed on the surface of a permissive host cell. Next, the virus-receptor complex is internalized by receptor-mediated endocytosis. Acidification of the endosome leads to fusion of the viral and endosomal membranes, particle disassembly and the release of the +ssRNA genome into the cytosol. Once the viral genome enters the cytosol an initial round of translation is carried out by host translational machinery, generating new structural and non-structural viral proteins. Next, the viral non-structural proteins form the replication complex (RC) by modifying host ER membranes and then act to generate new viral RNA genomes through an -ssRNA intermediate. Genomes are then packaged into new immature virion structures comprised of the structural proteins and a single copy of +ssRNA. Immature virions are transported through the ER and trans-Golgi network to the plasma membrane, simultaneously undergoing maturation processing mediated by Furin cleavage of prM to M. Finally, new mature virions are released by exocytosis to initiate a new cycle of infection [234].

ZIKV and DENV entry

The ability for both DENV and ZIKV to infect wide varieties of cell types largely depends on the host expression of each virus's entry receptor. The specific entry receptor for ZIKV and DENV have not yet been identified. This is likely because multiple molecules are used in

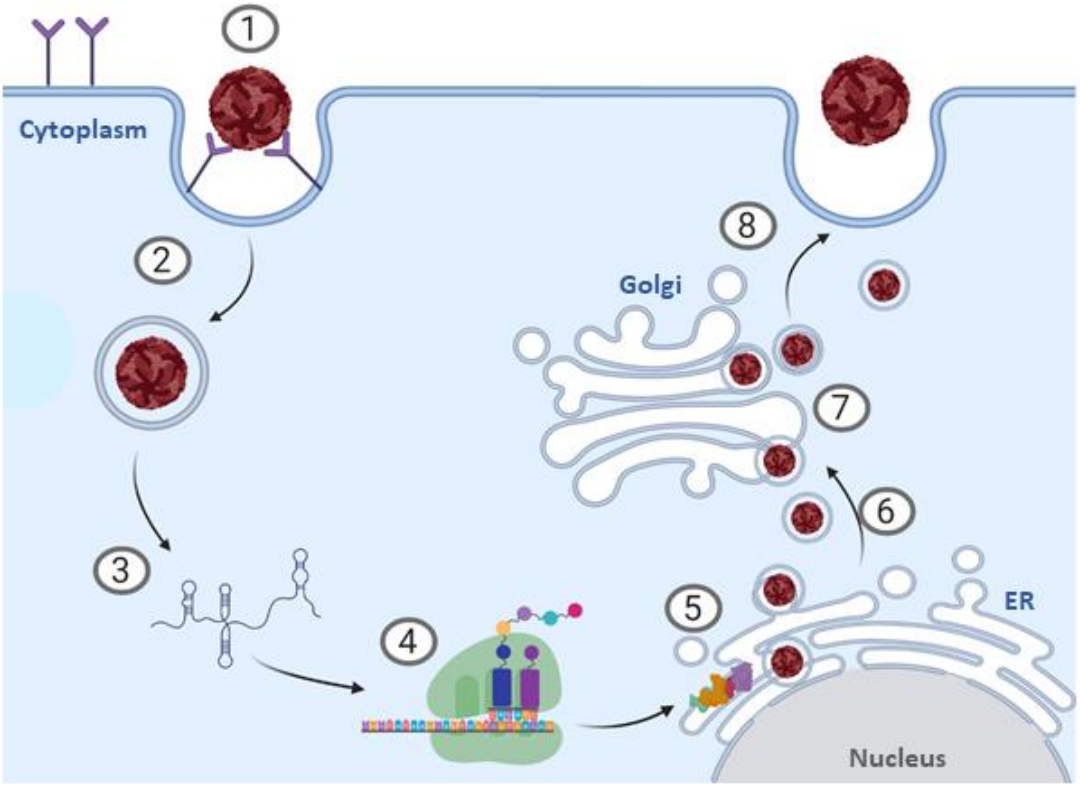

Figure 1.7: Stages of the *Flavivirus* lifecycle. 1) Attachment and receptor-mediated endocytosis. 2) Membrane fusion and particle disassembly. 3) Genome release into the cytoplasm. 4) Polyprotein translation. 5) Replication complex formation and genome replication. 6) Virion packaging. 7) Transportation through the trans-Golgi network and virion maturation. 8) Virion egress by exocytosis.

combination or in different cellular contexts for virus entry [3, 264]. Some of these molecules likely act as attachment factors rather than as entry receptors that directly facilitate virion uptake by the cell.

For flaviviruses the most common attachment factors are a family of receptor molecules called negatively charged glycosaminoglycans (GAGs), such as heparan sulphate [3]. These molecules are predicted to bind via electrostatic interactions with positively charged regions of the surface of the E protein [264]. Another family of cell surface receptor implicated in ZIKV and DENV attachment and entry are the C-type lectin receptors (CLRs). CLRs are a family of pattern recognition receptors (PRRs) that bind to carbohydrate pathogen associate molecular patterns (PAMPs) and are normally expressed on myeloid cells such as DC's and macrophages [264]. Normally they function to initiate innate immune responses and cause the uptake of PAMPs into endosomes for the purpose of antigen presentation. Flaviviruses exploit this interaction through binding through N-linked glycans on the E protein, facilitating attachment and potentially virion entry into endosomes [264]. The most implicated CLRs for *Flavivirus* entry is DC-SIGN (Dendritic cell-specific intercellular adhesion molecule-3-grabbing non-integrin). Expression of DC-SIGN in HEK293T cells was shown to enhance ZIKV infection [129]. Blocking of this interaction by anti-DC-SIGN antibodies has also been shown to decrease DENV infection in dendritic cells [344]. In addition to CLRs, two families of related transmembrane phosphatidylserine receptors the TIM (TIM1, TIM3 and TIM4) and TAM's (Tyro3, AXL and MER) have been implicated in both ZIKV and DENV attachment and entry. These bind either directly (TIM) or indirectly (TAM) to lipids such as phosphatidylserine (PS) embedded in the viral membrane [3]. Indirect binding of TAM receptors is mediated through extracellular bridging molecules such as Gas6 or protein-S [215]. Meertens *et al*. demonstrated ectopic expression of TIM and TAM receptors in 293T cells, and their natural expression levels in cell types demonstrably correlates with DENV infection [215]. Another publication by Hamel *et al*. demonstrated similar results with ZIKV using overexpression the TAM receptor AXL [129]. Interestingly, the role of AXL mediating ZIKV attachment and entry seems to be cell type specific, suggesting that multiple receptors are responsible for ZIKV attachment and entry. Wells *et al.* demonstrated the genetic ablation of the AXL receptor had no effect on ZIKV infection of neural progenitor cells and Hastings *et al*. demonstrated the TAM receptors were non-essential for ZIKV infection in mice [137].

After virion attachment and entry receptor engagement the virion enters the host cell via clathrin-mediated endocytosis [3]. This is a process where the virion-entry receptor complex is trafficked to clathrin-coated pits on the host cell membrane. This initiates membrane invagination, constriction and pinching off the membrane vesicle forming clathrin-coated vesicles containing the virion [233]. Once inside the cell the clathrin-coated vesicle is processed to form an early endosome, these then fuse with lysosomes to form late-endosomes [233]. The low pH environment of the late-endosome drives conformational changes in the virus E protein exposing the fusion peptide, leading to membrane fusion, uncoating and release of the +ssRNA genome into the cytoplasm [234].

ZIKV and DENV genome translation and replication

After the viral +ssRNA genome gains access to the cytosol viral replication is initiated by direct translation by host translational machinery to form a polyprotein that is inserted into the ER membrane [234]. This polyprotein is then proteolytically cleaved to form three structural (C, prM and E) and seven non-structural (NS1, NS2A, NS2B, NS3, NS4A, NS4B and NS5) proteins [289]. Together multiple NS proteins interact with host factors to induce changes in the structure of the ER membranes generating the viral RC [289]. The RC acts to concentrate viral and host proteins that are essential for viral genome replication and also functions to hide the replicating viral RNA from cytosolic PRR recognition detection [184, 289]. Ultrastructural analysis shows that ZIKV and DENV induce similar RC structures. They are both formed from the invagination of the rough ER membrane into the ER lumen generating a series of convoluted membranes and vesicle packets that contain the viral RNA and replication machinery [58]. Following formation of the replication complex, the +ssRNA genome is copied through a -ssRNA intermediate by the RdRp function of NS5 in coordination with other essential host and viral factors. The progeny genomes (+ssRNA) then exit vesicle packets through the vesicle pore and interact with capsid protein that forms the nucleocapsid encasing a single copy of the +ssRNA genome [289].

ZIKV and DENV virion maturation and egress

To generate new infectious virions the nucleoprotein complex buds into the ER-derived membranes [238]. These membranes are embedded with viral prM–E heterodimers that coat the newly enveloped immature virion upon budding into the ER [234]. After entering the ER lumen, the immature *Flavivirus* particle is shuttled through the secretory pathway. During this process, the virion undergoes a maturation process mediated by the acid-induced

rearrangement of the E protein and subsequent cleavage of the prM protein to M by host furin protease in the late Golgi compartment [387]. After maturation new virions are released from the host cell by fusion of secretory vesicles to the host membrane [238].

1.2 The innate immune response to viral infection overview

The innate immune response is the first line of defence against viral pathogens and has been reviewed extensively in [214]. This arm of the immune system generates a rapid, non-specific response aiming to control infection. The innate immune response also plays a crucial role in establishing adaptive immune responses, leading to pathogen specific and long-lasting immunological memory [214]. In general, the innate immune response is initiated by recognition of "non-self" molecules by the host. These evolutionarily conserved "non-self" molecules are called pathogen associated molecular patterns (PAMPS) and include a range of pathogen associated molecules such as lipids, polysaccharides, nucleic acids, and protein. PAMPs bind to host germline encoded pattern recognition receptor (PRRs) on the cell surface, within endosomes or in the cytoplasm. The location of PRR engagement by PAMPs depends on the lifecycle of the pathogen and helps to broadly direct the innate immune response. For intracellular pathogens such as viruses PAMPs accumulate inside cellular compartments such as the cytosol or endosomes. PRR binding to PAMPs causes cellular signalling pathways to be activated, leading to the upregulation of multiple innate immune effector molecules and cytokines. These act directly or indirectly control infection, promote inflammation, and manage the immune response appropriately. The most important class of cytokine involved in the innate response against viral pathogens are the interferons (IFN). These cytokines are responsible for orchestrating an antiviral state within infected cells, in neighbouring cells and in directing immune cell activation or trafficking to control viral infection.

1.2.1 Recognition of flaviviruses by innate immune pattern recognition receptors

Typically, ZIKV and DENV are recognized by PRRs that bind to RNA PAMPs generated as a by-product of vRNA replication. The main class of PRR that recognize *Flavivirus* RNA PAMPs are members of the the DExD/H box RNA helicase family of RIG-I-like receptors (RLRs) located in the cytoplasm [122]. *Flavivirus* RNA detection can also occur in the endosomal compartment by the membrane associated Toll-like receptors-3 or 7 (TLR) [214]. Most recently it has been found that both DENV and ZIKV infection results in mitochondrial DNA (mitoDNA) release that

is sensed by Cyclic GMP-AMP synthase (cGAS) and signals through the ER associated intermediate Stimulator of Interferon Genes (STING) [5, 214, 395]. Each of these pathways culminates in the phosphorylation and subsequent activation of the signalling intermediaries TANK-binding kinase 1 (TBK1) and IκB kinase-ε (IKKε). Following their activation, TBK1 and IKKε phosphorylate IFN-regulatory factor-3 or 7 (IRF) [214]. Additionally, IKKε phosphorylates the inhibitory subunit of nuclear factor-κB (NF-κB), leading to inhibitor degradation and subsequent activation of NF-κB [162]. Activated IRFs and NF-κB translocate to the nucleus where they act as transcription factors to promote expression of the IFNs and a small subset of antiviral or proinflammatory genes [182]. Figure 1.8 summarizes these pathways that are discussed in more depth below.

RIG-I like receptors

The main drivers of the innate immune response against flaviviruses are the ubiquitously expressed RLRs, retinoic acid-induced gene I (RIG-I) and melanoma differentiation-associated gene 5 (MDA5). RIG-I recognizes short 5'-triphosphorylated ssRNA and short dsRNAs whereas MDA5 is implicated in recognition of longer dsRNA products [161, 175, 303]. In structure these PRRs contain two N-terminal caspase recruitment and activation domains (CARDs) followed by an RNA helicase domain [175]. PAMP binding causes a conformational change in the receptor that exposes the CARD interaction domains and facilitates interactions with translocation mediators such as TRIM25 and members of the 14-3-3 family of proteins [162]. The RLR translocase complex is then shuttled to the mitochondrial associated membranes where the exposed CARD domains interact with the complementary CARD domain of signalling intermediate mitochondrial antiviral signalling protein (MAVS) [162]. This interaction triggers MAVS activation leading to subsequent activation of cytosolic kinases TBK1 and IKKε [214]. Interestingly, CRISPR/Cas9-mediated knockout of RIG-I but not MDA5 led to significantly increased ZIKV replication in A549 cells compared to control, indicating that RIG-I is the main sensor of ZIKV infection in these cells [302]. Furthermore, knockout of the RLR signalling intermediate MAVS was shown to enhance ZIKV infection in human placental trophoblast cell lines [200]. Similarly, siRNA mediated knockdown of RIG-I and MDA5 in the Huh7 cell line rendered them highly susceptible to DENV infection [243]. Collectively these studies demonstrate the importance of the RLRs in detection of both ZIKV and DENV infection.

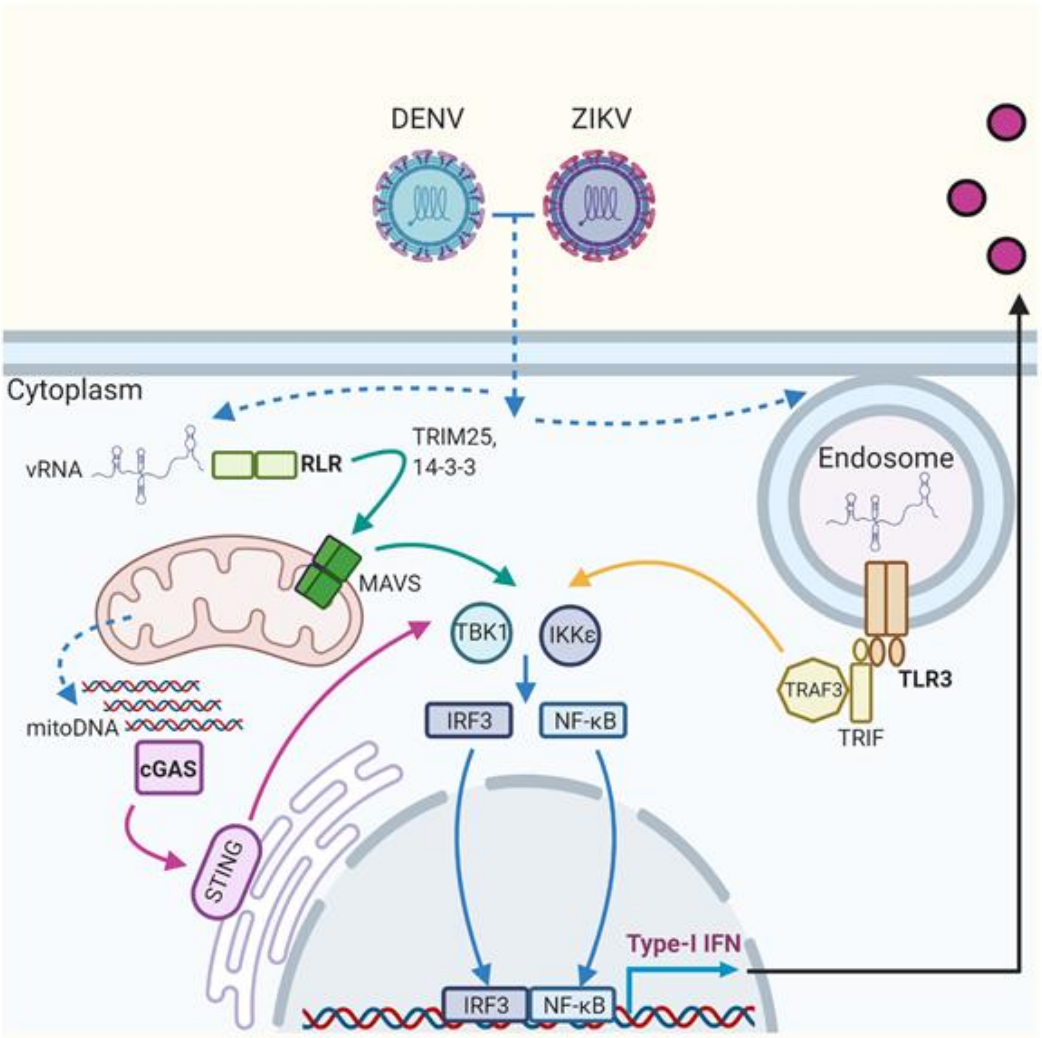

Figure 1.8: Recognition of RNA viruses by host pattern recognition receptors. Viral RNA (vRNA) is recognised in the cytosol by RIG-I or MDA5, or in the endosome by TLR3/7. RNA viruses like ZIKV and DENV also cause activation of STING at the endoplasmic reticulum via the release of mitochondrial DNA into the cytosol leading to formation of cGAMP. Each of these pathways culminates in activation of downstream transcription factors (IRF's and NF-κB) that promote transcription of the type-I and III IFNs.

Toll like receptors

In addition to cytosolic PRR activation, ZIKV and DENV RNA generated during the viral lifecycle can be recognized in the endosomal compartment by toll-like receptor 3 or 7 (TLR3/7) [245, 349]. TLR3 is more widely expressed and recognizes dsRNA whereas TLR7 is mainly expressed in specialised IFN producing cells (plasmacytoid DCs) and is activated by ssRNA [175]. Signalling downstream of activated TLR3 is initiated by binding of the cytoplasmic TIR domain of TLR3 to the complementary TIR domain containing adapter protein (TRIF). Next, TRIF interacts with TNF receptor associated factors (TRAF3/6) and with receptor interacting proteins (RIP1/3). Collectively these interacting partners activate TBK1 and IKKε. Comparatively TLR7 activates a MYD88 dependent pathway that culminates in TRAF6 signalling and subsequent TBK1 and IKKε activation [175, 245]. Evidence that TLR3 plays a significant role in ZIKV recognition is given by siRNA mediated gene silencing in HFF1 cells (foreskin fibroblast) increasing their permissive to ZIKV infection [129]. Additionally, HEK 293 cells heterologously expressing either TLR3 or TLR7 demonstrated elevated levels of downstream cytokine release following DENV infection [349].

cGAS-STING

Other than RNA mediated PRR activation of the innate immune response, DENV and ZIKV infection also causes the release of mitoDNA into the cytoplasm [5, 395]. The presence of mitoDNA in the cytoplasm is a hallmark of cellular damage and acts as a potent stimulator of apoptosis and innate immune responses [232]. Release of mitoDNA during DENV infection is likely caused by disruption of normal mitochondrial function. Specifically, the DENV M protein disrupts mitochondrial membrane potential [43]. Also, the DENV NS2B/3 protease cleaves important mitofusion proteins (MFN1 and MFN2) that are important for membrane fusion and mitochondrial homeostasis [386]. ZIKV is also known to impair mitochondrial function [183], but the molecular mechanisms that drive the release of mitoDNA during ZIKV infection remain unknown. Once released into the cytoplasm in response to viral infection, mitoDNA can bind directly to the cytosolic DNA sensor cGAS. DNA binding to cGAS causes a conformational change allowing it to catalyse the conversion of GTP and ATP to produce the second messenger cyclic GMP–AMP (cGAMP). Next, cGAMP binds to the STING located in the ER membrane. Upon cGAS binding, STING oligomerizes and translocates to the Golgi, where it activates TBK1 and IKKε [232]. Importantly knockout of cGAS in PMBCs renders these cells more susceptible to ZIKV infection and limits IFNβ production in infected cells [395].

Moreover, various human cell lines lacking STING demonstrate enhanced DENV replication *in vitro* [4].

Each of these pathways stimulates the transcription and translation of the IFNs by infected cells. In turn the IFNs are secreted from the cell to orchestrate and amplify a broader antiviral response both within infected cells and in neighbouring cells and tissues.

1.2.2 The Interferons

The IFNs are antiviral cytokines generally produced by the host in response to sensing of viral pathogens. They are grouped into type – I, II or III, based on sequence homology and their cognate receptors [182]. Type – I and III IFNs incite a cell intrinsic antiviral state and are widely produced in the body. Comparatively, type – II IFNγ is produced by specialized immune cells including innate natural killer (NK) cells and certain subsets of adaptive T-cells [306]. IFNγ acts as a pro-inflammatory and immunoregulatory cytokine and play a role in the adaptive response to viral infections [11]. The following section will focus on the shared and distinct roles of the type-I and III IFNs as innate antiviral effectors.

1.2.2.1 Type-I Interferons

In humans, the type-I IFNs are encoded by a cluster of related genes located on chromosome 9 [147]. They include 14 subtypes of IFNα and a single gene encoding IFNβ, IFNε, IFNκ and IFNω. In mice type-I IFNs are encoded on a related region on chromosome 4 and have the same subtypes except for their lack of IFNω, expressing IFNζ instead [133]. IFNα and IFNβ are the main IFNs produced downstream of PRR activation, and therefore are also the most heavily studied. In general, IFNα expression is dependent on the activation of IRFs (especially IRF7) whereas efficient IFNβ expression requires both IRF3/7 and NF-κB activation. The nuances of IRF-mediated type-I IFN expression regulation have been extensively reviewed elsewhere [343]. The type-I IFNs are classified by their ability to signal through the type-I IFN receptor that is composed of two heterodimeric subunits (IFNAR1 and IFNAR2) and is almost ubiquitously expressed throughout the body [70].

1.2.2.1.1 Signalling from the type-I IFN receptor

Once produced and secreted from infected cells, type-I IFNs bind to the extracellular domains of the cognate type-I IFN receptor (IFNAR1/2). Receptor binding can occur on the same cell

or on neighbouring cells to initiating autocrine or paracrine signalling, respectively. Importantly most cell types respond to type-I IFNs due to the almost ubiquitous expression of IFNAR1/2 [70, 155]. Ligand binding causes hetero-dimerization of the receptor subunits bringing the intracellular domains of the receptor into close proximity [179]. Each of the IFNAR1 and IFNAR2 intracellular domains are pre-associated with tyrosine kinases that are activated upon receptor dimerization by close proximity trans-phosphorylation [147]. IFNAR1 is associated with Tyrosine Kinase 2 (TYK2) and IFNAR2 is associated with Janus Kinase 1 (JAK1) respectively [81, 377]. Once activated JAK1 and TYK2 phosphorylate the intracellular domains of the IFNAR subunits, allowing docking of signal transducer and activator (STAT) proteins via their SH2 domains. The canonical STAT proteins downstream of IFNAR signalling are STAT1 and STAT2. Once docked to the receptor, JAK1 and TYK2 phosphorylate STAT1 and STAT2 at tyrosine residues Y701 or Y690 respectively [214]. STAT1/2 phosphorylation results in the formation of STAT1/2 heterodimers, nuclear translocation, and subsequent complexing with IRF9 [155]. This hetero-trimeric complex (ISGF3) then binds to IFN-stimulated response elements (ISRE) in the proximal promoter regions of over 100 interferon stimulated genes (ISGs), up-regulating their transcription and translation [304]. Figure 1.9 shows a summary of the type-I IFN signalling pathway. ISGs encode various proteins that act directly or indirectly to inhibit viral replication and spread [214]. These proteins carry out a range of effector or regulatory functions that give rise to an appropriately managed antiviral state. Effector functions are varied and include inhibition of viral entry, inhibition of protein synthesis, alterations to cellular metabolism, degradation of viral proteins or genetic material and inhibition of viral egress [304]. Regulatory ISGs include PRRs and signalling intermediaries of these pathways as well as immune modulatory molecules and negative regulators responsible for returning the cell to homeostasis [278].

1.2.2.1.2 Switching off the type-I IFN response

Negative regulation of the IFN pathway is essential for returning the body to homeostasis after infection is cleared, preventing over-activation of inflammatory pathways. Unchecked type-I IFN responses can lead to a range of auto-inflammatory conditions called “interferonopathies” including systemic lupus erythematosus, Sjogren's syndrome, rheumatoid arthritis, Aicardi-Goutières syndrome, and Pseudo-TORCH syndrome in pregnant

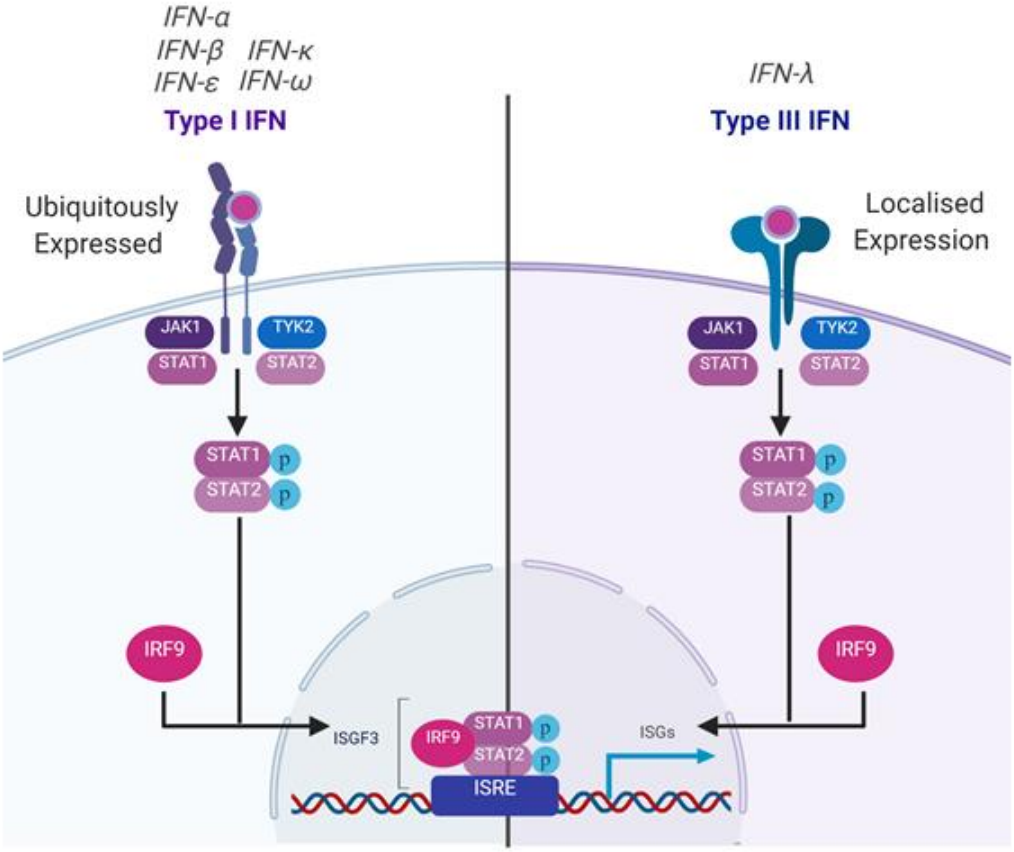

Figure 1.9: Type-I and type-III IFN signalling pathways. Both the ubiquitously expressed type-I receptor (IFNAR1/2) and type-III receptor (IL-10R/IFNLR) are pre-associated with cytosolic kinases JAK1 and TYK2. Upon ligand binding the receptors dimerise, activating JAK1 and TYK2 that phosphorylate downstream STAT1 and STAT2 proteins. Phosphorylated STAT1 and STAT2 heterodimerise and translocate to the nucleus where they associate with IRF9 to form the ISGF3 signalling complex. ISGF3 binds to ISRE elements, activating the transcription of ISGs.

women [59]. As a result, there are several negative feedback mechanisms that switch off type-I IFN responses.

One mechanism of negative regulation is the immediate ligand-stimulated downregulation of the type-I IFN receptor at the cell surface [14]. Upon ligand binding, the ligand-receptor complex is rapidly internalised by endocytosis [70]. Once internalized the IFNAR1 subunit is degraded in a lysosome dependent manner. This effect is mediated by a serine protein kinase called PKD2 [394]. PDK2 is activated in response to IFN signalling and mediates phosphorylation of IFNAR1 leading to its ubiquitination, internalisation by endocytosis and subsequent lysosomal degradation [394]. The IFNAR2 subunit is either recycled to the cell surface or degraded [70]. The fate of IFNAR2 after ligand binding appears to rely on the strength of the ternary structure formed between the ligand and the two receptor subunits. Weaker binding by IFNα results in recycling to the cell surface but stronger binding by IFNβ leads to receptor degradation along with IFNAR1 [207].

Another method of shutting off the IFN response is via the suppressor of cytokine signalling (SOCS) proteins. SOCS proteins (e.g., SOCS1) are also ISGs that are upregulated early in response to, and can negatively regulate both type-I and type-III IFN mediated JAK/STAT signalling [27, 333]. SOCS1 protein contains an N-terminal kinase inhibitory region (KIR), a central SH2 phospho-protein interaction domain, and a C-terminal SOCS box involved with ubiquitination of proteins for targeted degradation [385]. SOCS1 directly interacts with activated TYK2 protein that is associated with the IFNAR1 subunit of the receptor. By associating with TYK2 SOCS1 prevents the phosphorylation and activation of STAT proteins through the coordinated action of the SH2 and KIR domains [269]. In addition to this action on STAT phosphorylation, SOCS1 also inhibits the Lys-63 ubiquitination mediated stabilisation of TYK2 protein [269]. Prevention of this Lys-63 ubiquitination event likely destabilises the TYK2-IFNAR1 interaction resulting in reduced IFNAR1 surface expression. As an ISG, expression of SOCS proteins occurs rapidly after IFN signalling is initiated by ligand binding [385]. However, SOCS mediated negative regulation is short lived with most of these proteins having half-lives of less than two hours [322].

Additionally, the IFN response can also be switched off by the actions of the negative regulator Ubiquitin Specific Peptidase 18 (USP18). Like the SOCS proteins USP18 is an ISG that is produced in response to type-I and type-III IFN signalling [99]. In addition to causing degradation of IFN pathway proteins such as ISG15 via ubiquitination, USP18 expression also

leads to long-term receptor desensitisation [14]. Once accumulated in the cell USP18 protein interacts with STAT2. This STAT2 mediated interaction recruits USP18 to the receptor complex and facilitating its subsequent interaction with JAK1 [13]. Interaction with JAK1 at the IFNAR2 receptor subunit results in destabilisation of the ligand-receptor heterotrimeric complex preventing downstream signal transduction [369]. Unlike SOCS mediated desensitisation that is short lived, USP18 mediated desensitization lasts several days [95, 100]. Importantly, USP18 mediated receptor desensitisation is not equally applicable for all IFNs. For example, IFNβ is not susceptible to USP18 mediated desensitisation as a result of its stronger binding affinities for individual receptor subunits, partially explaining its differing signalling properties compared to IFNα [369].

1.2.2.1.3 Differential type-I IFN signalling

Many of the genes upregulated by type-I IFNs are the same because of their shared receptor and downstream signalling pathway. However, type-I IFNs exhibit both overlapping and distinct biological activities. A key example of differential biological activity is the ability of IFNβ to induce stronger pro-apoptotic and antiproliferative activity compared to IFNα despite eliciting the same antiviral protection on multiple cell lines [207]. Importantly the unique biological activities displayed by type-I IFN subtypes underpins their different clinical applications for treatment of viral infections [107], cancers [361] and multiple sclerosis [281]. Consequently, there is considerable interest in uncovering the molecular mechanisms that drive these differential properties. There is growing evidence implicating differences between IFN subtypes in their receptor binding kinetics to differential downstream effects. The general model for receptor engagement is that type-I IFNs first dimerize with a high affinity interaction to the IFNAR2 subunit. Subsequently, a lower affinity interaction to IFNAR1 recruits this subunit to the signalling complex and initiates signalling [39]. The binding of IFNAR1 is the rate limiting step for classical signalling to progress [196]. Interestingly, the affinity and dissociation constants for type-I IFNs with each receptor subunit differs between IFN subtypes. Notably, the binding affinities of IFNβ are stronger than for IFNα for both receptor subunits. Specifically, IFNβ binds the IFNAR2 ectodomain with ~100 pM affinity compared to IFNα binding in the nanomolar range [179]. For the interaction with the IFNAR1 ectodomain IFNβ exhibits ~260 nM binding affinity compared to IFNα binding in the micromolar range [71]. The tighter binding of IFNβ to the IFNAR1 subunit is demonstrated to

drive non-canonical signalling independent of IFNAR2 activation. This IFNβ-IFNAR1 signalling axis was shown to drive pathological toxicity in a mouse model of LPS-induced septic shock [71]. Additionally, IFNβ's higher affinity interaction to the IFNAR1 subunit also acts to prevent USP18 mediated receptor desensitization for IFNβ but not IFNα. This occurs as a result of the ability of IFNβ to efficiently recruit IFNAR1 causing greater stability of the ternary ligand-receptor complex that resists USP18 mediated receptor-ligand complex destabilisation [369]. Greater complex stability mediated by IFNβ but not IFNα is shown to result in prolonged ISG upregulation, including genes with pro-apoptotic function [100]. Understanding the molecular basis that drives the distinct properties the type-I IFN subtypes is important to tailor their therapeutic uses.

1.2.2.2 IFN-epsilon overview

IFN-epsilon (IFNε) is the most recently identified member of the type-I IFN family. Both the mouse and human IFNε gene were first annotated in a 2004 paper by Hardy *et al.* [133], however it was not until 2013 that it was more fully characterised [105]. Like others in the family, IFNε signals through the type-I IFN receptor (IFNAR1/2) to elicit its antiviral effect [105]. Unlike the classical type-I IFNs (α or β) that are mainly produced in reaction to sensing viral pathogens, IFNε displays the unique characteristic of being constitutively expressed in tissues of the female reproductive tract (FRT) [133]. Instead of regulation by PRR recognition the expression of IFNε is controlled by cycling female sex hormones and thus the level of IFNε change over the menstrual cycle and during pregnancy [105, 250]. This places IFNε in a unique position to pre-emptively control infection in the FRT. This aspect of IFNε's biology is especially important considering the ability of viruses to evade IFN response and cause disease after infection is established. A significant portion of this thesis will examine the antiviral properties of IFNε in control of viral infection in the FRT. The following section will discuss the current literature surrounding the biology, regulation, and antiviral effect of IFNε.

1.2.2.2.1 Discovery of IFNε

Both the mouse and human genes for IFNε (IFNe1) were discovered in 2004 by characterisation of novel gene sequences surrounding the type-I IFN locus [133]. The IFNe1 gene was found to have a similar structure and sequence to other members of the type-I IFN family. Specifically, human IFNε has 32% and 36% amino acid identity with human IFNα-2A

and IFNβ, respectively. This compares to 33% identity between IFNα-2A and IFNβ [133]. Interestingly, human IFNε has a high level of relatedness to the mouse gene with 58% sequence identity plus 15% amino acid similarity [133]. From this study, sequence alignments and modelling indicated that the expressed protein from the IFNe1 gene likely displayed conserved folding and domain structure to other type-I IFNs, including the predicted binding site for the IFNAR1/2 receptor. Despite the similarities in their coding regions, analysis of the IFNe1 proximal promoter region revealed divergence from canonical transcription factor (TF) elements normally found in canonical type-I IFN promoters. Importantly, the IFNe-1 promoter lacks conventional type-I IFN TF binding sites downstream of PRR or IFN signalling pathways such as IRFs, NF-kB or ISGF3 [105]. Instead of these conventional binding sites, the promoter contains a progesterone response element (PGR) that is conserved between the mouse and human genes.

1.2.2.2.2 Expression of IFNε

IFNε displays unique regulation and expression patterns *in vivo* as a result of differences in the promoter of the IFNe1 gene compared to other type-I IFNs. IFNε expression is tissue specific and most highly expressed in the FRT of both mice and humans [105]. Several others have reported detectable mRNA or protein expression of IFNε in the gut, brain, lung and in the male reproductive tissues of either humans, mice or rhesus macaques [73, 133, 145].

Unlike other type-I and type-III IFNs which illicit a reactionary response to viral infection IFNε expression is constitutive and mainly controlled by the levels of female sex hormones estrogen and progesterone [105]. In humans this means that IFNε expression changes over the menstrual cycle, is reduced in post-menopausal women and during early pregnancy [105, 250]. Importantly, IFNε is the only IFN to be expressed constitutively in the non-pregnant human FRT [253]. Consequently, this places IFNε in a unique position to activate IFN signalling prior to viral infection, potentially circumventing many viral evasion strategies (discussed in the following section 1.3) that rely on first establishing the transcription and translation of viral proteins. On the other hand, this means when expression of IFNε is low the female reproductive tract may be more susceptible to viral or bacterial infections.

The hormonal regulation of IFNε differs slightly between mouse and humans as illustrated in Figure 1.10. In the mouse, IFNε expression is highest during estrous and lowest during diestrus across both the lower and upper FRT (unpublished work, Hertzog *et al.*). In the context of

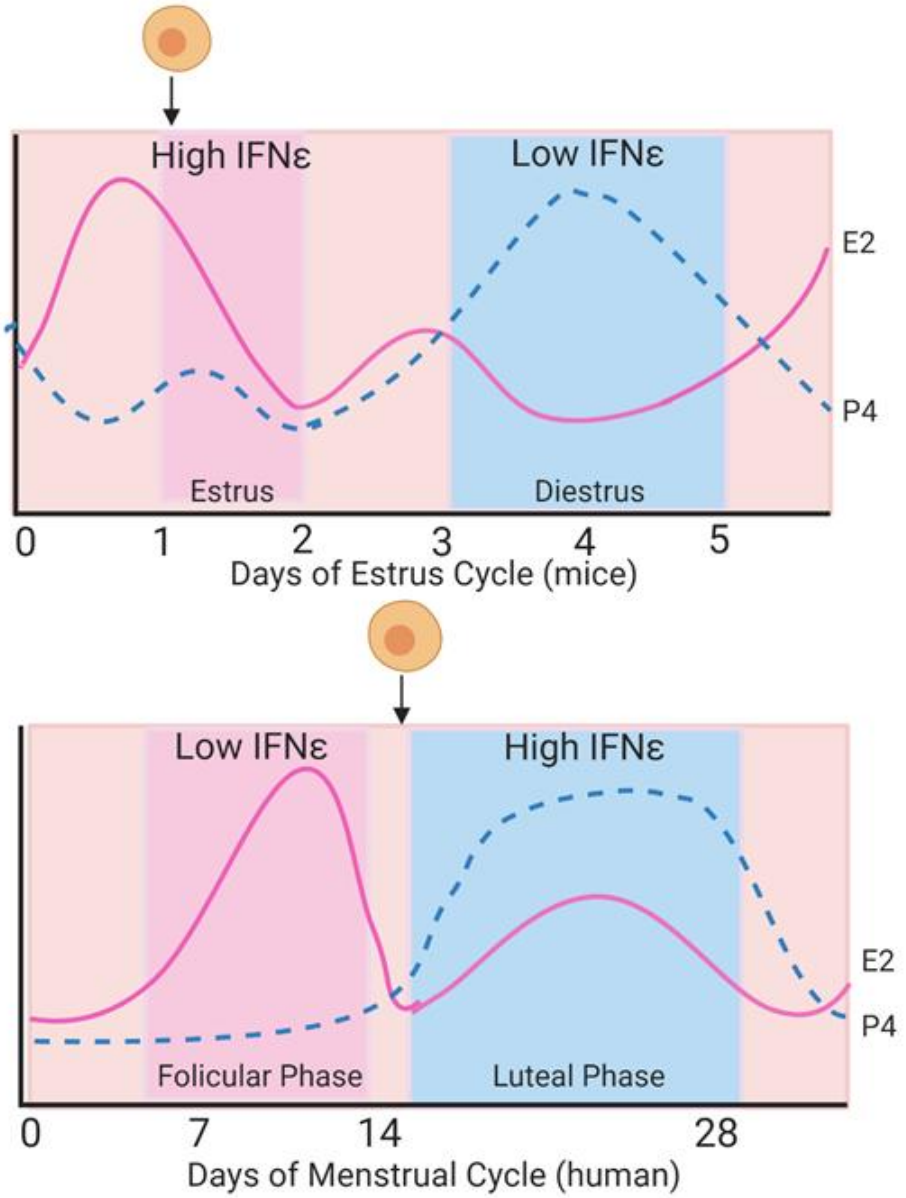

Figure 1.10: Hormonal regulation of IFNε in mice and humans. Levels of the female sex hormones estrogen (E2) and progesterone (P4) change over the estrus or menstrual cycle in mice and humans respectively. This leads to differences in the expression of IFNε. In mice IFNε is high during estrus and low during diestrus. In humans IFNε is low in the follicular phase and high in the luteal phase of the menstrual cycle.

pregnancy, murine IFNε expression is reduced in early pregnancy (d4.5) and increases gradually at later time points of gestation (d12.5, d18.5) [105]. On the other hand, the most recent work by Nollaig *et al*. on IFNε expression in humans indicates there are differences in regulation between upper and lower FRT [253]. In contrast to observations in mice, IFNε protein is highly expressed in the basal epithelium of the lower FRT (vagina and the ectocervix) and this stays constant throughout the menstrual cycle. However, in the endometrium (upper FRT) IFNε protein levels are significantly higher during the luteal phase compared to the follicular phase of the menstrual cycle [253]. Another study investigating IFNε expression in human pregnancy found that the concentrations of IFNε in vaginal secretions were lowest in early pregnancy and then increased throughout pregnancy similar to the expression pattern seen in mice [250].

In addition to *in vivo* expression patterns, studies in human cell lines have demonstrated regulation of IFNε *in vitro*. Consistent with its hormonal control, human IFNε promoter activity was shown to decrease following stimulation with progesterone in a hormone responsive endometrial cell line (ECC1) [253]. Additionally, treatment of HeLa cells with TNFα increased the expression of IFNε leading to an increase in downstream RIG-I expression [210]. Furthermore, IFNε mRNA expression was increased in an ectocervical cell line (Ect1) by exposure to semen [316]. IFNε expression can also be post-transcriptionally controlled by molecular transporter importin 9 that binds the 5' UTR of IFNε message acting to limit translation [211]. Together the unique expression pattern and regulation of IFNε suggests it has an important role balancing antiviral protection and normal biological function of the FRT.

1.2.2.2.3 Properties of recombinant human and mouse IFNε protein

Like all the type-I IFNs, both the human and mouse IFNε signal through the IFNAR1/2 receptor to initiate ISG expression and induce an antiviral state [105]. However, as the most recently discovered member of the type-I IFN family there is less known about the basic biology of IFNε compared to IFNα or IFNβ. In general, functional studies investigating the properties of the human IFNε protein have been hindered by difficulties in expressing the recombinant human IFNε protein and lack of commercially available antibody reagents [134]. Currently two groups have reported the successful expression of recombinant human IFNε protein. The first group (our collaborators led by Paul Hertzog at the Hudson Institute of Medical Research) published in 2017 on the anti-HIV properties of human IFNε *in vitro* using protein expressed

and refolded from bacteria [110]. The second group published in 2018 also expressed the protein in bacteria and used it to investigate binding properties to the type-I IFN receptor [134].

This latter study found that human IFNε displayed a-typical receptor binding kinetics with regards to the individual IFNAR1/2 receptor subunits. IFNε bound with significantly lower affinity to the extracellular domain of IFNAR2 compared to the equivalent interaction with IFNα. On the other hand, IFNε was able to bind with greater affinity to the IFNAR1 subunit compared to IFNα. Figure 1.11 compares the binding affinities of human type-I IFNα, IFNβ and IFNε with the individual receptor subunits. This data suggests IFNε has evolved to maintain a high affinity interaction with IFNAR1 compared to its reduced efficiency binding IFNAR2. This study also found that human IFNε is roughly 1000-fold less potent in biological assays compared to IFNα2, likely because of the lower affinity for IFNAR2.

The properties of recombinant murine IFNε protein have also been investigated [335]. Consistent with the study of the human protein, murine IFNε displayed the non-canonical binding affinities for the individual receptor subunits. Murine IFNε bound with higher affinity to IFNAR1 than IFNAR2. Compared to IFNα, murine IFNε bound to IFNAR2 with 3000-fold lower affinity and to IFNAR1 with a 4-fold higher affinity compared IFNα. This was consistent with a roughly 100 – 1000-fold reduced potency in biological assays for antiviral, anti-proliferative and anti-bacterial activities. Intriguingly murine IFNε was found to exhibit cross-species reactivity on human cells, displaying 100-fold greater activity than on mouse cells.

Taken together these studies highlight the subtle differences in type-I IFN biology. IFNε appears to be less potent compared to canonical type-I IFNs in biological assays. Furthermore, the abnormal binding kinetics to the IFNAR1/2 receptor suggests the potential for IFNε having unique signalling properties compared to other type-I IFNs. These unusual characteristics of IFNε biology appear to be conserved between the mouse and human proteins. The differences in biological activity and unique expression pattern of IFNε suggests it likely plays a role in FRT innate immunity that is not yet fully understood.

1.2.2.2.4 IFNε antiviral activity

There is growing evidence that IFNε protects against sexually transmitted viral and bacterial pathogens. In a mouse model, Fung *et al*. demonstrated that IFNε knockout ($IFN\varepsilon^{-/-}$) rendered mice more susceptible to HSV and *Chlamydia muridarum* vaginal infections compared to

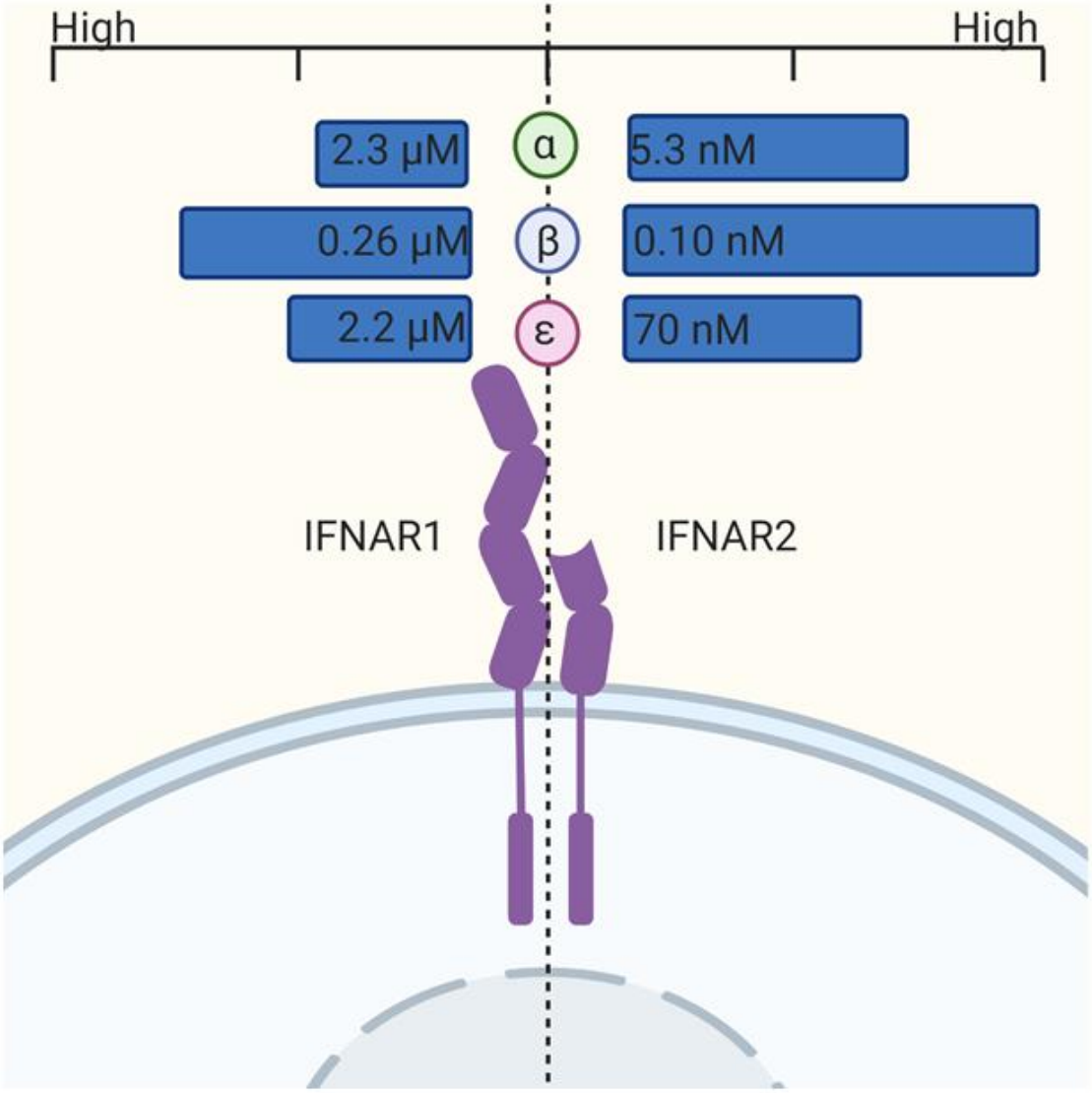

Figure 1.11: Binding kinetics of the IFNs with the type-I IFN receptor. The relative binding affinities and equilibrium dissociation constants (*KD*) of human IFN subtypes for the ectodomains of IFNAR1 or IFNAR2. Blue bars represent relative affinity, with larger bars (Smaller *KD*) indicating tighter binding. Sources: Harris, et al. (2018) de Weerd, et al. (2013) Lamken, et al. (2004).

wildtype counterparts [105]. Interestingly, a pilot study in humans observed IFNε protein levels in the cervical-vaginal secretions of pregnant women were inversely correlated to HSV infection status [250]. It is unclear at this stage if low IFNε levels promote HSV infection during pregnancy or if HSV infection reduces expression of IFNε in the human FRT to promote viral replication.

In addition to mouse models of infection, *in vitro* assays using reporter cell lines show that recombinant IFNε can protect against late-stage HIV replication events as a result of the upregulation of host restriction factors that block HIV infection [110]. Interestingly, this correlates with findings in a cohort of high exposure risk HIV negative female sex workers [1]. In this study the group of HIV negative sex workers had greater levels of IFNε expression compared to a low risk (non sex worker) control group. Interestingly, the levels of IFNε in the FRT positively correlated with increased exposure to semen. This suggests IFNε may contribute to cervical-vaginal immunity reducing susceptibility for HIV-1 infections in high risk groups. Taken together, *in vitro* experiments, *in vivo* mouse models and patient data imply IFNε has role in the protecting the FRT from sexually transmissible pathogens. Continued exploration into the host-virus interactions between IFNε with a diverse range of viral and bacterial pathogens that can infect the FRT are required for us to fully understand this aspect of mucosal innate immunity.

1.2.2.3 Similarities and differences between type-I and type-III IFN signaling

Other than the classical type-I IFNs, the type-III IFN family was discovered more recently by two independent groups in 2003 [174, 318]. They are related to the IL-10 family cytokines and are genetically distinct from the type-I IFNs [318]. In humans there are three functional subtypes IFNλ-I, IFNλ-II and IFNλ-III as well as one pseudogene IFNλ-IV. In mice only IFNλ-II and IFNλ-III are functionally expressed, and IFNλ-I is a pseudogene [182]. Like other IL-10 related cytokines, the type-III IFN receptor is a heterodimer made up of the shared IL-10 receptor chain β (IL-10RB) and the cytokine specific receptor chain (IFNLR1) [318]. Type-III IFNs initially bind to their receptor with a high-affinity interaction to the specific IFNLR1 subunit and then trimerize with the lower affinity IL-10R subunit [32]. Although type-I and type-III IFNs are genetically distinct and act through different receptors they display many overlapping functions. This is because of similarities in the pathways downstream of receptor binding (see Figure 1.9). Like the type-I IFN receptor, binding of type-III IFNs to the IL-10RB/

IFNLR1 initiates typical JAK/STAT signalling leading to the formation of STAT1/2 heterodimers and subsequent ISG induction [255]. As a result, transcriptional profiling has revealed that the vast majority of genes induced by type-III IFNs are the same as those induced by type-I IFNs [36, 98, 397]. However, despite their similarities these IFN families play non-redundant roles in controlling viral infection due to their differing special-temporal expression and activities.

1.2.2.3.1 Production of type-III IFN

Like type-I IFNs, type-III IFNs are produced in response to sensing viral infection. This occurs via the same PRRs (RIG-I, MDA5 and TLRs) as with type-I IFN [255]. However, type-I and III IFNs are not uniformly produced in response to viral infection. Interestingly, differentiated epithelial cells favour the production of type-III IFNs. This occurs because of the alternate sub-cellular localizations of the RLR signal intermediate MAVS to either the mitochondrial or peroxisomal membrane [79]. Whereas mitochondrial MAVS favours type-I IFN production, MAVS that localizes to peroxisomes promotes greater levels of type-III IFN production [255]. Importantly, epithelial cell differentiation has been shown to lead to an increased abundance of peroxisomes that is associated with an increase in type-III IFN responses in these cells [254].

1.2.2.3.2 Type-III receptor localization

The main driver of different biological function between type-I and III IFNs is the limited localization of the type-III IFN receptor. Although the shared IL-10B subunit is expressed widely throughout the body, the expression of the IFNLR1 subunit is tightly regulated and limited to epithelial cells or neutrophils [182]. Comparatively both subunits of the IFNAR1/2 receptor are expressed almost ubiquitously throughout the body. As a result, type-III IFNs act primarily at mucosal surfaces such as the lung, gut, and reproductive tract whereas type-I IFNs can have broad systemic effects [172, 182, 255].

1.2.2.3.3 Switching off the type-III IFN response

The other main difference of type-III IFNs is the kinetics of gene induction following receptor binding. Type-III IFNs display a slower onset and more sustained ISG induction compared to type-I IFNs in cell lines [28, 98]. The mechanisms driving differential kinetics of gene induction are likely due to differences in negative regulation of these pathways. As discussed previously, type-I IFNs are shut off by both short-term SOCS and long-term USP18 negative regulation.

Conversely, there is evidence suggesting that type-III IFNs respond to SOCS but are resistant to USP18 mediated regulation leading to a sustained ISG induction profile [27]. This is demonstrated in cell culture by IFN induced USP18 expression shutting off IFNα but not IFNβ or IFNλ signalling [99]. Additionally, IFNλ mediated ISG induction was enhanced in SOCS1 but not USP18 knockout cell lines [27]. However, this evidence is contrasted by results in USP18 knockout mice that were hypersensitive to both type-I and type-III IFN signalling, leading to improved outcomes in an epithelial breast cancer model [34]. Additionally, overexpression of both SOCS1 and USP18 in cell lines was able to inhibit type-I and III IFN signalling equally [27]. This contrasting evidence seems to imply there are situation dependent differences in type-III IFN responsiveness to USP18 mediated desensitisation. These differences could result from differences in the concentration of USP18 (overexpressed versus endogenous) or type-III IFN receptor expression in individual cell lines or model systems.

1.2.2.3.4 Physiological outcomes of type-I and III IFN signalling

As a result of the different spatial-temporal gene induction profiles mediated by type-I and III IFNs they have distinct role in controlling viral infection. There is evidence showing that type-III IFNs have a lower propensity to activate inflammatory pathways compared to type-I IFNs [32, 66, 98]. This effect is proposed to reduce the impact of type-III IFNs on barrier integrity of epithelial surfaces, making it more suitable for protecting mucosal surfaces from viral infection [32]. In a mouse model, treatment with both type-I and III IFNs were found to protect the mice equally well from Influenza A Virus (IAV) infection. However, in the process type-I IFNα induced greater levels of inflammatory cytokines, immune cell infiltration and epithelial cell death compared to type-III IFN treatment [66]. Importantly, despite type-I and III IFNs inducing identical responses in lung epithelial cells in this model, only type-I IFN treatment activated tissue resident immune cells leading to the release of pro-inflammatory cytokines. This example of different cell types responding to type-I or III IFN shows how differing receptor expression is a key driver of the biological differences between these IFN families. However, the tendency of type-III IFNs to incite lower levels of inflammation may be dependent on the biological context. For example, studies have shown that type-III IFNs are elevated in serum of systemic lupus erythematosus (SLE) autoimmune disease patients [190]. Additionally, mouse models of SLE showed that deletion of the IFNLR1 gene protects mice from organ damage [113]. This effect was driven by IFNλ mediated production of pro-

inflammatory chemokines (CXCL9, CXCL10 and CXCL11) in keratinocytes. Another example of how cell-type specific responses differentiate the function of type-I and III IFNs *in vivo* is comparing their efficacy in clearance of local or systemic viral infections. In a separate mouse model of IAV infection, IFNλ was found to offer greater protection in the upper airways compared to type-I IFNs. However, when IAV was inoculated directly into the lung, only mice deficient in IFNAR1 and not IFNLR1 were more susceptible to IAV infection compared to WT [172]. This indicates that once infection has bypassed mucosal epithelial surfaces, type-I IFNs contribute more to clearing viral infection than type-III IFNs. Another example of differential functions between type-I and III IFNs is the longevity of the antiviral response induced at mucosal surfaces. This is exemplified in mouse models where intranasal treatment with IFNλ provided longer lasting protection against IAV infection in the upper respiratory tract compared to similarly administered IFNα treatment [172]. The longevity of antiviral protection of type-III compared to type-I IFNs is likely dependent on differing properties regarding their negative regulation.

Together this information highlights the role of type-III IFNs as antiviral protectors of mucosal epithelial surfaces. Additionally, this implies the importance of type-I IFNs in protecting against infections that spread beyond the epithelial cell layers.

1.2.3 Inhibition of ZIKV and DENV infection by Interferon

Both type-I and III IFNs are important in controlling *Flavivirus* infection through the production of ISGs. These genes play a wide variety of roles in the innate antiviral response and have been extensively reviewed elsewhere [305]. Some ISGs are important for sensing viral pathogens, such as RIG-I or the IRF proteins while others are important in directing immune cell trafficking, such as the chemokine CXCL10 that recruits antiviral effector NK cells to the site of infection. Importantly, some ISGs can act directly to inhibit various stages of the virus lifecycle. Some of these direct acting ISGs have been determined for ZIKV and DENV and their mechanism of action will be described in the following sections.

1.2.3.1 Interferon stimulated genes that inhibit ZIKV and DENV

Two complementary studies have demonstrated that Interferon Stimulated Gene 15 (ISG15) protects against ZIKV infection [326, 327]. Mature ISG15 is a 15 kDa member of the ubiquitin family of proteins that plays various roles in the innate immune response that

have been extensively reviewed [266]. One of the main functions of ISG15 is the covalent modification of target proteins via ISG15 conjugation (ISGylation) disrupting target protein localization and protein-protein interactions. Additionally, ISG15 has immune modulatory functions through non-covalent protein interactions and by acting as an immune cell signalling molecule. One study found that ZIKV infected ISG15$^{-/-}$ mice had increased severity of retinal lesions and impaired antiviral responses compared to wildtype mice and this led to lower expression of other ISGs like RIG-I and IFI6 [325]. A follow-up study by the same group extended these observations to show that ZIKV infection in human primary corneal epithelial cells (HCEC) induced expression of ISG15 RNA and protein, and that siRNA mediated knockdown of this expression lead to increased ZIKV infection in these cells [327]. Conversely, heterologous expression of ISG15 protein was able to ameliorate this effect. Furthermore, this group found that ISG15 expression was important for both reducing ZIKV entry into host cells, and for inhibiting viral replication once inside the cell. Similarly, ISG15 inhibits DENV infection. DENV infection has been shown to upregulate expression of ISG15 in RAW264.7 cells, and its silencing increased DENV replication in these cells [64]. Furthermore, infection with DENV increased the total amount of ISGylated proteins in the cell, suggesting a link between the ISG conjugation activity of ISG15 with the observed antiviral effect [64].

Members of the Interferon-Inducible Transmembrane (IFITM) protein family also protect against both ZIKV and DENV infection. As their name suggests these proteins are found inserted into cellular membranes, most commonly localising in late endosomes, and can interfere with fusion of viral and host membranes following viral entry [19]. Importantly, siRNA mediated knockdown of IFITM1 or 3 was shown to increase ZIKV infection in human cell lines [300]. This effect could be rescued with overexpressed protein but relied on the protein's endosomal localisation. Consistent with their localisation to endosomal membranes, knockdown of IFITM1 or 3 was shown to impact very early steps in the viral replication cycle following entry [300]. Likewise ectopically expressed IFITM2 or IFITM3 have been shown to reduce DENV infection in human cell lines to similar levels to those observed when treating cells with 100 U/mL IFNα [157]. Like ZIKV, this inhibitory effect was observed to impact the DENV lifecycle at a step prior to the initial round of viral RNA translation.

Another ISG shown to directly inhibit ZIKV and DENV infection is interferon alpha-inducible protein 6 (IFI6). IFI6 is a 13 kDa protein that is known to be involved in cell survival and

counteracting virus-mediated apoptosis [275]. Increased expression of IFI6 was shown to reduce ZIKV replication and prevented ZIKV mediated cell death in the Huh7 (liver origin) cell line [89]. In this study, IFI6 localised to the ER near ZIKV RCs suggesting that it may play a role in inhibiting viral replication or virion production. Furthermore, this antiviral effect of IFI6 was independent of ZIKV protein stability or polyprotein processing. Likewise, Huh7.5 cells stably transduced with a lentivirus IFI6 expression vector demonstrated decreased DENV replication compared to an empty vector control [285]. This study also demonstrated that CRISPR-mediated knockout of endogenous IFI6 expression increased DENV replication in infected cells.

Furthermore, the virus inhibitory endoplasmic reticulum associated interferon inducible protein (Viperin) has been shown in multiple studies to reduce ZIKV and DENV replication [141, 259, 354]. Viperin is a 42 kDa protein and as the name suggests is normally associated with ER membranes. Importantly, Viperin has antiviral effects against a wide range of viruses in both RNA and DNA families [140, 142, 244]. The first study to investigate the importance of Viperin in ZIKV infection found that Viperin was induced in response to ZIKV infection and overexpressed Viperin restricted ZIKV replication in human cell lines [354]. Additionally, murine embronic fibroblasts (MEFs) derived from Viperin knockout mice were more permissive to ZIKV replication compared to wildtype MEFs. Furthermore, the anti-ZIKV action of Viperin relied on the highly conserved C-terminal end of the protein [142]. A second study confirmed Viperin's antiviral effect, finding that Viperin interacted directly with the ZIKV NS3 protein resulting in its degradation and reduced viral replication [259]. Similarly, DENV inhibition by Viperin is also dependent on the C-terminal region of the protein and its interaction with the DENV NS3 protein [141].

Aside from these ISGs that are known to inhibit both ZIKV and DENV infection, other direct acting ISGs have been independently validated for either virus. Future studies may prove these ISGs are effective against both viruses, or they may reveal virus-specific activity. One of these ISGs is interferon-inducible factor 16 (IFI16). This ISG has multiple roles in modulating expression of viral proteins and activating the STING pathway during infection [77]. Overexpressed IFI16 was shown to reduce infection of both the +ssRNA alphavirus chickungunya virus (CHIKV) and ZIKV in human skin fibroblasts [368]. No specific mechanism for this effect was investigated. To our knowledge, IFI16 has not been independently

validated for its antiviral activity against DENV infection. However, the role of IFI16 in promoting STING activation suggests that this is a strong possibility.

Other ISGs known to inhibit DENV infection are the ArfGAP with dual pleckstrin homology (PH) domains 2 (ADAP2) protein and the tripartite motif 69 protein (TRIM69). ADAP2 is most highly expressed in the heart, and skeletal muscle and is known to regulate the ADP ribosylation factor (Arf) family of proteins via its GTPase activating protein (GAP) function [132]. Arf proteins are involved in regulating vesicular trafficking and cytoskeletal organization. Importantly, ectopically expressed ADAP2 has been demonstrated to restrict DENV infection by inhibiting GAP mediated trafficking of incoming DENV containing vesicles [320]. TRIM69 mediates protein ubiquitination through its E2 conjugation enzymatic activity. It localizes to the cytoplasm and inside the nucleus of cells [131]. TRIM69 has been shown to directly interact with DENV NS3, resulting in its polyubiquitination and subsequent degradation to inhibit DENV replication [358]. To our knowledge, the roles of both ADAP2 and TRIM69 in protection against ZIKV infection have not been investigated.

In the context of natural infection, multiple ISGs are expressed in concert and as a result target many of the stages of DENV and ZIKV replication simultaneously. The combined effects of ISGs to inhibit ZIKV and DENV infection has applied strong selective pressure on these viruses to evolve mechanisms to evade detection by the cell or prevent the production of ISGs through blocking the IFN signalling pathway.

1.3 DENV and ZIKV mediated evasion of the IFN response

The IFN response is a barrier that viruses must overcome to cause infection, replicate, and spread. Not surprisingly, because of this strong selective pressure viruses have evolved ways to counteract IFN responses allowing them to gain a foothold and cause infection. Flaviviruses such as ZIKV and DENV are no exception. They have evolved a complex web of interactions with the host innate immune response to undermine both the production and downstream signalling of the IFNs. Some of these evasion mechanisms are common amongst flaviviruses but many are species specific and are yet to be fully elucidated. Discovery of new immune evasion mechanisms underpins the rational design of immune modulatory treatments or live-attenuated vaccine candidates.

1.3.1 Common strategies between flaviviruses

As obligate intracellular pathogens, flaviviruses have evolved many ways to avoid detection by host intracellular PRRs. For example, the 7-methylguanylate cap that is incorporated on the 5' end of the +ssRNA *Flavivirus* genome by the NS5 MTase domain mimics the appearance of host mRNA [234]. 5' capping assists host translational initiation factors to bind the viral RNA and prevents RNA degradation by exonucleases in the cytoplasm [295]. Importantly, 5' capping also interferes with the recognition of vRNA as 'non-self' by the MDA5 PRR, limiting the production of IFN by infected cells [399]. In addition to hiding from detection, capping also avoids the antiviral effects of the interferon induced protein with tetratricopeptide repeats (IFIT) protein family that can bind to and sequester vRNA of uncapped or cap mutant *Flavivirus* genomes [170].

The second mechanism commonly used by flaviviruses to avoid detection is the induction of membrane rearrangements allowing for the formation of the RC as part of the virus lifecycle [224]. As mentioned previously, for flaviviruses these structures are formed from modified ER membranes by the coordinated action of multiple host and viral proteins. Replication organelles form as a series of membranes that surround the dsRNA replication intermediate, acting to physically segregate this potent viral PAMP from detection by cytoplasmic PRRs like RIG-I [7, 310]. In addition, these replication organelles limit the antiviral activity of the ISG encoded MXA protein, likely by blocking MXA-mediated recognition of the forming viral nucleocapsid [149]. Evidence in support of this theory is provided in one study comparing DENV to JEV replication where they observed a greater degree of dsRNA in the cytosol during JEV infection compared to DENV and this correlated to increased IFN production in JEV infected cells [351]. Ultrastructural analysis of the ZIKV RC shows it to be highly similar to that of DENV, suggesting their related function [58].

Aside from genome capping and the formation of replication organelles, several flaviviruses evade IFN production by expression of subgenomic *Flavivirus* RNA (sfRNA) [51]. *Flavivirus* sfRNAs are formed from the incomplete degradation of the viral genome by cellular 5' to 3' exonucleases [212]. Specifically, conserved stem-loop (SL) or dumbbell (DB) RNA structures within the 3'UTR stall exonuclease activity and result in the production of short RNA sequences [106]. Importantly sfRNAs generated during ZIKV infection antagonize the activity of both RIG-I and MDA5 [82], although a full mechanism of action has not been elucidated for this interaction. Likewise, DENV sfRNA inhibits RIG-I mediated IFN production. This effect

is governed by a sequence-specific interaction between DENV sfRNA and the tripartite motif containing 25 protein (TRIM25) [202]. TRIM25 functions as an RNA binding protein and a ubiquitin ligase, responsible for the polyubiquitination of activated RIG-I leading to sustained signal transduction [162].

1.3.2 ZIKV specific mechanisms to evade IFN responses

In addition to strategies common to all flaviviruses, some evasion mechanisms have been characterised for ZIKV that may be unique for this virus. These mechanisms prevent ISG production by interfering with PRR-mediated IFN production, or by directly targeting signalling intermediaries downstream of the IFNAR1/2 receptor.

One mechanism that limits the production of IFN is mediated by ZIKV NS4A that inhibits RIG-I and MDA5 signalling and has been demonstrated independently by two groups [200, 249]. Collectively these studies found that ectopically expressed NS4A binds directly to the N-terminal CARD domain MAVS. This binding competitively inhibited MAVS interaction with activated RIG-I or MDA5, leading to potent inhibition of downstream type-I IFN production. ZIKV can also prevent the translocation of activated RIG-I and MDA5 to the mitochondrial membranes by acting on members of the 14-3-3 protein family. These proteins (14-3-3ε and 14-3-3η) act as mitochondrial targeting chaperones that are required for translocation of RIG-I and MDA5 respectively, facilitating their interaction with MAVS [188, 192]. Importantly, overexpressed ZIKV NS3 protein in HEK 293T cells was able to competitively bind to both 14-3-3ε and 14-3-3η via a conserved binding motif (64-RLDP-67) [286]. This sequence was found to contain a central negatively charged Aspartic acid residue (D66) that acted as a phospho-mimetic to compete with RIG-I or MDA5 binding. Mutation of this binging motif within the full length ZIKV genome attenuated viral replication compared to wildtype virus in A549 cells [286].

ZIKV can also inhibit the cGAS-STING pathway via the actions of NS1. One study found that ectopically expressed ZIKV NS1 interacts directly with host de-ubiquitinase USP8 to facilitate the deubiquitination of caspase-1, increasing its stability [395]. In turn caspase-1 proteolytically cleaves cGAS, reducing the production of IFN in the cell. Additionally, the ZIKV protease NS2B/3 mediates STING cleavage. Using exogenous expression in HEK 293T cells it was shown that ZIKV NS2B/3 cleaved human but not mouse STING [78]. This study extended these observations to natural ZIKV infection in human fibroblasts by detection of

STING cleavage products during infection. The reduction of cGAMP mediated STING activation as a result of ZIKV infection inhibited the production of IFN by infected cells. Other NS proteins also contribute to limit IFN production downstream of MAVS, TLR and cGAS-STING pathways by targeting the shared signalling intermediaries TBK1, IKKε or IRF3. Ectopically expressed NS1 and NS4B interact directly with TBK1, preventing TBK1 oligomerization and phosphorylation mediated activation [374]. Interestingly, another study found that NS1 mediated TBK1 inhibition was specific to recent outbreak strains that had evolutionarily acquired a 188-Val substitution mutation [375]. Additionally, overexpressed ZIKV NS5 in HEK 293 cells was demonstrated to directly interact with IKKε [198]. This direct interaction resulted in reduced IKKε protein levels and phosphorylation, thereby preventing the activation of IRF3. In another study, NS5 was also shown to inhibit IRF3 activation by direct binding to endogenous IRF3 in studies involving co-immunoprecipitation of overexpressed NS5 protein [375].

Downstream of the IFN receptor, ZIKV also acts to suppress JAK-STAT signal transduction. The best characterized of these mechanisms is the ZIKV NS5 mediated degradation of STAT2 protein. ZIKV NS5 can bind to STAT2 and initiate its degradation in a proteasome dependent manner [121]. Interestingly, this occurs with human but not mouse STAT2 protein, partially explaining the difference in species adaptation of ZIKV and difficulties associated with infecting IFN competent mice [231]. A separate study found that overexpression of NS5 leading to STAT2 degradation also resulted in reduced STAT1 phosphorylation in cells overexpressing NS5 [146]. One study also demonstrated that ZIKV NS2B/3 expression induced the degradation of JAK1 protein in a proteasome-dependent manner leading to a reduction in IFN mediated ISG expression [374]. In addition to the roles of NS proteins in inhibition of IFNAR signalling, ZIKV binding to the attachment factor Axl on the cell surface also inhibits IFN signalling. In a study using microglial cell lines, ZIKV binding was shown to activate the C-terminal kinase domain of Axl that in turn acted to negatively regulate the type-I signalling pathway via induction of SOCS1 protein expression [216].

1.3.3 DENV specific mechanisms to evade the IFN response

Some of the mechanisms that govern DENV-mediated IFN evasion closely reflect those of ZIKV, demonstrating their close evolutionary relationship. These tend to be evasion strategies mediated by the more conserved viral proteins, such as the NS3 helicase/protease

and NS5 RdRp/MTase. However, there are also mechanisms that differ entirely in their action and are unique to DENV.

One mechanism preventing the production of IFN by DENV is mediated by NS2B. Overexpressed DENV NS2B directly interacts with cGAS and causes its degradation by auto-phagolysosomes, reducing STING-mediated IFN production [5].

Additionally, DENV NS2B/3 proteolytically cleaves human but not mouse STING in a similar manner to ZIKV [4]. This species-specific cleavage was dependent on the presence of an NS3 cleavage site in human STING. Mutation of this cleavage site was able to restore DENV-mediated induction of IFNβ. DENV NS3 also contributes to evasion of IFN by non-proteolytic actions. HEK 293T cells expressing DENV NS3 demonstrated impaired RIG-I translocation to MAVS in response to Sendai Virus infection. Like ZIKV, this interaction was also dependent on inhibition of RIG-I binding to 14-3-3ε via a conserved phospho-mimetic binding motif at the same location within NS3 (64-RxEP-67) [44]. However, the charged residue mimicking the natural phosphorylation site was found to be a Glutamic acid (Glu66) rather than Aspartic acid residue as was found for the ZIKV NS3 protein. Furthermore, DENV NS2A and NS4B from multiple DENV serotypes inhibit PRR mediated IFN production via targeting TBK1 and IRF3. Ectopically expressed DENV NS2A and NS4B were shown to specifically inhibit TBK1 auto-phosphorylation, and reduced total IRF3 protein levels [65]. Moreover, this same study found that NS4A from serotype-1 was in addition uniquely able to contribute to TBK1 inhibition [65]. This additional evasion mechanism may contribute to the enhanced virulence of DENV1. Overexpressed DENV NS2B/3 in HEK 293/TLR3 expressing cells also directly interacts with the N-terminal Kinase domain of IKKε, inhibiting kinase activity and reducing IFN production [10].

Downstream of IFN receptor activation DENV NS4B blocks STAT1 phosphorylation and nuclear translocation [236]. DENV NS2A and NS4A were also shown to inhibit ISRE promoter activity downstream of IFNβ signalling in HEK 293T cells [236]. For NS4B this effect was later found to depend on the N-terminal signal peptide of the NS4B protein and was enhanced by natural cleavage between the NS4A-2K-NS4B fragment [235]. For NS2A and NS4A the mechanism driving their IFN evasion properties has not yet been elucidated. Finally, similar to ZIKV, DENV NS5 mediates STAT2 degradation in a proteasome dependent manner [16]. However, in contrast to ZIKV this requires natural viral processing of NS5 from the polyprotein and is dependent on the ubiquitin ligase UBR4 [230].

During natural infection multiple genetic elements and NS proteins work synergistically to counteract the IFN responses in cells. Most of these studies described here investigated virus mediated IFN evasion by ectopic expression of individual viral genetic elements. However, many of the essential functions performed *flaviviral* NS proteins or genetic elements are not recapitulated by their individual expression [167]. For this reason, it is important to perform mutational studies on fully infectious viral model systems to further our understanding of this complex aspect of DENV and ZIKV biology. This intricate web of molecular interactions between these viruses with the host innate immune system generates a balance between a state of virus induced immune evasion or an antiviral state. This balance largely determines the outcome between viral persistence or clearance by the immune system.

1.4 Experimental model systems used in this thesis

Studying the molecular interactions of flaviviruses with the type-I IFN response requires understanding of both viral and host biology. The following section will detail background information relating to the main model systems and experimental methods used in this thesis. These include methods to study the impact of changes to viral genetics on IFN evasion, and *in vivo* infection models to assess host innate responses.

1.4.1 Reverse genetics systems as tools for mutational profiling of viral genomes

A key method used to study the function of viral proteins or genetic elements is the targeted introduction of mutations within the viral genome. To do this requires viral expression systems that are genetically stable, can be faithfully propagated, manipulated, and cloned. For RNA viruses that have an inherently unstable genome this is underpinned by the development of reverse genetics systems [30]. In essence a reverse genetics system is a DNA vector containing reverse transcribed complementary DNA (cDNA) generated from the viral RNA genome under the control of a suitable promoter [17]. In general, two types of promoters have been utilised in these systems their different uses are illustrated in Figure 1.12. The first of these is a mammalian promoter, such as the Cytomegalovirus (CMV) promoter. These promoters utilize host cell transcriptional machinery and initiate the production of functional +ssRNA by direct transfection into mammalian cells [17]. The other type of promoter commonly used in reverse genetics systems are bacteriophage promoters, such as T7 or SP6. These are used to generate *in vitro* transcribed +ssRNA that can be

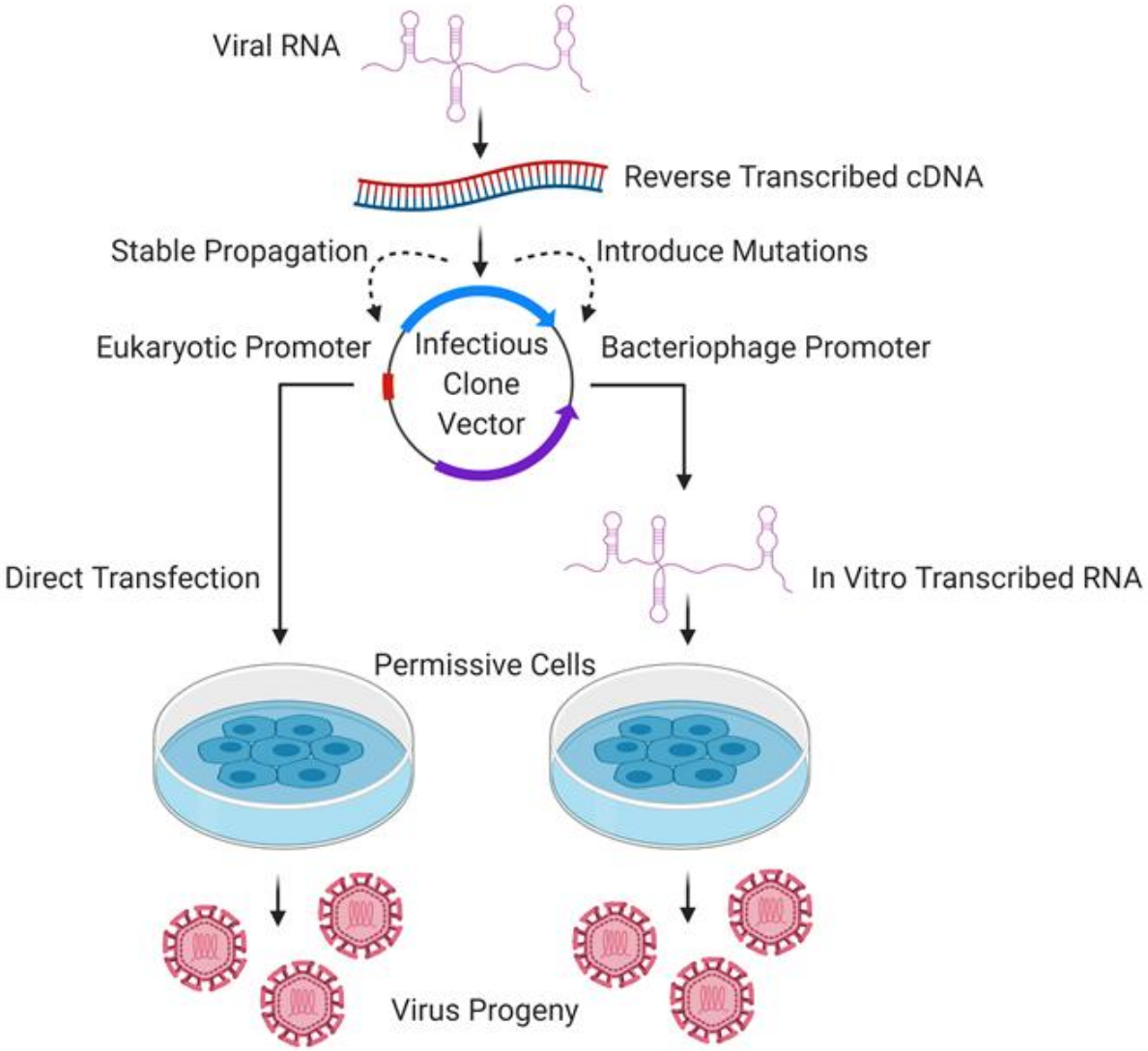

Figure 1.12: Uses of reverse genetics systems for *de novo* generation of infectious virus. First viral RNA is reverse transcribed to cDNA and cloned into a stable vector. This allows for modification to the viral sequence and propagation of the infectious clone. Depending on the type of promoter infectious clones can be directly transfected (eukaryotic promoter) or used to generate *in vitro* transcribed RNA (bacteriophage promoter) that is transfected into permissive cells. This initiates production of new infectious virions carrying genomes that maintain the genetics of the infectious clone sequence.

transfected into permissive cells to initiate *de novo* virus production in mammalian or insect cells [17].

Since flaviviruses have a non-segmented RNA genome that is a manageable size for cloning, reverse genetics systems have been extensively used in the field of *Flavivirus* molecular biology. The full-length cDNA genome of a *Flavivirus* incorporated into a reverse genetics system is termed an infectious clone. Infectious clones can independently initiate replication and production of infectious virus in permissive cells from a stable genetic starting point. As a result, infectious clone technology has revolutionized the study of flaviviruses. They have allowed the for controlled mutation of *Flavivirus* genomes and study of their effect on their biology and pathogenesis.

In addition to providing a stable genetic starting point for mutational studies, full-length infectious clones also overcome complications with over-expression of individually expressed viral proteins. Flaviviruses have a limited genetic capacity compared to eukaryotic organisms. However, the complexity of the *Flavivirus* lifecycle that requires replication, immune evasion and spread in both vertebrate and invertebrate hosts is remarkable compared to the size of their genomes. To achieve this complexity, flaviviruses rely on interactions involving multiple viral proteins and host factors to perform their complete lifecycle. As a result, many of the essential functions performed by *Flavivirus* proteins or genetic elements are not recapitulated by their individual expression [194]. Accordingly, there is a need to perform mutational profiling in infectious clones to see the full impact these mutations have on the virus lifecycle. Despite the obvious advantages when performing mutational studies on *Flavivirus* biology, the use of full-length infectious clones often presents a unique set of challenges. These challenges largely result from propagation of infectious clones in bacterial cells. Harbouring full-length *Flavivirus* genome sequence is often detrimental to bacterial cells, causing slow growth or genetic instability of the infectious clone as a result of bacterial recombination [292]. This is because *Flavivirus* genomes contain cryptic bacterial promoters that lead to expression of toxic viral gene products when introduced into bacterial cells [17, 185]. To overcome these challenges several strategies are employed to reduce bacterial toxicity and improve infectious clone stability. Most infectious clones use low-copy vectors to reduce the amount of toxic expression products that accumulate in bacteria [292]. Additionally, toxic sequences can be identified and disrupted by chimeric introns [17, 350]. These introns are present in bacterial hosts but are spliced out when introduced into eukaryotic cells due to

their different RNA processing capability. Alternatively, the full-length genome can be separated across multiple vectors, independently propagated, and then stitched back together by *in vitro* methods such as overlapping PCR or *in vitro* ligation [17, 74]. Despite these challenges, infectious clones are valuable tools for studying *Flavivirus* biology.

1.4.2 Transposon mutagenesis as a method for high-throughput genome wide mutational profiling

Mu transposon mutagenesis is a molecular tool used to efficiently construct insertional mutant libraries for functional analyses of protein coding and regulatory regions [348]. The process of generating these insertional mutant libraries is illustrated in Figure 1.13 and described here in brief. First, the target DNA, such as infectious clone cDNA, is subjected to a MuA transposase reaction. In this reaction purified MuA transposase enzyme catalyses the insertion of a transposon randomly into the target DNA at a frequency of approximately one insert per clone. This transposon consists of an encoded selection marker (Kanamycin resistance) flanked by two unique *NotI* restriction sites. Incorporation of the transposon into the infectious cDNA clone, followed by their introduction into bacteria allows for selection of successfully mutagenized infectious clones on dual antibiotic plates (Ampicillin and Kanamycin). After selection, the bacteria are pooled, and the plasmid DNA extracted. Next, the pooled library is further processed by *NotI* restriction digestion to remove the bulk of the transposon body. Re-ligation of the *NotI* sites results in the formation of a 15 bp insert made up of 10 bp from the transposon and 5 bp from the target site duplication. After re-ligation, the mutant library is re-introduced into bacteria using single antibiotic selection. Then the mutant clones are again pooled, and the plasmid DNA extracted to generate the final purified library. If the insertion occurs in a protein coding region, an extra 5 amino acids (sequence dependent on the reading frame) are inserted. Importantly, insertions are designed to prevent premature stop codons in all 6 reading frames. These 15 bp insertion mutations act to disrupt normal sequence of translated protein or untranslated RNA allowing for their functional profiling.

Compared to targeted mutational studies that use conventional labour-intensive molecular cloning methods, MuA transposon mutagenesis allows for the rapid generation of mutations across the entire viral genome [348]. Alternative high-throughput techniques for functional profiling of viral genomes include alanine scanning mutagenesis [373] or random point

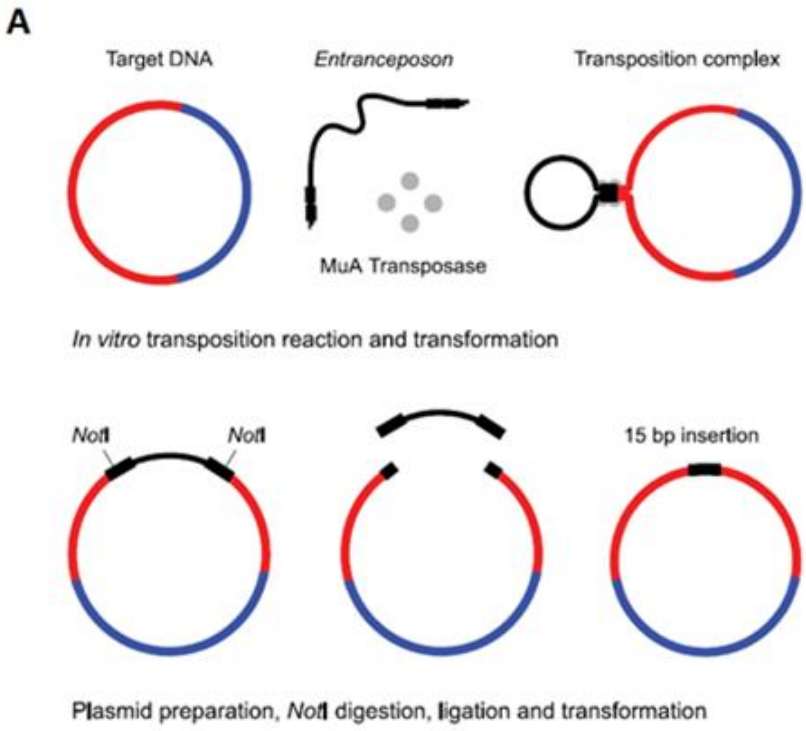

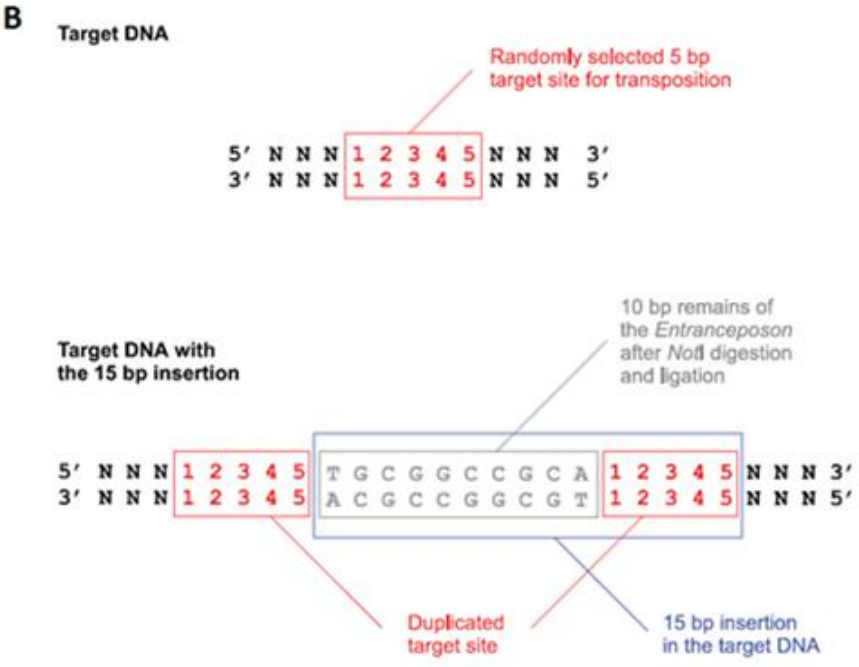

Figure 1.13: MuA transposon mutagenesis. Generation of 15 bp insertions to target DNA by MuA in vitro transposition and NotI digest (A). The 15 bp insertion remaining within target DNA following mutagenesis (B). Adapted from: Mutation Gneration System Kit: Technical Manual, Thermo Fisher, 2012.

mutagenesis [312, 371]. Each of these methods allows for high-resolution mutational studies that resolve to the individual nucleotide level. However, until recently these deep mutational scanning (DMS) methods were limited to investigating smaller regions of viral genomes in part due to their reliance on new high-throughput sequencing technologies [12]. In comparison to DMS, the 15 bp insertion-scar generated by MuA transposon mutagenesis allows for easy detection of mutations using readily available sequencing methods, such as the Illumina NextSeq 500 platform [94]. However, as new sequencing technologies are developed DMS methods will likely become more widely applicable. Indeed, one recent study utilised a DMS method to perform a genome-wide functional screen on the Influenza genome [84]. Aside from the benefit of performing genome-wide mutational studies using readily available sequencing platforms, the MuA transposon method allows for simple pre-selection of successfully mutagenized clones based on the presence of dual antibiotic resistance encoded within the transposon body. This therefore reduces the contribution of wildtype genomes to mutant library population genetics [348]. Comparatively, DMS methods require sequencing of clones to confirm their mutation status. One downside of the MuA transposon mutagenesis method is the potential for insertion bias introduced by the Mu transposase enzyme. Studies in bacterial genomes have shown that Mu transposases displays bias toward GC-rich sequences leading to less uniform spacing of insertions in AT-rich genomes [123]. However, one study on adeno-associated virus vectors has demonstrated the level of MuA insertion bias to be relatively low in this context [277].

1.4.2.1 Applications of MuA transposon mutagenesis for high-throughput mutational studies of viral infectious clones

The MuA transposon mutagenesis method has been successfully applied to several RNA virus reverse genetics systems. These include Polio Virus, Norovirus, Influenza Virus and to flaviviruses such as Hepatitis C Virus (HCV), DENV and ZIKV [94, 103, 104, 139, 283, 346]. This method has allowed for high-throughput mutational screening of viral genomes. Importantly, these studies have provided insight into regions of the viral genome that are important for replication and infectious virus production, regions tolerant to small insertions or regions that are important in evading the IFN response.

In general, these screens function by generating a library of mutant virus from the mutagenized infectious clone and then placing the mutant library under selective conditions

in cell culture or *in vivo* model systems. Mutant viruses that are less fit under selection are outcompeted, reducing their frequency within the population. This process of selection coupled to Next Generation Sequencing (NGS) identifies the genomic position of the remaining insertions and allows for a functional map of the virus genome to be constructed.

The first use of this method to study *Flavivirus* biology was applied to HCV, published in 2014 by Remenyi *et al.* [283]. In this screen, a full-length infectious clone of HCV was mutagenized, RNA was *in-vitro* transcribed and the pooled RNA was transfected into Huh-7.5 cells for genetic selection. This pooled RNA was used to represent the input library of mutants prior to selection (Pool 0). The total cell associated RNA was then recovered at 96 h post-transfection (Pool 1), and then again following passaging of the *de novo* generated infectious virus on Huh-7.5 cells (Pool 2). The cell associated RNA was extracted and RT-PCR was performed to amplify the full-length HCV genome in overlapping fragments. A map was generated for each pool based on NGS sequencing data identifying the location and frequency of insertions at each position of the genome. This study found that the MuA transposon mutagenesis generated 7,978 unique insertion events that covered 88% of the HCV genome in Pool 0. Following selection, the percentage of total insertion positions was reduced to 55% in Pool 1 and 17% in Pool 2. This indicated effective selection was applied to the mutant virus population based on their ability to replicate RNA (Pool 1) or generate infectious virus (Pool 2). The functional map of the HCV genome demonstrated distinct patterns of selection separating proteins based on early or late-stage replicative function. This knowledge was applied to elucidate novel functions of viral proteins not associated with their traditional roles in the HCV lifecycle. Specifically, this knowledge was used to validate a novel function for NS4B in late-stage virus replication by individually cloning the insertion mutations into the original HCV reverse genetics system.

Another example of the use of MuA transposon mutagenesis to study *Flavivirus* biology was a study conducted in our laboratory by Eyre *et al.* published in 2017 [94]. Briefly, a full-length DENV2 infectious clone was subjected to MuA transposon mutagenesis resulting in a library of ~250,000 mutant clones. This library represented 4700 unique insertion positions in the DENV2 genome. A similar selection process was applied to the mutant library as described above. First, full-length *in vitro* transcribed RNA was generated (Pool 0) and transfected into Huh-7.5 cells (Pool 1) to initiate *de novo* virus production. The infectious virus produced as a result was passaged on naive Huh-7.5 cells (Pool 2). This enriched for mutants that were

replication competent (Pool 1) and able to generate infectious virus (Pool 2). After selection, the initial 4700 unique insertion events were reduced to 1122 and 1003 in Pools 1 and 2 respectively indicating successful selection. Regions that were highly tolerant to insertion after the second passage were selected for the rational design of tagged viruses. This allowed for the generation of multiple reporter-tags to be inserted into NS1 region for use in high-resolution and live cell imaging or protein-protein interaction studies.

Other than using this approach to study the role of viral proteins in replication or to generate tagged viruses, the MuA transposon mutagenesis method has been used to discover novel *Flavivirus* immune evasion mechanisms. In 2017 Qi *et al.* published their work on applying this method to discover novel anti-IFN functions of HCV proteins. This screen used the same library generation method as their previous publication described above (Remenyi *et al* 2014). The resultant *in vitro* transcribed RNA was transfected into Huh-7.5 cells to reconstitute mutant virus library. Next, the mutant virus library underwent two rounds of selection on Huh-7.5 cells that had either been pre-treated with IFNα at a concentration that reduced infection to 50% (IC_{50}) or untreated control cells. After selection, the remaining mutant insertions were mapped to the genome and their relative frequency at each genome position was compared between the treatment groups. Analysis revealed insertions in regions previously known to encode IFN evasion and in regions not previously identified. This led to the identification of specific mutations in the HCV p7 protein that conferred hypersensitivity to IFNα. Furthermore, mutant p7 HCV hypersensitivity could be rescued with the introduction of over-expressed wildtype p7 protein.

Together these examples demonstrate the broad applications of the MuA mutagenesis method when applied to infectious clone technology for functional screening of viral genomes. Importantly, it also validates this method as a way of finding novel immune evasion mechanisms encoded by flaviviruses. For these reasons this approach was applied in Chapters 3 and 4 of this thesis with the aim of investigating novel innate immune evasion mechanisms for both ZIKV and DENV.

1.4.3 Mouse models of ZIKV sexual transmission

Small animal models that recapitulate human disease are important for understanding the pathophysiology of viral infections. For viruses such as DENV that have strong host specificity and cause disease that is specific to host immune responses the difficulty in establishing small

animal models has been a significant challenge to development of new treatments and vaccines [56].

Fortunately, there have been significant developments in the space of small animal models for ZIKV infection since the 2015-16 outbreak. Initial attempts to infect immune competent "wildtype" (WT) mice (C57BL/6, BALB/c, or CD-1 mice) with ZIKV by intravenous (IV) or subcutaneous (SC) routes showed no disease signs and little to no detectable viral RNA in blood or tissues [231]. Unsurprisingly, due to the importance of the IFN response to *Flavivirus* infection the first susceptible mouse models developed for ZIKV were IFN pathway knockout (KO) mice [231]. Lazear *et al*. found male mice that cannot respond to type-I IFN ($IFNAR1^{-/-}$), or mice that produce almost no IFNα/β (IRF3/IRF5/IRF7 triple KO) or mice that cannot respond to type-I or type-II IFN (AG129) were highly vulnerable to SC or IV inoculation of 10^2 focus forming units (FFU) of ZIKV [181]. These mice displayed neurological symptoms, detectable viremia, and tissue tropism like those observed in humans including infection in the brain, spinal cord and testes. Similar results were seen by Rossi *et al*. in the IFNαβ receptor null A129 strain mice [290].

After validating these models for SC and IV inoculation, they were adapted to investigate alternative transmission modes of ZIKV, including sexual transmission. Several mouse models have been used to investigate ZIKV sexual transmission in the FRT using vaginal inoculation methods (iVag).

Unexpectedly these studies found that unlike for SC or IV inoculation, immune competent mice were susceptible to ZIKV via iVag inoculation [164, 342, 381]. Importantly all these iVag models involved treatment of mice with progesterone or the progesterone mimic Depomedroxyprogesterone acetate (DMPA) to synchronize the estrous cycle to the diestrus phase. In mice diestrus thins the epithelial cell layer of the lower reproductive tract, however this does not occur to the same extent humans [370]. This thinning of the epithelial barrier caused by DMPA treatment likely contributes to the increased susceptibility of mice to iVag inoculation several viruses including LCMV, HSV and ZIKV [105, 165, 341]. Furthermore, DMPA treatment has been shown by our collaborators to reduce expression of IFNε in the FRT of mice and this also may be a contributing factor to permissiveness of WT mice (Hertzog, unpublished data).

One of the first studies by Yockey *et al*. compared iVag to intraperitoneal (IP) ZIKV inoculation methods. In this model WT C57BL/6 virgin female mice were inoculated iVag with 2.5×10^4

PFU or IP with 1.5 × 10^5 PFU of Cambodian ZIKV strain FSS13025. Mice that received IP inoculation had undetectable levels of ZIKV viral RNA (vRNA) in the spleen and vagina by 3 dpi. Comparatively mice that were iVag inoculated had high levels of vRNA detected in both tissues that increased over time. Importantly this data demonstrates the FRT selectively supports ZIKV infection and that mice infected via this route are more susceptible than those inoculated systemically. Additionally, the susceptibility of WT mice was compared to IRF3/7$^{-/-}$ and IFNAR1$^{-/-}$ mice via iVag infection. It was found that mice with minimal ability to produce IFNα/β (IRF3/7$^{-/-}$) or those that could not signal via the type-I IFN receptor were more susceptible to ZIKV infection via the iVag route compared to WT mice. While WT mice had detectable vRNA in FRT tissues from day 1 to 4 post infection this was almost completely undetectable by 7 dpi. Whereas IFNAR1$^{-/-}$ remained infected through 7 dpi and succumbed to iVag infection with high dose challenge (5.2 X 10^5 PFU) of ZIKV [381].

Similar results were seen in C57BL/6N mice by Khan *et al*. following ZIKV iVag inoculation with 2 X 10^4 FFU of Puerto Rican ZIKV strain PRVABC59. ZIKV vRNA was detected in the LFRT and it increased roughly one log at day 2 compared to day 1 after iVag inoculation, indicative of productive infection. Despite the presence of replicating virus there was minimal induction of type-I or type-III IFN and corresponding ISG mRNA in these mice. In this model mice began to control infection by day 3, indicating that a minimal IFN response was sufficient to control ZIKV infection in the LFRT of mice [165].

Another study looking at ZIKV iVag infection of mice by Tang *et al*. compared susceptibility of mice in estrus-like or diestrus-like phases induced by injection of either pregnant mare serum gonadotropin (PMSG) or progesterone, respectively. In this study estrus-like or diestrus-like AG129 mice (type-I and III IFN receptor KO) were inoculated iVag with 1 X 10^5 FFU of ZIKV (strain FSS13025). Mice infected in the estrus-like phase were resistant to iVag infection. However, AG129 mice in diestrus-like phase became productively infected with peak viremia at 5 dpi and succumbed to infection by 10 dpi. This study demonstrates the influence of the hormonal environment on ZIKV permissiveness of the FRT [341].

Continuing this line of enquiry Caine *et al*. also found the hormone environment of the FRT could alter susceptibility to ZIKV iVag challenge. Like results in AG129 mice they found that estradiol pre-treatment protected IFNAR1$^{-/-}$ mice challenged with iVag administered ZIKV at 10^6 FFU (African strain Dakar 41525). On the other hand, these mice were highly permissive to infection when treated with progesterone as measured by the amount of vRNA detected

in the vagina at 6 dpi. In addition, this group also tested the impact of type-III IFN receptor KO (IFNLR1$^{-/-}$) on ZIKV permissiveness in the FRT of mice. In this model WT or IFNLR1$^{-/-}$ mice were treated with 1 mg of anti-IFNAR1 monoclonal antibody (mAb) to block type-I IFN one day prior to iVag infection with 10^6 FFU ZIKV Dakar. IFNLR1$^{-/-}$ mice had increased viral burden measured by detection of vRNA in the LFRT but no showed no difference in the UFRT compared to similarly treated WT controls. To further explore the role of type-III IFNs in ZIKV infection of the FRT WT mice treated with progesterone and anti-IFNAR1 mAb were given 25 µg of pegylated IFNλ2 intravaginally 8 h prior to iVag challenge with ZIKV. Interestingly, pre-treatment with recombinant IFNλ2 significantly protected the mice, minimizing infection in the LFRT and leading to less infection in the UFRT and peripheral tissues such as the brain [36].

Together these models of iVag ZIKV infection demonstrate the inherent permissiveness of the FRT to ZIKV. This is exemplified by ZIKVs ability to infect immune competent WT mice via this the iVag route when systemic inoculation methods are ineffectual. These models also demonstrate the importance of both type-I and III IFN signalling in the FRT to protect against ZIKV infection. However, although these IFNs protect against infection in the FRT, there are additional IFN-independent mechanisms that alter permissiveness to ZIKV. For example, changes mediated by estradiol treatment result in the absence of infection in mice regardless of type-I or type-III IFN signalling. The blockade of type-I IFN signalling appears to have a greater impact compared to type-III signalling, especially in the UFRT. Additionally, this data shows that treatment with recombinant type-III IFN is effective at controlling ZIKV infection. In combination, these experimental models of ZIKV iVag infection established the basis for the *in vivo* model of iVag infection to investigate the importance of IFNε that is described in Chapter 5 in detail.

1.5 Experimental rationale, hypotheses and aims

Type-I IFNs are key innate immune effectors involved in host antiviral defence, acting to protect the host from viral infection via the expression of hundreds of ISGs that have direct antiviral or immune regulatory functions. However, ZIKV and DENV have evolved mechanisms to evade the IFN response allowing them to cause disease in humans. Our existing knowledge surrounding virus-mediated IFN evasion is limited by the lack of mutational studies conducted in fully infectious systems and on a genome-wide scale. Additionally, type-I IFNs are either expressed by the host in response to viral infection, or IFNε is constitutively expressed in the FRT. The contribution of IFNε as a constitutively expressed IFN in the FRT to circumvent viral evasion of the IFN response, and in protecting against ZIKV sexual transmission is not yet known. Therefore, this thesis explores the virus dependent mechanisms that abrogate the type-I IFN response and characterises the role of novel IFNε in preventing ZIKV infection of the FRT. As a result, the following hypotheses and aims are proposed.

Hypothesis 1:

The ZIKV and DENV genomes contain undiscovered regions encoding evasion of the type-I IFN response.

Aim 1: To identify and characterize novel genetic elements that confer resistance to type–I IFN using a genome-wide insertional mutagenesis screen of a recent outbreak strain of ZIKV.

Hypothesis 2:

IFNε is an important type–I IFN that protects against ZIKV infection in the female reproductive tract.

Aim 2: To investigate the antiviral properties of IFNε and determine whether it effectively controls ZIKV infection in the female reproductive tract.

Chapter 2

Material and Methods

2.1 General laboratory methods

2.1.1 Bacterial transformation methods

2.1.1.1 Chemically competent cells

For standard plasmid transformations, Alpha-Select DH5α Escherichia coli (*E. coli*) Silver efficiency (Bioline) were used as per the manufacturer's instructions. Briefly, cells were thawed on ice and a 25 – 100 µL aliquot was placed into pre-chilled microcentrifuge tubes. Then DNA was added to the cells (either 1 ng of purified plasmid or <5 µL ligation reaction per 50 µL cells). The bacteria and DNA were gently mixed by flicking the tube and these were rested on ice for a further 30 min. Next, the cells were placed in a heat block set to 42^{o}C for 30 sec then were placed back on ice for a further 2 min. Following heat shock, 900 - 975 µL of Super Optimal broth with Catabolite repression (SOC) medium was added to the cells and the culture was placed at 37 ^{o}C for 1 h on a rotating spinner. Next, the suspensions were centrifuged at 2000 ×*g* for 2 min, the supernatant was removed, and the transformed cells were resuspended in approximately 100 µL of SOC medium. This suspension was plated onto Luria Bertani-Agar (LB-Agar) with antibiotic selection (ampicillin at 100 µg/ml or kanamycin at 50 µg/ml) using a sterile spreader and placed at either 30 ^{o}C or 37 ^{o}C until visible bacterial colonies formed (16 – 30 h).

For large plasmids requiring higher transformation efficiency, XL10-Gold Ultracompetent Cells (Stratagene/Agilent) were used. A similar method was used as for DH5α transformation, above, with the following exceptions. Firstly, after thawing cells on ice, 4 µL β-mercaptoethanol was added per 100 µL aliquot of cells and samples were incubated on ice for 10 min with gentle swirling every 2 min. Next, after incubation with β-mercaptoethanol the DNA was added (1 ng purified DNA or <2 µL ligation reaction per aliquot) and samples were incubated for 30 min on ice. After incubating on ice, the tubes were heat shocked in a 42 ^{o}C water bath for 30 sec. Heat shocked cells were placed on ice for 2 min and recovery in SOC at 37 ^{o}C and plating were done as previously mentioned.

2.1.1.2 Electro-competent cells

For cloning purposes requiring maximum transformation efficiency with reduced recombination, Endura™ electro-competent cells (Lucigen) were used. These cells were thawed on ice and a 25 µL aliquot was placed into a pre-chilled microcentrifuge tube. Next, 1 µL of ligation reaction was added and gently mixed. This mixture was then directly transferred to a chilled 1.0 mm gap cuvette (Bio-Rad) and flicked downwards to ensure that all of the liquid was inside the cuvette gap without air bubbles forming. Next the cuvette was electroporated using a Bio-Rad Gene Pulser II with the optimal setting (10 µF, 600 Ohms, 1800 Volts). Room temperature Lucigen recovery media (975 µL) was then added to the cuvette and all the liquid was transferred into a new 10 mL yellow cap polystyrene tube for recovery at 37^{o}C for 1 h (unless otherwise stated). Recovery and plating were done as previously mentioned.

2.1.2 DNA purification methods

2.1.2.1 Small-scale plasmid DNA extraction (mini-preparation)

To perform small scale plasmid preparations, individual transformed colonies were picked and inoculated into separate 10 mL yellow cap polystyrene tubes containing 5 – 10mL of LB broth containing the appropriate antibiotic selection (ampicillin at 100 µg/ml or kanamycin at 50 µg/ml). Bacteria were cultured at 37^{o}C overnight unless otherwise stated. After sufficient bacterial growth was observed (up to 24 h for low copy number plasmids), these cultures were centrifuged at 4000 ×*g* for 7 min and the supernatant was discarded. To extract and purify the plasmid DNA, the NucleoSpin® Plasmid EasyPure kit (Macherey-Nagel) was used as per manufacturer's instructions. Briefly, the bacterial pellet was resuspended in 250 µL of resuspension buffer (with RNAse added) and transferred to a fresh microcentrifuge tube. Following resuspension, 250 µL of lysis buffer was added and mixed by inversion. Cells were lysed for 5 min at room temperature prior to adding 300 µL of neutralization buffer and mixing by inversion. The lysate was pelleted at 11,000 ×*g* for 5 min prior to transferring supernatant to a spin column. This was then centrifuged at 11,000 ×*g* for 30 sec to bind DNA and flow through was discarded. Two wash steps were performed (11,000 ×*g*, 30 sec) with 700 µL of wash buffer. Next the column was transferred to a fresh collection tube and pre-heated 70^{o}C elution buffer was incubated on the membrane for 2 min. Low copy number plasmids were eluted in 30 µL volumes and high copy number plasmids were eluted in 50 µL volumes.

Purified DNA samples were analysed for DNA concentration and sample purity (A260/A280 ratio) using a NanoDrop 2000 Spectrophotometer (Thermo Fisher Scientific) and stored at -20°C until used in downstream applications.

2.1.2.2 Large-scale plasmid DNA extraction (maxi-preparation)

To perform large scale plasmid preparations, a single transformed colony was picked and inoculated into 500 – 1000 mL of LB broth with the appropriate antibiotic selection. Bacteria were cultured at 37^{o}C overnight unless otherwise stated. After sufficient bacterial growth was observed (up to 24 h for low copy plasmids), these cultures were centrifuged at 6000 ×*g* for 15 min and the supernatant was discarded. These bacterial pellets were then stored frozen at -20^{o}C or used immediately for plasmid preparation using the NucleoBond Xtra Maxi kit (Macherey-Nagel) as per manufacturer's instructions. Briefly, for each sample the bacterial pellet was resuspended in 12 mL resuspension buffer with RNAse added. Following resuspension, 12 mL of lysis buffer was added and sample was mixed by inversion and cells were lysed for 5 min prior to adding 12 mL of neutralization buffer and mixing by inversion. The lysate was then transferred to 50 mL tubes and pelleted at 4000 ×*g* for 5 min prior to transferring the supernatant to the column filter that was pre-equilibrated with 25 mL of equilibration buffer. DNA within the supernatant was bound to the column by gravity flow-through. Next, two wash steps were performed; first with 15 mL of equilibration buffer and then with 25 mL of wash buffer. Following washes, the DNA was eluted from the column in 15 mL pre-heated (70^{o}C) elution buffer into a 30 mL centrifuge tube. 10.5 mL of room temperature isopropanol was added and samples were vortexed prior to centrifugation at 20,000 ×*g* for 1 h at 4^{o}C to pellet the DNA precipitate. After precipitation most of the supernatant was removed, and the pellet was resuspended in the remaining 1 mL of supernatant and transferred to a microcentrifuge tube. The DNA pellet was re-formed by centrifuging at 10,000 ×*g* for 5 min. Next, two washes were performed using 1mL of 70 % ethanol and centrifugation at 10,000 ×*g* for 3 min each. After washing the ethanol was removed and DNA pellets were air dried and resuspended to a concentration of approximately 1 µg/µL in nuclease-free (NF) water (Invitrogen). Purified DNA samples were analysed for DNA concentration and sample purity (A260/A280 ratio) using a NanoDrop 2000 Spectrophotometer (Thermo Fisher Scientific) and stored at -20°C until used in downstream applications.

2.1.2.3 Gel extraction

A UV light box was used to visualize DNA that was separated on a 1% agarose gel containing 1× RedSafe Nucleic Acid Staining Solution (iNtRON Biotechnology). The desired band was cut out using a clean scalpel blade and transferred to a pre-weighed microcentrifuge tube. Gel extractions were performed with the Isolate II PCR / Gel clean-up kit (Bioline) as per the manufacturer's instructions. Briefly, 200 µL of binding buffer was added per 100 µg of agarose gel and this was heated at 60 ^{o}C for 10 min with regular mixing by vortex. For dissolving agarose gel to extract large DNA fragments (>10 kbp), samples were placed in binding buffer and heated to 60 ^{o}C and mixed by gentle inversion to prevent shearing of the DNA. This mixture was transferred directly to the column and centrifuged at 11,000 ×*g* for 30 sec to bind DNA to the column and the flow through was discarded. Next, the column was washed twice with 700 µL of wash buffer via centrifugation at 11,000 ×*g* for 30 sec and the flow through was discarded. Following washes, the column was dried by centrifuging at 11,000 ×*g* for 2 min and then transferred to a new collection tube. For elution, the elution buffer was pre-heated to 70 ^{o}C and 15 -30 µL was incubated on the membrane for 2 min prior to centrifugation at 11,000 ×*g* for 1 min. For maximal recovery, the eluate was re-incubated on the membrane for a further 2 min prior to centrifugation at 11,000 ×*g* for 1 min to collect the final extracted DNA. Purified DNA samples were analysed for DNA concentration and sample purity (A260/A280 ratio) using a NanoDrop 2000 Spectrophotometer (Thermo Fisher Scientific) and stored at -20°C until used in downstream applications.

2.1.2.4 Column purification reaction clean-up

The Bioline Isolate II PCR / Gel clean-up kit as per the manufacturer's instructions. Briefly, 200 µL of binding buffer was added per 100 µL of reaction volume. This mixture was transferred directly to the column and spun at 11,000 ×*g* for 30 sec to bind DNA to the column and the flow through discarded. Next, the column was washed twice with 700 µL of wash buffer each spun at 11,000 ×*g* for 30 sec and the flow through was discarded. Following washes, the column was dried by centrifuging at 11,000 ×*g* for 2 min and then transferred to a new collection tube. For elution, the elution buffer was pre-heated to 70 ^{o}C and 15 -30 µL was incubated on the membrane for 2 min prior to centrifugation at 11,000 ×*g* for 1 min. Purified DNA samples were analysed for DNA concentration and sample purity (A260/A280 ratio)

using a NanoDrop 2000 Spectrophotometer (Thermo Fisher Scientific) and stored at -20°C until used in downstream applications.

2.1.2.5 Ethanol DNA precipitation reaction clean-up

To precipitate the DNA first a 1/10th volume of 3 M sodium acetate (pH 5.5) was added to the reaction mixture (i.e. 2 µL per 20 µL reaction). Next, 2.5 volumes of 94% ethanol were added and mixed by pipetting. This mixture was incubated at -20 ^{o}C for 20 minutes prior to centrifugation at 15,000 ×*g* for 30 min at 4 ^{o}C. Supernatant was removed and the pellet rinsed carefully with 500 µL 75% ethanol. After completely removing the ethanol, the DNA was air dried and re-suspended to the required concentration with deionised water. Purified DNA samples were analysed for DNA concentration and sample purity (A260/A280 ratio) using a NanoDrop 2000 Spectrophotometer (Thermo Fisher Scientific) and stored at -20°C until used in downstream applications.

2.1.3 Recombinant DNA cloning methods

2.1.3.1 Restriction enzyme digestion

To perform restriction digests 250 ng – 5 µg of purified plasmid DNA was added per 20 µL reaction containing 0.5 – 2 units of restriction enzyme (NEB), 2 µL 10x buffer and the remaining volume of water. These were incubated at the recommended temperature for 3 – 16 h using a Bio-Rad thermal cycler depending on required completeness of cutting. All reactions were carried out using the BioRad S1000 Thermal Cycler or equivalent.

2.1.3.2 Primer design

Primers for recombinant DNA cloning were designed using NCBI GenBank sequences that were visualized using SnapGene software to derive complementary annealing sequences and overlap extensions. These sequences were then assessed using the OligoAnalyzer online tool (IDT) to predict internal secondary structures, self and hetero-dimerisation based on free energy changes (ΔG). The primer annealing temperature was determined using the NEB Tm calculator. Primers pairs had a maximum difference of annealing temperature of 2 ^{o}C. For custom qRT-PCR primers, these were designed using the NCBI primer database, specifying product size between 80-120 bp, annealing temperatures between 59-61 degrees with no

more than 2 degrees difference between primer pairs. All primers were made by Sigma Aldrich and diluted to 20 µM in NF water. Primers were stored at -20°C.

2.1.3.3 Q5 High-fidelity Polymerase Chain Reaction (PCR)

Unless otherwise stated all PCR reactions were performed using the Q5 High-Fidelity 2 X Master Mix (NEB). PCR was performed as per the manufacturer's instructions with the appropriate annealing temperature for individual primers determined by the NEB Q5 Tm calculator. Briefly, each reaction contained 12.5 µL of 2 X Master Mix, 1.25 µL of forward and reverse primer (10 µM), DNA template (1 ng purified DNA or 1 µL cDNA) and water to 25 µL total volume. Annealing time per cycle was 30 sec, extension time per cycle was 30 sec/kb and a minimum of 35 cycles were run. All reactions were carried out using the Bio-Rad S1000 Thermal Cycler or equivalent.

2.1.3.4 Agarose gel electrophoresis

All agarose gels were made with molecular grade 1% w/v Agarose (Bioline) in 1 x TAE buffer, with 5 µL RedSafe™ Nucleic Acid Staining Solution (iNtRON Biotechnology) added per 100 mL of molten Agarose solution. These gels were immersed in 1 x TAE running buffer in a Bio-Rad gel tank. DNA or RNA was pre-mixed with 6 x loading dye (NEB) and loaded into the wells, with a 1 kb ladder to determine product size (NEB). Gels were run at 100 – 120 V for approximately 30 min to 1 h to achieve appropriate separation. For separation of *in vitro* transcribed RNA fresh agarose solution was made with autoclaved dH_2O and the gel-tank was washed first with ethanol and then with autoclaved dH_2O. Also, separate loading dye was used that had only NF pipette tips used. Gel images were taken using the ChemiDoc XRS+ (Bio-Rad) and accompanying image analysis software using the Gel Red nucleic acid setting.

2.1.3.5 DNA ligation

T4 DNA ligase (NEB) was used for DNA ligations as per the manufacturer's instructions. Briefly, each reaction contained 2 µL T4 DNA Ligase Buffer (10X), 50 ng of vector DNA, insert DNA, 1 µL T4 DNA ligase and water to 20 µL, assembled at room temperature. Overnight incubations at 16 ^{o}C were routinely used. For ligations used for electrocompetent *E.coli* transformation, NEB ElectroLigase® was used as per the manufacturer's instructions. Briefly, each reaction contained 50 ng of vector DNA, insert DNA, 5 µl ElectroLigase Reaction Buffer, 1 µL

ElectroLigase and water to 10 µL assembled on ice. Reaction incubation was for 1 h at room temperature prior to heat inactivation at 65 ^{o}C for 15 min. Insert-to-vector ratios of 3:1 or 5:1 were routinely used for ligations. All reactions were carried out using the Bio-Rad S1000 Thermal Cycler or equivalent.

2.1.3.6 Gibson assembly

Gibson Assembly Master Mix (NEB) was used as per the manufacturer's instructions. Each reaction contained 10 µL Gibson Assembly Master Mix (2X), 50 ng vector DNA, insert DNA and water to 20 µL. Insert-to-vector ratios of 3:1 or 5:1 were used and each reaction was performed at 50 ^{o}C for 1 h. All reactions were carried out using the Bio-Rad S1000 Thermal Cycler or equivalent.

2.1.3.7 Plasmid DNA Sanger sequencing

Approximately 1 µg of the purified plasmid DNA was added to two separate microcentrifuge tubes. Alternatively, if the concentration of DNA was too low for 1 µg per reaction the maximum volume (12 µL) per tube was added. To each tube 1 µL of 10 µM primer was added either in the forward or reverse orientation. Volumes were adjusted to 13 µL with dH_2O water and dispatched to AGRF for sequencing. FASTA format files were aligned to the expected sequence using SnapGene.

2.1.4 Total RNA extraction

2.1.4.1 TRIsure (Bioline)

The supernatants from cell monolayers were removed and the cells were then washed once with 1x PBS. Next, cells were lysed in 500 µL of TRIsure per 12 well or scaled accordingly. To ensure complete lysis a pipette was used to rinse the lysate over the well several times prior to transferring to a labelled nuclease-free microcentrifuge tube. This lysate was either stored frozen (-80 ^{o}C) or used directly to extract RNA. To extract total RNA, lysates were defrosted and brought to room temperature for 5 min prior to adding 200 µL chloroform per 1 mL TRIsure. Samples were mixed by vigorous shaking for 15 sec and then left to rest for 5 min at room temperature. Once settled, tubes were centrifuged at 4 ^{o}C, 20,000 ×*g* for 15 min. Next the clear aqueous layer (approximately 400 µL per 1 mL TRIsure) was transferred to a fresh labelled NF microcentrifuge tube. Then 500 µL of ice-cold isopropanol was added per tube,

these were mixed by inversion and incubated to precipitate RNA, either for 10 min at room temperature or for 30 min on ice. To pellet the precipitate, tubes were centrifuged at 4 ^{o}C, 20,000 ×*g* for 15 - 30 min. Once pelleted, the supernatant was carefully removed and replaced with 75 % ethanol, then tubes were re-centrifuged briefly for 3 min at 4 ^{o}C, 10,000 ×*g* and this process was repeated. After washing, the ethanol was removed and the pellet was air dried and resuspended in NF water to the appropriate concentration. Purified RNA samples were analysed for RNA concentration and sample purity (A260/A280 ratio) using a NanoDrop 2000 Spectrophotometer (Thermo Fisher Scientific) and stored at -80°C until used in downstream applications.

2.1.4.2 NucleoZOL (Macherey Nagel)

The supernatants were removed from cell monolayers, then cells were washed once with 1x PBS and lysed in 250 µL of NucleoZOL per 24 well or scaled accordingly. To ensure complete lysis a pipette was used to rinse the lysate over the well several times prior to transferring to a labelled nuclease-free microcentrifuge tube. This was either stored frozen (-80 ^{o}C) or used directly to extract total RNA. Where required, NucleoZOL lysates were defrosted and brought to room temperature for 5 min prior to adding 100 µL of chloroform per 250 µL NucleoZOL. This was mixed by vigorous shaking for 15 sec and then left to rest for 5 min at room temperature. Once settled, samples were centrifuged at room temperature, at 16,000 ×*g* for 15 min. After pelleting cell debris, the clear supernatant (approx. 250 µL) was transferred to a fresh labelled NF microcentrifuge tube. Next, an equal volume of room temperature isopropanol was added per tube and these were mixed by inversion. This mixture was then incubated to precipitate RNA for 10 min at room temperature. To pellet the precipitate, these samples were centrifuged at room temperature at 16,000 ×*g* for 10 min. Once pelleted, the supernatant was carefully removed and replaced with 75 % ethanol, then tubes were re-centrifuged briefly for 3 min at RT, 10,000 ×*g* and this process was repeated. After washing, the ethanol was removed and the pellet was air dried and resuspended in NF water to the appropriate concentration, measured using a using a NanoDrop 2000 Spectrophotometer (Thermo Fisher Scientific), as detailed above. Samples were stored at -80°C until used in downstream applications.

2.1.4.3 RNeasy Mini Kit (Qiagen) with or without DNase treatment

For cell monolayers (RNA preparation for NextSeq 550 Illumina sequencing)

First, fresh RLT lysis buffer was prepared by adding β-mercaptoethanol (10µL per 1mL). Then, the supernatants were removed from cell monolayers, cells were then washed once with 1x PBS and 350 µL of lysis buffer was added per well of a 6 well try. To ensure complete lysis, a pipette was used to rinse the lysate over the well several times prior to transferring to a labelled nuclease-free microcentrifuge tube. This was either stored frozen (-80 ^{o}C) or used directly. The lysate was then homogenized by passing through a 20-gauge (0.9 mm) needle attached to a sterile plastic syringe at least 5–10 times. Next, 1 volume of 70% ethanol was added to the homogenized lysate and mixed well by pipetting. From here, 700 µL of lysate mixture was transferred to a pre-labelled RNeasy Mini column and centrifuged for 15 sec at 10,000 ×*g* , afterwards discarding the flow-through. Subsequent wash steps were performed as per the RNeasy Mini Kit instructions. Briefly, 700 µl Buffer RW1 was added to the RNeasy spin column and centrifuged for 30 sec at 10,000 ×*g* and the flow through discarded into a waste container for appropriate disposal. At this stage if DNase treatment was required, 80 µl of pre-diluted RNase-Free DNase solution (Qiagen) was applied to the column and incubated at RT for 15 min. Again, 700 µl Buffer RW1 was added to the RNeasy spin column and centrifuged for 30 sec at 10,000 ×*g* and the flow through discarded into a waste container for appropriate disposal. Next, the column was washed twice with 500 µl RPE buffer solution by centrifuging for 30 sec at 10,000 ×*g* and the flow through was discarded. To elute the RNA, 40 µL of NF water was applied to the column, incubated for 2 min and centrifuged for 1 min at 10,000 ×*g*. This eluate was then re-applied to the column and the process repeated.

For extraction of RNA from solid tissues

Frozen tissues stored in nuclease-free microcentrifuge tubes (at -80^{o}C) were transferred to fresh tubes to dry. To each tube, 500 µL of TRIsure was added and frozen tissues were then immediately homogenized using an RNase-free tissue grinder (Kimble-Chase). Once sufficiently homogenized these lysates were transferred to wet ice. An additional 500 µL of TRIsure was added and this was briefly vortexed, centrifuged and left to rest at room temperature for 5 min. Next, 200 µL chloroform was added per 1 mL of TRIsure. This was mixed by vigorous shaking for 15 sec and then left to rest for 5 min at room temperature. Once settled, this was centrifuged at 4 ^{o}C, 20,000 ×*g* for 15 min. Next, the upper clear aqueous layer (approximately 400 µL per 1 mL TRIsure) was transferred to a fresh labelled NF

microcentrifuge tube. To this, 500 µL of 100% ethanol was added per 1 mL TRIsure. Each sample was then mixed by pipetting and immediately transferred to a pre-labelled RNeasy Mini column. The RNA was bound to the column by centrifuging for 15 s at 10,000 ×*g*, afterwards discarding the flow-through. This process was repeated with any remaining aqueous phase liquid. Washing and elution was done as described above and RNA quantification and storage was similarly performed as described above.

2.1.5 Nucleic acid quantification

DNA or RNA samples were routinely quantified using the NanoDrop spectrophotometer (Thermo Scientific) based on the 260/280 absorbance ratio. For low concentrations of nucleic acids requiring high-sensitivity (HS) detection ether the Qubit dsDNA or RNA HS Assay Kits (Thermo Scientific) were used. Briefly, 1 µL of 200 x concentrate detection reagent was diluted in 200 µL of buffer per sample at room temperature (including extra for standards). Next, volumes between 2 – 10 µL of sample were diluted in the 1 X detection reagent to a final volume of 200 µL aliquoted in a Qubit® assay tube. Following dilution of standards and samples, these were loaded onto the Qubit® Fluorometer for determination of concentration based on fluorescence readings.

2.1.6 cDNA synthesis

2.1.6.1 M-MLV reverse transcriptase cDNA preparation (Promega)

For standard applications, cDNA synthesis was performed using M-MLV reverse transcriptase (Promega). Reactions contained either 500 ng or 1000 ng of RNA (dependent on the lowest RNA yield in a sample cohort for consistency). 500 ng of random hexamer (IDT) was added to the RNA and then this mixture was diluted to 14 µL with NF water and incubated at 70 ^{o}C for 5 min. Next, a master mix was made containing the 5 µL of 5x reaction buffer, 1.25 µL of 10 nM dNTP mix, 0.5 µL of RNasin inhibitor, 1 µL of RT enzyme and 3.25 µL of NF water. 11 µL of master mix was added to each tube, samples were mixed and this was incubated at 42 ^{o}C for 1 h. These cDNA mixtures were then stored at -20 ^{o}C or diluted 1 in 4 with NF water for use. All reactions were carried out using the Bio-Rad S1000 Thermal Cycler or equivalent.

2.1.6.2 SuperScript™ III first-strand synthesis (Invitrogen)

For high quality cDNA preparations (viral cloning or sequencing purposes) the SuperScript™ III First-Strand Synthesis kit was used. First, a total of 1 – 5 µg of total RNA was incubated with 1 µL primer*, 1 µL 10mM dNTP and NF water to 10 µL at 65 ^{o}C for 5 min.

*For full-length DENV first strand synthesis 1 µL of 20 µM specific reverse primer binding to the end of the 3' UTR was used.

*For all other first strand synthesis reactions 1 µL of 50 ng/µL of random hexamer was used.

Next, a master mix containing 2 µL of 10X RT buffer, 4 µL of 25mM $MgCl_2$, 2 µL of 0.1 M DTT, 1 µL of 40 U/µL RNaseOUT and 1 µL of SuperScript III RT (200 U/µL) was added per tube. For specific primed reactions, the reaction was carried out at 50 ^{o}C for 50 min. For random primed reactions, first the reaction was placed at 25 ^{o}C for 10 min then the temperature was increased to 50 ^{o}C and samples were incubated for 50 min. Reactions were stopped by heating at 85 ^{o}C for 5 min and chilled on ice prior to adding 1 µL RNase H and returning the tubes to 37^{o}C for 20 min. All reactions were carried out using the Bio-Rad S1000 Thermal Cycler or equivalent.

2.1.7 Real-Time Quantitative PCR (qRT-PCR)

2.1.7.1 FastStart Universal SYBR Green Master (Rox) (Roche)

For cDNA samples the FastStart Universal SYBR Green Master (Rox) qRT-PCR system was used. First, a master mix was made for each primer set containing 5µL of SYBR Green Master mix, 0.15 µL of each gene specific forward and reverse primer (at 20 µM) and 2.2 µL of NF H_20 per reaction. 7.5 µL of master mix of this was added per tube in 8 tube-strips, 96-well plates or 384-well plates (Applied Biosystems). Next, 2.5 µL of diluted cDNA was added per reaction. Cycling conditions were as follows:

<u>pre-cycling:</u> 50 ^{o}C for 2 min then 95 ^{o}C for 10 min,

<u>cycling (40 cycles)</u>: 95 ^{o}C for 15 sec then 60 ^{o}C for 1 min.

At the end of 40 cycles a melt curve was run for each product with images taken every 0.5 sec. Reactions were carried out using the QuantStudio™ 7 Flex Real-Time PCR amplifier (Applied Biosystems).

2.1.7.2 Luna® Universal One-Step qRT-PCR (NEB)

For RNA samples the Luna® Universal One-Step qRT-PCR kit was used. First a master mix was made for each primer set containing 5 µL of Luna Universal One-Step Reaction Mix (2X), 0.2 µL of each gene specific forward and reverse primer (at 20 µM), 0.5 µL of Luna RT Enzyme Mix (20X) and 1.6 µL of NF H_20 per reaction. 7.5 µL of master mix of this was added per tube in 8 tube-strips, 96- or 384-well plates (Applied Biosystems). Next, 2.5 µL of diluted cDNA was added per reaction. Cycling conditions were as follows:

pre-cycling: 55 ^oC for 10 min then 95 ^oC for 1 min,

cycling (40 cycles): 95 ^oC for 10 sec then 60 ^oC for 1 min.

At the end of 40 cycles a melt curve was run for each product with images taken every 0.5 sec. Reactions were carried out using the QuantStudio™ 7 Flex Real-Time PCR amplifier, as above.

2.1.8 SDS-PAGE western blot assay

To perform Western blot assays, cell monolayers were washed in 1 X PBS prior to adding 200 µL of lysis buffer (RIPA) containing 2 µL of protease inhibitor cocktail (Sigma-Aldrich) per well of a 6-well try, or scaled accordingly. Complete lysis was done on ice for 20 min. Next the wells were scraped with a pipette and lysates were transferred to individual labelled microcentrifuge tubes. Lysates were homogenized by pipetting using a 1000 µL pipette tip and then by passing through a 25 G needle 10 times. For each sample, cell debris was pelleted by centrifugation at 16,000 ×*g* at 4 ^oC for 10 min and the supernatant was transferred to a fresh labelled microcentrifuge tube. Next, 1 part of 4 x SDS-PAGE reducing loading buffer was added to 3 parts of cleared protein lysate in a fresh microcentrifuge tube and this mixture was boiled at 95 ^oC for 5 m using a heat block. These samples were then cooled on ice prior to loading into a Mini-PROTEAN® TGX™ Precast Gel (Bio-Rad) suspended in 1 X SDS-PAGE running buffer. To separate proteins the gel was run for 90 min at 100 V. Next, protein was transferred to a nitrocellulose membrane using the Trans-Blot Turbo Transfer system and transfer buffer (Bio-Rad) using the mixed molecular weight setting for one gel (7 min transfer). After transfer, the membrane was blocked for 1 h in 5% w/v skim milk diluted in TBS-T (see appendix). Following blocking, primary antibody to the protein of interest was diluted to an appropriate concentration (see Appendix III) in 1% w/v skim milk diluted in TBS-T. This was incubated overnight with agitation at 4 ^oC. The following day membranes were washed in

TBS-T for 10 minutes 3 times prior to incubating for 1 h at room temperature in HRP-conjugated secondary antibody that was reactive against the primary antibody species diluted in 1% w/v skim milk. Next, the membranes were washed 5 times in TBS-T for 10 minutes per wash. After washing the membranes were developed using Clarity Western ECL Substrate (Bio-Rad) mix for 5 min at room temperature. Images were taken using the ChemiDoc XRS+ (Bio-Rad) and accompanying image analysis software using the Chemi or Colorimetric settings for blots. To strip and re-probe membranes, developed nitrocellulose membranes were washed 3 x for 5 min per wash in TBS-T then were incubated in Western blot stripping buffer at 60^{o}C for 30 min with gentle shaking. Stripped membranes were again washed 3 x for 10 min in TBS-T prior to returning to 5% w/v skim milk to block, as above.

2.1.9 Dual luciferase assay (Promega)

For dual luciferase assays, HeLa cells were seeded at 8 X 10^4 cells/well in 12-well trays or scaled accordingly and cultured overnight. The following day, cells were co-transfected with 500 ng of the ISRE firefly luciferase reporter construct (ISRE-luc), 500ng of the according plasmid of interest, and 10 ng of the constitutive *Renilla* luciferase reporter plasmid (pRL-TK) per 12 well using Lipofectamine 2000 (Life Technologies). Each transfection condition was carried out in triplicate. 24 hours following stimulation with IFN (or control media), cells were lysed in 1 x Passive Lysis Buffer (Promega; diluted from 5x in dH_2O) and stored at -20°C in plates. To detect luciferase activity in samples, 20 µL of each sample was aliquoted into a white-well Optiplate 96 (Perkin Elmer). To these wells, 50 µL of each 1 X luciferase assay reagent II (LARII) and 1 X Stop and Glow reagent (Promega) were added sequentially using the GloMax luminometer and luciferase activity was recorded, as per manufacturer's instructions. ISRE promoter activity was determined by normalising *Firefly* luciferase values to *Renilla* luciferase values and expressed as relative light units (RLU) (*Firefly*/*Renilla* = RLU) or these values were converted to a percentage of control by normalising to control sample RLU (RLU experimental / RLU control average x 100). Data were analyzed using GraphPad Prism 8 software.

2.1.10 Immunofluorescence staining

To perform immunofluorescent staining, cultured cells were fixed with a 1:1 ratio of ice cold acetone:methanol solution for 10 minutes on ice. After washing twice with 1X PBS, samples

were blocked in 5% w/v BSA diluted in 1X PBS for 30 min at room temperature. After blocking, the BSA solution was removed and replaced with primary antibody (for specific usage see Appendix III) diluted in 1% w/v BSA in PBS for 1 h at room temperature. After washing twice with 1X PBS, cells were incubated with Alexa Fluor-conjugated secondary antibody diluted 1:200 in 1% w/v BSA for 1 h at 4 °C in the dark. Samples were then washed three times with 1X PBS and incubated with DAPI (Sigma-Aldrich, diluted in PBS to 1 µg/ml) for 5 min at room temperature in the dark. Samples were then washed three times with 1X PBS. Images were acquired using a Nikon TiE inverted fluorescent microscope. Contrast was applied using the 'Autoscale' function of the NIS Elements program (Nikon).

2.2 Tissue culture methods

2.2.1 Tissue culture medium, cell culture reagents and recombinant interferons

Cultures of HeLa, Huh-7, Huh-7.5, Ishikawa, 293T and Vero cells were maintained in Dulbecco's Modified Eagle Medium (DMEM) containing 4.5 g/L D-Glucose, 25 mM HEPES and 2 mM L-glutamine (Gibco, Invitrogen) supplemented with 10% (v/v) foetal calf serum (FCS; Corning Life Sciences), Penicillin (Invitrogen; 100 U/ml) and Streptomycin (Invitrogen; 100 µg/ml). Culture of HTR8 cells was maintained in RPMI-1640 Medium (Gibco BRL, Invitrogen) supplemented antibiotics and with 10% (w/v) foetal calf serum (FCS; Corning Life Sciences), Cultures of Ect1 and VK2 cells were maintained Keratinocyte-Serum Free medium (Gibco, Invitrogen) with 0.1 ng/ml human recombinant EGF (Gibco, Invitrogen), 0.05 mg/ml bovine pituitary extract (Gibco, Invitrogen), and additional calcium chloride to 44.1 mg/L (final concentration 0.4 mM).

Lyophilized human recombinant IFNα-2A was purchased from Peprotech (lot #090CY28) and was diluted in sterile NF water to a concentration of 20,000 U/µL. Frozen 2 µL aliquots were stored at -20^{o}C until use. Progesterone was purchased from Sigma Aldrich as a powder and was diluted in ethanol to a concentration of 1 mg/mL stock solution. This was filtered using a sterile 0.2 µm cellulose acetate Minisart syringe filter (Sartorius) and stored at -80 °C until use. Cell culture treatments of progesterone were prepared by performing serial dilutions of the stock solution (or ethanol vehicle control) in appropriate cell culture media to a final concentration of 10 µM prior to use. Human recombinant IFNε was made by our collaborators at the Hudson Institute of Medical Research refolded from bacteria as described previously [110]. Frozen 10 µL aliquots were stored at -80^{o}C until use. Recombinant human IL-28B (IFNλ-

III) protein was purchased from R & D systems (cat# 5259-IL-025) diluted to 100 ng/µL. Frozen 10 µL aliquots were stored at -80^{o}C until use. Human recombinant IFNβ (Rebif) was provided by our collaborators purchased from Merck as a stock at 24, 000 U/µL. Liquid solution was stored at 4^{o}C as per the manufacturers instructions. Murine recombinant IFNε was made by our collaborators at the Hudson Institute of Medical Research refolded from bacteria as described previously [105]. Frozen 30 µL aliquots were stored at -80^{o}C until use.

2.2.2 Cell maintenance

Cell lines were maintained in vent capped tissue culture flasks (25 cm^2, 75 cm^2, or 175 cm^2) (Corning). When cells reached 80-90% confluence they were sub-cultured into new flasks. First the culture medium was removed and the cell monolayer was washed once with 1X PBS. Next, Trypsin-EDTA was used to cover the cell monolayer in a volume of 1 mL per 75 cm^2 flask or scaled accordingly (see Appendix II). Cells were incubated for 5-15 minutes (dependent on cell line) at 37^{o}C until they started to detach from the flask. To completely detach the cells, flasks were agitated by tapping on the sides. Next, trypsinization was halted by the addition of fresh culture media containing FCS and cells were resuspended by pipetting. For cells cultured in FCS free media (Ect1 and VK2 cells) the cell suspension was centrifuged at 150 ×*g*for 5 min at RT, the supernatant was removed, and the cells were resuspended in appropriate culture media. A portion of the cell suspension (1/3rd upto 1/10th) was transferred to a new flask and topped-up with fresh culture media to cover the bottom of the flask (12 mL total volume for 75 cm^2 flasks or scaled accordingly). After transferring the cells to a new flask they were returned to a 37 °C incubator with 5% CO_2. Cells were passaged every 2-3 days or as required.

2.2.3 Enumeration of cells - trypan blue exclusion

To determine the concentration of cells in suspension an aliquot of inactivated trypsinised cells (10 µL) was transferred to a microcentrifuge tube. Next, an equal volume of Trypan Blue Stain solution was added to the cells and mixed by pipetting. 10µL of this solution was loaded into one chamber of a Neubauer Hemocytometer and the number of live cells (not dark blue) in one triple lined grid section were counted using a clicker counter. To calculate the concentration of cells per mL the following calculation was used: cell count per 5 x 5 grid x ½ x number of 5 x 5 grids counted x 10^4 = cell/mL.

2.2.4 Cryopreservation of cells

For cryopreservation, cells that were at maximal growth rate (~80% confluent) were harvested by trypsinization, as described in 2.2.2 'Cell Maintenance'. Cell suspensions were centrifuged at ~200 ×*g* for 5 min to pellet cells. The supernatant was removed and cells were resuspended in an appropriate volume of complete cell culture medium. Next, an equal volume of filter-sterilised 2 x freeze mixture containing 50% DMEM or RPMI media (as appropriate), 30 % FCS and 20 % DMSO was added to the cells. 1 mL of resuspended cells were aliquoted into each sterile labelled cryopreservation tube (CryoTube vials, NUNC). These cryotubes were transferred immediately to a freezing chamber (Nalgene) containing fresh isopropanol and placed in a -80^{o}C freezer overnight. After overnight freezing, cells were transferred to liquid nitrogen for long-term storage.

2.2.5 Resuscitating cells from cryopreservation

Cryopreserved vials of cells were defrosted in a 37^{o}C water bath. Once defrosted these cells were immediately transferred to a new vent-capped flask (75cm^2) pre-filled with warmed culture media. Cells were returned to culture in a humidified 37^{o}C/5% CO_2 incubator to enable adherence to the flask. Following adherence, the media was removed and replaced with fresh culture media and cells were returned to culture.

2.2.6 Transient transfection of plasmid DNA or poly I:C (Lipofectamine 2000, Invitrogen)

To transfect cells with either plasmid DNA or polyI:C reagent (Sigma-Aldrich) Lipofectamine 2000 (Invitrogen) transfection reagent was used, as per manufacturer's instructions. First, cells were seeded one day prior to reach 90% confluence on the day of transfection. Then, 1 X 50 µL aliquot of Opti-MEM reduced serum media (Gibco, Invitrogen) was added to a microcentrifuge tube for each well of a 12-well tray to be transfected. To this aliquot 2 µL of Lipofectamine 2000 was added, the tube (tube A) was mixed by flicking and briefly centrifuged and incubated at room temperature for 5 min. In a separate tube (tube B) another 50 µL aliquot of Opti-MEM was added for each well of a 12-well tray to be transfected. Up to 1 µg of total plasmid DNA or polyI:C was added to tube B and mixed. Following the 5 min incubation the contents of tube A was combined with that of tube B, and again this was mixed by flicking the tube and briefly centrifuging to collect the liquid. This mixture was incubated

at room temperature for 15 min and then added dropwise to the cells in 12-well culture plates (100 µL per well of a 12-well tray). For smaller sized wells, the protocol was scaled down accordingly.

2.2.7 Transient siRNA transfection (RNAiMAX, Invitrogen)

For siRNA transfection RNAiMAX transfection reagent (Invitrogen) was used. One day prior to transfection, cells were seeded to be 90% confluent on the day of transfection. The following day the transfection was performed as follows. First, 1 X 100 µL aliquot of Opti-MEM reduced serum media (Gibco, Invitrogen) was added to a microcentrifuge tube for each well of a 12-well tray to be transfected. To this aliquot, 3 µL of RNAiMAX (Invitrogen) was added, the tube (tube A) was mixed by flicking and briefly centrifuged and incubated at room temperature for 5 min. In a separate tube (tube B) another 100 µL aliquot of Opti-MEM was added for each well to be transfected. To this tube, 1 µL of gene specific siRNA or non-targeting control siRNA (Dharmacon; 20 µM in siRNA resuspension buffer) was added and mixed to combine. Following the 5 min incubation, the contents of tube A were combined with that of tube B, and again this was mixed by flicking the tube and briefly centrifuging to collect the liquid. This mixture was incubated at room temperature for 5 min prior to adding dropwise to the cells in 12 well culture plates (200 µL per 12 well). For smaller wells, the protocol was scaled down accordingly.

2.2.8 Concentration of protein in cell-culture supernatant

To assess the antiviral properties of Ect1 cell culture supernatant it was first necessary to concentrate proteins in the size range of interest. Secreted IFNε has a molecular weight of approximately 20 kDa. Ect1 cells were cultured in a 75 cm^2 flask until 90% confluent on the day of the experiment. The overlaying media (12 mL) or an equivalent volume of fresh Keratinocyte Serum Free Media (KSFM) were filtered using a sterile 0.2 µm cellulose acetate Minisart syringe filter (Sartorius) to remove cell debris. The filtered culture media or KFSM were then placed in the top of a 10,000 molecular weight cut-off Vivaspin TURBO 15 concentrator (Sartorius) that had been pre-rinsed twice with 15 mL sterile dH_2O water at 4000 ×*g*. The concentrator containing either filtered culture media or KFSM were centrifuged at 4000 ×*g* for 10 min at room temperature. After centrifugation ~1.5 mL remained in the top of the concentrator, and the flow through was discarded. 500 µL per well of concentrated

filtered culture media or KFSM were applied in triplicate to Huh-7 cells seeded one day prior at 5 x 10^4 cells/well in 24 well plates.

2.2.9 Amplification of viral seed stocks

Following generation of DENV or ZIKV infectious clone viral seed stocks from *in vitro* transcribed RNA or plasmid DNA transfections, these virus stocks were amplified to generate larger volume stocks. Vero cells were seeded at 6 x 10^6 cells in a 175cm^2 flask. The following day the cells were inoculated at a MOI of 0.1 in a 10 mL volume and returned to culture. After 2 h the inoculum was removed and replaced with 15 mL of fresh culture media. Flasks were returned to culture at 37°C for 4-5 days. After 4-5 days the supernatant was collected, centrifuged at 4000 ×*g* for 5 min to clear cellular debris and aliquoted in 1 mL aliquots for storage at -80 ^oC. The viral stock was titrated for infectious virus by focus forming assay (DENV and ZIKV) and by plaque assay (ZIKV only).

2.2.10 Plaque assay

To assess the level of ZIKV in samples a plaque assay was used. First, Vero cells were seeded at a density of 2 X 10^5 cells/well in a 12 well plate or scaled accordingly. After overnight culture, neat viral stocks or cell culture supernatants were defrosted and serially diluted (1 in 10 dilutions) using fresh culture media to a total volume of 1mL. Next, the overlaying media was removed from the Vero cell monolayers and replaced with the 500µL of the diluted sample containing virus. Plates were returned to the 37°C incubator for 1 h to allow viral adherence and entry. Following 1 h inoculation, the overlay was replaced with fresh DMEM containing a final concentration of 2% FCS v/v and 1.5 % w/v carboxymethylcellulose sodium salt high viscosity (Sigma Aldrich). Plates were returned to culture at 37°C for 5 days. After 5 days, plates were fixed with 10 % v/v buffered formalin completely filling the wells. These were mixed by gentle swirling and then left in a fume hood at room temperature for 3 h. After fixation, plates were extensively washed with gentle flowing RO water until all residue had been removed (approximately 4 – 5 washes). Next, cell monolayers were stained using ~0.1% (w/v) crystal violet (CV) in a 10% (v/v) ethanol solution diluted in water for 20 minutes. Again, plates were extensively washed with gentle flowing RO water until all CV solution was removed. Plaques were visualized using a light box and enumerated by manual counting.

2.2.11 Focus forming assay

To titer the level of infectious DENV or ZIKV in supernatant samples, a focus forming assay was used. Huh7.5 cells were seeded at 2 X 10^4 cell/well in a total volume of 150 µL/well in 96 well plates. The following day culture media was removed and the cells were inoculated with 40 µL of 10-fold serially diluted viral supernatants for 3 h at 37 °C with manual agitation of the plate every 20 minutes. After 3h, the inoculum was removed, monolayers were washed with PBS, and replaced with 100 µL fresh culture medium and then returned to culture at 37 °C. After culturing, cells were fixed with a 1:1 ratio of ice cold acetone:methanol for 10 min on ice. For ZIKV, cells were fixed at 48 hpi, whereas for DENV cells were fixed at 72 hpi. Following fixation, ZIKV/DENV infection was detected via indirect immunofluorescence staining using the 4G2-pan-*Flavivirus* anti-E primary antibody. Foci were enumerated by observation under a fluorescent microscope and were defined as more than 3 infected cells in a distinct cluster. Virus infectivity in each sample was calculated based on biological triplicates (with technical duplicates for each diluted virus sample) and then expressed as Focus Forming Units (FFU) per mL.

2.3 Specific protocols for mutagenesis and mutant screening (Chapters 3 and 4)

2.3.1 Generation of viral seed stocks from DNA transfection of ZIKV infectious clones

To generate a viral seed stock from the pZIKV-ICD infectious clone Vero cells were seeded in 6 well plates at 2 x 10^5 cells/well. The following day the cells were transfected with the pZIKV-ICD plasmid using lipofectamine 2000 as described in section 2.2.6 with the following alterations: 200 µL Opti-MEM, 8 µL Lipofectamine 2000 reagent, and 2 µg pZIKV-ICD per well of a 6-well tray. At 96 h post-transfection the supernatants were collected, centrifuged at 4000 ×*g* for 5 min to clear cellular debris and aliquoted for storage at -80 ^{o}C. The seed stock was titrated for infectious virus by focus forming assay. To generate larger volume stocks, the 'amplifying viral stock protocol' (section 2.2.9) was used.

2.3.2 Half maximal inhibitory concentration (IC_{50}) assay for IFNα treatment

To perform an IC_{50} assay either Huh-7 or Huh-7.5 cells were seeded at 1 X 10^5 cells/well in a 12 well plate (or scaled accordingly). The following day, cells were treated in triplicate with increasing concentrations of IFNα (0, 0.01, 0.1, 1, 10, 25, 50, 100, 250, 500, 1000 U/mL) diluted in fresh culture media. After 6 h the IFNα treatment was removed and cells were inoculated

with either ZIKV or DENV at MOI = 0.2. The following morning, the inoculum was removed, and the media was replaced with the appropriate concentrations of IFNα diluted in fresh media. Cells were returned to culture for 48 h in a 37 ^{o}C incubator. 48 h post-infection, supernatants containing infectious virus were collected and stored frozen at -80 ^{o}C. These supernatants containing infectious virus were then titrated using a Focus Forming Assay in technical duplicates and used to calculate FFU/mL. Raw FFU/mL titers were normalized to the average raw titers at the minimum (0 U/mL) and maximum (1000 U/mL) inhibition concentrations of IFNα using the GraphPad Prism v8 "data normalization" function. Next the normalized data was used to fit a dose-response curve using the [inhibitor] vs normalized response non-linear regression analysis model. The IC_{50} was interpolated from the curve and is defined as the concentration of IFNα where the antiviral response was reduced by half. All normalization and statistical analysis were performed using GraphPad Prism v8 software.

2.3.3 Cloning the ZIKV MuA transposon insertion mutant library (Mutation Generation System Kit, Thermo Scientific)

To generate the ZIKV transposon insertion mutant library the Mutation Generation System Kit (Thermo Scientific) was used as per the manufacturer's instructions and is described here in brief [348]. Each MuA transposase reaction contained 0.6 µg of target DNA (pZIKV-ICD) to control the transposition rate to one insertion event per clone. To this, 4 µL of 5X Reaction Buffer, 1 µL of Entranceposon (M1-KanR), 1 µL MuA Transposase enzyme mix and water to a total volume of 20 µL were added to a PCR tube. This was briefly mixed and incubated at 30 ^{o}C for 1 h and afterwards the reaction was stopped at 75 ^{o}C for 10 min, prior to chilling on ice. Next, the reaction was purified (see section 2.1.2.5 Ethanol DNA precipitation) and resuspended in 15 µL NF water. The purified DNA was aliquoted into separate 5 µL volumes before storing frozen at -20 ^{o}C prior to use. Next, the purified DNA was transformed by electroporation into Endura (Lucigen) electro-competent cells (see section 2.1.1.2) using 1 µL of reaction mixture per 25 µL of cells. 5 transformations were performed concurrently to prevent freeze-thawing of the reaction mixture. Transformed cells were serially diluted and plated onto 15 cm^2 LB Agar plates (3-5 plates per transformation) containing a final concentration of 20 µg/mL Kanamycin (Kan) and 100 µg/mL Ampicillin (Amp), or plates containing only Amp for determination of reaction efficiency. Transformation plates were placed in a 30 ^{o}C incubator for a minimum of 24 h to allow for bacterial growth. The following

day the number of bacterial colonies formed on the Kan/Amp compared to the Amp only plates were enumerated by manual counting of the dilution plates. Then bacterial colonies on the Kan/Amp plates were pooled in LB broth by scraping plates with a sterile cell spreader and the liquid was transferred to 250 mL centrifuge bottles, centrifuged at 6000 ×*g* for 15 min, the supernatant removed and the pellet stored frozen at -20 ^{o}C prior to use. This process was repeated for the remaining 2 x 5 µL aliquots of transposon reaction mixture. Following transformation and harvesting of bacteria harboring the transposon, the three frozen bacterial pellets were pooled and used to isolate plasmid DNA by maxi-preparation (see section 2.1.2.2). Next the purified target DNA containing the transposon insertion was subjected to restriction digest by *Not*I-HF enzyme to remove the 1kb transposon body (see section 2.1.3.1). Two separate restriction digests were performed each containing 5 µg of purified DNA and 2 µL of *Not*I-HF per digest. Both digests were run on a 1% agarose gel and the high-molecular weight band containing the mutagenized target DNA was gel-extracted (see section 2.1.2.3) in 15 µL of elution buffer. Next, 375 ng of digested purified DNA was ligated using Electro-Ligase (see section 2.1.3.5) in a total reaction volume of 10 µL at 25 ^{o}C for 1 h, then inactivated at 65 ^{o}C for 15 min prior to chilling on ice. Two identical ligation reactions were performed and pooled. 1.5 µL of reaction mixture was transformed directly into each 25 µL aliquot of Endura electro-competent cells in 15 separate transformation reactions. Transformed cells were serially diluted and plated onto 15 cm^{2} LB Agar plates (3-5 plates per transformation) containing a final concentration of 100 µg/mL Ampicillin. Transformation plates were placed in a 30 ^{o}C incubator for a minimum of 24 h to allow for bacterial growth. The following day the number of bacterial colonies formed on the Amp plates were enumerated by manual counting of the dilution plates. Then bacterial colonies on the Amp plates were pooled in LB broth by scraping with a sterile cell spreader and the liquid was transferred to 250 mL centrifuge bottles, centrifuged at 6000 ×*g* for 15 min, the supernatant removed and the pellet stored frozen at -20 ^{o}C prior to use. Following transformation and harvesting of bacteria harbouring the transposon the frozen bacterial pellets were pooled and used to isolate plasmid DNA by maxi-preparation.

2.3.4 DENV mutant screening

2.3.4.1 Recovery of library from frozen stock

To recover the initial mutant library from frozen stock (Passage 0) Huh-7.5 cells were seeded into six 75cm^2 flask at 2x10^6 cells per flask in a 12 mL volume. The following day three flasks (n=3) were treated with IFNα at 1 U/mL diluted in fresh media and three flasks were left untreated for 6h. After 6 h of pre-treatment, all flasks were inoculated with the defrosted DENV mutant virus stock diluted 1:1 with fresh media in a total volume of 12 mL per flask. In parallel, an aliquot of the frozen virus stock was used in a Focus Forming Assay (section 2.2.11) to retrospectively determine the MOI for this passage. After overnight incubation of the flasks, the inoculum was removed and replaced with IFNα at 1 U/mL diluted in fresh media. Once the titer had been determined by Focus Forming Assay (72 h post-infection), the supernatant containing infectious virus was collected and cleared of cellular debris by centrifugation (4000 ×*g*, 5 min). Supernatant from each triplicate was divided in half and separately aliquoted into two 14 mL tubes (Corning). Additionally, smaller 1 mL volumes of each replicate were aliquoted into microcentrifuge tubes to titer the virus by Focus Forming Assay prior to use in the next passage. After removing infectious supernatant, the cell monolayer was washed with 1 X PBS and total RNA was harvested in 4 mL TRIsure reagent (Bioline) per 75cm^2 flask. Both supernatants and RNA samples were stored frozen at -80 ^{o}C until further use.

2.3.4.2 Passaging of the recovered mutant library

To perform subsequent passages (Passage 1 and Passage 2), Huh-7.5 cells were again seeded into six 75cm^2 flask at 2x10^6 cells per flask in a 12 mL volume. Additionally, 100 µL of diluted cells were seeded in 6 wells of a 96 well tray. The cells in 96 well trays were treated equivalently to the experimental replicates throughout the screen. This allowed monitoring of the rate of infection by indirect immunofluorescence using the 4G2 anti-E primary antibody. On the morning after seeding, cells were again treated with IFNα at 1 U/mL diluted in fresh media and three flasks were left untreated for 6h. Then all flasks were inoculated with a MOI = 0.2 of the mutant DENV from the previous passage. Replicates were not pooled between passages. 48 h post-infection, the supernatant containing infectious virus was collected and cleared of cellular debris by centrifugation (4000 ×*g*, 5 min). Supernatants from each replicate were divided in half and separately aliquoted into two 14 mL tubes (Corning).

Additionally, smaller 1 mL volumes of each replicate were aliquoted into microcentrifuge tubes to titer the virus by Focus Forming Assay prior to use in the next passage. After removing infectious supernatant, the cell monolayer was washed with 1 X PBS and total RNA was harvested in 4 mL of TRIsure reagent (Bioline) per 75cm^2 flask. Both supernatants and RNA samples were stored frozen at -80 ^{o}C until further use. Additionally, on the morning of the second day post-infection the parallel 96 well plates were fixed for anti-E immunofluorescence. This process was then repeated for an additional round of selection.

2.3.4.3 Genome sample preparation and NGS

To prepare samples of the selected DENV mutant library for NGS the following procedure was used. Briefly, total RNA was extracted separately from each replicate in passage 1 and 2 by standard TRIsure methods (section 2.1.4.1). Then this was used in a Superscript reverse-transcriptase III high-fidelity first strand synthesis (Life Technologies) reaction (section 2.1.6.2) performed using a reverse primer that bound specifically to the extreme 3' end of the DENV2 genome to amplify the full-length genome (see Appendix I). Next, full-length DENV cDNA from each replicate was used as a template to PCR amplify 6 overlapping fragments covering the entire length of the DENV genome using the high-fidelity Q5 polymerase (section 2.1.3.3; see Appendix I for primer sequences). Each PCR product was gel-extracted and purified (section 2.1.3.2). The resultant concentration of PCR product from each sample was determined using the Qubit dsDNA HS (High Sensitivity) Assay Kit (section 2.1.5). Subsequently, the 6 overlapping PCR fragments covering the full-length genome were pooled in equimolar ratios (0.1pmol of each fragment) as calculated by the molecular weight of each fragment using the Promega online Biomath calculator. This was performed separately for each independent replicate. These samples were then sent to collaborators at UNSW and the Ramaciotti Centre for Genomics, where NGS libraries for each pool were prepared using the Nextera XT (Illumina) and sequenced on the NextSeq500 platform.

2.3.5 Preparation of DENV infectious clone plasmids and *in vitro* synthesis of viral RNA (mMESSAGE mMACHINE® SP6, Invitrogen)

To generate *in vitro* transcribed RNA for DENV infectious clones the mMESSAGE mMACHINE® SP6 kit (Invitrogen) was used. Initially 2- 5 µg of the parent pFK-DVs plasmid or equivalent mutant infectious clone was linearized by overnight *Xba*I restriction digestion, cleaving at the

extreme 3' terminus of the DENV genome. Following overnight digestion, the linearized plasmid was column purified as described previously in section 2.1.2.4 (Bioline) and eluted in 15 µL of NF water. Next, the SP6 reaction was set up in PCR tubes containing 10 µL of NTP/Cap 2 X mixture, 2 µL of 10 X reaction buffer, 1.5 µL of GTP (20 mM), 4.5 µL of linearized purified plasmid template and 2 µL of SP6 enzyme mix. The reaction was briefly mixed by pipetting and incubated at 37^{o}C for 3 h using the Bio-Rad S1000 Thermal Cycler. Then 1 µL of Turbo DNase was added per tube and returned to incubate for a further 15 min at 37^{o}C. To purify the RNA the entire 20 µL reaction was spiked into 1 mL of TRIsure (Bioline) and the RNA was extracted as described in section 2.1.4.1.

2.3.6 Transfection of *in vitro* transcribed RNA for viral production kinetics assays and the propagation of DENV infectious virus stocks (DMRIE-C, Invitrogen)

One day prior to transfection, Huh7.5 cells were seeded at 2 X 10^5 cells/well in a 6 well plate. The following day the transfection mixture containing 1 mL Opti-MEM (Gibco, Invitrogen), 6 µL DMRIE-C (Invitrogen) and 5 µg *in vitro* transcribed and purified RNA was made up in a microcentrifuge tube. Next, culture media was removed from the cells, then they were washed once with 1 X PBS prior to adding the entire transfection mixture onto the cells directly. These plates were returned to culture for 3 h at 37^{o}C. After incubation, the transfection mixture was removed and replaced with fresh culture media (3 mL). Each day post transfection 250 µL of culture supernatant was collected from each well and stored frozen at -80 ^{o}C. After 3 days of culture the transfected Huh-7.5 cells had reached confluence and were harvested by trypsinisation, prior to application of equal volumes of the cell suspension from each well into a 25 cm^2 flask and a 6 well plate. The virus-containing supernatant was diluted 1:1 with fresh media and divided equally between the T25 and the 6 well dish. A small portion of the transfected cells (100 µL) were concurrently seeded into 96 well plates and left to attach to the wells prior to fixing with acetone/methanol. These 96 well replicates were used the following day to estimate the rate of infection at 72 hpi by immunofluorescent labelling of E-protein. After re-seeding, 250 µL of culture supernatant was collected from each well of the 6 well tray, each day until 7 dpi and stored frozen at -80 ^{o}C. After the 7-day time point had elapsed, these frozen aliquots were used to determine the level of infectious virus in the supernatant at each time point by focus forming assay.

2.3.7 IFN sensitivity assay

To perform an IFN sensitivity assay Huh-7.5 cells were seeded at 1 X 10^5cells/well in a 12 well plate (or scaled accordingly). The following day cells were treated in triplicate with increasing concentrations of IFNα diluted in fresh culture media or left untreated. After 6 h the IFNα treatment was removed and cells were inoculated with either ZIKV or DENV at an MOI of 0.2. The following morning, the inoculum was removed, and the media was replaced with the appropriate concentrations of IFNα diluted in fresh media. Cells were returned to culture for 48 h in a 37 ^{o}C incubator. 48 h post-infection, supernatants containing infectious virus were collected and stored frozen at -80 ^{o}C. These supernatants containing infectious virus were then titrated using a Focus Forming Assay in technical duplicates and used to calculate FFU/mL. Raw FFU/mL titers were normalized to the average titer of infectious virus generated by the untreated cells. Statistical analyses were performed on the normalized data using one-way AVOVA compared to untreated using the GraphPad Prism v8 software.

2.4 Cultured Cell lines

2.4.1 Ect1

The ectocervical Ect1/E6E7 cell line was established in 1996 from normal epithelial tissue taken from a premenopausal woman. Cells at passage 3 were immortalized by transduction with the retroviral vector LXSN-16E6E7 [96]. These cells were generously provided by Sarah Robertson of the Robinson Research Institute, Adelaide, Australia.

2.4.2 HeLa

The HeLa cell line is derived from cervical cancer cells isolated from Henrietta Lacks a 31 year old African American woman [301].

2.4.3 Huh-7

The Huh7 cell line is a hepatocellular carcinoma cell line of epithelial origin isolated from a 57 year old Japanese male [242].

2.4.4 Huh-7.5

The Huh-7.5 cell line is derived from the Huh-7 cells which used to harbour replication of an HCV subgenomic replicon but were cured after IFN-α treatment [26] and are defective in RIG-

I signalling [336]. These cells were kindly provided by Charles Rice, Rockefeller University, New York, USA.

2.4.5 HTR8

The HTR-8/SVneo cell line was derived by transfecting the cells that grew out of chorinic villi explants of human first-trimester placenta with the gene encoding for simian virus 40 large T antigen [120]. These cells were generously provided by Claire Roberts, Flinders University, Adelaide, Australia.

2.4.6 HEK 293T

The HEK 293T cell line is derived from the human HEK 293 cell line of embryonic kidney epithelial origin with the addition of the SV40 large T antigen [85].

2.4.7 Ishikawa

The Ishikawa cell line is derived from endometrial adenocarcinoma in a 39 year old pre-menopausal woman [252]. These cells were generously provided by Sarah Robertson of the Robinson Research Institute, Adelaide, Australia.

2.4.8 Vero

The Vero cell line was isolated from the kidney of a normal adult African green monkey and were established in 1962 by Y. Yasumura and Y. Kawakita at the Chiba University in Chiba, Japan.

2.4.9 VK2

The VK2/E6E7 cell line was established in 1996 from the normal vaginal mucosal tissue taken from a premenopausal woman. Cells at passage 3 were immortalized by transduction with the retroviral vector LXSN-16E6E7 in the presence of polybrene [96]. These cells were generously provided by Sarah Robertson of the Robinson Research Institute, Adelaide, Australia.

Chapter 3

Construction of a ZIKV transposon mutant library

3.1 Introduction

The ability to evade the type-I IFN response is crucial to ZIKV infection and associated disease in humans. This is demonstrated by the difference in host adaption between primates that are naturally susceptible to ZIKV and mice that are the main small animal model used for ZIKV research. Immune competent mice are not susceptible to ZIKV infection by intravenous inoculation but IFNAR receptor knockout mice, which are readily infected and can succumb to the associated disease [181, 209, 231]. This stark difference in species adaptation and susceptibility to infection is primarily dependent on ZIKV NS5 mediated degradation of human but not mouse STAT2, resulting in blockade of the human IFN pathway [121]. Importantly, transgenic mice expressing human STAT2 demonstrate increased susceptibility to infection, implying ZIKV blockade of IFN signalling is the main barrier to infection in mice [115]. Together this data highlights the importance of IFN in prevention of ZIKV infections and suggests this axis of host-virus interaction can be exploited to improve patient outcomes. In addition to species adaption, the importance of the IFN response is illustrated by ZIKV having evolved multiple strategies to evade both IFN production and signalling downstream of the IFNAR receptor. Several studies (detailed in section 1.3) have elucidated roles of NS1, NS4A, NS2A and NS5 and others in preventing induction of IFN downstream of the RIG-I/MAVS pathway [189, 200, 249, 374, 393]. Other studies have discovered evasion mechanisms downstream of IFNAR activation. Aside from NS5 mediated degradation of STAT2 these include NS2B/3 mediated degradation of JAK1 [374] and ZIKV increasing levels of the negative regulator SOCS1 after binding with the proposed attachment factor AXL on the cell surface [47, 216]. Each of these studies shares a similar limitation in that they rely on over-expression of isolated viral proteins. As a result, they do not accommodate for potential synergistic effects of other viral proteins or untranslated genetic elements that are part of the full ZIKV lifecycle. This is especially important since the functions of individually expressed *Flavivirus* proteins have a limited capacity to recapitulate natural functions within the full lifecycle [167]. Furthermore, most studies have resolved only to the whole protein level, or at best to the domain level and

have not pinpointed the exact encoded region responsible for these evasion mechanisms. Another poorly understood area is the contribution of the ZIKV UTRs to IFN evasion. *Flavivirus* UTRs produce functionally significant sub-genomic *Flavivirus* RNAs (sfRNA) that can antagonise IFN [379]. The IFN evasion capacity of DENV sfRNAs has been well established and was shown to depend on preventing activation of RIG-I in a TRIM25 dependent manner [35, 202]. Recently, ZIKV sfRNA was also shown to inhibit RIG-I and MDA5, however these experiments relied on transient transfection of 3'UTR elements [82]. Additionally, WNV sfRNA was shown to inhibit signalling downstream of activated IFNAR1/2 [307]. Knowledge of ZIKV IFN evasion by viral proteins and UTR elements could be improved by testing these mechanisms within a fully infectious system.

For these reasons, the primary aim of this chapter was to discover novel sequence elements within the ZIKV genome (both in translated and in un-translated regions) that contribute to evasion of the IFN response downstream of the IFNAR1/2 receptor. To address this topic, we aimed to generate a high-throughput random transposon mutagenesis library of a full-length infectious cDNA clone of ZIKV. The underlying rationale was that the randomly distributed 15 bp inserts generated by the MuA transposon mutagenesis process would create loss-of-function mutations when sequences that were essential under the IFN selection condition were interrupted. This would result in a reduced fitness of these viral mutants and consequently a reduced frequency under selection when compared to the control (no IFN) environment. This knowledge could be useful in understanding *Flavivirus* immune evasion and may enable generation of attenuated virus strains for use in targeted vaccine development. In support of this approach, a ZIKV reverse genetics system has recently been used to test an IFN hypersensitive mutant as a live attenuated vaccine in mice [18, 186].

3.2 Results

3.2.1 Testing ZIKV reverse genetics systems

Recently our laboratory was gifted two different ZIKV infectious cDNA clones. These are described in full by their respective creators in the publications by Tsestarkin *et al*. (2016) and Schwarz *et al*. (2016) and are represented diagrammatically in Figure 3.1 [309, 350]. Briefly, the first clone named pZIKV-ICD [350] was generated by incorporating full-length ZIKV cDNA into a low copy number vector pACNR1811 (Fig. 3.1a). The viral cDNA for this clone was isolated by reverse transcription from a female ZIKV patient with febrile illness in Brazil, 2015

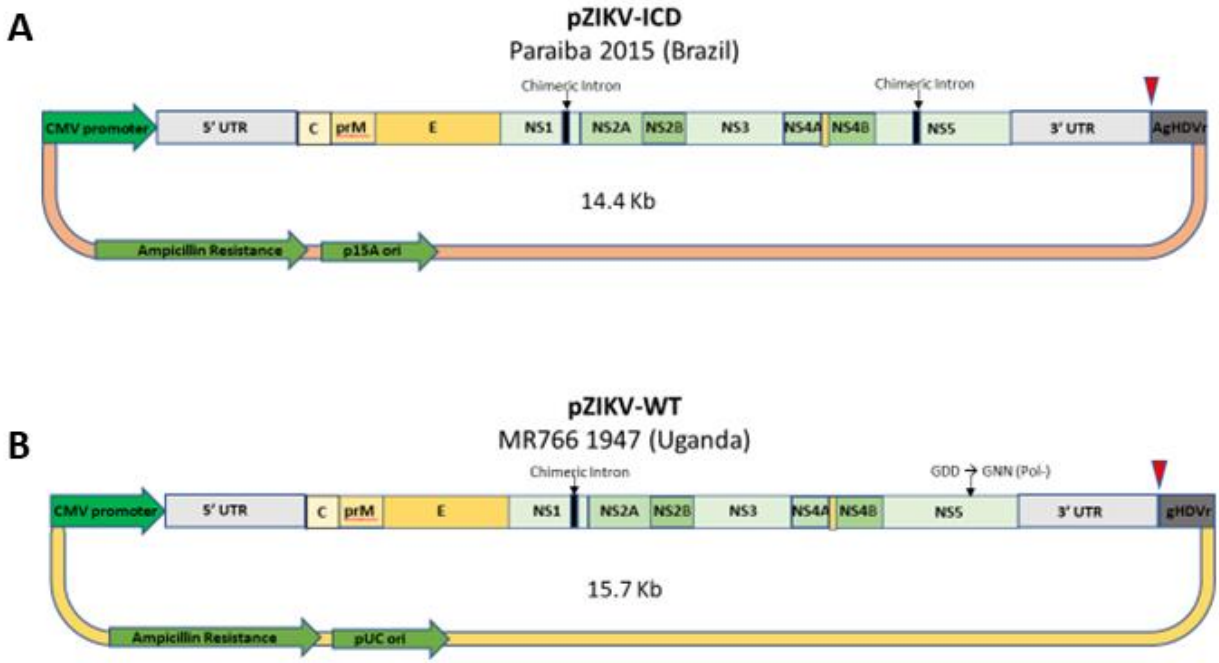

Figure 3.1: Schematic representation of the ZIKV infectious clones pZIKV-ICD and pZIKV-MR766-WT. For additional sequence details see Appendix IV.

(strain: Paraiba_2015) [59]. Following transfection of the plasmid into eukaryotic cells, the initial transcription of full-length positive sense ZIKV RNA is driven by the eukaryotic RNA polymerase II cytomegalavirus (CMV) promoter. Authentic 3' ends are generated by the anti-genomic hepatitis delta virus ribozyme (agHDVR) sequence downstream of the viral 3' UTR region that auto cleaves after it is transcribed. Additionally, to minimize toxicity of viral sequence and to enhance plasmid stability in *Escherichia coli* (*E. coli*) two chimeric introns were introduced at nucleotide positions 2711 (NS1) and 8882 (NS5). The second clone named pZIKV-MR766-WT was generated from cDNA of the historical African strain MR766 first discovered in Uganda in 1947. This cDNA was cloned into the high-copy-number vector pCDNA6.2 (Fig. 3.1b) [309]. Like pZIKV-ICD this clone utilizes a eukaryotic CMV promoter to drive transcription of viral sequence and a genomic HDVR (gHDVR) for generation of authentic 3' ends. Interestingly, this clone only required a single insertion of a chimeric intron in NS1 at nucleotide position 3127 for plasmid stability. To validate these clones for generation of infectious virus each plasmid was transfected into Huh-7 cells that are permissive to the related DENV [94]. Figure 3.2 shows following transfection of these clones they successfully initiated transcription and translation of the viral proteins as determined by immunofluorescent detection of ZIKV E-protein in transfected cells (Fig. 3.2a). The ZIKV E-protein was first detected at 48 hours post transfection (hpt) and increased by 72 hpt. Importantly, transfection of these plasmids resulted in the production of infectious virions in the supernatant 48 hpt detected by plaque assay on Vero cells (Fig. 3.2b). The ability of these virus particles to infect Vero cells and spread independently of plasmid transfection indicated *de novo* virions were packaged and exported with a full-length copy of the +ssRNA ZIKV genome. Collectively this data confirms the ability of these infectious clones to initiate the complete virus lifecycle after direct transfection into mammalian cell culture. Due to a concurrent publication by Fulton *et al*. (2017) utilizing the pZIKV-MR766-WT clone for transposon mutagenesis screening [104] and the enhanced relevance of the pZIKV-ICD clone to the recent outbreak it was decided to continue further experiments with the pZIKV-ICD clone.

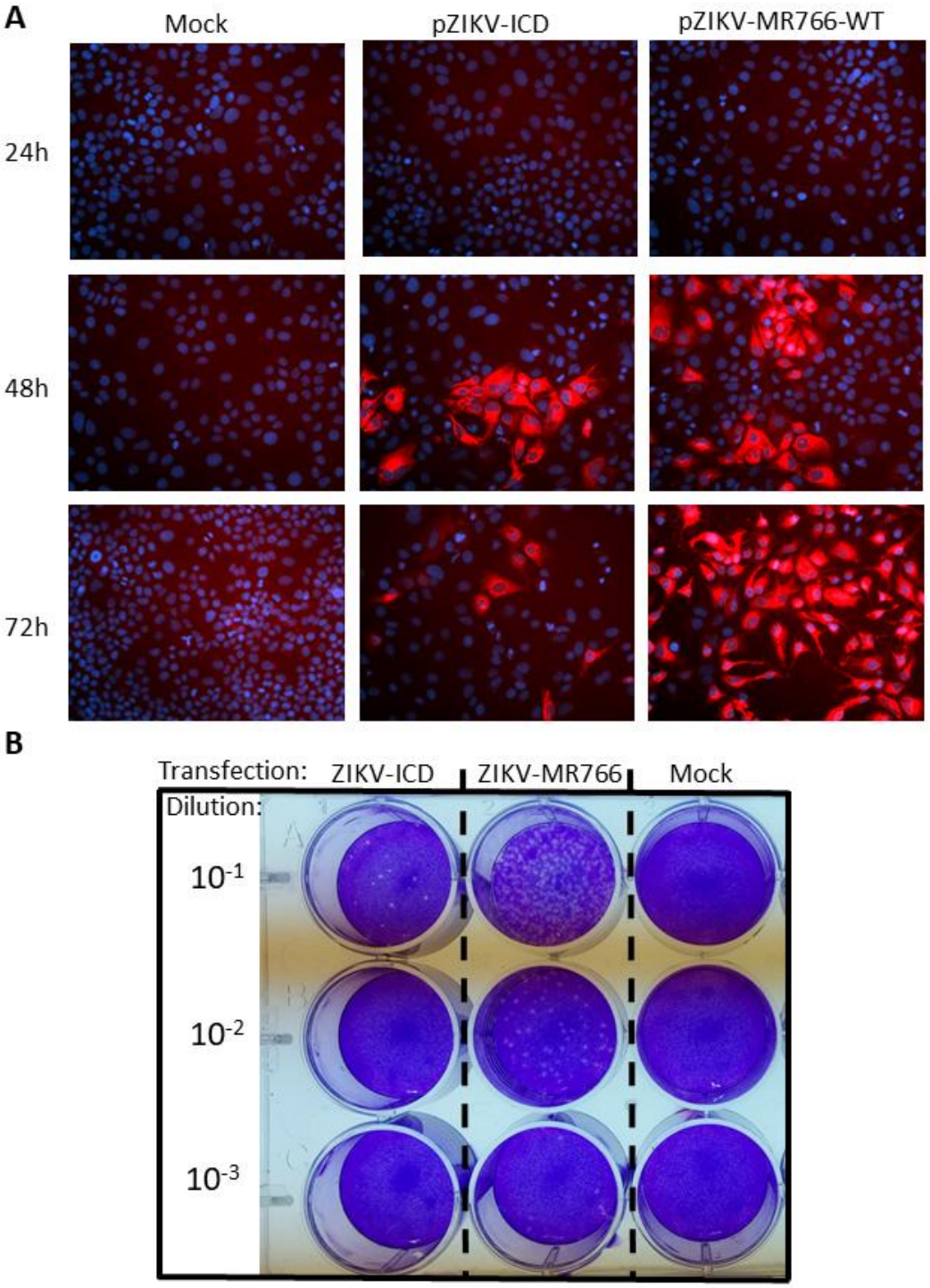

Figure 3.2: Transfection of the infectious clone pZIKV-ICD or pZIKV-MR766-WT into permissive cells initiates the complete ZIKV lifecycle. A) Huh7 cells were transfected with the indicated plasmids and fixed with acetone:methanol at 24, 48 or 72 h post transfection points to detect ZIKV infected cells by immunofluorescent staining using the 4G2 anti-*flavivirus* E protein and cell nuclei using DAPI (blue). B) Huh7 cells were transfected with the indicated infectious clone plasmids and supernatants were collected at 48 h post-transfection to detect infectious virus in the supernatant by plaque assay.

3.2.2 Optimization of screening conditions

Following validation of the pZIKV-ICD reverse genetics system for production of infectious virus the next step was to select the appropriate cell type for use in the screen. The ideal cell type for the screen was one of human origin to rule out species-specific differences with the IFN pathway. Also, cells were required to have an intact IFN signalling pathway downstream of the type-I IFN receptor. Additionally, it was desirable that these cells have a low level of endogenous IFN production to the limited unintended induction of viral associated immune pathways in the untreated group. Huh-7 cells used in our laboratory to culture flaviviruses such as DENV represented an ideal choice. These cells are of human liver origin, are known to respond well to IFN, have defects in IFN production pathways and are permissive to ZIKV [163, 354].

Other considerations for the screen related to the generation of the initial seed stock from transfection of plasmid DNA into mammalian cells. This step of transfecting the library into mammalian cells was a potential bottleneck that could constrict the diversity of the mutant virus represented in the subsequent passages. Therefore, to maximise mutant virus diversity from the cDNA library we aimed to optimise transfection efficiency for the pZIKV-ICD clone and quantify the impact on virus production. Furthermore, we wanted to determine the cell lines that are most permissive to ZIKV infection for use in subsequent passages. Virus production by 48 hpt and spread by 72 hpt was compared in the indicated cell lines following transfection of the pZIKV-ICD clone. Virus production was monitored over time by detection of infected cells using the 4G2 anti- E protein and immunofluorescence microscopy. These cell lines (Huh-7, Vero and 293T) were selected based on their use in either the Tsestarkin *et al*. publication or in the mutant screen by Fulton *et al.*, respectively, to generate high virus titres. Figure 3.3a demonstrated that at 48 hpt, 293T cells clearly have greater numbers of infected cells producing virus E protein compared to both Huh-7 and Vero cells at the same time point indicating their improved transfection efficiency. However, the spread of virus by 72 h post transfection was limited in 293T cells and was greatly improved in Huh-7 and Vero cells,

indicating that these cell types are more permissive to ZIKV infection after virus production was established. To confirm this differing permissiveness independent of transfection efficiency, all three cell types were infected with a virus stock of the MR766 strain at an MOI of 1 FFU/mL. Figure 3.3b shows at 48 and 72 h post infection Huh-7 cells are the most

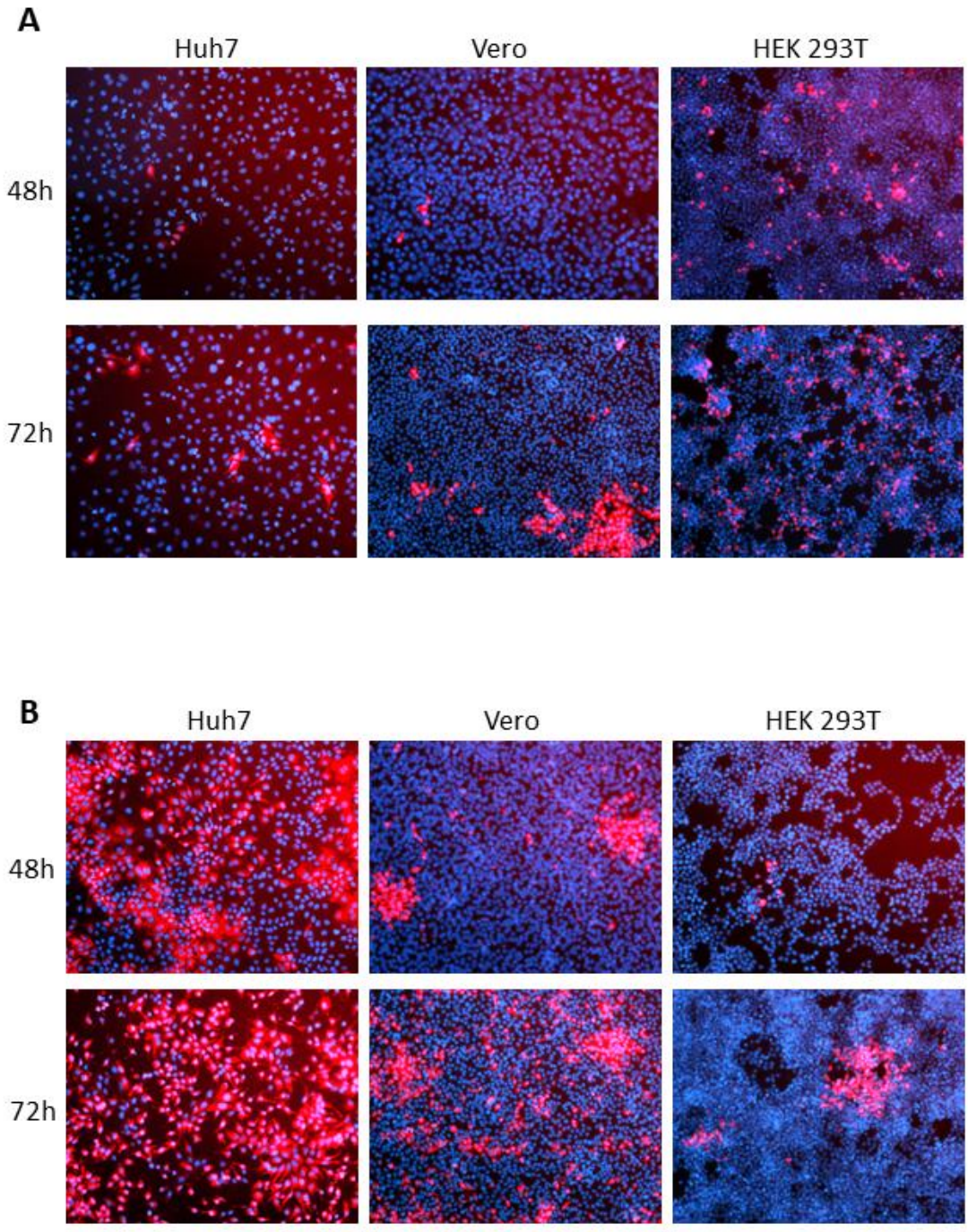

Figure 3.3: The spread of infection following pZIKV-ICD transfection and the permissiveness of cells to ZIKV infection varies between cell lines. A) Huh7, Vero or 293T cells were transfected with the pZIKV-ICD infectious clone or B) infected with ZIKV MR766 virus at an MOI of 1. Cells were fixed with acetone:methanol at the indicated time points to detect ZIKV infected cells by immunofluorescent staining using the 4G2 anti-*flavivirus* E protein (red) and cell nuclei using DAPI (blue).

permissive followed by Vero cells and then 293T cells based on the number of E-protein positive cells. Next, to quantify the impact of transfection efficiency and permissiveness on virus production, Huh-7, Vero, 293T and HeLa cells were transfected with pZIKV-ICD. Supernatants were collected at 24 h intervals following transfection, and the level of infectious virus was quantified by focus forming assay on Huh7.5 cells. Corresponding with the immunofluorescence data, Huh-7 cells (Fig 3.4a) had low quantities ($5x10^2$ FFU/mL) of virus produced at 48 h indicating poor transfection efficiency and by 72 h infectious virus levels of approximately 7.5 x 10^2 FFU/mL were produced. 293T cells produced 1.3 x 10^3 FFU/mL at 48 hpt, presumably reflecting their improved transfection efficiency compared to Huh-7 cells (Fig. 3.4c). The subsequent plateau in virus production of 1.1 x 10^3 FFU/mL at 72 h and the maximum of 2.3 x 10^4 FFU/mL recorded at one-week post transfection suggested that 293T cells do not support efficient virus replication and/or virus production. Vero cells started with the lowest recorded virus titer at 48 hpt (3.6 x 10^2 FFU/mL) but then rapidly generated higher levels of infectious virus (2.3 x 10^4 FFU/mL) at 72 hpt before a plateau at approximately 3.3 x 10^5 FFU/mL after one week (Fig. 3.4d). Comparatively, the titers generated following transfection of Vero cells with the same plasmid, transfection reagent and cell line were much lower than those reported in publication by Tsestarkin *et al*. (reportedly 1 $x10^4$ PFU/mL at 24 hpt and a maximum of 3x 10^6 PFU/mL at 72 hpt). Interestingly, HeLa cells had the highest initial titer at 48h of approximately 2.3 x 10^4 FFU/mL and the highest at 72 hpt (6.3 x 10^4 FFU/mL) compared to other cell lines (Fig. 3.4b). From this data it was concluded out of the cell lines tested, HeLa cells had the preferred characteristics to generate a virus seed stock of the mutant library, as they generated the highest titer of virions following direct transfection and therefore would limit the bottleneck on mutant diversity following transfection. However, HeLa cells can mount a full IFN response to virus (see results Chapter 6). To reduce the impact of endogenous IFN production on the screen it was decided that virus library seed stock would be generated in HeLa cells for 48 h to generate an input pool of mutant virus (Pool 0). This seed stock would then be passaged onto Huh-7 cells for the subsequent Pools 1 and 2 to apply selective pressure to the mutant library in conditions with or without IFN.

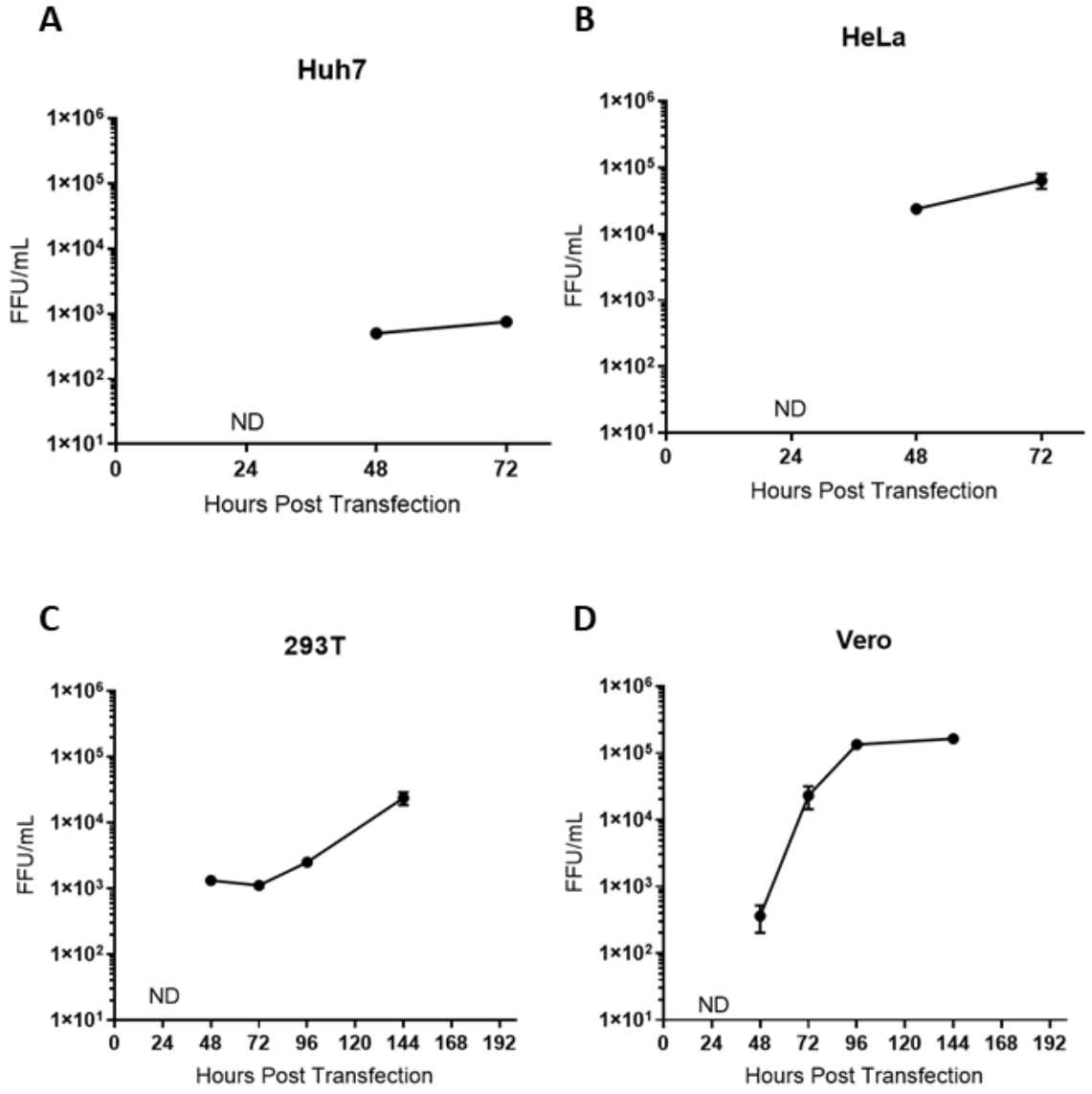

Figure 3.4: The kinetics of infectious virus production following transfection with the pZIKV-ICD infectious clone in various cell lines. The pZIKV-ICD infectious clone was transfected into A) Huh7, B) HeLa, C) 293T or D) Vero cells. Supernatants from transfected cells were collected at the indicated time points and the level of infectious virus in supernatant was quantified by focus forming assay. Data are presented as means +/- s.d.

The final consideration for the screening conditions was the concentration and timing of IFN treatments applied to the cells in following passages. Ideally this treatment would give adequate selection pressure to reduce the frequency of IFN sensitive mutants without dramatically reducing library diversity within the IFN treated pools. For this reason, the concentration of IFNα that inhibited ZIKV production by 50 % (IC_{50}) was determined for Huh-7 cells (see Materials and Methods section 2.3.2 for details). Based on a similar screen by Qi *et al.* (2017) uncovering HCV IFN sensitive mutants, it was decided that a low multiplicity of infection (MOI = 0.2) would be used for passaging to prevent co-infection with multiple mutant or wildtype viruses [274]. To determine the IC_{50} of IFNα for the screen, Huh-7 cells were treated with increasing concentrations of IFNα for 6 or 18 h (overnight) prior to infection with ZIKV (MOI of 0.2). 48 h post infection (hpi) supernatants were collected, and infectious virus was enumerated by focus forming assay to calculate the FFU/mL. Raw FFU/mL values were then normalized to the average of the untreated control (maximum infection) and expressed as a percentage of the infectious virus titer of the untreated control. These normalized values were then used to determine the IC_{50} by non-linear regression analysis. Figures 3.5a and 3.5b show that the IC_{50} for IFNα was inversely related to the length of pre-treatment. We hypothesized that this was likely a result of elevated ISG protein expression over the longer timeframe, improving antiviral protection against ZIKV infection. It was decided to continue the screen using the 6 h pre-treatment IC_{50} as this was the most convenient timing for the screen and closely reflected the IFN concentration used in the afore-mentioned HCV screen (4 U/mL vs 1 U/mL) [274].

3.2.3 Generation of the ZIKV MuA transposon mutant library

After selecting, validating, and optimising the experimental conditions related to the use of the pZIKV-ICD infectious clone for the screen, construction of the transposon mutant library was initiated using the Thermo Fisher Mutation Generation System Kit (see Materials and Methods section 2.3.3 for details). The aim was to generate a library containing between 250,000 to 1,000,000 individual mutant clones as had been reported for similar MuA transposon mutagenesis studies on flaviviruses [94, 104, 274] thereby providing good coverage of all possible transposon insertion events across the genome. The first step in the generation of the mutant library was the MuA transposase reaction to insert the 1.2 Kbp transposon containing a Kanamycin selection cassette (KanR) randomly into the pZIKV-ICD

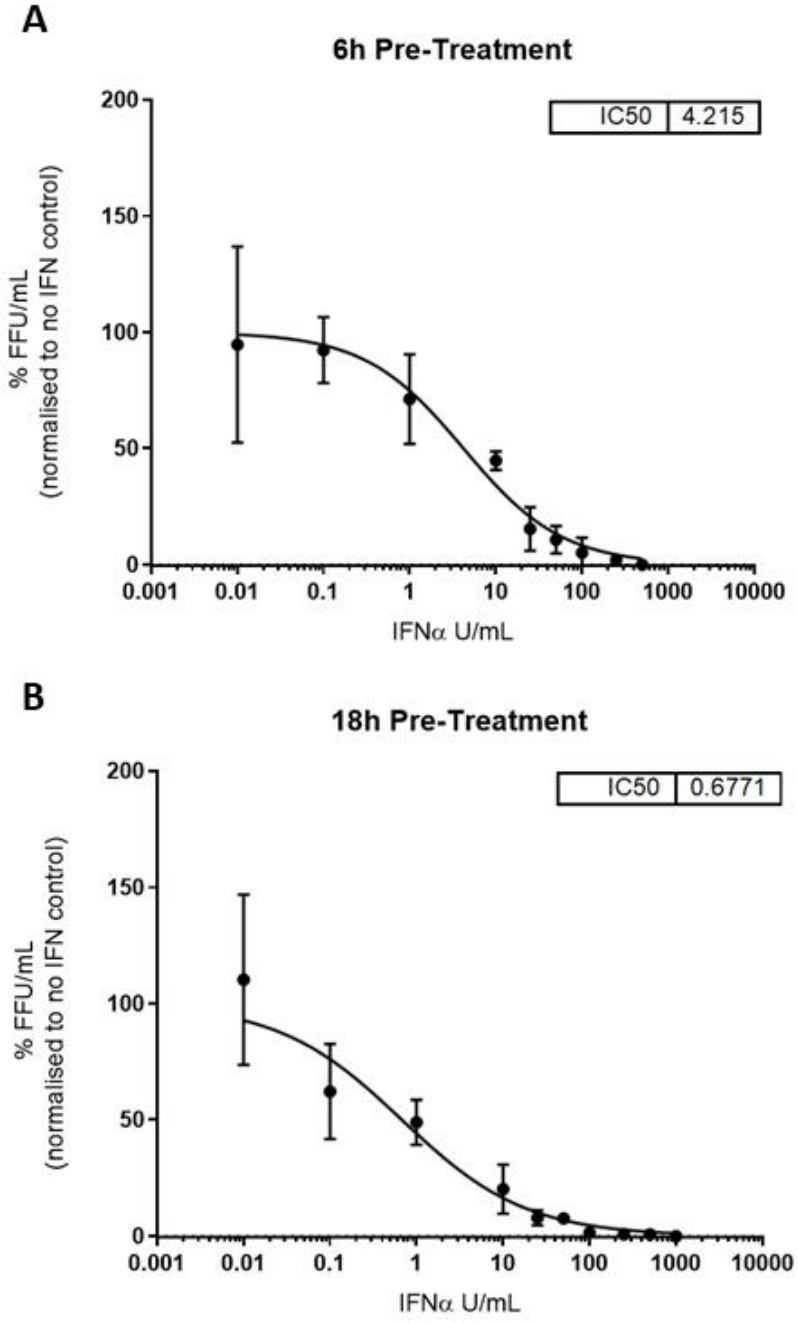

Figure 3.5: Determination of the IC50 concentration of IFNα for inhibition of ZIKV replication. Huh7 cells were treated with the indicated concentrations of IFNα for 6 h A) or 18 h B) prior to infection with ZIKV-ICD virus at an MOI of 0.5. 48 h post-infection supernatants were collected to determine the level of infectious virus in the cell supernatant by focus forming assay. Data is represented as % FFU/mL normalised to the maximum and minimum inhibitory concentrations of IFNα treatment. Data are presented as means +/- s.d.

clone. Initial attempts to recover mutant clones (KanR, AmpR) after bacterial transformation by methods previously optimized for the DENV mutant library generation by Eyre *et al.* were unsuccessful (summarised in Table 3.1) [94]. The recovery of mutant colonies per transformation was too low (1000 clones per transformation) to adequately address the aim of comprehensively exploring all regions of the ZIKV genome that are involved with IFN evasion. Additionally, diagnostic restriction digests performed on individual plasmid clones revealed deletions of large fragments of DNA that was characteristic of bacterial recombination events (results not shown). The frequency of plasmid recombination in multiple randomly selected mutant clones was considered too high (43% of individual mutant clones) to be practical within a pooled mutant library. To improve these outcomes multiple systematic attempts to optimise the transformation conditions were made. Factors optimised for transformation efficiency included, (i) improved input plasmid purity, (ii) decreasing the concentration of Kanamycin antibiotic on Agar plates, (iii) introducing a purification step after the MuA transposase reaction prior to transformation and (iv) changing the competent cells to electro-competent cells that were specialised for viral sequence stability (detailed in Table 3.1). Further optimization to reduce the percentage of recombinant clones included reducing the temperature of bacterial recovery and out-growth to 30 ^{o}C for 24 h instead of 37 ^{o}C for 16 h. These combined variables resulted in significantly improved recovery of mutants as measured by the number of dual resistance mutants on Kanamycin / Ampicillin plates compared to Ampicillin only selection (see Fig. 3.6a & b). Furthermore, the frequency of recombination occurring in randomly selected individual clones was reduced more than 2.5-fold. After performing multiple transformations (15 in total) approximately 385,000 individual mutant clones were transformed. These bacterial clones were then pooled from all the dual selection plates and plasmid DNA was purified. To assess the pooled plasmid DNA preparation for signs of recombination and for successful insertion of the 1.2 kb insert, a *NotI* restriction digest was performed to release the transposon body from the pooled mutant pZIKV-ICD DNA (see Fig 3.6c). The clearly defined upper band in lane 4 that was the same size as the full-length linear pZIKV-ICD plasmid in lane 3 indicated that most mutants within the library retained full-length ZIKV sequence (not recombined). The lower band in lane 4 present at the expected 1.2 kb size indicated successful incorporation of the transposon containing the Kanamycin resistance cassette. Together this process generated an intermediate pooled mutant library containing ~385,000 individual mutant clones meeting the requirement of

Table 3.1: Summary of the initial and optimised reaction conditions for bacterial transformations of the ZIKV-ICD MuA transposase reaction.

	Reaction preparation method for transformation	Competent Cells	[Kanamycin] of transformation plates	# Mutants per transformation (Kan/Amp resistant)	# Transformants (Amp resistant)	Recombination frequency of randomly selected clones
Initial	Dilute reaction 1/10	Aligent XL-10 Gold Chemically Competent (5×10^9 cfu/µg)	50 µg/mL	1000	Confluent (Neat only)	43%
Optimised	Sodium Acetate/ Ethanol cleanup	Lucigen Endura Electro Competent (1×10^{10} cfu/µg)	20 µg/mL	12,000-50,000	Confluent (Neat only)	17%

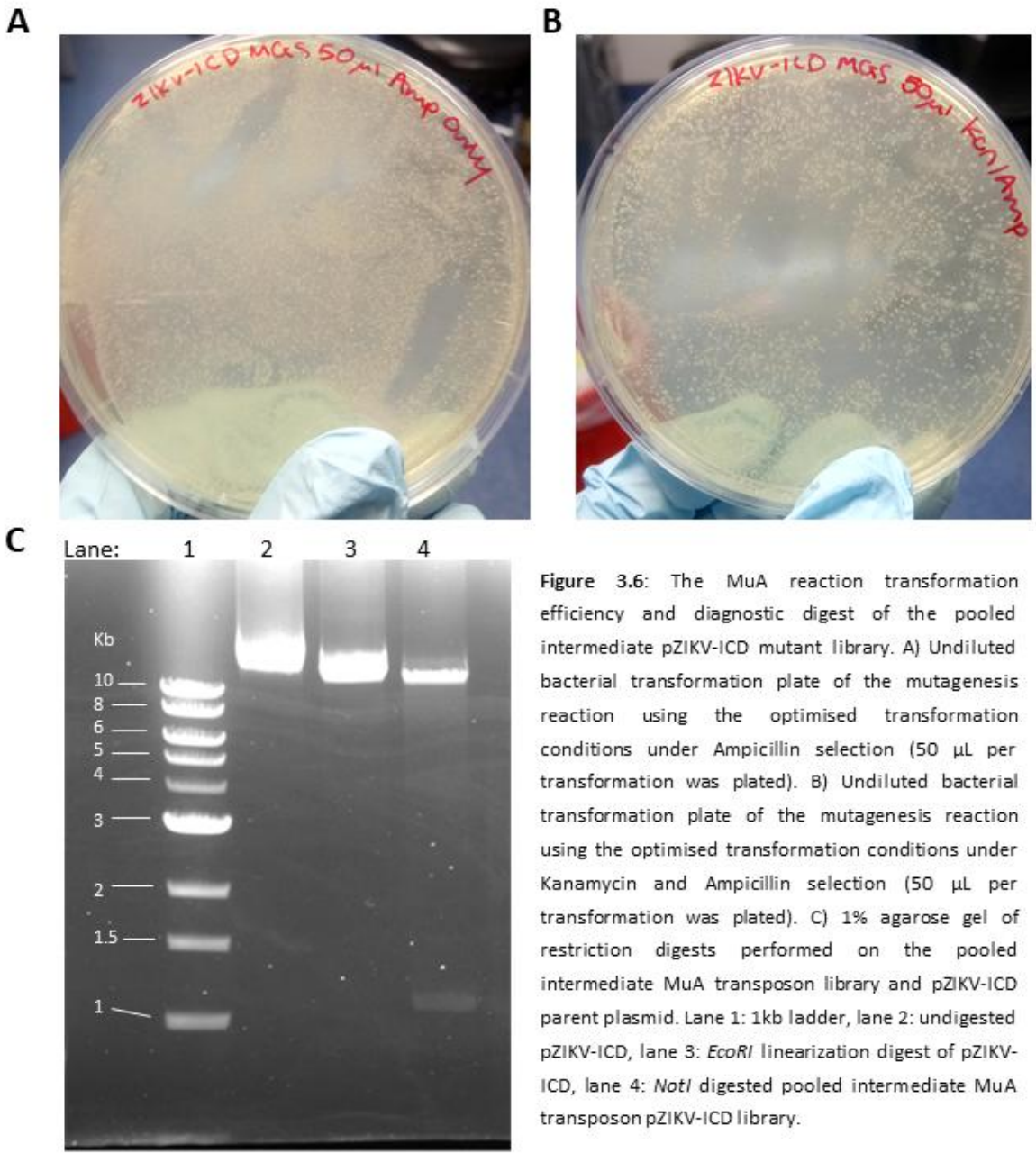

Figure 3.6: The MuA reaction transformation efficiency and diagnostic digest of the pooled intermediate pZIKV-ICD mutant library. A) Undiluted bacterial transformation plate of the mutagenesis reaction using the optimised transformation conditions under Ampicillin selection (50 µL per transformation was plated). B) Undiluted bacterial transformation plate of the mutagenesis reaction using the optimised transformation conditions under Kanamycin and Ampicillin selection (50 µL per transformation was plated). C) 1% agarose gel of restriction digests performed on the pooled intermediate MuA transposon library and pZIKV-ICD parent plasmid. Lane 1: 1kb ladder, lane 2: undigested pZIKV-ICD, lane 3: *EcoRI* linearization digest of pZIKV-ICD, lane 4: *NotI* digested pooled intermediate MuA transposon pZIKV-ICD library.

between 250,000 – 1,000,000 mutant clones to adequately cover the ZIKV genome. This intermediate library was not substantially contaminated with recombinant clones and contained the expected transposon insert.

The next step in library preparation was to remove the transposon body by *NotI* restriction digestion and then to re-ligate the full-length mutant pZIKV-ICD sequence, leaving behind the final 15 bp mutant insertion. Initial attempts were hampered by low yield of DNA recovered after gel-extraction of the mutant pZIKV-ICD sequence and additionally after purification of the T4 ligation reaction prior to electroporation. To overcome this barrier, NEB ElectroLigase was used because it does not require an additional purification step prior to transformation into electro-competent cells. Table 3.2 shows that after transformation with the optimised recovery and outgrowth at 30 ^{o}C comparable numbers of mutant clones were recovered for each transformation (~20,000 – 30,000). After performing multiple transformations, a total of ~300,000 mutant colonies were recovered, indicating maintenance of the library diversity generated in the intermediate cloning step. To assess the outcome of the re-ligation a panel of randomly selected individual plasmid clones were subjected to restriction digest with *NotI*. Unfortunately, restriction digest screening of individual clones revealed widespread recombination as indicated by bands of smaller than expected size. A staggering 90% of individual clones harboured recombinant plasmid DNA. The combined effect of this can be observed in the gel image of the pooled library digested with *NotI* (Fig. 3.7). Instead of appearing on the gel as a clearly defined band at the same size as the *NotI* digested intermediate transposon insertion library (lane 2) or the linearized pZIKV-ICD parent DNA (lane 3) the mutant library appeared as a smear (lane 1). This indicated significant proportions of the mutant clones had lost segments of the plasmid DNA due to recombination following bacterial transformation. Multiple systematic attempts were made to reduce the recombination frequency such as by reducing recovery and out-growth temperatures (25 ^{o}C), and the use of different competent cells reported to be more stable for viral sequences (Stable 3, Invitrogen). Unfortunately, none of the optimization attempts were able to significantly reduce the recombination frequency of the pZIKV-ICD mutant library.

Table 3.2: Summary of the initial and optimised reaction conditions for bacterial transformations of the final ligation reaction of the pZIKV-ICD mutant library.

	Ligation	Reaction preparation method for transformation	Yield after purification	Competent Cells	# Mutants per transformation (Amp resistant)	Recombination frequency of randomly selected clones
Initial	NEB T4 ligase, overnight 16°C	Purification by Sodium Acetate / Ethanol Precipitation	4 ng/µL	Lucigen Endura Electro Competent (1×10^{10} cfu/µg)	NA	NA
Optimised	NEB ElectroLigase 1h 25°C	NA	37.5 ng/µL	Lucigen Endura Electro Competent (1×10^{10} cfu/µg)	20,000–30,000	90%

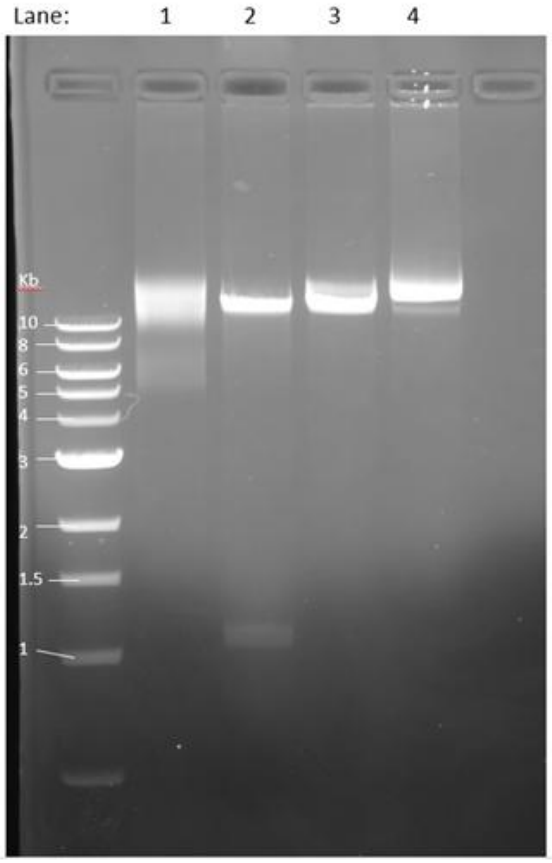

Figure 3.7: Diagnostic restriction digest to detect recombination in the final pooled pZIKV-ICD mutant library. 1% agarose gel of restriction digests performed on the pooled ligated pZIKV-ICD mutant library, the pooled MuA transposon insert pZIKV-ICD library and the pZIKV-ICD parent strain. Lane 1: *NotI* digested pooled mutant library (post-ligation), lane 2: *NotI* digested pooled MuA transposon pZIKV-ICD library, lane 3: *EcoRI* linearization digest of pZIKV-ICD, lane 4: undigested pZIKV-ICD

3.2.4 Testing the ZIKV MuA transposon mutant library for viability

To determine if the final pZIKV-ICD mutant library was able to initiate virus replication or infectious virus production even in the face of significant plasmid recombination the pooled library was transfected into HeLa cells in parallel with the parent pZIKV-ICD plasmid. Figure 3.8a shows markedly reduced ZIKV E-protein detected by immunofluorescence at 24, 48 or 72 hpt from cells transfected with the pooled mutant library compared to the parent plasmid. The distribution of E-protein positive cells in wells transfected with the mutant library was limited to sparsely distributed individual cells at 24 hpt that expanded to sparsely distributed foci of infected cells by 72 hpt. This pattern implied initiation of virus replication was a result of rare non-recombined plasmids within the library, and that the majority of the pooled plasmid stock was non-functional. Comparatively, the parent plasmid pZIKV-ICD transfection resulted in frequent detection of E-protein positive cells that were evenly distributed throughout the culture at 24h and increased in frequency over time at 48 and 72h. Together, this indicated a severely diminished frequency of transfection events initiating viral replication and protein production by the pooled mutant library compared to the parent plasmid as a result of non-functional recombined plasmid clones. To confirm and quantify this effect the level of infectious virus in cell culture supernatants were enumerated by focus forming assay on Huh7.5 cells for parallel cultures of transfected cells. Figure 3.8b shows that the parent pZIKV-ICD transfection was able to initiate robust production of infectious virus that increased steadily over time to comparable titers previously observed in HeLa cells. On the other hand, the mutant library produced levels of infectious virus titers that were 3-logs lower at all time points. Interestingly, the related study involving mutagenesis of the MR766 clone by Fulton et al. [103] also found a 3-log reduction compared to wildtype, validating our experimental procedure. However, in combination, the high frequency of recombination in the pooled mutant library reduced the estimated percentage of functional plasmids capable of generating *de novo* virus production by 90% of those recovered. This corresponded to ~30,000 viable mutants in the pool. Consequently, when the mutant library was transfected into cells it produced approximately 3-log lower levels of infectious virus. Some loss of function was expected in the screening process since not all mutants would be replication competent. However, it was of major concern that the theoretical coverage of the 11 kb genome was reduced to less than 3 times. This level of coverage reduced the likelihood of

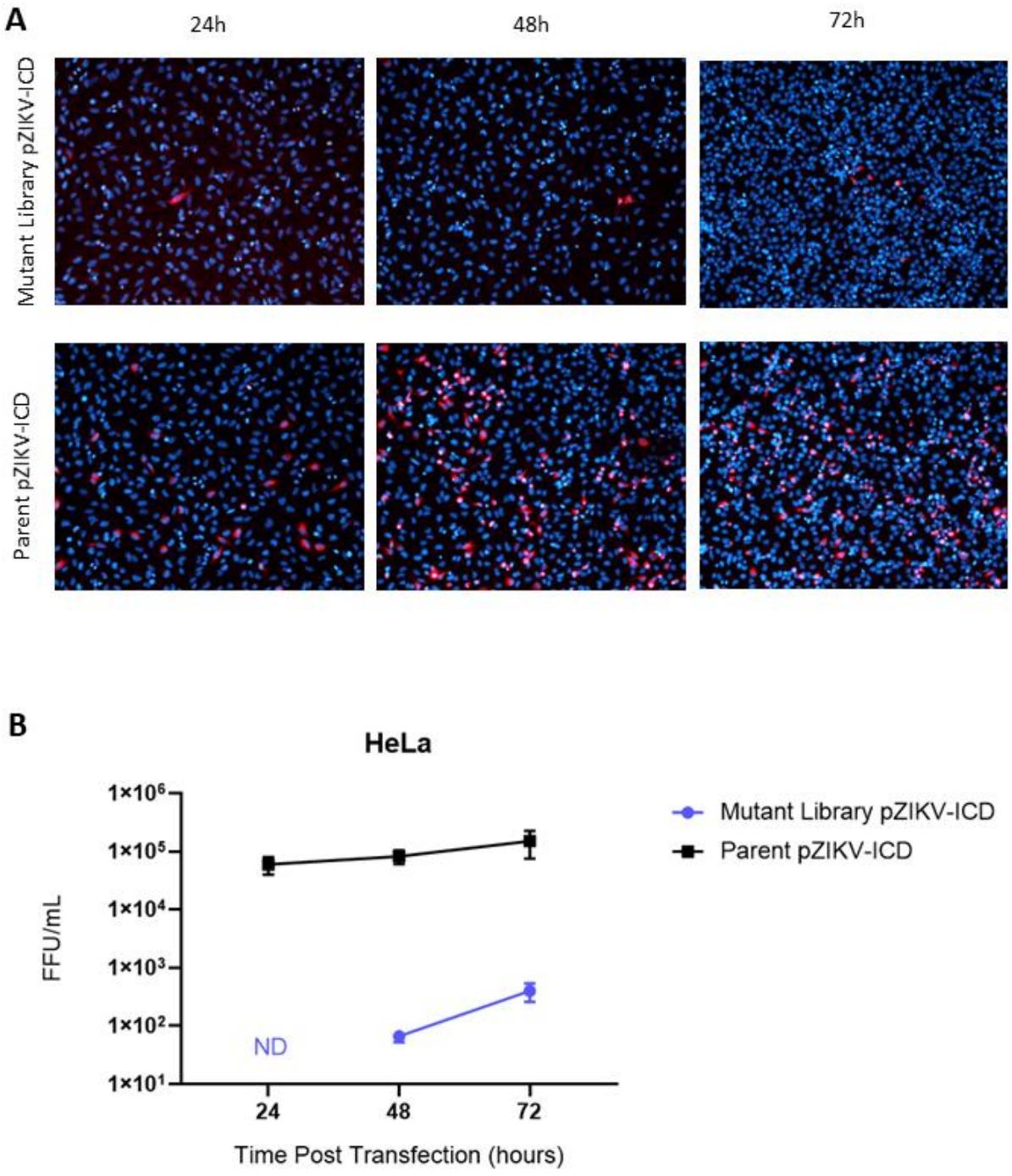

Figure 3.8: Transfection efficiency and infectious virus production are impaired following transfection of the final pooled pZIKV-ICD mutant library. A) HeLa cells were transfected with the mutant library or parent pZIKV-ICD and at 24, 48 and 72h post transfection cells were fixed with acetone:methanol. ZIKV infected cells were detected by immunofluorescent staining using the 4G2 anti-*flavivirus* E protein (red) and cell nuclei using DAPI (blue). B) HeLa cells were transfected with the mutant library or parent pZIKV-ICD infectious clone and the level of infectious virus in supernatant was measured by focus forming assay. Data are presented as means +/- s.d.

targeting each residue in the genome and limited the screening power to a point not appropriate for continuation. Unfortunately, due to these significant experimental issues and time constraints the decision was made to discontinue work on ZIKV transposon mutagenesis. Instead, a related line of investigation to detect *Flavivirus* IFN evasion genetic elements was initiated as outlined in the following Chapter 4.

3.3 Discussion

The ability of ZIKV to evade the type-I IFN response is key to it causing infection and disease in humans. Specific components encoded within the ZIKV genome are responsible for this IFN evasion. To date, studies examining ZIKV IFN evasion have focused on expression of individual viral proteins or UTR elements and lack the context of the full virus lifecycle. This limitation means there are likely undiscovered genetic regions that are important for ZIKV IFN evasion. To address this gap in knowledge we aimed to generate a transposon mutant library of an infectious full-length ZIKV cDNA clone. This mutant library was then to be subjected to selection in mammalian cell culture under conditions with or without IFN prior to the analysis of the impact of each mutation on IFN sensitivity. Together, this high-throughput mutagenesis and selection approach coupled with NGS sequencing intended to reveal novel genetic elements involved in ZIKV IFN evasion.

In preparation for screening a reverse genetics system was validated for generation of *de novo* virus production. This system (pZIKV-ICD) was chosen based on its utility in initiating generation of infectious virus, its relevance to the recent outbreak strain and its novelty compared to an infectious clone based on the prototypical MR766 Uganda strain. Initially, there were challenges regarding the amount of infectious virus generated from transfection into cells used by other groups for similar screens (Huh-7, Vero or 293T) [94, 104, 350]. This was found to depend on balancing transfection efficiency and permissiveness of cell lines. Of the cell lines tested, HeLa cells provided the best compromise, generating the highest titers of virus from direct transfection. This was an important consideration for the desired use of the plasmid in a high-throughput mutagenesis approach, as low transfection efficiency would create a genetic bottleneck in library diversity entering cells. A better approach, rather than directly transfecting a full-length cDNA plasmid that relies on CMV driven RNA transcription, could be to generate *in vitro* transcribed RNA from a bacteriophage promoter similar to that used by Eyre *et al.* in a recent DENV mutagenesis screen [94]. This would likely improve

transfection efficiency since the +ssRNA can directly initiate viral replication in the cytoplasm rather than requiring plasmid DNA entry into the nucleus as for DNA based expression systems. Further steps in preparation for the screen included determining the optimal treatment condition for IFN. As done previously for a relevant HCV mutagenesis screen using IFN selection, the IC_{50} was determined [274]. The IC_{50} value was found to be dependent on the duration of IFN pre-treatment, likely as a result of accumulation of antiviral proteins in response to IFN stimulation. A 6 h treatment at 4 U/mL of IFNα on Huh-7 cells was selected based on practical considerations for the screen.

After validating the screening conditions, mutant library preparation was attempted. Briefly this required two cloning steps. The first step involved random insertion of transposon cassettes into the ZIKV genome that were then selected for based on Kanamycin resistance. The second step was removal of the bulk transposon body, ligating together a 15 bp insert that would disrupt essential sequence elements in both coding and non-coding regions. We aimed to generate a library with between 250,000 to 1,000,000 individual mutants in order to provide adequate coverage of the 11 kb genome as reported by other groups with similar high throughput screening methods [94, 104, 274]. Unfortunately, due to widespread recombination in the library, it was deemed unfit for purpose. This brought the theoretical number of successfully mutated clones down to approximately 30,000 which was well below the required number. When transfected into HeLa cells the library failed to initiate efficient virus production, suggesting that the virus produced was from rare transfection events that would restrict mutant diversity in the screen.

When working with the ZIKV infectious clone recombination was a continuous barrier to ZIKV plasmid manipulation and propagation. This has been extensively documented with similar *Flavivirus* reverse genetics systems and is reviewed by Aubry *et al*. (2015) [17]. The fundamental problem that causes plasmid instability in bacteria is unanticipated expression of viral cDNA encoding products toxic to the bacterial host. This can occur from cryptic bacterial promoters within viral sequences or from mammalian promoters (CMV) and is less commonly seen with bacteriophage promoters (SP6 or T7) [17, 273]. Consequently, *Flavivirus* clones are often difficult to maintain in *E. coli* due to spontaneous recombination or acquiring stabilizing mutations [292]. Several strategies to limit this problem had already been employed with the pZIKV-ICD clone [350]. These included placing the viral cDNA in a low copy vector and the insertion of chimeric introns. These are only spliced out following transcription

in eukaryotic cells and therefore can disrupt toxic sequences in bacteria [17]. Considering the difficulty of stably cultivating the pZIKV-ICD clone in bacteria, other approaches could have been taken to limit recombination. This however, would have required a full restructure of the infectious clone and subsequent mutagenesis cloning strategy which was beyond the scope of this project aims and timeframe. One strategy could be to employ a bacteria free approach to generate a full-length clone. This would require splitting the viral cDNA into multiple vector backbones, limiting toxicity in bacteria of each individual plasmid. Then these plasmids would be separately cultivated and mutagenized. To reform the full viral sequence a Circular Polymerase Extension Reaction (CPER) could be used to PCR amplify and join each segment of viral cDNA, including a mammalian promoter directly upstream of the 5' UTR for transcription. This method has been applied successfully to ZIKV reverse genetics systems by Setoh *et al.* (2017) [311]. This protocol results in the generation of a circular DNA product that is then transfected into mammalian cells, initiating *de novo* virus production.

3.4 Conclusions

The aim of this chapter was to determine novel sequence elements in the ZIKV genome that confer IFN resistance. To address this aim it was intended that a high throughput random transposon mutagenesis approach would be applied to a ZIKV infectious clone reverse genetics system. The resultant mutant library was then to be subjected to selection in conditions with or without IFN and the impact of each mutation on IFN sensitivity was to be analysed by NGS. Unfortunately, due to the low number of functional mutant clones generated by the transposon mutagenesis approach the resultant mutant library did not adequately cover the full-length ZIKV genome at a depth appropriate for the screen. This occurred largely as a result of plasmid instability in *E.coli* that caused approximately 90% of recovered plasmid clones to have lost large fragments of DNA, rendering them non-functional. Therefore, a decision was made to adopt a related line of inquiry looking for mutations that confer IFN sensitivity in the closely related DENV as outlined in the following Chapter 4.

Chapter 4

Screening a DENV transposon mutant library to identify mutations that confer IFN sensitivity

4.1 Introduction

The type-I IFN response plays a crucial role in the host control and pathogenesis of DENV. Like ZIKV, DENV replication exposes dsRNA replication intermediates to detection by cytosolic RLR PRRs as detailed in the introduction (section 1.2.1) [214]. In addition to detection by RLR, DENV infection results in the release of mitochondrial DNA (mitoDNA) into the cytosol. This serves to activate the cyclic GMP–AMP synthase and stimulator of interferon genes (cGAS/STING) pathway [5]. Briefly, cytosolic DNA activates cGAS and leads to the generation of cyclic GMP–AMP that acts as a second messenger to activate STING. Both RLR and STING activation leads to downstream activation of TBK1 and IRF3 resulting in the production of IFN [232]. The involvement of multiple pathways in sensing DENV infection implies a critical importance of the IFN response in protecting against this viral pathogen. Like ZIKV, type-I IFNs significantly inhibit DENV replication and spread when cells are treated prior to infection [75]. This effect is mediated through the actions of ISGs upregulated in response to IFN. For example, members of the IFITM family disrupt early stages of the virus lifecycle [157] (virus entry and uncoating) or Viperin [141] and ISG20 [157] that inhibit later stage processes such as viral protein or RNA biosynthesis. To overcome this barrier to replication DENV has evolved strategies to circumvent IFN mediated antiviral immunity. As a pathogen of global concern, the ability of DENV to evade the IFN response has been extensively studied in the hope of discovering druggable targets to improve patient outcomes, as reviewed in [229] and [52]. However, most of these studies utilise overexpression of individual viral proteins and do not recapitulate the complex roles of these proteins within the virus lifecycle [167]. Strategies that DENV uses to evade the IFN response involve several NS proteins targeting multiple stages of the IFN production or signalling downstream of receptor binding and are discussed in depth in the Introduction. Briefly these strategies include, DENV NS2B mediated lysosomal degradation of cGAS [5], NS2A and NS4B mediated inhibition of TBK1 phosphorylation [65], DENV NS4B blockade of STAT1 phosphorylation downstream of IFNAR1/2 receptor activation

[235] and akin to ZIKV, DENV NS5 mediated STAT2 degradation [108]. Importantly, this NS5-mediated degradation only occurs in the context of the natural cleavage and processing of NS5 from the viral polyprotein. As a result, this activity cannot be recapitulated by NS5 overexpression alone [16]. The requirement for NS5 polyprotein processing for STAT2 degradation relies on recruitment of a pro-viral host factor UBR4, that preferentially binds to processed NS5 and facilitates STAT2 degradation [230]. The reliance of NS5 mediated STAT2 degradation on natural polyprotein cleavage is an important example demonstrating the benefit of a fully infectious system in discovery of viral evasion mechanisms. Utilizing a high-throughput mutational screening method applied to the entire full-length DENV genome has the potential to reveal novel evasion mechanisms previously undetected in overexpression studies. Additionally, this technique may assist in pinpointing specific genetic regions responsible for already known evasion strategies as identified in previous targeted mutational studies.

Previously, our laboratory developed a high-throughput random mutagenesis library of a cloned DENV serotype 2 viral genome using the MuA transposon mutagenesis approach described in the previous chapter [94]. This was created with the aim of mapping regions in the DENV2 genome that are tolerant to insertions in a fully infectious system. Briefly, the pFK-DVs infectious clone containing the full-length DENV2 genome under the control of bacteriophage SP6 promoter was subjected to MuA transposon mutagenesis resulting in a library of ~250,000 mutant clones [94]. From this library, full-length *in vitro* transcribed RNA was generated and transfected into Huh-7.5 cells to initiate *de novo* virus production. The infectious virus produced from the RNA transfection was subjected to two subsequent rounds of passaging on naive Huh-7.5 cells. This enriched for mutants that were replication-competent and able to generate infectious virus. After selection, the relative fitness of the remaining mutants was determined with respect to the input virus pool. This was done by isolating intracellular RNA, subjecting the RNA to first-strand cDNA synthesis using a DENV2 specific reverse primer, PCR amplifying across the full-length DENV genome and performing NGS sequencing to detect the location of the 15 bp transposon insertion scars within the DENV genome. Mapping the individual transposon insertions to their position within the DENV genome allowed an assessment of their frequency within the remaining virus population compared to the input library. This map of relative insertion frequencies in the DENV genome was used to identify regions highly tolerant to insertions (regions of genetic

flexibility) and led to the rational design of tagged viruses for rapid and simple detection of DENV infection levels for a variety of purposes. Supernatant from the final passage contained a pool of mutant viruses that were replication-competent and able to generate infectious virus in the Huh-7.5 cell line. The aim of this chapter was to repurpose this library of replication-competent and infectious insertion mutant viruses, further selecting these based on their differing ability to support the full virus lifecycle either in the presence or absence of type-I IFN. This was coupled with NGS to pinpoint regions of the DENV genome that are key for IFN evasion. Mutations discovered to impact on DENV mediated IFN evasion were individually assessed and their mechanism of action defined.

4.2 Results

4.2.1 Optimisation of screening conditions

In a similar approach to chapter 3, the IC_{50} value for IFNα treatment against DENV infection at a low MOI was determined for use in the screen. Huh-7.5 cells were treated with increasing concentrations of IFNα for 6h prior to infection with DENV2 at MOI 0.2. Approximately 24 h post IFN treatment, the virus inoculum in each well was removed and replaced with fresh media containing IFNα or left untreated as required. 48 hpi supernatants were collected to enumerate the level of infectious virus in the supernatant by focus forming assay. Raw FFU/mL values were then normalised to the average of the untreated control (maximum infection) and transformed to a percentage of maximum. These normalised values were then used to determine the IC_{50} by non-linear regression analysis using the [inhibitor] vs normalised response model of GraphPad Prism v8. The data represented in Figure 4.1 are a result of two independent experiments. From the curve the IC_{50} for DENV2 was calculated to be approximately 1 U/mL of IFNα. This coincides with expected results based on the reported IC_{50} of IFNα against the related virus HCV (1 U/mL) that was also determined using the Huh-7.5 cell line [274]. In addition, the DENV IC_{50} closely resembled the IC_{50} for ZIKV (4 U/mL) determined in the previous chapter using the related Huh-7 cells. Following determination of the IC_{50} of IFNα against DENV, NGS-dependent screening of the impact of transposon insertions on IFN sensitivity was undertaken.

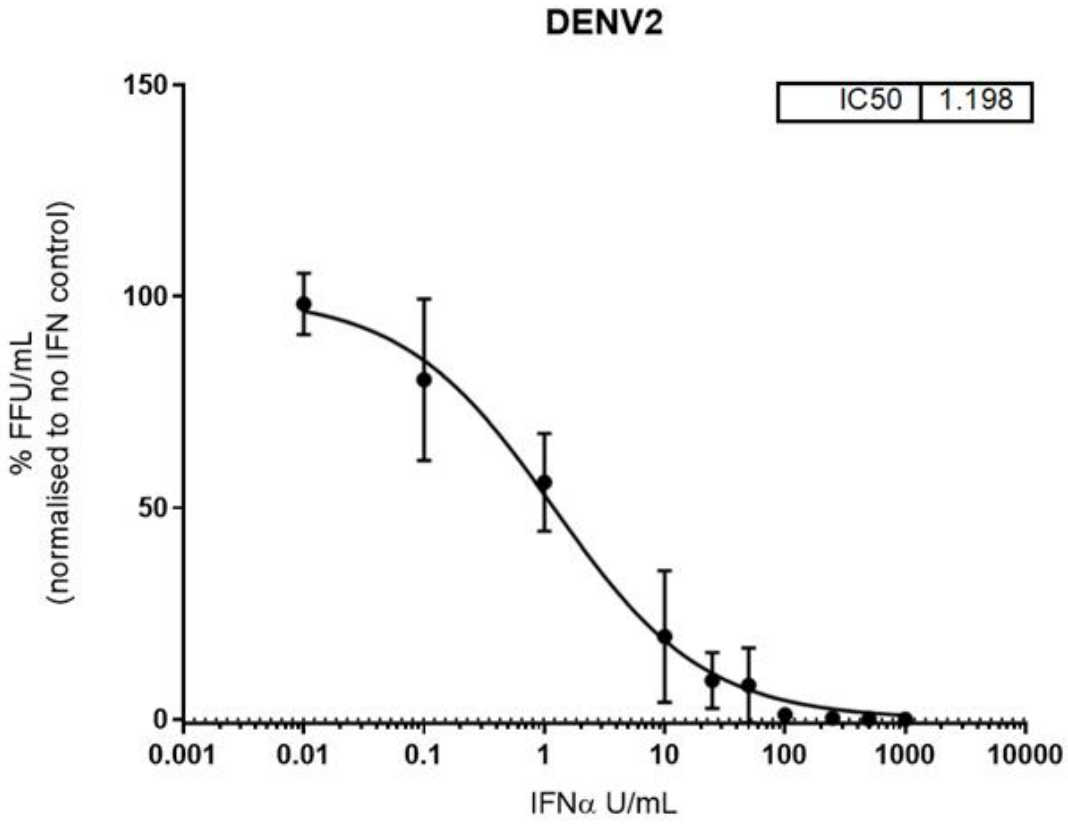

Figure 4.1: Determination of the IC_{50} concentration of IFNα treatment against DENV infection. Huh7.5 cells were treated with increasing concentrations of IFNα for 6h prior to infection with DENV2 at an MOI of 0.2. After overnight inoculation, the inoculation media was replaced with fresh media containing the appropriate concentration of IFNα. 48 h post-infection supernatants were collected to quantify the levels of infectious virus in supernatant by focus forming assay. Data is represented as % FFU/mL normalised to the maximum and minimum inhibitory concentrations of IFNα treatment.. This data is a result of two independent experiments and is represented as means +/- s.d.

4.2.2 Recovery of the DENV2 insertion library

Figure 4.2 shows the passaging strategy used for the screen. First, to repurpose the insertion library it was necessary to recover the frozen supernatant from passage 2 of the previous screen that was generated by passaging on untreated Huh7.5 cells (see Figure 2a). The library had been stored in a single 40 mL aliquot of unknown titer and therefore resuscitation of the library relied on estimated infection rates for the initial passage (passage 0). This estimate was based on the passaging strategy employed by Eyre *et al.* where viral supernatants were diluted 1:1 with fresh media between passages [94]. As detailed in the Materials and Methods (section 2.3) the DENV mutant library was recovered from frozen stock (Passage 0). Briefly, this was done by pre-treating Huh-7.5 cells either with media containing IFNα at 1 U/mL or leaving them untreated for 6h prior to inoculation with the defrosted DENV mutant library diluted 1:1 with fresh media before returning to culture. On the same day, without additional freeze-thaws, 10-fold serial dilutions of the mutant virus stock were procured for determination (in triplicate) of infectious virus via focus forming assay, enabling the retrospective titration of the stock. Approximately 24 h post IFN treatment, virus inoculum on each flask was removed and replaced with fresh media containing IFNα at 1 U/mL or untreated media as appropriate. After 72 hpi a focus forming assay performed in parallel was used to retrospectively determine the titer of virus and resultant MOI for passage 0. Surprisingly, the virus titer was higher than anticipated at approximately ~3x 10^6 FFU/mL. This meant that the MOI calculated retrospectively for this passage was 30 times greater (MOI = 6) than intended based on the IFNα IC_{50} assay optimized for an MOI of 0.2. As a result of this high rate of infection the viral supernatant from each replicate was harvested at this time to minimize the impact of unwanted cytopathic effects on the screen. Supernatant from each replicate was independently collected and a smaller volume aliquoted for quantification of infectious virus. For subsequent passages (passage 1 and 2, see Figure 4.2) this allowed the titer of each replicate to be determined by FFA prior to inoculation onto naïve cells. Once the titer of infectious virus in the supernatant was determined from each replicate they were diluted to the appropriate concentration for the next passage. Then, naive Huh-7.5 cells were treated with or without IFNα for 6h and inoculated with DENV mutant virus at an MOI of 0.2. Each treatment group and replicate were maintained independently of one another without pooling supernatants. This process was then repeated for an additional round of selection. After each passage total RNA was harvested from the infected cell monolayer and at the same

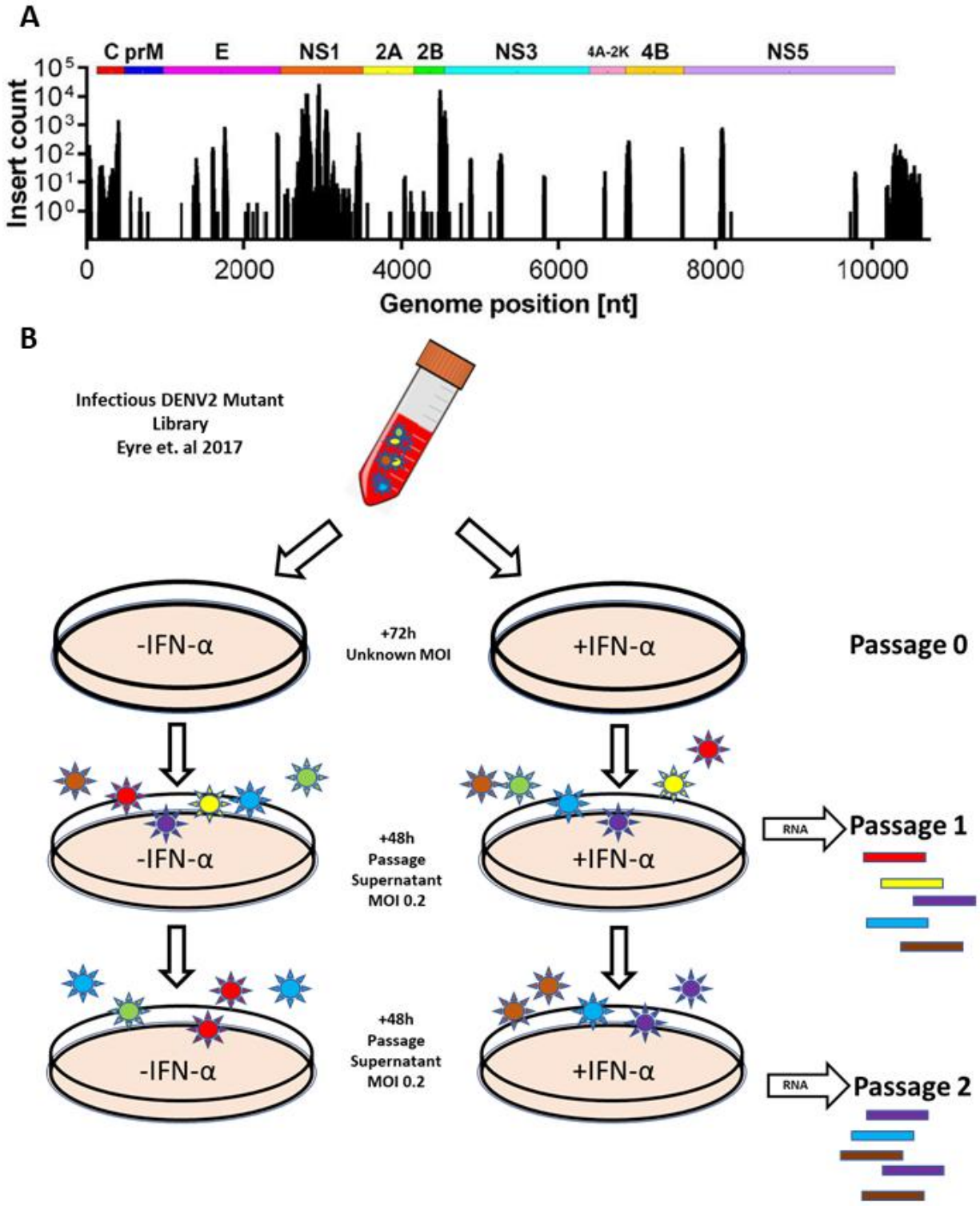

Figure 4.2: Re-purposing the DENV2 MuA mutant library to identify mutations that alter DENV IFN evasion. A) Graphic representation of the position and frequency of insertion mutations following pre-selection for replication competence and infectious virus production in the original mutant library . B) The passaging strategy for recovery of the frozen mutant library to select for loss of fitness mutations in the presence of type-I IFN. This figure was partially adapted from [94].

time supernatants were taken. The excess supernatant and the total RNA were aliquoted and stored at -80^{o}C for later processing.

Alongside passage 1 and 2, small scale replicates in 96 well plates were treated and infected in parallel to monitor the rate of infection by detection of infected cells expressing the DENV E-protein prior to harvesting the supernatant at 48 hpi for the next passage. On the morning of the second day post infection, these parallel replicates were fixed and stained with 4G2 IgG anti-*Flavivirus* E primary antibody and fluorescent secondary (red). Figures 4.3d shows representative images for each replicate highlighting the extent of DENV infection amongst the cells of each passage on the morning prior to harvesting the supernatants. As expected, IFNα pre-treatment resulted in a lower rate of infection in both passages as indicated by less frequent detection of E-protein positive cells (Figure 4.3d). Interestingly, despite inoculating with the same MOI for both passages the spread of infection appears greater in passage 2 compared to passage 1 at the same time post infection. In passage 1, DENV infection resulted in clustered foci of infected cells. Conversely, passage 2 resulted in extensive and uniform spread of infection that was no longer clearly defined in distinct clusters. This likely demonstrates enhanced cell-to-cell spread of the selected virus between the passages. The reduced level of infection in the presence of IFNα pre-treatment and the enhanced replication fitness comparing virus from passage 1 and indicated that the screening process was successful in applying selective pressure upon the genetic diversity of the DENV mutant virus populations and validated continuation of the screening process.

In addition to monitoring infection rate by immunofluorescent detection of E protein positive cells, the level of infectious virus present in supernatant was quantified by focus forming assay between each passage. Figure 4.3a shows that for passage 0 there was no detectable difference in the amount of infectious virus determined by focus forming assay in the treated and untreated groups. This indicated the IFN concentration used (1 U/mL) did not provide adequate selective pressure to the virus library in this initial passage. It was inferred that this was a result of the high MOI (MOI = 30) used to infect cells of this passage therefore causing the IFN pathway to be overwhelmed by virus mediated evasion. In contrast, after equalizing the MOI to 0.2 in Passage 1 and treating with the same amount of IFN, the amount of infectious virus detected in the supernatant was reduced by approximately 50% at 48 hpi (Figure 4.3b). This coincided with the expected result based on the IC_{50} assay and validated that the concentration of IFNα used provided adequate selective pressure upon the pooled

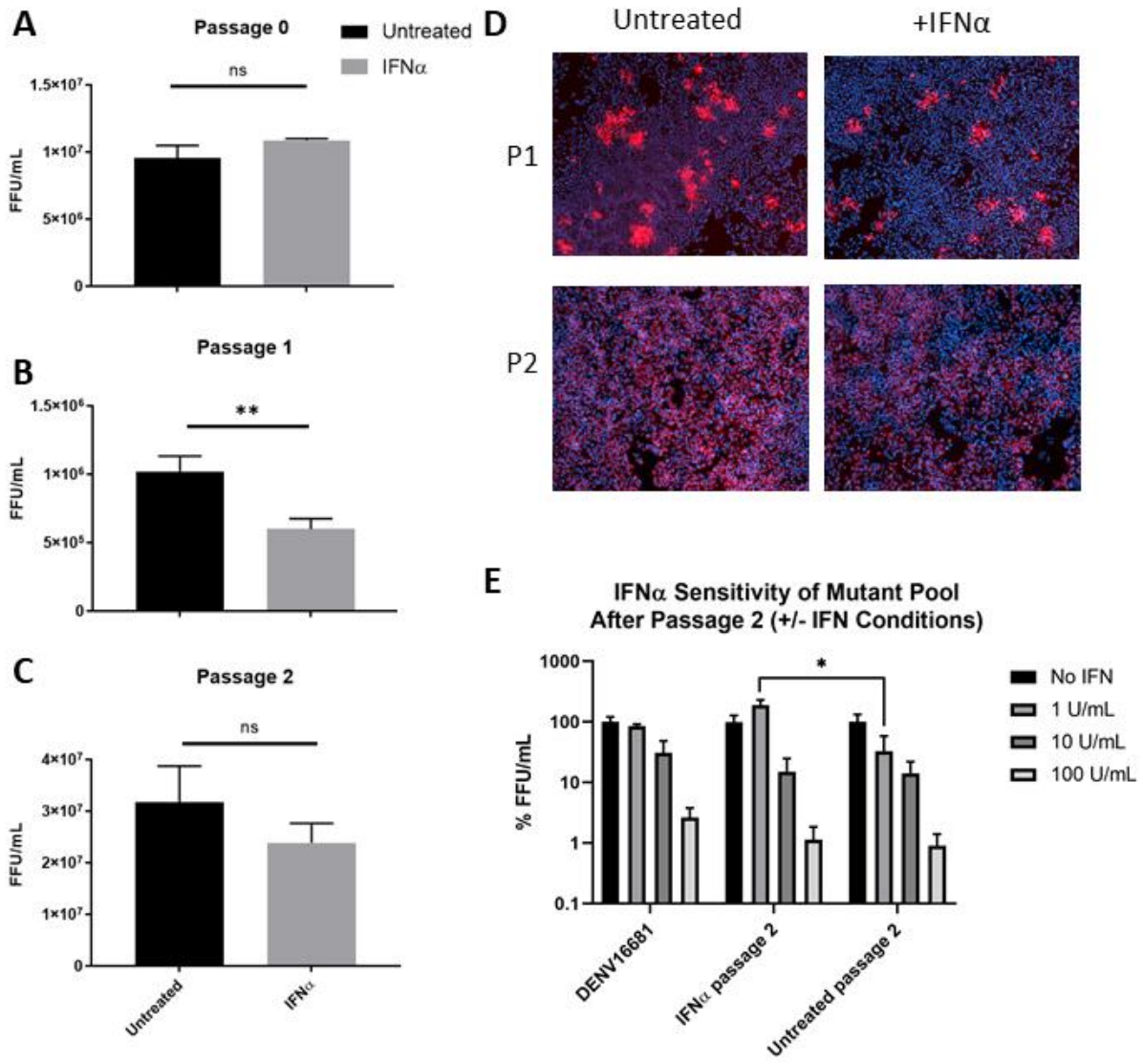

Figure 4.3: IFN selection of the DENV mutant library. A, B & C) Following each passage of the screen, cell supernatants were harvested from both treatment conditions (+/- IFNα) in triplicate. An aliquot of each replicate was titrated using focus forming assay to determine the level of infectious virus in the supernatant of each sample. This titer was then used to determine the appropriate inoculum for the subsequent passage (MOI = 0.2). Statistics are by two-tailed T-test (* $P < 0.05$, ** $P < 0.01$). D) Immunofluorescent detection of E-protein positive cells in parallel conditions to screening passages 1 and 2. E) Huh-7.5 cells were pre-treated with the indicated concentration of IFNα for 6h prior to overnight inoculation with either the pooled virus population of IFNα passage 2, pooled population of untreated passage 2 or the parent DENV strain. After overnight inoculation the inoculum was replaced with fresh treatment media. Then, at 48 hpi supernatants were collected and the levels of infectious virus in supernatants were quantified by focus forming assay. Statistics are performed using an ordinary Two-Way ANOVA (* $P < 0.05$, ** $P < 0.01$) all other comparisons are non-significant). Data are presented as means +/- s.d.

virus population. Interestingly, after repeating this process for passage 2, Figure 4.3c shows that the mean level of infectious virus from each treatment group was reduced by only ~25% under IFNα treated conditions (mean untreated = 3.2 x 10^7 FFU/mL vs IFNα treated 2.4 x 10^7 FFU/mL). The difference between the means were not statistically significant comparing the IFNα and untreated samples in this passage. This data indicated a shift in the population genetics of the selected mutant virus pool compared to the input mutant pool towards IFN resistance. This was likely due to IFN hypersensitive mutations being selected out of the pool because of passaging in the presence of IFN. This quantifiable data agrees with the estimated observed rate of infection by immunofluorescence comparing untreated cells to IFNα treated cells as seen in Figure 4.3d. In addition to the expected selection pressure applied by IFNα treatment, the titer of infectious virus recovered in supernatant after 48h was higher in passage 2 compared to passage 1 for both the treated and untreated conditions (see Figure 4.3b compared to 4.3c). Again, this agreed with the observed rate of infection by immunofluorescence comparing untreated cells to IFNα treated cells as seen in Figure 4.3d. In combination this data indicated that the virus population was better adapted to replication in the Huh-7.5 cell line after multiple passages on the same cell type. The impact on selective adaptation to the Huh-7.5 cell-line was not further investigated as it was assumed to have equal impact on IFNα treated and untreated conditions.

To investigate whether passaging the pooled mutant library in the presence of IFNα had resulted in adaptation of the population to these conditions, an IFN sensitivity assay was performed. The pooled mutant virus generated after passage 2 from untreated or IFNα treated groups were used to inoculate Huh-7.5 cells (MOI = 0.2) pre-treated for 6h with increasing concentrations of IFNα. At 48 hpi, supernatants were collected and virus titer determined by FFA. Figure 4.3e shows that the IFNα treated virus pool was significantly more resistant to IFN at the concentration of IFN used in the screen (1 U/mL IFNα). Importantly this data confirmed the successful selection of the mutant virus population of virus after IFN passaging. Interestingly, this effect was not observed when higher concentrations of IFNα were applied. This may reflect the ability of IFN to activate expression of different virus-controlling genes at higher concentrations. These genes, termed “tuneable” ISGs, have a higher threshold for promoter activation and as a result only are activated by high concentrations of IFN [352]. This may mean that the mutant library was selected for based on a set of genes expressed at 1 U/mL but not for genes that require higher concentrations of

IFN for activation. This data indicated the mutant library had successfully undergone selection based on its sensitivity to IFNα at the concentration used in the screen.

4.2.3 Sample preparation and NGS analysis

Once the passaging and selection under IFNα conditions were complete, the diversity and frequency of remaining DENV mutant genomes after selection was determined. Briefly this was achieved by extracting the total RNA from the cell monolayers of each passage and performing DENV specific RT-PCR to prepare each sample for NGS sequencing. Since Passage 0 showed no sign of IFN selection pressure this was excluded from the NGS analysis.

Figure 4.4a shows the processing pipeline. Briefly, total RNA was extracted separately from each replicate in passage 1 and 2. Then this was used in a first strand cDNA synthesis reaction using a reverse primer that was complementary to the extreme 3' terminus of the DENV2 UTR in order to amplify the full-length genome using a high-fidelity RT-DNA polymerase as described in methods section 2.1.6.2. Next, full-length DENV cDNA from each replicate was used as a template to PCR amplify 6 overlapping fragments covering the entire length of the DENV genome. Each PCR product was gel-extracted, purified, quantified, and pooled in equimolar ratios for each independent replicate. These samples were then shipped to collaborators (R. Bull, UNSW) for NGS library preparation (Nextera XT Illumina) and sequencing on the NextSeq500 platform. Each sample was analysed as an independent replicate and these had on average 27 million reads per sample (Figure 4.4b). Of these total reads, ~44 thousand mutant insertion events were detected on average for each sample (Figure 4.4c). These individual insertion events were assigned to their nucleotide position based on the surrounding sequence alignment to the DENV2 genome. The analysis method used to convert raw insert counts at each nucleotide position into a measure of IFN sensitivity is described here in brief. First, to enable relative frequencies of insertions to be calculated, even in instances where insertion events were not measurable in the virus pools, 1 insert count was added for each nucleotide position, increasing the baseline in an even manner. Then, to remove bias of a 'global' reduction in insert counts in the independent replicates the insert frequency at each nucleotide position was divided by the total number of insert counts at all nucleotide positions in that replicate. This essentially gave a percentage or raw frequency of insertion at each position in the genome. To generate the graph of IFN sensitivity, the corresponding triplicates were averaged. Then the average frequency of

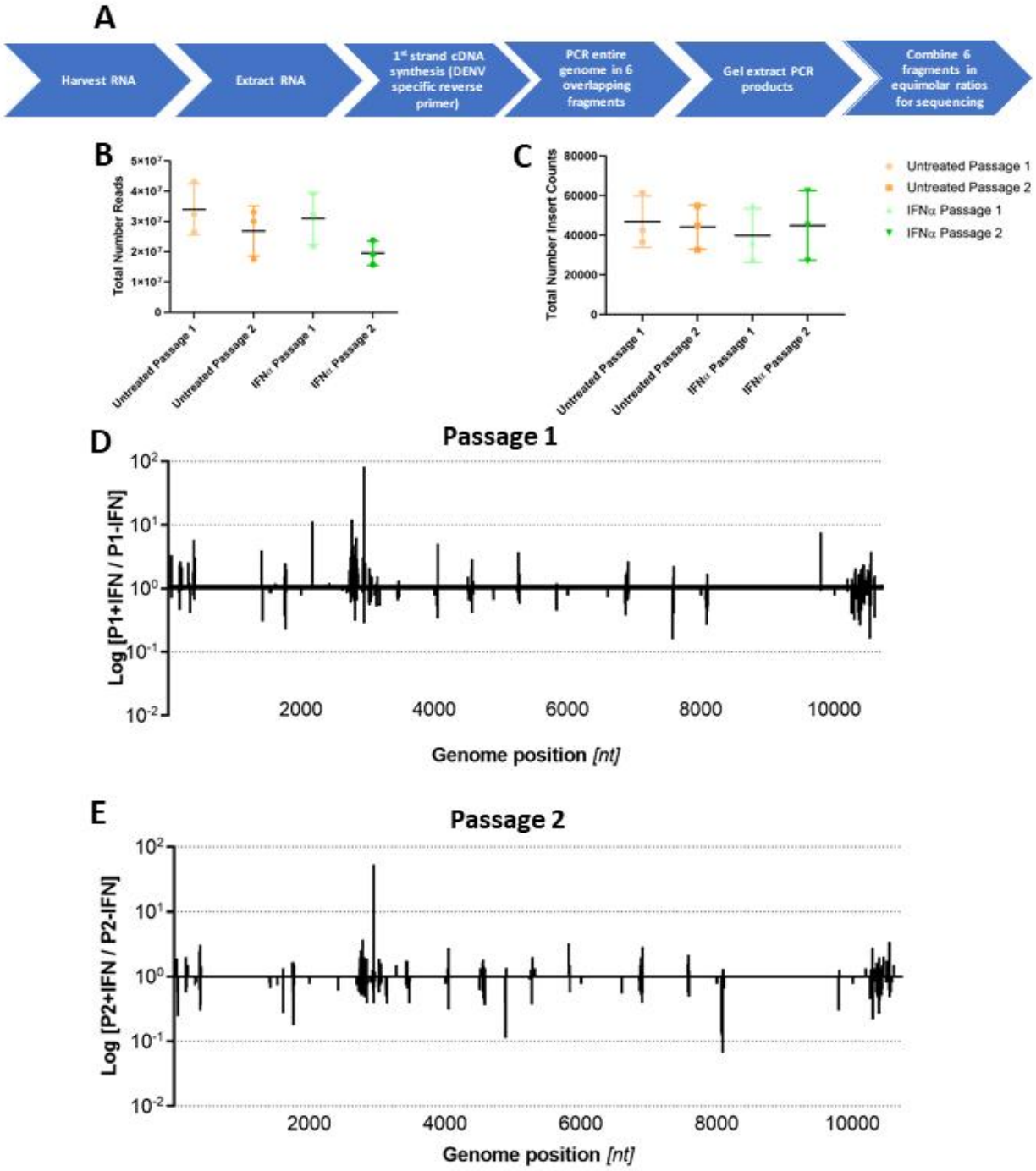

Figure 4.4: Next generation sequencing of the selected DENV mutant library. A) RNA processing pipe-line prior to NGS sequencing to determine insertion location and frequency. The total number of reads B) or insertion events detected C) in each sample group by NGS analysis. D & E) The ratio of insertion frequencies at each nucleotide position between IFNα treated to untreated replicates for passage 1 and 2 respectively. Values below the line indicate positions of inserts that potentially contribute to increased IFN sensitivity.

insertion in IFNα passages were divided by the average frequency of insertion in the untreated passages. These frequency ratios were then log10 transformed and data was represented as Log10[IFNα/untreated] for each passage 1 and passage 2 in Figure 4.4d and 4.4e respectively. Essentially, this means that if an insert at any given genome position were selected against in IFN conditions this resulted in log10 values represented by bars below the line. Figures 4.4d and 4.4e show the overall pattern of insertions that are differentially selected in untreated compared to IFN treated conditions across the genome by nucleotide position. This revealed a spread of insertions with differing frequencies between the treatment groups throughout the genome in both translated and untranslated regions. Some of these regions clustered into peaks, implying similar functional effects of closely positioned insertion mutations at these locations. In addition to regions negatively selected in IFN conditions there were also regions in which insertion mutations were enriched under IFN treatment, suggesting a selective advantage over other mutants in the pool. This could reflect the relative fitness compared to other mutants and as such may not reflect a gain in fitness compared to wildtype DENV. Since this sequencing does not detect the presence of wildtype virus the contribution of wildtype virus to the pool cannot be determined using this analysis method. Importantly, there appears to be a narrowing of peaks, an overall trend for a greater proportion of the peaks to exist below log 0, and for peaks to reach stronger negative log powers in passage 2 compared to passage 1. In combination, this implied additional selection between the two passages, further validating the selection conditions. Figure 4.5 shows selected zoomed regions from passage 2 that contained the 10 insertions that were most strongly selected against in the presence of IFN. Sequence specific information for each of these insertion mutations is given in Table 1 Appendix V. These regions were in the 5' UTR, E, NS3, NS5 and the 3' UTR. In addition, the NS1 region also contained a peak existing above the line that was of interest. Importantly, 3 peaks that were most strongly selected against in the presence of IFN were clustered at positions 8069, 8077 and 8086. These all fell within the DENV NS5 protein which is known to be an important effector in DENV mediated shutdown of the IFN signalling pathway [213].

The overall pattern and specific location of inserts in passage 2 compared to passage 1 demonstrated the selection process occurred as expected. This was further validated by detecting multiple insertions that were most strongly selected against in the presence of IFN

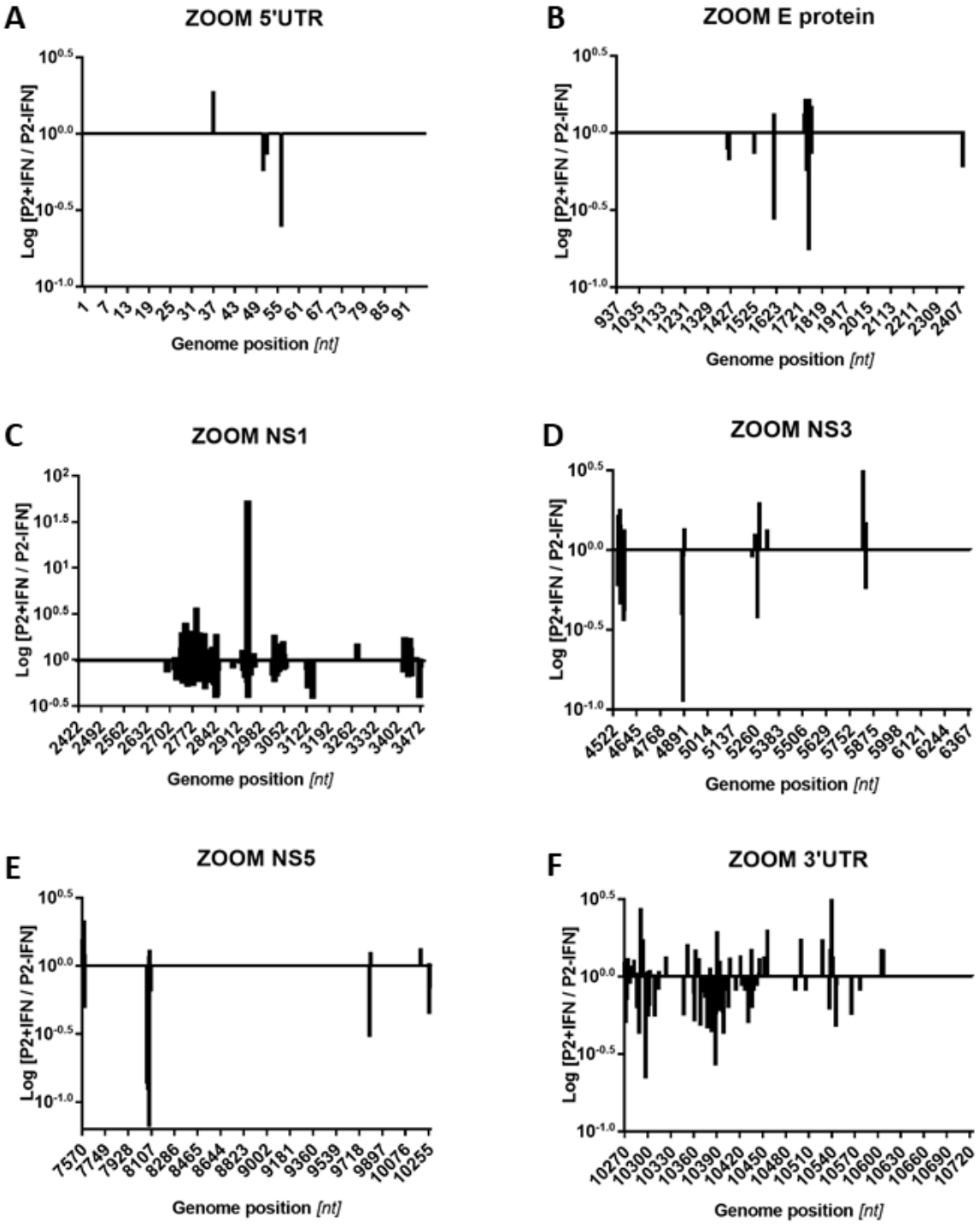

Figure 4.5: Zoomed insets of specific regions of interest from passage 2. A) 5' UTR, B) E-protein, C) NS1, D) NS3, E) NS5, F) 3' UTR.

clustering within NS5, a known IFN evasion mediator. This meant that further characterization of insertions was viable.

4.2.4 Identification of mutants that are likely to enhance DENV IFN sensitivity

To statistically analyse the difference in insert frequency between the IFN treated and untreated group, the % insertion frequencies for each independent replicate were graphed for the insertions that were most strongly selected against in IFN conditions. We also compared the frequency of insertions as a percentage between passages 1 and 2, to identify evidence of consistent and increasing selection between the passages. Figure 4.6a shows a single insertion at nucleotide position 8086 within NS5 that was statistically significantly different between the two treatments in passage 1. Interestingly, although position 8086 was the most strongly selected against in both passage 1 and 2, the difference between the two treatments was not statistically significant in passage 2. Figure 4.6b shows that two alternative insertion events within NS5 at nucleotide positions 8077, 8069 and one peak in the 3' UTR at position 10,297 were statistically significantly different between the two treatment conditions in passage 2. The strongly enriched for insertion at position 2941 within NS1 was not statistically significant between treatment groups despite having the largest difference between means. This data indicated increasing negative selection between passage 1 and passage 2. Furthermore, this data highlights NS5 at positions between 8069 to 8086 as a likely genomic region that contributes towards IFN evasion. Due to the large variance in between the triplicates, additional replicates or a repeat screen would have been ideal to confirm these findings.

4.2.5 Cloning individual mutations into the full-length DENV genome

After selecting a panel of potential hits from the screen, the next step was to confirm the IFNα sensitization phenotype of each mutation by individually cloning these mutations into a DENV infectious clone (pFK-DVs) and then to test these individual mutations for IFN sensitivity. To achieve this aim, synthetic dsDNA constructs containing the desired mutations within the DENV genome sequence were purchased (GeneWorks). These fragments contained the 15 bp insertion mutation at nucleotide positions 1610 and 1760 within E, 2941 within NS1, 4884 within NS3, 8069, 8077 and 8086 within N-terminus of NS5 and 9795, 10297 and 10388 within the C-terminal region of NS5 or the 3'UTR (see Appendix V). Whenever possible these

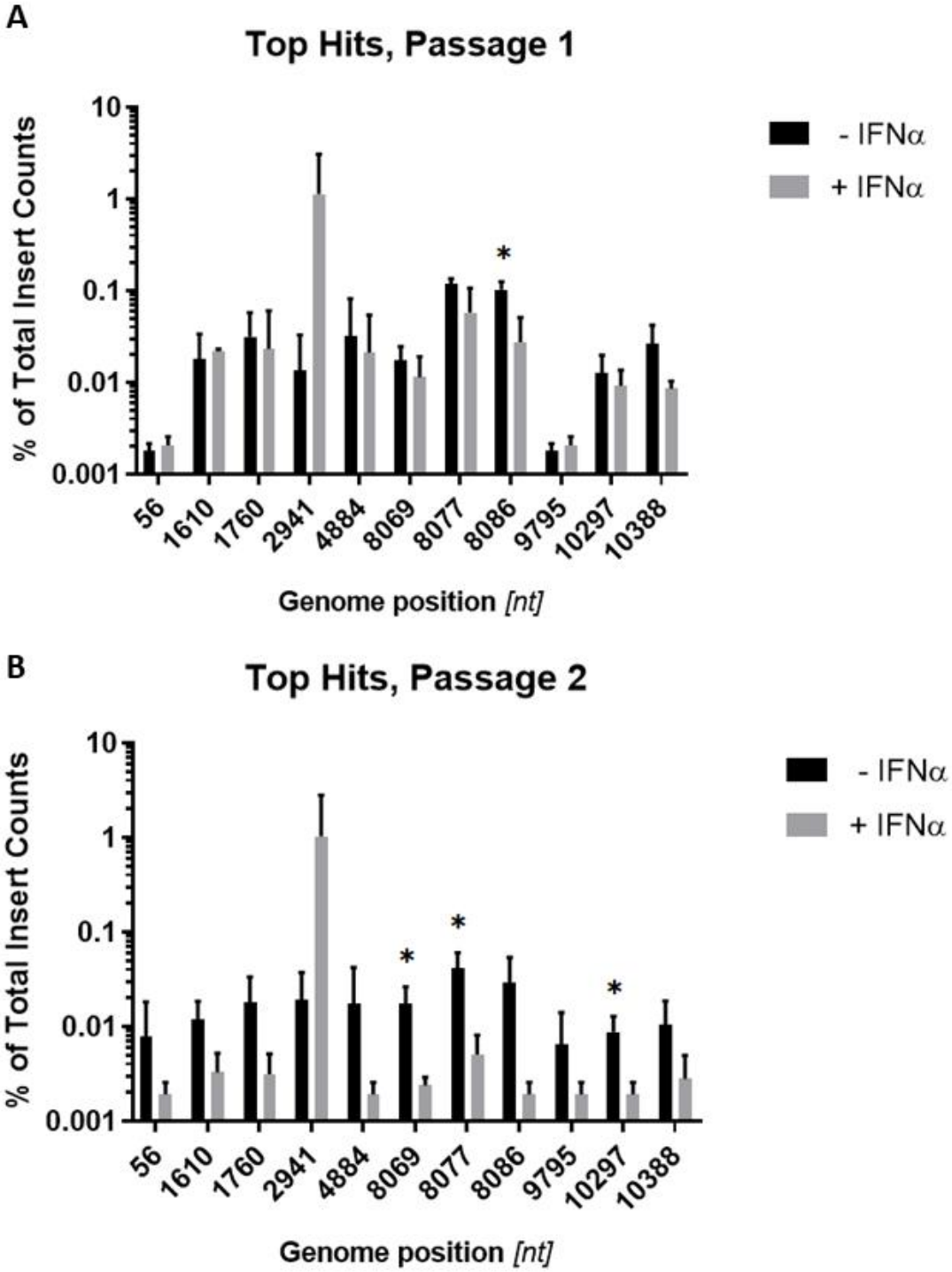

Figure 4.6: Statistical analysis of the top hits for IFN hypersensitive mutations as determined by NGS. A & B) The raw insertion frequencies for peaks of interest in each triplicate to determine statistical significance in passage 1 and 2, respectively. Statistical analysis was performed by independent two-tailed T-test, (* $P < 0.05$). Data are presented as means +/- s.d.

constructs were designed to exploit pre-existing unique restriction (natural restriction) sites within the DENV2 genome. However, for the N-terminal NS5 (NS5) mutations and the C-terminal NS5/3'UTR (UTR) mutations, the large distance between naturally occurring unique restriction sites necessitated the introduction of synthetic mutations to generate unique restriction sites. For this reason, a larger region between naturally occurring unique restriction sites was selected to be synthesized within a sequenced pUC57 intermediate cloning plasmid. Within each of these plasmids (pUC-57-BmtI-AvrII-NS5-silents, and pUC-57-AvrII-XbaI-UTR-silents) two restriction sites flanking the 15 bp insertion region were generated using synthetic mutations that maintained the amino acid sequence within the translated region. It was necessary to include one synthetic mutation within the 3'UTR, in this case only a single nucleotide was altered to minimize the impact of alterations the sequence. In addition, data from the transposon insertion screen by Eyre *et al.* indicated this region as being highly tolerant to insertions, hence implying its genetic flexibility and further supporting that changes to sequence within this region of the 3'UTR can be accommodated in an infectious system [94]. Diagrammatic representations of the pFK-DVs plasmid showing natural restriction sites, the intermediate cloning pUC57 plasmids and the structure of the synthetic dsDNA mutant fragments with specific restriction sites are given in Appendix V.

To clone the individual mutants the first step was to insert each NS5 or UTR mutation into their respective pUC57 intermediate cloning vector, the methods used to achieve this goal are summarised in Table 4.1. Initially, attempts were made to complete this task by simple restriction enzyme cloning methods. Briefly, both the plasmid and the insert were digested with the indicated restriction enzymes. The inserts were column purified and the vector backbone was gel-extracted and purified. Then, T4 DNA ligase was used in an overnight ligation prior to transformation. This process was successful for sub-cloning insertion mutations at nucleotide positions 8069, 9795, 10297 and 10388. Alternatively, when restriction cloning was unsuccessful after the second attempt (8077 and 8086), Gibson Assembly was used with the primer sequences shown in Appendix I. Each clone was confirmed by diagnostic restriction digest (not shown) and by Sanger sequencing to ensure there were no sequence errors in the synthetic dsDNA fragment prior to performing large scale plasmid purification.

The next step was to subclone the individual insertion mutations into the pFK-DVs destination vector, the methods used to achieve this goal are summarised in Table 4.2. Restriction cloning

Table 4.1: Summary of methods used to subclone insertion mutations with synthetic restriction sites into the respective pUC57 intermediate vectors

Mutation Insert Position	pUC-57 Plasmid Intermediate (NS5/UTR)	Silent Restriction Sites	Restriction Cloning Attempt? (Yes/No)	Restriction Cloning Success? (Yes/No)	Gibson Cloning Attempt? (Yes/No)	Gibson Cloning Success? (Yes/No)
8069	NS5	*PstI/ClaI*	Yes	Yes	-	-
8077	NS5	*PstI/ClaI*	Yes	No	Yes	Yes
8086	NS5	*PstI/ClaI*	Yes	No	Yes	Yes
9795	UTR	*AcsI/BsiWI*	Yes	Yes	-	-
10297	UTR	*AcsI/BsiWI*	Yes	Yes	-	-
10388	UTR	*AcsI/BsiWI*	Yes	Yes	-	-

Table 4.2: Summary of methods used to subclone insertion mutations (either directly from a synthetic dsDNA fragment or from the pUC57 intermediate vector) into the pFK-DVs destination vector

Mutation Insert position OR Wildtype silent mutation	Cloning from G-block OR pUC57 Intermediate Plasmid	Unique Restriction Sites	Restriction Cloning Attempt? (Yes/No)	Restriction Cloning Success? (Yes/No)	Gibson Cloning Attempt? (Yes/No)	Gibson Cloning Success? (Yes/No)
1610	G-block	*SphI/BamHI*	Yes	Yes	-	-
1760	G-block	*SphI/BamHI*	Yes	Yes	-	-
2941	G-block	*MluI/KasI*	Yes	Yes	-	-
4884	G-block	*NsiI/XhoI*	Yes	Yes	-	-
UTR-WT-s.m	pUC57-UTR	*AvrII/XbaI*	Yes	No	Yes	Yes
9795	pUC57-UTR	*AvrII/XbaI*	No	-	Yes	Yes
10297	pUC57-UTR	*AvrII/XbaI*	No	-	Yes	Yes
10388	pUC57-UTR	*AvrII/XbaI*	No	-	Yes	Yes
NS5-WT-s.m	pUC57-NS5	*BmtI/AvrII*	Yes	No	Yes	Yes
8069	pUC57-NS5	*BmtI/AvrII*	No	-	Yes	Yes
8077	pUC57-NS5	*BmtI/AvrII*	No	-	Yes	Yes
8086	pUC57-NS5	*BmtI/AvrII*	No	-	Yes	Yes

was successful for all synthetic dsDNA fragments directly cloned into pFK-DVs. On the other hand, restriction enzyme subcloning between the pUC57 intermediate vector and pFK-DVs was not successful and instead the Gibson Assembly method was used. This method successfully generated the remaining pFK-DVs individual mutant clones, which were confirmed by diagnostic restriction digest (not shown) and Sanger sequencing prior to large scale DNA preparation. The resulting plasmid DNA was compared to the parent pFK-DVs plasmid by diagnostic restriction digest (see Figure 4.7a-g) to rule out any bacterial recombination following transformation and outgrowth that is regularly observed when transforming this infectious clone system.

4.2.6 Testing the replication kinetics of the individual DENV mutants

After successfully generating the plasmid clones of each individual mutant it was then necessary to produce a working stock of each virus mutant, test each mutant for viability and assess their replication fitness compared to the parent virus strain. To perform this task, *in vitro* transcribed RNA was generated from each plasmid of the mutant, corresponding wildtype (synthetic mutation) and the original pFK-DVs parent plasmid. A portion of purified *in vitro* transcribed RNA generated from each plasmid was separated on a non-denaturing 1 % agarose gel and visualised to confirm the quality of the RNA. Appendix V shows that each mutant clone generated high quality *in vitro* transcribed RNA that was indistinguishable in appearance to that of the parent (pFK-DVs) transcribed RNA indicating that full-length product had been generated. In addition, this RNA appeared as a single defined band on the gel indicating that it was not degraded or fragmented by the purification process.

Once the quality of the RNA was confirmed it was then transfected in biological duplicates into Huh-7.5 cells (see Materials and Methods section 2.3.6). Each mutant cohort was transfected concurrently along with the DENV2 RNA generated from the parent pFK-DVs plasmid, a mock transfection control and a wildtype (synthetic mutant) RNA when appropriate.

Following RNA transfection, samples of culture supernatant were collected at 24 h intervals for a one-week period and stored at -80^{o}C. At 72 hpt confluent cells were split and re-seeded diluted 1:1 with fresh media. Concurrently, a fraction of the transfected cells was seeded for immunofluorescence-based analysis of the rate of transfection/infection at 72 hpt (96 well trays) and collection of working virus stocks (25 cm^2 flask) at 4-5 days post-transfection. These

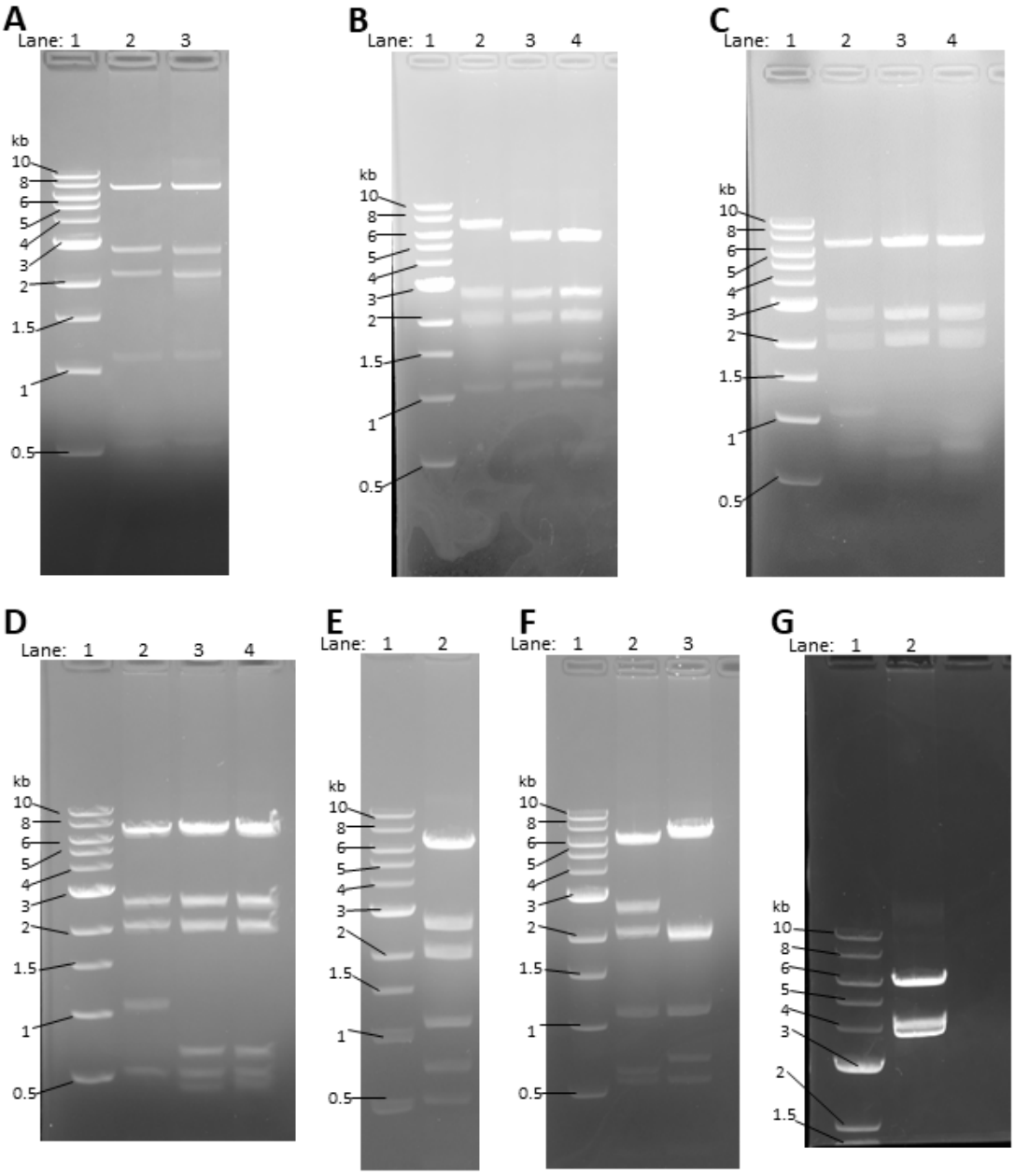

Figure 4.7: 1% Agarose gel-electrophoresis for visualisation of diagnostic restriction digests performed for each final preparation of pFK-DVs parent, Wildtype synthetic mutation (WT-s.m) or insertion mutant plasmid. **A)** Lane 1: 1 kb ladder, Lane 2: pFK-DVs-UTR-WT-s.m digested with *EcoRI*, Lane 3: pFK-DVs-9795 digested with *EcoRI*. **B)** Lane 1: 1 kb ladder, Lane 2: pFK-DVs digested with *EcoRI* and *NotI* (non-cutter), Lane 3: pFK-DVs-10297 digested with *EcoRI* and *NotI*, Lane 4: pFK-DVs-10388 digested with *EcoRI* and *NotI*. **C)** Lane 1: 1 kb ladder, Lane 2: pFK-DVs digested with *EcoRI, NotI* and *ClaI* (non-cutters), Lane 3: pFK-DVs-NS5-WT-s.m digested with *EcoRI* and *ClaI*, Lane 4: pFK-DVs-10388 digested with *EcoRI* and *NotI*. **D)** Lane 1: 1 kb ladder, Lane 2: pFK-DVs digested with *EcoRI* and *NotI* (non-cutter), Lane 3: pFK-DVs-8077 digested with *EcoRI* and *NotI*, Lane 4: pFK-DVs-8086 digested with *EcoRI* and *NotI*. **E)** Lane 1: 1 kb ladder, Lane 2: pFK-DVs-1610 digested with *EcoRI* and *NotI*. **F)** Lane 1: 1 kb ladder, Lane 2: pFK-DVs-1760 digested with *EcoRI* and *NotI* , Lane 3: pFK-DVs-4884 digested with *EcoRI* and *NotI*. **G)** Lane 1: 1 kb ladder, Lane 2: pFK-DVs-2941 digested with *NotI, NheI* and *XbaI*. All banding patterns were assessed in comparison to predicted digest patterns using SnapGene Simulate Agarose Gel function.

working stocks of *de novo* generated virus were used in subsequent experiments for IFN sensitivity. Culture supernatant samples were used to determine the level of infectious virus generated at each time point by focus forming assay. Results from these assays are presented in Figures 4.8, 4.9 and 4.10 below and are representative of two independent experiments.

Figure 4.8 shows the immunofluorescent detection of infected cells at 72 hpi and the replication kinetics of infectious virus production for mutant viruses with insertions at nucleotide positions 1610, 1769, 2941 and 4884 compared to the parent strain. Figure 4.8a shows that each mutant virus construct was able to successfully initiate virus replication after transfection into Huh-7.5 cells, as indicated by a large proportion of E-protein positive cells. All of these mutant viruses were able to initiate the expected log phase growth kinetics at early time points (24 – 48 hpi) compared to the pFK-DVs parent virus (Figure 4.8b). The NS3 4884 virus displayed indistinguishable replication kinetics from the parent strain whereas the E 1610 and 1760 mutant viruses had slightly lower peak virus titers at 96 hpt compared to the parent strain. Interestingly, the NS1 2941 mutant virus produced appreciably higher titers of infectious virus compared to the parent strain in the Huh-7.5 cell line as indicated by rapid virus replication between 48 – 72 hpt and by higher peak titers at 96 hpt. This data indicated that the introduction of these 15 bp insertions to the DENV genome was associated with unchanged (4884 mutant), reduced (1610 and 1760 mutants) or enhanced (2941 mutant) viral replicative fitness compared to the parent strain.

Figure 4.9 shows the corresponding set of data for all mutant viruses generated using the synthetic mutation N-terminal NS5 pUC57 intermediate cloning vector compared to the parent stain pFK-DVs. Figure 4.9a shows that unlike the parent strain, wildtype (synthetic mutation) or the NS5 8086 RNA transfections, there were no cells with positive E staining detected for the NS5 8069 or 8077 mutants at 72 hpt. This result indicated a critical defect in the replication of these two mutant viruses compared to the parent strain that was independent of the synthetic mutation introduced in the cloning process. This finding was substantiated by the lack of infectious virus detected in the culture supernatant of cells transfected with the 8069 or 8077 RNA up to one-week post transfection (Figure 4.9b). Conversely, both the 8086 mutant and the wildtype (synthetic mutant) clones were able to generate comparable levels of infectious virus to the parent strain over this time course. This result was unexpected since both the 8069 and 8077 insertion mutations were detected in the final population of insertion mutants after multiple rounds of selection on the Huh-7.5

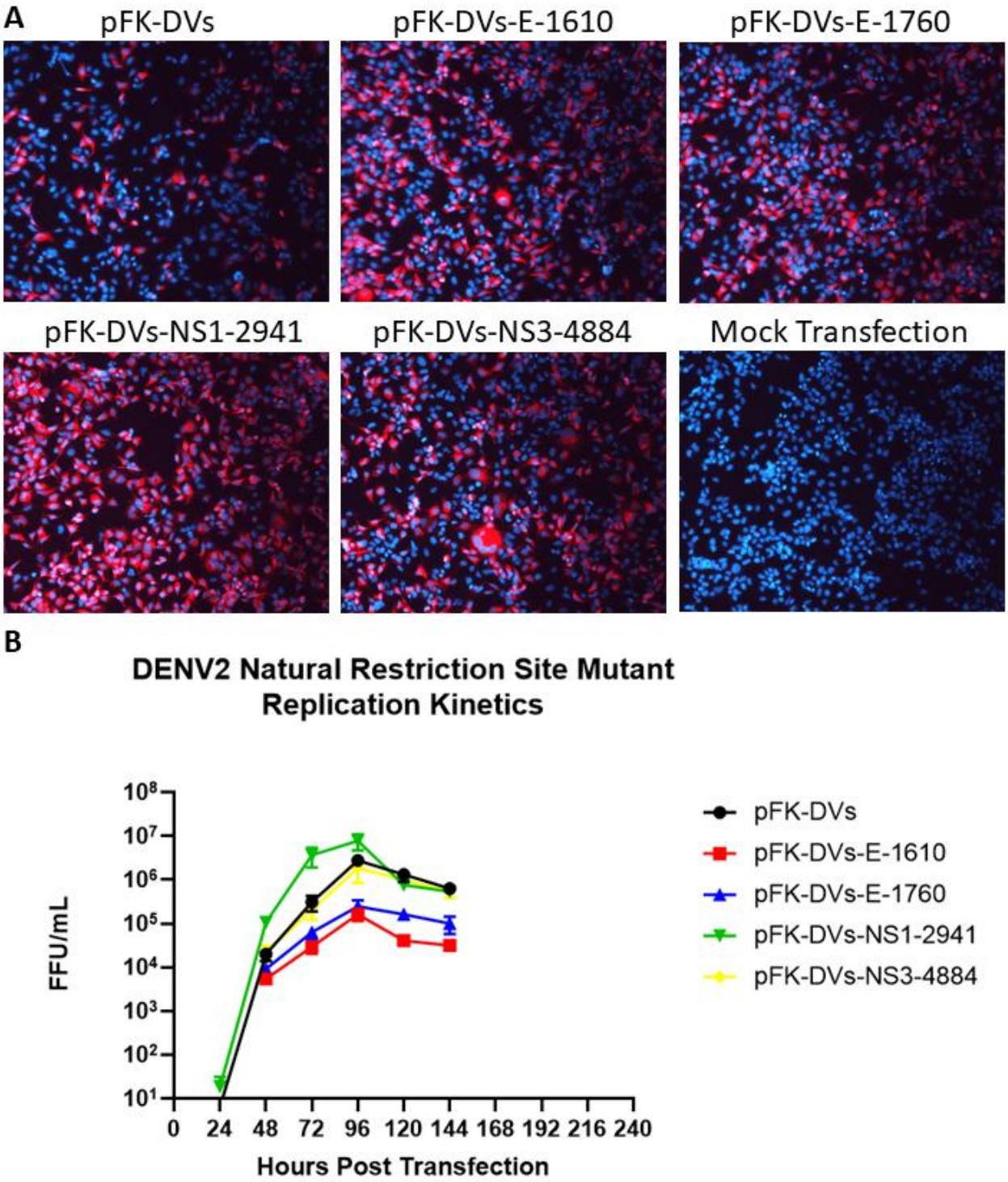

Figure 4.8: Replication kinetics of individual mutant viruses containing transposon insertions at nucleotide positions 1610, 1760, 2941 and 4884 within the DENV2 genome. A) DENV infected Huh7.5 cells 72 h after transfection with *in vitro* transcribed RNA generated from the indicated mutant plasmid, detected by staining with 4G2 *flavivirus* E protein (red) and cell nuclei by DAPI (blue) . B) *In vitro* transcribed RNA was transfected into Huh7.5 cells in duplicate and supernatants were collected from transfected cells every 24 h over the course of one week. The quantity of infectious virus in these supernatants were then determined by focus forming assay and expressed as FFU/mL. Data are represented as means +/- s.d.

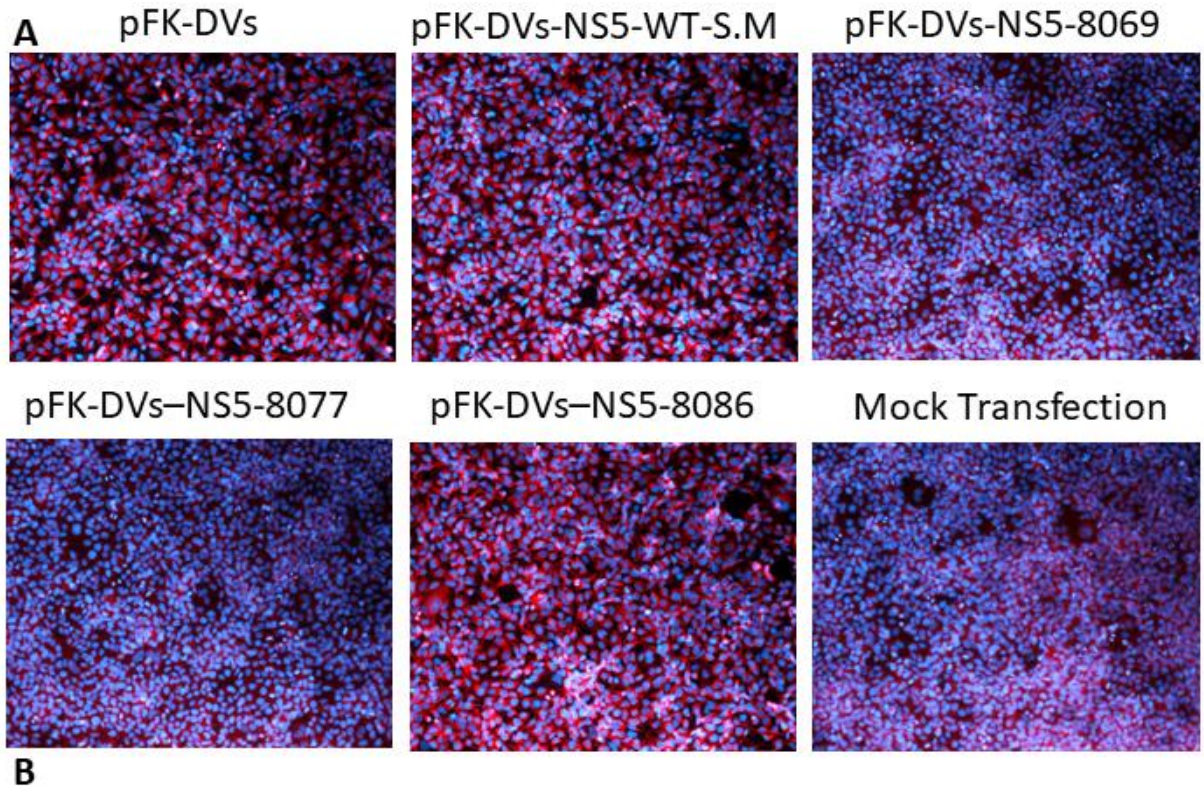

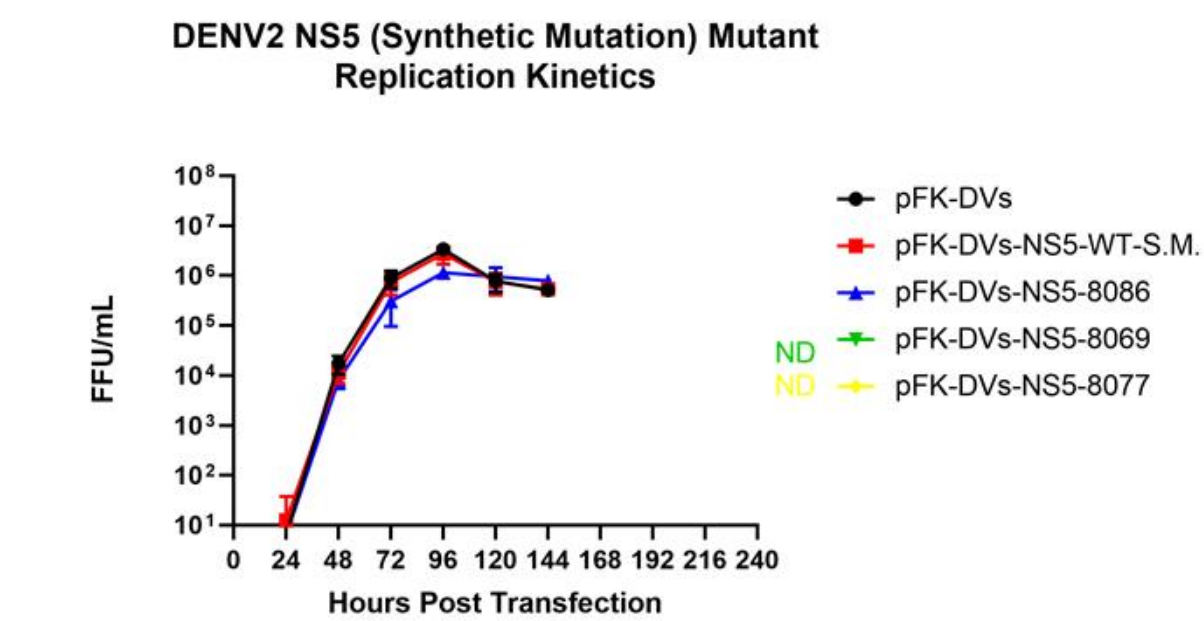

Figure 4.9: Replication kinetics of individual mutant viruses containing transposon insertions at nucleotide positions 8069, 8077 and 8086 within the DENV2 genome including the corresponding parental WT clone with synthetic mutations. A) DENV infected Huh7.5 cells 72 h after transfection with *in vitro* transcribed RNA generated from the indicated mutant plasmid, detected by staining with 4G2 *flavivirus* E protein (red) and cell nuclei by DAPI (blue) . B) *In vitro* transcribed RNA was transfected into Huh7.5 cells in duplicate and supernatants were collected from transfected cells every 24 h over the course of one week. The quantity of infectious virus in these supernatants were then determined by focus forming assay and expressed as FFU/mL. Data are represented as means +/- s.d.

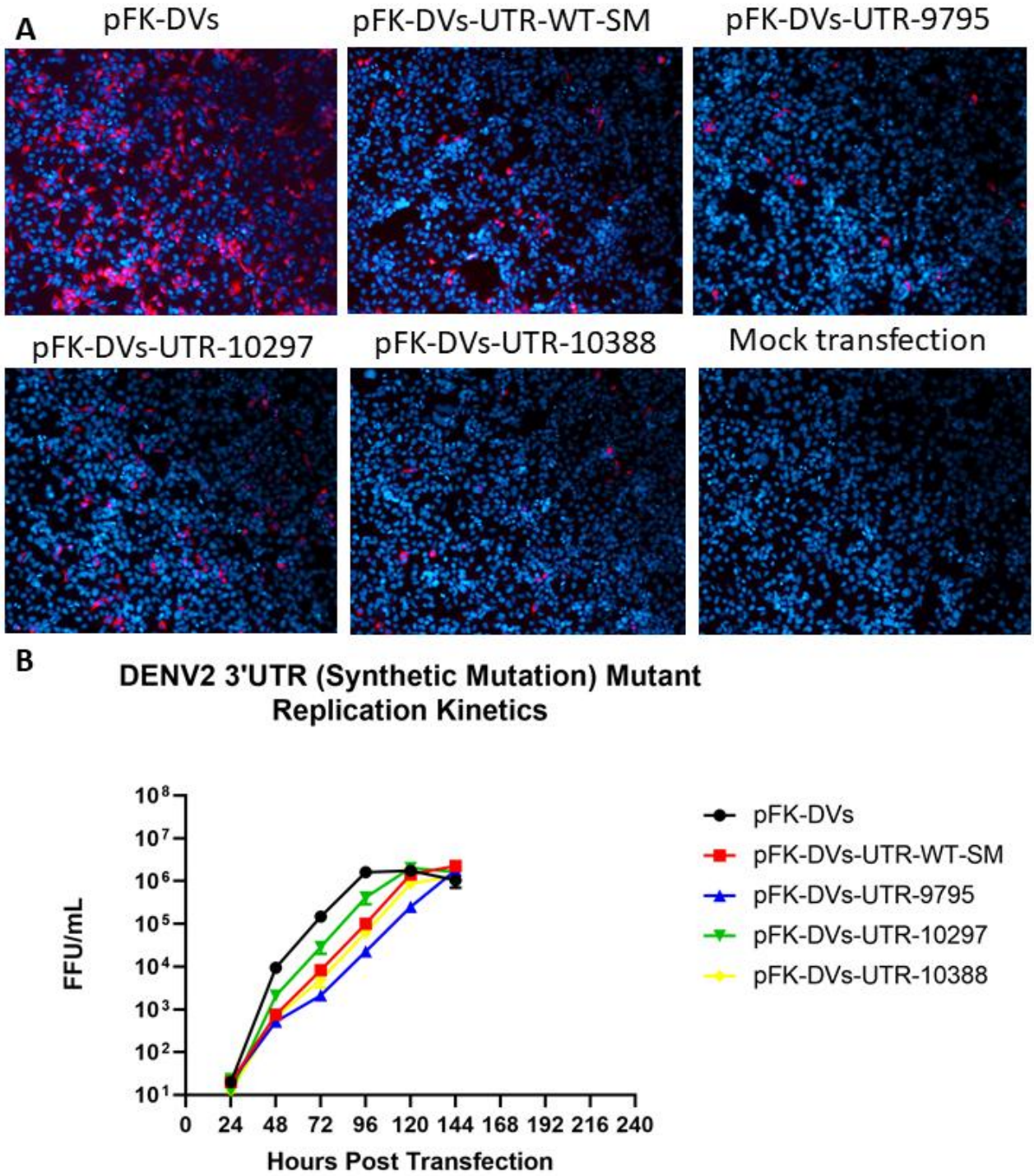

Figure 4.10: Replication kinetics of individual mutant viruses containing transposon insertions at nucleotide positions 9795, 10297 and 10388 within the DENV2 genome including the corresponding parental WT clone with synthetic mutations. A) DENV infected Huh7.5 cells 72 h after transfection with *in vitro* transcribed RNA generated from the indicated mutant plasmid, detected by staining with 4G2 *flavivirus* E protein (red) and cell nuclei by DAPI (blue) . B) *In vitro* transcribed RNA was transfected into Huh7.5 cells in duplicate and supernatants were collected from transfected cells every 24 h over the course of one week. The quantity of infectious virus in these supernatants were then determined by focus forming assay and expressed as FFU/mL. Data are represented as means +/- s.d.

cell line, including the initial passaging by Eyre *et al.* to enrich for replication competent and infectious virus [94]. However, as outlined in the introduction, the NS5 protein is essential for viral RNA capping and replication via a -ssRNA intermediate. The complete lack of virus replication from these clones strongly indicated the insertion mutations at nucleotide positions 8069 and 8077 interfered with at least one of these essential processes. Therefore, further experiments for this cohort of mutant viruses were focused on the NS5 8086 mutant for characterization.

Finally, Figure 4.10 shows the replication kinetics data for the group of mutant viruses generated using the UTR synthetic mutation that was introduced for cloning of insertion sequences into the pFK-DVs plasmid. All the mutant viruses in this group supported viral RNA replication (Figure 4.10a) as indicated by positive E staining in all but the mock transfected panel. However, for each of the mutant viruses and the wildtype (synthetic mutation) there was clearly a lower rate of virus replication in transfected cells at this time point compared to the parent pFK-DVs transfected cells. This data is concordant with that of Figure 4.10b, showing that of all the mutant viruses had delayed replication kinetics leading to an approximately 1 log reduction in the levels of infectious virus in supernatants at 96 hpt. This data indicated that there was a significant reduction in viral fitness as a result of the synthetic mutation introduced to clone these mutants (pFK-DVs compared to pFK-DVs-UTR-WT-SM). Despite the reduction in replication fitness, all of the mutant viruses displayed log phase growth kinetics and were able to reach equivalent titers compared to the pFK-DVs parent strain by day 7 post transfection. Together this data demonstrated that these mutant viruses were replication-competent and were able to progress to further testing for IFN sensitivity. However, the delayed growth kinetics conferred by the synthetic mutations that were introduced for cloning purposes would need to be accounted for in controlled experiments to draw comparisons with the 15 bp insertion mutant viruses.

4.2.7 Testing the IFN sensitivity of the individual DENV mutants

After confirming the replication fitness of each mutant virus, it was then possible to individually test these mutants for changes to IFN sensitivity predicted by the screening process. The first experiments designed to test IFN sensitivity, replicated the conditions of the screen to confirm these results. Huh-7.5 cells were pre-treated for 6 h with increasing concentrations of IFNα prior to inoculating with each mutant virus at an MOI of 0.2. After overnight inoculation, the media was replaced with media containing the appropriate concentration of IFNα. Then, 48 hpi supernatants were harvested to determine the level of infectious virus in each treatment group by focus forming assay. Levels of infectious virus in supernatant were normalized independently to the untreated control group of each virus strain and were represented as a percentage of the levels of infectious virus for the untreated controls. This normalisation was essential to account for differences in replication fitness of the individual mutant virus strains compared to the parent DENV 16682 strain. Each IFN sensitivity experiment was conducted in biological triplicate and each focus forming assay was conducted in technical duplicates. For each cohort of mutants (natural restriction site, NS5 synthetic mutation and UTR synthetic mutation), these experiments were conducted alongside the parent strain of DENV and the appropriate wildtype (synthetic mutation) counterpart generated from *de novo* RNA transfection from the same controlled experiment. Each figure represents two independent experiments for each group of viruses. Figure 4.11 shows the IFN sensitivity assays for all mutant viruses generated using natural restriction site cloning into the pFK-DVs plasmid. Figure 4.12 shows the IFN sensitivity assays for all mutant viruses generated using the NS5 synthetic mutation cloning strategy while Figure 4.13 shows the IFN sensitivity assays for the group of mutant viruses generated using the UTR synthetic mutation cloning strategy. As expected, these experiments revealed dose-dependent reductions in the levels of wildtype and mutant infectious viruses present in the supernatants of infected cells that were treated with IFNα. The reduction in the levels of infectious virus was equivalent to that of the parent DENV strain for all viruses generated using natural restriction site cloning and those generated using the NS5 synthetic mutation cloning strategy. Conversely, for viruses generated using the UTR synthetic mutation cloning strategy there was a statistically significant difference at all three doses of IFNα in the IFN dependent reduction of infectious virus compared to the parent strain. Interestingly, this difference in IFN sensitivity was detected for the wildtype (synthetic mutation) clone, and this effect was

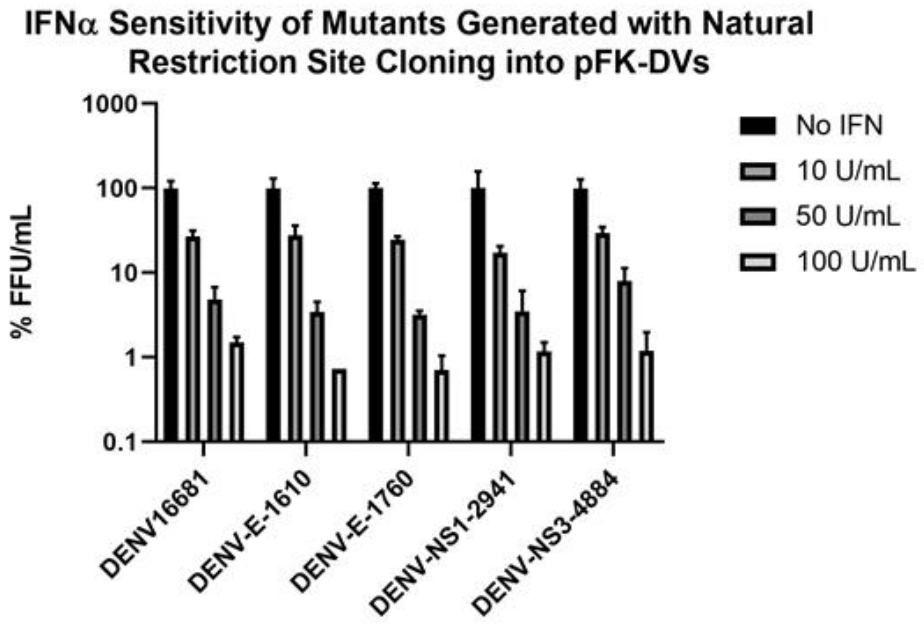

Figure 4.11: IFN sensitivity assay of mutant viruses containing transposon insertions at nucleotide positions 1610, 1760, 2941 and 4884 within the DENV2 genome. Huh7.5 cells were pre-treated with IFNα at the indicated concentration for 6 h prior to inoculation with the parent (DENV16681) or mutant strain of DENV at MOI of 0.2. After overnight inoculation, supernatants were removed and replaced with the appropriate fresh treatment media. After 48 hpi supernatants were collected and the quantity of infectious virus in supernatants were determined by focus forming assay and expressed as FFU/mL. Statistical analysis was performed using standard 2-way ANOVA (* $P < 0.05$, ** $P < 0.01$, all other unmarked comparisons are non-significant). Data are represented as means +/- s.d.

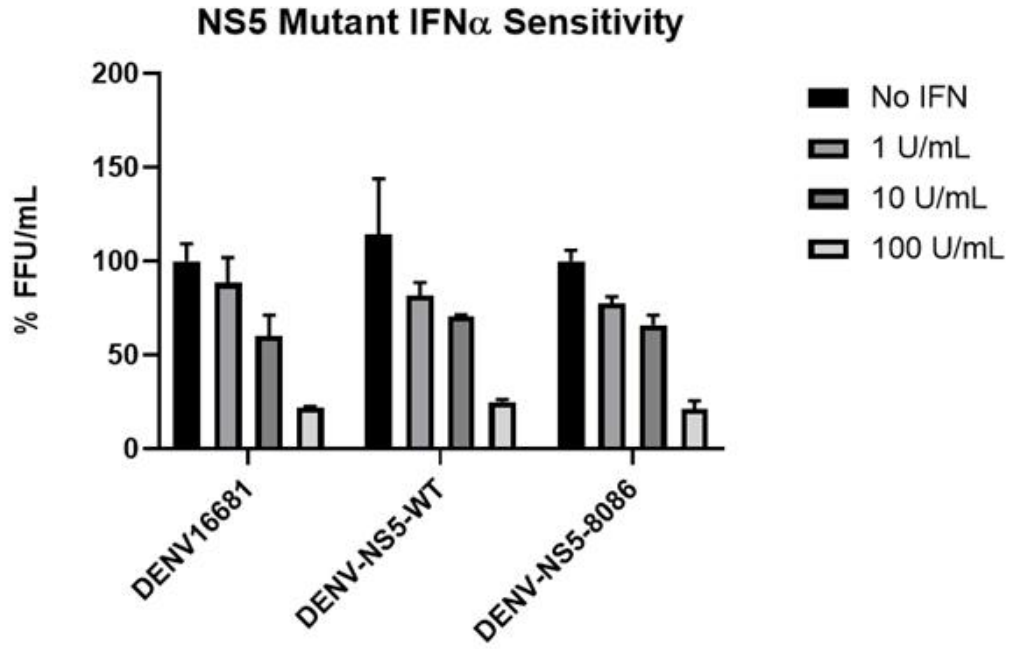

Figure 4.12: IFN sensitivity assay of mutant viruses containing a transposon insertion mutation at nucleotide position 8086 within the DENV2 genome and including the synthetic mutation (WT) counterpart. Huh7.5 cells were pre-treated with IFNα at the indicated concentration for 6 h prior to inoculation with the parent (DENV16681) or mutant strain of DENV at MOI of 0.2. After overnight inoculation, supernatants were removed and replaced with the appropriate fresh treatment media. After 48 hpi supernatants were collected and the quantity of infectious virus in supernatants were determined by focus forming assay and expressed as FFU/mL. Statistical analysis was performed using standard 2-way ANOVA (* $P < 0.05$, ** $P < 0.01$, all other unmarked comparisons are non-significant). Data are represented as means +/- s.d.

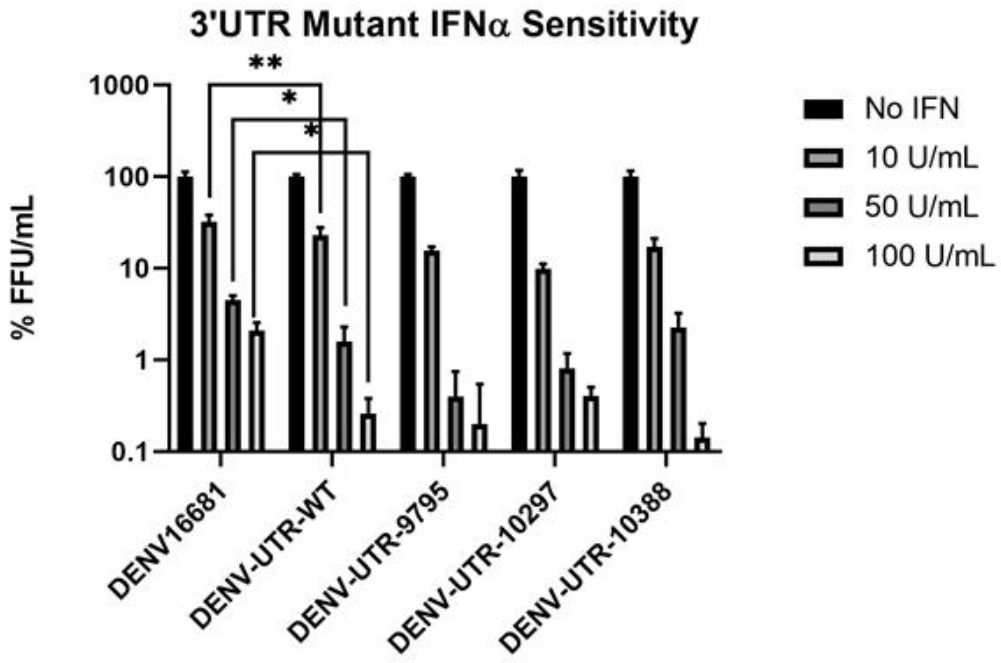

Figure 4.13: IFN sensitivity assay of mutant viruses containing transposon insertions at nucleotide positions 9795, 10297 and 10388 within the DENV2 genome including the corresponding WT clone with synthetic mutations. Huh7.5 cells were pre-treated with IFNα at the indicated concentration for 6 h prior to inoculation with the parent (DENV16681) or mutant strain of DENV at MOI of 0.2. After overnight inoculation, supernatants were removed and replaced with the appropriate fresh treatment media. After 48 hpi supernatants were collected and the quantity of infectious virus in supernatants were determined by focus forming assay and expressed as FFU/mL. Statistical analysis was performed using standard 2-way ANOVA (* $P < 0.05$, ** $P < 0.01$, all other unmarked comparisons are non-significant). Data are represented as means +/- s.d.

consistent across the mutants generated from this clone. This data implied that one or both silent single nucleotide substitutions used to generate this cohort of viruses contributed to IFN sensitization of these clones. Collectively, this data demonstrated there were no changes to IFN sensitivity of mutant viruses based on the presence of the transposon insertion mutations predicted to cause this outcome by the screening process.

Given that none of the viruses encoding transposon insertion mutations displayed differences in IFN sensitivity in experiments that were designed to mirror the screening conditions it was possible that the insertion mutations that appeared to cause this effect in the screen were a result of experimental variability. This is consistent with the demonstration that most of these mutations were not statistically significantly different between the treated and untreated conditions of the screening replicates. Additionally, the two most likely candidates for modulating IFN sensitivity based on statistical significance in the screen (mutants 8069 and 8077) could not be tested for IFN sensitivity since they produced no infectious virus. Because all of the hits from the screen were not associated with altered IFN sensitivity in dose-response validation experiments, it was no longer viable to pursue this line on inquiry to discover DENV mutants with enhanced IFN sensitivity.

4.3 Discussion

DENV is a significant human pathogen, infecting approximately 390 million people resulting in more than 21, 000 deaths annually [127]. In addition, DENV is responsible for generating a considerable economic burden due to the high rate of hospitalizations for serious DENV infections [125]. Currently there is a deficiency in safe and effective antiviral treatments and vaccines available to manage DENV infection globally. Importantly, the ability of DENV to evade the innate immune response is crucial to establishing infection and causing disease in humans. In particular, the type-I IFN response effectively controls DENV infection when activated prior to infection. To overcome this barrier DENV has evolved multiple evasion strategies targeting the IFN pathway in humans. Understanding the specific mechanisms and genetic determinants of these viral evasion strategies underpins the development of efficient immune modulating treatments, antivirals, and live attenuated vaccines. As a result, this axis of DENV host-virus interaction has been extensively studied. Specific NS proteins including the NS5 RdRp are known to contribute to IFN evasion through a range of molecular mechanisms detailed in the Introduction (section 1.3). However, the knowledge of

mechanisms used by DENV to evade the IFN response is likely incomplete. This is because much of the research conducted on DENV evasion of the IFN response investigates mechanisms of individually expressed viral proteins. As a result, there is a need to perform mutational studies on the complete DENV genome in the context of a fully infectious system to further elucidate novel evasion mechanisms. For this reason, the aim of this chapter was to find novel mechanisms of DENV IFN evasion based on a high-throughput genome wide mutational screening approach. Briefly, this approach utilized a pre-existing library of replication competent and infectious DENV insertion mutants generated using a fully infectious clone by Eyre *et al*. [94]. This library then underwent passaging in conditions with or without type-I IFN to select for mutants based on their sensitivity to type-I IFN. This process allowed the identification of potential mutations causing a deficit of virus fitness under IFN conditions. After identifying potential hits from the screen, these mutations were re-introduced into the full-length infectious clone of DENV allowing testing of their IFN sensitivity.

To achieve the aim of this Chapter it was first necessary to establish a screening platform that was able to apply adequate selective pressure by IFN treatment to the population of mutant DENV. To this end the IC_{50} for IFNα treatment against DENV infection at low MOI was determined on the Huh-7.5 cell line as done previously for a related HCV mutagenesis screen that had successfully discovered novel evasion mechanisms [274]. This level of IFNα stimulation was decided upon to give appropriate activation of the innate antiviral response without completely overwhelming the entire virus population. The IC_{50} for IFNα treatment against DENV was found to be approximately 1 U/mL when IFNα treatment was applied for 6 h prior to infection. This was consistent with the IC_{50} for IFNα treatment against HCV [274] and was close to the IC_{50} for ZIKV determined in the previous Chapter.

Initially the library of replication competent and infectious DENV insertion mutants required resuscitation from frozen storage. Since the titer of the frozen mutant library was unknown this required estimating the rate of infection based on its use in the previous screen. The frozen library was diluted 1:1 with fresh media and passaged onto cells treated with or without the calculated IC_{50} of IFNα diluted in fresh media. Unfortunately, due to the unexpectedly high titer of the frozen stock the IFN treatment applied in this initial passage (passage 0) was inefficient at reducing DENV infection to the expected 50 % compared to levels of infectious virus in untreated controls. The most likely explanation for this effect was

that the IFN pathway was effectively shut-off by the high titer infection of DENV. According to this model, the higher titer of virus would lead to a greater multiplicity of infection per cell, greater levels of DENV protein expression and resultantly a greater level of inhibition of IFN signalling than anticipated. Importantly, while the impact of IFN treatment at the bulk population level was not apparent it is possible that individual mutations that conferred high sensitivity to IFN were underrepresented in the total virus population after this passage.

Following this initial recovery passage, each of the IFNα treated and the untreated populations of mutant virus were passaged under the same condition with replicates maintained independently of one another. To ensure the efficacy of the IFN pre-treatment, the MOI was scaled back to the intended 0.2 units of infectious virus per cell. This resulted in the expected degree of selection pressure in passage 1 determined by an observed 50 % reduction in the levels of infectious virus in supernatant of the IFNα treated group compared to the untreated group. Interestingly, when this process was repeated for passage 2 using the same infection conditions and the same concentration of IFN this resulted in a smaller reduction of DENV infection between the two treatments. Instead of a 50% reduction in the level of infectious virus in the supernatant from this passage, the mean difference was approximately 25%. Importantly, this data implied a shift in the genetics of the library at the population level to be more resistant to IFN treatment. This likely resulted from IFN sensitive mutants being outcompeted by IFN resistant mutants in the population. This rapid desensitization of the DENV population to IFN treatment could be exploited in future screens of this nature. Improved selection may have been possible by progressively increasing the IFN concentration between the passages to again achieve an approximately 50 % reduction in virus infection levels in the treated group. A greater degree of selective pressure on the population of mutant viruses would increase the likelihood of IFN sensitive mutants being removed from the population. This would have made the comparison between the remaining virus populations in different treatment groups more clearly defined and therefore improved the likelihood of detecting IFN sensitive mutations following NGS analysis. In addition to the IFN mediated selective pressure there was also evidence that both the IFNα treated and untreated populations had adapted to replication in the Huh-7.5 cell line after multiple rounds of passaging. This was demonstrated by the higher titers generated following passage 2 compared to passage 1 despite infecting at the same MOI and collecting supernatants at the same time post infection. As this effect was balanced in both the treatment groups the

assumption was made that this would not impact on the analysis of the screen. However, this data highlights the importance of validating results of individual mutations in multiple cell lines to ensure this is not specific to the Huh-7.5 cell line. Importantly, comparison between the levels of infectious virus produced after each passage in either the IFNα treated or untreated conditions indicated the progressive negative selection of mutants with reduced fitness in IFN conditions.

Comparison of the relative frequency of mutations remaining following each passage revealed a spread of mutations across both translated and untranslated regions of the genome. The effect of IFN-mediated selection was demonstrated by the progressive narrowing breadth of mutation frequencies represented in subsequent passages. Additionally, there was a general trend towards under-representation of mutations that were passaged in IFNα treatment conditions compared to the untreated controls.

Analysis of specific regions revealed nucleotide positions of interest that demonstrated a lower frequency of mutations in IFN treated compared to untreated conditions. The exception to this was the insertion at nucleotide position 2941 (NS1) that showed a greater frequency of mutations in IFN treated compared to untreated conditions. Broadly the insertions of interest were found in regions of the E protein, NS1, NS3, NS5 and the 3' UTR. Each of these regions are known to contribute to the ability of flaviviruses to modulate innate antiviral responses, giving weight to the possibility of their involvement in IFN pathway evasion. For example, the E protein of WNV inhibits TLR mediated IFN production through inhibition of NF-κB activation [15]. NS1 is known to have multiple roles in immune modulation depending on the virus. The secreted form of DENV NS1 is known to modulate immune responses through binding TLR4, activating cytokine production [225]. Conversely, ZIKV NS1 dampens IFN production through TBK1 inhibition [176]. Additionally, the DENV NS2B/3 protein complex inhibits production of type-I IFN via interaction with Ikκ-ε [10]. The 3' UTR of each DENV and ZIKV are known to generate sfRNA's that inhibit RIG-I dependent signalling [82, 202]. Of special interest, 4 out of 10 top hits were found within the NS5 protein (nucleotide positions 8069, 8077, 8086 and 9795). This was significant because DENV NS5 protein is known to directly inhibit signalling downstream of the type-I IFN receptor via degradation of the STAT2 protein [213]. As a result, it was anticipated that NS5 mutations would be highly represented amongst viruses with altered IFN sensitivity.

In addition to assessing the validity of potential hits based on the supporting literature, the impact of the top 10 insertions of interest were evaluated statistically. This was done by directly comparing the insertion frequencies from the IFNα treated to the untreated pool of mutants, considering the standard deviation between the triplicates. Of the 10 insertion events assessed, 3 were significantly different between the groups after the second round of passaging. These 3 insertions occurred at nucleotide positions 8069, 8077 within NS5 and 10297 within the 3' UTR. To validate the apparent effect of these insertions on IFN sensitivity the top 10 nucleotide position insertions were individually cloned into the pFK-DVs parent. This allowed testing of each mutation independently of the pooled population for their sensitivity to IFNα.

After each mutation was independently cloned into the parent plasmid it was then necessary to confirm the replication fitness of each virus. Of the 10 individual mutations introduced into pFK-DVs, 8 produced replication competent viruses. Notably, the insertion mutations at positions 8069 and 8077 resulted in deleterious effects on DENV replication fitness. This is likely due to the impact of these insertions on the MTase domain of the NS5 protein. The catalytic site (K61-D146-K180-E216) of this domain is formed by interacting amino acids at the centre of a β-sheet extending from nucleotide positions 7750 to 8220 [171]. Interestingly, the mutant containing a 15 bp insertion at position 8086 was not similarly impacted. This indicated that insertions within this β-sheet region had differing effects on replication fitness based on their exact position. Importantly, the 8077 and 8086 had highly similar amino acid insertions (MRPQE vs MRPQL) likely ruling out the impact of specific chemical properties of the inserted amino acids causing this change (see Appendix V, Table 1 for sequence details). A more likely explanation was that the insertions at 8069 and 8077 caused a steric change due to the additional 5 amino acids added and this reduced β-sheet integrity, leading to the disruption of the MTase active site formation and producing a replication deficient mutation. Since the full-length NS5 DENV crystal structure is available [392], it would be interesting to add these insertions *in silico* to observe any changes in the overall structure or free-energy of the MTase domain.

In addition to specific 15 bp insertions causing changes to replication fitness there was also a decrease in replication fitness caused by the single nucleotide change introduced into the 3' UTR for cloning purposes. The effect of these synthetic mutations was consistent between the wildtype and the corresponding insertion mutants cloned through this intermediate. One

of these mutations within the NS5 coding region was designed to introduce the *AscI* site between positions 9776 – 9783 while maintaining amino acid sequence (gcagagcc → ggcgcgcc). The other mutation was a single nucleotide substitution within the 3'UTR region to create a *BsiWI* site between positions 10476 – 10481 (tgtacg → cgtacg). Since the mutation in the NS5 region was a silent mutation it is unlikely this resulted in the observed reduction in replication fitness. It is more likely that the single nucleotide change within the 3' UTR was responsible for the observed effect. After assessing the sequence change in more depth it was discovered that this substitution (t → c) occurred within the conserved loop structure of the DB1 region of the 3' UTR [68]. This region is directly involved with long range RNA:RNA interactions between DB1 and the C1 sequence (RNA structure within the capsid coding region) required for DENV genome cyclization, and is essential for RNA replication [67]. A single nucleotide substitution in this region likely caused weaker RNA interactions and therefore impeded the replication fitness of these mutant viruses. However, these viruses were able to generate equivalent titers of infectious virus in the supernatant of transfected cells to the parent pFK-DVs despite delayed replication kinetics. Therefore, these mutants were considered sufficiently replication competent to test for effects of the insertions on IFN sensitivity.

Following assessment of viral replication fitness, the remaining replication competent mutant viruses were tested for their sensitivity to IFNα treatment. The ability of each mutant to replicate in a range of IFNα concentrations was tested. The IFNα treatment was administered to Huh-7.5 cells prior to infection to recapitulate the conditions of the screen for testing the individual virus mutants. The levels of infectious virus in the supernatant after 48 h was compared to the appropriate wildtype or parent strain. From this analysis no evidence was found that any of the 15 bp insertion mutations resulted in increased IFNα sensitivity as predicted by the screen. However, unexpectedly synthetic mutations introduced into the 3' UTR of wildtype virus for cloning purposes enhanced IFN sensitivity. All the mutants generated from this cloning strategy displayed the same sensitization effect indicating that this was an effect of the common synthetic mutation and not of the 15 bp insert. It is plausible that the increased IFN sensitivity resulted from the single nucleotide substitution within the DB1 structure of the 3' UTR as DB1 acts to inhibit host 5' exonuclease activity leading to the production of sfRNAs that are involved in IFN evasion [51]. DENV sfRNAs are known to reduce the production of type-I IFN downstream of PRR activation [202]. Additionally, a mutational

study showed that sfRNA deficient WNV virus was more sensitive to pre-treatment with IFNα, akin to the effect we observed in our screen [307] [51]. Future experiments to determine the impact of this single nucleotide substitution on the stability of DB1, RNA:RNA interactions and sfRNA formation could provide new insights into DENV pathogenesis and IFN evasion.

In light of these combined results, it was determined that none of the 15 bp insertion mutations tested increased IFN sensitivity in a fully infectious DENV model system. This suggests that a more refined screening approach may be required to definitively map mutations that influence IFN sensitivity.

One hypothesis explaining these results is that unintended naturally occurring mutations were introduced into the mutant virus population after multiple rounds of passaging. In general RNA viruses have high mutation rates (between 10^{-6} to 10^{-4} substitutions per nucleotide per cell infection) as a result of their error prone RdRp activity [298]. This leads to accumulation of mutations in the genome that, in nature, are important for population diversity and viral evolution [180]. If these mutations were linked to a transposon insertion mutation, they would be co-selected for during the screen. Therefore, it is plausible that these unintended mutations impacted the apparent relationship between the frequency of a given transposon mutation under IFN treated and untreated conditions.

Logically, these mutations were likely introduced during passage 0 of the current screen or accumulated in the original screen performed by Eyre *et al.* [94]. This is because in these scenarios the MOI and hence the rate of coinfection was not controlled for. This assumption is supported by both genetic studies and mathematical modelling on the impact of coinfection on RNA virus population genetics. One study investigating the impact of coinfection on RNA virus population genetics found that high coinfection rates reduced the clearance of deleterious mutants in RNA virus populations [102]. Importantly this was caused by complementation of deleterious mutations with replication competent viruses infecting the same cell. In addition, mathematical modelling shows that high coinfection rates leading to complementation increase the frequency of mutations accumulating in RNA virus populations over time [109]. In combination, these two forces mediated by the effect of high coinfection rate increase the likelihood of complementation that in turn leads to greater accumulation and sustained diversity of mutations (deleterious or otherwise) within viral populations over time [109].

Therefore, it is plausible that deleterious transposon mutations (such as those occurring in NS5) were able to persist when the rate of coinfection (MOI) was high due to complementation. In turn, this increased the likelihood of these mutants accumulating compensatory mutations that rescued the deleterious phenotype conferred by the transposon mutation. Therefore, these transposon mutants could have survived when subjected to subsequent passages even at low MOI. These combined effects may account for the representation of deleterious insertion mutations in the analysis of the screen. Alternatively, the accumulation of naturally occurring mutations could have led to altered fitness under IFN selection irrespective of a linked transposon mutation. Therefore, transposon mutations could have 'piggybacked' on linked naturally occurring mutations that altered IFN sensitivity. These transposon mutations would have then appeared to alter fitness under IFN selection in the analysis despite not conferring this function, as was shown in our validation studies using a number of highly-represented transposon mutations.

Evidence supporting this theory is given by the results of an alanine-scanning mutagenesis screen investigating the function of the DENV NS2A protein. This study by Wu *et al*. [373] subjected a the N-terminal domain of NS2A within a full-length infectious clone of the DENV2 genome to alanine substitution mutation. These mutants were then individually screened for their ability to yield infectious virus and to cause cytopathic effect (CPE). NS2A alanine mutants that displayed a lethal phenotype were then subjected to passaging in cells trans-complemented with expressed wildtype NS2A. Interestingly, after only 3 – 5 passages on NS2A transfected cells, 45% of the tested alanine mutants had accumulated compensatory mutations that rescued their lethal phenotype. This demonstrates that the natural mutation rate of DENV2 is sufficient to introduce adaptive compensatory mutations within the time frame of our screen (including the initial screen by Eyre *et al.* [94]).

One way to confirm this theory would be to perform trans-complementation experiments on the deleterious NS5 transposon mutants 8069 and 8077 to experimentally observe the accumulation of compensatory mutations over time. This would require co-expressing mutant NS5 RNA with wildtype NS5 protein, allowing the generation of infectious virus that could be used in multiple passages. However, this approach is complicated by the fact that NS5 is notoriously difficult to trans-complement due to its essential enzymatic function within the *Flavivirus* lifecycle. To date, mutations within the RdRp domain but not those in the MTase domain (covering the 8069 and 8077 mutations) of the *Flavivirus* NS5 have been trans-

complemented by NS5 expression constructs [166]. However, NS5 mutations can be trans-complemented by stably expressed DENV replicon RNA containing the full-complement of NS proteins able to initiate viral RNA replication without the production of infectious virus [83]. Therefore, these experiments would require first generating a stably expressing DENV replicon cell line and therefore are beyond the scope of this current project. However, if this strategy were applied and revealed compensatory mutations for the NS5 transposon mutants, these adapted viruses could be used to test whether the transposon mutations genuinely conferred IFN sensitivity.

Another important consideration for this theory is the proximity of accumulated mutations to the transposon insertion site. Interestingly, in the study by Wu *et al*. on NS2A function, the accumulated compensatory mutations were all detected within the NS2A region [372]. However, a similar study involving passaging replication impaired HIV mutants showed that mutations accumulated at distal sites of the viral genome were also able to compensate function [187]. This shows that accumulation of both short- and long-range mutations can act to compensate for deleterious mutations or those impacting viral fitness. Consequently, further investigation of accumulated mutations in our screen or future screens of a similar nature would benefit greatly from new long-read sequencing technology. Such technology, like the Nanopore system, is now able to continuously sequence sections over 10 kbp in a single read without compromising on the number of reads [205]. This new technology would provide valuable insight into the rate of accumulating mutations and linkage of unintentional mutations with transposon insertions under IFN selection.

In addition to using new sequencing technology, future screens of this nature would benefit from *de novo* generation of the mutant library from the plasmid stock rather than pre-selecting for replication fitness. This would limit the number of passages and therefore reduce the likelihood of accumulation of unanticipated mutations. Additionally, this data highlights the importance of performing mutational screens at low MOI (≤ 1) to limit the rate of coinfection and complementation leading to accelerated accumulation of mutations in the viral population.

Moreover, increasing the strength of selection could be used to limit unwanted compensatory mutations accumulating in future high-throughput mutant screens. Modelling shows that increased selection pressure weakens the impact of complementation on maintaining mutant diversity in viral populations [109]. This theory supports that sequentially increasing the

concentration of IFNα would have benefited this screen. Alternatively using an IC_{80} instead of an IC_{50} concentration of IFNα treatment, as was applied in one influenza mutant screen differentiating based on IFN sensitivity [84], could have been another way of limiting accumulated mutations.

4.4 Conclusions

The aim of this chapter was to find novel mechanisms of DENV IFN evasion based on a high-throughput genome wide mutational screening approach. To address this aim, a library of replication competent and infectious transposon insertion mutant DENV was re-purposed from a previous screen performed in our laboratory [94]. This library was subjected to selection by passaging in conditions with or without type-I IFNα and the impact of this selection was assessed by determining the frequency of remaining insertion events at each position in the genome by NGS. The frequency of mutations at each genome position was then compared between the treatment groups to assess their impact on IFN sensitivity. Mutations of interest were then re-introduced into the full-length infectious clone of DENV allowing testing of their IFN sensitivity independently. Unfortunately, none of the individually cloned 15 bp insertion mutants displayed increased IFN sensitivity as predicted by the screen. This may have been a result of introduction of compensatory mutations resulting in non-replication competent virus being detected by the screen and/or transposon insertion-linked mutations that confounded interpretation of the impact of transposon insertion during the screen. The results of this screen highlight the complexity of high-throughput mutational studies on RNA virus genomes and have provided constructive recommendations to improve similar work conducted in the future. These include reducing accumulated mutations by lowering the number of non-essential passages, reducing co-infection, and increasing selection pressure applied to the mutant population. Additionally, the added power given by new long-read sequencing technology could greatly benefit future screens of this nature by identifying linked compensatory mutations in viral genomes.

Statement of Authorship

Title of Paper	**IFN-epsilon is a distinct constitutively expressed type-I IFN in the female reproductive tract that protects against ZIKV infection**
Publication Status	☐ Published ☐ Accepted for Publication ☑ Submitted for Publication ☐ Unpublished and Unsubmitted work written in manuscript style
Publication Details	The immunological surveillance factors controlling the vulnerability of the female reproductive tract (FRT) to viral sexually transmitted infection are not well understood. Interferon-epsilon (IFNε) is a distinct, immunoregulatory type I IFN that is constitutively expressed by FRT epithelium, not regulated by pathogens like other antiviral IFNs α, β and λ. We show the necessity of IFNε for ZIKV protection by: susceptibility of IFNε$^{-/-}$ mice; their "rescue" by intravaginal recombinant IFNε; and blockade of protective endogenous IFNε by neutralising antibody. Complementary studies in human FRT cell lines showed IFNε had potent anti ZIKV activity, induced similar genes to IFNλ but not some IFNα-induced proinflammatory genes. IFNε activated, similar to IFNα and λ, the STAT1/2 pathways which were inhibited by ZIKV-encoded non-structural (NS) proteins. Importantly in contrast, constitutive IFNε was not inhibited by ZIKV NS proteins which did block the PRR-induction of IFNα, β or λ. The constitutive nature and resistance to virus blockade of IFNε enables it to precede virus and maximise antiviral activity. These results show that the unique spatiotemporal properties of IFNε provides an innate immune surveillance network to govern viral infection with important implications for prevention and therapy.

Principal Author

Name of Principal Author (Candidate)	Rosa C. Coldbeck-Shackley		
Contribution to the Paper	Intellectual input Experimental design and data analysis Sample processing and analysis for animal experiments and in vitro experiments Assisting with animal experiments Writing the original draft, edits and data presentation		
Overall percentage (%)	80%		
Certification:	This paper reports on original research I conducted during the period of my Higher Degree by Research candidature and is not subject to any obligations or contractual agreements with a third party that would constrain its inclusion in this thesis. I am the primary author of this paper.		
Signature		Date	31/01/2021

Co-Author Contributions

By signing the Statement of Authorship, each author certifies that:

i. the candidate's stated contribution to the publication is accurate (as detailed above);

ii. permission is granted for the candidate in include the publication in the thesis; and

iii. the sum of all co-author contributions is equal to 100% less the candidate's stated contribution.

Name of Co-Author	Michelle D. Tate		
Contribution to the Paper	Intellectual input Experimental design for animal experiments Sample processing and analysis for animal experiments Coordinated, supervised, and carried out animal experiments		
Signature		Date	02/10/2020

Name of Co-Author	Sarah Rosli		
Contribution to the Paper	Assisting with animal experiments		
Signature		Date	05/10/2020

Name of Co-Author	Linden J. Gearing		
Contribution to the Paper	RNA sequencing experiment, bioinformatics analysis, report preparation and data presentation		
Signature		Date	03/10/2020

Name of Co-Author	Jodee A. Gould		
Contribution to the Paper	RNA sequencing experiment library preparation, quality control, analysis and report preparation		
Signature		Date	02/10/2020

Name of Co-Author	San S. Lim		
Contribution to the Paper	Production and quality control of specialised in-house reagents including recombinant IFNε protein and neutralising antibodies		
Signature		Date	07/10/2020

Name of Co-Author	Kylie H. Van der Hoek		
Contribution to the Paper	Intellectual input Assistance with qRT-PCR setup and standard curve analysis protocols		
Signature		Date	15/02/21

Name of Co-Author	Nicholas S. Eyre		
Contribution to the Paper	Intellectual input Production and quality control of viral stocks		
Signature		Date	2/02/21

Name of Co-Author	Byron Shue		
Contribution to the Paper	Creation of expression plasmids encoding ZIKV NS-proteins		
Signature		Date	15/02/21

Name of Co-Author	Sarah A. Robertson		
Contribution to the Paper	Intellectual input Providing female reproductive tract cell lines		
Signature		Date	4 February 2021

Name of Co-Author	Sonja M. Best		
Contribution to the Paper	In-situ hybridisation for ZIKV RNA in FRT tissue Intellectual input Supplier of anti-NS5 antibody		
Signature		Date	4/2/21

Name of Co-Author	Paul J. Hertzog		
Contribution to the Paper	Intellectual input Experimental design Editing manuscript		
Signature		Date	8/10/2020

Name of Co-Author	Michael R. Beard		
Contribution to the Paper	Intellectual input Experimental design Editing manuscript Funding and supervision		
Signature		Date	15/02/2021

Chapter 5

(Manuscript in Submission)

IFN-epsilon (IFNε) is a distinct constitutively expressed type-I IFN in the female reproductive tract that protects against ZIKV infection

Rosa C. Coldbeck-Shackley[1], Michelle D. Tate[2,3], Sarah Rosli[2,3], Linden J. Gearing[2,3], Jodee A. Gould[2,3], San S. Lim[2,3], Kylie H. Van der Hoek[1], Nicholas S. Eyre[1], Byron Shue[1], Sarah A. Robertson[4], Sonja M. Best[5], Paul J. Hertzog[2,3] and Michael R. Beard[1]

[1] Research Centre for Infectious Diseases, School of Biological Sciences, The University of Adelaide, SA, Australia.

[2] Centre for Innate Immunity and Infectious Diseases, Hudson Institute of Medical Research, VIC, Australia.

[3] Department of Molecular and Translational Sciences, Monash University, VIC, Australia.

[4] Robinson Research Institute, The University of Adelaide, SA, Australia.

[5] National Institutes of Health, Rocky Mountain Laboratories, Montana, USA

Correspondence to be addressed to:

Professor Michael Beard,

Research Centre for Infectious Diseases, School of Biological Sciences, The University of Adelaide, SA, Australia.

The University of Adelaide, North Terrace Campus, Adelaide, SA, 5005

Email: michael.beard@adelaide.edu.au

Professor Paul Hertzog,

Centre for Innate Immunity and Infectious Diseases, Hudson Institute of Medical Research, VIC, Australia.

27-31 Wright St, Clayton, Victoria, 3168

Email: paul.hertzog@hudson.org.au

Key words: Zika, ZIKV, Interferon epsilon, IFNE, innate immunity, sexual transmission, female reproductive tract

5.1 Abstract

The immunological surveillance factors controlling vulnerability of the female reproductive tract (FRT) to sexually transmitted viral infections are not well understood. Interferon-epsilon (IFNε) is a distinct, immunoregulatory type I IFN that is constitutively expressed by FRT epithelium and is not regulated by pathogens like other antiviral IFNs α, β and λ. We show the necessity of IFNε for Zika Virus (ZIKV) protection by: susceptibility of IFNε$^{-/-}$ mice; their "rescue" by intravaginal recombinant IFNε treatment and blockade of protective endogenous IFNε by neutralising antibody. Complementary studies in human FRT cell lines showed IFNε had potent anti-ZIKV activity, induced similar genes to IFNλ but not some IFNα-induced proinflammatory genes. IFNε activated, similar to IFNα and λ, the STAT1/2 pathways which were inhibited by ZIKV-encoded non-structural (NS) proteins. Importantly in contrast, constitutive IFNε expression was not inhibited by ZIKV NS proteins which did block the PRR-induction of IFNα, β or λ. The constitutive nature and resistance to virus blockade of IFNε enables it to precede virus and maximise antiviral activity. These results show that the unique spatiotemporal properties of IFNε provides an innate immune surveillance network in the FRT to govern viral infection with important implications for prevention and therapy.

5.2 Introduction

Zika virus (ZIKV) is a mosquito-borne *Flavivirus* that can also be transmitted sexually [296], and *in utero* [270] leading to foetal infection and congenital symptoms in neonates [279] including microcephaly, intrauterine growth restriction, as well as ocular and cognitive impairment [284, 294].

The innate immune response to ZIKV is critical for controlling infection [156] particularly at the mucosa of the female reproductive tract (FRT) where transmission to offspring occurs. Type-I and type-III IFNs, are the body's premier antiviral cytokines that protect against viral infection at mucosal surfaces [214]. Type-I and III IFNs orchestrate the cellular antiviral response via binding cognate receptors, IFNAR1/2 or IFNLR1/IL10Rβ, respectively. Receptor binding activates JAK/STAT signalling (as reviewed in [182]) leading to activation of thousands

of Interferon Stimulated Genes (ISGs) [293]. These ISGs encode effector proteins including Viperin, IFITM family, ISG15 and IFI6 that directly inhibit ZIKV [89, 129, 300, 354], or those with immune regulatory function [156]. Importantly, ZIKV is exquisitely sensitive to the biological effect of type-I and III IFNs evidenced by its enhanced replication in IFN receptor knockout mouse models [36, 181]. Normally, these IFNs are only produced after detection of viral infection by pattern recognition receptors (PRRs) such as by the cytosolic PRR retinoic acid-inducible gene-I RIG-I [224, 302]. This delay between pathogen detection and establishment of the IFN-mediated antiviral state is exploited by ZIKV that, after entering the cell, translates non-structural (NS) proteins that can inhibit the pathway and promote infection [52].

Unlike the typical type-I and type III IFNs, that are for the most part only expressed following viral detection, the unique type-I IFN, IFN-epsilon (IFNε) expression is constitutive, not reliant on pathogen detection pathways and is regulated by female sex hormones [105]. IFNε is produced primarily by the mucosal epithelium of the FRT in both mice and humans [105, 133] and like other type-I IFNs, signals via IFNAR1/2 to induce expression of ISGs [105, 335]. This constitutive expression is important for protective mucosal immune responses to bacterial (chlamydia) and viral (HSV2) infection of the FRT [105]. Additionally, IFNε demonstrates *in vitro* activity that inhibits multiple steps of the HIV lifecycle [110]. Our current knowledge of the role of IFNs in protection from ZIKV infection of the FRT has been elegantly investigated largely by the use of IFNAR1 [381] and IFNLR1 [36] null mice, however the particular ligands that act to protect the ZIKV infected FRT through these receptors are not well characterised. In this study we demonstrate the importance of IFNε as a major contributor to protecting the FRT from ZIKV infection.

5.3 Results

5.3.1 ZIKV replication is inhibited by endogenous IFNε in a mouse model of vaginal transmission

To determine the contribution of endogenous IFNε expression in the FRT, relative to other (conventional) type-I IFNs to prevent ZIKV infection, we compared the outcomes of intravaginal (iVag) infection [105] of wildtype (WT), IFNε$^{-/-}$ or IFNAR1$^{-/-}$ mice with 5 X 10^5 FFU of ZIKV Brazilian stain PRVABC59 (Fig. 5.1a).

In the absence of IFNε, mice were more susceptible to ZIKV infection in tissues of the reproductive tract with higher viral titres in vaginal washes (VW) 3, 5 and 7 days post-infection (dpi) (Fig. 5.1b). Interestingly, the levels of infectious virus in VW at 5 dpi of IFNε$^{-/-}$ mice were similar to that of IFNAR1$^{-/-}$ mice. Higher viral load in VW correlated with increased viral RNA (vRNA) detected by qRT-PCR in both the uterus and ovary on 5 (Fig. 5.1d & e) and 7 dpi (Sup. 5.1). Interestingly, no significant difference was detected in the vagina (Fig. 5.1c) of IFNε$^{-/-}$ mice compared to WT mice that had much greater levels of infection in the vagina (5.06 Log10) compared to both the uterus (3.19 Log10) and ovary (2.28 Log10). The vagina had apparently lower IFNε RNA levels than the uterus and ovary but this was not statistically significant (Sup. 5.2). Additionally, we performed in-situ hybridisation on FRT tissues at 5 dpi (Sup. 5.3). ZIKV RNA was detected in the lower FRT (LFRT) of WT, IFNε$^{-/-}$ and IFNAR1$^{-/-}$ mice, however this was below the limit of detection in the upper FRT (UFRT) except for IFNAR1$^{-/-}$ mice. Unexpectedly, the absence of IFNε also led to greater spread of virus to the draining illiac lymph node and spleen by 5 dpi (Fig. 5.1f & g & h) despite these tissues having no detectable or very low levels of IFNε mRNA (Sup. 5.2). Similar to previous reports [133, 145], we found detectable levels of IFNε mRNA in the brain of WT mice, and in the absence of IFNε, mice displayed greater levels of infection in the brain by 5 dpi. However, unlike the uterus and ovary that remained infected in the absence of IFNε, by 7 dpi the levels of ZIKV RNA detected in the lymph node, spleen and brain were equivalent to WT (Sup. 5.1). In contrast to WT and IFNε$^{-/-}$ mice, the high level of infection seen in all tissues of IFNAR1$^{-/-}$ mice at 5 and 7 dpi illustrated the major contribution of all type-I IFNs in protecting against the systemic spread of ZIKV infection. Collectively this data emphasises the importance of type-I IFNs, and specifically of IFNε, in early protection of the FRT from ZIKV infection and in limiting spread to other tissues via this route.

To further characterise the role of IFNε in control of viral infection of the FRT, IFNε$^{-/-}$ mice were reconstituted with intravaginal treatments of recombinant mIFNε or buffer alone 6 h prior to infection with ZIKV. As expected, mice treated with mIFNε had lower levels of infectious ZIKV in VW (Fig. 5.1i) and this effect seemed to be limited to the lower reproductive tract observed by qRT-PCR (results not shown). To further characterise this response, we treated uninfected IFNε$^{-/-}$ mice with recombinant mIFNε or mIFNλ-2 (4μg) and assessed antiviral ISG expression in the lower FRT (LFRT) (Fig. 5.1J) and upper FRT (UFRT) (Sup. 5.4) 6 h post-treatment. We observed ISG induction induced by both recombinant mIFNε and mIFNλ-

2 importantly in the vagina but not uterus or ovary that is consistent with the antiviral effect of recombinant IFNε noted above.

To further investigate the compartmentalisation of these intravaginal treatments to the LFRT, WT mice were injected with an IFNε blocking antibody which led to increased viral titres in comparison to the isotype controls. This effect was evident in vaginal samples (Fig. 5.1k&l), but not in samples from the UFRT, nor distant organs (Sup. 5.5). In the UFRT mice controlled the infection in part due to competent IFN signalling in these tissues [165], also likely indicating the instilled IFN or antibody treatments did not reach the UFRT.

Together, this data demonstrates endogenous IFNε expression in the FRT has a significant impact on local ZIKV infection and viral dissemination at early times post infection. This effect is added to by other type-I IFNs controlling infection especially at in peripheral tissues at later timepoints.

5.3.2 Antiviral effect of IFNε on cells of vaginal and cervical origin

Having demonstrated that IFNε plays an important role in control of ZIKV infection in our mouse model it was important to determine the effect and mechanism of action in human, for which we tested vaginal and cervical epithelial cells - the first infected by sexually transmitted pathogens [2].

We initially determined these cell types were permissive to infection by inoculating primary transformed ectocervical (Ect1) or vaginal keratinocyte (VK2) cells with increasing MOI of ZIKV (PRVABC59) and detection of infected cells by E-antigen immunofluorescence staining (Fig. 5.2a), or titrating infected cell supernatants by plaque assay (Fig. 5.2b &c). We then evaluated the impact of recombinant IFNε on ZIKV infection in these cells, compared to other IFNs that are important modulators of antiviral activity at mucosal surfaces (IFNα and IFNλ) [182]. IFNε treatment inhibited viral infection of both Ect1 and VK2 cells by ~90%, whether determined by plaque assay or viral RNA (Ect1 vRNA: 88% reduced) (Fig. 5.2b-e). Similar reduction in viral titres or vRNA were elicited by IFNα (Ect1 vRNA: 78%) and IFNλ (Ect1 vRNA: 83%) (Fig. 5.2b-g), indicating that IFNε can generate an antiviral state similar to that of IFNα or IFNλ in epithelial FRT cell lines.

To further investigate their antiviral functions, we compared the responses to these IFNs in FRT cells using whole transcriptome profiling by RNAseq analysis (NextSeq550 V2.5). Interestingly, IFNε and IFNλ-III had almost indistinguishable gene signatures at this time point (Fig. 5.3a, Sup. 5.6) which contrasts recent reports comparing type-I, IFNβ, and type-III IFNs

that found several differently regulated ISGs [36, 98]. As expected, all IFN treatments significantly upregulated a number of canonical ISGs in both cell types compared to untreated controls (Fig. 5.3b, c & d). Consistent with the reported specific activities of these IFNs [134, 318, 335], IFNα induced the strongest response, upregulating greater numbers and magnitude changes of responsive genes (See Fig 5.3b).

Next, we performed qRT-PCR analysis to confirm expression of key antiviral (Fig. 5.3e & f) or proinflammatory (Fig. 5.4g & h) genes. Key ISGs that protect against ZIKV infection (Viperin [354], ISG15 [327], IFITM1[300], IFI6 [89]) were upregulated in all three treatments. We also noted that while both type-I and type-III IFNs were able to induce expression of the proinflammatory CXCR3 ligands, CXCL10 and CXCL11, but that their expression was significantly lower in IFNε and IFNλ treatments. Interestingly, a recent report has suggested that temporal ISG induction by type-I and III IFNs provides a collaborative antiviral response, with type-I IFNβ promoting inflammation via an IRF-1 dependant inflammatory response [98]. Consistent with this observation we also noted an increase in IRF-1 expression in Ect1 and VK2 cells stimulated with IFNα as compared to stimulation with IFNε and IFNλ-III (Fig. 5.3a, h,i). This increase in IRF-1 expression for IFNα suggests that IFNα, like IFNβ, drives a greater proinflammatory phenotype in comparison to IFNε and IFNλ-III that is reflected by increased expression proinflammatory ISGs like CXCL10 and CXCL11.

To further understand the spatiotemporal action of IFNε in the FRT we compared ISG induction in Ect1 cells responding to IFNε, IFNα-2A, and IFNλ-III treatments over time. IFNε induced an early but transient induction of ISGs (ISG15, Viperin, CXCL10) while IFNα induced early induction of ISGs that was maintained over the 24 h time course (Fig. 5.3i, j &k) and IFNλ a gradual induction of ISGs over 24 hrs as seen previously in liver and lung epithelial cell lines [28, 98, 158, 172, 206, 356]. Collectively this suggests that these IFNs have evolved to perform specialised functions to coordinate antiviral responses spatiotemporally to combat viral infection of the FRT. Of these functions the apparent ability of IFNε to induce lower levels of the transcription factor IRF1 and proinflammatory genes in the FRT, like IFNλ rather than IFNα, warrants further investigation.

5.3.3 Treatment of cells with IFNε prior to infection precedes ZIKV evasion of type-I and type-III IFN signalling pathways

To understand the impact of IFNε's unique constitutive expression on ZIKV evasion of IFN responses in humans that are mediated by viral NS proteins [121, 176, 374], we treated the

placental trophoblast cell line HTR8, with IFNε or IFNα either pre- or post-infection with ZIKV (Fig. 5.4a). When administered at later time points post-infection (24 hpi), both IFNε and IFNα treatments were less efficient at controlling ZIKV infection compared to early treatments (3 hpi), leading to greater levels of vRNA in cells or levels of infectious virus in supernatants (Fig. 5.4 b&c). However, compared to pre-treated conditions, early post-infection treatment was significantly less effective at limiting ZIKV infection. This observation is consistent with similar studies for other flaviviruses, showing a rapid shut-down of IFN signalling following viral entry and detectable NS protein expression as early as 3 hpi [16]. As expected, this effect was also observed for IFNλ-III, since this relies on a similar signalling pathway to type-I IFNs (Fig. 5.4d &e).

To observe the molecular target of ZIKVs evasion downstream of IFNε we first investigated STAT1/2 nuclear translocation by immunofluorescence, and STAT1/2 phosphorylation 30 min post-treatment by western blotting in HeLa cells infected with ZIKV. Cells infected with ZIKV had a reduced capacity for STAT1 nuclear translocation (Fig. 5.5a) in comparison to uninfected cells and this correlated with a reduction in STAT1-Y701P phosphorylation (Fig. 5.5c) post stimulation with IFNε. Importantly, STAT2 nuclear translocation (Fig. 5.5b), phosphorylation (STAT2-Y690P) and total protein levels (Fig. 5.5c) were more potently reduced by ZIKV infection compared to the observed effects on STAT1. This effect on STAT1 and STAT2 phosphorylation following ZIKV infection was comparable after stimulation with IFNα (Fig. 5.5d), indicating a similar mechanism of ZIKV-mediated evasion was responsible for inhibiting the pathway downstream of both IFNs.

Next, we determined if inhibition of STAT2 activation by IFNε was driven by the same ZIKV factors as previously described for IFNα [121]. HeLa cells transfected with plasmids expressing ZIKV NS5, or an empty vector were stimulated with IFNε or IFNα and 30 minutes post stimulation, STAT1/STAT2 activation was assessed as above. In the presence of NS5 protein and IFNε stimulation, total STAT2 protein was reduced that corresponded to a concomitant decrease in STAT2 phosphorylation with no impact on STAT1 phosphorylation (Fig. 5.6a). A similar picture was also seen for IFNα stimulation (Fig. 5.6b). Interestingly, total STAT1 and phosphorylated STAT1 in the presence of ZIKV NS2B/3 and IFNs remained constant despite previous findings that ectopic expression of NS2B/3 protein inhibits STAT1 activation [374]. To confirm the impact of reduced STAT2 phosphorylation on downstream signalling we performed a dual luciferase assay for ISRE activity and qRT-PCR for ISGs. Accordingly, Figure

5.6c shows NS5 expression also inhibits downstream ISRE and concomitant ISG expression (representative gene ISG15 shown for simplicity) in HeLa cells in a dose dependent fashion (Fig. 5.6d).

Taken together this data demonstrates the potent ability of ZIKV to shut-down type-I and III IFN responses after infection is established, primarily via ZIKV NS5 induced STAT2 degradation. This highlights the importance of priming with IFN before infection is established to limit virus spread and therefore implies the likely significance of IFNε as the only constitutively expressed IFN detectable in the non-pregnant FRT.

5.3.4 IFNε constitutive expression is not inhibited by ZIKV infection or NS proteins

The expression of IFNε in the FRT prior to viral infection is hypothesised by us and others [62] to circumvent pathogen-mediated IFN evasion helping to protect the FRT from viral and bacterial infections. However, this assumes infection cannot inhibit IFNε expression, therefore we asked if ZIKV infection could inhibit the expression of IFNε.

HeLa cells are known to express IFNε RNA at levels similar to FRT cell lines [105], therefore we used these to investigate expression of IFNε compared to other type-I and III IFNs in response to ZIKV infection or poly I:C stimulation (viral mimic). At a basal level, we found that IFNε was highly expressed compared to other type-I and III IFNs (Fig. 5.7a). Consistent with previous reports [105] we saw minimal induction of IFNε in HeLa cells in response to either ZIKV infection or poly I:C transfection. Conversely, PRR-mediated induction of type-I IFNβ and type-III IFNλ was required to generate expression levels equivalent to basal IFNε in these cells. Interestingly, we did not see ZIKV mediated dampening of poly I:C induced IFNβ induction when cells were infected prior to poly I:C stimulation as reported previously by our group [354] and others [374]. However, these experiments were conducted in either Huh-7 or A549 cells, suggesting the PRR pathways that contribute to HeLa cell IFN expression may differ and are not as efficiently inhibited by ZIKV.

To isolate on the main pathway responsible for inducing IFN expression in response to ZIKV infection (RIG-I/MAVS) [302, 381] we co-transfected HeLa cells with a plasmid expressing constitutively active RIG-I (RIG-I-N [384]) and either vectors expressing ZIKV-NS1/NS4A/NS2B-3/NS5-FLAG or an empty vector control (see Sup. 5.7 for protein expression levels). These NS proteins are known to restrict the expression of other type-I IFNs in response to viral infection [176, 189, 198, 200, 375]. Expression of RIG-I-N alone resulted in the upregulation of IFNβ and type-III IFNλ and this was restricted by the presence of co-expressed ZIKV-NS1, NS4A, NS5 but

not NS2B/3 (Fig. 5.7b). Conversely the constitutive expression of IFNε RNA was unaffected by RIG-I pathway stimulation or by the presence of NS proteins in these cells.

Together this data demonstrates IFNε constitutive expression is not altered following ZIKV infection. This contrasts with other type-I and III IFNs (IFNβ and IFNλ-I) that rely on PRR activation for their expression and are therefore susceptible to inhibition by ZIKV NS-proteins.

5.4 Discussion

ZIKV is the only *Flavivirus* known to transmit both sexually and in utero, making it a unique threat to the FRT immunological niche, both during pregnancy and under normal physiological conditions. Here we demonstrate the non-redundant role of a novel type-I IFN; IFNε, in protecting the FRT from ZIKV infections both in vitro and in a mouse model of vaginal transmission.

To assess the contribution of endogenous IFNε in controlling ZIKV FRT infections we used a murine model of vaginal transmission. In this model DMPA treatment was used to synchronise mice to diestrus, rendering mice susceptible to ZIKV iVag infection as reported by other groups [36, 341, 381]. Since IFNε is hormonally regulated its expression is reduced during diestrus and pregnancy in mice [105]. This reduction in IFNε may contribute to the natural susceptibility of WT mice during diestrus [341, 381] and pregnancy [381] to iVag ZIKV infection compared to systemic inoculation methods. Importantly, this means our data must be viewed as “no” versus “low” IFNε in the FRT when comparing IFNε$^{-/-}$ to WT mice. ZIKV infection via iVag inoculation was compared between WT, IFNε$^{-/-}$ and IFNAR1$^{-/-}$ mice.

Although WT mice expressed suboptimal levels of IFNε, we found that its presence in the FRT was sufficient to offer significant protection against ZIKV iVag infection compared to mice lacking IFNε. This protection was most significant during the early stages of infection as indicated by the high levels of infectious virus recovered in the VW of IFNε$^{-/-}$ mice that closely mirrored levels observed in the highly susceptible IFNAR1$^{-/-}$ mice. Interestingly, the antiviral activity of endogenous IFNε primarily acted in the UFRT tissues and not the vagina, despite the vagina expressing high levels of IFNε mRNA compared to peripheral tissues such as the spleen. Notably, there was also a smaller difference in vRNA levels between WT and IFNAR1$^{-/-}$ mice in this tissue compared to upper FRT tissues. This demonstrates a lesser overall impact of type-I IFN signalling in the vagina and agrees with recent reports showing a small impact of

IFNAR1$^{-/-}$ in ZIKV infected lower FRT (LFRT) compared to the upper FRT (UFRT) in mice, reportedly due to lower relative PRR expression in LFRT [165]. Our data suggests the LFRT is highly susceptible to ZIKV infection independent of endogenous or induced IFN expression, potentially explaining ZIKVs aptitude for sexual transmission in humans. Comparatively we demonstrate that IFNε expressed in the UFRT, the site of *in utero* transmission, is essential for ZIKV infection control.

In apparent contrast to our observations that indicate IFNε plays a significant role in protecting the FRT from ZIKV infection, multiple groups have observed type-I and III IFN independent protection of the FRT during estrus in mice [36, 61]. This appears counterintuitive to IFNε playing a significant role since mice in estrus have the highest levels of IFNε expression in FRT tissues [105]. This mechanism of estrus dependent, IFN independent protection against ZIKV infection in mice is yet to be fully characterised. However, one plausible theory is that this effect is mediated by thickening of the epithelial layer during estrus in both upper and lower reproductive tract of mice, presenting an additional physical barrier to infection. Comparatively in humans, the epithelium of the lower reproductive tract remains constant over the menstrual cycle [370]. This additional barrier during estrus may mask the contribution of IFNε during this stage of the cycle in mice. Therefore, it is plausible the effect of IFNε may be more significant in human sexual transmission due to physiological differences in FRT biology. Additionally, ZIKV NS5 mediated evasion of human but not mouse IFN signalling via STAT2 degradation [121] likely enhances the antiviral efficacy of ZIKV-induced IFNs in WT compared to IFNAR/IFNLR$^{-/-}$ mouse models.

Interestingly, IFNε also significantly decreased the dissemination of ZIKV to the peripheral tissues in WT mice by 5 dpi. Since IFNε is primarily expressed in the FRT it was surmised this effect resulted from additional replication in the FRT driving increased circulation of the virus to the peripheral organs. However, unlike the spleen and lymph node that do not express IFNε, we detected relatively high levels of IFNε mRNA in the brain (see Sup. 5.1) consistent with reports by others [133, 262]. If IFNε protein is functionally expressed in the brain it may have a role in protecting against ZIKV as a neurotropic *Flavivirus*. Interestingly, one study in humans has linked a polymorphism of IFNε to cerebral haemorrhage, indicating it may be functionally expressed in this tissue [169]. Studies to determine the antiviral role of IFNε in the brain would be an area of interest to ZIKV and other neurotropic viruses.

Collectively this data has demonstrated that IFNε plays a significant and non-redundant role at physiological levels during early infection of the FRT and in preventing systemic dissemination in non-pregnant adult female mice.

Understanding the capacity to modulate immune responses is the first step towards developing new immune therapies. Here we have shown modulation of IFNε levels in the lower FRT can alter the infectivity of mice by ZIKV intravaginal infection. Antibody mediated neutralisation of IFNε in WT mice significantly increased infection. On the other hand, iVag treatment with IFNε was able to restore antiviral activity in IFNε$^{-/-}$ mice. Furthermore, we investigated the immune stimulatory properties of intravaginally administered recombinant IFNε. This produced increased ISG expression in the vagina without significantly inducing ISGs in the UFRT. This indicates short iVag IFN treatments mainly act to prevent establishment of infection in the LFRT likely protecting against ascending infection and female to male sexual transmission.

To extend these observations to human cell culture we next investigated the antiviral properties of IFNε on FRT cell lines. Pre-treatment with either IFNε, IFNα or IFNλ3 protected Ect1 and VK2 cells from ZIKV infection, indicating the importance of both type-I and III IFNs in protection of the FRT in humans. We found that IFNε generated antiviral responses in FRT Ect1 and VK2 cell lines by inducing a typical IFN antiviral signature, including upregulation of several ISGs known to inhibit ZIKV infection. Interestingly, the gene signature of IFNε treatment was almost indistinguishable to IFNλ at this time point (6 h) despite signalling through different receptors. Both IFNε and IFNλ were found to induce lower levels of the transcription factor IRF1 and proinflammatory genes compared to conventional type-I IFNα treatment at the same concentration. Confirmation by qRT-PCR of key anti-ZIKV ISGs or proinflammatory genes indicated fold induction consistent with the reported specific activities of these IFNs, with IFNα inducing a more potent response than either IFNε or IFNλ at the same ng/mL concentration. Together this data shows at early times post-stimulation, IFNε induces a typical antiviral gene signature in FRT cell lines, and like type-III IFNs may have a lower propensity to induce inflammation via CXCR3 ligand regulation compared to conventional type-I IFNs. We propose the lower specific activity of IFNε provides an evolutionary advantage because of its constitutive presence in the FRT, striking a balance between limiting infection, inflammation, and normal reproductive function in these tissues.

Additionally, we found that the kinetics of gene induction in response to IFNε in FRT cell line was rapid, having highest levels of ISGs at early times and waning by 24 h. Comparatively, IFNλ displayed typical type-III induction having gradually increasing gene expression with the greatest levels of gene induction at 24 h. This suggests that type-I and type-III IFNs likely have differing spatial-temporal roles in controlling ZIKV infection and most likely other infections of the FRT.

The importance of both type-I and type-III IFNs protecting against ZIKV infection is now well established in mice [36, 87, 231, 341, 381]. However, in humans and other primates, ZIKV has adapted to evade IFN responses via multiple host-viral interactions that restrict the effectiveness of IFN mediated protection [121, 176, 216, 374]. Understanding and exploiting this axis of host-virus interaction is therefore important to improve patient outcomes. Here we have shown ZIKV can evade both type-I and III IFN mediated antiviral activities downstream of receptor binding within hours after infection is established. ZIKV was able to limit the induction of ISGs via blocking both STAT1 and STAT2 activation. The key molecular mechanism underlying this effect was found to be NS5 mediated degradation of STAT2 protein as previously described for IFNα [121]. Importantly this effect was equally applicable to IFNα, IFNε, and IFNλ. Equivalent viral evasion highlights the similarities between the type-I and III IFN signalling pathways that contribute to anti-ZIKV activity. Furthermore, ZIKVs efficient evasion of both type-I and III IFN antiviral activity after infection is established, highlights the importance of a rapid induction of ISGs or priming cells with IFN to effectively prevent infection. This also suggests that at times when IFNε is reduced, such as early pregnancy [105, 250], the FRT is likely more vulnerable to ZIKV infection. Importantly, IFNε is the only IFN known to be produced constitutively by mucosal surfaces of the non-pregnant FRT [253] suggesting it may have a significant impact on human FRT infections.

Additionally, we characterised the constitutive nature of IFNε expression under viral infection and showed that in contrast to type-I and III IFNs, endogenous expression of IFNε was not susceptible to ZIKV-mediated evasion. This demonstrates for ZIKV infections, the FRT can be pre-emptively tuned to an antiviral state and that it appears to be a unique property of IFNε, stemming from the different regulatory pathways that govern its expression. Further exploration into the stimuli and pathways that regulate IFNε expression in the human FRT will therefore be important to downstream therapeutic applications.

5.5 Conclusion

In summary we have shown that IFNε is an important mediator of antiviral activity in the FRT of both mice and humans. This activity is effective to reduce ZIKV iVag transmission in mice and infection in FRT cell lines. The constitutive presence of IFNε in the non-pregnant FRT is likely significant in human infections as ZIKV can effectively evade post-infection IFN responses but is strongly inhibited by prophylactic treatment.

5.6 Methods and Materials

5.6.1 Virus. Low passage ZIKV strain PRVABC59 was propagated in C6/36 mosquito larvae cells. Infectious virus stock titres were determined by Focus Forming Assay on Huh7.5 cells.

5.6.2 Cell lines, reagents and recombinant IFNs. HeLa and Vero E6 cells were cultured in DMEM supplemented with 10% FCS and 1% Penicillin/Streptomycin. HTR8 cells were maintained in RMPI with 10% FCS and 1% Penicillin/Streptomycin. Ect1 and VK2 cells were cultured in Keratinocyte Serum Free Media supplemented with 0.1 ng/mL human recombinant EGF, 0.05 mg/mL bovine pituitary extract, additional calcium chloride 44.1 mg/mL and 1% Penicillin/Streptomycin. All cell lines were cultured at 37 °C with 5% CO_2. Mouse and human recombinant IFNε protein (mIFNε, hIFNε) were made in house as previously described [110, 335]. Commercial IFNs were hIFNα-2A (PeproTech), hIL-28B (R&D systems) and mIFNλ2 (PeproTech). Due to the limited supply of hIFNε, large scale *in vitro* experiments on HTR8 or HeLa cells used mIFNε (10 U/mL) and hIFNα-2A (500 U/mL). These concentrations were titered by direct comparison of receptor activation levels and antiviral properties (see Supl. Fig. 5.8). For specific use of antibodies see supplementary methods.

5.6.3 Mice. Sexually mature female mice aged between 6 – 12 weeks at the time of infection were used in these experiments. Mice from each genetic background were age matched between experiment groups to minimise the impact of differing susceptibility. C57BL/6 (WT) mice were purchased from Monash Animal Services and acclimatised for one week prior to infection. IFNε$^{-/-}$ and IFNAR1$^{-/-}$ mice on C57BL/6 background were maintained in house.

5.6.4 Intravaginal infection and treatments of mice. All mice were treated with 2 mg Depo-ralovera DMPA (Kenral) subcutaneously 5 days prior to infection to synchronize the estrus cycle into diestrus phase on the day of infection as previously described [105]. On day 0 mice were anesthetised using isoflurane then inoculated intravaginally with 5 x 10^5 FFU ZIKV in 10

µL PBS, then kept under aesthetic for 2-3 minutes to promote viral adherence. Mice were monitored daily to assess clinical signs of disease: 0, no apparent signs of disease; 1, genital redness or minor genital swelling; 2, genital redness and genital swelling, huddled and inactive; 3, severe lethargy and little response to handling. At day 5 or 7 mice were culled, and tissues were extracted. Tissues for RNA extraction were flash frozen in liquid nitrogen and tissues for IHC or ISH staining were fixed in 10% neutral buffered formalin for a minimum of 24 h prior to embedding in paraffin. Treatments with 4 µg mIFNε or 100 µg IFNε neutralising antibody (made in house) were administered intravaginally 6 h prior to infection (or tissue collection) and again on day 3 post infection. Control groups were treated with either buffer or an IgG isotype control antibody equivalently.

5.6.5 Plaque Assay – detection of infectious virus and collection of vaginal wash samples. Vaginal washes were collected by pipetting 30 µL of PBS into the vaginal cavity. Washes were performed twice for each mouse and pooled. Samples were immediately transferred to dry ice and stored at -80°C until ready for use. Then Vero cells in 12-well trays at approximately 90% confluency were infected with 300 µL of serially-diluted virus-containing supernatants for 1 hour at 37 °C. Supernatants were then replaced with a 1mL overlay of complete media containing 1.5% (w/v) carboxymethylcellulose (CMC) (Sigma) and cells returned to culture for 5 days. Cell monolayers were then fixed with 10% formalin and incubation for 1 h. The CMC overlay was then removed, and plaques were visualised via crystal violet stain. Plaques were enumerated, and virus infectivity expressed as plaque-forming units (PFU) per mL.

5.6.6 Tissue RNA extractions and cDNA preparation and qRT-PCR. 500 µL of TRISURE reagent was added to each frozen tissue and these were dissociated in an RNAse free microcentrifuge tube (Eppendorf) using a homogenisation pestle. A further 500µL of TRISURE was added prior to the addition of 200 µL chloroform and separation of the aqueous phase by cold centrifugation. The aqueous layer was reserved and 500 µL 100% ethanol was added. This was then transferred to an RNAeasy column (QIAGEN) for final RNA isolation as per manufacturer's instructions. cDNA synthesis was performed using MMLV-reverse transcriptase (Promega), reactions contained either 500 ng or 1000 ng RNA (dependent on the lowest RNA yield in a tissue cohort for consistency) and primed with 500ng random hexamer. cDNA were diluted 1 in 4 prior to use. qRT-PCR was performed with Roche FastStart Universal SYBR green (ROX) reagent using the QuantStudio 7 Real-Time PCR System (Applied Biosystem).

5.6.7 Quantification and analysis of viral RNA (vRNA) genome copies per µg RNA determination of lower LOD for uninfected tissues. A plasmid containing the full-length genome of a Brazilian ZIKV (Paraiba_2015) was used to generate a standard curve for qRT-PCR analysis [350]. First the plasmid was linearised using EcoRV and column purified. The number of genome copies per ng of plasmid was enumerated based on the molecular weight of the plasmid. Serial dilutions on a log2 scale were used to place the curve within a detectable range (between 13 – 36 cycles). A standard curve containing 8 dilutions (including blank) was run with each tissue cohort. Raw CT values were plotted against log2 transformed genome copies and CT values from each tissue cohort were interpolated using the standard curve. Log2 interpolated values were then transformed to a linear scale and normalised to µg RNA used in total cDNA preparation. To achieve normal distributions and equal standard deviations between genotypes, data was log10 transformed and represented as log10 genome copies per µg RNA. Determination of the limit of detection for uninfected tissues was performed by qRT-PCR analysis of treatment, genotype and tissue matched uninfected samples (5 per group) using the same ZIKV PCR primers. CT values from uninfected tissues were compared between genotypes and tissues to ensure consistency in primer background. The earliest detected CT value for all uninfected tissues was determined to be 36.4. This value was then applied to each tissues standard curve to give the minimum value for infected tissue detection. Mice were determined to be uninfected by assessment of melt curves in both technical duplicates and their CT value compared to uninfected controls.

5.6.8 Viral RNA *In Situ* Hybridization. RNA ISH was performed on formalin fixed paraffin embedded sections (5 µM) using RNAscope 2.5 HD (Brown) (Advanced Cell Diagnostics) according to the manufacturer's instructions and as previously described [115].

5.6.9 RNAseq sample preparation and analysis. Ect1 and VK2 cells seeded to 90% confluency in 6 well plates were treated with hIFNε, hIFNα-2a or hIFNλ-3 (100 ng/mL) diluted in fresh culture media or left untreated (n = 4) for 6 h prior to harvesting RNA in RLT buffer (Qiagen) with added β-ME. Lysates were homogenized by passing through a 20-gauge needle attached to a sterile plastic syringe. Total RNA were extracted from lysates using the Qiagen RNeasy kit, including removal of DNA contamination using the Qiagen RNase free DNase set as per the manufacturers instructions. Library preparation and RNASeq analysis (Illumina NextSeq550 V2.5) were performed using a novel in house RNA-seq pipeline (ACRF, Medical

Genomics Facility, Monash). Differentially expressed genes were determined with a 1.2-fold cut-off and adjusted p-value < 0.05.

5.6.10 Focus forming assay – detection of infectious virus. Vero or Huh 7.5 cells were seeded in 96 well plates (90% confluence for infection) were inoculated with 40 µL of serially diluted viral supernatants for 3 hours at 37 °C with manual agitation every 20 minutes. Inoculum was removed and replaced with 100 µL fresh culture medium for 48 hours in a level incubator without shaking. Cells were fixed with acetone/methanol prior to indirect immunofluorescence detection of ZIKV protein using the 4G2-pan *Flavivirus* E primary antibody and fluorescently labelled secondary antibody. Foci were enumerated by observation under a fluorescent microscope and were defined as more than 3 infected cells in a distinct cluster. Each sample was calculated based on biological triplicates with technical duplicates then expressed as Focus Forming Units (FFU) per mL.

5.6.11 Plasmids and transfections. Non-structural proteins were PCR amplified from an infectious clone of a Brazilian isolate of ZIKV (Paraiba_2015) [350] and cloned into the expression plasmid pCDNA6.2 by Gibson Assembly using primers containing 3' FLAG extension. Empty vector was used as a control in all expression experiments or as a filler for co-transfection in dose dependent assays.

NS1

F ACCGATCCAGCCTCCGGACTCTAGAatggatgtggggtgctc

R TCAGTTAGCCTCCCCCGTTTAAACTTACTTGTCGTCATCGTCTTTGTAGTCtgcagtcaccactg

NS2B/3

F ACCGATCCAGCCTCCGGACTCTAGAatgagctggcccccta

R TCAGTTAGCCTCCCCCGTTTAAACTTACTTGTCGTCATCGTCTTTGTAGTCtcttttcccagcgg

NS4A

F ACCGATCCAGCCTCCGGACTCTAGAatgggagcggcttttgg

R TCAGTTAGCCTCCCCCGTTTAAACTTACTTGTCGTCATCGTCTTTGTAGTCtctttgcttttctggctca

NS5

F GGGACCGATCCAGCCTCCGGACTCTAGAATGgggggtggaacag

R GTTTCAGTTAGCCTCCCCCGTTTAAACTTACTTGTCGTCATCGTCTTTGTAGTCcagcactccaggtg

Plasmids containing constitutively active RIG-I-N or ISRE-Luciferase have been described previously [354, 384]. Transfections were performed using with a 2:1 ratio of lipofectamine 2000 reagent (Invitrogen) to DNA.

5.6.12 Dual luciferase assay. HeLa cells were co-transfected with the ISRE-luciferase reporter construct, the constitutive renilla luciferase reporter pRL-TK (Promega) as a transfection control and the according pCDNA6.2-NS expression construct or empty vector (total DNA 1µg per 12 well). Each transfection condition was carried out in triplicate. 24 hours following stimulation with IFN cells were harvested in 1 x passive lysis buffer (Promega) and stored at -20°C. For luciferase assays, the samples were thawed and aliquoted in technical duplicates for detection of firefly and renilla luciferase activity using the Dual-Luciferase Reporter Assay kit using the GloMax luminometer to the manufacturer's specifications (Promega). Promoter activity was determined by normalising firefly luciferase values to renilla luciferase values and expressed as relative light units (RLU).

5.6.13 Immunofluorescence microscopy. Briefly, cells were grown in culture plates and fixed with ice-cold acetone:methanol (1:1) for 10 minutes at 4 °C. After washing twice with PBS, samples were blocked with 5% BSA in PBS for 30 min at room temperature and incubated with primary antibody (for specific usage see Sup.) diluted in PBS/1% BSA for 1 h at room temperature. After washing twice with PBS, cells were incubated with Alexa Fluor-conjugated secondary antibody diluted 1:200 in PBS/1%BSA for 1 h at 4 °C in the dark. Samples were then washed with PBS and incubated with DAPI (Sigma-Aldrich, 1 µg/ml) for 5 min at room temperature. Samples were then washed with PBS. Images were then acquired using a Nikon TiE inverted fluorescent microscope. Contrast was applied using the 'Autoscale' function of NIS.

5.6.14 Western blot for STAT1/STAT2 phosphorylation. HeLa cells were seeded in 6 well trays to be approximately 80 % confluent for transfections. Transfections of NS protein expression constructs or empty vector control were performed as previously described using lipofectamine 2000. 24 h post transfection HeLa cells were stimulated with type-I IFN at the indicated concentrations, 30 minutes later protein was harvested in lysis buffer and left in the well on ice for 10 minutes prior to transfer into a new tube. Lysates were then homogenised by 10 passages through a 25 G needle prior to clearing cellular debris by centrifugation (16,000 RCF for 10 minutes at 4°C). Cleared lysate was diluted with reducing loading dye (3:4) and heated at 95 °C for 5 minutes prior to loading into SDS acrylamide gel and run for 90 minutes. Separate gels were run for each protein of roughly the same molecular weight on the same day to prevent freeze / thaw degradation. Membrane transfer was done for 1 h in

cold transfer buffer. Primary antibodies were applied at 1: 1000 (or to the recommended dilution) overnight in 1 % skim milk at 4°C with agitation. The following day secondary HRP conjugated antibodies were applied to the manufacturers specification for 1 h at room temperature with agitation. SuperSignal™ West Femto Maximum Sensitivity Substrate (ThermoFisher) was used to detect HRP signal using the BioRad gel dock imager.

5.6.15 Statistical analyses. For in vivo analysis of vaginal washes the ordinary two-way ANOVA was used on log10 transformed data comparing independent time points. For qRT-PCR analysis of vRNA the ordinary one-way ANOVA was used on log10 transformed data compared to wildtype. All graphing and statistical analyses were performed using GraphPad Prism 8.0. For *in vitro* experiments the analysis method is described in the figure legend.

5.6.16 Acknowledgements:

For conducting ISH experiments we would like to acknowledge Greg Saturday and Rebecca Rosenke (Rocky Mountain Veterinary Branch, RML, NIAID).

5.6.17 Funding:

This research was funded by the National Health and Medical Research Council (NHMRC) of Australia, awarded to M.R.B (APP1145613). Additionally, this work was supported by the Victorian State Government Operational Infrastructure Scheme. M.D.T was supported by an NHMRC Career Development Fellowship (1123319). Also, this study was supported in part by the Division of Intramural Research, National Institutes of Health, National Institute of Allergy and Infectious Diseases.

5.7 Figures

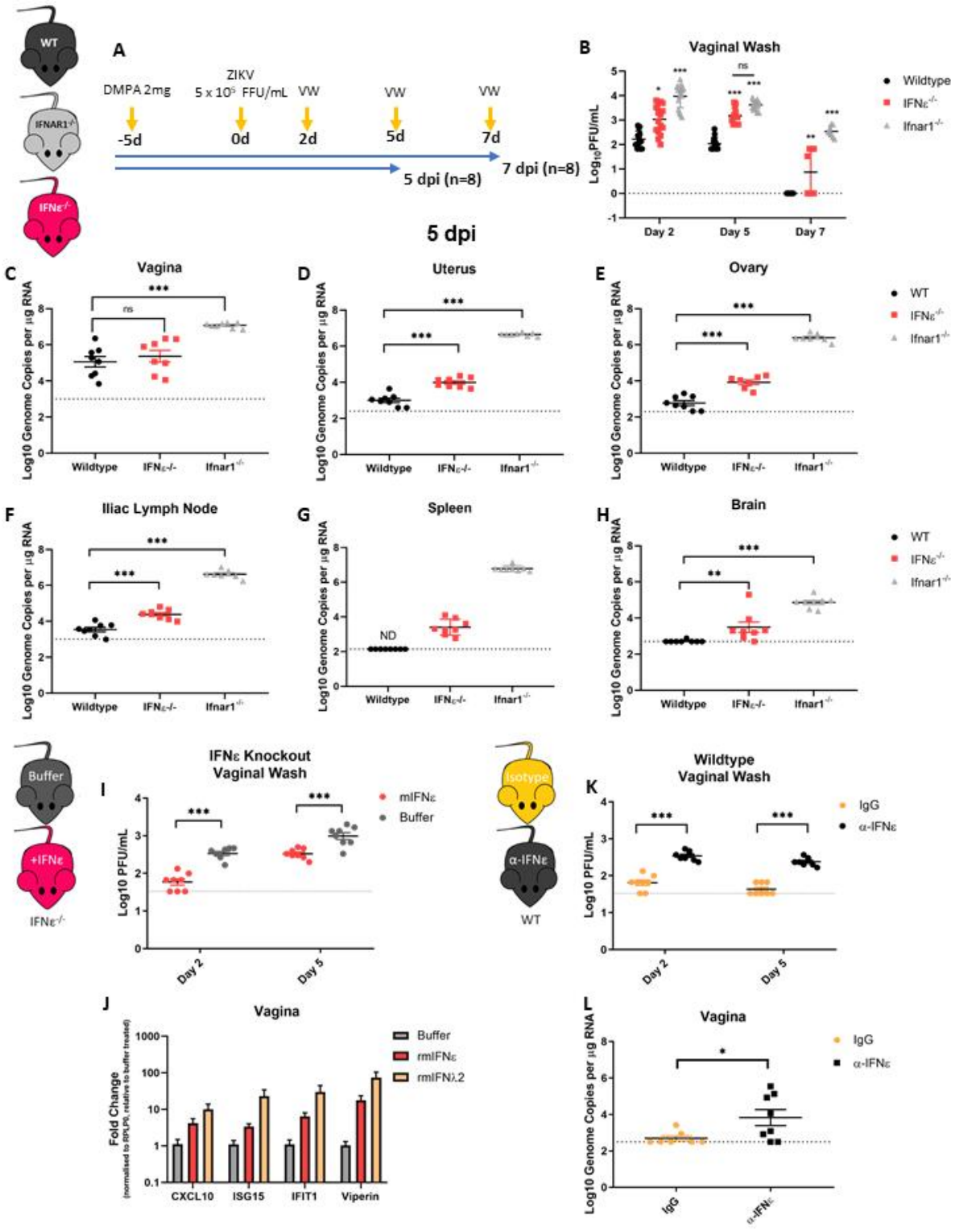

Figure 5.1: ZIKV replication is inhibited by IFNε in a mouse model of vaginal transmission. A) Experimental time-line of WT (black), mice lacking IFNε (IFNε-/-) (red) or mice lacking the type-I IFN receptor (IFNAR1-/-) (grey) were infected with ZIKV at 5 x 10^5 FFU iVag 5 days post DMPA treatment and vaginal washes were taken at 2, 5, 7 dpi. Groups of 8 mice were culled

at 5 dpi and 8 were culled at 7 dpi. B) Infectious virus was measured from vaginal washes by plaque assay at 2, 5, 7 dpi. C, D, E, F, G & H) Tissues taken at 5 dpi were used to harvest RNA for analysis of viral RNA by qRT-PCR in the vagina, uterus, ovary, illiac lymph node spleen and brain respectively. I) IFNε-/- mice were treated for 6h with either mIFNε or buffer prior to iVag infection with ZIKV, Infectious virus was measured from vaginal washes by plaque assay at 2 and 5 dpi. J) IFNε-/- mice were treated iVag with either mIFNε, mIFNλ2 or buffer for 6h prior to harvesting FRT tissues to determine the level of ISGs by qRT-PCR. K) WT mice mice were treated for 6h with either IFNε neutralising antibody (α-IFNε) or an isotype control (IgG) prior to iVag infection with ZIKV, Infectious virus was measured from vaginal washes by plaque assay at 2 and 5 dpi. Additionally, L) tissues taken at 5 dpi were used to harvest RNA for analysis of viral RNA by qRT-PCR in the vagina.

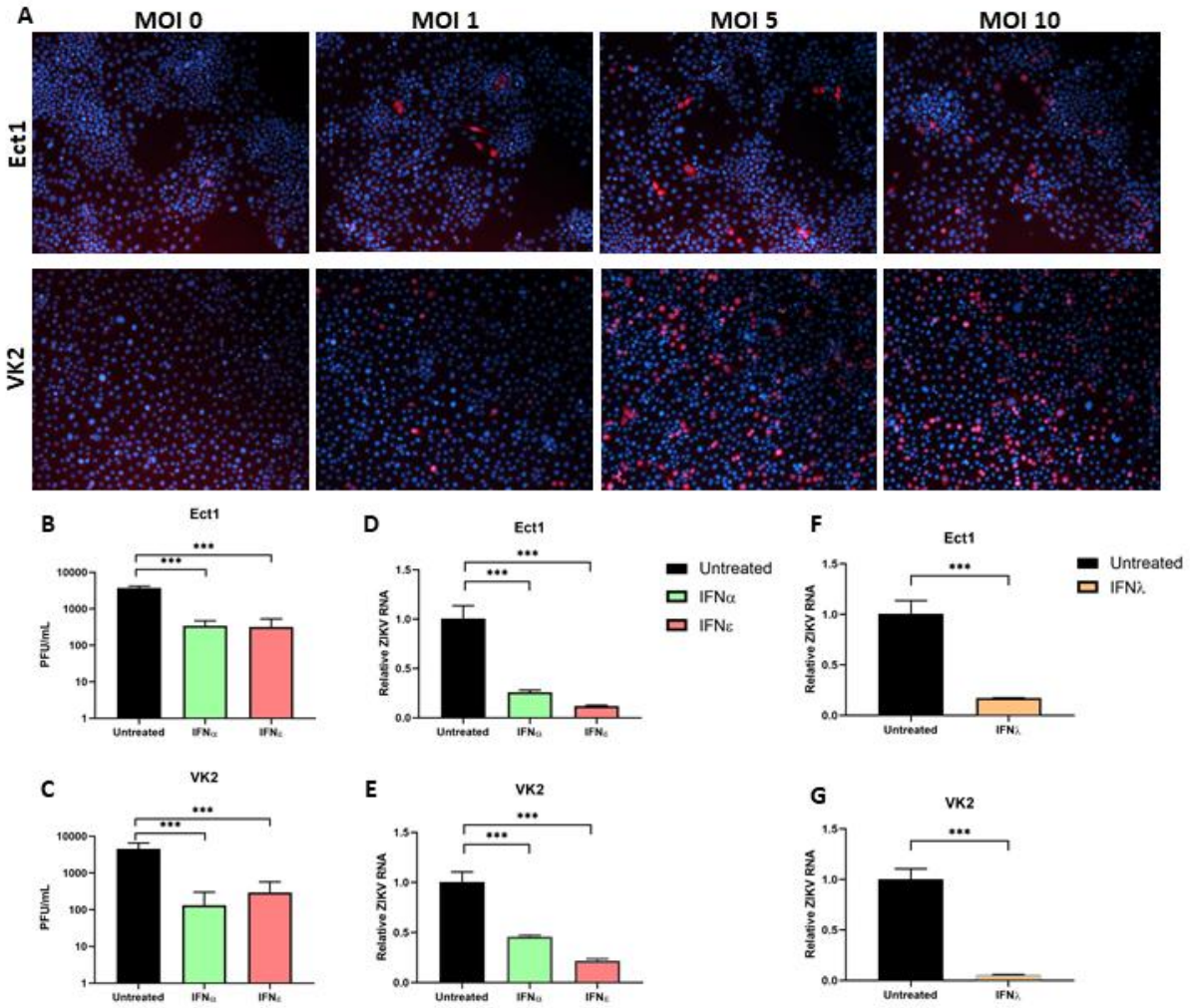

Figure 5.2: Ectocervical and Vaginal cell lines are permissive to ZIKV infection and treatment with IFNε is antiviral. A) Ect1 or VK2 cells were infected with ZIKV PRVABC59 at the indicated MOI for 24h prior to staining, anti-flavi E staining (red), DAPI (blue). Ect1 or VK2 cells were treated overnight with 100 U/mL rhIFNε, rhIFNα-2A then infected with MOI 10 or 5 respectively for a further 48h prior to collecting supernatant and RNA for plaque assay (B & C) detection of infectious virus or qRT-PCR detection (D & E) of vRNA. F & G) Ect1 or VK2 cells were treated overnight with 100 ng/mL rhFNλ-III then infected with MOI 10 or 5 respectively for a further 48h prior to harvesting RNA for detection of vRNA by qRT-PCR. Statistical analyses are performed by one-way ANOVA compared to the untreated control (b-e) or by two tailed t-test (f &g), (n.s non-significant, * $P < 0.05$, ** $P < 0.01$). Data are presented as means +/- S.D.

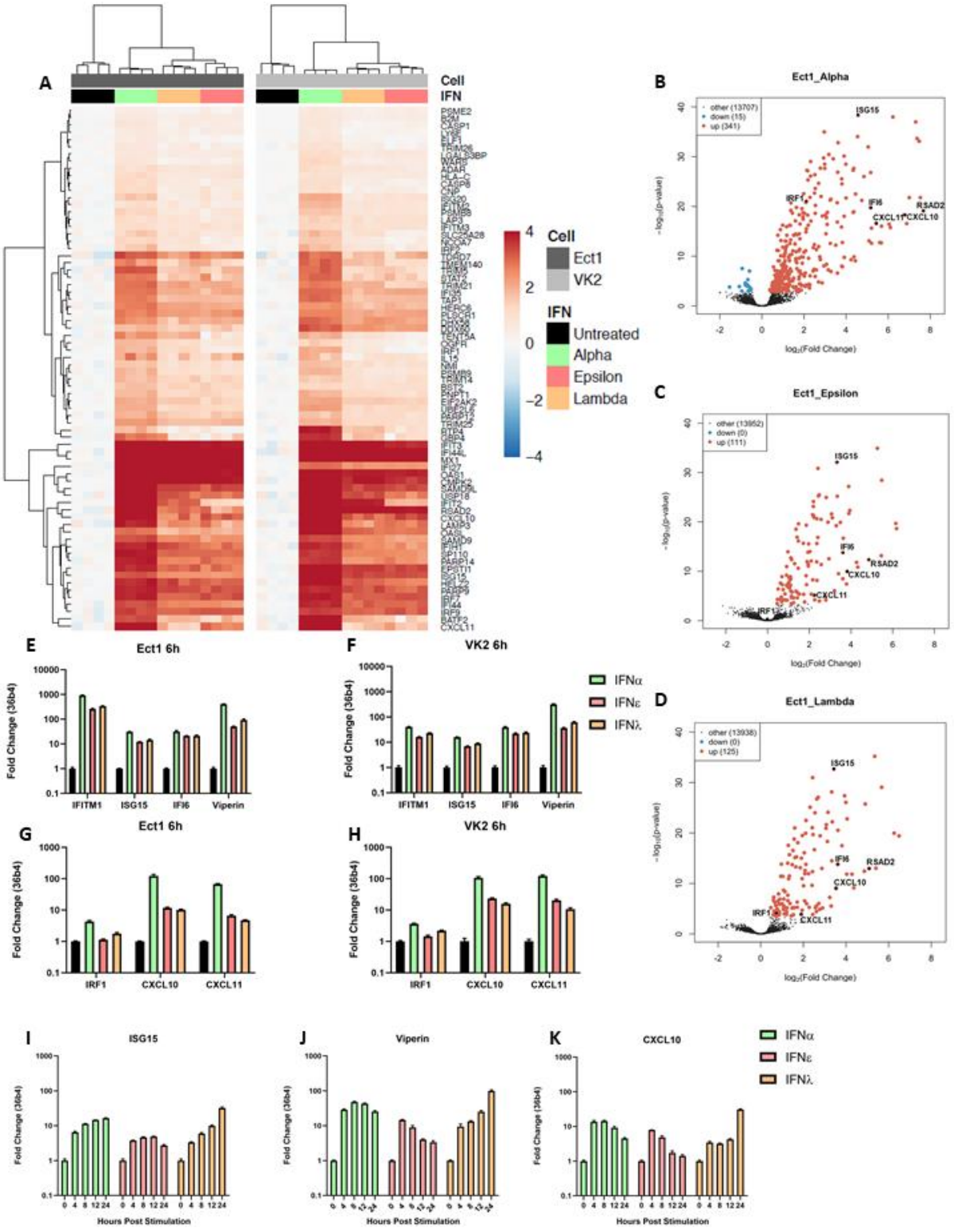

Figure 5.3: IFNε displays typical type-I IFN kinetics but induces an antiviral gene signature like IFNλ-3 at early time points in ectocervical and vaginal cells. Ect1 and VK2 cells were treated with IFNε, IFNα-2a or IFNλ-3 (100 ng/mL) or left untreated (n = 4) for 6hr prior to RNASeq analysis (NextSeq550 V2.5). Differentially expressed genes were determined with a 1.2-fold cut-off and adjusted p-value < 0.05. A) Heat map showing expression of key ISGs. B, C & D)

Volcano plots indicating up or downregulation of genes after IFNα-2a, IFNε or IFNλ-3 treatment, respectively. E & F) Confirmation of anti-ZIKV ISGs (ISG15, IFI6, IFITM1, Viperin) expression by qRT-PCR. G & H) Confirmation of pro-inflammatory ISGs (IRF1, CXCL10, CXCL11) expression by qRT-PCR. I, J & K) Ect1 cells were treated with IFNε, IFNα-2a or IFNλ-3 (100 ng/mL) and RNA was harvested from untreated cells (t = 0) and at the indicated time points post stimulation. qRT-PCR was performed to detect expression of ISG15, Viperin and CXCL10.

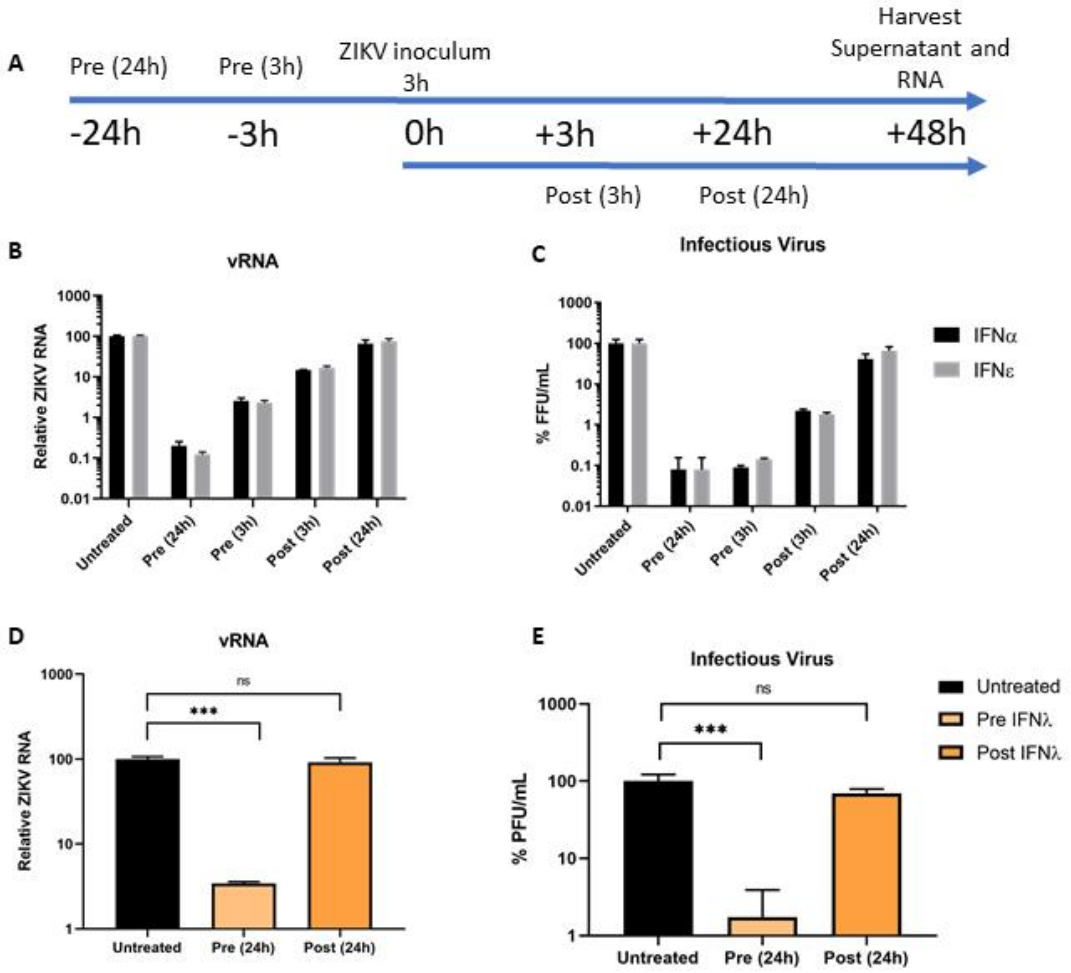

Figure 5.4: ZIKV evades type-I and III IFN antiviral activity post-infection. A) Timeline for IFN treatment regimes in HTR8 cells. B & C) HTR8 cells were infected with ZIKV PRVABC59 at a MOI of 1, cells were either primed with the indicated IFN (mIFNε 10 U/mL or hIFNα-2A 500 U/mL) or treated post infection. 48 hpi supernatants and RNA were harvested for determination of infectious virus by Focus Forming Assay or quantification of viral RNA by qRT-PCR. D & E) HTR8 cells were infected with ZIKV PRVABC59 at a MOI of 1, cells were either primed for 24h with hIFN λ-III (100 ng/mL) or treated post 24h post infection. Viral RNA and supernatant were collected 48hpi for determination of infectious virus by Focus Forming Assay or quantification of viral RNA by qRT-PCR. Statistical analyses are performed by or one-way ANOVA compared to the untreated control, (n.s non-significant, * $P < 0.05$, ** $P < 0.01$). Data are presented as means +/- S.D.

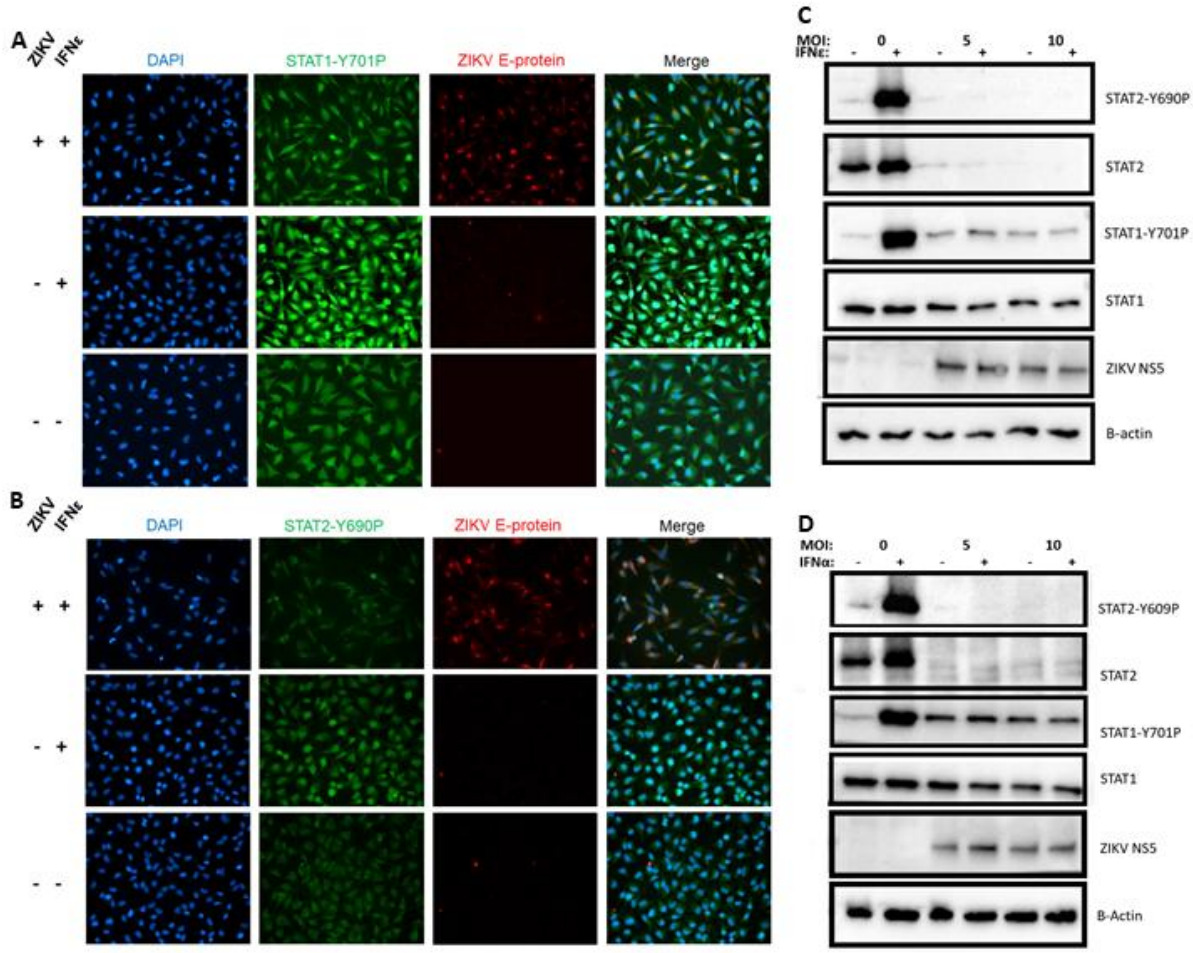

Figure 5.5: Antiviral protection mediated by IFNε and other type-I IFNs is potently inhibited due to ZIKV inhibition of STAT1/2 signalling. A & B) HeLa cells were infected with ZIKV MOI of 10, 24h post infection cells were stimulated with mIFNε (10 U/mL) for 30 min then fixed with acetone/methanol for detection of ZIKV E antigen (Red) and phosphorylated STAT1 or STAT2 proteins (Green) by indirect immunofluorescence, DAPI (Blue). C & D) HeLa cells were infected at the indicated MOI of ZIKV 24h prior to stimulation with the either mIFNε (10 U/mL) or hIFNα-2A (500 U/mL) for 30 min, lysates were harvested for immunoblot of STAT1/2 protein and phosphorylated STAT1/2 proteins.

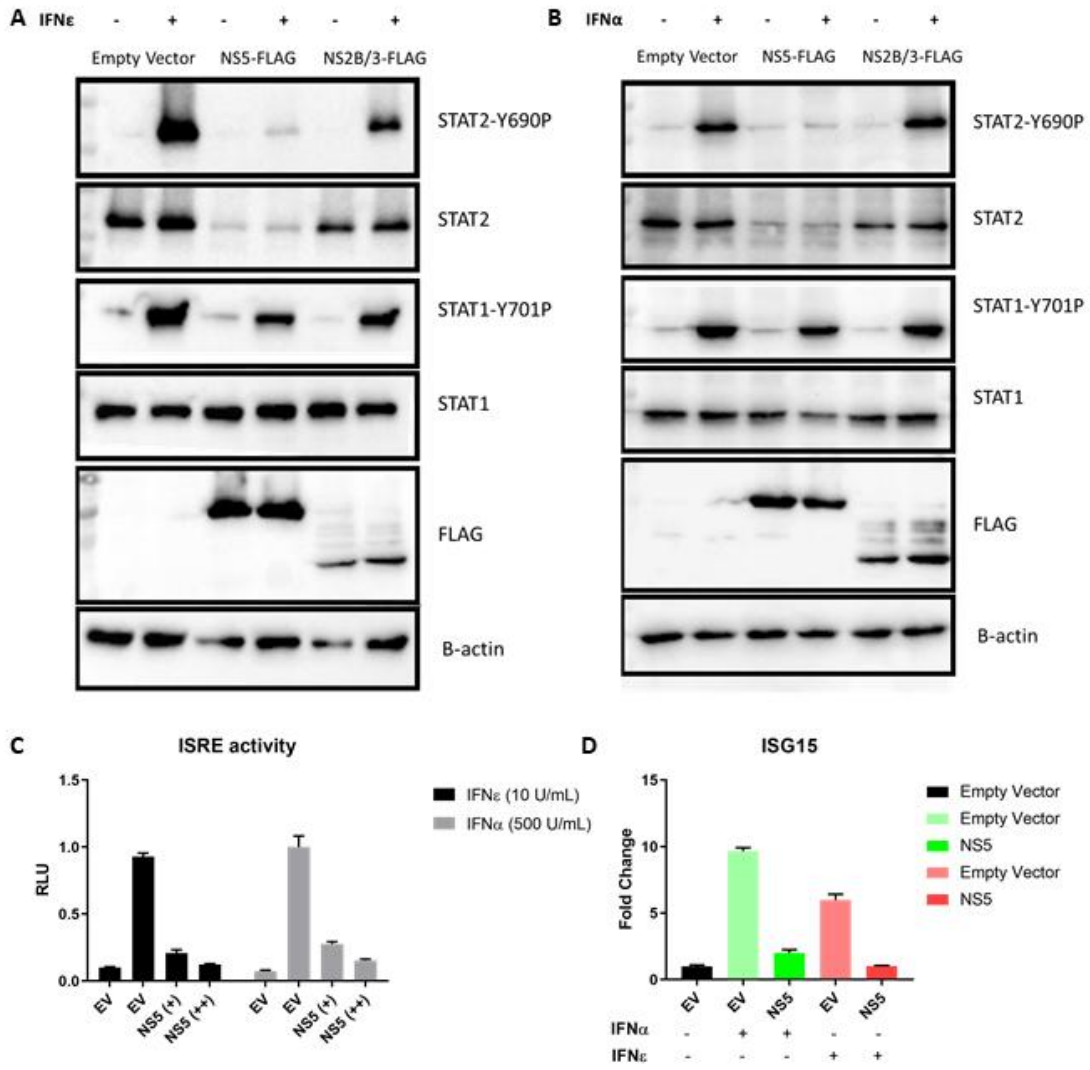

Figure 5.6: Evasion of IFNε antiviral activity is mediated by ZIKV NS5 degradation of STAT2. **A & B)** HeLa cells were transfected with pCDNA6.2-ZIKV-NS5-FLAG, NS2B/3-FLAG or empty vector control and 24 h later stimulated for 30min with the indicated IFN prior to assessing total and phosphorylated STAT1/2 by immunoblotting. **C)** ISRE promoter activity was assessed following 24 h IFNε stimulation in the presence or absence of ZIKV NS5A expression. **D)** HeLa cells were transfected with pCDNA-NS5-FLAG expression plasmid or an empty vector control (EV), 24h post transfection cells were stimulated with the indicated type-I IFN for 6 h prior to harvesting RNA for qRT-PCR analysis of ISG15 expression.

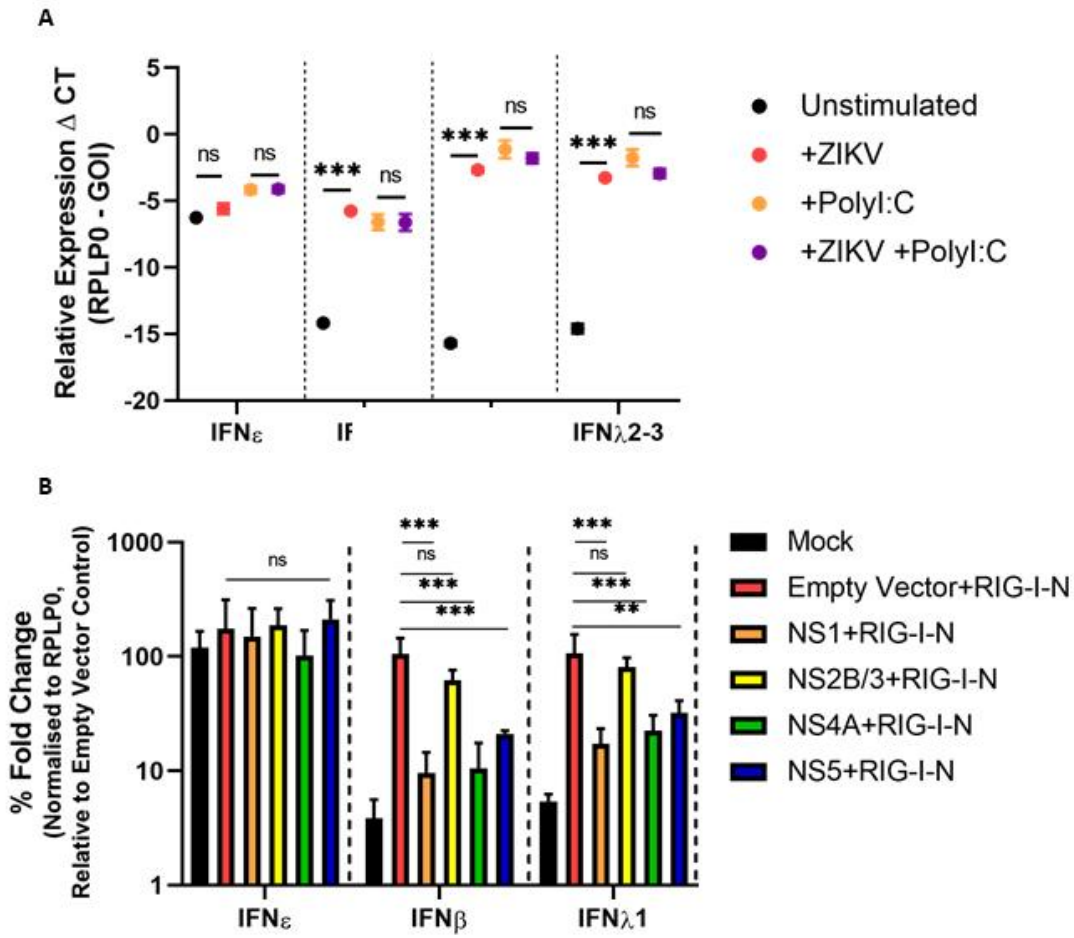

Figure 5.7: IFNε RNA expression is not reduced by ZIKV infection or NS protein expression. A) HeLa cells infected for 16h MOI 1 ZIKV PRV prior to stimulation with Poly I:C 1 µg for 8 h prior to assessing IFN gene induction by qRT-PCR. B) HeLa cells were co-transfected with expression plasmids encoding ZIKV NS1/2B/3/4A/5 or empty vector (pCDNA6.2) and the RIG-I-N plasmid or were mock transfected (Lipofectamine only), 24 h later RNA was harvested prior to assessing induction of type-I and type-III IFNs by qRT-PCR. Statistical analyses are performed by two-way ANOVA (a) or one-way ANOVA compared to the empty vector control (b), (n.s non-significant, * $P < 0.05$, ** $P < 0.01$). Data are presented as means +/- S.D.

5.8 Supplementary Figures

Supplementary 1

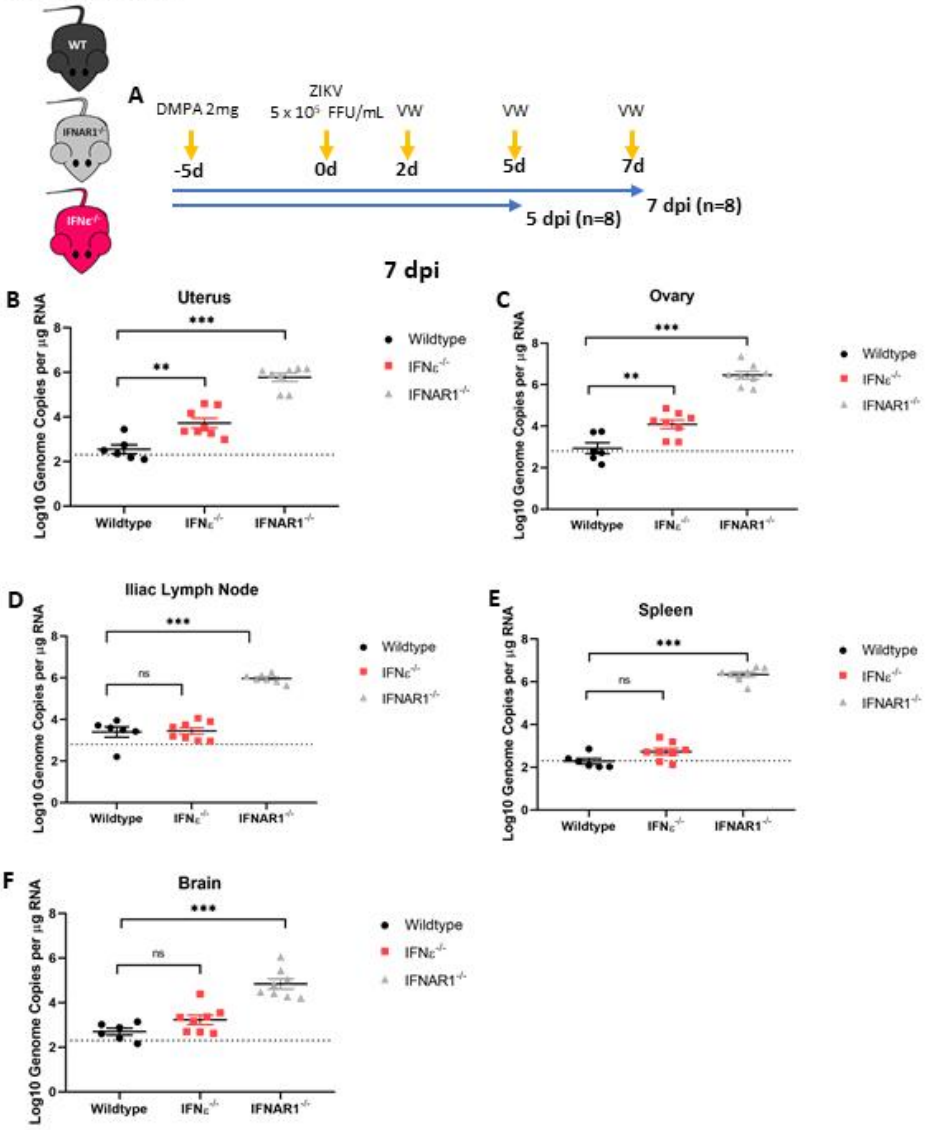

Supplementary Figure 5.1: ZIKV replication is inhibited by IFNε in a mouse model of vaginal transmission. A) Experimental time line of WT (black), mice lacking IFNε (IFNε-/-) (red) or mice lacking the type-I IFN receptor (IFNAR1-/-) (grey) were infected with ZIKV at 5 X10^5 FFU 5 days post DMPA treatment and vaginal washes were taken at 2, 5, 7 dpi. 8 mice were culled at 5 dpi and 8 were culled at 7 dpi. B, C, D, E, & F) Tissues taken at 7 dpi were used to harvest RNA for analysis of viral RNA by qRT-PCR in the uterus, ovary, illiac lymph node spleen and brain respectively.

Supplementary 2

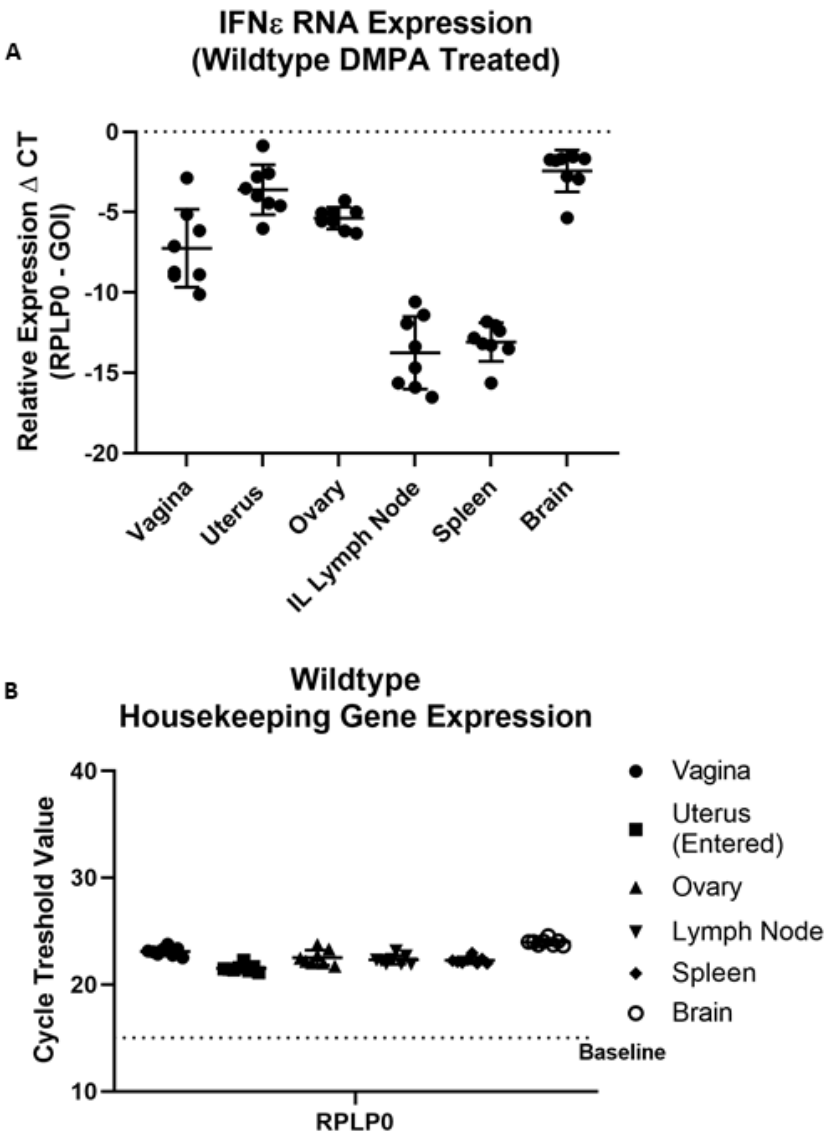

Supplementary Figure 5.2: IFNε is highly expressed by tissues of the FRT and in the brain of WT mice. A) Uninfected mice (n=8) were culled 10 days post DMPA treatment to mirror the timeline of the experiment shown in Figure 1 and tissues were collected as previously described. A) the level of IFNε RNA was determined by qRT-PCR and was expressed as ΔCT normalised to expression of the housekeeping gene RPLP0 (36B4). B) Expression of RPLP0 was compared between the tissues by qRT-PCR and expressed as raw cycle threshold value.

Supplementary 3

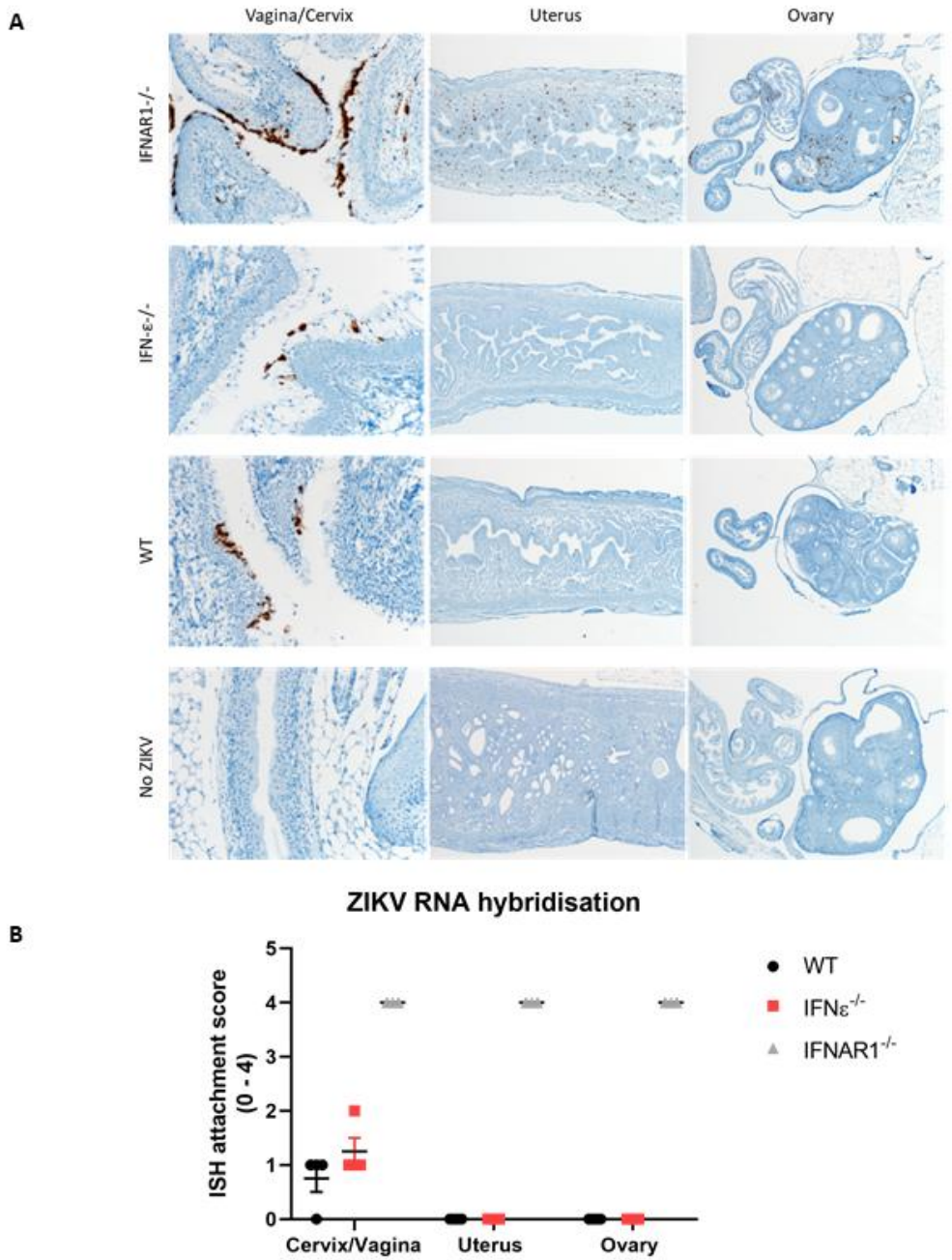

Supplementary Figure 5.3: RNAscope in-situ hybridisation (ISH) of ZIKV RNA in FRT tissues at 5 dpi (n = 4). Whole FRT tissues (vagina, cervix, uterus and ovary) were fixed in formalin for 24 h prior to paraffin embedding and sectioning (5 µM), The RNAscrope protocol was used to the manufacturers specifications to detect ZIKV infection using a probe specific to ZIKV –ssRNA. A) Representative ISH images detecting from WT, IFNε-/- and IFNAR-/- mice (ZIKV in brown). B) Pathologist scoring of ISH attachment (0 = none, 1 = rare/few, 2 = scattered, 3 = moderate, 4 = numerous).

Supplementary 4

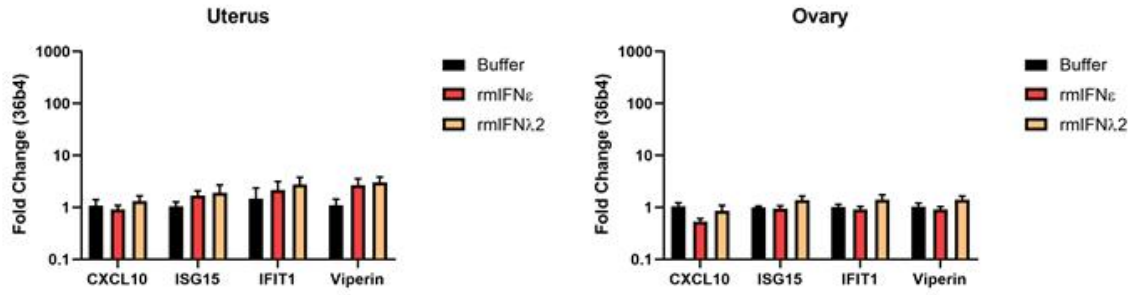

Supplementary Figure 5.4: A & B) ISG induction in the uterus and ovary in DMPA treated uninfected IFNε-/- mice following 6 h iVag treatment with the indicated IFN or buffer control.

Supplementary 5

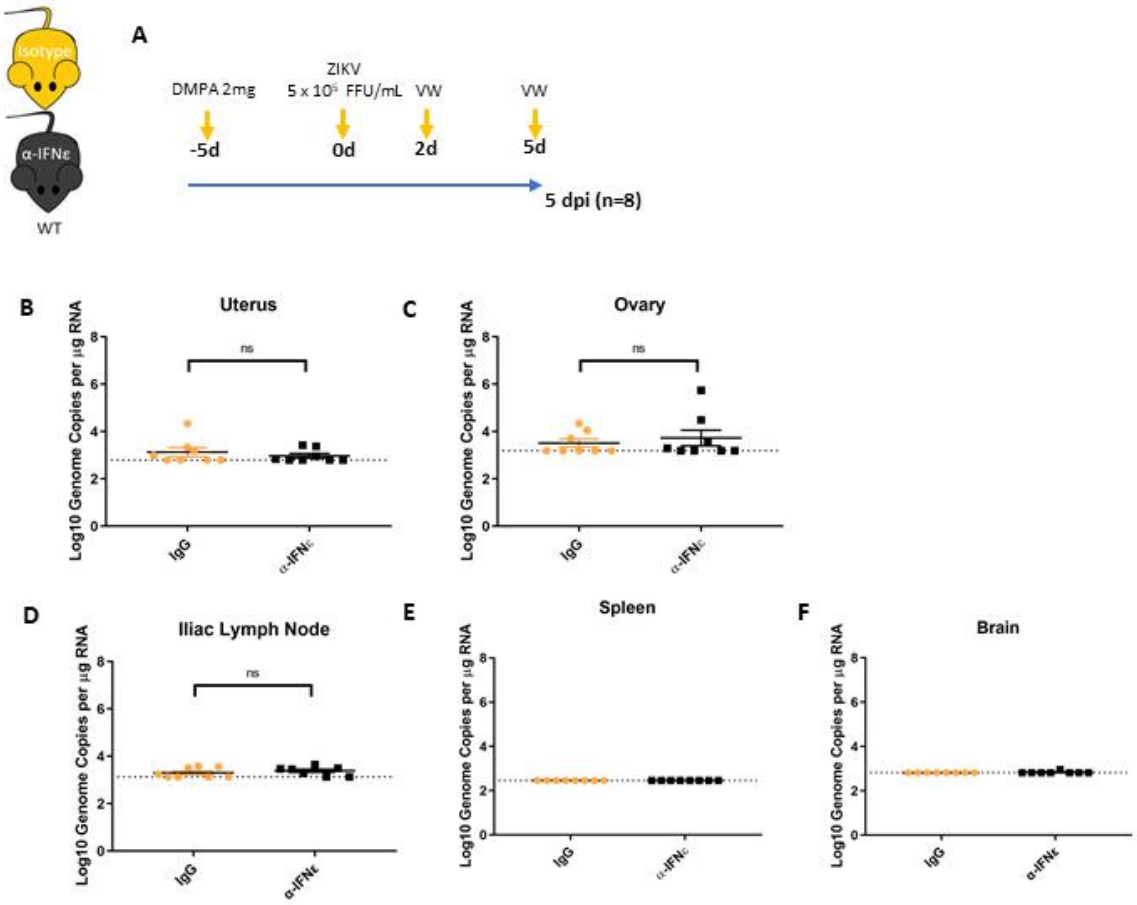

Supplementary Figure 5.5: iVag treatment of wildtype mice with IFNε neutralising antibody enhances ZIKV infection in the vagina (Fig. 1) but not in other tissues. **A)** Experimental time line of (WT mice were treated 6 h prior to infection with 100 ug anti-IFNε or isotype control, then infected with ZIKV at 5 X10^5 FFU 5 days post DMPA treatment and vaginal washes were taken at 2, 5, mice were culled at 5 dpi. **B, C, D, E)** Tissues taken at 5 dpi were used to harvest RNA for analysis of viral RNA by qRT-PCR in the uterus, ovary, illiac lymph node spleen and brain respectively.

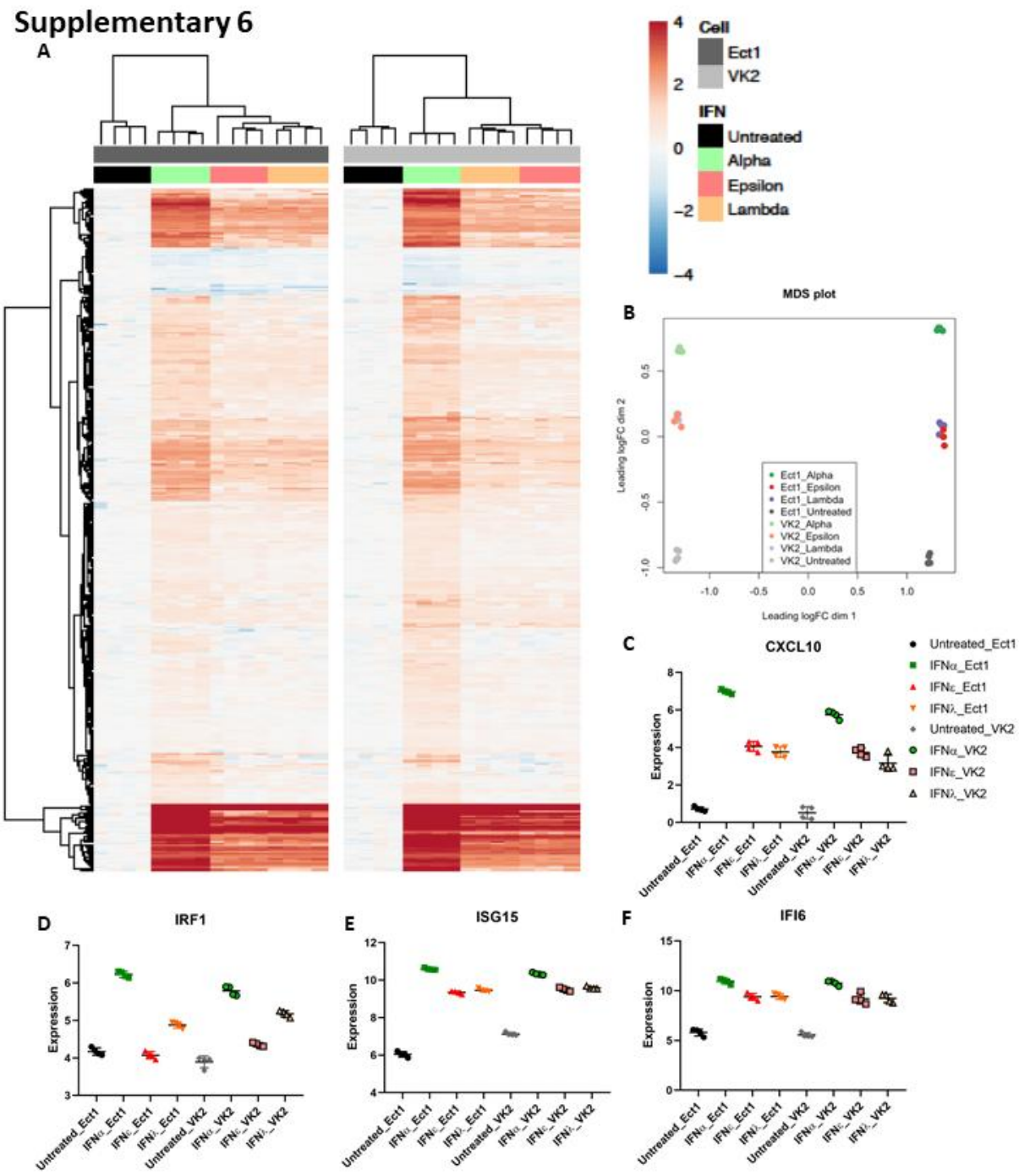

Supplementary Figure 5.6: Ect1 and VK2 cells were treated with IFNε, IFNα-2a or IFNλ-3 (100 ng/mL) or left untreated (n = 4) for 6hr prior to RNASeq analysis (NextSeq550 V2.5). Differentially expressed genes were determined with a 1.2-fold cut-off and adjusted p-value < 0.05. A) Heat map showing expression of all differentially regulated genes. B) MDS plot showing the relationship between samples based on the top 500 most variable genes. C, D, E & F) Expression plots for CXCL10, IRF1, ISG15 and IFI6 respectively in Ect1 or VK2 cells.

Supplementary 7

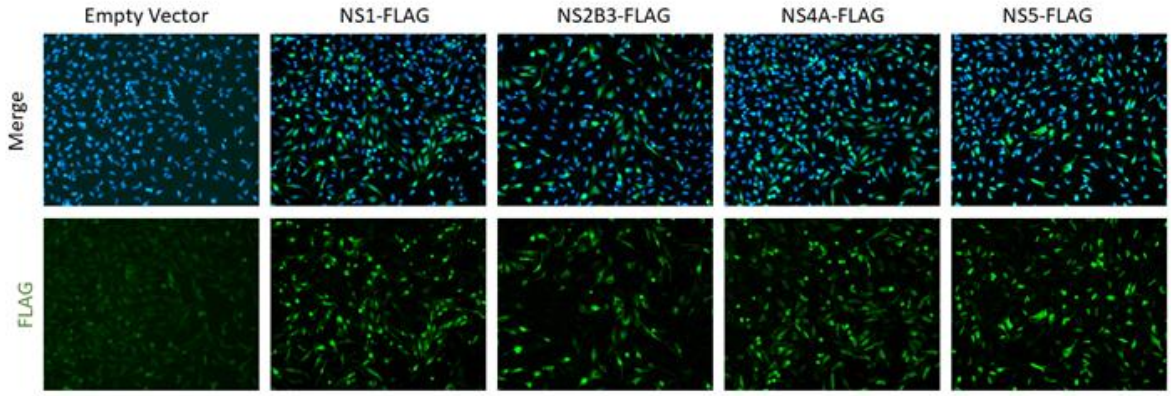

Supplementary Figure 5. 7: Protein expression for ZIKV NS-FLAG expression constructs as indicated by immunofluorescence staining of FLAG protein. Transfections were performed in parallel to the data presented in Fig. 5.7b.

Supplementary 8

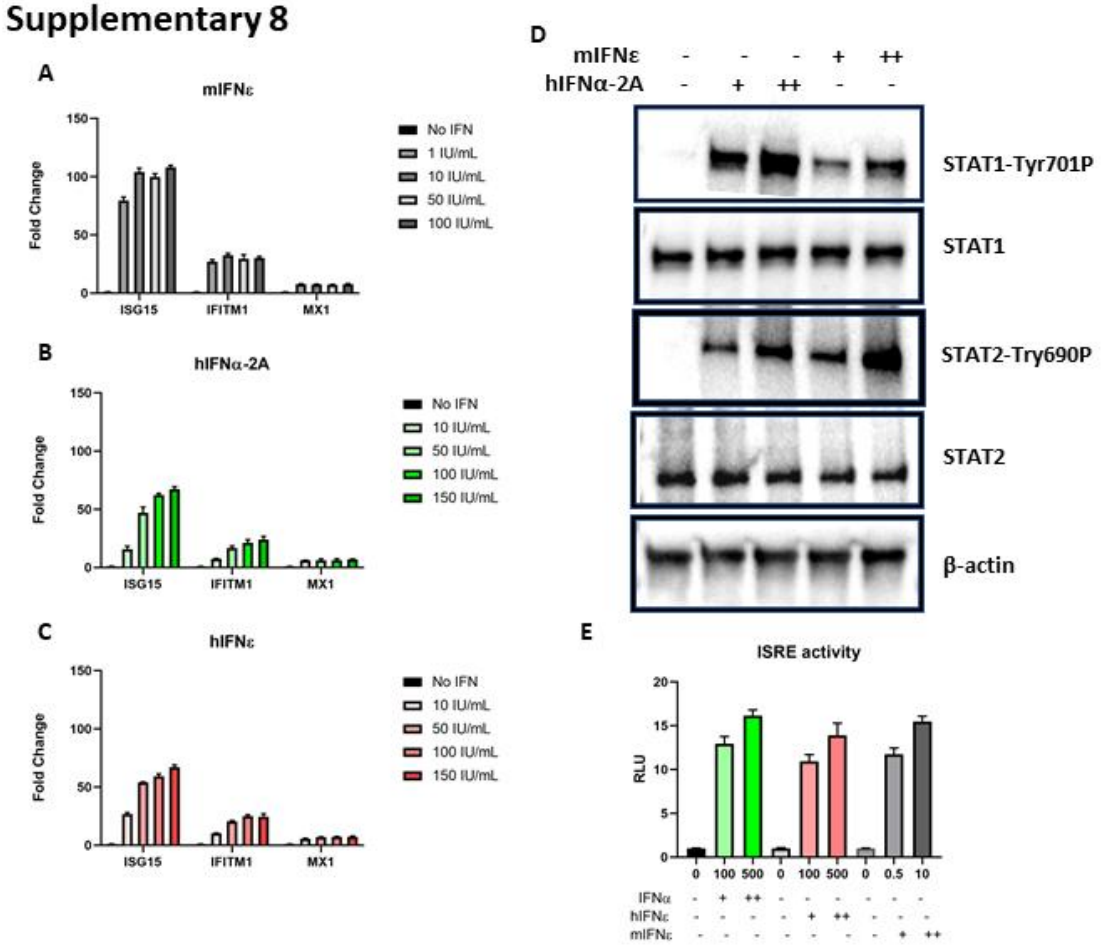

Supplementary Figure 5.8: Murine IFNε stimulate the ISG expression in human cell lines via ISRE driven JAK/STAT pathway activation. **A, B & C)** Dose dependent ISG induction in HTR8 cells following 6h stimulation with indicated amounts of type-I IFNs, data is expressed as fold change relative to untreated cells. **D)** Immunoblot of STAT1/STAT2 phosphorylation in HeLa cells 30 minutes post stimulation with mIFNε (0.5 or 10 U/mL) or hIFNαt-2A(100 or 500 U/mL). **E)** ISRE promoter activity in HeLa cells transfected with an ISRE luciferase reporter was measured by dual luciferase assay in relative light units (RLU) 8 h post stimulation with the indicated amounts of mIFNε.

Chapter 6

Characterising the regulation and intrinsic properties of IFNε *in vitro*

6.1 Introduction

As explored in the previous chapter, IFNε is a constitutively expressed type-I IFN in the FRT that contributes to the local antiviral state and protects against ZIKV infection in mice and humans. *In vivo* expression patterns of IFNε indicate that it is predominantly controlled by changing levels of female sex hormones, Estrogen (E2) and Progesterone (P4), over the estrus or menstrual cycle and during pregnancy [105]. Accordingly, the proximal promoter of the gene that encodes IFNε (IFNe1) contains a putative response element for the Progesterone Receptor (PR) that is conserved between mice and humans [133]. The presence of this response element in the proximal promoter region suggests that the PR acts to directly control IFNe1 expression at the transcriptional level. Despite similarities in the proximal promoter of the mouse and human IFNe1 gene the expression pattern of IFNε in the FRT is different between these species. In mice, the levels of IFNε are highest during estrus (high E2, low P4) and are lowest during diestrus (low E2, high P4) [105]. These changes occur uniformly across the upper and lower reproductive tract (UFRT and LFRT). However, in humans the levels of IFNε are increased during the luteal phase (mid E2, high P4) and are reduced in the follicular phase (increasing E2, low P4) of the menstrual cycle [253]. These changes in humans occur only in the UFRT, whereas the LFRT maintains high levels of IFNε protein regardless of cycle stage [253]. These unexplained differences between expression of IFNε in mice and humans highlights how little is known about the regulation of this important antiviral cytokine. In general, hormonal control of gene expression is notoriously complex. For example, E2 and P4 are steroid hormones that primarily act through their cognate steroid nuclear hormone receptors. For E2 these are estrogen receptor-α (ERα) and ERβ, transcribed from two separate genes [91]. P4 also has two nuclear receptor isoforms called PRA and PRB, encoded as long and short transcripts from the same gene [160]. Receptor subtypes have distinct and overlapping expression patterns, display differential gene activation and many of their physiological roles are poorly understood [91]. Gene expression in response to P4 is further complicated by the direct transcriptional control of both PRA and PRB by the ERs and

the hormonal environment of the FRT [160]. In addition to the hormonal control of IFNε there are other factors including seminal plasma [316] and TNFα [210] detailed in the Introduction (section 1.2.2.2) that can alter expression of IFNε at the RNA level. Currently the molecular mechanisms, signalling pathways, transcription factors and interactions between competing stimuli that govern IFNε expressed are unknown. In addition to stimuli normally present in the FRT, the impact of ZIKV infection on the expression of IFNε is poorly defined. ZIKV has evolved multiple evasion strategies to effectively restrict the production of other type-I and III IFNs in response to viral infection [176, 200]. Since IFNε protects against ZIKV when administered prophylactically (chapter 5), the question remains if ZIKV has evolved strategies to evade the constitutive expression of this key antiviral cytokine in the human FRT. Viral evasion of constitutively expressed IFN is not unprecedented, as human papillomavirus (HPV) can dampen IFNκ constitutively expressed by keratinocytes of the skin [282]. Understanding the pathways that regulate IFNε will underpin its clinical use and improve existing *in vivo* model systems. Currently there is a lack of *in vitro* model systems that recapitulate endogenous IFNε expression patterns. Establishing *in vitro* model systems would enhance our capacity to dissect the pathways that govern IFNε expression at the molecular level. As a result, this chapter aims to establish *in vitro* models of endogenous IFNε expression and regulation.

Another poorly understood aspect of IFNε biology is its ability to signal constitutively *in vivo.* Chapter 5 demonstrated that FRT cell lines displayed transient gene induction kinetics in response to a single treatment of IFNε. In a similar pattern to other type-I IFNs [98], these cells displayed high levels of ISG induction in response to IFNε at early time points that waned by 24 h post stimulation. This pattern of expression is indicative of negative regulation of the pathway. As detailed in the Introduction (section 1.2.2.1.2) there are several ways the type-I IFN pathway can be switched off. Two main mechanisms involve the accumulation of the regulatory ISGs, SOCS1 and USP18. Whereas SOCS1 inhibition is short lived and is responsible for rapidly returning ISG expression to baseline [322], USP18 mediated desensitization can last days [100]. Importantly, the effect of USP18 mediated desensitization on IFNAR1/2 dependent signalling is observed in cells responding to IFNα, but not to IFNβ *in vitro* [99]. This differential signalling property is driven by IFNβs higher affinity for the IFNAR1 receptor subunit compared to IFNα [369]. This higher affinity interaction facilitates the formation of the ternary receptor-ligand complex despite the presence of USP18, that otherwise

destabilises the complex [369]. Notably, IFNε shares greater sequence homology with IFNβ than IFNα [133]. Furthermore, the ratio of affinity for IFNε binding to each individual receptor subunit closely resembles that of IFNβ (these interactions are summarised in the introduction Figure 1.11). Specifically, IFNε has a high affinity for IFNAR1 and a weaker binding affinity for IFNAR2 compared to IFNα [134]. Together this information suggests that IFNε may signal via the IFNAR1/2 receptor constitutively despite the presence of IFN induced USP18 expression. Understanding this aspect of IFNε biology is important as it may change our understanding of viral infections of the FRT. For example, if cells responding to IFNε in the FRT become desensitized over a long period they may remain vulnerable to infection even when IFNε levels are high. Alternatively, if cells can respond to IFNε via the IFNε-IFNAR1/2 receptor complex in the presence of USP18 then they may be constitutively protected against infection. Collectively, this Chapter investigates models of endogenous IFNε regulation and demonstrates preliminary results indicating that IFNε can signal constitutively *in vitro*.

6.2 Results

6.2.1 Cell lines of FRT origin express high levels of IFNε RNA

The first step in establishing an *in vitro* model of endogenous IFNε regulation was to find cell line that naturally express IFNε mRNA. To this end the basal level of IFNε mRNA was compared between cell lines of non-FRT and FRT origin by qRT-PCR. Figure 6.1a shows the expression level of IFNε mRNA in Huh7 (liver), Ishikawa (endometrial adenocarcinoma), HTR8 (transformed primary placental trophoblast) and HeLa (cervical adenocarcinoma) cell lines. As expected Huh7 cells expressed the lowest amount of IFNε mRNA. This coincides with other reports finding little to no IFNε expression in the liver [133, 145]. Comparatively, cell lines from FRT origin had greater levels of IFNε mRNA. HeLa cells expressed the greatest levels of IFNε followed by HTR8 and then Ishikawa cells. Because these cell lines were derived from adenocarcinomas or the placenta and are not normally present in the FRT it was important to compare the expression of IFNε mRNA in more relevant FRT cell lines. To address this need, the basal level of IFNε mRNA was compared between HeLa cells and Ect1 (ectocervical), or VK2 (vaginal keratinocyte) primary transformed cells [96] by qRT-PCR. Figure 6.1b shows that both Ect1 and VK2 cells expressed high levels of IFNε mRNA that were comparable to those observed in HeLa cells. Together this data confirmed the cell type specific expression of IFNε. Importantly this implies that IFNε expression is subject to endogenous control measures that

A

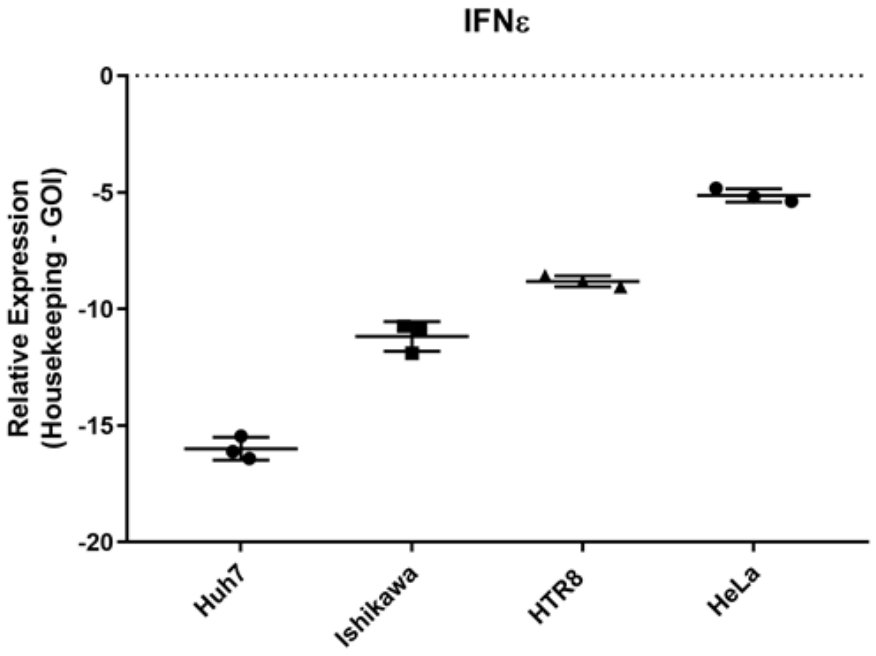

B

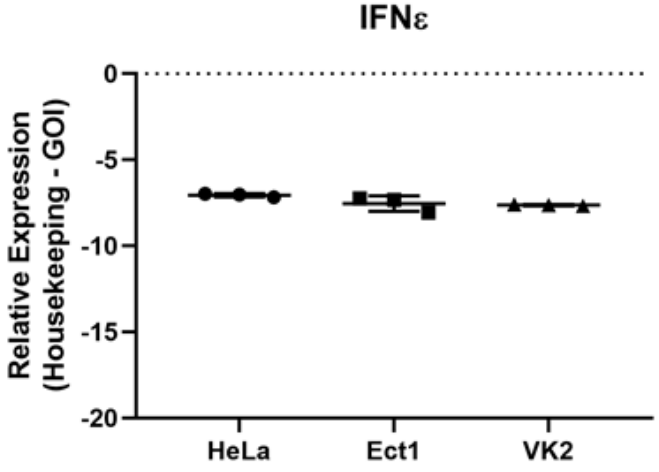

Figure 6.1: Cell lines of female reproductive tract origin express high levels of IFNε mRNA. Basal levels of IFNε RNA measured by qRT-PCR in A) Huh7, Ishikawa, HTR8 and HeLa cells or B) HeLa, Ect1 and VK2 cells. Data are displayed as delta CT values and are normalised to expression of the housekeeping gene (36B4) that is represented as the dotted line.

are cell type specific. Additionally, this data demonstrates that HeLa, Ect1 and VK2 cells express high levels of IFNε mRNA relative to other cell lines of FRT and non-FRT origin. These cell lines may prove to be useful to investigate endogenous regulation of IFNε.

6.2.2 Primary transformed FRT cell lines express high basal levels of ISGs

After determining cell lines that express high levels of IFNε mRNA it was important to determine if this mRNA was translated into functional protein, as there are post-transcriptional controls in place for IFNε protein expression. For example, one study found that protein expression of IFNε was limited by the molecular transporter Importin 9 [211]. In this study, Importin 9 was found to associate with the 5' UTR of IFNε mRNA, preventing its translation into functional protein in HeLa cells at a basal state. Currently, there are no commercially available antibodies to detect endogenous IFNε protein. Therefore, measuring the downstream effect of IFNε on ISG expression was used as an indirect method of assessing protein function. In theory, if IFNε protein was produced by these cells, the basal levels of ISG expression would increase due to autocrine signalling. To test this hypothesis, we first compared the baseline levels of a commonly upregulated ISG (ISG15) between Huh7, HeLa, Ect1 and VK2 cells by qRT-PCR. Interestingly, both Ect1 and VK2 cells but not HeLa cells had significantly higher basal levels of ISG15 compared to Huh7 cells (Figure 6.2a). This supports the possibility that IFNε is translated into functional protein in Ect1 and VK2 cells. To extend these observations, the levels of multiple ISGs were assessed in these cells both at baseline and in response to a 6h treatment with 1000 U/mL of IFNα. Figure 6.2 shows that both Ect1 (Fig. 6.2c) and VK2 cells (Fig. 6.2d) displayed higher basal levels of the ISGs MX1 and ISG15 compared to HeLa cells (6.2b). In addition, VK2 cells displayed higher basal levels of IFITM1. This correlates with previous studies demonstrating some cells of epithelial origin have increased basal expression of the IFITM family proteins [19]. Moreover, these cells increased ISG expression in response to IFNα treatment, confirming the ability of both Ect1 and VK2 cells to respond to type-I IFN. Together this data supports that Ect1 and VK2 cells may produce functional IFNε protein, that can act in autocrine by increasing the basal levels of ISGs. In correlation with the higher basal level of ISGs observed in these cells, Ect1 and VK2 cells were less permissive to infection compared to HeLa cells. Figure 6.3 shows the level of ZIKV infection by staining for cells expressing ZIKV E-protein (red) at 24 hpi by immunofluorescence. This demonstrated that Ect1 cells were the least permissive to ZIKV

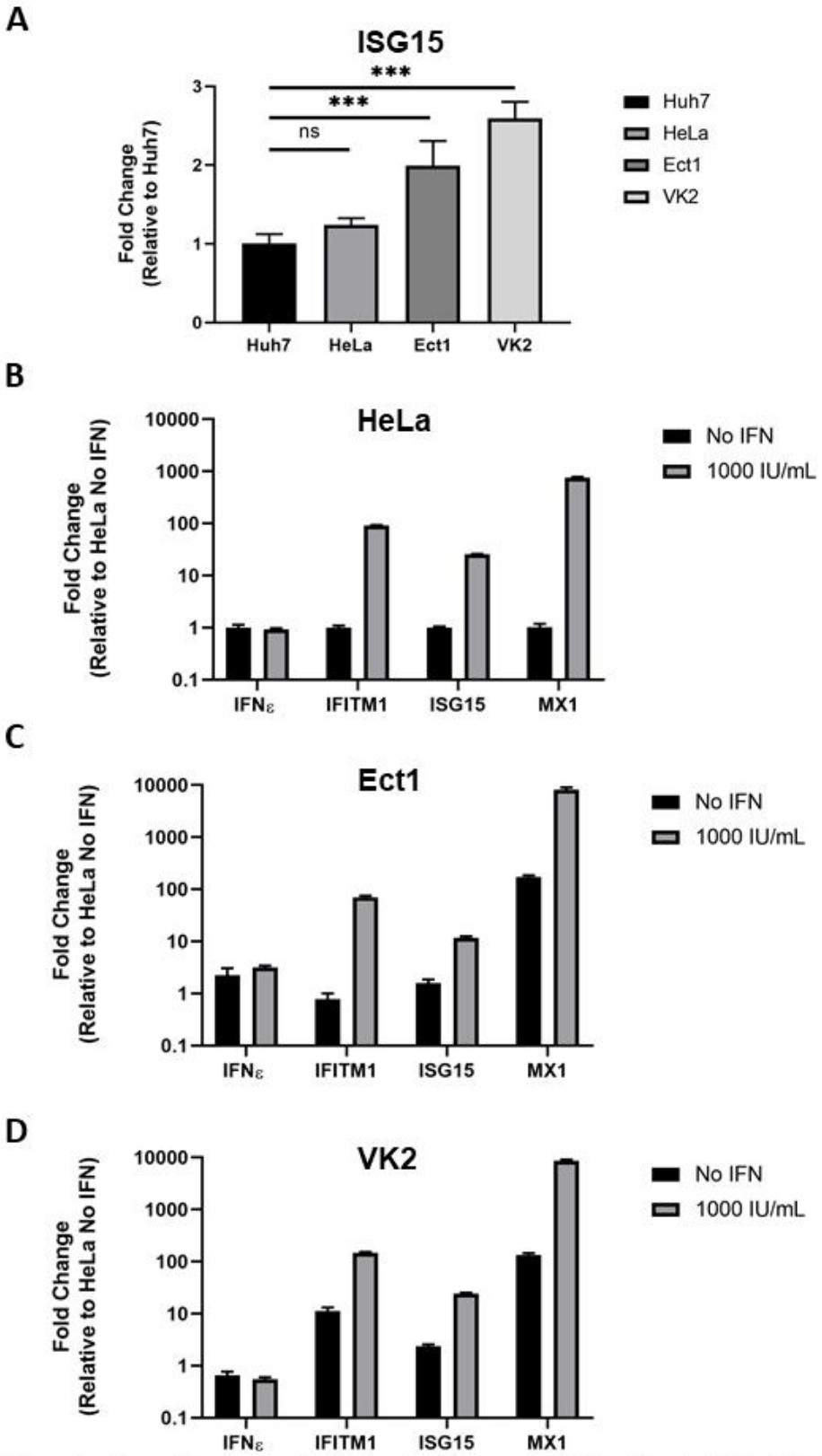

Figure 6.2: Primary transformed female reproductive tract cell lines express high basal levels of ISGs. A) The basal expression of ISG15 RNA in Huh7, HeLa, Ect1 and VK2 cells determined by qRT-PCR. B) HeLa cells, C) Ect1 cells or D) VK2 cells were left untreated or stimulated with 1000 U/mL of IFNα for 6 h prior to harvesting RNA. The RNA levels of IFNε and ISGs (IFITM1, ISG15, MX1) were measured by qRT-PCR. The data is expressed as a fold change in gene expression relative to untreated HeLa cells. Statistics were performed by one-way ANOVA analysis, (* $P < 0.05$, ** $P < 0.01$, *** $P < 0.001$).

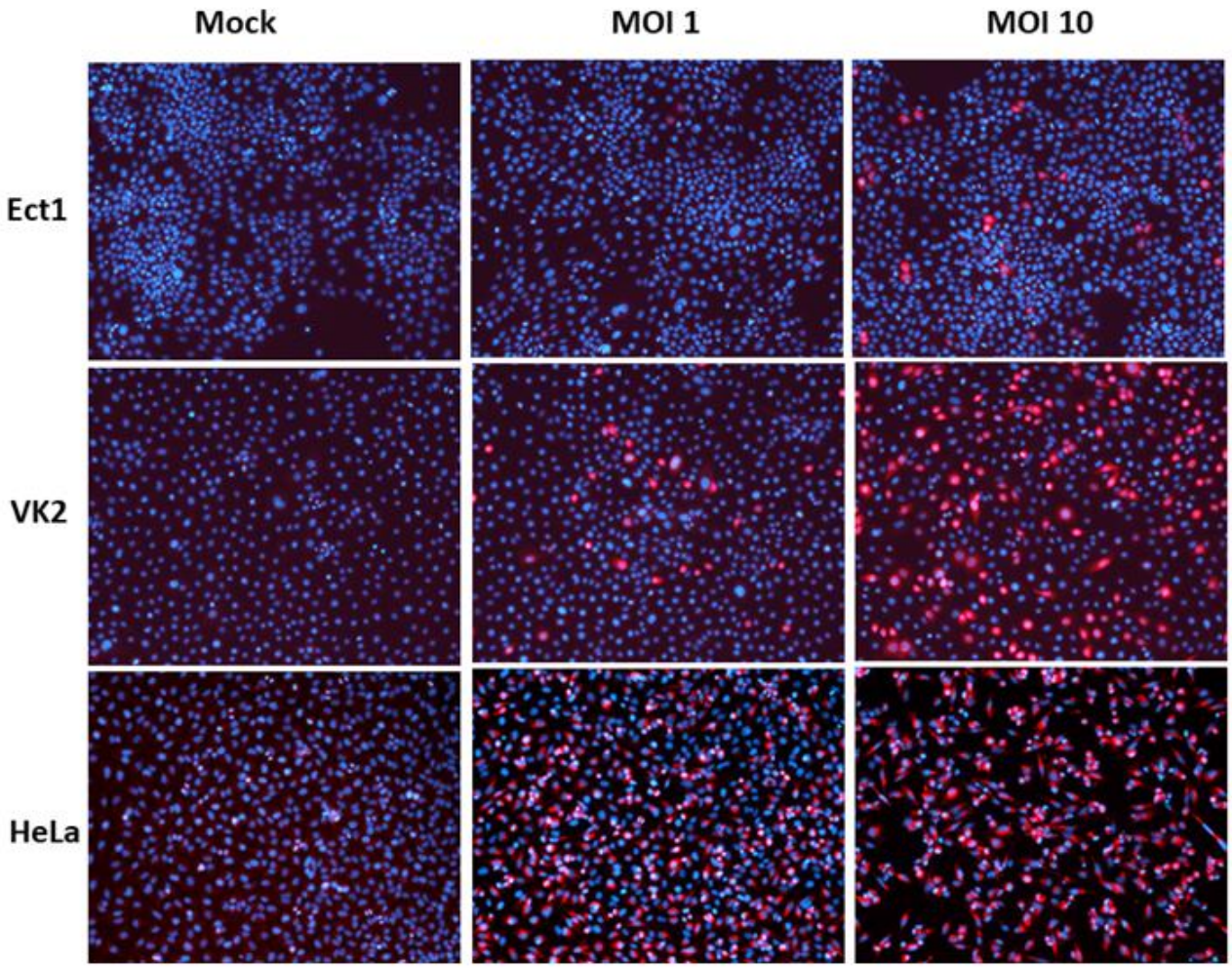

Figure 6.3: Primary transformed female reproductive tract cell lines are naturally resistant to ZIKV infection. Ect1, VK2 and HeLa cells were infected with the indicated MOI of ZIKV (PRVABC59) for 24 h prior to fixing with acetone:methanol. Infected cells were detected by immunofluorescent staining using the 4G2 anti-*flavivirus* E antibody (red) and cell nuclei by DAPI (blue).

infection followed by VK2 and HeLa cells, respectively. Together this suggests that Ect1 and VK2 are less permissive to ZIKV infection, potentially due to their higher baseline expression of ISGs compared to other cell lines. In turn, it is possible that the higher basal level of ISG expression observed in these cells is driven by endogenous expression of IFNε protein. However, this experimental model does not rule out intrinsic differences in gene expression that are independent from expression of IFNε protein.

6.2.3 Huh7 cells upregulate expression of ISGs in response to Ect1 cell culture supernatant

Next, to determine if any potential IFNε expressed by these cells could regulate ISG expression, in the absence of intrinsic cell line differences, it was logical to assess the antiviral properties of supernatant from these FRT cells. This is because any prospective IFNε protein produced by FRT cells may display paracrine activity on another cell line. However, it has been demonstrated that IFNε protein is inefficiently secreted from cells compared to other type-I IFNs [145]. This study found that poor secretion was a result of inefficient cleavage of the IFNε protein signal peptide in fibroblast cell lines. Importantly, this indicates the paracrine antiviral activity of IFNε protein may be limited in cell culture. To investigate any potential paracrine activity from cell culture supernatant we utilised the Huh7 cells that have a low baseline levels of IFNε and ISG mRNA expression but can respond to type-I IFN. Huh7 cells were treated for 6h with concentrated Ect1 culture supernatant (Ect1 SN) as described in Materials and Methods (section 2.2.8), similarly concentrated Huh7 supernatant (H7 SN), or similarly concentrated Keratinocyte Serum Free Media (KSFM) as controls prior to harvesting total RNA to detect expression of ISGs by qRT-PCR. Huh7 cells were also treated with 100 U/mL of IFNα as to confirm these cells were IFN responsive. Figure 6.4a shows that in response to Ect1 supernatant, Huh7 cells significantly increased the expression of ISG15 compared to H7 SN, or KSFM treated controls. Although this was only a small increase (3-fold compared to H7 SN treated Huh7 cells) it should be noted that treatment with 100 U/mL of IFNα only resulted in a modest induction at this time point. Additionally, while the difference in Viperin expression was non-significant a similar trend was observed for the Ect1 supernatant treated cells (Figure 6.4b). To confirm this observation a dual luciferase assay was used to determine ISRE promoter activity in response to an 8h treatment of Ect1 supernatant. Figure 6.5 showed a small but significant increase in the levels of ISRE promoter activity in response to Ect1 supernatant that was consistent with the changes in ISG expressed observed by qRT-PCR.

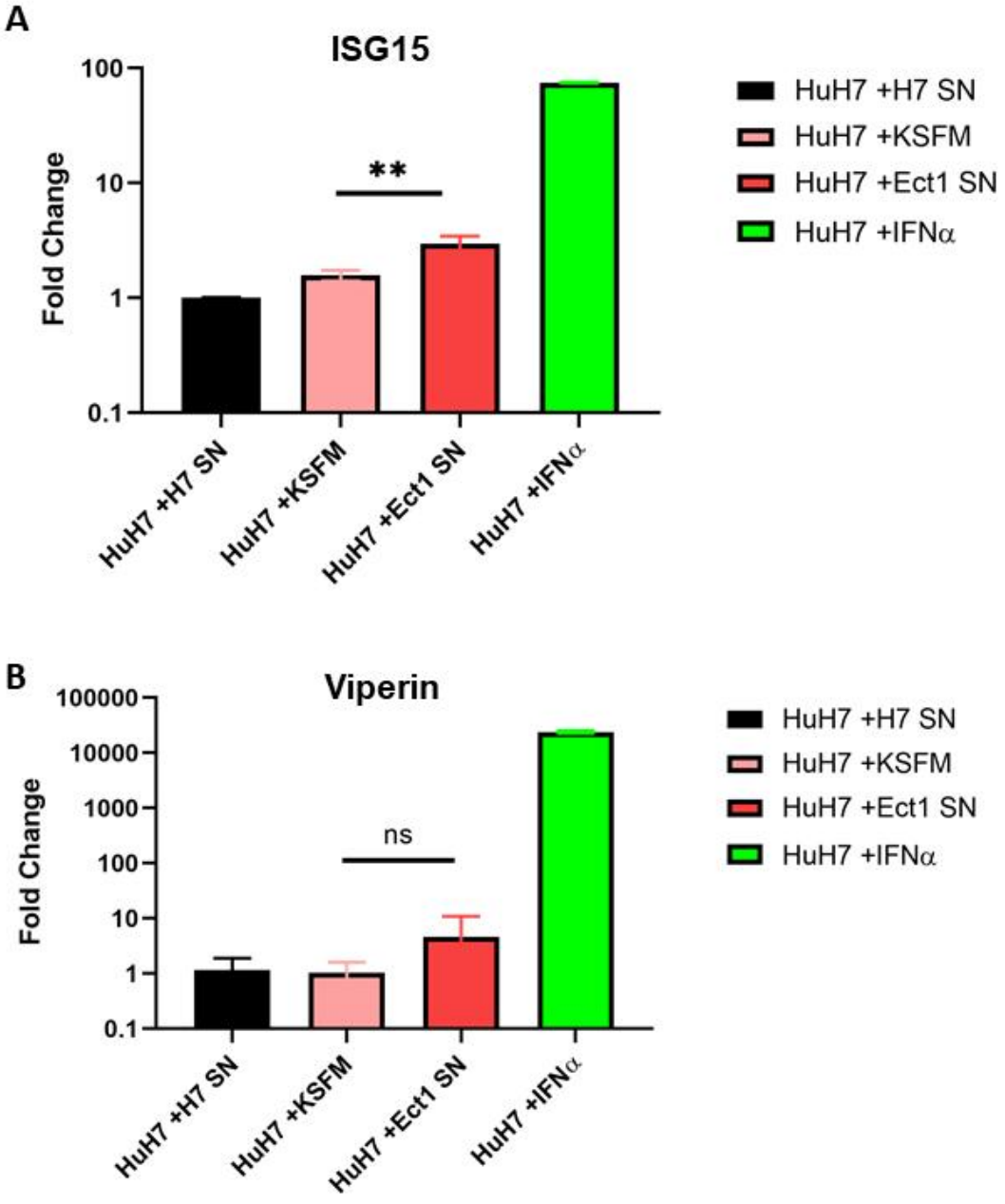

Figure 6.4: Huh7 cells upregulate expression of ISGs in response to supernatant from primary transformed female reproductive tract cell lines. Huh7 cells were treated with concentrated Ect1 supernatant (Ect1 SN), similarly concentrated Keratinocyte Serum Free Media (KSFM), 100 U/mL IFNα or Huh7 supernatant (H7 SN). 8 h post stimulation RNA was harvested to detect the expression level of A) ISG15 or B) Viperin. The data is expressed as a fold change in gene expression relative to untreated Huh7 cells (Huh7 +H7 SN). Statistics were performed by one-way ANOVA analysis, (* $P < 0.05$, ** $P < 0.01$, *** $P < 0.001$).

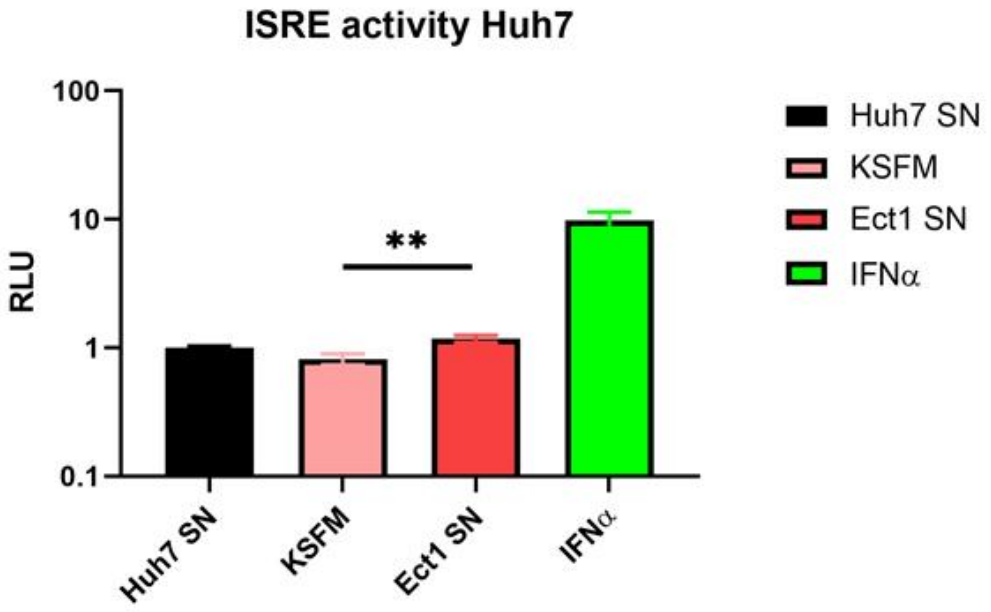

Figure 6.5: Treatment of Huh7 cells with Ect1 supernatant increases ISRE promoter activity. Huh7 cells were co-transfected with ISRE-luc and pTK-RL one day prior to treatment with concentrated Ect1 supernatant (Ect1 SN), similarly concentrated Keratinocyte Serum Free Media (KSFM), 100 U/mL IFNα or Huh7 supernatant (H7 SN). 8 h post stimulation protein was harvested to detect ISRE promoter activity by dual luciferase assay. Units are expressed as relative light units (RLU) normalised to renilla activity. Statistics were performed by one-way ANOVA analysis, (* $P < 0.05$, ** $P < 0.01$, *** $P < 0.001$).

Although this experimental model does not preclude other immune effector molecules that may be present in Ect1 cell supernatant, the data supports the possibility of functional IFNε protein that is secreted by Ect1 cells that can act in paracrine to upregulate ISG expression.

6.2.4 Transfection of siRNA targeting IFNε does not alter the levels of endogenous IFNε RNA, ISG expression, or ZIKV infection in Ect1 cells

To establish a direct link between Ect1 IFNε mRNA expression with protein function, attempts were made to knockdown IFNε expression by an siRNA-mediated knockdown approach. A pooled siRNA that specifically targeted 4 different sites of the IFNε mRNA (Dharmacon) was introduced into cells by transfection using RNAiMAX (Invitrogen) as outlined in the Materials and Methods (section 2.2.7). To confirm the activity of the siRNA, a CMV promoter IFNε-FLAG expression construct was used for simple detection of exogenous IFNε protein expression (see Appendix VII for sequence details). The IFNε-FLAG expression construct was introduced into HeLa (Figure 6.6a) or Ect1 cells (Figure 6.6b) by transfection (Lipofectamine 2000) 6 h prior to siRNA transfection (RNAiMAX) with a non-targeting control (NTC) or the pooled IFNε siRNA reagent. Following siRNA transfection, cells were fixed at 24 h or 48 h for detection of exogenous IFNε protein levels by immunofluorescence using an anti-FLAG antibody. Figures 6.6a & b show that exogenously expressed IFNε-FLAG protein was reduced in both HeLa and Ect1 at 24 and 48 h post transfection compared to NTC. This confirmed the ability of the siRNA pool to knockdown IFNε protein expression. Next, the effect of IFNε siRNA knockdown on endogenous expression was assessed in Ect1 cells. Figure 6.7 shows the level of IFNε (Fig. 6.7a) and downstream ISGs mRNAs (Fig. 6.7b & c) following transfection of IFNε siRNA for 24, 48 and 72 h by qRT-PCR. Unexpectedly, in contrast to the efficient knockdown observed for IFNε-FLAG protein no difference was observed in the levels of endogenous IFNε mRNA or downstream ISGs (ISG15 and MX1) in IFNε siRNA compared to NTC transfected cells. This result was consistent between two independent experiments. Notably, siRNAs can act by reducing translation of protein without impacting of mRNA stability [42]. Therefore, it was possible that the siRNA reduced endogenous IFNε protein without an observed effect on mRNA levels. In an attempt to measure functional changes to IFNε expression in response to siRNA knockdown, the relative permissiveness of Ect1 cells to ZIKV infection was assessed. If IFNε protein was expressed and siRNA knockdown was able to reduce IFNε protein levels one would expect these cells to be more permissive to ZIKV infection. However, Figure 6.8a & b

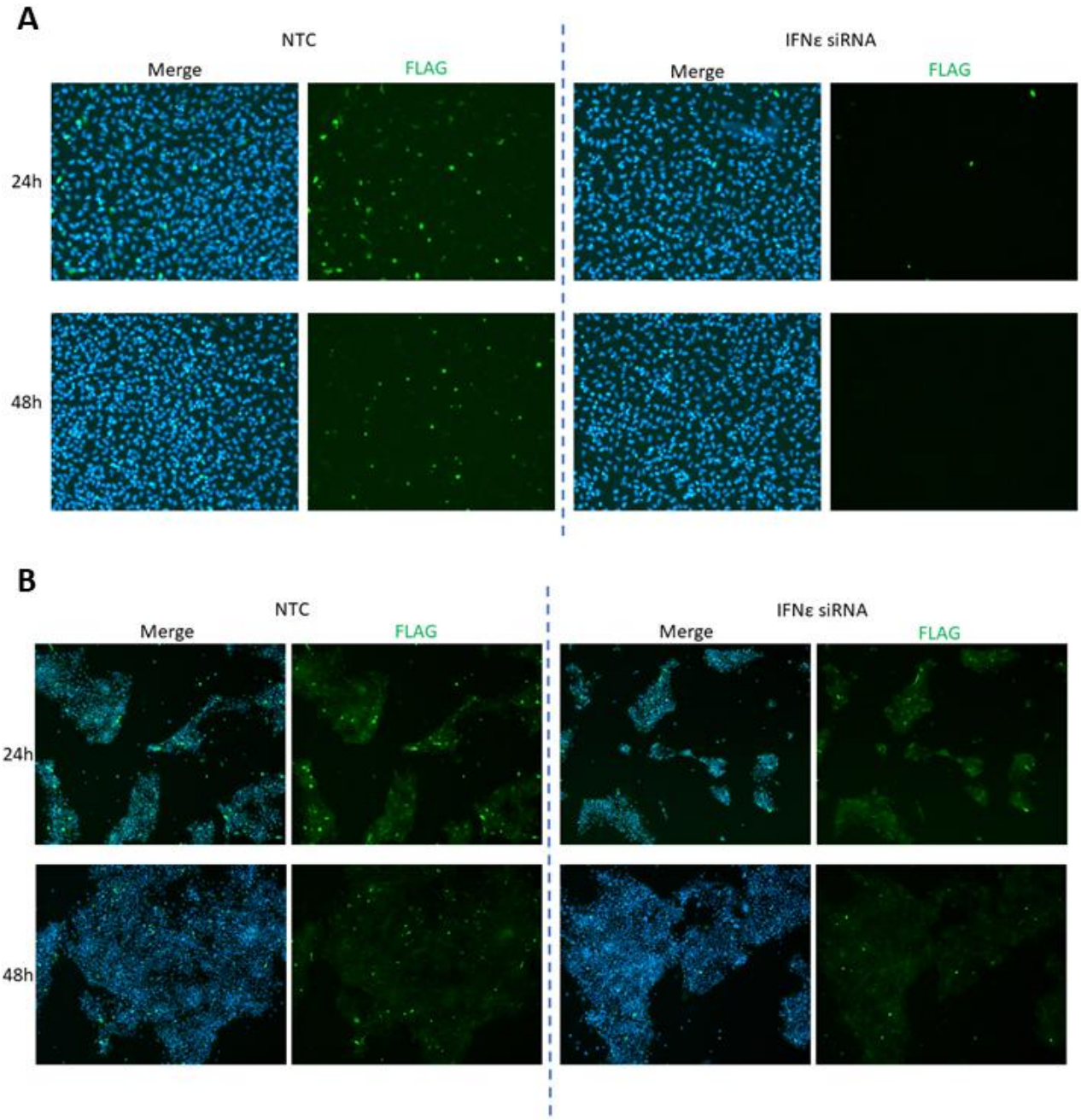

Figure 6.6: Transfection of IFNε siRNA reduces the levels of overexpressed IFNε-FLAG protein. A) HeLa or B) Ect1 cells were transfected with pLenti6.2- IFNε-FLAG 6 h prior to transfection with IFNε siRNA or non-targeting control siRNA (NTC). 24 or 48 h post siRNA transfection cells were fixed with acetone:methanol for immunofluorescent detection of IFNε-FLAG protein using an anti-FLAG antibody (green) and cell nuclei by DAPI (blue).

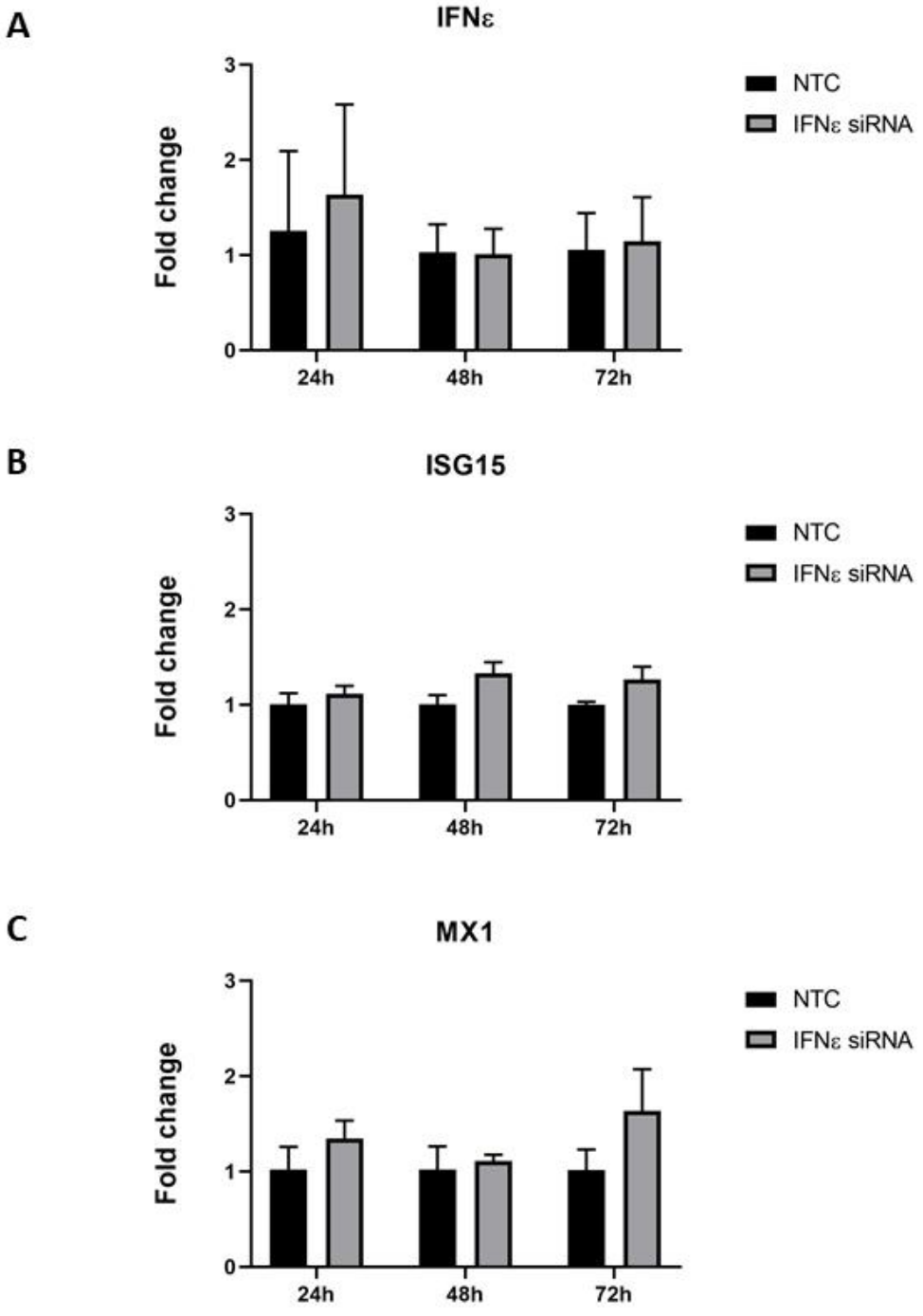

Figure 6.7: Transfection of siRNA targeting endogenous IFNε does not alter the levels of IFNε RNA, ISG RNA expression in Ect1 cells. Ect1 cells were transfected with IFNε siRNA or non-targeting control (NTC) and RNA was collected at 24, 48 and 72h post transfection to detect RNA levels of IFNε A) ISG15 B) or MX1 C) by qRT-PCR. Data are expressed as a fold change relative to the NTC at each time point. All changes are non-significant.

showed there was no significant difference in ZIKV infection in IFNε siRNA compared to NTC transfected Ect1 cells. This result was consistent with the level of ZIKV RNA detected by qRT-PCR (Fig. 6.8a) and the frequency of infected cells detected by immunofluorescence (Fig. 6.8b). Collectively these results did not confirm the expression of IFNε protein by Ect1 cells. This may indicate that IFNε protein is not expressed in these cells, and that the higher basal level of ISGs and antiviral activity previously observed resulted from unrelated factors. Alternatively, it is possible that the siRNA was able to efficiently knockdown exogenous protein expression but not the endogenous expression of IFNε mRNA or protein. Unfortunately, this limited the use of Ect1 cells as an *in vitro* model to observe changes in IFNε expression at the mRNA level.

6.2.5 IFNε RNA is regulated by progesterone *in vitro*

Despite not confirming the expression of endogenous IFNε protein in Ect1 cells, these and other cell lines may be used to assess transcriptional control of IFNε mRNA expression. This was significant, as currently there is limited understanding of endogenous IFNε expression control in relevant FRT cell lines (see section 1.2.2.2.2 for a review of the current literature). Therefore, the level of IFNε mRNA expression in response to progesterone (P4) was assessed in FRT cell lines. P4 was chosen because it purportedly acts as the main regulator of IFNε transcription *in vivo*. Each HeLa, HTR8, Ect1 and VK2 cells (Figures 6.9a, b, c & d respectively) were treated with 10 µM of P4 or vehicle control diluted in fresh media for 24 h and the level of IFNε mRNA was observed by qRT-PCR. Interestingly, we saw differing effects of P4 treatments on the level of IFNε mRNA that were cell line dependent. Both HeLa and HTR8 cells significantly reduced expression of IFNε mRNA in response to P4, correlating with previous reports using an IFNε promoter reporter assay in ECC1 cells [253]. Unexpectedly, the opposite effect was observed in both Ect1 and VK2 cells that significantly increased the level of IFNε mRNA in response to P4 treatment. However, both Ect1 and VK2 cell lines are derived from the LFRT (ectocervix and vagina). As noted in the chapter 6 introduction, the *in vivo* expression pattern of IFNε differs between the upper and lower FRT. Therefore, this observation may be a genuine effect of P4 transcriptional control in isolated primary transformed cell lines that is representative of human LFRT expression patterns *in vivo*. One hypothesis explaining the observed difference in IFNε regulation between cell lines in response to P4 treatment is that these cells express differing ratios of either the PRA or PRB

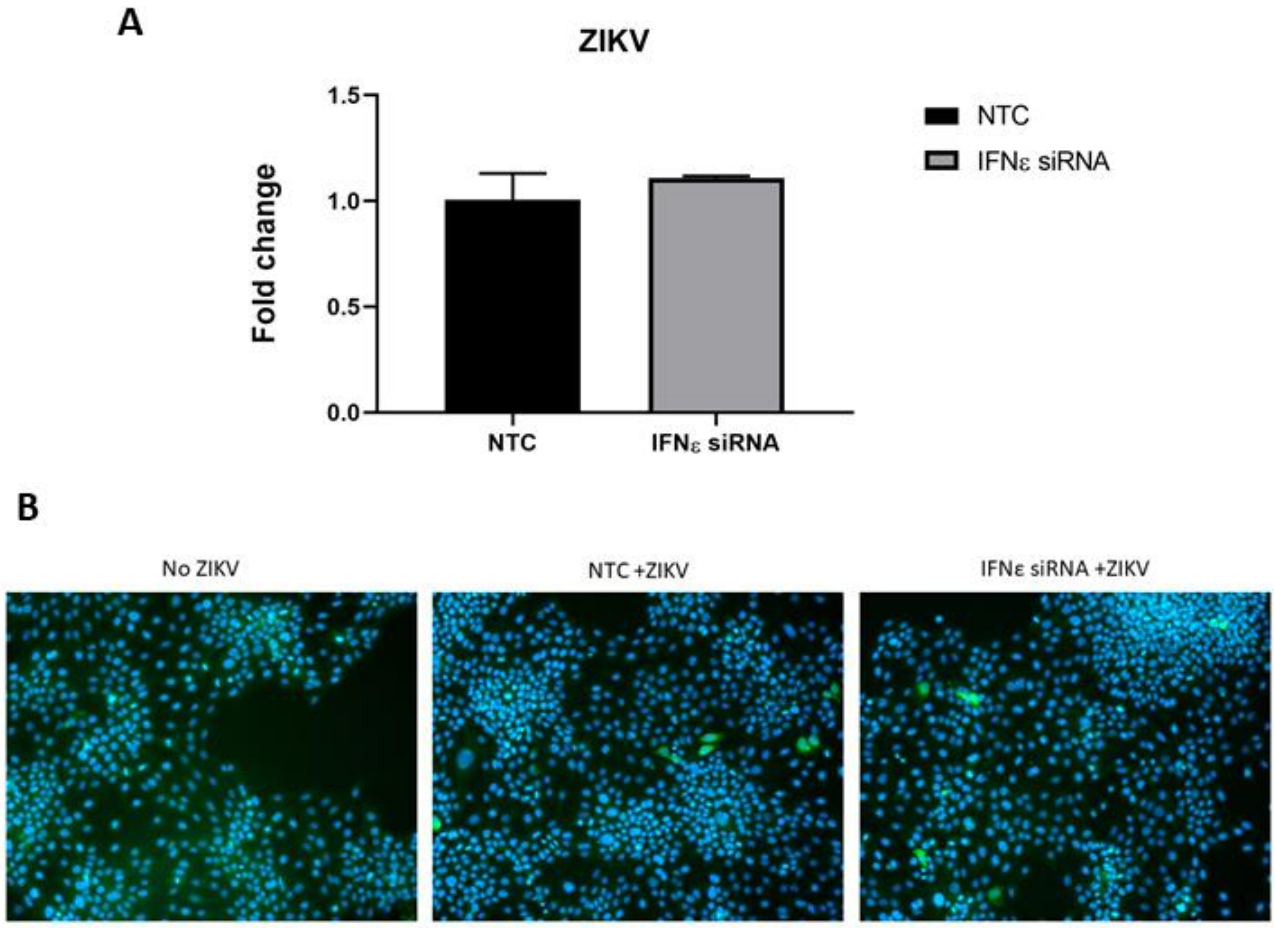

Figure 6.8: Transfection of siRNA targeting endogenous IFNε does not alter the levels of ZIKV infection in Ect1 cells. Ect1 cells were transfected with IFNε siRNA or non-targeting control (NTC). 24 h post-transfection cells were infected with ZIKV PRVABC59 (MOI 5). 24 h post-infection RNA was harvested to detect A) the levels of ZIKV vRNA by qRT-PCR or B) cells were fixed with acetone:methanol for immunofluorescent detection of infected cells using 4G2 anti-*flavivirus* E (green) and cell nuclei by DAPI (blue).

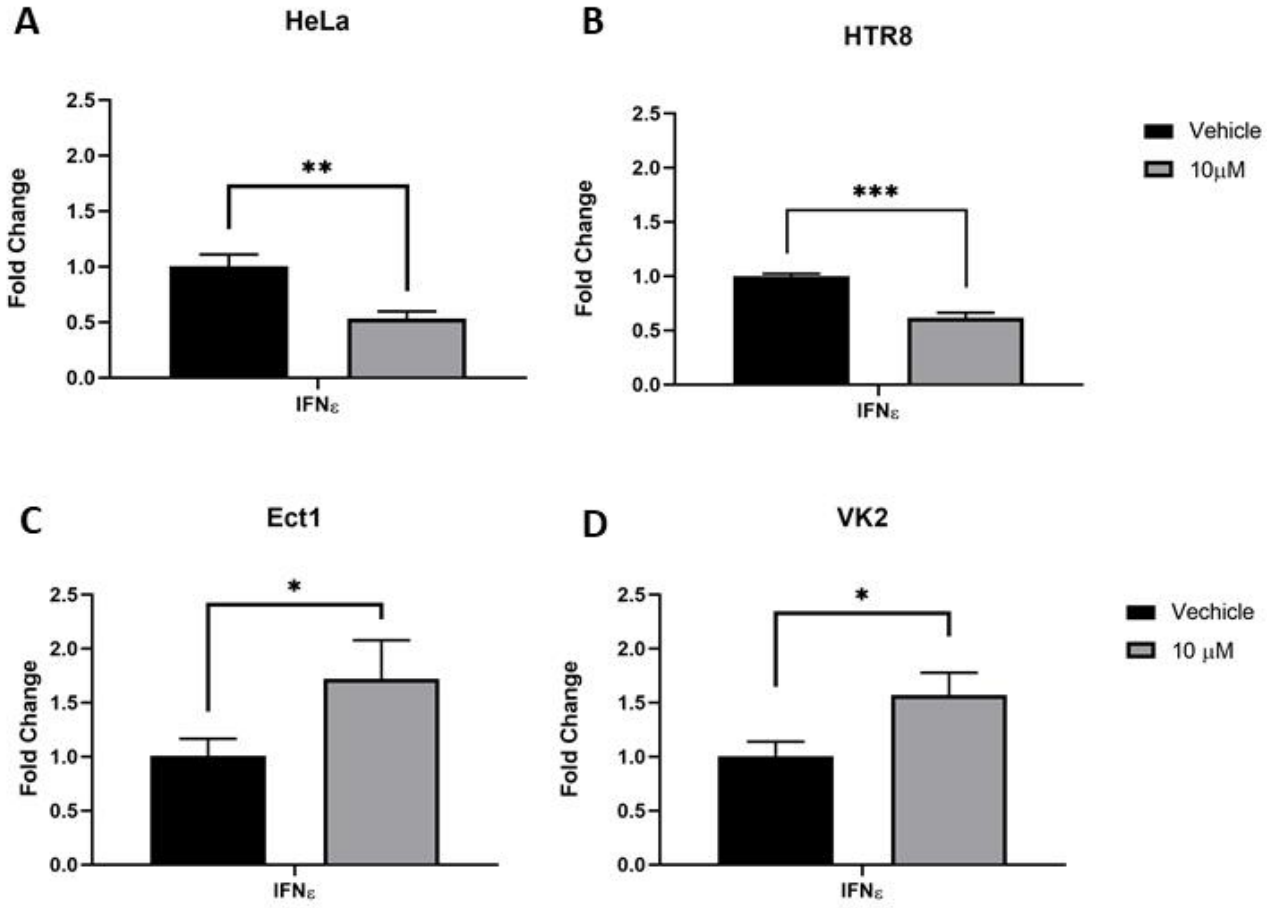

Figure 6.9: IFNε RNA is regulated by progesterone *in vitro*. HeLa A), HTR8 B), Ect1 C) or VK2 D) cells were treated with 10 μ*M* of progesterone or vehicle control. 24 h post-treatment RNA was harvested to detect the levels of IFNε RNA by qRT-PCR. The data is expressed as a fold change in gene expression relative to the vehicle control. Statistics were performed by two-tailed T-test analysis, (* $P < 0.05$, ** $P < 0.01$, *** $P < 0.001$).

receptor isoforms. To determine if the observed differences in IFNε mRNA regulation were due to differing expression of PR isoforms, primers specific to the long (PRB) and short (PRA) isoform of the PR were used in qRT-PCR on these samples (see Appendix I for sequences). Unfortunately, neither primer set was able to amplify the PRA or PRB isoform and displayed poor melt curves indicating non-specific amplification (data not shown). This data confirms that P4 influences endogenous IFNε expression at the mRNA level. However, the mechanism that drives this effect appears to be cell type specific and may rely on the expression of different PR isoforms. Future investigation into the impact of different PR isoforms on IFNε expression would be required to confirm this conjecture.

6.2.6 The constitutive expression of IFNε RNA is not altered by ZIKV infection in FRT cell lines

Aside from regulation by P4, ZIKV infection may alter the constitutive expression of IFNε. The majority of RNA viruses, including ZIKV, can induce IFN expression but also limit the production of other type-I and III IFNs by inhibiting pathways downstream of PRR activation. Specifically, ZIKV NS4A is shown to inhibit RLR signalling by preventing MAVS activation [200]. Additionally, NS1 inhibits IRF3 phosphorylation by preventing TBK1 activation [176]. NS5 also inhibits TBK1 and IRF3 activation [189, 375]. In chapter 5 we demonstrated that ZIKV infection or individually expressed viral proteins did not alter IFNε mRNA levels in HeLa cells. To extend these observations to primary transformed cells, Ect1 and VK2 cells were infected with ZIKV at increasing MOI or mock infected for 24 h prior to harvesting RNA to detect the levels of IFNε, IFNβ or IFNλI genes by qRT-PCR. Figure 6.10a & b showed that IFNε remained highly expressed irrespective of ZIKV infection. This contrasts with IFNβ and IFNλ-I that displayed low basal levels of mRNA expression in uninfected cells compared to IFNε. This data agrees with the lower level of other type-I and III IFN expression compared to IFNε observed in biopsies from the vagina, ectocervix and endometrial tissue of healthy women in previous studies [253]. In contrast to IFNε, the levels of IFNβ and IFNλ-I expression were upregulated in response to ZIKV infection suggesting that ZIKV does not entirely block PRR-mediated IFN production in these FRT cell lines. Comparatively, ZIKV infection does not reduce the constitutive expression of IFNε in FRT cell lines at the mRNA level. This highlights the unique position of IFNε being present prior to infection compared to other type-I and III IFNs that are only produced after infection is established. Collectively, this data has characterised cell lines

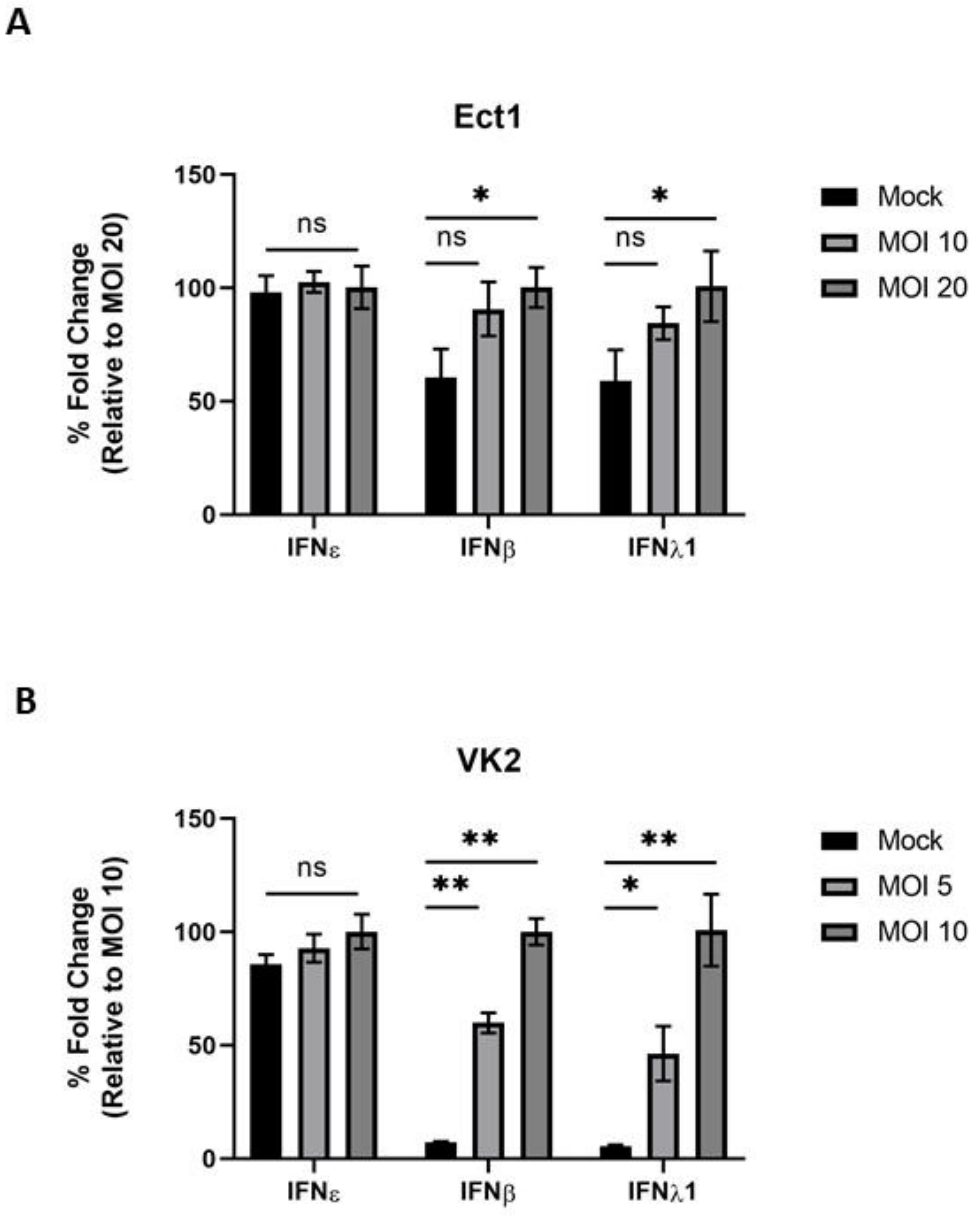

Figure 6.10: The constitutive expression of IFNε RNA in primary transformed FRT cell lines is not altered by ZIKV infection like other type-I and III IFNs. A) Ect1 or B) VK2 cells were infected with the indicated MOI of ZIKV PRVABC59. 24 h post-infection RNA was harvested to detect the levels of IFNε, IFNβ, IFNλ1 or ZIKV RNA by qRT-PCR. The data is expressed as a % fold change in gene expression relative to mock infected cells. Statistics were performed by one-way ANOVA analysis, (* $P < 0.05$, ** $P < 0.01$, *** $P < 0.001$).

as *in vitro* model systems that allow monitoring of endogenous IFNε expression levels. Despite not detecting expression of endogenous protein, these cell lines have shown promise in observing changes to IFNε expression at the mRNA level. Further characterization of these models, including determining the PR isoforms present and their effect on IFNε expression in these cell lines, would improve these models for future use.

6.2.7 Human recombinant IFNε is resistant to long-term receptor desensitization compared to IFNα *in vitro*

Another unanswered question regarding IFNε biology is the mechanism underlying its constitutive activity *in vivo*. In the previous chapter, it was demonstrated that gene induction in response to a single treatment of IFNε is subject to short-term negative regulation, returning ISG expression to baseline 24 h post-stimulus. However, it is unknown if IFNε is regulated by long-term receptor desensitization mediated by the ISG USP18 like the related IFNα. To begin investigations into this novel line of enquiry, an assay that measures receptor desensitization was developed based on the seminal work by Francois-Newton *et al*. on USP18 mediated receptor desensitization of IFNα [99]. Because of the limited supply of human recombinant IFNε protein this assay was optimised using readily available sources of IFNα and IFNβ (see Materials and Methods section 2.2.1 for details). Figure 6.11a outlines the timeline for this experiment. HeLa cells were either left untreated (naïve) or treated with IFNα (primed) for 8 h to induce expression of the negative regulator USP18. Figure 6.11b confirms that after 8 h of priming with IFNα, USP18 expression was upregulated compared to naïve cells by qRT-PCR. Following priming, the IFN stimulus was removed by washing and the cells were returned to culture overnight. During this resting phase, the level of receptor activation was allowed to return to baseline. Following overnight culture, naïve or primed cells were introduced to a booster treatment of either IFNα or IFNβ at 800 U/mL. 30 minutes afterwards cellular protein was harvested for western blot analysis to detect STAT1 and STAT2 protein phosphorylation status downstream of receptor activation. Figure 6.11c compares the levels of STAT1 and STAT2 phosphorylation between naïve and primed cells following a booster treatment with IFNα or IFNβ. Naïve cells responded robustly to both IFNα and IFNβ (lane 2 and 3) by increased levels of STAT phosphorylation compared to untreated cells (lane 1). However, in response to IFNα the levels of STAT1 and STAT2 phosphorylation in primed cells (lane 5) were reduced compared to the levels observed in naïve cells (lane 2). Conversely, in

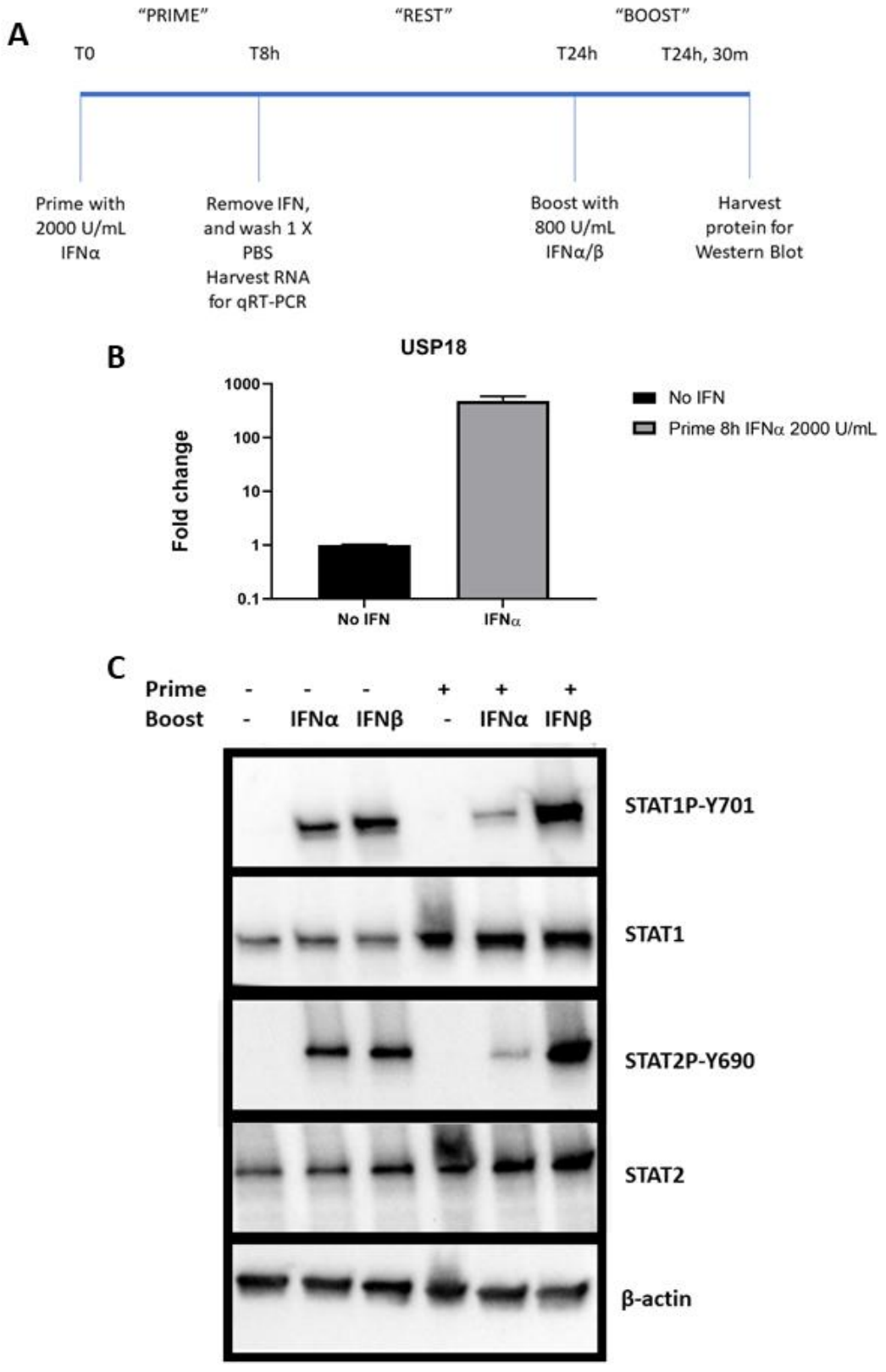

Figure 6.11: IFNα but not IFNβ signal transduction is regulated by long-term, IFN-induced receptor desensitization. A) Experimental timeline. B) HeLa cells were treated with 2000 U/mL IFNα for 8 h. RNA was harvested to determine the level of USP18 upregulation by qRT-PCR. C) HeLa cells were primed with 2000 U/mL IFNα for 8 h, rested overnight and then treated with IFNα or IFNβ (800 U/mL) for 30 minutes. Lysates were harvested for immunoblot of STAT1/2 protein and phosphorylated STAT1/2 proteins.

response to IFNβ the levels of STAT1 and STAT2 phosphorylation were enhanced in primed cells (lane 6) compared to the response in naïve cells (lane 3). The increase in STAT phosphorylation observed in primed cells when treated with IFNβ was likely a combined result of increased STAT1 and STAT2 protein expression and insensitivity to USP18 mediated desensitization. Importantly, these results are consistent with previous findings that IFNα but not IFNβ signalling is impacted by the build-up of long-term negative regulators such as USP18 leading to receptor desensitization over this time period [99]. After validating an assay that compared susceptibility of different IFN subtypes to long-term receptor desensitization, this was applied to assess the properties of IFNε. Figure 6.12a shows the experimental timeline. The protocol for priming and resting cells was maintained but in this experiment two booster treatment concentrations (100 and 600 U/mL) of IFNα, IFNβ or human recombinant IFNε were tested to see if the observed effect was consistent at lower concentrations. The results are shown in Figure 6.12b. Naïve cells responded to both concentrations of IFNα, IFNβ and IFNε booster treatments (Lanes 2-7) as indicated by robust STAT1 and STAT2 phosphorylation compared to untreated cells (Lane 1). As observed previously, the response to IFNα in primed cells was weaker than that of naïve cells (Lanes 2,3 compared to Lanes 9,10), implying desensitization. Both IFNβ treatments displayed increased levels of STAT phosphorylation after priming compared to naïve cells, indicating resistance to desensitization (Lanes 4,5 compared to Lanes 11,12). Interestingly, both treatments of IFNε were resistant to this effect of desensitization (lanes 6,7 compared to lanes 13,14) as indicated by greater levels of STAT1/2 phosphorylation in primed cells compared to naïve cells, like the observed result for IFNβ. This data implies that the human IFNε protein is resistant to long-term receptor desensitization like IFNβ. Importantly, this data provides preliminary evidence suggesting that IFNε can signal constitutively via the type-I IFN receptor. This finding has implications for the constitutive control of viral infections of the FRT.

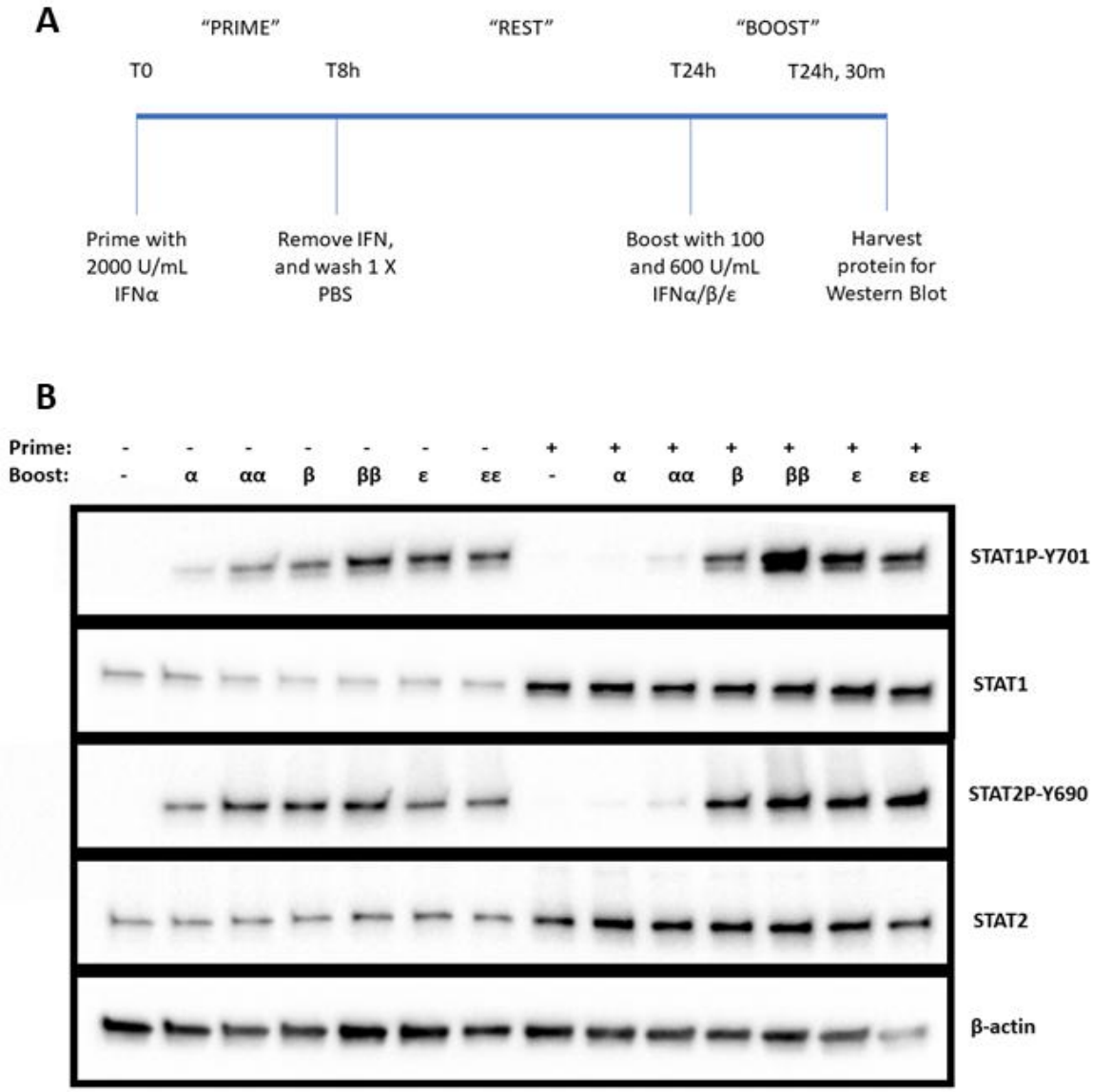

Figure 6.12: Human recombinant IFNε is resistant to long-term, IFN-induced receptor desensitization compared to IFNα in vitro. A) Experimental timeline. B) HeLa cells were primed with 2000 U/mL IFNα for 8 h, rested overnight and then treated with IFNα, IFNβ or IFNε (100 or 600 U/mL) for 30 minutes. Lysates were harvested for immunoblot of STAT1/2 protein and phosphorylated STAT1/2 proteins.

6.3 Discussion

As the most recently discovered member of the type-I IFN family less is known about the endogenous regulation and signalling properties of IFNε compared to the canonical examples IFNα and IFNβ. IFNε is a unique type-I IFN because it is constitutively expressed in the FRT and is regulated by female sex hormones rather than by viral recognition [105]. These unique aspects of IFNε's biology raise questions surrounding the mechanisms that govern its expression and signalling properties despite negative regulation of the type-I IFN pathway. This chapter aimed to address these unknowns, first by attempting to validate a cell culture model of endogenous IFNε expression and by investigating the effect of IFN-induced receptor desensitization on IFNε signal transduction *in vitro*.

Initially, to validate a cell culture model of IFNε expression, cell lines were identified that expressed high levels of IFNε mRNA. In accordance with previous *in vivo* studies of IFNε expression patterns, cell lines of FRT origin were found to express high levels of IFNε mRNA [133, 145]. The cell lines expressing the highest level of IFNε mRNA were HeLa (cervical adenocarcinoma), Ect1 (ectocervical primary transformed) and VK2 (vaginal keratinocyte primary transformed) cells. For isolated cells in culture to maintain IFNε expression patterns outside of the structural and hormonal environment of the FRT indicates there are cell intrinsic regulation mechanisms imposed on IFNε expression. This supports the concept that IFNε evolved to be specifically expressed by cells at mucosal surfaces, such as the FRT, that are at increased risk of encountering pathogens. This unique and deliberate expression pattern implies IFNε plays a non-redundant role as a type-I IFN in specific biological contexts and tissue locations. In apparent contrast, genetics studies on whole populations have found that the IFNe1 gene displays high rates of homozygous nonsense mutations, suggesting a level of functional redundancy and an evolutionary shift towards pseudogenization [203]. However, this study did not divide the cohort into population subsets, including not differentiating based on gender. Therefore, it is possible IFNε may be non-redundant within subsets of the population, such as in women but not in men, suggesting an evolutionarily refined role. Further studies into the tissue specific expression of IFNε and the genetic constraints especially comparing between men and women would be an interesting line of enquiry shedding light on its evolutionary role.

After identifying cells expressing high levels of IFNε mRNA attempts were made to characterize whether this was expressed as functional protein. Interestingly, Ect1 and VK2

cells displayed elevated levels of ISGs, both at baseline and in response to stimulation with IFNα compared to HeLa cells. This elevated level of ISG expression was inversely correlated with permissiveness to ZIKV infection. Additionally, Ect1 cell supernatant demonstrated an ability to stimulate low levels of ISG expression when applied in-trans to non-FRT cells. Collectively this data provided circumstantial evidence that primary transformed FRT cells may produce and secrete functional IFNε protein. This data is in line with IFNε protein acting to initiate a low level of "tonic" pathway activation that protects the mucosal epithelium and adjacent tissues against viral infection *in vivo* (chapter 5). Currently, the concept of tonic signalling by type-I IFNs is limited to IFNβ. Studies have demonstrated the presence of constitutive IFNβ expression at levels below assay detection in healthy animals [117]. This constitutive expression is important for maintaining a basal level of IFN-inducible signalling intermediaries such the STAT proteins [116]. Importantly, cells lacking constitutive IFNβ are more susceptible and have diminished innate responses to viral infections [268]. Currently, the importance of constitutively expressed IFNε and its potential role in tonic IFN signalling in the FRT has not been explored.

To address this dearth of information an attempt was made to link the elevated levels of ISG expression in Ect1 cells to IFNε directly by siRNA mediated gene silencing. Unfortunately, despite observing efficient knockdown of overexpressed IFNε protein no reduction of endogenous IFNε expression was characterized at the mRNA level, or via an effect on downstream ISG expression and antiviral activity. Failure to detect the expected reduction in IFNε expression or activity was likely caused by one of two reasons. Firstly, that a mechanism unrelated to endogenous IFNε expression was responsible for the observed heightened ISG expression and antiviral effect in Ect1 cells. Another possibility is that siRNA knockdown was inefficient at reducing endogenous IFNε expression compared to overexpressed protein. One theory explaining the latter cause may be due to differences in the abundance of mRNA expressed from the endogenous promoter compared to the IFNε-FLAG expression construct. This is because siRNA knockdown of gene expression is most effective on highly expressed transcripts [151]. Therefore, overexpressed IFNε-FLAG RNA may have been more susceptible to siRNA knockdown compared to endogenous IFNε transcripts. Continuing this line of enquiry would be greatly assisted by the development of new tools and antibodies to study this novel type-I IFN. In future, to directly compare the effect of endogenous IFNε expression on the basal levels of ISGs would require generating an IFNε knockout Ect1 cell line using

CRISPR gene editing technology. Alternatively, murine FRT cells could be isolated from WT and IFNε$^{-/-}$ mice and used to a similar effect. Overall, these experiments have left an unanswered question regarding the importance of IFNε in tonic signalling in Ect1 cells.

Despite an inability to detect changes in IFNε protein and downstream signalling, progress was made using these cell lines to characterize responses at the transcriptional level. Here it was shown that various cell lines (HTR8, HeLa, Ect1 and VK2) responded differently to stimulation by P4 in their regulation of IFNε expression levels. Interestingly, primary transformed cell lines derived from LFRT tissues increased expression of IFNε mRNA in response to P4. This result was counterintuitive based on data in mice showing low levels of IFNε in response to diestrus (high P4, low E2) [105], and previous promoter assays in ECC1 cells [253]. However, one study in humans found differences in IFNε regulation between the upper and lower FRT. In particular, this study demonstrated a stronger correlation between IFNε expression with levels of the level of the PR rather than the P4 hormone [253]. As mentioned previously, the levels of PRA and PRB are also hormonally regulated. Currently it is unknown how the expression and regulation of different PR isoforms by the hormonal environment and other competing stimuli impacts upon IFNε expression levels. To address this unknown, primers specific to both isoforms of the PR were used to assess their levels in different cell lines in response to P4 treatment. Unfortunately, these primers were not able to efficiently amplify PR isoform transcripts by qRT-PCR. In the future, characterization of expression of PR isoforms, how they are altered in response to different hormone environments and if this is correlated with IFNε expression *in vitro* and *in vivo* would be valuable in understanding the hormonal regulation of IFNε in more detail.

After confirming that endogenous IFNε mRNA levels are regulated in response to environmental stimuli, the impact of ZIKV infection on IFNε constitutive expression was investigated in FRT cell lines. This data adds to the results from chapter 5 that showed ZIKV infection or NS protein expression did not alter IFNε expression in HeLa cells. Ect1 and VK2 primary transformed cells are likely a better model of endogenous IFNε expression as they closely resemble normal FRT cell function [96] and are not cancer derived lines that often have different signalling capabilities [313]. Using these cell culture models it was confirmed that ZIKV infection did not alter (reduce or increase) the constitutive expression of IFNε at the mRNA level. The inability of ZIKV to evade IFNε production agrees with the observed antiviral effect of constitutively expressed IFNε in wildtype mice (chapter 5, Fig. 5.1) and extends these

observations to human cell lines. Furthermore, the lack of virus mediated induction of IFNε expression confirms the absence of response elements downstream of PRR signalling pathways in the IFNe1 gene promoter [133]. This unique characteristic of IFNε to be constitutively expressed in cells of the FRT during viral infection contrasts with other type-I and III IFNs. The basal levels of IFNβ or IFNλI mRNA were consistently lower than IFNε in FRT cell lines. However, the expression of IFNβ and IFNλI was induced by ZIKV infection indicating that PRR-mediated signalling is not fully blocked by ZIKV NS-protein expression in these cells at this time point. This incomplete blockade of PRR-mediated signalling by ZIKV infection likely reflects the inbuilt redundancy of multiple PRR pathways to sense infection and implies that viral NS-protein mediated inhibition of IFN production (as seen in chapter 5, Fig. 5.7) has evolved to reduce or delay rather than completely block IFN production in humans. This contrasts with the stark inhibition downstream of IFNAR1/2 receptor activation mediated by ZIKV NS5 that almost completely ablates the effect of type-I IFN treatment *in vitro* (chapter 5, Fig. 5.5 and Fig. 5.6). Collectively, this ability of ZIKV to delay PRR-mediated IFN production and then to block IFN-mediated signalling highlights the importance of priming cells with IFN prior to infection. Collectively, this suggests that prophylactic expression of IFNε may significantly contribute to anti-ZIKV protection in the human FRT.

The constitutive expression of IFNε makes it unique amongst other IFNs. To date, research surrounding this unique IFN has implicitly assumed that IFNε is able to signal via the IFNAR1/2 receptor constitutively. This would offer comprehensive protection to cells in the FRT to viral infection. However, the constitutive activity of IFNε contrasts the classical model of type-I IFN signalling, whereby the signal leads to accumulation of negative regulators that switch off the response and prevent overt immune activation [70]. In the previous chapter it was demonstrated that a single dose of IFNε led to transient induction of ISGs implying the pathway was susceptible to short-term negative regulation. However, it remained to be seen if this effect translated to long-term receptor desensitization, as previously observed for type-I IFNα [95, 99]. Alternatively, more recent modelling has demonstrated that type-I IFNβ present at low levels is able to constitutively induce “tonic” levels of ISGs that are required to mount an effective immune response to viruses [217]. Correlating with this activity, IFNβ signal transduction is not dependent on USP18 receptor desensitization [99]. Furthermore, these differing susceptibilities to long-term receptor desensitization have been linked to these IFNs differential receptor binding kinetics to the individual subunits of the IFNAR1/2

receptor [369]. For the first time, the ability of IFNε to signal constitutively via the IFNAR1/2 receptor despite accumulation of long-term negative regulators was demonstrated with experimental evidence. This preliminary data supports the potential of an evolved link between the unusual receptor binding kinetics of IFNε with its unique biological properties. It would be valuable in future to extend these observations to effects on long term downstream ISG expression. Additionally, this model could be improved by repeating these experiments in cell lines that express USP18 in an IFN-independent manner, directly linking this effect to the long-term negative regulator. Moreover, molecular modelling to compare receptor dimerization upon binding of IFNε, IFNβ or IFNα in the presence or absence of USP18 should be conducted. These experiments could be modelled on the fluorescence-based co-locomotion assays used by Wilmes *et. al* to determine the frequency of IFNAR1/IFNAR2 dimerization upon ligand binding in the presence or absence of USP18 expression in live cells [369].

6.4 Conclusion

IFNε is unique amongst the type-I IFNs, most prominently because of its constitutive hormonally regulated expression. As a result, there is limited information regarding the mechanisms that govern its expression. Additionally, as the most recently discovered member of the family questions remain about the fundamental biology of this IFN such as how it can signal constitutively. In response to these gaps in knowledge, the aim of this chapter was to find models of endogenous regulation of IFNε expression and to determine its constitutive signalling properties *in vitro.* Cell lines of FRT origin were identified that express high levels of IFNε RNA. Accordingly, primary transformed FRT cell lines were found to have heightened basal expression of ISGs and intrinsic antiviral activity. However, due to the inability to monitor changes in endogenous IFNε mRNA or protein expression following siRNA knockdown it remains unclear if these properties are directly linked to these cell lines expressing functional IFNε protein. Despite being unable to confirm IFNε protein expression in these cells, these *in vitro* models were used to assess the impact of P4 on IFNε RNA expression. This led to the novel finding of cell lines responding differently to this environmental stimulus, opening discussion on further research into the impact of PR isoforms on IFNε expression. These cells were also used to confirm that ZIKV is unable to evade the constitutive production of IFNε RNA in human cell lines. This was an important

finding for future infection modelling experiments. Together these results have made headway into uncovering useful *in vitro* model systems to easily assess the impact of competing stimuli on IFNε expression. Future advances in this line of enquiry would benefit greatly from the development of commercially available antibodies to detect endogenous IFNε protein expression in cell culture. Moreover, for the first-time experimental evidence demonstrated that IFNε can signal independently of long-term receptor desensitization. This is likely a result of the unique binding characteristics of IFNε for the individual subunits of the IFNAR1/2 receptor, leading to USP18 insensitivity. Future experiments to confirm a direct link between USP18 expression and IFNε's signalling properties would provide valuable insights into the biological actions of this unique type-I IFN.

Chapter 7

Conclusions and Future Directions

Dengue virus (DENV) and Zika virus (ZIKV) are two closely related flaviviruses that infect humans. Although most infections are asymptomatic, these viruses can cause severe life threatening or debilitating disease. DENV has the greatest disease burden of all flaviviruses, infecting more than 390 million people and causing approximately 21,000 deaths annually [127]. Comparatively, ZIKV causes far fewer deaths but infection during pregnancy can result in foetal infection, early pregnancy loss, or developmental and neurological impairment in newborns [53]. To date there are no specific antiviral treatments or approved vaccines for ZIKV [365], and the approved vaccine for DENV (Dengvaxia®) has continuing issues surrounding safety and applicability for high-risk groups [364]. The lack of effective treatments and vaccines for these viruses places the burden of controlling infection directly on the individual host immune response. Type-I IFNs are a crucial host front-line immune defence that protect against a broad range of viral pathogens. The IFNs are normally produced in response to sensing viral infection within cells [175]. Once secreted from infected cells these antiviral cytokines bind their cognate receptor to induce expression of hundreds of ISGs, including some that directly inhibit ZIKV and DENV replication such as Viperin [141, 354], ISG15 [64, 327] and members of the IFITM family [157, 300]. Aside from their direct antiviral roles, several ISGs regulate the innate and adaptive immune responses, giving rise to an appropriately managed antiviral state [305]. To counter the potent antiviral activity mediated by the IFNs, most, if not all, viruses have evolved ways to overcome this response. Consequently, viral evasion of the IFN pathway directly underpins the ability of these viruses to cause infection and disease. Likewise, to counter viral evasion the host must utilize the IFN response with the right spatiotemporal controls to bring infection under control whilst limiting damage to host tissues. This balance between viral immune evasion and an effectively managed innate immune response often determines the outcome of disease for the host. This thesis aimed to enhance our understanding of the molecular mechanisms that govern the interactions between the host innate immune response and these flaviviruses from the perspective of both the virus and of the host. It is hoped that an improved understanding of

these interactions will aid in the design of new therapeutics or vaccines that can shift the balance in favour of the host immune response and help to prevent disease.

As detailed in Chapter 1, flaviviruses such as ZIKV and DENV have evolved a complex web of molecular interactions to undermine both the production and downstream signalling of the IFNs. Some of these mechanisms have been characterized [52]. However, to date most studies investigating mechanisms of innate immune evasion by ZIKV and DENV have relied on overexpressed viral proteins or genetic elements. Importantly the functions of individually expressed viral proteins are often not representative of their role within the complete virus lifecycle [167]. As a result, we hypothesized that the ZIKV and DENV genomes contain undiscovered regions that encode type-I IFN response evasion mechanism. To test this hypothesis, in chapter 3 and 4 of this thesis, we aimed to perform genome-wide mutational studies in the context of the full virus lifecycle to uncover novel evasion mechanisms used by ZIKV and DENV to counter the type-I IFN response. The methodology for this work was preceded by a genome-wide mutagenesis screen performed by Qi *et al*. to detect novel HCV IFN evasion mechanisms [274]. This study utilized the MuA transposon mutagenesis method to create an HCV mutant library that was selected for in conditions with or without exogenous IFN treatment (IFNα IC_{50}, 1 U/mL), revealing novel mutations that conferred IFN hypersensitivity and, by inference, viral determinants of IFN resistance. Accordingly, to address our aim the MuA transposon mutagenesis approach was applied initially to a ZIKV infectious clone (pZIKV-ICD). The results of chapter 3 revealed major challenges associated with instability and recombination of the ZIKV clone within bacteria indicating that this infectious clone was unsuitable for high-throughput mutagenesis approaches that require the use of bacteria for plasmid propagation. Unfortunately, approximately 90% of the mutant clones in the final transposon library displayed large deletions of viral sequences due to bacterial recombination, resulting in non-functional clones and reducing the theoretical coverage of mutations across the genome to numbers below those that are practical or meaningful for this type of study [94, 104, 274]. Despite multiple attempts to correct this issue, this project was deemed unviable for the timeframe. Within the field, multiple studies have reported that cloned *Flavivirus* genomes are toxic in bacteria due to the presence of cryptic bacterial promoters and are unstable due to the presence of highly repetitive sequences [17]. Interestingly however, during the course of this thesis an identical mutagenesis approach was successfully applied to a ZIKV infectious clone harbouring the

historical African strain MR766 [104]. Importantly, there is approximately 10% sequence divergence at the nucleotide level between the MR766 strain compared to the Paraiba_2015 strain used in this thesis to [389]. This level of sequence divergence is sufficient to account for phenotypic differences in viral replication observed by us (Figure 3.2) and others [9, 319] in various cell lines. The data from chapter 3 implies that this sequence divergence may also be responsible for the differing stability of these infectious clones in bacteria. Further evidence supporting this theory was given by the MR766 infectious clone being stable with only a single chimeric intron [309], as opposed to the two required to generate the original full-length pZIKV-ICD clone in bacteria [350]. This suggests that the Paraiba_2015 strain sequence incorporated in the pZIKV-ICD clone may be inherently less stable compared to the MR766 strain in bacteria. At the time of writing, other infectious clones have become available for multiple different strains of ZIKV [49, 74, 241, 311]. It is possible that one of these clones may be better suited to the MuA transposon mutagenesis method. Aside from using a different infectious clone system, future attempts to apply this method to the ZIKV genome would benefit from bacteria-free cloning methods. This approach would negate the impact of toxicity of viral sequences in bacteria and therefore reduce recombination of the final mutant library [17]. Individually mutagenized viral genome segments could then be used to generate full-length sequence by methods such as circular polymerase extension reaction (CPER) [311] or *in vitro* ligation approaches [74] to generate full-length ZIKV mutant libraries. Collectively, this data highlights the importance of selecting highly stable infectious clones for use in high-throughput mutagenesis approaches.

To substitute for the ZIKV mutant library, a DENV MuA transposon mutant library was repurposed for the screen. This mutant library was pre-selected based on replication competence and ability to produce infectious virus in a previous screen by Eyre *et al.* [94]. This library was then further selected and screened for relative sensitivity to type-I IFN. The results of chapter 4 showed selection of the library was achieved using a pre-treatment of 1 U/mL of IFNα (Figure 4.3). NGS analysis of the selected mutant library generated a functional map of the DENV genome, highlighting regions likely to confer IFN evasion (Figure 4.4). Based on this functional map, several specific mutations were selected to test their ability to encode an IFN hypersensitive phenotype. These included two promising hits at nucleotide positions 8069 and 8077 within the MTase domain of NS5. To our surprise, the results of chapter 4 revealed that none of these mutations were able to confer IFN hypersensitivity when

introduced into the genome of the parent DENV2 strain (Figures 4.9, 4.10 & 4.11). We hypothesized that these unexpected results were due to naturally occurring mutations that accumulated after multiple passages and confounded the apparent impact of individual transposon insertions. These mutations, if present, most likely arose during high MOI passages that facilitated co-infection and complementation of mutant viral genomes, leading to accumulated compensatory mutations [109]. Evidence supporting this hypothesis is provided by an alanine scanning DENV2 mutant screen. In this screen, trans-complementation using heterologously expressed wildtype NS2 protein allowed compensatory mutations to accumulate after only three passages on the same cells [372]. These compensatory mutations were shown to rescue deleterious mutations introduced within the NS2 region. As detailed in Chapter 4, testing this theory for deleterious mutations occurring within the NS5 MTase domain would require the development of a stable DENV replicon cell line because the MTase domain of NS5 cannot be trans-complemented by individual protein overexpression [83, 167]. Additionally, in future studies compensatory mutations could be detected using long-read sequencing technology [205]. Other approaches to improve whole-genome high-throughput screening of RNA virus genomes relate to reducing the likelihood of accumulated mutations. This could be achieved by reducing the number of passages, limiting the rate of co-infection by controlling MOI and increasing selection pressure on the virus population when performing screens [109]. One point of interest arising from this Chapter was the discovery of a synthetically introduced SNP at nucleotide position 10476 in the 3'UTR that conferred a weak IFN hypersensitive phenotype. Analysis determined this SNP occurred within a conserved loop of DB1 within the 3'UTR that was important for both vRNA replication [67] and inhibition of the IFN response via generation of sfRNAs [51]. Despite not aiming to detect this mutation as part of the transposon insertion screen it would be interesting in future to independently characterize the impact of this mutation on DENV IFN sensitivity. Currently, DENV sfRNA is known to inhibit IFN production downstream of RIG-I by binding to the RIG-I translocase protein TRIM25 [202]. However, our screen circumvented the RIG-I pathway by applying exogenous IFN treatment directly to cells. Interestingly, mutations in the 3' UTR of WNV are also known to confer an IFN hypersensitive phenotype downstream of the activated type-I IFN receptor [307]. Currently the mechanism underlying WNV sfRNA-mediated evasion of type-I IFN signalling has not yet been elucidated. Importantly our data indicates the DENV 3' UTR not only inhibits signalling downstream of RIG-I, but that like WNV, it also inhibits

downstream of IFNAR1/2 receptor activation, shifting our current understanding of DENV UTR-mediated evasion. The mechanism of DENV sfRNA mediated evasion of IFNAR1/2 signalling may be common amongst flaviviruses (such as WNV) or may have a different mechanism of action. Future experiments to validate and determine the mechanism whereby this SNP confers IFN hypersensitivity are required. These experiments could include generating individually expressed 3'UTR mutant constructs for DENV, WNV and ZIKV. These constructs could then be used to determine the impact that these mutations have on ISG expression and the phosphorylation status and/or stability of signalling intermediaries downstream of type-I IFN receptor activation compared to WT sfRNA. This hypothesis could be further explored by generating an SNP mutant library targeting the 3' UTR using error-prone PCR methods and screening in conditions with and without IFN to determine if other mutations in these RNA structures confer similar phenotypes. Indeed, this deep-mutational scanning approach was successfully performed by Du *et al.* (2017) on the Influenza H1N1 genome [84]. In this study a SNP mutant library was generated by error prone PCR on small 240 segments of the influenza genome. The library of H1N1 mutants were then passaged in A549 cells with or without exogenous IFN treatment (IFNα at IC_{80}). Deep sequencing (Illumina PE250) revealed specific mutations within NS1 that had reduced fitness under IFN treated conditions. More recently, another study utilized a cDNA mutant library containing synthetically engineered mutations representing all possible codon substitutions in the C-terminal of the ZIKV E-protein [312]. This library was selected in mammalian or mosquito cells leading to the discovery of mutations conferring host-specific adaptations. This study utilized barcoded sub-amplicon sequencing coupled to the Illumina MiSeq v3.2 platform. Importantly, this method led to discovery of strains that were attenuated in mouse models of infection. Both studies exemplify the future of functional screening under selection conditions. New technology such as improved error prone PCR methods, lower costs of synthetic DNA generation and new sequencing technologies are shifting this field towards mutational studies that resolve to the individual nucleotide level. In combination, although the MuA transposon mutagenesis approach to screening was unsuccessful at discovering novel IFN evasion mechanisms for ZIKV or DENV, this information contributes to the body of knowledge on whole-genome high-throughput screening methods for flaviviruses under selective conditions.

On the other side of the evolutionary arms race, the host has evolved multiple families and subtypes of IFNs (see introduction section 1.1.2) to control viral infection in a range of biological contexts. Typically, the classical type-I IFNs like IFNα and IFNβ are produced in response PRR detection [214]. The ubiquitous expression of the IFNAR1/2 receptor allows the type-I IFNs to protect against both local and systemic viral infections [214]. Aside from the broad acting IFNα and IFNβ, other IFNs have evolved to contribute towards local protection in tissues with a higher risk of infection [203]. These include the type-III IFNs that act almost exclusively on epithelial cells at mucosal surfaces due to the restricted expression of IFNLR1 receptor subunit [143]. Type-III IFNs are the first IFNs produced by infected epithelial cells [254] and provide localized antiviral protection without causing overt inflammation at mucosal surfaces in tissues such as the lung [66, 98, 182]. Therefore, it has been proposed by others that type-III IFNs protect at the site of infection while having minimal impact on mucosal barrier integrity, preventing pathogens from entering more distant tissues [182]. However, as is the case for IFNα and IFNβ, expression of type-III IFNs is reliant on pathogen detection [182]. Also, there is conflicting evidence regarding the impact of type-III IFN on inflammation in different biological contexts. Type-III IFNs appear to limit inflammation in the lung and in the gut [50, 66]. However, studies in both mice [113] and humans [190] link type-III IFNs to immune dysregulation in systemic lupus erythematosus via promoting inflammatory cytokine release from skin and kidney keratinocytes. Importantly, the impact that type-III IFNs have on inflammatory pathways in the FRT are not yet understood.

Another example of a specialized, locally acting IFN is IFNε. IFNε is a type-I IFN produced primarily by the mucosal epithelium of the FRT in both mice and humans [105, 133]. Whereas other type-I and type-III IFNs are produced in response to viral infection, IFNε is unique because it is constitutively expressed in the FRT where it maintains a basal level of ISG expression and can protect against STIs [105]. For example, IFNε protects against HSV infection in the FRT of mice [105]. Furthermore, IFNε inhibits multiple steps of the HIV lifecycle in cell culture [110]. It is now known that ZIKV preferentially infects the FRT and it is capable of transmitting sexually even in asymptomatic cases [101]. Additionally, ZIKV evades both the production and downstream signalling of the classical type-I and III IFNs due to the combined actions of multiple viral NS proteins (detailed in the introduction section 1.3 and reviewed in [52]). Coupled with the fact that the most severe foetal pathologies of ZIKV infection occur via infection of the FRT [288], we propose that the constitutive expression of IFNε may be

especially important for the host to control ZIKV infection in this biological niche. Therefore, we aimed to investigate the antiviral properties of IFNε and determine if it controls ZIKV infection in the FRT. The results of chapter 5 revealed that IFNε is unequivocally important to protect the FRT from viral infection. Endogenous IFNε expression significantly limited viral infection in WT mice compared to IFNε$^{-/-}$ mice (Figure 5.1a - h). Complementary experiments demonstrated the prophylactic potential of IFNε by iVag administration of exogenous rIFNε protein (Figure 5.1i - J). In FRT cell lines we showed that IFNε induced a gene profile involving hundreds of ISGs that protected against ZIKV infection when administered prior to infection (Figure 5.2 & 5.3). Interestingly our RNAseq analysis and ISG induction kinetics assays showed that IFNε induced lower levels of pro-inflammatory genes such as the transcription factor IRF1, and chemokines CXCL10 and CXCL11 compared to those induced by other type-I and III IFNs at an early time point (6 h) and over an extended timeframe (4 - 24 h). Interestingly, however, the antiviral response to IFNε treatment was dampened by ZIKV NS5-mediated evasion to a similar degree to that of IFNα when administered post-infection (Figure 5.5 & 5.6). Conversely, the constitutive expression of IFNε was impervious to ZIKV NS4A-, NS1- and NS5-mediated inhibition, that delayed the production of other type-I and III IFNs downstream of activated RIG-I (Figure 5.7). Collectively, this data highlights the prophylactic potential of constitutively expressed IFNε in protecting the FRT from ZIKV sexual transmission, as it is the only type-I or III IFN expressed prior to infection in the non-pregnant human FRT [253]. This finding adds to our understanding of FRT immunobiology. The current model of immunity in the FRT implies that host-mediated viral defences are organised into tiers that are activated in a distinct, sequential order. The first tier is comprised of the physical defences of the mucosal epithelium lining the upper and lower FRT. These defences include secreted mucus, commensal bacteria, low pH, the LFRT stratified epithelium and UFRT epithelial tight-junctions [317]. Collectively, the mucosal epithelium acts as a continuous physical barrier that non-specifically impedes pathogen access to target cells and deeper tissues [321, 370]. If viruses overcome this first layer and colonize cells of the mucosal epithelium, they are recognized by PRRs, activating the second tier of innate immune defence [317]. PRRs that sense RNA viral pathogens (RLRs, TLRs) are expressed in cells of both the upper and lower FRT in humans [111, 135]. Viral recognition leads to the secretion of classical type-I and III IFNs and other key cytokines or chemokines that have direct antiviral effects, cause inflammation and mediate immune cell activation and recruitment to the site of infection [317]. If viral

pathogens are not cleared by innate defences, the adaptive immune response is initiated and modulated by the innate immune response as the third tier of defence to control infection. Clearly, this archetypic model of immune protection is ineffective for viral infections like ZIKV that preferentially infect the mucosa of the FRT and efficiently evade IFN responses [41, 152]. Studies in mice [164] and humans [152] show that PRR-mediated IFN production is delayed during ZIKV infection, including in the FRT. This delay likely facilitates the persistence of ZIKV in the FRT [63]. However, our data challenges this established view of FRT immunobiology, shifting it away from a reliance on reactionary responses (such as by other type-I and type-III IFNs) to one of pre-emptive protection against viral infection. IFNε uniquely activates a pre-emptive immunological barrier to infection with both direct antiviral and immune modulatory functions. Our data implies that without endogenous IFNε in the human FRT, ZIKV sexual and *in utero* transmission may be even more prevalent. Studies investigating the expression of IFNε in the FRT of ZIKV infected patients could help to clarify the importance of IFNε.

So far, our research has not addressed the antiviral potential of IFNε in the context of pregnancy. This will be an important avenue of research in the future because ZIKV infection can cross the placenta and cause birth defects [53]. Studies in humans [250] and mice [105] show that the levels of IFNε increase during the late stages of pregnancy. Furthermore, HSV infection during pregnancy in humans correlates to lower levels of IFNε compared to those of healthy women [250]. Collectively, this data implies that IFNε plays an important antiviral role in the context of pregnancy. Currently, there are conflicting views on the role of type-I IFN during pregnancy. Type-I IFNs are thought to play an essential role during the early stages of pregnancy following implantation. In both humans and mice type-I IFNα is upregulated during early pregnancy [46]. Additionally, mice lacking the type-I IFN receptor have abnormal pregnancy-associated changes to the spiral arterioles, suggesting that this pathway is important for development of the early maternal decidua [237]. Moreover, functional type-I IFN signalling can protect both the mother and foetus from viral infection during pregnancy. *In vivo* infection modelling has shown that pregnant IFNAR1$^{-/-}$ mice have a greater susceptibility to Herpes Virus (MHV68) infection [276]. This led to greater levels of virus in maternal circulation, in the placenta and in the foetal compartment of these mice compared to WT counterparts. Similar results were seen for ZIKV infected pregnant mice [221]. In this study ZIKV infection in IFNAR1$^{-/-}$ mothers led to greater levels of viral infection, more severe placental damage and increased frequencies of foetal demise compared to WT mice.

Moreover, IFNα treatment trialled in human pregnancies for women with essential thrombocythemia was well-tolerated and did not alter the rate of miscarriage beyond the population average [22, 378]. Conversely, overactive type-I IFN responses are known to have detrimental outcomes in pregnancy. For example, genetic deficiencies in the type-I IFN negative regulator USP18 can lead to interferonopathy, foetal brain damage and pseudo-TORCH syndrome in humans [218]. Additionally, high levels of IFNβ induced by TLR4 in response to bacterial LPS can lead to foetal demise in mouse models [178]. Similarly, pregnant IFNAR1$^{-/-}$ mice mated to immune competent IFNAR1$^{+/+}$ males that were challenged with ZIKV displayed increased resorption in the presence of functional type-I IFN signalling in the foetal compartment (IFNAR1$^{+/-}$) compared to IFNAR1$^{-/-}$ littermates [383]. Collectively these studies imply there is a time, a place, and an extent of IFN signalling that is beneficial in protecting against infection and promoting healthy pregnancy.

In light of the above data, other studies have proposed that type-III IFNs would provide safer protection during pregnancy against ZIKV infections due to their reduced capacity to incite general inflammation in other tissues such as the lung [66, 98, 182]. Evidence supporting this theory was provided by investigations involving a non-pregnant mouse model. In this study IFNLR1 KO mice were more susceptible to ZIKV infection in the LFRT [36]. However, this effect was mostly lost in UFRT tissues, the site where trans-placental infection occurs. Additionally, studies have found that isolated primary human trophoblasts [21] and mid-gestation organotypic placental explants [57] constitutively release type-III IFNs that protect against ZIKV infection. However, this effect has not yet been confirmed in the hormonal and tissue micro-environment of natural pregnancy. Moreover, our data (Figure 5.3k) indicated that type-III IFN treatment induced greater expression of the inflammatory cytokine CXCL10 over a 24 h period in FRT epithelial cells compared to IFNε treatment that was applied at the same concentration of protein. Combined with ZIKV-mediated evasion of type-III IFN production, this suggests that further investigation into the importance of type-III IFN protecting against ZIKV infection in pregnancy are required to support these assertions. Collectively, this data suggests that because IFNε is present during normal pregnancy and has a lower propensity to incite inflammation in FRT epithelial cells, it may be the most appropriate IFN to be explored as a therapeutic agent regarding safety and efficacy to prevent ZIKV infections in pregnancy. Testing this theory would require modelling iVag ZIKV infection during pregnancy and comparing infection outcomes between WT, IFNε$^{-/-}$, IFNAR1$^{-/-}$ and IFNLR$^{-/-}$ mice. Further

experiments could use iVag treatment with recombinant IFNε or IFNλ during different stages of pregnancy in mice to compare their impact on tissue inflammation and normal pregnancy. In humans, the immune environment of the UFRT and LFRT are controlled hormonally, by damage signals and by recognition of foreign agents like viruses, sperm or the semi-allogenic foetus [317]. These alterations to the immune environment are essential to support the normal biological functions of the FRT [382]. IFNε expression is also controlled by hormones, semen and other immune modulatory molecules like TNFα [105, 210, 316]. As a newly discovered IFN, less is known about the basic biology that allows IFNε to function constitutively without adverse effects in this biologically important tissue. The inter-relatedness of competing stimuli, the biological properties of IFNε, and their intersection with the normal reproductive process are not well characterised. This is in part due to a lack of *in vitro* models that recapitulate human IFNε expression patterns, and this concept was explored in chapter 6. Here we developed *in vitro* models that allowed observation of IFNε regulation at the RNA level in response to progesterone (Figure 6.9). This was a significant issue to address because previous studies that have investigated progesterone-mediated IFNε regulation have only examined *in vivo* expression patterns or utilized promoter reporter assay systems [105, 253]. These studies were limited by the inability to control for multiple competing stimuli within a complex living system and by our current limited understanding of the IFNε gene promoter, respectively. Additionally, our *in vitro* models were used to demonstrate that ZIKV infection did not alter the expression of IFNε (Figure 6.11). With further optimization our *in vitro* model systems can serve as tools to complement *in vivo* and patient studies on IFNε expression. These models will improve our ability to dissect the pathways, transcription factors and promoter elements that control IFNε expression. Collectively this data highlights the importance of the unique properties of IFNε, shedding light on its evolved function to protect against viral infection in the FRT. In future, these models could be applied to investigate other stimuli that regulate IFNε expression at the RNA level. This could include investigation of the effects of combinations of hormones that better reflect the complex hormonal environments of the menstrual cycle or pregnancy. Likewise, investigation of the impact of hormonal contraceptives on expression of IFNε would be an important future avenue of research. If IFNε is regulated by hormonal contraceptives, this may help to explain observations that such contraceptives alter the permissiveness of the FRT to other viral infections like HIV [154]. Additionally, chromatin immunoprecipitation (ChIP)

assays combined with mass spectroscopy could be used to determine the transcription factors and promoter elements that are important for the regulation of IFNε expression in the context of different stimuli.

Additionally, this thesis provided preliminary evidence that IFNε signals constitutively via the IFNAR1/2 receptor, giving insight into the unique biological properties that allow it to protect the FRT from viral infection. This was a significant finding because signalling induced by canonical type-I IFNα is switched off by negative feedback loops involving the SOCS and USP18 proteins. Unlike the short-lived receptor desensitization that is mediated by SOCS proteins [322], USP18 desensitization is sustained over several days [99]. Importantly this has implications for the usage of IFNα as an antiviral therapy because USP18-mediated receptor desensitization leads to unresponsiveness to prolonged IFNα treatment in mice [299]. Conversely, IFNβ can signal constitutively despite USP18-mediated desensitization [99] and shares greater sequence homology to IFNε than to IFNα [133]. Here we demonstrated for the first time that unlike IFNα, recombinant IFNε activates the type-I IFN receptor in cells that were primed with IFN over an extended period (Figure 6.13). This data highlights the importance of the evolutionary closeness of IFNε with IFNβ, that both signal constitutively via the IFNAR1/2 receptor. Interestingly, there is growing evidence that IFNβ is responsible for inducing basal levels of ISGs in healthy animal models, similar to the role of IFNε in the FRT of mice [105, 117]. Notably, these and other distinct functional properties of IFNβ have been linked to the higher binding affinity of IFNβ to the type-I IFN receptor, and especially to the IFNAR1 subunit of the receptor complex [71, 369]. This higher affinity binding by IFNβ to the IFNAR1 subunit promotes the formation of ligand-IFNAR1/2 complexes despite expression of USP18, that otherwise destabilises the signalling complex when weaker interactions are in effect [100, 369]. Although IFNε is roughly 1000-fold less potent than IFNβ in both mice and humans [134, 335], IFNε has a similar affinity ratio for binding to the individual IFNAR1 and IFNAR2 subunits as compared to those of IFNβ [134, 179]. Therefore, our preliminary findings lead to the hypothesis that IFNε has evolved unique binding affinities to the IFNAR1/2 receptor subunits thereby allowing its constitutive, low potency signalling in the FRT which leads to a basal antiviral state with limited induction of damaging inflammation. A graphical model of this working hypothesis, that ties together experimental observations from chapters 5 and 6, is presented in Figure 7.1. Future studies to develop this hypothesis could involve performing these experiments in the context of heterologous USP18 expression that is

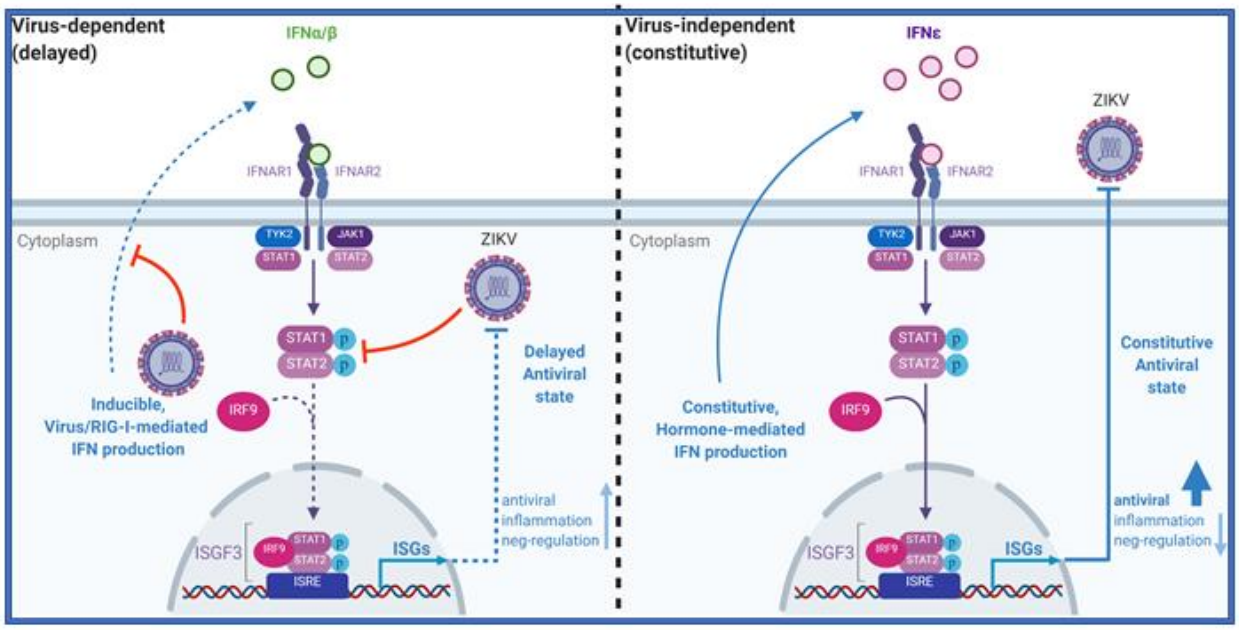

Figure 7.1: Working model of IFNε-mediated protection of the FRT from ZIKV infection, compared to canonical type-I IFN(α/β). The left side depicts the canonical virus-dependent mechanism of type-I IFN-mediated antiviral protection. Expression of IFN is only induced after viral infection, due to RIG-I recognising viral PAMPs within the cell. This delay is exploited by ZIKV, allowing sufficient time to translate viral proteins (such as NS1, NS4A and NS5). These viral proteins then inhibit the RIG-I-mediated IFN production pathway and JAK/STAT signalling downstream of IFNAR1/2 receptor activation. Viral inhibition of the IFN pathway leads to dampened and delayed antiviral responses that are less effective at controlling ZIKV infection. The right side depicts the virus-independent mechanism of IFNε-mediated antiviral protection. Rather than being dependent on viral recognition, IFNε expression is constitutive and is controlled hormonally in the FRT. IFNε produced by cells of the FRT can act on the same cell or neighbouring cells to stimulate JAK/STAT signalling and production of ISGs, leading to the activation of a constitutive antiviral state that protects against ZIKV infection. This antiviral state appears to bias expression of antiviral over pro-inflammatory ISG profiles. Additionally, cellular responses to type-I IFNα loose efficacy over the long-term (days following infection) due to susceptibility to long-term receptor desensitisation, likely mediated by USP18. in contrast, IFNε appears able to signal constitutively, without loosing efficacy due to constant signalling via the IFNAR1/2 receptor, despite the accumulation of long-lasting negative regulators of the IFN pathway.

independent of other upregulated ISGs. Additionally, molecular modelling to compare IFNAR1/2 receptor dimerization upon binding of IFNε, IFNβ or IFNα in the presence or absence of USP18 should be conducted to further explore the mechanism of receptor engagement and stability of receptor complexes for IFNε compared to IFNβ or IFNα [369]. Furthermore, the impact of sustained iVag treatment with IFNε, IFNβ, IFNα and IFNλ should be compared in mice to measure ISG profile, IFN induced desensitization and to compare the level of inflammatory pathway activation in the FRT. Collectively, this could clarify the relative impact of these IFNs on FRT antiviral immunity and tissue inflammation in the context of constitutive pathway activation.

In summary, genome-wide mutational analysis was used as a tool to study the molecular aspects of viral IFN evasion. Despite not finding novel ZIKV- or DENV-mediated innate immune evasion mechanisms by this method, unintentionally a SNP within the DB1 region of the 3' UTR of the DENV genome was found to confer a weak IFN hypersensitive phenotype. The findings of our screen and the recommendations arising from this thesis will contribute towards future studies using deep-mutational screening of viral genomes under various innate immune selection conditions. Additionally, we have shown that constitutively expressed IFNε prophylactically protects the FRT from ZIKV infection. This finding has shifted the paradigm of antiviral protection of the FRT, demonstrating that constitutive protection, rather than reactionary IFN responses, can effectively protect against ZIKV sexual transmission. We have shown that the antiviral protection afforded by IFNε is able to circumvent ZIKV IFN evasion via its unique constitutive expression that is not dependent on viral recognition pathways unlike other type-I and III IFNs. When combined with the ability of IFNε to signal constitutively via the IFNAR1/2 receptor this allows IFNε to support a basal antiviral state in the FRT that protects against ZIKV infection. Collectively, this project has made progress in characterizing the molecular interactions of the host innate immune response with two globally significant flaviviruses in relevant physiological contexts on both sides of the evolutionary arms race.

Appendices

Appendix I: Primer sequences used in this thesis

qRT-PCR primer sequences (F, forward, R, reverse)

Gene/Target	Sequence (5' to 3')
36B4 or RPLP0 (mouse and human)	F – AGA TGC AGC AGA TCC GCA T R – GGA TGG CCT TGC GCA
Human IFNε	F – TCA GCC TCT TCA GGG CAA ATA R – GAG GAA TTT CTC CGT GTG GTT T
Human IFNβ	F – GCA GTC TGC ACC TGA AAA GAT ATT R – TGT ACT CCT TGG CCT TGA GGT A
Human IFNλ1	F – GGA AGA GTC ACT CAA GCT GAA AAA C R – AGA AGC CTC AGG TCC CAA TTC
Human IFNλ2-3	F – CAG CTG CAG GTG AGG GA R – GCG GTG GCC TCC AGA ACC TT
Human ISG15	F – TGG CGG GCA ACG AAT T R – GGG TGA TCT GCG CCT TCA
Human IFIT1	F – AAC TTA ATG CAG GAA GAA CAT GAC AA R – CTG CCA GTC TGC CCA TGT G
Human Viperin	F – GTG AGC AAT GGA AGC CTG ATC R – GCT GTC ACA GGA GAT AGC GA
Human CXCL10 (IP-10)	F – TCC ACG TGT TGA GAT CAT TGC R – TCT TGA TGG CCT TCG ATT CTG
Human CXCL11	F – CCT TGG CTG TGA TAT TGT GTG C R – CCA CTT TCA CTG CTT TTA CCC C
Human IRF1	F – CCA GCC CTG ATA CCT TCT CTG A R – AAG TCC TGC ATG TAG CCT GGA A
Human IFI6	F – CTG AAG ATT GCT TCT CTT CTC R – CAC TTT TTC TTA CCT GCC TC
Human PR isoform A (KiCqStart™ Primers, Sigma Aldrich)	F – GCA TGA TCT TGT CAA ACA AC R – TCT GGA AAT TCA ACA CTC AG
Human PR isoform B (KiCqStart™ Primers, Sigma Aldrich)	F – ATT CAC TTT TTC ACC AGG TC R – AAC CTG GCA ATG ATT TAG AC
Murine IFNε	F – GAA ACG GAT TCC CTT CCA AT R – ACT GCT GGA CTG ACG AGC TT
Murine IFNα	F – CTG CCT GAA GGA CAG GAA GG R – GTC ATT GAG CTG CTG GTG GA
Murine IFNβ	F – AGA AAG GAC GAA CAT TCG GAA A R – CCG TCA TCT CCA TAG GGA TCT T

Murine IFNλ2	F – CCA CAT TGC TCA GTT CAA GTC TCT R – TCC TTC TCA AGC AGC CTC TTC T
Murine ISG15	F – GGG GCC ACA GCA ACA TCT AT R – AGC CAG AAC TGG TCT TCG TG
Murine IFIT1	F – TGG CGT AGA CAA AGC TCT TCA TC R – TAG CAG AGC CCT TTT TGA TAA TGT AA
Murine Viperin	F – TTG GGC AAG CTT GTG AGA TTC R – TGA ACC ATC TCT CCT GGA TAA GG
Murine HPRT	F – AAG CTT GCT GGT GAA AAG GA R – TTG CGC TCA TCT TAG GCT TT
Murine CXCL10	F – ATG ACG GGC CAG TGA GAA TG R – ATG ATC TCA ACA CGT GGG CA
ZIKV PRVABC59 – prM specific	F – GTG TGA TGC CAC CAT GAG CTA R – TGG CAG GTT CCG TAC ACA AAC

Gibson assembly primers for subcloning mutations into the pUC57-BmtI-AvrII-NS5-s.m intermediate cloning vector (F, forward, R, reverse)

Mutation Insert Position	**pUC-57 Plasmid Intermediate Plasmid**	**Synthetic Restriction Sites (used to digest vector)**	**Gibson Assembly Primer Sequence (5'-3') (complementary overhang in lower case)**
8077	pUC57-NS5	PstI/ClaI	F - atgtcaacatatgggtggaatctAGTGCGTCTGCAGAG R- gctcgtaagtggctttcttgtatctcATTGTAAATCGATTGATCAACATCC
8086	pUC57-NS5	PstI/ClaI	F - atgtcaacatatgggtggaatctAGTGCGTCTGCAGAG R- gctcgtaagtggctttcttgtatctcATTGTAAATCGATTGATCAACATCC

Gibson assembly primers for subcloning mutations into the pFK-DVs destination vector (F,forward, R, reverse)

Mutation Insert position OR Wildtype silent mutation (s.m)	**pUC57 Intermediate Plasmid**	**Unique Restriction Sites (used to digest vector)**	**Gibson Assembly Primer Sequence (5'-3') (complementary overhang in lower case)**
UTR-WT-s.m	pUC57-UTR	AvrII/XbaI	F-tgtggcttggagcacgcttcttagagtTTGAAGCCCTAGGATTCTTAAATGAAG R- aagaattgaattaaccctcactaaaggGACTAGTTCTAGAACCTGTTGATTCAAC
9795	pUC57-UTR	AvrII/XbaI	F-tgtggcttggagcacgcttcttagagtTTGAAGCCCTAGGATTCTTAAATGAAG R- aagaattgaattaaccctcactaaaggGACTAGTTCTAGAACCTGTTGATTCAAC
10297	pUC57-UTR	AvrII/XbaI	F-tgtggcttggagcacgcttcttagagtTTGAAGCCCTAGGATTCTTAAATGAAG R- aagaattgaattaaccctcactaaaggGACTAGTTCTAGAACCTGTTGATTCAAC
10388	pUC57-UTR	AvrII/XbaI	F-tgtggcttggagcacgcttcttagagtTTGAAGCCCTAGGATTCTTAAATGAAG

			R- aagaattgaattaaccctcactaaaggGACTAGTTCTAGAACCTGTTGATTCAAC
NS5-WT-s.m	pUC57-NS5	BmtI/AvrII	F- atgaccctgggaatgtgctgcatAATCACGGCTAGCATCCTC R- ctctctggagaaccagtgatcttcattTAAGAATCCTAGGGCTTCAAACTC
8069	pUC57-NS5	BmtI/AvrII	F- atgaccctgggaatgtgctgcatAATCACGGCTAGCATCCTC R- ctctctggagaaccagtgatcttcattTAAGAATCCTAGGGCTTCAAACTC
8077	pUC57-NS5	BmtI/AvrII	F- atgaccctgggaatgtgctgcatAATCACGGCTAGCATCCTC R- ctctctggagaaccagtgatcttcattTAAGAATCCTAGGGCTTCAAACTC
8086	pUC57-NS5	BmtI/AvrII	F- atgaccctgggaatgtgctgcatAATCACGGCTAGCATCCTC R- ctctctggagaaccagtgatcttcattTAAGAATCCTAGGGCTTCAAACTC

Primers used to clone ZIKV NS-FLAG sequences from the pZIKV-ICD clone into the pcDNA6.2 expression vector between the XbaI and PmeI restriction sites by Gibson Assembly (F, forward, R, reverse)

NS protein	Primers (3' - 5')
NS1	F – ACCGATCCAGCCTCCGGACTCTAGAatggatgtggggtgctc R- TCAGTTAGCCTCCCCCGTTTAAACTTACTTGTCGTCATCGTCTTTGTAGTCtgcagtcaccactg
NS2B3	F – ACCGATCCAGCCTCCGGACTCTAGAatgagctggcccccta R - TCAGTTAGCCTCCCCCGTTTAAACTTACTTGTCGTCATCGTCTTTGTAGTCtcttttcccagcgg
NS4A	F – ACCGATCCAGCCTCCGGACTCTAGAatgggagcggcttttgg R - TCAGTTAGCCTCCCCCGTTTAAACTTACTTGTCGTCATCGTCTTTGTAGTCtctttgcttttctggctca
NS5	F – GGGACCGATCCAGCCTCCGGACTCTAGAATGgggggtggaacag R - GTTTCAGTTAGCCTCCCCCGTTTAAACTTACTTGTCGTCATCGTCTTTGTAGTCcagcactccaggtg

Primers used for amplifying full-length DENV2 sequence for NGS application

Primer Name	Primer Sequence (5'-3')
DV2NGS1F	agttgttagtctacgtggaccg
DV2NGS1R	cgaatggaggttctgcttctatgt
DV2NGS2F	gcagaaacacaacatggaacaatag
DV2NGS2R	cctaaggctaacgcatcagtc
DV2NGS3F	tgtcctttagagacctgggaag
DV2NGS4F	cagcaagtatagcagctagagga
DV2NGS4R	tttcccttctggtgtgaccatg
DV2NGS5F	ctcaagtattgatgatgaggactacatg
DV2NGS5R	acttgtgtccaatcattccatcc
DV2NGS6F	ccgcaggatgggatacaaga
DV2NGS6R	agaacctgttgattcaacagcac

Primers used to clone human IFNE-FLAG sequence into the pLenti6-V5-D-TOPO vector between the EcoRI and MluI restriction sites by restriction cloning (F, forward, R, reverse)

cDNA target	Primer Sequence (3'- 5')
Human IFNE1 gene	F – tcgatcGAATTCaccatgattatcaagcac R - TAGTCTacgcgtctaCTTGTCGTCATCGTCTTTGTAGTCcctcgggcttctaaac

Appendix II: General Solutions and Buffers

The following solutions were obtained from the Central Services Unit (CSU) and Tissue Culture Services Unit (TSU), School of Biological Sciences, The University of Adelaide.

- 0.85% saline solution
- 10x Tris-glycine-SDS (TGS) buffer
- 10x Tris-buffered-saline (TBS) buffer
- 20x Tris-acetate-EDTA (TAE) buffer
- 1x Phosphate-buffered-saline (PBS) solution
- 20% Glucose solution
- 80% Glycerol solution
- 4M NaCl solution
- 3M Sodium Acetate (NaAc) pH 5.5 solution
- Ampicillin 1 mg/ml
- Ethylenediaminetetraacetic acid (EDTA) (different concentration and pH)
- Dimethyl sulfoxide (DMSO)
- Kanamycin 1 mg/ml
- L-Agar + ampicillin plates
- Luria agar plates
- Luria Broth
- Sodium dodecyl sulfate (SDS)
- Super Optimal broth with Catabolite repression (SOC) media
- Tris solutions (different concentration and pH)
- Penicillin/streptomycin
- Trypan blue
- Trypsin-EDTA
- Foetal calf serum (FCS)

Prepared Solutions	**Components**
RIPA Cell lysis Buffer (40 ml)	• 150mM NaCl (1.5ml of 4M NaCl) • 0.5% deoxycholate = 0.2g • 0.1% SDS (0.4ml of 10% SDS) • 1% NP-40 (0.4 ml of NP-40) • 50mM Tris (2 ml of 1M Tris) • dH2O 35.7 ml

SDS-PAGE 4 x Reducing Loading Buffer	• 500mM dithiothreitol (DTT) • 0.5% bromophenol blue • 50% glycerol • 10% SDS • 250mM Tris-HCl (pH 6.8) • dH2O
SDS-PAGE Running Buffer	• 2.9% Tris Base • 14.14% glycine • 1% SDS • dH2O
SDS-PAGE Transfer Buffer	• 0.3% Tris Base • 1.44% glycine • 20% (v/v) methanol • dH2O
Western Blot TBS-T washing solution	• 1x TBS buffer in dH2O • 0.1 % Tween® 20 • dH2O
Western Blot membrane stripping buffer	• 2% SDS • 62.5mM Tris-HCl (pH 6.7) • 100mM 2-mercaptoethanol
Acetone:Methanol	• 50% acetone • 50% methanol
1% Agarose	• 1g Agarose • 100ml 1xTAE buffer
1% BSA	• 1 g of Bovine serum albumin (BSA) • 100 ml of 1X PBS
5% BSA	• 5 g of BSA • 100 ml of 1X PBS
2x Cell cryopreservation solution	• 50% complete DMEM • 30% FCS • 20% DMSO

Appendix III: Antibodies

Antibody	Usage	Primary (1^o) or Secondary (2^o)	Dilution	Incubation	Supplier
Mouse anti - *Flavivirus* E (4G2) hybridoma supernatant	Immunofluorescence	1^o	1/5	RT 1h	Made in house from hybridoma HB-112
Mouse anti – FLAG	Immunofluorescence	1^o	1:200	RT 1h	Sigma Aldrich
Rabbit anti – STAT2-Y690P (#D3P2P)	Immunofluorescence	1^o	1:100	4 ^oC overnight	Cell Signaling
Rabbit anti – STAT1-Y701P (#58D6)	Immunofluorescence	1^o	1:100	4 ^oC overnight	Cell Signaling
Goat anti-Mouse IgG, Alexa Fluor 555 linked	Immunofluorescence	2^o	1:200	On ice 1h	Invitrogen
Goat anti-Mouse IgG, Alexa Fluor 488 linked	Immunofluorescence	2^o	1:200	On ice 1h	Invitrogen
Rabbit anti – STAT2-Y690P (#D3P2P)	Western Blot	1^o	1:1000	4 ^oC overnight	Cell Signaling

Chicken anti – NS5	Western Blot	1^{o}	1:1000	4 ^{o}C overnight	Sonja Best, Rocky Mountains, NIH
Mouse anti – FLAG	Western Blot	1^{o}	1:1000	4 ^{o}C overnight	Sigma Aldrich
Mouse anti – βactin	Western Blot	1^{o}	1:10000	4 ^{o}C overnight	Sigma Aldrich
Rabbit anti – STAT1-Y701P (#58D6)	Western Blot	1^{o}	1:1000	4 ^{o}C overnight	Cell Signaling
Rabbit anti – STAT2 (#D9JL)	Western Blot	1^{o}	1:1000	4 ^{o}C overnight	Cell Signaling
Rabbit anti – STAT1 (#D1K9Y)	Western Blot	1^{o}	1:1000	4 ^{o}C overnight	Cell Signaling
Goat anti-mouse IgG (H+L), HRP linked	Western Blot	2^{o}	1:10000	RT 1h	Invitrogen
Goat anti-rabbit IgG, HRP linked (#7074)	Western Blot	2^{o}	1:1000	RT 1h	Cell Signaling

Appendix IV: ZIKV infectious clone plasmid maps

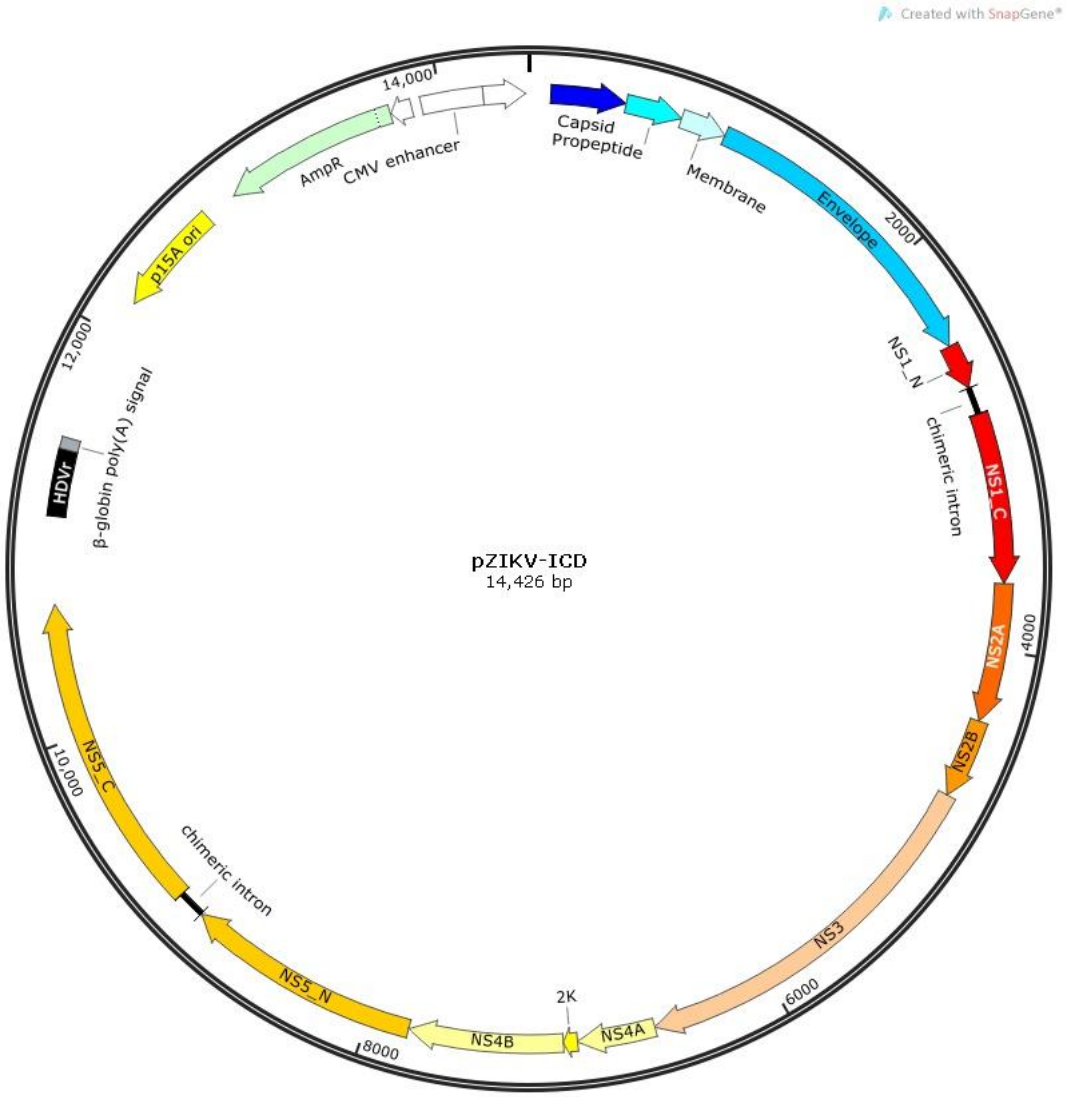

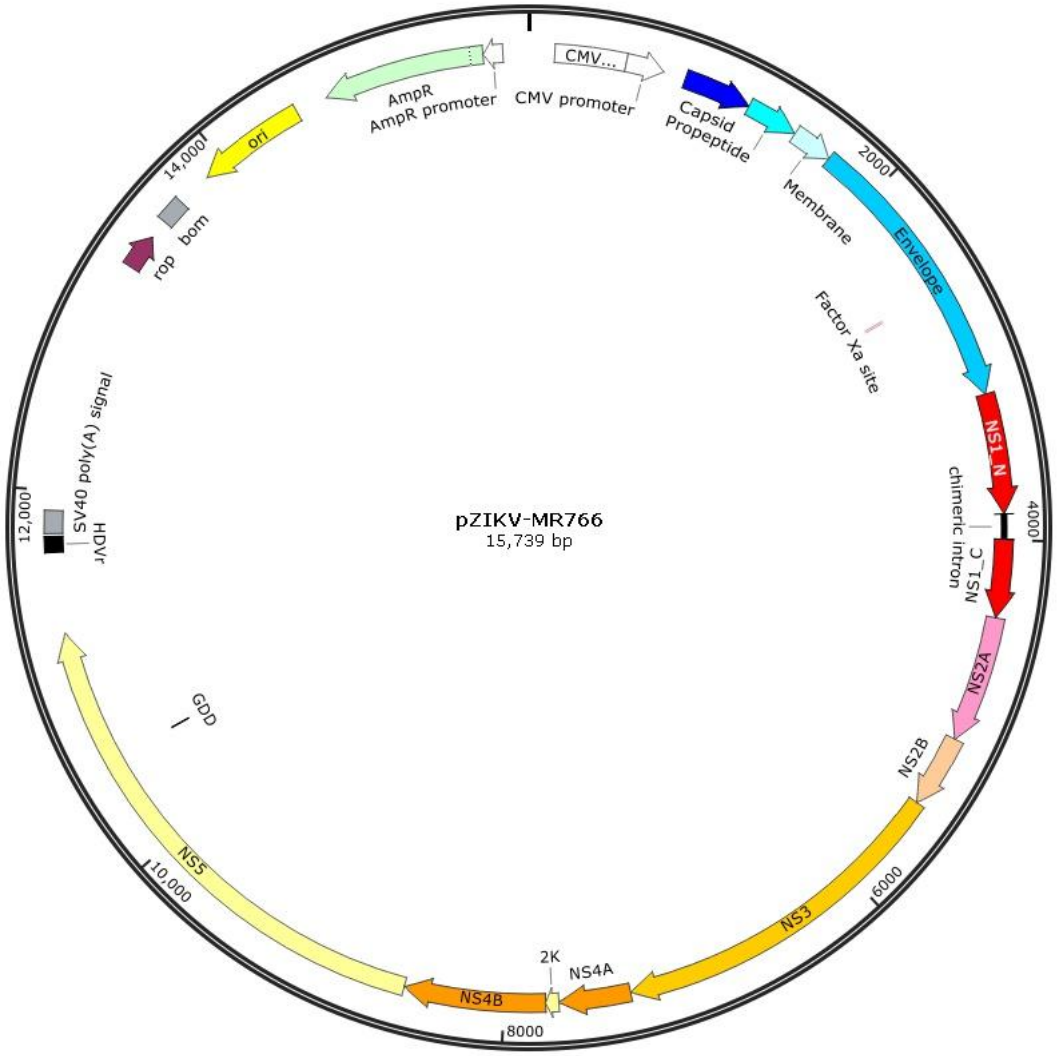
Created with SnapGene®
pZIKV-MR766
15,739 bp
CMV...
AmpR
AmpR promoter
CMV promoter
Capsid
Propeptide
Membrane
Envelope
Factor Xa site
NS1_N
NS1_C
chimeric intron
NS2A
NS2B
NS3
2K
NS4A
NS4B
NS5
GDD
HDVr
SV40 poly(A) signal
rop
bom
ori
2000
4000
6000
8000
10,000
12,000
14,000

Appendix V: DENV infectious clone and intermediate cloning vector plasmid maps, synthetic dsDNA for insertion mutation cloning and specific sequences changes for mutations and 1 % agarose gel images for in vitro RNA

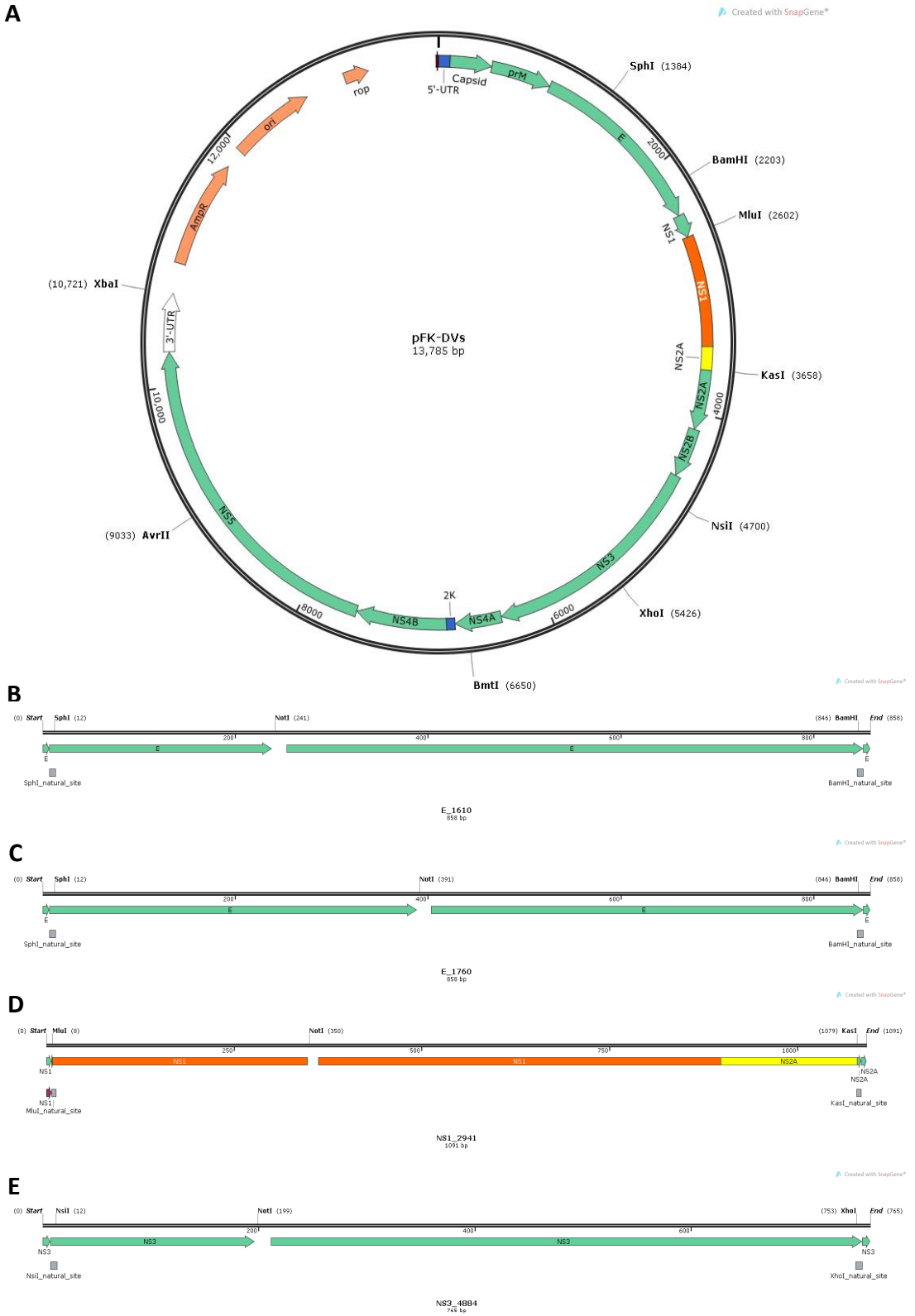

Figure 1: A) Diagrammatic representation of the pFK-DVs infectious clone harbouring the full-length genome of the DENV2 16681 strain. The location of naturally occurring unique restriction sites used for cloning individual insertion mutants are shown for reference. B – E) Diagrammatic representations of the G-Blocks used for cloning individual mutants at nucleotide positions 1610, 1760 flanked by *SphI* and *BamHI*, 2941 flanked by *MluI* and *KasI* and 4884 flanked by *NsiI* and *XhoI* within the DENV genome. Each insert contains a 15 bp insertion mutation denoted by the *NotI* restriction site and the two flanking unique restriction sites for their subcloning into pFK-DVs.

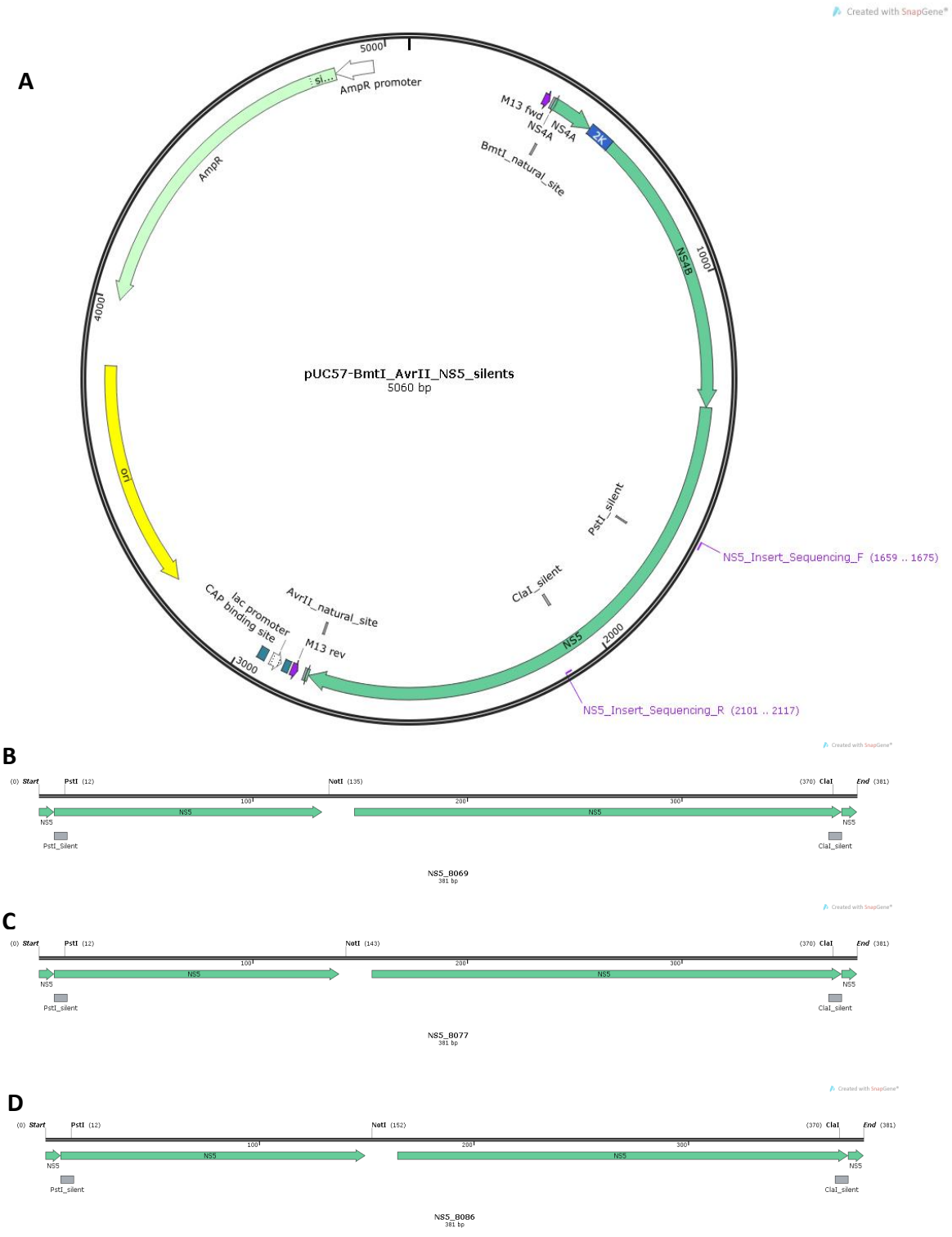

Figure 2: A) Diagrammatic representation of the intermediate cloning vector pUC-57 containing the C-terminus of NS5 of the DENV genome between the *BmtI* and *AvrII* restriction sites that are naturally occurring in the DENV2 16681 sequence. The location of synthetic mutations included to generate unique restriction sites used for cloning individual insertion mutants are shown for reference (*PstI* and *ClaI*). B – D) Diagrammatic representations of the synthetic dsDNA fragments used for cloning individual mutants at nucleotide positions 8069, 8077, and 8086 within the DENV genome. Each insert contains a 15 bp insertion mutation denoted by the *NotI* restriction site and the two flanking unique silent mutation restriction sites (*PstI* and *ClaI*) for

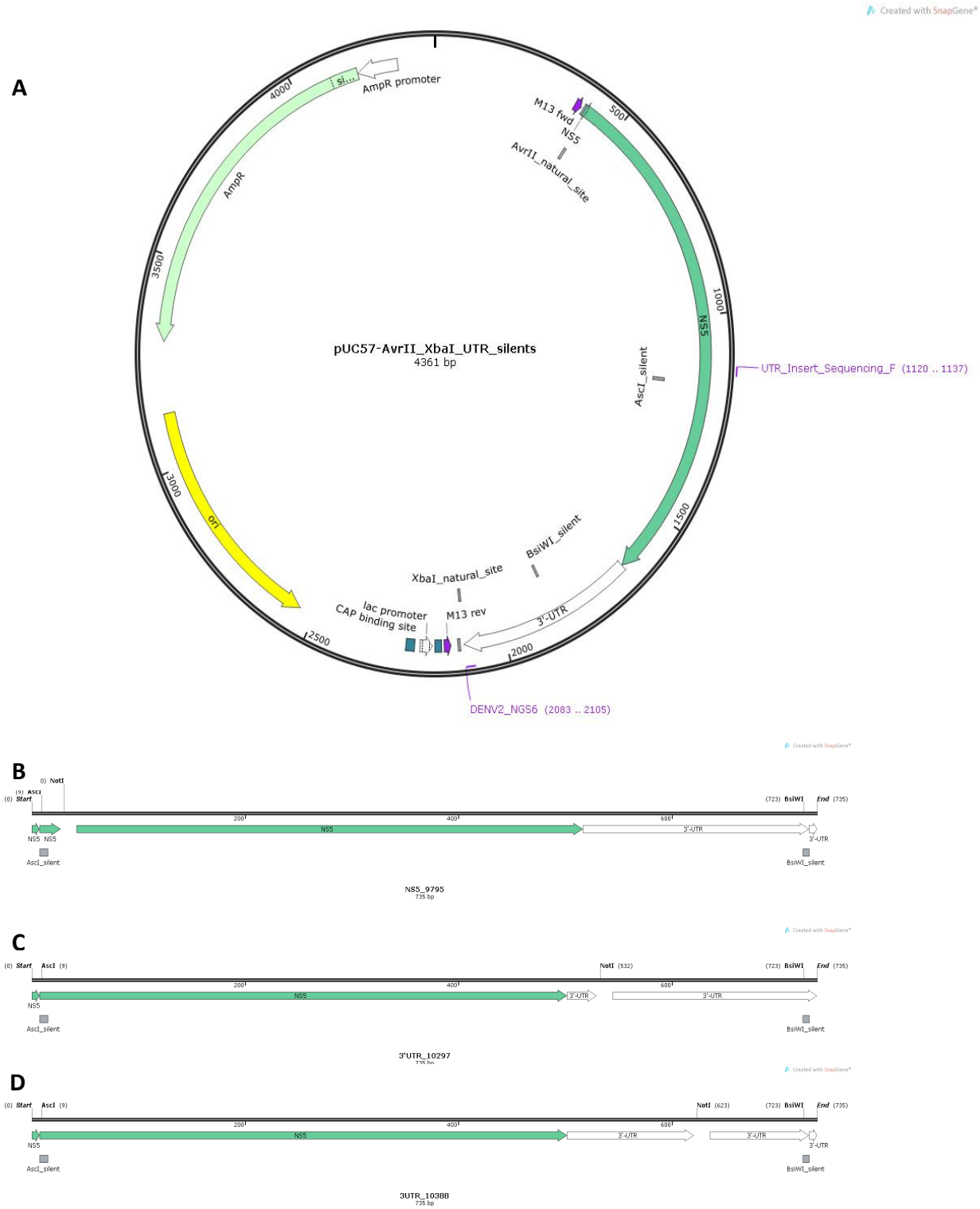

Figure 3: A) Diagrammatic representation of the intermediate cloning vector pUC-57 ordered from GeneWorks containing the N-terminus of NS5 and the complete 3' UTR of the DENV genome between the *AvrII* and *XbaI* restriction sites that are naturally occurring in the DENV2 16681 sequence. The location of synthetic mutations included to generate unique restriction sites used for cloning individual insertion mutants are shown for reference (*AscI* and *BsiWI*). B – D) Diagrammatic representations of the synthetic dsDNA fragments used for cloning individual mutants at nucleotide positions 9795, 10297, and 10388 within the DENV genome. Each insert contains a 15 bp insertion mutation denoted by the *NotI* restriction site and the two flanking unique silent mutation restriction sites (*AscI* and *BsiWI*) for subcloning into the intermediate pUC-57 vector in (A).

Table I: Specific sequence changes to the each of the top hits identified from selection after passage 2

Nucleotide Position (*nt*)	Genomic Region	Log10 [IFNαp2/UTp2]	Amino Acid Sequence Before Insertion	Amino Acid Sequence After Insertion (Hydrophobic, Negative, Positive, Uncharged, Special Cases)	Nucleotide Sequence Containing 15 bp Insertion Mutation (tgcggccgca)
1610	E	-0.56	GADT	GADAAAADT	tgcggccgcagcgga
1760	E	-0.75	SGNL	SGAAASGNL	tgcggccgcatcagg
2941	NS1	1.7	KEKQ	KEMRPQEKQ	tgcggccgcaagaaa
4884	NS3	-0.95	AGTI	AGCGRTGTI	tgcggccgcaccgga
8069	NS5	-0.86	LNLV	LNFAAANLV	tgcggccgcaaactt
8077	NS5	-0.91	VENW	VEMRPQENW	tgcggccgcaagaaa
8086	NS5	-1.18	WLNN	WLMRPQLNN	tgcggccgcagttga
9795	NS5	-0.52	SQGA	SQCGRTQGA	tgcggccgcacccaa
10297	3'UTR	-0.65	N/A	N/A	tgcggccgcacaagg
10388	3'UTR	-0.57	N/A	N/A	tgcggccgcacatca

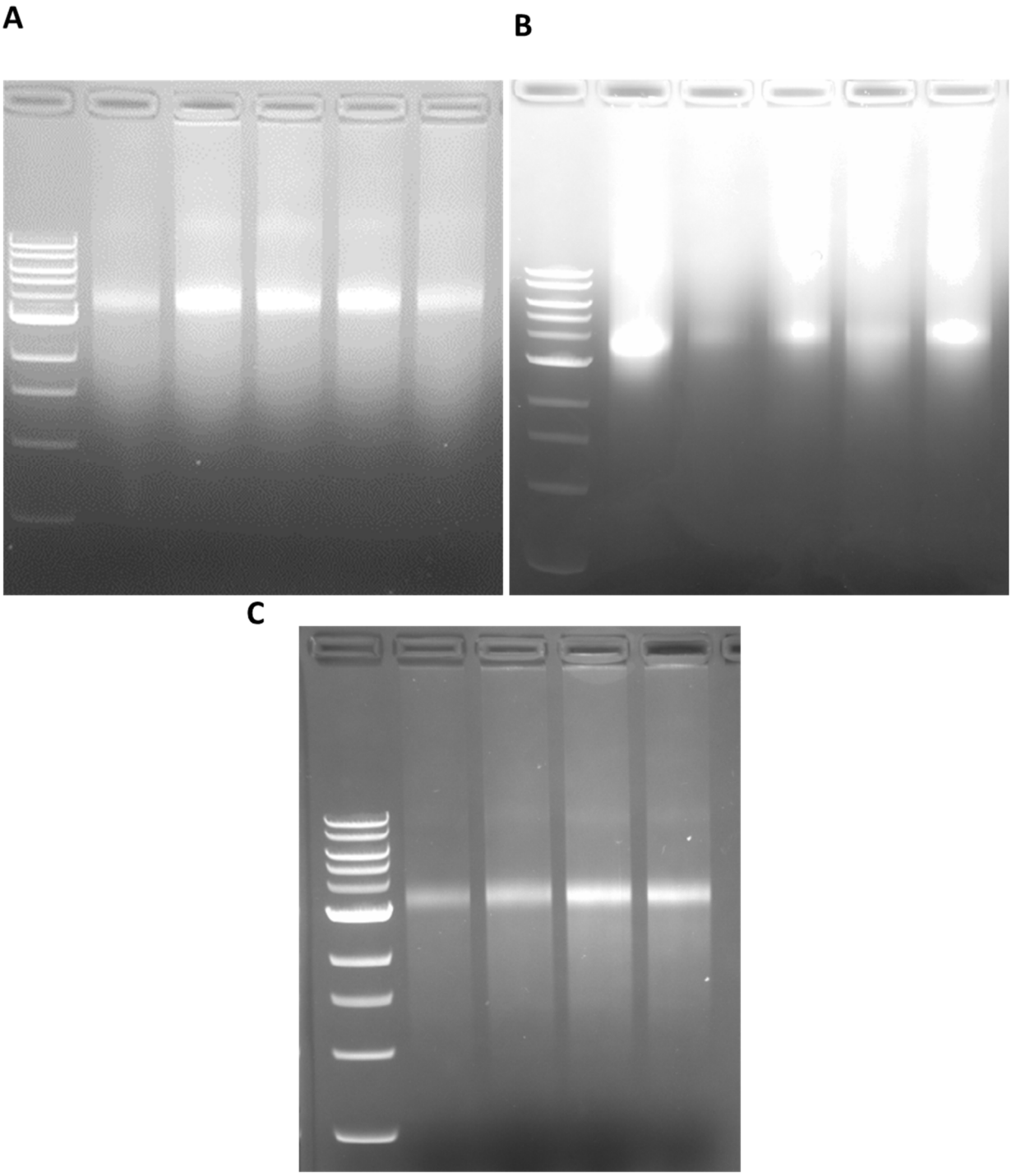

Figure 4) A - C) Non-denaturing 1% Agarose gel electrophoresis of RNA generated from SP6 *in vitro* transcription from linearized template pFK-DVs full-length individual mutant clones as templates.

A) RNA from mutant plasmids generated by cloning directly into pFK-DVs by naturally occurring unique restriction sites. Lane 1: 1 kb ladder, lane 2: parent pFK-DVs, lane 3: pFK-DVs-E-1610, lane 4: pFK-DVs-E-1760, lane 5: pFK-DVs-NS1-2941, lane 6: pFK-DVs-NS3-4884. **B)** RNA from mutant plasmids generated by subcloning into pFK-DVs from the C-terminal NS5 pUC-57 intermediate containing silent mutations (s.m), including a wildtype (WT) with silent mutations as a control. Lane 1: 1 kb ladder, lane 2: parent pFK-DVs, lane 3: pFK-DVs-NS5-WT-s.m, lane 4: pFK-DVs-NS5-8069, lane 5: pFK-DVs-NS5-8077, lane 6: pFK-DVs-NS5-8086. **C)** RNA from mutant plasmids generated by subcloning into pFK-DVs from the N-terminal of NS5 and 3'UTR pUC-57 intermediate containing silent mutations (s.m), including a wildtype (WT) with silent mutations as a control. Lane 1: 1 kb ladder, lane 2: pFK-DVs-UTR-WT-s.m, lane 3: pFK-DVs-UTR-9795, lane 4: pFK-DVs-UTR-10297, lane 5: pFK-DVs-UTR-10388.

Appendix VI: Mammalian expression plasmids for ZIKV non-structural (NS) proteins

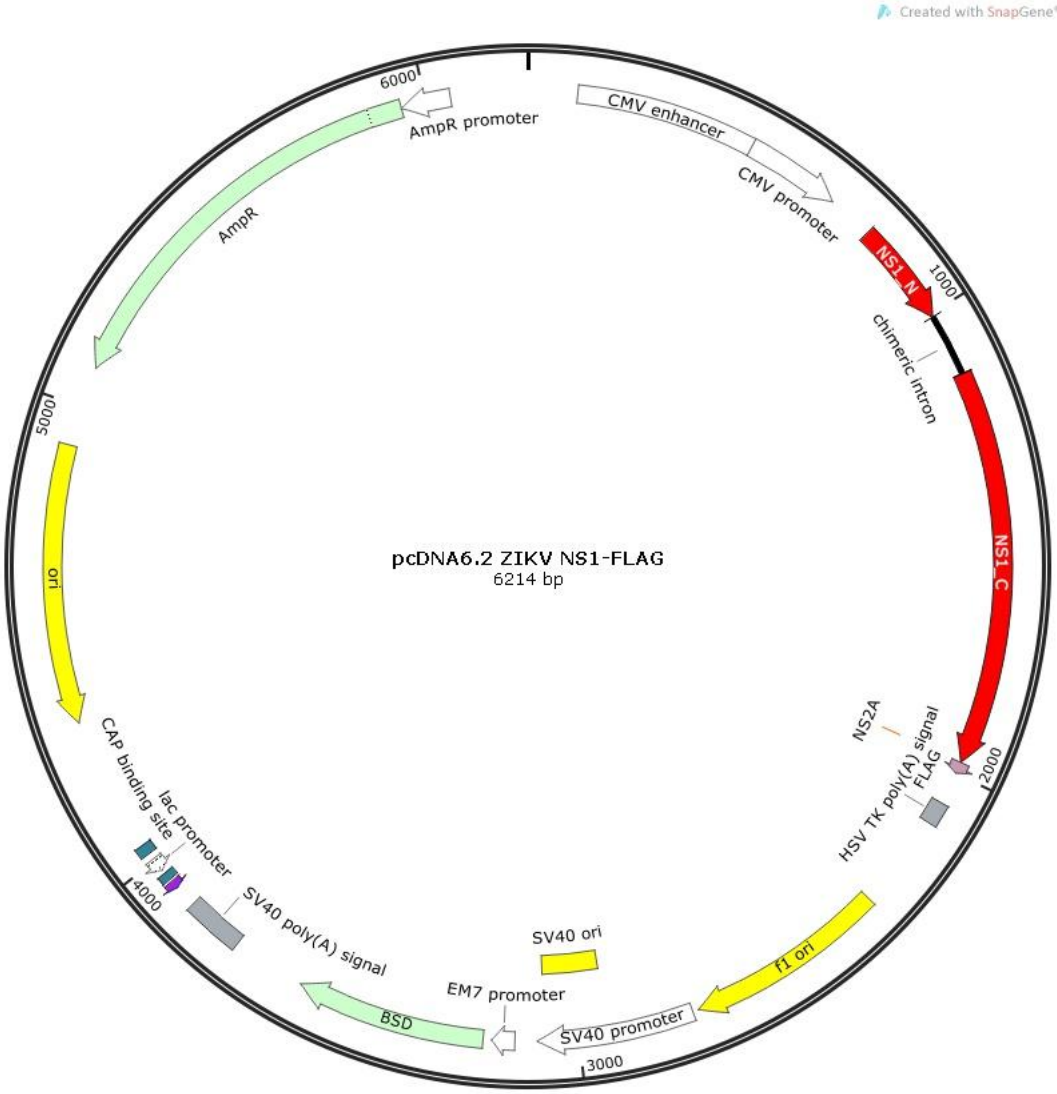

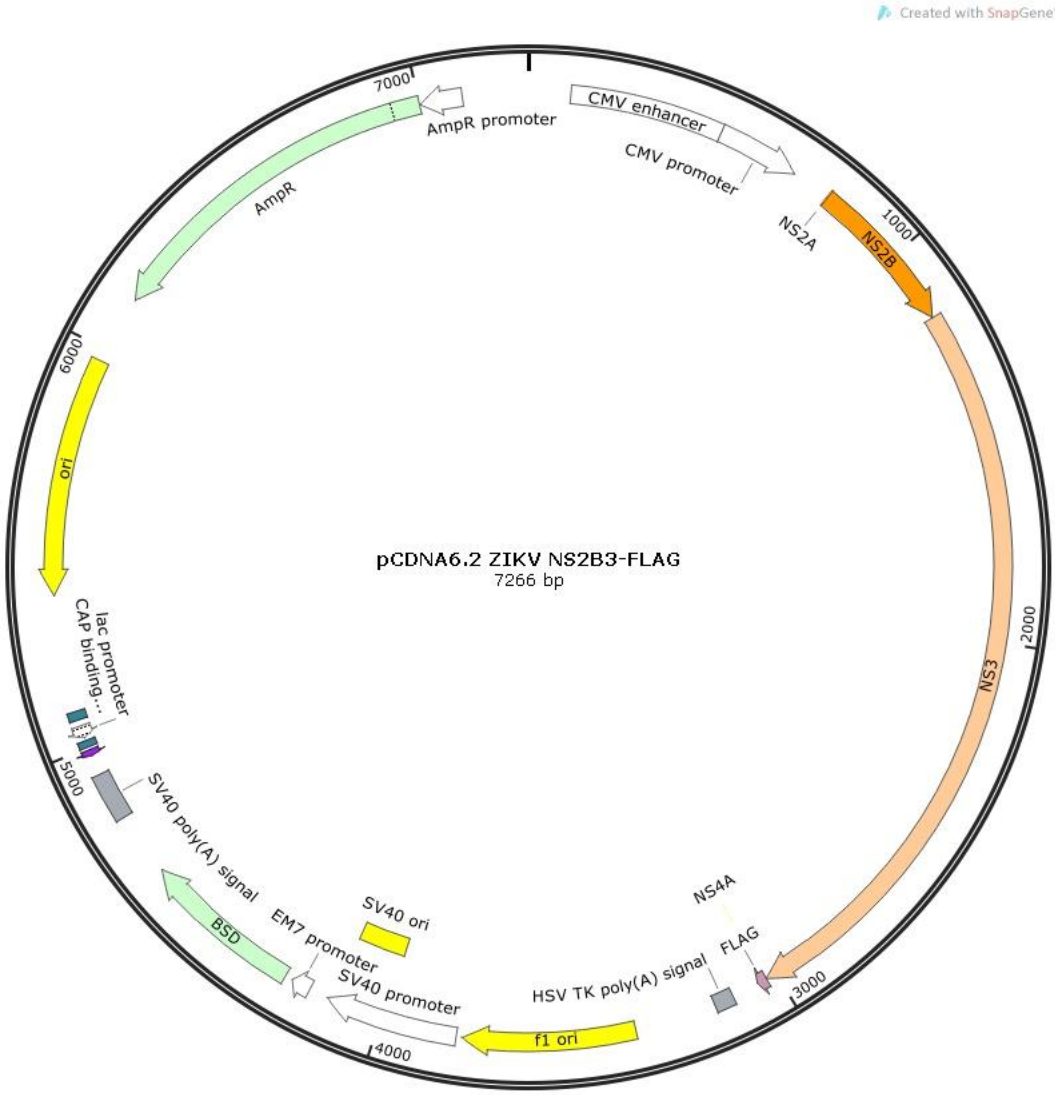
Created with SnapGene®
pCDNA6.2 ZIKV NS2B3-FLAG
7266 bp
7000
AmpR promoter
CMV enhancer
CMV promoter
1000
NS2A
NS2B
NS3
2000
AmpR
6000
ori
lac promoter
CAP binding...
5000
SV40 poly(A) signal
BSD
EM7 promoter
SV40 ori
SV40 promoter
4000
f1 ori
HSV TK poly(A) signal
NS4A
FLAG
3000


Created with SnapGene®
pcDNA6.2 ZIKV NS4A-FLAG
5406 bp
5000
si...
AmpR promoter
AmpR
CMV enhancer
CMV promoter
1000
NS4A
FLAG
HSV TK poly(A) signal
f1 ori
2000
SV40 promoter
SV40 ori
EM7 promoter
BSD
3000
SV4...
M13 rev
lac promoter
CAP binding site
4000
ori

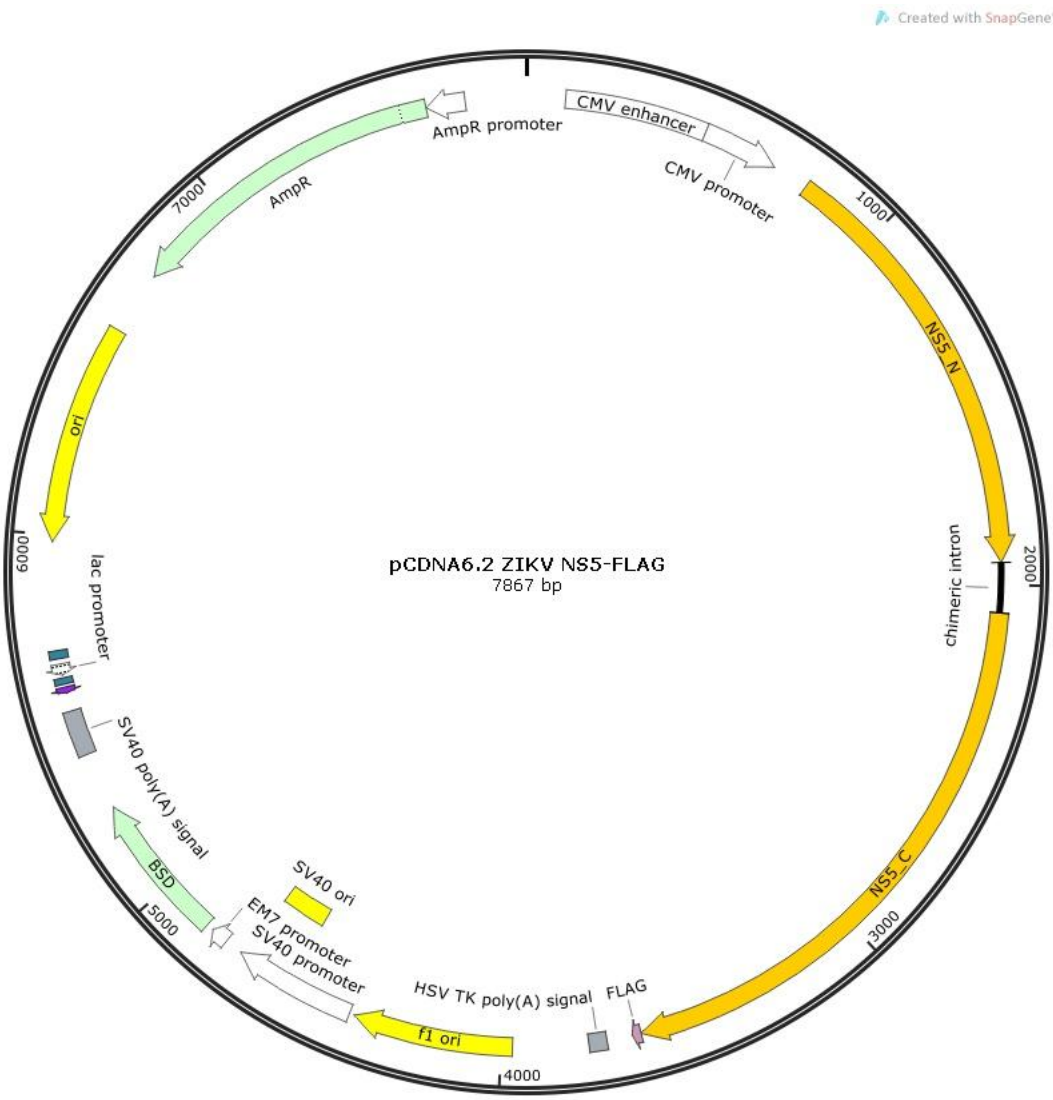
Created with SnapGene®
pCDNA6.2 ZIKV NS5-FLAG
7867 bp
CMV enhancer
CMV promoter
NS5_N
chimeric intron
NS5_C
FLAG
HSV TK poly(A) signal
f1 ori
SV40 promoter
EM7 promoter
SV40 ori
BSD
SV40 poly(A) signal
lac promoter
ori
AmpR
AmpR promoter
1000
2000
3000
4000
5000
6000
7000

Appendix VII: Mammalian expression plasmid for the human IFNε-FLAG protein

Statement of Authorship

Title of Paper	**The molecular interactions of ZIKV and DENV with the type-I IFN response (Review)**
Publication Status	☑ Published ☐ Accepted for Publication ☐ Submitted for Publication ☐ Unpublished and Unsubmitted work written in manuscript style
Publication Details	Published: Vaccines. 2020 Sep 14;8(3):530. doi: 10.3390/vaccines8030530. PMID: 32937990; PMCID: PMC7565347. Abstract: Zika Virus (ZIKV) and Dengue Virus (DENV) are two related flaviviruses that cause significant disease in humans. Existing control measures have been ineffective at curbing the increasing global incidence of infection for both viruses and they are therefore prime targets for new vaccination strategies. Type-I interferon (IFN) responses are important in clearing viral infection and for generating efficient adaptive immune responses towards infection and vaccination. However, ZIKV and DENV have evolved a myriad of molecular mechanisms to evade type-I IFN production. This review covers the molecular interactions, from detection to evasion, of these viruses with the type-I IFN response. Additionally, we discuss how this knowledge can be exploited to improve the design of new vaccine strategies.

Principal Author

Name of Principal Author (Candidate)	Rosa C. Coldbeck-Shackley		
Contribution to the Paper	Intellectual input Research of literature Writing the original draft and editing Generating Figures		
Overall percentage (%)	%80		
Certification:	This paper reports on a literature review I conducted during the period of my Higher Degree by Research candidature and is not subject to any obligations or contractual agreements with a third party that would constrain its inclusion in this thesis. I am the primary author of this paper.		
Signature		Date	05/02/2021

Co-Author Contributions

By signing the Statement of Authorship, each author certifies that:

i. the candidate's stated contribution to the publication is accurate (as detailed above);

ii. permission is granted for the candidate in include the publication in the thesis; and

iii. the sum of all co-author contributions is equal to 100% less the candidate's stated contribution.

Name of Co-Author	Nicholas S. Eyre		
Contribution to the Paper	Intellectual input Drafting text		
Signature		Date	2/02/21

Name of Co-Author	Michael R. Beard		
Contribution to the Paper	Intellectual input Drafting text		
Signature		Date	17/02/21

Appendix VIII: Published first author manuscript

vaccines

MDPI

Review

The Molecular Interactions of ZIKV and DENV with the Type-I IFN Response

Rosa C. Coldbeck-Shackley [1], Nicholas S. Eyre [2] and Michael R. Beard [1,*]

[1] School of Biological Sciences, Research Centre for Infectious Diseases, The University of Adelaide, Adelaide, SA 5005, Australia; rosa.coldbeck-shackley@adelaide.edu.au

[2] College of Medicine and Public Health, Flinders University, Bedford Park, SA 5042, Australia; nicholas.eyre@flinders.edu.au

* Correspondence: michael.beard@adelaide.edu.au; Tel.: +61-88313-5522

Received: 28 August 2020; Accepted: 11 September 2020; Published: 14 September 2020

Abstract: Zika Virus (ZIKV) and Dengue Virus (DENV) are related viruses of the *Flavivirus* genus that cause significant disease in humans. Existing control measures have been ineffective at curbing the increasing global incidence of infection for both viruses and they are therefore prime targets for new vaccination strategies. Type-I interferon (IFN) responses are important in clearing viral infection and for generating efficient adaptive immune responses towards infection and vaccination. However, ZIKV and DENV have evolved multiple molecular mechanisms to evade type-I IFN production. This review covers the molecular interactions, from detection to evasion, of these viruses with the type-I IFN response. Additionally, we discuss how this knowledge can be exploited to improve the design of new vaccine strategies.

Keywords: ZIKV; DENV; innate immunity; interferon; IFN; evasion

1. Introduction

Dengue Virus (DENV) and Zika Virus (ZIKV) are closely related viruses of the *Flavivirus* genus and although most infections in humans are asymptomatic, both viruses can cause severe life threatening or debilitating disease. DENV includes four serotypes (DENV-1-4) and collectively causes the greatest disease burden of all flaviviruses, infecting more than 390 million people causing 21,000 deaths annually [1]. Comparatively, ZIKV is mono-serotypic and causes far fewer deaths, but infection during pregnancy can result in infection of the developing fetus, early pregnancy loss, or developmental and neurological impairment in newborns [2]. The primary mode of ZIKV and DENV transmission is via mosquitoes of the *Aedes* species. As a result of their shared vector, both viruses co-circulate in tropical and sub-tropical regions of Africa, Asia and the Americas [3]. It is estimated that more than one third of the world population lives in areas with high risk of DENV infection [4]. Worryingly, both of these viruses have rapidly expanded their geographic range in recent years as a result of factors such as climate change and globalization [5]. Currently, there are no specific antiviral treatments for either infection despite DENV and ZIKV posing serious threats to human health and placing large socio-economic burdens on many of the world's most under-developed nations. To date there are no approved vaccines for ZIKV, but several vaccine candidates are currently being investigated and as of late 2019, the WHO listed 15 vaccine candidates in phase I/II clinical trials [6]. These include DNA, RNA, recombinant protein, recombinant viral vector, and inactivated whole virus vaccines. As for DENV, there is an approved vaccine (Dengvaxia®) developed by Sanofi Pasteur; however, it is not recommended for children under 9 years of age and has been associated with safety concerns due to its ability to increase the risk of severe disease in people who are seronegative when receiving

vaccination [7]. Despite its limited applicability, Dengvaxia® generates immune responses against all four serotypes and reduces the incidence of severe complications associated with DENV infection [8]. Development of specific, effective, and safe treatments and vaccines for the prevention of both ZIKV and DENV requires understanding of their fundamental biology, pathogenesis, and molecular interactions with the host immune response.

The type-I IFNs are produced in response to sensing viral infection within cells and act as a crucial front-line defense against a broad range of viral pathogens [9]. Once produced and secreted by infected cells these antiviral cytokines can act on the same cell or neighboring cells expressing their cognate receptor to initiate signaling that leads to the production of hundreds of interferon stimulated genes (ISGs) [10]. These ISGs carry out a range of direct antiviral, regulatory or immunomodulatory functions giving rise to an antiviral state within host cells and tissues [11]. Importantly this IFN response shapes aspects of the adaptive immune response to viruses, leading to improved cell mediated and humoral responses [12]. As a result, the IFN response is a barrier that viruses must overcome to cause infection, replicate, and spread. Not surprisingly, because of this strong selective pressure many viruses have evolved mechanisms to counteract IFN responses, allowing them to gain a foothold and cause infection. For example, flaviviruses such as ZIKV and DENV have evolved a complex array of molecular interactions with the host innate immune response to undermine both the production and downstream signaling of IFNs.

This review aims to summarize the current knowledge of the molecular interactions between ZIKV and DENV with the type-I IFN response. Furthermore, we discuss how this knowledge can be exploited in the development of safe and effective vaccines.

2. DENV/ZIKV Virology and Lifecycle

The design of new therapeutics and vaccines is underpinned by understanding the fundamental biology and lifecycle of the virus. In the following section we explain the relevant aspects of *Flavivirus* virology and lifecycle.

2.1. Phylogeny and Genome Structure

The *Flavivirus* are a genus of primarily arthropod borne, enveloped, non-segmented positive-sense single-stranded RNA (+ssRNA) viruses that include several major human pathogens such as Yellow Fever Virus (YFV), Japanese Encephalitis Virus (JEV), West Nile Virus (WNV), DENV and ZIKV. Within the *Flavivirus* genus DENV and ZIKV are closely related, sharing on average 55% amino acid identity [13]. Both the +ssRNA genomes for DENV and ZIKV are approximately 11kb in size, are flanked by 5′ and 3′ untranslated regions (UTRs) and contain a central open reading frame (ORF) encoding the structural (Capsid (C), pre-Membrane (prM) and Envelope (E)) and non-structural (NS1, NS2A, NS2B, NS3, NS4A, NS4B, NS5) viral proteins (Figure 1). The 5′ end of the genome terminates in a type-I cap, mimicking the structure of host mRNA [14]. Both the 5′ and 3′ UTR's are predicted to form extensive RNA secondary structures that are conserved among flaviviruses [15]. These RNA structures are critical for genome replication and also evasion of host immune responses [16]. In general, the structural proteins are involved with infectious particle (virion) production, virus attachment, entry and uncoating. The NS proteins play various roles in the intracellular aspects of the virus lifecycle, including genome replication, translation, processing of the viral polyprotein, membrane rearrangements, virion assembly, and evasion of the innate immune response.

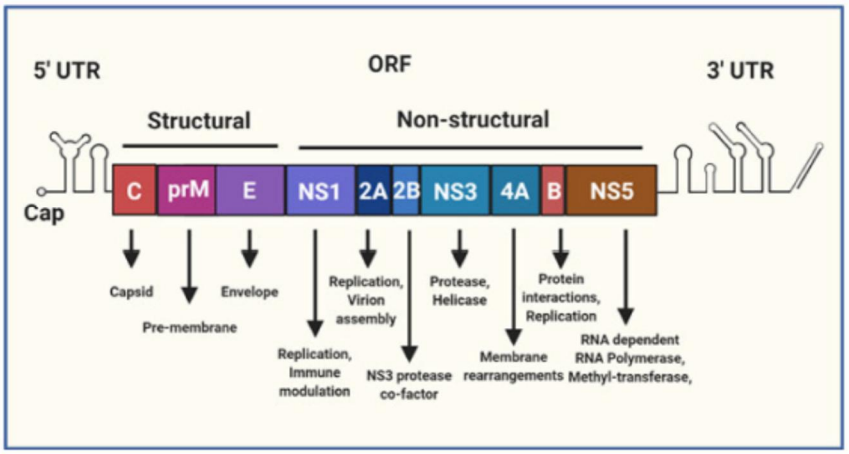

Figure 1. A schematic representation of the Flavivirus genome. The genome is a single positive-sense single-stranded RNA (+ssRNA) molecule that is roughly 11 kb in size, capped at the 5′ terminus and flanked by 5′ and 3′ untranslated regions (UTR). The central open reading frame (ORF) encodes a polyprotein that is cleaved into individual structural and non-structural (NS) viral proteins, the text below lists some of their known functions as reviewed in [17].

2.2. *Lifecycle*

As closely related flaviviruses, ZIKV and DENV share many aspects of their lifecycle within host cells. The *Flavivirus* lifecycle is carried out in several stages: Attachment, entry, fusion and uncoating, initial translation of the viral proteins, generation of the replication complex and replication of new viral genomes, assembly, maturation, and egress [18], summarized in Figure 2.

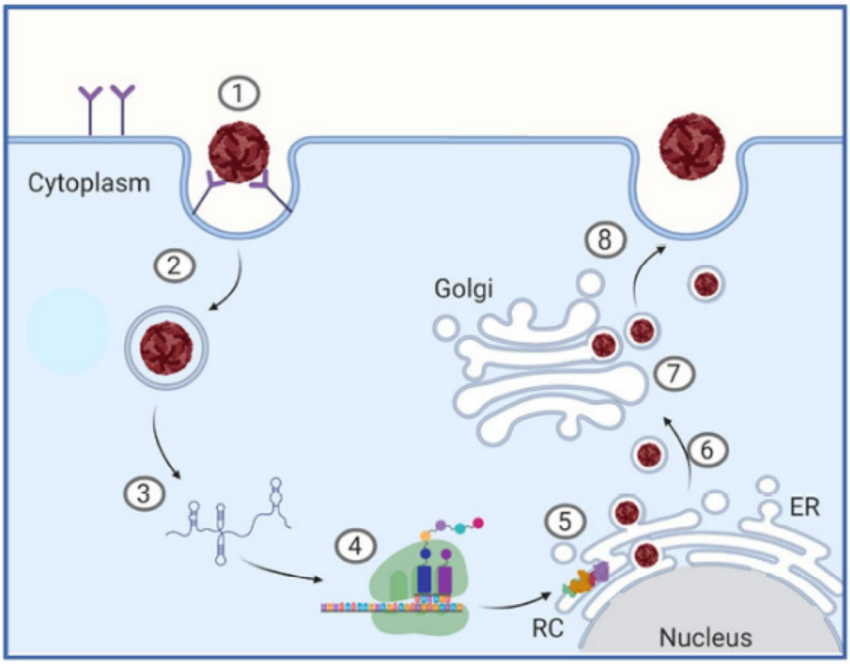

Figure 2. Stages of the *Flavivirus* lifecycle. (1) Attachment and receptor-mediated endocytosis. (2) Membrane fusion and particle disassembly. (3) Genome release into the cytoplasm. (4) Polyprotein translation. (5) Replication complex (RC) formation and genome replication. (6) Virion packaging. (7) Transportation through the trans-Golgi network and virion maturation. (8) Virion egress by exocytosis.

Initially virions attach to host cells via interactions with host cell surface receptors to gain entry to the cell. Virion attachment and entry involves multiple host surface receptors [19,20]. Some of the known attachment factors for DENV and ZIKV include glycosaminoglycans (GAGs), such as heparan sulphate [19], C-type Lectin Receptors (CLRs) such as DC-SIGN [21] and members of the TIM (TIM1, TIM3, and TIM4) and TAM (Tyro3, Axl, and Mer) family of receptors [21,22]. Following attachment, the virion enters the host cell via clathrin-mediated endocytosis [19]. The clathrin-coated vesicle is processed to form an early endosome, these are then increasingly acidified to form late-endosomes [23]. The low pH environment of the late-endosome drives conformational changes in the E protein present on the virion surface leading to membrane fusion, uncoating and release of the +ssRNA genome into the cytoplasm [18]. In the cytosol, viral replication is initiated by direct translation of the +ssRNA by the host ribosome machinery that recognizes the type-I cap in the 5′ UTR [18]. The ORF is translated as a single multi-pass transmembrane polyprotein imbedded into the endoplasmic reticulum (ER) membrane. Following and during translation, the polyprotein is cleaved by host and viral proteases (NS3) to liberate the individual viral proteins [15]. Together, multiple NS proteins interact with host factors to induce changes in the structure of the ER membranes to generate replication organelles or "vesicle packets" that house the viral replication complex (RC) [24]. The RC acts to concentrate viral and host proteins that are essential for viral genome replication and also functions to hide the replicating viral RNA from innate immune detection [24,25]. Following formation of the RC, the +ssRNA genome is copied through a -ssRNA intermediate by the NS5 RNA dependent RNA polymerase (RdRp) in coordination with other essential host and viral factors. The progeny genomes are capped by the NS5 methyl-transferase (MTase) domain and exit the vesicle packets through the vesicle pore where a single +ssRNA copy interacts with multiple copies of the C protein to form the nucleocapsid [24]. Next, this nucleoprotein complex buds into the ER-derived membrane imbedded with viral prM–E protein heterodimers that coat the newly enveloped immature virion [18,26]. After entering the ER lumen, the immature *Flavivirus* particle is shuttled through the secretory pathway. Here the virion undergoes maturation involving the acid-induced rearrangement of E protein and subsequent cleavage of the prM protein by furin into the mature M protein, forming a smooth outer coat [27]. Interestingly, some immature prM also remains on the surface of virions [28] and during DENV infection, heterotypic cross-reactive antibodies raised against prM promote antibody-dependent enhancement of severe dengue disease [29] as reviewed in [30]. After maturation, new virions are released from the host cell by exocytosis [26].

Importantly, the intracellular *Flavivirus* lifecycle is vulnerable to detection and inhibition by the innate immune response. As a result, DENV and ZIKV have evolved subterfuge strategies to avoid detection or prevent the actions of the innate immune response.

3. The Innate Immune Response to RNA Viruses

The innate immune response is the first line of defense against invading viral pathogens. This arm of the immune system generates a rapid, non-specific response aiming to control infection. The innate immune response also plays a crucial role in establishing adaptive immune responses, leading to pathogen specific and long-lasting immunological memory [31]. In general, the innate immune response is initiated by recognition of microbial components or pathogen associated molecular patterns (PAMPs) that accumulate during infection. PAMPs bind to host germline encoded pattern recognition receptors (PRRs) on the cell surface, within endosomes or in the cytoplasm, leading to recognition leads to activation of complex signaling pathways and the upregulation of multiple innate immune effector molecules and cytokines. These act directly or indirectly to control infection and promote inflammation in a temporally controlled manner. The most important class of cytokine involved in the innate response against viral pathogens are the interferons (IFN). These cytokines are responsible for orchestrating an antiviral state within infected cells, in neighboring cells and in directing immune cell activation or trafficking to control viral infection.

3.1. Recognition of DENV and ZIKV by the Innate Immune System

Single-stranded or double-stranded RNAs (ssRNA or dsRNA) produced as by-products of viral genome replication are commonly recognized PAMPs during *Flavivirus* infections. For DENV and ZIKV these RNA PAMPs are mainly recognized by members of the DExD/H box RNA helicase family of RIG-I like receptors (RLRs) located in the cytoplasm [32]. Detection of viral RNAs can also occur in the endosomal compartment by the membrane associated Toll-like receptors-3 or 7 (TLR) [31]. Additionally, both ZIKV and DENV infection results in host mitochondrial DNA (mitoDNA) release that is sensed by cyclic GMP-AMP synthase (cGAS) and signals through the ER associated intermediate stimulator of interferon genes (STING) [31,33,34]. Each of these pathways culminates in the phosphorylation and subsequent activation of the signaling intermediaries TANK-binding kinase 1 (TBK1) and IκB kinase-ε (IKKε). Following their activation, TBK1 and IKKε phosphorylate IFN-regulatory factors-3/7 (IRF) [31]. Additionally, IKKε phosphorylates the inhibitory subunit of nuclear factor-κB (NF-κB), leading to inhibitor degradation and subsequent activation of NF-κB [35]. Activated IRF3 and NF-κB translocate to the nucleus where they act as transcription factors to promote expression mainly of type-I IFNβ and a small subset of antiviral or proinflammatory genes [36]. Figure 3 summarizes these pathways that are discussed in more depth below.

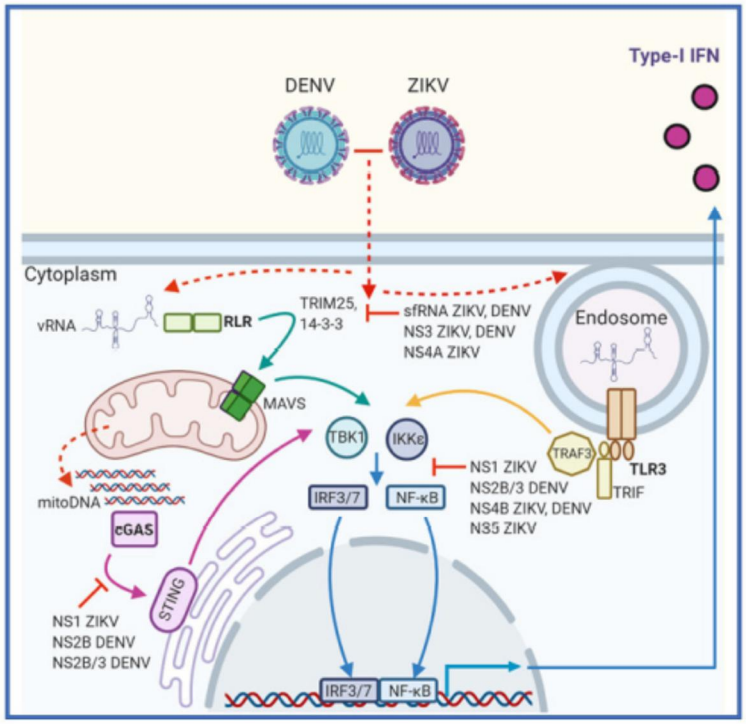

Figure 3. Recognition of Zika Virus (ZIKV) and Dengue Virus (DENV) by the innate immune system and viral evasion of pattern recognition receptor (PRR)-mediated interferons (IFN) production. ZIKV and DENV infections are sensed by multiple PRRs inside the cell. or pathogen associated molecular pattern (PAMP) vRNA from the replication stage of the virus lifecycle activates RLRs in the cytosol (green arrows) or Toll-like receptors (TLRs) in the endosome (gold arrows). Alternatively, both ZIKV and DENV infection results in release to mitoDNA into the cytoplasm that is sensed by cyclic GMP-AMP synthase (cGAS), activating stimulator of interferon genes (STING) (purple arrows). Each of these pathways leads to phosphorylation of kinases TBK1 and IKKε that activate IRF3/7 and NF-κB. These transcription factors then upregulate the production of type-I IFNβ (blue arrows). However, ZIKV and DENV have evolved evasion mechanisms (red) to prevent IFN production that target multiple stages of these pathways.

3.2. RIG-I Like Receptors

The main drivers of the innate immune response against flaviviruses are the ubiquitously expressed RLRs, retinoic acid-induced gene I (RIG-I) and melanoma differentiation-associated gene 5 (MDA5) (Figure 3). RIG-I recognizes short 5′-triphosphorylated ssRNA and short dsRNAs whereas MDA5 is implicated in recognition of longer dsRNA products [9,37,38]. In structure, these PRRs contain two N-terminal caspase recruitment and activation domains (CARDs) followed by an RNA helicase domain [9]. PAMP binding causes a conformational change in the receptor that exposes the CARD interaction domains and facilitates interactions with translocation mediators such as TRIM25 and members of the 14-3-3 family of proteins [35]. The RLR translocase complex is then shuttled to the mitochondrial associated membranes where the exposed CARD domains interact with the complimentary CARD domain of signaling intermediate mitochondrial antiviral signaling protein (MAVS) [35,39]. This interaction triggers MAVS activation leading to subsequent activation of cytosolic kinases TBK1 and IKKε [31]. Interestingly, CRISPR/Cas9-mediated knockout of RIG-I but not MDA5 led to significantly increased ZIKV replication in A549 cells compared to control, indicating that RIG-I is the main sensor of ZIKV infection in these cells [40]. Furthermore, knockout of the RLR signaling intermediate MAVS was shown to enhance ZIKV infection in human placental trophoblast cell lines [41]. Similarly, siRNA mediated knockdown of RIG-I and MDA5 in the Huh7 cell line rendered them highly susceptible to DENV infection [42]. Collectively these studies demonstrate the importance of the RLRs in detection of both ZIKV and DENV infection.

3.3. Toll-Like Receptors

In addition to cytosolic PRR activation, viral RNAs can accumulate in the endosomal compartment where they are recognized by toll-like receptor 3 or 7 (TLR3/7) (Figure 3) [43,44]. TLRs are transmembrane glycoproteins containing an N-terminal ligand binding ectodomain, a single transmembrane domain and a C-terminal toll/interleukin-1 receptor (TIR) homology domain located in the cytoplasm [44]. Ligand binding causes receptor dimerization and the recruitment of signal transducers to the TIR domain [45]. TLR3 is more widely expressed and recognizes dsRNA whereas TLR7 is mainly expressed in plasmacytoid dendritic cells (DCs) and is activated by ssRNA [9,46]. After ligand binding and receptor dimerization the cytoplasmic TIR domain of TLR3 interacts with the TIR domain containing adapter inducing interferon-β protein (TRIF). Next, TRIF interacts with TNF receptor associated factors (TRAF3/6) and with receptor interacting proteins (RIP1/3). Comparatively, TLR7 activates a MYD88 dependent pathway that culminates in TRAF6 signaling and subsequent TBK1 and IKKε activation [9,44]. Evidence that TLR3 plays a significant role in ZIKV recognition is given by siRNA mediated gene silencing in HFF1 (foreskin fibroblast) cells rendering these cells more permissive to ZIKV [21]. Interestingly, mice deficient in TLR7 ($TLR7^{-/-}$) supported equivalent levels of ZIKV replication compared to wildtype mice [47]. However, in this study ZIKV replication was significantly enhanced in $TLR7^{-/-}$/$MAVS^{-/-}$ double-knockout mice compared to wildtype and $MAVS^{-/-}$ single-knockout mice, indicating a degree of functional redundancy between the TLR and RLR pathways. Additionally, HEK 293 cells exogenously expressing either TLR3 or TLR7 demonstrated elevated levels of downstream cytokine release following DENV infection [43].

3.4. cGAS-STING

Other than RNA PAMP activation of the innate immune response, DENV and ZIKV infection also results in the release of mitochondrial DNA (mitoDNA) into the cytoplasm of infected cells (33, 34). The presence of mitochondrial DNA in the cytoplasm is a hallmark of cellular damage where it acts as a potent stimulator of apoptosis and innate immune responses (Figure 3) [48]. Release of mitoDNA during DENV infection results from disruption of normal mitochondrial function. This is likely mediated by the DENV M protein that disrupts mitochondrial membrane potential [49], while the DENV NS2B/3 protease also cleaves important mitofusion proteins (MFN1 and MFN2) that are

important for mitochondrial membrane fusion and homeostasis [50]. ZIKV is also known to impair mitochondrial function [51], but the molecular mechanisms that drive the release of mitoDNA during ZIKV infection are unknown. However, it is possible that these mechanisms are similar to those of DENV. Once in the cytoplasm, mitoDNA can bind directly to the cytosolic DNA sensor cGAS, resulting in a conformational change allowing cGAS to catalyze the conversion of GTP and ATP to produce the second messenger cyclic GMP–AMP (cGAMP). Next, cGAMP binds to STING located in the ER membrane causing oligomerization and translocation to the Golgi, where it activates TBK1 and IKKε [48]. Importantly knockout of cGAS in PMBCs renders these cells more susceptible to ZIKV infection and limits IFNβ production in infected cells [34]. Moreover, various human cell lines lacking STING demonstrate enhanced DENV replication in vitro [52].

Each of the above-mentioned pathways stimulates the transcription and translation of type-I IFN by infected cells. In turn the IFNs are secreted from the cell to orchestrate and amplify a broader antiviral response both within infected cells and in neighboring cells and tissues.

3.5. Type-I Interferons

In humans, the type-I IFNs are encoded by a cluster of related genes located on chromosome 9 [53]. They include 14 subtypes of IFNα and a single gene encoding each of IFNβ, IFNε, IFNκ, and IFNω. IFNα and IFNβ are the main IFNs produced downstream of PRR activation. In general, IFNα expression is dependent on the activation of IRFs (especially IRF7) whereas efficient IFNβ expression requires both IRF3/7 and NF-κB activation. The nuances of IRF-dependent type-I IFN expression regulation have been extensively reviewed elsewhere [54]. Collectively, the type-I IFNs are defined by their ability to signal through the type-I IFN receptor that is composed of two heterodimeric subunits (IFNAR1 and IFNAR2) and is almost ubiquitously expressed throughout the body [55].

3.6. Signalling from the Type-I IFN Receptor

Once produced in response to detection viral infection, secreted type-I IFN binds to the extracellular domains of its cognate receptor (IFNAR1/2) expressed on the same cell or on neighboring cells (Figure 4). Importantly, most cell types respond to type-I IFNs due to the almost ubiquitous expression of IFNAR1/2 [55,56]. Ligand binding causes hetero-dimerization of the receptor subunits bringing the intracellular domains of the receptor into close proximity [57]. Each of the IFNAR1 and IFNAR2 intracellular domains are pre-associated with tyrosine kinases that are activated upon receptor dimerization by close proximity trans-phosphorylation [53]. IFNAR1 is associated with tyrosine kinase 2 (TYK2) and IFNAR2 is associated with janus kinase 1 (JAK1) respectively [58,59]. Once activated JAK1 and TYK2 phosphorylate the intracellular domains of the IFNAR subunits, allowing docking of signal transducer and activators (STAT1 and STAT2). Once docked to the receptor, JAK1 and TYK2 phosphorylate STAT1 and STAT2 at tyrosine residues Y701 or Y690 respectively [31]. Phosphorylation leads to the formation of STAT1/2 heterodimers, nuclear translocation and subsequent complexing with IRF9 [56]. This hetero-trimeric complex called interferon stimulated gene factor 3 (ISGF3) then binds to IFN-stimulated response elements (ISRE) in the proximal promoter regions of over 100 ISGs, up-regulating their transcription and translation [11]. ISGs encode various proteins that carry out a range of effector or regulatory functions [31]. Effector functions are varied and include inhibition of viral entry, inhibition of protein synthesis, alterations to cellular metabolism, degradation of viral proteins or genetic material and inhibition of viral egress [11]. Regulatory ISGs include PRRs and signaling partners of these pathways as well as immunomodulatory molecules and negative regulators responsible for controlling immune cell activation and trafficking or returning the cell to homeostasis, respectively [60].

3.7. Inhibition of ZIKV and DENV Infection by Interferon Stimulated Genes

Type-I IFNs are important in controlling *Flavivirus* infection through the production of ISGs. These ISGs play a wide variety of roles in the innate antiviral response and have been extensively reviewed

elsewhere [11]. Importantly, some ISGs can act directly to inhibit various stages of the ZIKV and DENV virus lifecycle. Due to the shared aspects of their lifecycles some of these ISGs are similarly effective against both viruses. Several of these direct acting ISGs are known and their mechanisms of action are described below.

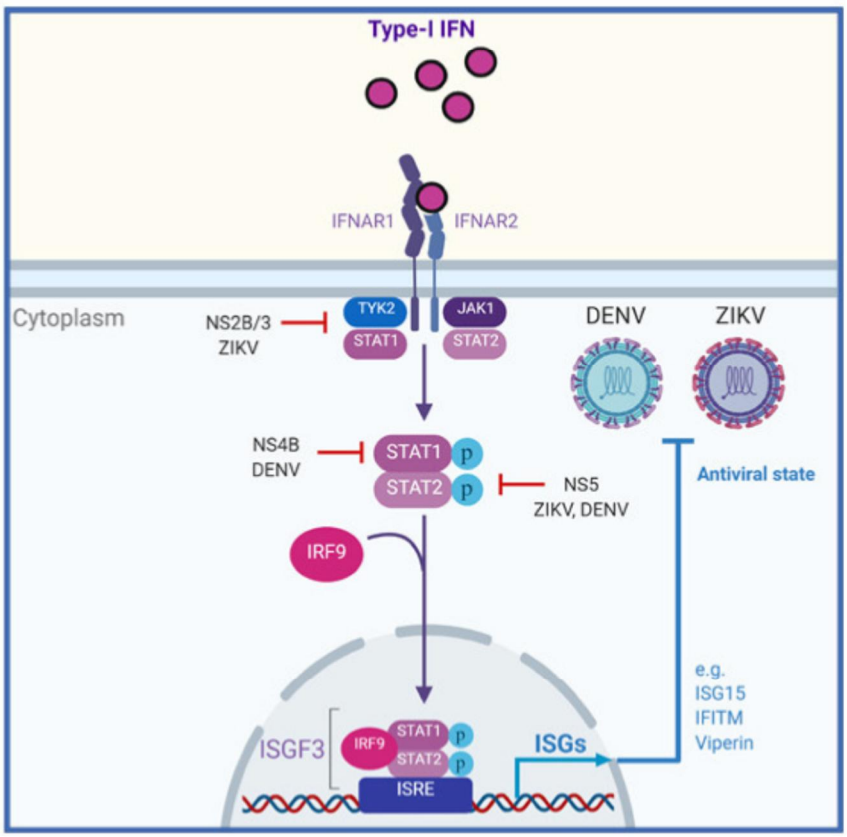

Figure 4. The molecular interactions of ZIKV and DENV with the type-I IFN pathway. Once produced and secreted from infected cells type-I IFNs bind to their cognate cell surface receptor, activating janus kinase-signal transducer and activator (JAK-STAT) signaling (black arrows). This leads to the phosphorylation of STAT1 and STAT2, their heterodimerzation and subsequent complexing with IRF9 to form the complex ISGF3. ISGF3 then transcriptionally upregulates interferon stimulated genes (ISGs) that have antiviral effects against ZIKV and DENV. Several stages of the IFN pathway are inhibited by ZIKV and DENV mediated evasion mechanisms (red).

Two complimentary studies have demonstrated that Interferon Stimulated Gene 15 (ISG15) protects against ZIKV infection [61,62]. Mature ISG15 is a 15 kDa member of the ubiquitin family of proteins that plays various roles in the innate immune response that have been extensively reviewed [63]. One of the main functions of ISG15 is the covalent modification of target proteins via ISG15 conjugation (ISGylation) disrupting target protein localization and protein-protein interactions. Additionally, ISG15 has immune modulatory functions through non-covalent protein interactions and by acting as an immune cell signaling molecule. One study found that ZIKV infected ISG15$^{-/-}$ mice had increased severity of retinal lesions and impaired antiviral responses compared to wildtype mice and this led to lower expression of other ISGs like RIG-I and IFI6 [62]. A follow-up study by the same group extended these observations to show that ZIKV infection in human primary corneal epithelial cells (HCEC) induced expression of ISG15 RNA and protein, and that siRNA mediated knockdown of this expression lead to increased ZIKV infection in these cells [62]. Conversely, heterologous expression of ISG15 protein was able to ameliorate this effect. Furthermore, this group found that ISG15 expression was important for both reducing ZIKV entry into host cells, and for inhibiting viral replication once

inside the cell. Similarly, ISG15 inhibits DENV infection. DENV infection has been shown to upregulate expression of ISG15 in RAW264.7 cells, and its silencing increased DENV replication in these cells [64]. Furthermore, infection with DENV increased the total amount of ISGylated proteins in the cell, suggesting a link between the ISG conjugation activity of ISG15 with the observed antiviral effect [64].

Members of the Interferon-Inducible Transmembrane (IFITM) protein family also protect against both ZIKV and DENV infection. As their name suggests these proteins are found inserted into cellular membranes, most commonly localizing in late endosomes, and can interfere with fusion of viral and host membranes following viral entry [65]. Importantly, siRNA mediated knockdown of IFITM1 or 3 was shown to increase ZIKV infection in human cell lines [66]. This effect could be rescued with overexpressed protein but relied on the protein's endosomal localization. Consistent with their localization to endosomal membranes, knockdown of IFITM1 or 3 was shown to impact very early steps in the viral replication cycle following entry [66]. Likewise ectopically expressed IFITM2 or IFITM3 have been shown to reduce DENV infection in human cell lines to similar levels to those observed when treating cells with 100 U/mL IFNα [67]. Like ZIKV, this inhibitory effect was observed to impact the DENV lifecycle at a step prior to the initial round of viral RNA translation.

Another ISG shown to directly inhibit ZIKV and DENV infection is interferon alpha-inducible protein 6 (IFI6). IFI6 is a 13 kDa protein that is known to be involved in cell survival and counteracting viral-mediated apoptosis [68]. Increased expression of IFI6 was shown to reduce ZIKV replication and prevented ZIKV mediated cell death in the Huh7 (liver origin) cell line [69]. In this study, IFI6 localized to the ER near ZIKV RCs suggesting that it may play a role in inhibiting viral replication or virion production. Furthermore, this antiviral effect of IFI6 was independent of ZIKV protein stability or polyprotein processing. Likewise Huh7.5 cells stably transduced with a lentivirus IFI6 expression vector demonstrated decreased DENV replication compared to an empty vector control [70]. This study also demonstrated that CRISPR-mediated knockout of endogenous IFI6 expression increased DENV replication in infected cells.

Furthermore, the virus inhibitory endoplasmic reticulum associated interferon inducible protein (Viperin) has been shown in multiple studies to reduce ZIKV and DENV replication [71–73]. Viperin is a 42 kDa protein and as the name suggests is normally associated with ER membranes. Importantly, Viperin has antiviral effects against a wide range of viruses in both RNA and DNA families [74–76]. The first study to investigate the importance of Viperin in ZIKV infection found that Viperin was induced in response to ZIKV infection and overexpressed Viperin restricted ZIKV replication in human cell lines [71]. Additionally, murine embryonic fibroblasts (MEFs) derived from Viperin knockout mice were more permissive to ZIKV replication compared to wildtype MEFs. Furthermore, the anti-ZIKV action of Viperin relied on the highly conserved C-terminal end of the protein [74]. A second study confirmed Viperin's antiviral effect, finding that Viperin interacted directly with the ZIKV NS3 protein resulting in its degradation and reduced viral replication [72]. Similarly, DENV inhibition by Viperin is also dependent on the C-terminal region of the protein and its interaction with the DENV NS3 protein [73].

Aside from these ISGs that are known to inhibit both ZIKV and DENV infection, other direct acting ISGs have been independently validated for either virus. Future studies may prove these ISGs are effective against both viruses, or they may reveal virus-specific activity. One of these ISGs is interferon-inducible factor 16 (IFI16). This ISG has multiple roles in modulating expression of viral proteins and activating the STING pathway during infection [77]. Overexpressed IFI16 was shown to reduce infection of both the +ssRNA alphavirus chickungunya virus (CHIKV) and ZIKV in human skin fibroblasts [78]. No specific mechanism for this effect was investigated. To our knowledge, IFI16 has not been independently validated for antiviral activity against DENV infection. However, the role of IFI16 in promoting STING activation suggests that this is a strong possibility.

Other ISGs known to inhibit DENV infection are the ArfGAP with dual pleckstrin homology (PH) domains 2 (ADAP2) protein and the tripartite motif 69 protein (TRIM69). ADAP2 is most highly expressed in the heart, and skeletal muscle and is known to regulate the ADP ribosylation factor (Arf)

family of proteins via its GTPase activating protein (GAP) function [79]. Arf proteins are involved in regulating vesicular trafficking and cytoskeletal organization. Importantly, ectopically expressed ADAP2 has been demonstrated to restrict DENV infection by inhibiting GAP mediated trafficking of incoming DENV containing vesicles [80]. TRIM69 mediates protein ubiquitination through its E2 conjugation enzymatic activity. It localizes to the cytoplasm and inside the nucleus of cells [81]. TRIM69 has been shown to directly interact with DENV NS3, resulting in its polyubiquitination and subsequent degradation to inhibit DENV replication [82]. To our knowledge, the roles of both ADAP2 and TRIM69 in protection against ZIKV infection have not been investigated.

In the context of natural infection, multiple ISGs are expressed in concert and as a result target many of the stages of DENV and ZIKV replication simultaneously. The combined effects of ISGs to inhibit ZIKV and DENV infection has applied strong selective pressure on these viruses to evolve mechanisms to evade detection by the cell or prevent the production of ISGs through blocking the IFN signaling pathway.

4. Common Strategies Employed by Flaviviruses to Evade the IFN Response

As obligate intracellular pathogens, flaviviruses have evolved many ways to avoid detection by host intracellular PRRs. For example, the 7-methylguanylate cap that is incorporated on the 5′ end of the +ssRNA genome by the NS5 MTase domain mimics the appearance of host mRNA (18). 5′ capping assists host translational initiation factors to bind the viral RNA and prevents RNA degradation by endonucleases in the cytoplasm [83]. Importantly, 5′ capping also interferes with the recognition of vRNA as 'non-self' by the MDA5 PRR, limiting the production of IFN by infected cells [84]. In addition to hiding from detection, capping also avoids the antiviral effects of the interferon induced protein with tetratricopeptide repeats (IFIT) protein family that can bind to and sequester vRNA of uncapped or cap mutant *Flavivirus* genomes [85].

The second mechanism commonly used by flaviviruses to avoid detection is the induction of membrane rearrangements allowing for the formation of the RC as part of the virus lifecycle [86]. As mentioned previously, for flaviviruses these structures are formed from modified ER membranes by the coordinated action of multiple host and viral proteins. Replication organelles form as a series of membranes that surround the dsRNA replication intermediate, acting to physically segregate this potent viral PAMP from detection by cytoplasmic PRRs like RIG-I [87,88]. In addition, these replication organelles limit the antiviral activity of the ISG encoded MXA protein, likely by blocking MXA-mediated recognition of the forming viral nucleocapsid [89]. Evidence in support of this theory is provided in one study comparing DENV to JEV replication where they observed a greater degree of dsRNA in the cytosol during JEV infection compared to DENV and this correlated to increased IFN production in JEV infected cells [90]. Ultrastructural analysis of the ZIKV RC shows it to be highly similar to that of DENV, suggesting their related function [91].

Aside from genome capping and the formation of replication organelles, several flaviviruses evade IFN production by expression of subgenomic *Flavivirus* RNA (sfRNA) [92]. *Flavivirus* sfRNAs are formed from the incomplete degradation of the viral genome by cellular 5′ to 3′ exonucleases [93]. Specifically, conserved stem-loop or dumbbell RNA structures within the 3′UTR stall exonuclease activity and result in the production of short RNA sequences [94]. Importantly sfRNAs generated during ZIKV infection antagonize the activity of both RIG-I and MDA5 [95], although a full mechanism of action has not been elucidated for this interaction. Likewise, DENV sfRNA inhibits RIG-I mediated IFN production. This effect is governed by a sequence-specific interaction between DENV sfRNA and the tripartite motif containing 25 protein (TRIM25) [96]. TRIM25 functions as an RNA binding protein and a ubiquitin ligase, responsible for the polyubiquitination of activated RIG-I leading to sustained signal transduction [35].

4.1. ZIKV-Specific Mechanisms to Evade IFN Responses

In addition to strategies common to all flaviviruses, some evasion mechanisms have been characterized for ZIKV that may be unique for this virus. These mechanisms prevent ISG production by interfering with PRR-mediated IFN production, or by directly targeting signaling intermediaries downstream of the IFNAR1/2 receptor.

One mechanism that limits the production of IFN is mediated by ZIKV NS4A that inhibits RIG-I and MDA5 signaling and has been demonstrated independently by two groups [41,97]. Collectively these studies found that ectopically expressed NS4A binds directly to the N-terminal CARD domain MAVS. This binding competitively inhibited MAVS interaction with activated RIG-I or MDA5, leading to potent inhibition of downstream type-I IFN production.

ZIKV can also prevent the translocation of activated RIG-I and MDA5 to the mitochondrial membranes by acting on members of the 14-3-3 protein family. These proteins (14-3-3ε and 14-3-3η) act as mitochondrial targeting chaperones that are required for translocation of RIG-I and MDA5 respectively, facilitating their interaction with MAVS [98,99]. Importantly, overexpressed ZIKV NS3 protein in HEK 293T cells was able to competitively bind to both 14-3-3ε and 14-3-3η via a conserved binding motif (64-RLDP-67) [100]. This sequence was found to contain a central negatively charged Aspartic acid residue (D66) that acted as a phospho-mimetic to compete with RIG-I or MDA5 binding. Mutation of this binging motif within the full length ZIKV genome attenuated viral replication compared to wildtype virus in A549 cells [100].

ZIKV can also inhibit the cGAS-STING pathway via the actions of NS1. One study found that ectopically expressed ZIKV NS1 interacts directly with host de-ubiquitinase USP8 to facilitate the deubiquitination of caspase-1, increasing its stability [34]. In turn caspase-1 proteolytically cleaves cGAS, reducing the production of IFN in the cell. Additionally, the ZIKV protease NS2B/3 mediates STING cleavage. Using exogenous expression in HEK 293T cells it was shown that ZIKV NS2B/3 cleaved human but not mouse STING [101]. This study extended these observations to natural ZIKV infection in human fibroblasts by detection of STING cleavage products during infection. The reduction of cGAMP mediated STING activation as a result of ZIKV infection inhibited the production of IFN by infected cells.

Other NS proteins also contribute to limit IFN production downstream of MAVS, TLR and cGAS-STING pathways by targeting the shared signaling intermediaries TBK1, IKKε, or IRF3. Ectopically expressed NS1 and NS4B interact directly with TBK1, preventing TBK1 oligomerization and phosphorylation mediated activation [102]. Interestingly, another study found that NS1 mediated TBK1 inhibition was specific to recent outbreak strains that had evolutionarily acquired a 188-Val substitution mutation [103]. Additionally, overexpressed ZIKV NS5 in HEK 293 cells was demonstrated to directly interact with IKKε [104]. This direct interaction resulted in reduced IKKε protein levels and phosphorylation, thereby preventing the activation of IRF3. In another study, NS5 was also shown to inhibit IRF3 activation by direct binding to endogenous IRF3 in studies involving co-immunoprecipitation of overexpressed NS5 protein [103].

Downstream of the IFN receptor, ZIKV also acts to suppress JAK-STAT signal transduction. The best characterized of these mechanisms is the ZIKV NS5 mediated degradation of STAT2 protein. ZIKV NS5 can bind to STAT2 and initiate its degradation in a proteasome dependent manner [105]. Interestingly, this occurs with human but not mouse STAT2 protein, partially explaining the difference in species adaptation of ZIKV and difficulties associated with infecting IFN competent mice [106]. A separate study found that overexpression of NS5 leading to STAT2 degradation also resulted in reduced STAT1 phosphorylation in cells overexpressing NS5 [107]. One study also demonstrated that ZIKV NS2B/3 expression induced the degradation of JAK1 protein in a proteasome-dependent manner leading to a reduction in IFN mediated ISG expression [102]. In addition to the roles of NS proteins in inhibition of IFNAR signaling, ZIKV binding to the attachment factor Axl on the cell surface also inhibits IFN signaling. In a study using microglial cell lines, ZIKV binding was shown to activate the

C-terminal kinase domain of Axl that in turn acted to negatively regulate the type-I signaling pathway via induction of SOCS1 protein expression [108].

4.2. DENV-Specific Mechanisms to Evade the IFN Response

Some of the mechanisms that govern DENV-mediated IFN evasion closely reflect those of ZIKV, demonstrating their close evolutionary relationship. These tend to be evasion strategies mediated by the more conserved viral proteins, such as the NS3 helicase/protease and NS5 RdRp/MTase. However, there are also mechanisms that differ entirely in their action and are unique to DENV.

One mechanism preventing the production of IFN by DENV is mediated by NS2B. Overexpressed DENV NS2B directly interacts with cGAS and causes its degradation by auto-phagolysosomes, reducing STING-mediated IFN production [33].

Additionally, DENV NS2B/3 proteolytically cleaves human but not mouse STING in a similar manner to ZIKV [52]. This species-specific cleavage was dependent on the presence of an NS3 cleavage site in human STING. Mutation of this cleavage site was able to restore DENV-mediated induction of IFNβ. DENV NS3 also contributes to evasion of IFN by non-proteolytic actions. HEK 293T cells expressing DENV NS3 demonstrated impaired RIG-I translocation to MAVS in response to Sendai Virus infection. Like ZIKV, this interaction was also dependent on inhibition of RIG-I binding to 14-3-3ε via a conserved phospho-mimetic binding motif at the same location within NS3 (64-RxEP-67) [109]. However, the charged residue mimicking the natural phosphorylation site was found to be a Glutamic acid (Glu66) rather than Aspartic acid residue as was found for the ZIKV NS3 protein. Furthermore, DENV NS2A and NS4B from multiple DENV serotypes inhibit PRR mediated IFN production via targeting TBK1 and IRF3. Ectopically expressed DENV NS2A and NS4B were shown to specifically inhibit TBK1 auto-phosphorylation, and reduced total IRF3 protein levels [110]. Moreover, this same study found that NS4A from serotype-1 was in addition uniquely able to contribute to TBK1 inhibition [110]. This additional evasion mechanism may contribute to the enhanced virulence of DENV1. Overexpressed DENV NS2B/3 in HEK 293/TLR3 expressing cells also directly interacts with the N-terminal Kinase domain of IKKε, inhibiting kinase activity and reducing IFN production [111].

Downstream of IFN receptor activation DENV NS4B blocks STAT1 phosphorylation and nuclear translocation [112]. DENV NS2A and NS4A were also shown to inhibit ISRE promoter activity downstream of IFNβ signaling in HEK 293T cells [112]. For NS4B this effect was later found to depend on the N-terminal signal peptide of the NS4B protein and was enhanced by natural cleavage between the NS4A-2K-NS4B fragment [113]. For NS2A and NS4A the mechanism driving their IFN evasion properties has not yet been elucidated. Finally, similar to ZIKV, DENV NS5 mediates human STAT2 degradation in a proteasome dependent manner [114]. This similarity is highlighted by a recent study that found the specific interacting residues of NS5 and its binding mode with human STAT2 were highly conserved between ZIKV and DENV [115]. However, in contrast to ZIKV this requires natural viral processing of NS5 from the polyprotein and is dependent on the ubiquitin ligase UBR4 [116].

Importantly, this intricate web of viral:host molecular interactions for both ZIKV and DENV means the innate immune system competes with the virus in a race to establish an antiviral state or a state of immune-suppressed infection. The outcome of this race largely determines the outcome of natural infection or responses to vaccination. A summary of ZIKV and DENV mediated IFN-evasion mechanisms is given in Table 1 below.

Table 1. Summary of virus specific IFN evasion mechanisms for both ZIKV and DENV

ZIKV-Mediated IFN Evasion Mechanisms			
Viral Factor	**Immune Pathway**	**Host Target**	**References**
NS4A	RLR	Binds directly to MAVS	[41,97]
NS3	RLR	Competitively binds to both 14-3-3ε and 14-3-3η	[100]
NS1	cGAS-STING	Binds USP8 leading to cGAS cleavage	[34]
NS1 and NS4B	RLR, TLR, cGAS-STING	Interacts with TBK1	[102]
NS5	RLR, TLR, cGAS-STING	Interacts with IKKε	[104]
NS5	RLR, TLR, cGAS-STING	Direct binding to IRF3	[103]
NS5	IFNAR1/2	STAT2 degradation	[105]
NS2B/3	IFNAR1/2	JAK1 degradation	[102]
Viral attachment	IFNAR1/2	Binding to Axl on the cell surface inducing SOCS1 expression	[108]
DENV-Mediated IFN Evasion Mechanisms			
Viral Factor	**Immune Pathway**	**Host Target**	**References**
NS2B	cGAS-STING	cGAS degradation	[33]
NS2B/3	cGAS-STING	STING cleavage	[52]
NS3	RLR	Competitively binds to both 14-3-3ε	[109]
NS2A and NS4B	RLR, TLR, cGAS-STING	TBK1 inhibition and reduced IRF3 protein levels	[110]
NS2B/3	RLR, TLR, cGAS-STING	Interacts with IKKε	[111]
NS4B	IFNAR1/2	Blocking STAT1 phosphorylation	[112]
NS5	IFNAR1/2	STAT2 degradation	[114]

5. Exploitation of Enhanced Type-I IFN Responses for Effective Vaccine Development

Aside from directly controlling viral replication, the type-I IFNs also have a significant role in enhancing adaptive immune responses to viral pathogens. Expression of the type-I receptor on both T and B cells is required for efficient activation of antibody responses in mice [117,118]. Additionally, type-I IFN enhances isotype switching via activation of antigen-presenting dendritic cells (DCs) [119]. Because several of the ISGs that are expressed in response to IFNs are chemokines and chemokine receptors, type-I IFNs also influence immune cell migration and recruitment. For example, in the presence of type-I interferon, DCs express greater levels of chemokine receptor CCR7 which is important in the generation of primary immune responses, and greater levels of CXCL10 that are required for recruitment of Th1 memory lymphocytes [120]. Furthermore, type-I IFN influences cytotoxic T cell expansion and memory formation [121]. Our understanding of the effect that type-I IFN has on immune responses to *Flavivirus* infection have vastly improved due to the development of immune-competent small animal models. While beyond the scope of this review, small animal models of DENV and ZIKV infection are of vital importance in pre-clinical testing of the efficacy and safety of vaccine candidates. Recent advances in this area have been comprehensively reviewed elsewhere [106,122,123].

Collectively, the combined action of type-I IFNs are important to promote efficient immune activation and therefore IFN or IFN-stimulating adjuvants are often used to enhance vaccine responses. For example, co-administrated type-I IFN can act as an adjuvant to improve vaccine responses against influenza in mice [124]. Furthermore, the cationic polysaccharide chitosan is an adjuvant currently used in vaccines that results in improved Th1 responses compared to other adjuvants like alum salts that promote mainly Th2 responses [125]. It was recently discovered that chitosan mediated this action by increasing type-I IFN production, influencing DC maturation and leading to improved antigen specific Th1 responses following vaccination [126]. Therefore, enhancing type-I IFN responses in vaccination settings is a proven way to enhance vaccine efficacy, especially where Th1 responses are important for effective control against viral pathogens [127].

Aside from its potential use as an adjuvant for vaccines, type-I IFN can also be induced naturally by live-attenuated vaccines leading to long lasting immunity. One example of this is the YF-17D vaccine licensed for YFV. One study investigating the transcriptomic profile of humans immunized with YF-17D found that the type-I IFN response was the most highly activated immune signaling pathway [128]. The type-I IFN response was induced early and transiently, returning to baseline by day 14. Importantly, the YF-17D vaccine is known to offer highly effective, lifelong protection in most patients [129].

Mutation of the genetic regions involved in viral evasion of the IFN response has shown promise in developing new live-attenuated vaccine candidates. One study performing functional profiling on the Influenza virus genome found a series of mutations within NS1 that conferred IFN hypersensitivity of these viruses [130]. When these IFN sensitive mutants were introduced into a lethal model of mouse influenza, the virus generated robust type-I IFN and adaptive immune responses but was highly attenuated, resulting in a 100% survival rate of infected mice. Inoculation with these IFN sensitive mutant virus strains protected against homologous and heterologous viral challenge in the lethal mouse model. Another example of this approach to generate potential live-attenuated vaccines was recently reported for ZIKV [131]. In this study, a full-length infectious clone of ZIKV was subjected to site directed mutagenesis focused on residues in ZIKV NS4B that are important for IFN evasion, namely a C100S mutation. These mutant viruses were propagated in Vero cells that are deficient in IFN production and used to infect mice. Whereas mice infected with wildtype virus displayed 100% lethality upon challenge, the C100S mutant virus did not result in significant weight loss or death, indicating that it was successfully attenuated. During infection, the C100S mutant was found to induce stronger type-I IFN and antigen specific T cell responses compared to the parent strain. Notably, vaccination with the C100S mutant protected mice from a lethal ZIKV challenge.

These examples demonstrate the importance of type-I IFN responses in generating protective immunity in vaccines. Furthermore, they highlight how the knowledge of viral evasion strategies can be used for the targeted, rational design of new live-attenuated vaccine candidates.

6. Conclusions

DENV and ZIKV are significant human pathogens that lack appropriate control measures. The development of safe and effective vaccines is important in the global fight against these pathogens. The immune response to both viruses is heavily underpinned by an appropriate type-I IFN response. However, both viruses have developed ways to counteract this aspect of innate immunity to cause infection and disease in humans. Understanding the molecular interactions of these viruses with the type-I IFN response is important and may assist in improving current vaccine strategies though adjuvants or aid in producing future mutant live-attenuated vaccine candidates that are unable to evade type-I IFN responses.

Author Contributions: R.C.C.-S. contributed to writing the manuscript while N.S.E. and M.R.B. provided input and edited the manuscript. All authors have read and agreed to the published version of the manuscript.

Funding: This research was funded by the National Health and Medical Research Council (NHMRC) of Australia, awarded to M.R.B (APP1145613) and N.S.E (APP1163662).

Acknowledgments: We thank Chuan Kok Lim and Thomas Burton for their assistance generating figures.

Conflicts of Interest: The authors declare no conflict of interest.

References

1. Guzman, M.G.; Harris, E. Dengue. *Lancet* **2015**, *385*, 453–465. [CrossRef]
2. Contreras-Capetillo, S.N.; Valadez-Gonzalez, N.; Manrique-Saide, P.; Carcano-Castillo, R.E.; Pacheco-Tugores, F.; Barrera-Perez, H.A.M.; Pinto-Escalante, D.; Lliteras-Cardin, M.; Hoil-Parra, J.A.; Caceres-Solis, J.L.; et al. Birth Defects Associated with Congenital Zika Virus Infection in Mexico. *Clin. Pediatr.* **2018**, *57*, 927–936. [CrossRef] [PubMed]
3. Lwande, O.W.; Obanda, V.; Lindstrom, A.; Ahlm, C.; Evander, M.; Naslund, J.; Bucht, G. Globe-Trotting Aedes aegypti and Aedes albopictus: Risk Factors for Arbovirus Pandemics. *Vector Borne Zoonotic Dis.* **2020**, *20*, 71–81. [CrossRef]
4. Best, S.M. Flaviviruses. *Curr. Biol. CB* **2016**, *26*, R1258–R1260. [CrossRef] [PubMed]
5. Gould, E.A.; Higgs, S. Impact of climate change and other factors on emerging arbovirus diseases. *Trans. R. Soc. Trop. Med. Hyg.* **2009**, *103*, 109–121. [CrossRef] [PubMed]
6. WHO. WHO Vaccine Pipeline Tracker. Available online: https://docs.google.com/spreadsheets/d/19otvINcayJURCMg76xWO4KvuyedYbMZDcXqbyJGdcZM/pubhtml# (accessed on 11 December 2019).
7. WHO. Revised SAGE Recommendation on Use of Dengue Vaccine. Available online: https://www.who.int/immunization/diseases/dengue/revised_SAGE_recommendations_dengue_vaccines_apr2018/en/ (accessed on 30 July 2020).
8. Villar, L.; Dayan, G.H.; Arredondo-García, J.L.; Rivera, D.M.; Cunha, R.; Deseda, C.; Reynales, H.; Costa, M.S.; Morales-Ramírez, J.O.; Carrasquilla, G.; et al. Efficacy of a tetravalent dengue vaccine in children in Latin America. *N. Engl. J. Med.* **2015**, *372*, 113–123. [CrossRef]
9. Koyama, S.; Ishii, K.J.; Coban, C.; Akira, S. Innate immune response to viral infection. *Cytokine* **2008**, *43*, 336–341. [CrossRef]
10. Rusinova, I.; Forster, S.; Yu, S.; Kannan, A.; Masse, M.; Cumming, H.; Chapman, R.; Hertzog, P.J. INTERFEROME v2.0: An updated database of annotated interferon-regulated genes. *Nucleic Acids Res.* **2013**, *41*, D1040–D1046. [CrossRef]
11. Schneider, W.M.; Chevillotte, M.D.; Rice, C.M. Interferon-stimulated genes: A complex web of host defenses. *Annu. Rev. Immunol.* **2014**, *32*, 513–545. [CrossRef] [PubMed]
12. Jain, A.; Pasare, C. Innate Control of Adaptive Immunity: Beyond the Three-Signal Paradigm. *J. Immunol.* **2017**, *198*, 3791–3800. [CrossRef]

13. Chang, H.H.; Huber, R.G.; Bond, P.J.; Grad, Y.H.; Camerini, D.; Maurer-Stroh, S.; Lipsitch, M. Systematic analysis of protein identity between Zika virus and other arthropod-borne viruses. *Bull. World Health Organ.* **2017**, *95*, 517i–525i. [CrossRef] [PubMed]
14. Ng, W.C.; Soto-Acosta, R.; Bradrick, S.S.; Garcia-Blanco, M.A.; Ooi, E.E. The 5′ and 3′ Untranslated Regions of the Flaviviral Genome. *Viruses* **2017**, *9*, 137. [CrossRef] [PubMed]
15. Yun, S.I.; Lee, Y.M. Zika virus: An emerging flavivirus. *J. Microbiol.* **2017**, *55*, 204–219. [CrossRef] [PubMed]
16. Thurner, C.; Witwer, C.; Hofacker, I.L.; Stadler, P.F. Conserved RNA secondary structures in Flaviviridae genomes. *J. Gen. Virol.* **2004**, *85*, 1113–1124. [CrossRef]
17. Perera, R.; Kuhn, R.J. Structural proteomics of dengue virus. *Curr. Opin. Microbiol.* **2008**, *11*, 369–377. [CrossRef]
18. Mukhopadhyay, S.; Kuhn, R.J.; Rossmann, M.G. A structural perspective of the flavivirus life cycle. *Nat. Rev. Microbiol.* **2005**, *3*, 13–22. [CrossRef]
19. Agrelli, A.; de Moura, R.R.; Crovella, S.; Brandao, L.A.C. ZIKA virus entry mechanisms in human cells. *Infect. Genet. Evol. J. Mol. Epidemiol. Evol. Genet. Infect. Dis.* **2019**, *69*, 22–29. [CrossRef]
20. Perera-Lecoin, M.; Meertens, L.; Carnec, X.; Amara, A. Flavivirus Entry Receptors: An Update. *Viruses* **2014**, *6*, 69–88. [CrossRef]
21. Hamel, R.; Dejarnac, O.; Wichit, S.; Ekchariyawat, P.; Neyret, A.; Luplertlop, N.; Perera-Lecoin, M.; Surasombatpattana, P.; Talignani, L.; Thomas, F.; et al. Biology of Zika Virus Infection in Human Skin Cells. *J. Virol.* **2015**, *89*, 8880–8896. [CrossRef]
22. Meertens, L.; Carnec, X.; Lecoin, M.P.; Ramdasi, R.; Guivel-Benhassine, F.; Lew, E.; Lemke, G.; Schwartz, O.; Amara, A. The TIM and TAM Families of Phosphatidylserine Receptors Mediate Dengue Virus Entry. *Cell Host Microbe* **2012**, *12*, 544–557. [CrossRef]
23. Mousavi, S.A.; Malerod, L.; Berg, T.; Kjeken, R. Clathrin-dependent endocytosis. *Biochem. J.* **2004**, *377*, 1–16. [CrossRef]
24. Roby, J.A.; Funk, A.; Khromykh, A.A. Flavivirus replication and assembly. In *Molecular Virology and Control of Flaviviruses*; Caister Academic Press: Norfolk, UK, 2012.
25. Lescar, J.; Soh, S.; Lee, L.T.; Vasudevan, S.G.; Kang, C.; Lim, S.P. The Dengue Virus Replication Complex: From RNA Replication to Protein-Protein Interactions to Evasion of Innate Immunity. *Adv. Exp. Med. Biol.* **2018**, *1062*, 115–129. [CrossRef] [PubMed]
26. Murray, C.L.; Jones, C.T.; Rice, C.M. Architects of assembly: Roles of Flaviviridae non-structural proteins in virion morphogenesis. *Nat. Rev. Microbiol.* **2008**, *6*, 699–708. [CrossRef] [PubMed]
27. Yu, I.M.; Zhang, W.; Holdaway, H.A.; Li, L.; Kostyuchenko, V.A.; Chipman, P.R.; Kuhn, R.J.; Rossmann, M.G.; Chen, J. Structure of the immature dengue virus at low pH primes proteolytic maturation. *Science* **2008**, *319*, 1834–1837. [CrossRef] [PubMed]
28. Zicari, S.; Arakelyan, A.; Fitzgerald, W.; Zaitseva, E.; Chernomordik, L.V.; Margolis, L.; Grivel, J.-C. Evaluation of the maturation of individual Dengue virions with flow virometry. *Virology* **2016**, *488*, 20–27. [CrossRef] [PubMed]
29. Dejnirattisai, W.; Jumnainsong, A.; Onsirisakul, N.; Fitton, P.; Vasanawathana, S.; Limpitikul, W.; Puttikhunt, C.; Edwards, C.; Duangchinda, T.; Supasa, S.; et al. Cross-reacting antibodies enhance dengue virus infection in humans. *Science* **2010**, *328*, 745–748. [CrossRef] [PubMed]
30. Diamond, M.S.; Pierson, T.C. Molecular Insight into Dengue Virus Pathogenesis and Its Implications for Disease Control. *Cell* **2015**, *162*, 488–492. [CrossRef] [PubMed]
31. McNab, F.; Mayer-Barber, K.; Sher, A.; Wack, A.; O'Garra, A. Type I interferons in infectious disease. *Nat. Rev. Immunol.* **2015**, *15*, 87–103. [CrossRef]
32. Green, A.M.; Beatty, P.R.; Hadjilaou, A.; Harris, E. Innate immunity to dengue virus infection and subversion of antiviral responses. *J. Mol. Biol.* **2014**, *426*, 1148–1160. [CrossRef]
33. Aguirre, S.; Luthra, P.; Sanchez-Aparicio, M.T.; Maestre, A.M.; Patel, J.; Lamothe, F.; Fredericks, A.C.; Tripathi, S.; Zhu, T.; Pintado-Silva, J.; et al. Dengue virus NS2B protein targets cGAS for degradation and prevents mitochondrial DNA sensing during infection. *Nat. Microbiol.* **2017**, *2*, 17037. [CrossRef]
34. Zheng, Y.; Liu, Q.; Wu, Y.; Ma, L.; Zhang, Z.; Liu, T.; Jin, S.; She, Y.; Li, Y.P.; Cui, J. Zika virus elicits inflammation to evade antiviral response by cleaving cGAS via NS1-caspase-1 axis. *EMBO J.* **2018**, *37*. [CrossRef]
35. Kell, A.M.; Gale, M. RIG-I in RNA virus recognition. *Virology* **2015**, *479–480*, 110–121. [CrossRef] [PubMed]
36. Lazear, H.M.; Schoggins, J.W.; Diamond, M.S. Shared and Distinct Functions of Type I and Type III Interferons. *Immunity* **2019**, *50*, 907–923. [CrossRef] [PubMed]

37. Kato, H.; Takeuchi, O.; Mikamo-Satoh, E.; Hirai, R.; Kawai, T.; Matsushita, K.; Hiiragi, A.; Dermody, T.S.; Fujita, T.; Akira, S. Length-dependent recognition of double-stranded ribonucleic acids by retinoic acid-inducible gene-I and melanoma differentiation-associated gene 5. *J. Exp. Med.* **2008**, *205*, 1601–1610. [CrossRef]
38. Schlee, M.; Roth, A.; Hornung, V.; Hagmann, C.A.; Wimmenauer, V.; Barchet, W.; Coch, C.; Janke, M.; Mihailovic, A.; Wardle, G.; et al. Recognition of 5′ triphosphate by RIG-I helicase requires short blunt double-stranded RNA as contained in panhandle of negative-strand virus. *Immunity* **2009**, *31*, 25–34. [CrossRef]
39. Vazquez, C.; Horner, S.M. MAVS Coordination of Antiviral Innate Immunity. *J. Virol.* **2015**, *89*, 6974–6977. [CrossRef]
40. Schilling, M.; Bridgeman, A.; Gray, N.; Hertzog, J.; Hublitz, P.; Kohl, A.; Rehwinkel, J. RIG-I Plays a Dominant Role in the Induction of Transcriptional Changes in Zika Virus-Infected Cells, which Protect from Virus-Induced Cell Death. *Cells* **2020**, *9*, 1476. [CrossRef]
41. Ma, J.; Ketkar, H.; Geng, T.; Lo, E.; Wang, L.; Xi, J.; Sun, Q.; Zhu, Z.; Cui, Y.; Yang, L.; et al. Zika Virus Non-structural Protein 4A Blocks the RLR-MAVS Signaling. *Front. Microbiol.* **2018**, *9*, 1350. [CrossRef]
42. Nasirudeen, A.M.; Wong, H.H.; Thien, P.; Xu, S.; Lam, K.P.; Liu, D.X. RIG-I, MDA5 and TLR3 synergistically play an important role in restriction of dengue virus infection. *PLoS Negl. Trop. Dis.* **2011**, *5*, e926. [CrossRef]
43. Tsai, Y.T.; Chang, S.Y.; Lee, C.N.; Kao, C.L. Human TLR3 recognizes dengue virus and modulates viral replication in vitro. *Cell. Microbiol.* **2009**, *11*, 604–615. [CrossRef]
44. Nazmi, A.; Dutta, K.; Hazra, B.; Basu, A. Role of pattern recognition receptors in flavivirus infections. *Virus Res.* **2014**, *185*, 32–40. [CrossRef]
45. Leifer, C.A.; Medvedev, A.E. Molecular mechanisms of regulation of Toll-like receptor signaling. *J. Leukoc. Biol.* **2016**, *100*, 927–941. [CrossRef] [PubMed]
46. Okahira, S.; Nishikawa, F.; Nishikawa, S.; Akazawa, T.; Seya, T.; Matsumoto, M. Interferon-beta induction through toll-like receptor 3 depends on double-stranded RNA structure. *DNA Cell Biol.* **2005**, *24*, 614–623. [CrossRef] [PubMed]
47. Yockey, L.J.; Varela, L.; Rakib, T.; Khoury-Hanold, W.; Fink, S.L.; Stutz, B.; Szigeti-Buck, K.; Van den Pol, A.; Lindenbach, B.D.; Horvath, T.L.; et al. Vaginal Exposure to Zika Virus during Pregnancy Leads to Fetal Brain Infection. *Cell* **2016**, *166*, 1247–1256. [CrossRef]
48. Motwani, M.; Pesiridis, S.; Fitzgerald, K.A. DNA sensing by the cGAS-STING pathway in health and disease. *Nat. Rev. Genet.* **2019**, *20*, 657–674. [CrossRef]
49. Catteau, A.; Roué, G.; Yuste, V.J.; Susin, S.A.; Desprès, P. Expression of dengue ApoptoM sequence results in disruption of mitochondrial potential and caspase activation. *Biochimie* **2003**, *85*, 789–793. [CrossRef]
50. Yu, C.Y.; Liang, J.J.; Li, J.K.; Lee, Y.L.; Chang, B.L.; Su, C.I.; Huang, W.J.; Lai, M.M.; Lin, Y.L. Dengue Virus Impairs Mitochondrial Fusion by Cleaving Mitofusins. *PLoS Pathog* **2015**, *11*, e1005350. [CrossRef]
51. Ledur, P.F.; Karmirian, K.; Pedrosa, C.d.S.G.; Souza, L.R.Q.; Assis-de-Lemos, G.; Martins, T.M.; Ferreira, J.d.C.C.G.; de Azevedo Reis, G.F.; Silva, E.S.; Silva, D.; et al. Zika virus infection leads to mitochondrial failure, oxidative stress and DNA damage in human iPSC-derived astrocytes. *Sci. Rep.* **2020**, *10*, 1218. [CrossRef]
52. Aguirre, S.; Maestre, A.M.; Pagni, S.; Patel, J.R.; Savage, T.; Gutman, D.; Maringer, K.; Bernal-Rubio, D.; Shabman, R.S.; Simon, V.; et al. DENV inhibits type I IFN production in infected cells by cleaving human STING. *PLoS Pathog.* **2012**, *8*, e1002934. [CrossRef]
53. Hertzog, P.J.; Williams, B.R.G. Fine tuning type I interferon responses. *Cytokine Growth Factor Rev.* **2013**, *24*, 217–225. [CrossRef] [PubMed]
54. Taniguchi, T.; Ogasawara, K.; Takaoka, A.; Tanaka, N. IRF family of transcription factors as regulators of host defense. *Ann. Rev. Immunol.* **2001**, *19*, 623–655. [CrossRef] [PubMed]
55. de Weerd, N.A.; Nguyen, T. The interferons and their receptors—Distribution and regulation. *Immunol. Cell Biol.* **2012**, *90*, 483–491. [CrossRef] [PubMed]
56. Ivashkiv, L.B.; Donlin, L.T. Regulation of type I interferon responses. *Nat. Rev. Immunol.* **2014**, *14*, 36–49. [CrossRef] [PubMed]
57. Lamken, P.; Lata, S.; Gavutis, M.; Piehler, J. Ligand-induced assembling of the type I interferon receptor on supported lipid bilayers. *J. Mol. Biol.* **2004**, *341*, 303–318. [CrossRef]
58. Yan, H.; Krishnan, K.; Lim, J.T.; Contillo, L.G.; Krolewski, J.J. Molecular characterization of an alpha interferon receptor 1 subunit (IFNaR1) domain required for TYK2 binding and signal transduction. *Mol. Cell. Biol.* **1996**, *16*, 2074–2082. [CrossRef]

59. Domanski, P.; Fish, E.; Nadeau, O.W.; Witte, M.; Platanias, L.C.; Yan, H.; Krolewski, J.; Pitha, P.; Colamonici, O.R. A region of the beta subunit of the interferon alpha receptor different from box 1 interacts with Jak1 and is sufficient to activate the Jak-Stat pathway and induce an antiviral state. *J. Biol. Chem.* **1997**, *272*, 26388–26393. [CrossRef]
60. Raftery, N.; Stevenson, N.J. Advances in anti-viral immune defence: Revealing the importance of the IFN JAK/STAT pathway. *Cell. Mol. Life Sci.* **2017**, *74*, 2525–2535. [CrossRef]
61. Singh, P.K.; Guest, J.-M.; Kanwar, M.; Boss, J.; Gao, N.; Juzych, M.S.; Abrams, G.W.; Yu, F.-S.; Kumar, A. Zika virus infects cells lining the blood-retinal barrier and causes chorioretinal atrophy in mouse eyes. *JCI Insight* **2017**, *2*, e92340. [CrossRef]
62. Singh, P.K.; Singh, S.; Farr, D.; Kumar, A. Interferon-stimulated gene 15 (ISG15) restricts Zika virus replication in primary human corneal epithelial cells. *Ocul. Surf.* **2019**. [CrossRef]
63. Perng, Y.-C.; Lenschow, D.J. ISG15 in antiviral immunity and beyond. *Nat. Rev. Microbiol.* **2018**, *16*, 423–439. [CrossRef]
64. Dai, J.; Pan, W.; Wang, P. ISG15 facilitates cellular antiviral response to dengue and west nile virus infection in vitro. *Virol. J.* **2011**, *8*, 468. [CrossRef] [PubMed]
65. Bailey, C.C.; Zhong, G.; Huang, I.C.; Farzan, M. IFITM-Family Proteins: The Cell's First Line of Antiviral Defense. *Ann. Rev. Virol.* **2014**, *1*, 261–283. [CrossRef] [PubMed]
66. Savidis, G.; Perreira, J.M.; Portmann, J.M.; Meraner, P.; Guo, Z.; Green, S.; Brass, A.L. The IFITMs Inhibit Zika Virus Replication. *Cell Rep.* **2016**, *15*, 2323–2330. [CrossRef] [PubMed]
67. Jiang, D.; Weidner, J.M.; Qing, M.; Pan, X.-B.; Guo, H.; Xu, C.; Zhang, X.; Birk, A.; Chang, J.; Shi, P.-Y.; et al. Identification of five interferon-induced cellular proteins that inhibit west nile virus and dengue virus infections. *J. Virol.* **2010**, *84*, 8332–8341. [CrossRef] [PubMed]
68. Qi, Y.; Li, Y.; Zhang, Y.; Zhang, L.; Wang, Z.; Zhang, X.; Gui, L.; Huang, J. IFI6 Inhibits Apoptosis via Mitochondrial-Dependent Pathway in Dengue Virus 2 Infected Vascular Endothelial Cells. *PLoS ONE* **2015**, *10*, e0132743. [CrossRef]
69. Dukhovny, A.; Lamkiewicz, K.; Chen, Q.; Fricke, M.; Jabrane-Ferrat, N.; Marz, M.; Jung, J.U.; Sklan, E.H. A CRISPR activation screen identifies genes protecting from Zika virus infection. *J. Virol.* **2019**. [CrossRef]
70. Richardson, R.B.; Ohlson, M.B.; Eitson, J.L.; Kumar, A.; McDougal, M.B.; Boys, I.N.; Mar, K.B.; De La Cruz-Rivera, P.C.; Douglas, C.; Konopka, G.; et al. A CRISPR screen identifies IFI6 as an ER-resident interferon effector that blocks flavivirus replication. *Nat. Microbiol.* **2018**, *3*, 1214–1223. [CrossRef]
71. Van der Hoek, K.H.; Eyre, N.S.; Shue, B.; Khantisitthiporn, O.; Glab-Ampi, K.; Carr, J.M.; Gartner, M.J.; Jolly, L.A.; Thomas, P.Q.; Adikusuma, F.; et al. Viperin is an important host restriction factor in control of Zika virus infection. *Sci. Rep.* **2017**, *7*, 4475. [CrossRef]
72. Panayiotou, C.; Lindqvist, R.; Kurhade, C.; Vonderstein, K.; Pasto, J.; Edlund, K.; Upadhyay, A.S.; Overby, A.K. Viperin restricts Zika virus and tick-borne encephalitis virus replication by targeting NS3 for proteasomal degradation. *J. Virol.* **2018**. [CrossRef]
73. Helbig, K.J.; Carr, J.M.; Calvert, J.K.; Wati, S.; Clarke, J.N.; Eyre, N.S.; Narayana, S.K.; Fiches, G.N.; McCartney, E.M.; Beard, M.R. Viperin is induced following dengue virus type-2 (DENV-2) infection and has anti-viral actions requiring the C-terminal end of viperin. *PLoS Negl. Trop. Dis.* **2013**, *7*, e2178. [CrossRef]
74. Helbig, K.J.; Beard, M.R. The role of viperin in the innate antiviral response. *J. Mol. Biol.* **2014**, *426*, 1210–1219. [CrossRef] [PubMed]
75. Nasr, N.; Maddocks, S.; Turville, S.G.; Harman, A.N.; Woolger, N.; Helbig, K.J.; Wilkinson, J.; Bye, C.R.; Wright, T.K.; Rambukwelle, D.; et al. HIV-1 infection of human macrophages directly induces viperin which inhibits viral production. *Blood* **2012**, *120*, 778–788. [CrossRef] [PubMed]
76. Helbig, K.J.; Eyre, N.S.; Yip, E.; Narayana, S.; Li, K.; Fiches, G.; McCartney, E.M.; Jangra, R.K.; Lemon, S.M.; Beard, M.R. The antiviral protein viperin inhibits hepatitis C virus replication via interaction with nonstructural protein 5A. *Hepatology* **2011**, *54*, 1506–1517. [CrossRef] [PubMed]
77. Diner, B.A.; Lum, K.K.; Toettcher, J.E.; Cristea, I.M. Viral DNA Sensors IFI16 and Cyclic GMP-AMP Synthase Possess Distinct Functions in Regulating Viral Gene Expression, Immune Defenses, and Apoptotic Responses during Herpesvirus Infection. *mBio* **2016**, *7*, e01553-16. [CrossRef] [PubMed]
78. Wichit, S.; Hamel, R.; Yainoy, S.; Gumpangseth, N.; Panich, S.; Phuadraksa, T.; Saetear, P.; Monteil, A.; Morales Vargas, R.; Misse, D. Interferon-inducible protein (IFI) 16 regulates Chikungunya and Zika virus infection in human skin fibroblasts. *EXCLI J.* **2019**, *18*, 467–476. [CrossRef]

79. Hanck, T.; Stricker, R.; Sedehizade, F.; Reiser, G. Identification of gene structure and subcellular localization of human centaurin alpha 2, and p42IP4, a family of two highly homologous, Ins 1,3,4,5-P4-/PtdIns 3,4,5-P3-binding, adapter proteins. *J. Neurochem.* **2004**, *88*, 326–336. [CrossRef]
80. Shu, Q.; Lennemann, N.J.; Sarkar, S.N.; Sadovsky, Y.; Coyne, C.B. ADAP2 Is an Interferon Stimulated Gene That Restricts RNA Virus Entry. *PLoS Pathog.* **2015**, *11*, e1005150. [CrossRef]
81. Han, Y.; Li, R.; Gao, J.; Miao, S.; Wang, L. Characterisation of human RING finger protein TRIM69, a novel testis E3 ubiquitin ligase and its subcellular localisation. *Biochem. Biophys. Res. Commun.* **2012**, *429*, 6–11. [CrossRef]
82. Wang, K.; Zou, C.; Wang, X.; Huang, C.; Feng, T.; Pan, W.; Wu, Q.; Wang, P.; Dai, J. Interferon-stimulated TRIM69 interrupts dengue virus replication by ubiquitinating viral nonstructural protein 3. *PLoS Pathog.* **2018**, *14*, e1007287. [CrossRef]
83. Saeedi, B.J.; Geiss, B.J. Regulation of flavivirus RNA synthesis and capping. *Wiley Interdiscip. Rev. RNA* **2013**, *4*, 723–735. [CrossRef]
84. Zust, R.; Cervantes-Barragan, L.; Habjan, M.; Maier, R.; Neuman, B.W.; Ziebuhr, J.; Szretter, K.J.; Baker, S.C.; Barchet, W.; Diamond, M.S.; et al. Ribose 2′-O-methylation provides a molecular signature for the distinction of self and non-self mRNA dependent on the RNA sensor Mda5. *Nat. Immunol.* **2011**, *12*, 137–143. [CrossRef] [PubMed]
85. Kimura, T.; Katoh, H.; Kayama, H.; Saiga, H.; Okuyama, M.; Okamoto, T.; Umemoto, E.; Matsuura, Y.; Yamamoto, M.; Takeda, K. Ifit1 inhibits Japanese encephalitis virus replication through binding to 5′ capped 2′-O unmethylated RNA. *J. Virol.* **2013**, *87*, 9997–10003. [CrossRef]
86. Miorin, L.; Maestre, A.M.; Fernandez-Sesma, A.; García-Sastre, A. Antagonism of type I interferon by flaviviruses. *Biochem. Biophys. Res. Commun.* **2017**, *492*, 587–596. [CrossRef]
87. Scutigliani, E.M.; Kikkert, M. Interaction of the innate immune system with positive-strand RNA virus replication organelles. *Cytokine Growth Factor Rev.* **2017**, *37*, 17–27. [CrossRef]
88. Aktepe, T.E.; Mackenzie, J.M. Shaping the flavivirus replication complex: It is curvaceous! *Cell. Microbiol.* **2018**, *20*, e12884. [CrossRef] [PubMed]
89. Hoenen, A.; Liu, W.; Kochs, G.; Khromykh, A.A.; Mackenzie, J.M. West Nile virus-induced cytoplasmic membrane structures provide partial protection against the interferon-induced antiviral MxA protein. *J. Gen. Virol.* **2007**, *88*, 3013–3017. [CrossRef] [PubMed]
90. Uchida, L.; Espada-Murao, L.A.; Takamatsu, Y.; Okamoto, K.; Hayasaka, D.; Yu, F.; Nabeshima, T.; Buerano, C.C.; Morita, K. The dengue virus conceals double-stranded RNA in the intracellular membrane to escape from an interferon response. *Sci. Rep.* **2014**, *4*, 7395. [CrossRef]
91. Cortese, M.; Goellner, S.; Acosta, E.G.; Neufeldt, C.J.; Oleksiuk, O.; Lampe, M.; Haselmann, U.; Funaya, C.; Schieber, N.; Ronchi, P.; et al. Ultrastructural Characterization of Zika Virus Replication Factories. *Cell Rep.* **2017**, *18*, 2113–2123. [CrossRef]
92. Clarke, B.D.; Roby, J.A.; Slonchak, A.; Khromykh, A.A. Functional non-coding RNAs derived from the flavivirus 3′ untranslated region. *Virus Res.* **2015**, *206*, 53–61. [CrossRef]
93. Mazeaud, C.; Freppel, W.; Chatel-Chaix, L. The Multiples Fates of the Flavivirus RNA Genome During Pathogenesis. *Front. Genet.* **2018**, *9*, 595. [CrossRef]
94. Funk, A.; Truong, K.; Nagasaki, T.; Torres, S.; Floden, N.; Balmori Melian, E.; Edmonds, J.; Dong, H.; Shi, P.-Y.; Khromykh, A.A. RNA structures required for production of subgenomic flavivirus RNA. *J. Virol.* **2010**, *84*, 11407–11417. [CrossRef] [PubMed]
95. Donald, C.L.; Brennan, B.; Cumberworth, S.L.; Rezelj, V.V.; Clark, J.J.; Cordeiro, M.T.; Freitas de Oliveira Franca, R.; Pena, L.J.; Wilkie, G.S.; Da Silva Filipe, A.; et al. Full Genome Sequence and sfRNA Interferon Antagonist Activity of Zika Virus from Recife, Brazil. *PLoS Negl. Trop. Dis.* **2016**, *10*, e0005048. [CrossRef] [PubMed]
96. Manokaran, G.; Finol, E.; Wang, C.; Gunaratne, J.; Bahl, J.; Ong, E.Z.; Tan, H.C.; Sessions, O.M.; Ward, A.M.; Gubler, D.J.; et al. Dengue subgenomic RNA binds TRIM25 to inhibit interferon expression for epidemiological fitness. *Science* **2015**, *350*, 217–221. [CrossRef] [PubMed]
97. Ngueyen, T.T.N.; Kim, S.J.; Lee, J.Y.; Myoung, J. Zika Virus Proteins NS2A and NS4A Are Major Antagonists that Reduce IFN-beta Promoter Activity Induced by the MDA5/RIG-I Signaling Pathway. *J. Microbiol. Biotechnol.* **2019**, *29*, 1665–1674. [CrossRef] [PubMed]

98. Lin, J.P.; Fan, Y.K.; Liu, H.M. The 14-3-3η chaperone protein promotes antiviral innate immunity via facilitating MDA5 oligomerization and intracellular redistribution. *PLoS Pathog* **2019**, *15*, e1007582. [CrossRef]
99. Liu, H.M.; Loo, Y.M.; Horner, S.M.; Zornetzer, G.A.; Katze, M.G.; Gale, M., Jr. The mitochondrial targeting chaperone 14-3-3ε regulates a RIG-I translocon that mediates membrane association and innate antiviral immunity. *Cell Host Microbe* **2012**, *11*, 528–537. [CrossRef]
100. Riedl, W.; Acharya, D.; Lee, J.H.; Liu, G.; Serman, T.; Chiang, C.; Chan, Y.K.; Diamond, M.S.; Gack, M.U. Zika Virus NS3 Mimics a Cellular 14-3-3-Binding Motif to Antagonize RIG-I- and MDA5-Mediated Innate Immunity. *Cell Host Microbe* **2019**, *26*, 493–503. [CrossRef]
101. Ding, Q.; Gaska, J.M.; Douam, F.; Wei, L.; Kim, D.; Balev, M.; Heller, B.; Ploss, A. Species-specific disruption of STING-dependent antiviral cellular defenses by the Zika virus NS2B3 protease. *Proc. Natl. Acad. Sci. USA* **2018**, *115*, E6310–E6318. [CrossRef]
102. Wu, Y.; Liu, Q.; Zhou, J.; Xie, W.; Chen, C.; Wang, Z.; Yang, H.; Cui, J. Zika virus evades interferon-mediated antiviral response through the co-operation of multiple nonstructural proteins in vitro. *Cell Discov.* **2017**, *3*, 17006. [CrossRef]
103. Xia, H.; Luo, H.; Shan, C.; Muruato, A.E.; Nunes, B.T.D.; Medeiros, D.B.A.; Zou, J.; Xie, X.; Giraldo, M.I.; Vasconcelos, P.F.C.; et al. An evolutionary NS1 mutation enhances Zika virus evasion of host interferon induction. *Nat. Commun.* **2018**, *9*, 414. [CrossRef]
104. Lundberg, R.; Melen, K.; Westenius, V.; Jiang, M.; Osterlund, P.; Khan, H.; Vapalahti, O.; Julkunen, I.; Kakkola, L. Zika Virus Non-Structural Protein NS5 Inhibits the RIG-I Pathway and Interferon Lambda 1 Promoter Activation by Targeting IKK Epsilon. *Viruses* **2019**, *11*, 1024. [CrossRef] [PubMed]
105. Grant, A.; Ponia, S.S.; Tripathi, S.; Balasubramaniam, V.; Miorin, L.; Sourisseau, M.; Schwarz, M.C.; Sanchez-Seco, M.P.; Evans, M.J.; Best, S.M.; et al. Zika Virus Targets Human STAT2 to Inhibit Type I Interferon Signaling. *Cell Host Microbe* **2016**, *19*, 882–890. [CrossRef] [PubMed]
106. Morrison, T.E.; Diamond, M.S. Animal Models of Zika Virus Infection, Pathogenesis, and Immunity. *J. Virol.* **2017**, 91. [CrossRef] [PubMed]
107. Hertzog, J.; Dias Junior, A.G.; Rigby, R.E.; Donald, C.L.; Mayer, A.; Sezgin, E.; Song, C.; Jin, B.; Hublitz, P.; Eggeling, C.; et al. Infection with a Brazilian isolate of Zika virus generates RIG-I stimulatory RNA and the viral NS5 protein blocks type I IFN induction and signalling. *Eur. J. Immunol.* **2018**. [CrossRef]
108. Meertens, L.; Labeau, A.; Dejarnac, O.; Cipriani, S.; Sinigaglia, L.; Bonnet-Madin, L.; Le Charpentier, T.; Hafirassou, M.L.; Zamborlini, A.; Cao-Lormeau, V.M.; et al. Axl Mediates ZIKA Virus Entry in Human Glial Cells and Modulates Innate Immune Responses. *Cell Rep.* **2017**, *18*, 324–333. [CrossRef]
109. Chan, Y.K.; Gack, M.U. A phosphomimetic-based mechanism of dengue virus to antagonize innate immunity. *Nat. Immunol.* **2016**, *17*, 523–530. [CrossRef]
110. Dalrymple, N.A.; Cimica, V.; Mackow, E.R. Dengue Virus NS Proteins Inhibit RIG-I/MAVS Signaling by Blocking TBK1/IRF3 Phosphorylation: Dengue Virus Serotype 1 NS4A Is a Unique Interferon-Regulating Virulence Determinant. *mBio* **2015**, *6*, e00553-15. [CrossRef]
111. Angleró-Rodríguez, Y.I.; Pantoja, P.; Sariol, C.A. Dengue virus subverts the interferon induction pathway via NS2B/3 protease-IκB kinase epsilon interaction. *Clin Vaccine Immunol* **2014**, *21*, 29–38. [CrossRef]
112. Muñoz-Jordan, J.L.; Sánchez-Burgos, G.G.; Laurent-Rolle, M.; García-Sastre, A. Inhibition of interferon signaling by dengue virus. *Proc. Natl. Acad. Sci. USA* **2003**, *100*, 14333–14338. [CrossRef]
113. Munoz-Jordan, J.L.; Laurent-Rolle, M.; Ashour, J.; Martinez-Sobrido, L.; Ashok, M.; Lipkin, W.I.; Garcia-Sastre, A. Inhibition of alpha/beta interferon signaling by the NS4B protein of flaviviruses. *J. Virol.* **2005**, *79*, 8004–8013. [CrossRef]
114. Ashour, J.; Laurent-Rolle, M.; Shi, P.Y.; Garcia-Sastre, A. NS5 of dengue virus mediates STAT2 binding and degradation. *J. Virol.* **2009**, *83*, 5408–5418. [CrossRef] [PubMed]
115. Wang, B.; Thurmond, S.; Zhou, K.; Sánchez-Aparicio, M.T.; Fang, J.; Lu, J.; Gao, L.; Ren, W.; Cui, Y.; Veit, E.C.; et al. Structural basis for STAT2 suppression by flavivirus NS5. *Nat. Struct. Mol. Biol.* **2020**. [CrossRef] [PubMed]
116. Morrison, J.; Laurent-Rolle, M.; Maestre, A.M.; Rajsbaum, R.; Pisanelli, G.; Simon, V.; Mulder, L.C.; Fernandez-Sesma, A.; Garcia-Sastre, A. Dengue virus co-opts UBR4 to degrade STAT2 and antagonize type I interferon signaling. *PLoS Pathog* **2013**, *9*, e1003265. [CrossRef] [PubMed]
117. Fink, K.; Lang, K.S.; Manjarrez-Orduno, N.; Junt, T.; Senn, B.M.; Holdener, M.; Akira, S.; Zinkernagel, R.M.; Hengartner, H. Early type I interferon-mediated signals on B cells specifically enhance antiviral humoral responses. *Eur. J. Immunol.* **2006**, *36*, 2094–2105. [CrossRef]

118. Le Bon, A.; Thompson, C.; Kamphuis, E.; Durand, V.; Rossmann, C.; Kalinke, U.; Tough, D.F. Cutting edge: Enhancement of antibody responses through direct stimulation of B and T cells by type I IFN. *J. Immunol.* **2006**, *176*, 2074–2078. [CrossRef] [PubMed]
119. Le Bon, A.; Schiavoni, G.; D'Agostino, G.; Gresser, I.; Belardelli, F.; Tough, D.F. Type i interferons potently enhance humoral immunity and can promote isotype switching by stimulating dendritic cells in vivo. *Immunity* **2001**, *14*, 461–470. [CrossRef]
120. Parlato, S.; Santini, S.M.; Lapenta, C.; Di Pucchio, T.; Logozzi, M.; Spada, M.; Giammarioli, A.M.; Malorni, W.; Fais, S.; Belardelli, F. Expression of CCR-7, MIP-3beta, and Th-1 chemokines in type I IFN-induced monocyte-derived dendritic cells: Importance for the rapid acquisition of potent migratory and functional activities. *Blood* **2001**, *98*, 3022–3029. [CrossRef]
121. Thompson, L.J.; Kolumam, G.A.; Thomas, S.; Murali-Krishna, K. Innate inflammatory signals induced by various pathogens differentially dictate the IFN-I dependence of CD8 T cells for clonal expansion and memory formation. *J. Immunol.* **2006**, *177*, 1746–1754. [CrossRef]
122. Mathew, A. Humanized mouse models to study human cell-mediated and humoral responses to dengue virus. *Curr. Opin. Virol.* **2017**, *25*, 76–80. [CrossRef]
123. Na, W.; Yeom, M.; Choi, I.K.; Yook, H.; Song, D. Animal models for dengue vaccine development and testing. *Clin. Exp. Vaccine Res.* **2017**, *6*, 104–110. [CrossRef]
124. Proietti, E.; Bracci, L.; Puzelli, S.; Di Pucchio, T.; Sestili, P.; De Vincenzi, E.; Venditti, M.; Capone, I.; Seif, I.; De Maeyer, E.; et al. Type I IFN as a natural adjuvant for a protective immune response: Lessons from the influenza vaccine model. *J. Immunol.* **2002**, *169*, 375–383. [CrossRef] [PubMed]
125. Mori, A.; Oleszycka, E.; Sharp, F.A.; Coleman, M.; Ozasa, Y.; Singh, M.; O'Hagan, D.T.; Tajber, L.; Corrigan, O.I.; McNeela, E.A.; et al. The vaccine adjuvant alum inhibits IL-12 by promoting PI3 kinase signaling while chitosan does not inhibit IL-12 and enhances Th1 and Th17 responses. *Eur. J. Immunol.* **2012**, *42*, 2709–2719. [CrossRef] [PubMed]
126. Carroll, E.C.; Jin, L.; Mori, A.; Muñoz-Wolf, N.; Oleszycka, E.; Moran, H.B.T.; Mansouri, S.; McEntee, C.P.; Lambe, E.; Agger, E.M.; et al. The Vaccine Adjuvant Chitosan Promotes Cellular Immunity via DNA Sensor cGAS-STING-Dependent Induction of Type I Interferons. *Immunity* **2016**, *44*, 597–608. [CrossRef] [PubMed]
127. Snell, L.M.; Osokine, I.; Yamada, D.H.; De la Fuente, J.R.; Elsaesser, H.J.; Brooks, D.G. Overcoming CD4 Th1 Cell Fate Restrictions to Sustain Antiviral CD8 T Cells and Control Persistent Virus Infection. *Cell Rep.* **2016**, *16*, 3286–3296. [CrossRef] [PubMed]
128. Hou, J.; Wang, S.; Jia, M.; Li, D.; Liu, Y.; Li, Z.; Zhu, H.; Xu, H.; Sun, M.; Lu, L.; et al. A Systems Vaccinology Approach Reveals Temporal Transcriptomic Changes of Immune Responses to the Yellow Fever 17D Vaccine. *J. Immunol.* **2017**, *199*, 1476–1489. [CrossRef]
129. Collins, N.D.; Barrett, A.D. Live Attenuated Yellow Fever 17D Vaccine: A Legacy Vaccine Still Controlling Outbreaks In Modern Day. *Curr. Infect. Dis. Rep.* **2017**, *19*, 14. [CrossRef]
130. Du, Y.; Xin, L.; Shi, Y.; Zhang, T.H.; Wu, N.C.; Dai, L.; Gong, D.; Brar, G.; Shu, S.; Luo, J.; et al. Genome-wide identification of interferon-sensitive mutations enables influenza vaccine design. *Science* **2018**, *359*, 290–296. [CrossRef]
131. Li, G.; Adam, A.; Luo, H.; Shan, C.; Cao, Z.; Fontes-Garfias, C.R.; Sarathy, V.V.; Teleki, C.; Winkelmann, E.R.; Liang, Y.; et al. An attenuated Zika virus NS4B protein mutant is a potent inducer of antiviral immune responses. *NPJ Vaccines* **2019**, *4*, 48. [CrossRef]

Bibliographic References

1. Abdulhaqq SA, Zorrilla C, Kang G, Yin X, Tamayo V, Seaton KE, Joseph J, Garced S, Tomaras GD, Linn KA, Foulkes AS, Azzoni L, VerMilyea M, Coutifaris C, Kossenkov AV, Showe L, Kraiselburd EN, Li Q, Montaner LJ (2016) HIV-1-negative female sex workers sustain high cervical IFNvarepsilon, low immune activation, and low expression of HIV-1-required host genes. Mucosal immunology 9:1027-1038
2. Africander D, Louw R, Verhoog N, Noeth D, Hapgood JP (2011) Differential regulation of endogenous pro-inflammatory cytokine genes by medroxyprogesterone acetate and norethisterone acetate in cell lines of the female genital tract. Contraception 84:423-435
3. Agrelli A, de Moura RR, Crovella S, Brandao LAC (2019) ZIKA virus entry mechanisms in human cells. Infection, genetics and evolution : journal of molecular epidemiology and evolutionary genetics in infectious diseases 69:22-29
4. Aguirre S, Maestre AM, Pagni S, Patel JR, Savage T, Gutman D, Maringer K, Bernal-Rubio D, Shabman RS, Simon V, Rodriguez-Madoz JR, Mulder LC, Barber GN, Fernandez-Sesma A (2012) DENV inhibits type I IFN production in infected cells by cleaving human STING. PLoS Pathog 8:e1002934
5. Aguirre S, Luthra P, Sanchez-Aparicio MT, Maestre AM, Patel J, Lamothe F, Fredericks AC, Tripathi S, Zhu T, Pintado-Silva J, Webb LG, Bernal-Rubio D, Solovyov A, Greenbaum B, Simon V, Basler CF, Mulder LC, Garcia-Sastre A, Fernandez-Sesma A (2017) Dengue virus NS2B protein targets cGAS for degradation and prevents mitochondrial DNA sensing during infection. Nature microbiology 2:17037
6. Akey DL, Brown WC, Dutta S, Konwerski J, Jose J, Jurkiw TJ, DelProposto J, Ogata CM, Skiniotis G, Kuhn RJ, Smith JL (2014) Flavivirus NS1 structures reveal surfaces for associations with membranes and the immune system. Science (New York, NY) 343:881-885
7. Aktepe TE, Mackenzie JM (2018) Shaping the flavivirus replication complex: It is curvaceous! Cellular microbiology 20:e12884
8. Akter R, Naish S, Gatton M, Bambrick H, Hu W, Tong S (2019) Spatial and temporal analysis of dengue infections in Queensland, Australia: Recent trend and perspectives. PLoS One 14:e0220134
9. Anfasa F, Siegers JY, van der Kroeg M, Mumtaz N, Stalin Raj V, de Vrij FMS, Widagdo W, Gabriel G, Salinas S, Simonin Y, Reusken C, Kushner SA, Koopmans MPG, Haagmans B, Martina BEE, van Riel D (2017) Phenotypic Differences between Asian and African Lineage Zika Viruses in Human Neural Progenitor Cells. mSphere 2
10. Angleró-Rodríguez YI, Pantoja P, Sariol CA (2014) Dengue virus subverts the interferon induction pathway via NS2B/3 protease-IκB kinase epsilon interaction. Clin Vaccine Immunol 21:29-38
11. Ank N, Paludan SR (2009) Type III IFNs: new layers of complexity in innate antiviral immunity. BioFactors (Oxford, England) 35:82-87
12. Araya CL, Fowler DM (2011) Deep mutational scanning: assessing protein function on a massive scale. Trends in biotechnology 29:435-442
13. Arimoto KI, Lochte S, Stoner SA, Burkart C, Zhang Y, Miyauchi S, Wilmes S, Fan JB, Heinisch JJ, Li Z, Yan M, Pellegrini S, Colland F, Piehler J, Zhang DE (2017) STAT2 is an

essential adaptor in USP18-mediated suppression of type I interferon signaling. Nature structural & molecular biology 24:279-289
14. Arimoto KI, Miyauchi S, Stoner SA, Fan JB, Zhang DE (2018) Negative regulation of type I IFN signaling. Journal of leukocyte biology
15. Arjona A, Ledizet M, Anthony K, Bonafe N, Modis Y, Town T, Fikrig E (2007) West Nile virus envelope protein inhibits dsRNA-induced innate immune responses. Journal of immunology (Baltimore, Md : 1950) 179:8403-8409
16. Ashour J, Laurent-Rolle M, Shi PY, Garcia-Sastre A (2009) NS5 of dengue virus mediates STAT2 binding and degradation. Journal of virology 83:5408-5418
17. Aubry F, Nougairède A, Gould EA, de Lamballerie X (2015) Flavivirus reverse genetic systems, construction techniques and applications: A historical perspective. Antiviral Research 114:67-85
18. Avila-Perez G, Nogales A, Park JG, Vasquez DM, Dean DA, Barravecchia M, Perez DR, Almazan F, Martinez-Sobrido L (2020) In vivo rescue of recombinant Zika virus from an infectious cDNA clone and its implications in vaccine development. Scientific reports 10:512
19. Bailey CC, Zhong G, Huang IC, Farzan M (2014) IFITM-Family Proteins: The Cell's First Line of Antiviral Defense. Annual review of virology 1:261-283
20. Barzon L, Percivalle E, Pacenti M, Rovida F, Zavattoni M, Del Bravo P, Cattelan AM, Palu G, Baldanti F (2018) Virus and Antibody Dynamics in Travelers With Acute Zika Virus Infection. Clinical infectious diseases : an official publication of the Infectious Diseases Society of America 66:1173-1180
21. Bayer A, Lennemann NJ, Ouyang Y, Bramley JC, Morosky S, Marques ET, Jr., Cherry S, Sadovsky Y, Coyne CB (2016) Type III Interferons Produced by Human Placental Trophoblasts Confer Protection against Zika Virus Infection. Cell host & microbe 19:705-712
22. Beauverd Y, Radia D, Cargo C, Knapper S, Drummond M, Pillai A, Harrison C, Robinson S (2016) Pegylated interferon alpha-2a for essential thrombocythemia during pregnancy: outcome and safety. A case series. Haematologica 101:e182-e184
23. Best SM (2016) Flaviviruses. Current biology : CB 26:R1258-r1260
24. Bhamarapravati N, Tuchinda P, Boonyapaknavik V (1967) Pathology of Thailand haemorrhagic fever: a study of 100 autopsy cases. Annals of tropical medicine and parasitology 61:500-510
25. Bhatnagar J, Rabeneck DB, Martines RB, Reagan-Steiner S, Ermias Y, Estetter LB, Suzuki T, Ritter J, Keating MK, Hale G, Gary J, Muehlenbachs A, Lambert A, Lanciotti R, Oduyebo T, Meaney-Delman D, Bolanos F, Saad EA, Shieh WJ, Zaki SR (2017) Zika Virus RNA Replication and Persistence in Brain and Placental Tissue. Emerging infectious diseases 23:405-414
26. Blight KJ, McKeating JA, Rice CM (2002) Highly permissive cell lines for subgenomic and genomic hepatitis C virus RNA replication. Journal of virology 76:13001-13014
27. Blumer T, Coto-Llerena M, Duong FHT, Heim MH (2017) SOCS1 is an inducible negative regulator of interferon lambda (IFN-lambda)-induced gene expression in vivo. The Journal of biological chemistry 292:17928-17938
28. Bolen CR, Ding S, Robek MD, Kleinstein SH (2014) Dynamic expression profiling of type I and type III interferon-stimulated hepatocytes reveals a stable hierarchy of gene expression. Hepatology (Baltimore, Md) 59:1262-1272

29. Bollati M, Alvarez K, Assenberg R, Baronti C, Canard B, Cook S, Coutard B, Decroly E, de Lamballerie X, Gould EA, Grard G, Grimes JM, Hilgenfeld R, Jansson AM, Malet H, Mancini EJ, Mastrangelo E, Mattevi A, Milani M, Moureau G, Neyts J, Owens RJ, Ren J, Selisko B, Speroni S, Steuber H, Stuart DI, Unge T, Bolognesi M (2010) Structure and functionality in flavivirus NS-proteins: perspectives for drug design. Antiviral Res 87:125-148
30. Boyer J-C, Haenni A-L (1994) Infectious Transcripts and cDNA Clones of RNA Viruses. Virology 198:415-426
31. Brinton MA, Basu M (2015) Functions of the 3' and 5' genome RNA regions of members of the genus Flavivirus. Virus research 206:108-119
32. Broggi A, Granucci F, Zanoni I (2019) Type III interferons: Balancing tissue tolerance and resistance to pathogen invasion. The Journal of Experimental Medicine 217
33. Brooks RB, Carlos MP, Myers RA, White MG, Bobo-Lenoci T, Aplan D, Blythe D, Feldman KA (2016) Likely Sexual Transmission of Zika Virus from a Man with No Symptoms of Infection - Maryland, 2016. MMWR Morbidity and mortality weekly report 65:915-916
34. Burkart C, Arimoto K-i, Tang T, Cong X, Xiao N, Liu Y-C, Kotenko SV, Ellies LG, Zhang D-E (2013) Usp18 deficient mammary epithelial cells create an antitumour environment driven by hypersensitivity to IFN-λ and elevated secretion of Cxcl10. EMBO molecular medicine 5:1035-1050
35. Bustos-Arriaga J, Gromowski GD, Tsetsarkin KA, Firestone CY, Castro-Jimenez T, Pletnev AG, Cedillo-Barron L, Whitehead SS (2018) Decreased accumulation of subgenomic RNA in human cells infected with vaccine candidate DEN4Delta30 increases viral susceptibility to type I interferon. Vaccine 36:3460-3467
36. Caine EA, Scheaffer SM, Arora N, Zaitsev K, Artyomov MN, Coyne CB, Moley KH, Diamond MS (2019) Interferon lambda protects the female reproductive tract against Zika virus infection. Nature communications 10:280
37. Calvet G, Aguiar RS, Melo AS, Sampaio SA, de Filippis I, Fabri A, Araujo ES, de Sequeira PC, de Mendonca MC, de Oliveira L, Tschoeke DA, Schrago CG, Thompson FL, Brasil P, Dos Santos FB, Nogueira RM, Tanuri A, de Filippis AM (2016) Detection and sequencing of Zika virus from amniotic fluid of fetuses with microcephaly in Brazil: a case study. The Lancet Infectious diseases 16:653-660
38. Campos GS, Bandeira AC, Sardi SI (2015) Zika Virus Outbreak, Bahia, Brazil. Emerging infectious diseases 21:1885-1886
39. Cao-Lormeau VM, Roche C, Teissier A, Robin E, Berry AL, Mallet HP, Sall AA, Musso D (2014) Zika virus, French polynesia, South pacific, 2013. Emerging infectious diseases 20:1085-1086
40. Cao-Lormeau VM, Blake A, Mons S, Lastere S, Roche C, Vanhomwegen J, Dub T, Baudouin L, Teissier A, Larre P, Vial AL, Decam C, Choumet V, Halstead SK, Willison HJ, Musset L, Manuguerra JC, Despres P, Fournier E, Mallet HP, Musso D, Fontanet A, Neil J, Ghawche F (2016) Guillain-Barre Syndrome outbreak associated with Zika virus infection in French Polynesia: a case-control study. Lancet (London, England) 387:1531-1539
41. Carroll T, Lo M, Lanteri M, Dutra J, Zarbock K, Silveira P, Rourke T, Ma Z-m, Fritts L, O'Connor S, Busch M, Miller CJ (2017) Zika virus preferentially replicates in the female reproductive tract after vaginal inoculation of rhesus macaques. PLoS Pathogens 13:e1006537

42. Carthew RW, Sontheimer EJ (2009) Origins and Mechanisms of miRNAs and siRNAs. Cell 136:642-655
43. Catteau A, Roué G, Yuste VJ, Susin SA, Desprès P (2003) Expression of dengue ApoptoM sequence results in disruption of mitochondrial potential and caspase activation. Biochimie 85:789-793
44. Chan YK, Gack MU (2016) A phosphomimetic-based mechanism of dengue virus to antagonize innate immunity. Nature immunology 17:523-530
45. Chang HH, Huber RG, Bond PJ, Grad YH, Camerini D, Maurer-Stroh S, Lipsitch M (2017) Systematic analysis of protein identity between Zika virus and other arthropod-borne viruses. Bulletin of the World Health Organization 95:517-525i
46. Chen HW, Chen JJ, Tzeng CR, Li HN, Chang SJ, Cheng YF, Chang CW, Wang RS, Yang PC, Lee YT (2002) Global analysis of differentially expressed genes in early gestational decidua and chorionic villi using a 9600 human cDNA microarray. Molecular human reproduction 8:475-484
47. Chen J, Yang YF, Yang Y, Zou P, Chen J, He Y, Shui SL, Cui YR, Bai R, Liang YJ, Hu Y, Jiang B, Lu L, Zhang X, Liu J, Xu J (2018) AXL promotes Zika virus infection in astrocytes by antagonizing type I interferon signalling. Nature microbiology
48. Chen LH, Hamer DH (2018) Zika virus and sexual transmission: updated preconception guidance. Journal of Travel Medicine 25
49. Chen Y, Liu T, Zhang Z, Chen M, Rong L, Ma L, Yu B, Wu, Zhang P, Zhu X, Huang X, Zhang H, Li YP (2018) Novel genetically stable infectious clone for a Zika virus clinical isolate and identification of RNA elements essential for virus production. Virus research
50. Chiriac MT, Buchen B, Wandersee A, Hundorfean G, Günther C, Bourjau Y, Doyle SE, Frey B, Ekici AB, Büttner C, Weigmann B, Atreya R, Wirtz S, Becker C, Siebler J, Neurath MF (2017) Activation of Epithelial Signal Transducer and Activator of Transcription 1 by Interleukin 28 Controls Mucosal Healing in Mice With Colitis and Is Increased in Mucosa of Patients With Inflammatory Bowel Disease. Gastroenterology 153:123-138.e128
51. Clarke BD, Roby JA, Slonchak A, Khromykh AA (2015) Functional non-coding RNAs derived from the flavivirus 3' untranslated region. Virus research 206:53-61
52. Coldbeck-Shackley RC, Eyre NS, Beard MR (2020) The Molecular Interactions of ZIKV and DENV with the Type-I IFN Response. Vaccines 8
53. Contreras-Capetillo SN, Valadez-Gonzalez N, Manrique-Saide P, Carcano-Castillo RE, Pacheco-Tugores F, Barrera-Perez HAM, Pinto-Escalante D, Lliteras-Cardin M, Hoil-Parra JA, Caceres-Solis JL, Pavia-Ruz N (2018) Birth Defects Associated With Congenital Zika Virus Infection in Mexico. Clinical pediatrics 57:927-936
54. Control E-ECfDPa (2015) Zika virus epidemic in the Americas: potential association with microcephaly and Guillain-Barré syndrome.
55. Control ECfDPa (2019) Sexual transmission of dengue in Spain.
56. Coronel-Ruiz C, Gutierrez-Barbosa H, Medina-Moreno S, Velandia-Romero ML, Chua JV, Castellanos JE, Zapata JC (2020) Humanized Mice in Dengue Research: A Comparison with Other Mouse Models. Vaccines 8
57. Corry J, Arora N, Good CA, Sadovsky Y, Coyne CB (2017) Organotypic models of type III interferon-mediated protection from Zika virus infections at the maternal–fetal interface. Proceedings of the National Academy of Sciences

58. Cortese M, Goellner S, Acosta EG, Neufeldt CJ, Oleksiuk O, Lampe M, Haselmann U, Funaya C, Schieber N, Ronchi P, Schorb M, Pruunsild P, Schwab Y, Chatel-Chaix L, Ruggieri A, Bartenschlager R (2017) Ultrastructural Characterization of Zika Virus Replication Factories. Cell reports 18:2113-2123
59. Crow YJ, Manel N (2015) Aicardi–Goutières syndrome and the type I interferonopathies. Nature Reviews Immunology 15:429
60. Cugola FR, Fernandes IR, Russo FB, Freitas BC, Dias JL, Guimaraes KP, Benazzato C, Almeida N, Pignatari GC, Romero S, Polonio CM, Cunha I, Freitas CL, Brandao WN, Rossato C, Andrade DG, Faria Dde P, Garcez AT, Buchpigel CA, Braconi CT, Mendes E, Sall AA, Zanotto PM, Peron JP, Muotri AR, Beltrao-Braga PC (2016) The Brazilian Zika virus strain causes birth defects in experimental models. Nature 534:267-271
61. Cumming HE, Bourke NM (2018) Type I IFNs in the female reproductive tract: The first line of defense in an ever-changing battleground. Journal of leukocyte biology
62. Cumming HE, Bourke NM (2018) Type I IFNs in the female reproductive tract: The first line of defense in an ever-changing battleground. Journal of leukocyte biology 0
63. da Cruz TE, Souza RP, Pelloso SM, Morelli F, Suehiro TT, Damke E, Bonfim-Mendonca PS, da Silva VRS, Consolaro MEL (2019) Case Reports: Prolonged Detection of Zika Virus RNA in Vaginal and Endocervical Samples from a Brazilian Woman, 2018. The American journal of tropical medicine and hygiene 100:183-186
64. Dai J, Pan W, Wang P (2011) ISG15 facilitates cellular antiviral response to dengue and west nile virus infection in vitro. Virology journal 8:468-468
65. Dalrymple NA, Cimica V, Mackow ER (2015) Dengue Virus NS Proteins Inhibit RIG-I/MAVS Signaling by Blocking TBK1/IRF3 Phosphorylation: Dengue Virus Serotype 1 NS4A Is a Unique Interferon-Regulating Virulence Determinant. mBio 6:e00553-00515
66. Davidson S, McCabe TM, Crotta S, Gad HH, Hessel EM, Beinke S, Hartmann R, Wack A (2016) IFNlambda is a potent anti-influenza therapeutic without the inflammatory side effects of IFNalpha treatment. EMBO molecular medicine 8:1099-1112
67. de Borba L, Villordo SM, Iglesias NG, Filomatori CV, Gebhard LG, Gamarnik AV (2015) Overlapping local and long-range RNA-RNA interactions modulate dengue virus genome cyclization and replication. Journal of virology 89:3430-3437
68. de Borba L, Villordo SM, Marsico FL, Carballeda JM, Filomatori CV, Gebhard LG, Pallarés HM, Lequime S, Lambrechts L, Sánchez Vargas I, Blair CD, Gamarnik AV (2019) RNA Structure Duplication in the Dengue Virus 3' UTR: Redundancy or Host Specificity? mBio 10:e02506-02518
69. de Paula Freitas B, de Oliveira Dias JR, Prazeres J, Sacramento GA, Ko AI, Maia M, Belfort R, Jr. (2016) Ocular Findings in Infants With Microcephaly Associated With Presumed Zika Virus Congenital Infection in Salvador, Brazil. JAMA ophthalmology 134:529-535
70. de Weerd NA, Nguyen T (2012) The interferons and their receptors--distribution and regulation. Immunology and cell biology 90:483-491
71. de Weerd NA, Vivian JP, Nguyen TK, Mangan NE, Gould JA, Braniff SJ, Zaker-Tabrizi L, Fung KY, Forster SC, Beddoe T, Reid HH, Rossjohn J, Hertzog PJ (2013) Structural basis of a unique interferon-beta signaling axis mediated via the receptor IFNAR1. Nature immunology 14:901-907
72. Delorme-Axford E, Sadovsky Y, Coyne CB (2014) The Placenta as a Barrier to Viral Infections. Annual review of virology 1:133-146

73. Demers A, Kang G, Ma F, Lu W, Yuan Z, Li Y, Lewis M, Kraiselburd EN, Montaner L, Li Q (2014) The mucosal expression pattern of interferon-epsilon in rhesus macaques. Journal of leukocyte biology 96:1101-1107
74. Deng C-L, Zhang Q-Y, Chen D-D, Liu S-Q, Qin C-F, Zhang B, Ye H-Q (2017) Recovery of the Zika virus through an in vitro ligation approach. Journal of General Virology 98:1739-1743
75. Diamond MS, Roberts TG, Edgil D, Lu B, Ernst J, Harris E (2000) Modulation of Dengue Virus Infection in Human Cells by Alpha, Beta, and Gamma Interferons. Journal of virology 74:4957-4966
76. Diamond MS, Pierson TC (2015) Molecular Insight into Dengue Virus Pathogenesis and Its Implications for Disease Control. Cell 162:488-492
77. Diner BA, Lum KK, Toettcher JE, Cristea IM (2016) Viral DNA Sensors IFI16 and Cyclic GMP-AMP Synthase Possess Distinct Functions in Regulating Viral Gene Expression, Immune Defenses, and Apoptotic Responses during Herpesvirus Infection. mBio 7:e01553-01516
78. Ding Q, Gaska JM, Douam F, Wei L, Kim D, Balev M, Heller B, Ploss A (2018) Species-specific disruption of STING-dependent antiviral cellular defenses by the Zika virus NS2B3 protease. Proceedings of the National Academy of Sciences of the United States of America 115:E6310-e6318
79. Dixit E, Boulant S, Zhang Y, Lee ASY, Odendall C, Shum B, Hacohen N, Chen ZJ, Whelan SP, Fransen M, Nibert ML, Superti-Furga G, Kagan JC (2010) Peroxisomes are signaling platforms for antiviral innate immunity. Cell 141:668-681
80. do Rosario MS, de Jesus PA, Vasilakis N, Farias DS, Novaes MA, Rodrigues SG, Martins LC, Vasconcelos PF, Ko AI, Alcantara LC, de Siqueira IC (2016) Guillain-Barre Syndrome After Zika Virus Infection in Brazil. The American journal of tropical medicine and hygiene 95:1157-1160
81. Domanski P, Fish E, Nadeau OW, Witte M, Platanias LC, Yan H, Krolewski J, Pitha P, Colamonici OR (1997) A region of the beta subunit of the interferon alpha receptor different from box 1 interacts with Jak1 and is sufficient to activate the Jak-Stat pathway and induce an antiviral state. The Journal of biological chemistry 272:26388-26393
82. Donald CL, Brennan B, Cumberworth SL, Rezelj VV, Clark JJ, Cordeiro MT, Freitas de Oliveira Franca R, Pena LJ, Wilkie GS, Da Silva Filipe A, Davis C, Hughes J, Varjak M, Selinger M, Zuvanov L, Owsianka AM, Patel AH, McLauchlan J, Lindenbach BD, Fall G, Sall AA, Biek R, Rehwinkel J, Schnettler E, Kohl A (2016) Full Genome Sequence and sfRNA Interferon Antagonist Activity of Zika Virus from Recife, Brazil. PLoS neglected tropical diseases 10:e0005048
83. Dong H, Chang DC, Xie X, Toh YX, Chung KY, Zou G, Lescar J, Lim SP, Shi PY (2010) Biochemical and genetic characterization of dengue virus methyltransferase. Virology 405:568-578
84. Du Y, Xin L, Shi Y, Zhang TH, Wu NC, Dai L, Gong D, Brar G, Shu S, Luo J, Reiley W, Tseng YW, Bai H, Wu TT, Wang J, Shu Y, Sun R (2018) Genome-wide identification of interferon-sensitive mutations enables influenza vaccine design. Science (New York, NY) 359:290-296
85. DuBridge RB, Tang P, Hsia HC, Leong PM, Miller JH, Calos MP (1987) Analysis of mutation in human cells by using an Epstein-Barr virus shuttle system. Molecular and cellular biology 7:379-387

86. Duffy MR, Chen TH, Hancock WT, Powers AM, Kool JL, Lanciotti RS, Pretrick M, Marfel M, Holzbauer S, Dubray C, Guillaumot L, Griggs A, Bel M, Lambert AJ, Laven J, Kosoy O, Panella A, Biggerstaff BJ, Fischer M, Hayes EB (2009) Zika virus outbreak on Yap Island, Federated States of Micronesia. The New England journal of medicine 360:2536-2543
87. Duggal NK, Ritter JM, Pestorius SE, Zaki SR, Davis BS, Chang G-JJ, Bowen RA, Brault AC (2017) Frequent Zika Virus Sexual Transmission and Prolonged Viral RNA Shedding in an Immunodeficient Mouse Model. Cell reports 18:1751-1760
88. Duggal NK, McDonald EM, Ritter JM, Brault AC (2018) Sexual transmission of Zika virus enhances in utero transmission in a mouse model. Scientific reports 8:4510
89. Dukhovny A, Lamkiewicz K, Chen Q, Fricke M, Jabrane-Ferrat N, Marz M, Jung JU, Sklan EH (2019) A CRISPR activation screen identifies genes protecting from Zika virus infection. Journal of virology
90. Duong V, Lambrechts L, Paul RE, Ly S, Lay RS, Long KC, Huy R, Tarantola A, Scott TW, Sakuntabhai A, Buchy P (2015) Asymptomatic humans transmit dengue virus to mosquitoes. Proceedings of the National Academy of Sciences of the United States of America 112:14688-14693
91. Edwards DP (2005) Regulation of signal transduction pathways by estrogen and progesterone. Annual review of physiology 67:335-376
92. El Costa H, Gouilly J, Mansuy J-M, Chen Q, Levy C, Cartron G, Veas F, Al-Daccak R, Izopet J, Jabrane-Ferrat N (2016) ZIKA virus reveals broad tissue and cell tropism during the first trimester of pregnancy. Scientific reports 6:35296
93. Esser-Nobis K, Aarreberg LD, Roby JA, Fairgrieve MR, Green R, Gale M, Jr. (2019) Comparative analysis of African and Asian lineage-derived Zika Virus strains reveals differences in activation of and sensitivity to antiviral innate immunity. Journal of virology
94. Eyre NS, Johnson SM, Eltahla AA, Aloi M, Aloia AL, McDevitt CA, Bull RA, Beard MR (2017) Genome-wide mutagenesis of dengue virus reveals plasticity of the NS1 protein and enables generation of infectious tagged reporter viruses. Journal of virology
95. Fan W, Xie S, Zhao X, Li N, Chang C, Li L, Yu G, Chi X, Pan Y, Niu J, Zhong J, Sun B (2016) IFN-lambda4 desensitizes the response to IFN-alpha treatment in chronic hepatitis C through long-term induction of USP18. The Journal of general virology 97:2210-2220
96. Fichorova RN, Rheinwald JG, Anderson DJ (1997) Generation of papillomavirus-immortalized cell lines from normal human ectocervical, endocervical, and vaginal epithelium that maintain expression of tissue-specific differentiation proteins. Biol Reprod 57:847-855
97. Fontes-Garfias CR, Shan C, Luo H, Muruato AE, Medeiros DBA, Mays E, Xie X, Zou J, Roundy CM, Wakamiya M, Rossi SL, Wang T, Weaver SC, Shi P-Y (2017) Functional Analysis of Glycosylation of Zika Virus Envelope Protein. Cell reports 21:1180-1190
98. Forero A, Ozarkar S, Li H, Lee CH, Hemann EA, Nadjsombati MS, Hendricks MR, So L, Green R, Roy CN, Sarkar SN, von Moltke J, Anderson SK, Gale M, Jr., Savan R (2019) Differential Activation of the Transcription Factor IRF1 Underlies the Distinct Immune Responses Elicited by Type I and Type III Interferons. Immunity
99. Francois-Newton V, Magno de Freitas Almeida G, Payelle-Brogard B, Monneron D, Pichard-Garcia L, Piehler J, Pellegrini S, Uze G (2011) USP18-based negative feedback

control is induced by type I and type III interferons and specifically inactivates interferon alpha response. PLoS One 6:e22200
100. Francois-Newton V, Livingstone M, Payelle-Brogard B, Uze G, Pellegrini S (2012) USP18 establishes the transcriptional and anti-proliferative interferon alpha/beta differential. The Biochemical journal 446:509-516
101. Freour T, Mirallie S, Hubert B, Splingart C, Barriere P, Maquart M, Leparc-Goffart I (2016) Sexual transmission of Zika virus in an entirely asymptomatic couple returning from a Zika epidemic area, France, April 2016. Euro surveillance : bulletin Europeen sur les maladies transmissibles = European communicable disease bulletin 21
102. Froissart R, Wilke CO, Montville R, Remold SK, Chao L, Turner PE (2004) Co-infection weakens selection against epistatic mutations in RNA viruses. Genetics 168:9-19
103. Fulton BO, Sachs D, Beaty SM, Won ST, Lee B, Palese P, Heaton NS (2015) Mutational Analysis of Measles Virus Suggests Constraints on Antigenic Variation of the Glycoproteins. Cell reports 11:1331-1338
104. Fulton BO, Sachs D, Schwarz MC, Palese P, Evans MJ (2017) Transposon mutagenesis of the Zika virus genome highlights regions essential for RNA replication and restricted for immune evasion. Journal of virology
105. Fung KY, Mangan NE, Cumming H, Horvat JC, Mayall JR, Stifter SA, De Weerd N, Roisman LC, Rossjohn J, Robertson SA, Schjenken JE, Parker B, Gargett CE, Nguyen HP, Carr DJ, Hansbro PM, Hertzog PJ (2013) Interferon-epsilon protects the female reproductive tract from viral and bacterial infection. Science (New York, NY) 339:1088-1092
106. Funk A, Truong K, Nagasaki T, Torres S, Floden N, Balmori Melian E, Edmonds J, Dong H, Shi P-Y, Khromykh AA (2010) RNA structures required for production of subgenomic flavivirus RNA. Journal of virology 84:11407-11417
107. Furusyo N, Hayashi J, Ohmiya M, Sawayama Y, Kawakami Y, Ariyama I, Kinukawa N, Kashiwagi S (1999) Differences between interferon-alpha and -beta treatment for patients with chronic hepatitis C virus infection. Digestive diseases and sciences 44:608-617
108. Gack MU, Diamond MS (2016) Innate immune escape by Dengue and West Nile viruses. Current opinion in virology 20:119-128
109. Gao H, Feldman MW (2009) Complementation and epistasis in viral coinfection dynamics. Genetics 182:251-263
110. Garcia-Minambres A, Eid SG, Mangan NE, Pade C, Lim SS, Matthews AY, de Weerd NA, Hertzog PJ, Mak J (2017) Interferon epsilon promotes HIV restriction at multiple steps of viral replication. Immunology and cell biology 95:478-483
111. Ghosh M, Shen Z, Fahey JV, Crist SG, Patel M, Smith JM, Wira CR (2013) Pathogen recognition in the human female reproductive tract: expression of intracellular cytosolic sensors NOD1, NOD2, RIG-1, and MDA5 and response to HIV-1 and Neisseria gonorrhea. American journal of reproductive immunology (New York, NY : 1989) 69:41-51
112. Giron S, Franke F, Decoppet A, Cadiou B, Travaglini T, Thirion L, Durand G, Jeannin C, L'Ambert G, Grard G, Noel H, Fournet N, Auzet-Caillaud M, Zandotti C, Aboukais S, Chaud P, Guedj S, Hamouda L, Naudot X, Ovize A, Lazarus C, de Valk H, Paty MC, Leparc-Goffart I (2019) Vector-borne transmission of Zika virus in Europe, southern France, August 2019. Euro surveillance : bulletin Europeen sur les maladies transmissibles = European communicable disease bulletin 24

113. Goel RR, Wang X, O'Neil LJ, Nakabo S, Hasneen K, Gupta S, Wigerblad G, Blanco LP, Kopp JB, Morasso MI, Kotenko SV, Yu ZX, Carmona-Rivera C, Kaplan MJ (2020) Interferon lambda promotes immune dysregulation and tissue inflammation in TLR7-induced lupus. Proceedings of the National Academy of Sciences of the United States of America 117:5409-5419
114. Goertz GP, Abbo SR, Fros JJ, Pijlman GP (2018) Functional RNA during Zika virus infection. Virus research 254:41-53
115. Gorman MJ, Caine EA, Zaitsev K, Begley MC, Weger-Lucarelli J, Uccellini MB, Tripathi S, Morrison J, Yount BL, Dinnon KH, 3rd, Ruckert C, Young MC, Zhu Z, Robertson SJ, McNally KL, Ye J, Cao B, Mysorekar IU, Ebel GD, Baric RS, Best SM, Artyomov MN, Garcia-Sastre A, Diamond MS (2018) An Immunocompetent Mouse Model of Zika Virus Infection. Cell host & microbe 23:672-685.e676
116. Gough DJ, Messina NL, Hii L, Gould JA, Sabapathy K, Robertson AP, Trapani JA, Levy DE, Hertzog PJ, Clarke CJ, Johnstone RW (2010) Functional crosstalk between type I and II interferon through the regulated expression of STAT1. PLoS biology 8:e1000361
117. Gough DJ, Messina NL, Clarke CJP, Johnstone RW, Levy DE (2012) Constitutive type I interferon modulates homeostatic balance through tonic signaling. Immunity 36:166-174
118. Gould EA, Solomon T (2008) Pathogenic flaviviruses. Lancet (London, England) 371:500-509
119. Gould EA, Higgs S (2009) Impact of climate change and other factors on emerging arbovirus diseases. Transactions of the Royal Society of Tropical Medicine and Hygiene 103:109-121
120. Graham CH, Hawley TS, Hawley RG, MacDougall JR, Kerbel RS, Khoo N, Lala PK (1993) Establishment and characterization of first trimester human trophoblast cells with extended lifespan. Experimental cell research 206:204-211
121. Grant A, Ponia SS, Tripathi S, Balasubramaniam V, Miorin L, Sourisseau M, Schwarz MC, Sanchez-Seco MP, Evans MJ, Best SM, Garcia-Sastre A (2016) Zika Virus Targets Human STAT2 to Inhibit Type I Interferon Signaling. Cell host & microbe 19:882-890
122. Green AM, Beatty PR, Hadjilaou A, Harris E (2014) Innate immunity to dengue virus infection and subversion of antiviral responses. Journal of molecular biology 426:1148-1160
123. Green B, Bouchier C, Fairhead C, Craig NL, Cormack BP (2012) Insertion site preference of Mu, Tn5, and Tn7 transposons. Mobile DNA 3:3
124. Grischott F, Puhan M, Hatz C, Schlagenhauf P (2016) Non-vector-borne transmission of Zika virus: A systematic review. Travel medicine and infectious disease 14:313-330
125. Gubler DJ (2012) The economic burden of dengue. The American journal of tropical medicine and hygiene 86:743-744
126. Guzman MG, Halstead SB, Artsob H, Buchy P, Farrar J, Gubler DJ, Hunsperger E, Kroeger A, Margolis HS, Martinez E, Nathan MB, Pelegrino JL, Simmons C, Yoksan S, Peeling RW (2010) Dengue: a continuing global threat. Nature reviews Microbiology 8:S7-16
127. Guzman MG, Harris E (2015) Dengue. Lancet (London, England) 385:453-465
128. Halstead SB (2007) Dengue. Lancet (London, England) 370:1644-1652
129. Hamel R, Dejarnac O, Wichit S, Ekchariyawat P, Neyret A, Luplertlop N, Perera-Lecoin M, Surasombatpattana P, Talignani L, Thomas F, Cao-Lormeau VM, Choumet V,

Briant L, Despres P, Amara A, Yssel H, Misse D (2015) Biology of Zika Virus Infection in Human Skin Cells. Journal of virology 89:8880-8896
130. Hammond SN, Balmaseda A, Perez L, Tellez Y, Saborio SI, Mercado JC, Videa E, Rodriguez Y, Perez MA, Cuadra R, Solano S, Rocha J, Idiaquez W, Gonzalez A, Harris E (2005) Differences in dengue severity in infants, children, and adults in a 3-year hospital-based study in Nicaragua. The American journal of tropical medicine and hygiene 73:1063-1070
131. Han Y, Li R, Gao J, Miao S, Wang L (2012) Characterisation of human RING finger protein TRIM69, a novel testis E3 ubiquitin ligase and its subcellular localisation. Biochem Biophys Res Commun 429:6-11
132. Hanck T, Stricker R, Sedehizade F, Reiser G (2004) Identification of gene structure and subcellular localization of human centaurin alpha 2, and p42IP4, a family of two highly homologous, Ins 1,3,4,5-P4-/PtdIns 3,4,5-P3-binding, adapter proteins. Journal of neurochemistry 88:326-336
133. Hardy MP, Owczarek CM, Jermiin LS, Ejdeback M, Hertzog PJ (2004) Characterization of the type I interferon locus and identification of novel genes. Genomics 84:331-345
134. Harris BD, Schreiter J, Chevrier M, Jordan JL, Walter MR (2018) Human interferon- and interferon-kappa exhibit low potency and low affinity for cell-surface IFNAR and the poxvirus antagonist B18R. The Journal of biological chemistry 293:16057-16068
135. Hart KM, Murphy AJ, Barrett KT, Wira CR, Guyre PM, Pioli PA (2009) Functional expression of pattern recognition receptors in tissues of the human female reproductive tract. J Reprod Immunol 80:33-40
136. Hasan S, Jamdar SF, Alalowi M, Al Ageel Al Beaiji SM (2016) Dengue virus: A global human threat: Review of literature. Journal of International Society of Preventive & Community Dentistry 6:1-6
137. Hastings AK, Yockey LJ, Jagger BW, Hwang J, Uraki R, Gaitsch HF, Parnell LA, Cao B, Mysorekar IU, Rothlin CV, Fikrig E, Diamond MS, Iwasaki A (2017) TAM Receptors Are Not Required for Zika Virus Infection in Mice. Cell reports 19:558-568
138. Hayashida E, Ling ZL, Ashhurst TM, Viengkhou B, Jung SR, Songkhunawej P, West PK, King NJC, Hofer MJ (2019) Zika virus encephalitis in immunocompetent mice is dominated by innate immune cells and does not require T or B cells. J Neuroinflammation 16:177
139. Heaton NS, Sachs D, Chen CJ, Hai R, Palese P (2013) Genome-wide mutagenesis of influenza virus reveals unique plasticity of the hemagglutinin and NS1 proteins. Proceedings of the National Academy of Sciences of the United States of America 110:20248-20253
140. Helbig KJ, Eyre NS, Yip E, Narayana S, Li K, Fiches G, McCartney EM, Jangra RK, Lemon SM, Beard MR (2011) The antiviral protein viperin inhibits hepatitis C virus replication via interaction with nonstructural protein 5A. Hepatology (Baltimore, Md) 54:1506-1517
141. Helbig KJ, Carr JM, Calvert JK, Wati S, Clarke JN, Eyre NS, Narayana SK, Fiches GN, McCartney EM, Beard MR (2013) Viperin is induced following dengue virus type-2 (DENV-2) infection and has anti-viral actions requiring the C-terminal end of viperin. PLoS neglected tropical diseases 7:e2178-e2178
142. Helbig KJ, Beard MR (2014) The role of viperin in the innate antiviral response. J Mol Biol 426:1210-1219

143. Hemann EA, Gale M, Jr., Savan R (2017) Interferon Lambda Genetics and Biology in Regulation of Viral Control. Frontiers in immunology 8:1707
144. Hennessey M, Fischer M, Staples JE (2016) Zika Virus Spreads to New Areas - Region of the Americas, May 2015-January 2016. MMWR Morbidity and mortality weekly report 65:55-58
145. Hermant P, Francius C, Clotman F, Michiels T (2013) IFN-epsilon is constitutively expressed by cells of the reproductive tract and is inefficiently secreted by fibroblasts and cell lines. PLoS One 8:e71320
146. Hertzog J, Dias Junior AG, Rigby RE, Donald CL, Mayer A, Sezgin E, Song C, Jin B, Hublitz P, Eggeling C, Kohl A, Rehwinkel J (2018) Infection with a Brazilian isolate of Zika virus generates RIG-I stimulatory RNA and the viral NS5 protein blocks type I IFN induction and signalling. European journal of immunology
147. Hertzog PJ, Williams BRG (2013) Fine tuning type I interferon responses. Cytokine & Growth Factor Reviews 24:217-225
148. Hilgenfeld R (2016) Zika virus NS1, a pathogenicity factor with many faces. The EMBO journal 35:2631-2633
149. Hoenen A, Liu W, Kochs G, Khromykh AA, Mackenzie JM (2007) West Nile virus-induced cytoplasmic membrane structures provide partial protection against the interferon-induced antiviral MxA protein. The Journal of general virology 88:3013-3017
150. Holmes EC, Twiddy SS (2003) The origin, emergence and evolutionary genetics of dengue virus. Infection, genetics and evolution : journal of molecular epidemiology and evolutionary genetics in infectious diseases 3:19-28
151. Hong SW, Jiang Y, Kim S, Li CJ, Lee D-k (2014) Target gene abundance contributes to the efficiency of siRNA-mediated gene silencing. Nucleic Acid Ther 24:192-198
152. Hu Y, Dong X, He Z, Wu Y, Zhang S, Lin J, Yang Y, Chen J, An S, Yin Y, Shen Z, Zeng G, Tian H, Cai J, Yang Y, Guan H, Wu J, Li M, Zhu X (2019) Zika virus antagonizes interferon response in patients and disrupts RIG-I-MAVS interaction through its CARD-TM domains. Cell & bioscience 9:46
153. Huang WC, Abraham R, Shim BS, Choe H, Page DT (2016) Zika virus infection during the period of maximal brain growth causes microcephaly and corticospinal neuron apoptosis in wild type mice. Scientific reports 6:34793
154. Huijbregts RP, Helton ES, Michel KG, Sabbaj S, Richter HE, Goepfert PA, Hel Z (2013) Hormonal contraception and HIV-1 infection: medroxyprogesterone acetate suppresses innate and adaptive immune mechanisms. Endocrinology 154:1282-1295
155. Ivashkiv LB, Donlin LT (2014) Regulation of type I interferon responses. Nature reviews Immunology 14:36-49
156. Jain A, Pasare C (2017) Innate Control of Adaptive Immunity: Beyond the Three-Signal Paradigm. Journal of immunology (Baltimore, Md : 1950) 198:3791-3800
157. Jiang D, Weidner JM, Qing M, Pan X-B, Guo H, Xu C, Zhang X, Birk A, Chang J, Shi P-Y, Block TM, Guo J-T (2010) Identification of five interferon-induced cellular proteins that inhibit west nile virus and dengue virus infections. Journal of virology 84:8332-8341
158. Jilg N, Lin W, Hong J, Schaefer EA, Wolski D, Meixong J, Goto K, Brisac C, Chusri P, Fusco DN, Chevaliez S, Luther J, Kumthip K, Urban TJ, Peng LF, Lauer GM, Chung RT (2014) Kinetic differences in the induction of interferon stimulated genes by

interferon-α and interleukin 28B are altered by infection with hepatitis C virus. Hepatology (Baltimore, Md) 59:1250-1261
159. Johansson MA, Mier-y-Teran-Romero L, Reefhuis J, Gilboa SM, Hills SL (2016) Zika and the Risk of Microcephaly. The New England journal of medicine 375:1-4
160. Kastner P, Krust A, Turcotte B, Stropp U, Tora L, Gronemeyer H, Chambon P (1990) Two distinct estrogen-regulated promoters generate transcripts encoding the two functionally different human progesterone receptor forms A and B. The EMBO journal 9:1603-1614
161. Kato H, Takeuchi O, Mikamo-Satoh E, Hirai R, Kawai T, Matsushita K, Hiiragi A, Dermody TS, Fujita T, Akira S (2008) Length-dependent recognition of double-stranded ribonucleic acids by retinoic acid-inducible gene-I and melanoma differentiation-associated gene 5. J Exp Med 205:1601-1610
162. Kell AM, Gale M, Jr. (2015) RIG-I in RNA virus recognition. Virology 479-480:110-121
163. Keskinen P, Nyqvist M, Sareneva T, Pirhonen J, Melén K, Julkunen I (1999) Impaired Antiviral Response in Human Hepatoma Cells. Virology 263:364-375
164. Khan S, Woodruff EM, Trapecar M, Fontaine KA, Ezaki A, Borbet TC, Ott M, Sanjabi S (2016) Dampened antiviral immunity to intravaginal exposure to RNA viral pathogens allows enhanced viral replication. The Journal of Experimental Medicine 213:2913
165. Khan S, Lew I, Wu F, Fritts L, Fontaine KA, Tomar S, Trapecar M, Shehata HM, Ott M, Miller CJ, Sanjabi S (2019) Low expression of RNA sensors impacts Zika virus infection in the lower female reproductive tract. Nature communications 10:4344
166. Khromykh AA, Sedlak PL, Westaway EG (1999) trans-Complementation analysis of the flavivirus Kunjin ns5 gene reveals an essential role for translation of its N-terminal half in RNA replication. Journal of virology 73:9247-9255
167. Khromykh AA, Sedlak PL, Westaway EG (2000) cis- and trans-acting elements in flavivirus RNA replication. Journal of virology 74:3253-3263
168. Killen H, O'Sullivan MA (1993) Detection of dengue virus by in situ hybridization. Journal of virological methods 41:135-146
169. Kim SK, Park HJ, Kim JW, Chung J-H, Yoo SD, Kim DH, Yun DH, Kim H-S (2014) T Allele of nonsense polymorphism (rs2039381, Gln71Stop) of interferon-ε is a risk factor for the development of intracerebral hemorrhage. Human Immunology 75:88-90
170. Kimura T, Katoh H, Kayama H, Saiga H, Okuyama M, Okamoto T, Umemoto E, Matsuura Y, Yamamoto M, Takeda K (2013) Ifit1 inhibits Japanese encephalitis virus replication through binding to 5' capped 2'-O unmethylated RNA. Journal of virology 87:9997-10003
171. Klema VJ, Ye M, Hindupur A, Teramoto T, Gottipati K, Padmanabhan R, Choi KH (2016) Dengue Virus Nonstructural Protein 5 (NS5) Assembles into a Dimer with a Unique Methyltransferase and Polymerase Interface. PLoS pathogens 12:e1005451-e1005451
172. Klinkhammer J, Schnepf D, Ye L, Schwaderlapp M, Gad HH, Hartmann R, Garcin D, Mahlakoiv T, Staeheli P (2018) IFN-lambda prevents influenza virus spread from the upper airways to the lungs and limits virus transmission. eLife 7
173. Kodati S, Palmore TN, Spellman FA, Cunningham D, Weistrop B, Sen HN (2017) Bilateral posterior uveitis associated with Zika virus infection. Lancet (London, England) 389:125-126
174. Kotenko SV, Gallagher G, Baurin VV, Lewis-Antes A, Shen M, Shah NK, Langer JA, Sheikh F, Dickensheets H, Donnelly RP (2003) IFN-lambdas mediate antiviral

protection through a distinct class II cytokine receptor complex. Nature immunology 4:69-77
175. Koyama S, Ishii KJ, Coban C, Akira S (2008) Innate immune response to viral infection. Cytokine 43:336-341
176. Kumar A, Hou S, Airo AM, Limonta D, Mancinelli V, Branton W, Power C, Hobman TC (2016) Zika virus inhibits type-I interferon production and downstream signaling. EMBO reports 17:1766-1775
177. Kumar A, Jovel J, Lopez-Orozco J, Limonta D, Airo AM, Hou S, Stryapunina I, Fibke C, Moore RB, Hobman TC (2018) Human Sertoli cells support high levels of Zika virus replication and persistence. Scientific reports 8:5477
178. Kwon JY, Aldo P, You Y, Ding J, Racicot K, Dong X, Murphy J, Glukshtad G, Silasi M, Peng J, Wen L, Abrahams VM, Romero R, Mor G (2018) Relevance of placental type I interferon beta regulation for pregnancy success. Cellular & molecular immunology
179. Lamken P, Lata S, Gavutis M, Piehler J (2004) Ligand-induced assembling of the type I interferon receptor on supported lipid bilayers. J Mol Biol 341:303-318
180. Lauring AS, Andino R (2010) Quasispecies theory and the behavior of RNA viruses. PLoS Pathog 6:e1001005
181. Lazear HM, Govero J, Smith AM, Platt DJ, Fernandez E, Miner JJ, Diamond MS (2016) A Mouse Model of Zika Virus Pathogenesis. Cell host & microbe 19:720-730
182. Lazear HM, Schoggins JW, Diamond MS (2019) Shared and Distinct Functions of Type I and Type III Interferons. Immunity 50:907-923
183. Ledur PF, Karmirian K, Pedrosa CdSG, Souza LRQ, Assis-de-Lemos G, Martins TM, Ferreira JdCCG, de Azevedo Reis GF, Silva ES, Silva D, Salerno JA, Ornelas IM, Devalle S, Madeiro da Costa RF, Goto-Silva L, Higa LM, Melo A, Tanuri A, Chimelli L, Murata MM, Garcez PP, Filippi-Chiela EC, Galina A, Borges HL, Rehen SK (2020) Zika virus infection leads to mitochondrial failure, oxidative stress and DNA damage in human iPSC-derived astrocytes. Scientific reports 10:1218-1218
184. Lescar J, Soh S, Lee LT, Vasudevan SG, Kang C, Lim SP (2018) The Dengue Virus Replication Complex: From RNA Replication to Protein-Protein Interactions to Evasion of Innate Immunity. Advances in experimental medicine and biology 1062:115-129
185. Li D, Aaskov J, Lott WB (2011) Identification of a cryptic prokaryotic promoter within the cDNA encoding the 5' end of dengue virus RNA genome. PloS one 6:e18197-e18197
186. Li G, Adam A, Luo H, Shan C, Cao Z, Fontes-Garfias CR, Sarathy VV, Teleki C, Winkelmann ER, Liang Y, Sun J, Bourne N, Barrett ADT, Shi PY, Wang T (2019) An attenuated Zika virus NS4B protein mutant is a potent inducer of antiviral immune responses. NPJ vaccines 4:48
187. Liang C, Rong L, Laughrea M, Kleiman L, Wainberg MA (1998) Compensatory point mutations in the human immunodeficiency virus type 1 Gag region that are distal from deletion mutations in the dimerization initiation site can restore viral replication. Journal of virology 72:6629-6636
188. Lin JP, Fan YK, Liu HM (2019) The 14-3-3η chaperone protein promotes antiviral innate immunity via facilitating MDA5 oligomerization and intracellular redistribution. PLoS Pathog 15:e1007582

189. Lin S, Yang S, He J, Guest JD, Ma Z, Yang L, Pierce BG, Tang Q, Zhang YJ (2019) Zika virus NS5 protein antagonizes type I interferon production via blocking TBK1 activation. Virology 527:180-187
190. Lin SC, Kuo CC, Tsao JT, Lin LJ (2012) Profiling the expression of interleukin (IL)-28 and IL-28 receptor α in systemic lupus erythematosus patients. European journal of clinical investigation 42:61-69
191. Lisova O, Belkadi L, Bedouelle H (2014) Direct and indirect interactions in the recognition between a cross-neutralizing antibody and the four serotypes of dengue virus. Journal of molecular recognition : JMR 27:205-214
192. Liu HM, Loo YM, Horner SM, Zornetzer GA, Katze MG, Gale M, Jr. (2012) The mitochondrial targeting chaperone 14-3-3ε regulates a RIG-I translocon that mediates membrane association and innate antiviral immunity. Cell host & microbe 11:528-537
193. Liu L, Chen Z, Zhang X, Li S, Hui Y, Feng H, Du Y, Jin G, Zhou X, Zhang X (2019) Protection of ZIKV infection-induced neuropathy by abrogation of acute antiviral response in human neural progenitors. Cell death and differentiation
194. Liu WJ, Wang XJ, Mokhonov VV, Shi P-Y, Randall R, Khromykh AA (2005) Inhibition of Interferon Signaling by the New York 99 Strain and Kunjin Subtype of West Nile Virus Involves Blockage of STAT1 and STAT2 Activation by Nonstructural Proteins. Journal of virology 79:1934-1942
195. Liu Y, Liu J, Du S, Shan C, Nie K, Zhang R, Li XF, Zhang R, Wang T, Qin CF, Wang P, Shi PY, Cheng G (2017) Evolutionary enhancement of Zika virus infectivity in Aedes aegypti mosquitoes. Nature 545:482-486
196. Lodeiro MF, Filomatori CV, Gamarnik AV (2009) Structural and functional studies of the promoter element for dengue virus RNA replication. Journal of virology 83:993-1008
197. Lovera D, Martinez de Cuellar C, Araya S, Amarilla S, Gonzalez N, Aguiar C, Acuna J, Arbo A (2016) Clinical Characteristics and Risk Factors of Dengue Shock Syndrome in Children. The Pediatric infectious disease journal 35:1294-1299
198. Lundberg R, Melen K, Westenius V, Jiang M, Osterlund P, Khan H, Vapalahti O, Julkunen I, Kakkola L (2019) Zika Virus Non-Structural Protein NS5 Inhibits the RIG-I Pathway and Interferon Lambda 1 Promoter Activation by Targeting IKK Epsilon. Viruses 11
199. Lwande OW, Obanda V, Lindstrom A, Ahlm C, Evander M, Naslund J, Bucht G (2020) Globe-Trotting Aedes aegypti and Aedes albopictus: Risk Factors for Arbovirus Pandemics. Vector borne and zoonotic diseases (Larchmont, NY) 20:71-81
200. Ma J, Ketkar H, Geng T, Lo E, Wang L, Xi J, Sun Q, Zhu Z, Cui Y, Yang L, Wang P (2018) Zika Virus Non-structural Protein 4A Blocks the RLR-MAVS Signaling. Frontiers in microbiology 9:1350
201. Maltepe E, Fisher SJ (2015) Placenta: the forgotten organ. Annual review of cell and developmental biology 31:523-552
202. Manokaran G, Finol E, Wang C, Gunaratne J, Bahl J, Ong EZ, Tan HC, Sessions OM, Ward AM, Gubler DJ, Harris E, Garcia-Blanco MA, Ooi EE (2015) Dengue subgenomic RNA binds TRIM25 to inhibit interferon expression for epidemiological fitness. Science (New York, NY) 350:217-221

203. Manry J, Laval G, Patin E, Fornarino S, Itan Y, Fumagalli M, Sironi M, Tichit M, Bouchier C, Casanova JL, Barreiro LB, Quintana-Murci L (2011) Evolutionary genetic dissection of human interferons. J Exp Med 208:2747-2759
204. Mansuy JM, Suberbielle E, Chapuy-Regaud S, Mengelle C, Bujan L, Marchou B, Delobel P, Gonzalez-Dunia D, Malnou CE, Izopet J, Martin-Blondel G (2016) Zika virus in semen and spermatozoa. The Lancet Infectious diseases 16:1106-1107
205. Mantere T, Kersten S, Hoischen A (2019) Long-Read Sequencing Emerging in Medical Genetics. Frontiers in genetics 10:426
206. Marcello T, Grakoui A, Barba-Spaeth G, Machlin ES, Kotenko SV, MacDonald MR, Rice CM (2006) Interferons alpha and lambda inhibit hepatitis C virus replication with distinct signal transduction and gene regulation kinetics. Gastroenterology 131:1887-1898
207. Marijanovic Z, Ragimbeau J, van der Heyden J, Uze G, Pellegrini S (2007) Comparable potency of IFNalpha2 and IFNbeta on immediate JAK/STAT activation but differential down-regulation of IFNAR2. The Biochemical journal 407:141-151
208. Martina BE, Koraka P, Osterhaus AD (2009) Dengue virus pathogenesis: an integrated view. Clinical microbiology reviews 22:564-581
209. Marzi A, Emanuel J, Callison J, McNally KL, Arndt N, Chadinha S, Martellaro C, Rosenke R, Scott DP, Safronetz D, Whitehead SS, Best SM, Feldmann H (2018) Lethal Zika Virus Disease Models in Young and Older Interferon α/β Receptor Knock Out Mice. Frontiers in Cellular and Infection Microbiology 8:117
210. Matsumiya T, Prescott SM, Stafforini DM (2007) IFN-epsilon mediates TNF-alpha-induced STAT1 phosphorylation and induction of retinoic acid-inducible gene-I in human cervical cancer cells. Journal of immunology (Baltimore, Md : 1950) 179:4542-4549
211. Matsumiya T, Xing F, Ebina M, Hayakari R, Imaizumi T, Yoshida H, Kikuchi H, Topham MK, Satoh K, Stafforini DM (2013) Novel role for molecular transporter importin 9 in posttranscriptional regulation of IFN-epsilon expression. Journal of immunology (Baltimore, Md : 1950) 191:1907-1915
212. Mazeaud C, Freppel W, Chatel-Chaix L (2018) The Multiples Fates of the Flavivirus RNA Genome During Pathogenesis. Frontiers in genetics 9:595
213. Mazzon M, Jones M, Davidson A, Chain B, Jacobs M (2009) Dengue Virus NS5 Inhibits Interferon-α Signaling by Blocking Signal Transducer and Activator of Transcription 2 Phosphorylation. The Journal of Infectious Diseases 200:1261-1270
214. McNab F, Mayer-Barber K, Sher A, Wack A, O'Garra A (2015) Type I interferons in infectious disease. Nature reviews Immunology 15:87-103
215. Meertens L, Carnec X, Lecoin Manuel P, Ramdasi R, Guivel-Benhassine F, Lew E, Lemke G, Schwartz O, Amara A (2012) The TIM and TAM Families of Phosphatidylserine Receptors Mediate Dengue Virus Entry. Cell host & microbe 12:544-557
216. Meertens L, Labeau A, Dejarnac O, Cipriani S, Sinigaglia L, Bonnet-Madin L, Le Charpentier T, Hafirassou ML, Zamborlini A, Cao-Lormeau VM, Coulpier M, Misse D, Jouvenet N, Tabibiazar R, Gressens P, Schwartz O, Amara A (2017) Axl Mediates ZIKA Virus Entry in Human Glial Cells and Modulates Innate Immune Responses. Cell reports 18:324-333

217. Messina NL, Clarke CJP, Johnstone RW (2016) Constitutive IFNα/β signaling maintains expression of signaling intermediaries for efficient cytokine responses. JAK-STAT 5:e1173804
218. Meuwissen MEC, Schot R, Buta S, Oudesluijs G, Tinschert S, Speer SD, Li Z, van Unen L, Heijsman D, Goldmann T, Lequin MH, Kros JM, Stam W, Hermann M, Willemsen R, Brouwer RWW, Van Ijcken WFJ, Martin-Fernandez M, de Coo I, Dudink J, de Vries FAT, Bertoli Avella A, Prinz M, Crow YJ, Verheijen FW, Pellegrini S, Bogunovic D, Mancini GMS (2016) Human USP18 deficiency underlies type 1 interferonopathy leading to severe pseudo-TORCH syndrome. The Journal of experimental medicine 213:1163-1174
219. Miagostovich MP, Ramos RG, Nicol AF, Nogueira RM, Cuzzi-Maya T, Oliveira AV, Marchevsky RS, Mesquita RP, Schatzmayr HG (1997) Retrospective study on dengue fatal cases. Clinical neuropathology 16:204-208
220. Miller S, Kastner S, Krijnse-Locker J, Buhler S, Bartenschlager R (2007) The non-structural protein 4A of dengue virus is an integral membrane protein inducing membrane alterations in a 2K-regulated manner. The Journal of biological chemistry 282:8873-8882
221. Miner JJ, Cao B, Govero J, Smith AM, Fernandez E, Cabrera OH, Garber C, Noll M, Klein RS, Noguchi KK, Mysorekar IU, Diamond MS (2016) Zika Virus Infection during Pregnancy in Mice Causes Placental Damage and Fetal Demise. Cell 165:1081-1091
222. Miner Jonathan J, Sene A, Richner Justin M, Smith Amber M, Santeford A, Ban N, Weger-Lucarelli J, Manzella F, Rückert C, Govero J, Noguchi Kevin K, Ebel Gregory D, Diamond Michael S, Apte Rajendra S (2016) Zika Virus Infection in Mice Causes Panuveitis with Shedding of Virus in Tears. Cell reports 16:3208-3218
223. Miner JJ, Diamond MS (2017) Zika Virus Pathogenesis and Tissue Tropism. Cell host & microbe 21 134-142
224. Miorin L, Maestre AM, Fernandez-Sesma A, García-Sastre A Antagonism of type I interferon by flaviviruses. Biochemical and Biophysical Research Communications
225. Modhiran N, Watterson D, Blumenthal A, Baxter AG, Young PR, Stacey KJ (2017) Dengue virus NS1 protein activates immune cells via TLR4 but not TLR2 or TLR6. Immunology and cell biology 95:491-495
226. Mor G (2016) Placental Inflammatory Response to Zika Virus may Affect Fetal Brain Development. American journal of reproductive immunology (New York, NY : 1989) 75:421-422
227. Mor G, Aldo P, Alvero AB (2017) The unique immunological and microbial aspects of pregnancy. Nature reviews Immunology 17:469-482
228. Moreira J, Peixoto TM, Siqueira AM, Lamas CC (2017) Sexually acquired Zika virus: a systematic review. Clinical microbiology and infection : the official publication of the European Society of Clinical Microbiology and Infectious Diseases 23:296-305
229. Morrison J, Aguirre S, Fernandez-Sesma A (2012) Innate Immunity Evasion by Dengue Virus. Viruses 4:397-413
230. Morrison J, Laurent-Rolle M, Maestre AM, Rajsbaum R, Pisanelli G, Simon V, Mulder LC, Fernandez-Sesma A, Garcia-Sastre A (2013) Dengue virus co-opts UBR4 to degrade STAT2 and antagonize type I interferon signaling. PLoS Pathog 9:e1003265
231. Morrison TE, Diamond MS (2017) Animal Models of Zika Virus Infection, Pathogenesis, and Immunity. Journal of virology 91

232. Motwani M, Pesiridis S, Fitzgerald KA (2019) DNA sensing by the cGAS-STING pathway in health and disease. Nature reviews Genetics 20:657-674
233. Mousavi SA, Malerod L, Berg T, Kjeken R (2004) Clathrin-dependent endocytosis. The Biochemical journal 377:1-16
234. Mukhopadhyay S, Kuhn RJ, Rossmann MG (2005) A structural perspective of the flavivirus life cycle. Nature reviews Microbiology 3:13-22
235. Munoz-Jordan JL, Laurent-Rolle M, Ashour J, Martinez-Sobrido L, Ashok M, Lipkin WI, Garcia-Sastre A (2005) Inhibition of alpha/beta interferon signaling by the NS4B protein of flaviviruses. Journal of virology 79:8004-8013
236. Muñoz-Jordan JL, Sánchez-Burgos GG, Laurent-Rolle M, García-Sastre A (2003) Inhibition of interferon signaling by dengue virus. Proceedings of the National Academy of Sciences of the United States of America 100:14333-14338
237. Murphy SP, Tayade C, Ashkar AA, Hatta K, Zhang J, Croy BA (2009) Interferon gamma in successful pregnancies. Biol Reprod 80:848-859
238. Murray CL, Jones CT, Rice CM (2008) Architects of assembly: roles of Flaviviridae non-structural proteins in virion morphogenesis. Nature reviews Microbiology 6:699-708
239. Murray NEA, Quam MB, Wilder-Smith A (2013) Epidemiology of dengue: past, present and future prospects. Clin Epidemiol 5:299-309
240. Musso D, Ko AI, Baud D (2019) Zika Virus Infection - After the Pandemic. The New England journal of medicine 381:1444-1457
241. Mutso M, Saul S, Rausalu K, Susova O, Zusinaite E, Mahalingam S, Merits A (2017) Reverse genetic system, genetically stable reporter viruses and packaged subgenomic replicon based on a Brazilian Zika virus isolate. The Journal of general virology 98:2712-2724
242. Nakabayashi H, Taketa K, Miyano K, Yamane T, Sato J (1982) Growth of human hepatoma cells lines with differentiated functions in chemically defined medium. Cancer Res 42:3858-3863
243. Nasirudeen AM, Wong HH, Thien P, Xu S, Lam KP, Liu DX (2011) RIG-I, MDA5 and TLR3 synergistically play an important role in restriction of dengue virus infection. PLoS neglected tropical diseases 5:e926
244. Nasr N, Maddocks S, Turville SG, Harman AN, Woolger N, Helbig KJ, Wilkinson J, Bye CR, Wright TK, Rambukwelle D, Donaghy H, Beard MR, Cunningham AL (2012) HIV-1 infection of human macrophages directly induces viperin which inhibits viral production. Blood 120:778-788
245. Nazmi A, Dutta K, Hazra B, Basu A (2014) Role of pattern recognition receptors in flavivirus infections. Virus research 185:32-40
246. Ng DHL, Ho HJ, Chow A, Wong J, Kyaw WM, Tan A, Chia PY, Choy CY, Tan G, Yeo TW, Leo YS (2018) Correlation of clinical illness with viremia in Zika virus disease during an outbreak in Singapore. BMC infectious diseases 18:301
247. Ng WC, Soto-Acosta R, Bradrick SS, Garcia-Blanco MA, Ooi EE (2017) The 5' and 3' Untranslated Regions of the Flaviviral Genome. Viruses 9:137
248. Ngo AM, Shurtleff MJ, Popova KD, Kulsuptrakul J, Weissman JS, Puschnik AS (2019) The ER membrane protein complex is required to ensure correct topology and stable expression of flavivirus polyproteins. eLife 8
249. Ngueyen TTN, Kim SJ, Lee JY, Myoung J (2019) Zika Virus Proteins NS2A and NS4A Are Major Antagonists that Reduce IFN-beta Promoter Activity Induced by the

MDA5/RIG-I Signaling Pathway. Journal of microbiology and biotechnology 29:1665-1674
250. Nickodem C, Criscitiello MF, Bazer F, Abiodun-Ojo O, Taylor BD (2018) Interferon epsilon in the reproductive tract of healthy and genital herpes simplex virus-infected pregnant women: Results of a pilot study. American journal of reproductive immunology (New York, NY : 1989) 80:e12995
251. Nielsen-Saines K, Brasil P, Kerin T, Vasconcelos Z, Gabaglia CR, Damasceno L, Pone M, Abreu de Carvalho LM, Pone SM, Zin AA, Tsui I, Salles TRS, da Cunha DC, Costa RP, Malacarne J, Reis AB, Hasue RH, Aizawa CYP, Genovesi FF, Einspieler C, Marschik PB, Pereira JP, Gaw SL, Adachi K, Cherry JD, Xu Z, Cheng G, Moreira ME (2019) Delayed childhood neurodevelopment and neurosensory alterations in the second year of life in a prospective cohort of ZIKV-exposed children. Nature Medicine
252. Nishida M, Kasahara K, Kaneko M, Iwasaki H, Hayashi K (1985) [Establishment of a new human endometrial adenocarcinoma cell line, Ishikawa cells, containing estrogen and progesterone receptors]. Nihon Sanka Fujinka Gakkai zasshi 37:1103-1111
253. Nollaig M. Bourke SLA, Stephanie U. Huang, Helen E. Cumming, Irene Papageorgio, Linden J. Gearing, Suruchi Thakore, Niamh E. Mangan, Sam Mesiano, Paul J. Hertzog (2018) Human IFNε: Spatiotemporal expression, hormone regulation and innate immunity in the female reproductive tract. bioRxiv
254. Odendall C, Dixit E, Stavru F, Bierne H, Franz KM, Durbin AF, Boulant S, Gehrke L, Cossart P, Kagan JC (2014) Diverse intracellular pathogens activate type III interferon expression from peroxisomes. Nature immunology 15:717-726
255. Odendall C, Kagan JC (2015) The unique regulation and functions of type III interferons in antiviral immunity. Current opinion in virology 12:47-52
256. Oliveira ERA, Mohana-Borges R, de Alencastro RB, Horta BAC (2017) The flavivirus capsid protein: Structure, function and perspectives towards drug design. Virus research 227:115-123
257. Pagani I, Ghezzi S, Ulisse A, Rubio A, Turrini F, Garavaglia E, Candiani M, Castilletti C, Ippolito G, Poli G, Broccoli V, Panina-Bordignon P, Vicenzi E (2017) Human Endometrial Stromal Cells Are Highly Permissive To Productive Infection by Zika Virus. Scientific reports 7:44286
258. Paixao ES, Leong WY, Rodrigues LC, Wilder-Smith A (2018) Asymptomatic Prenatal Zika Virus Infection and Congenital Zika Syndrome. Open forum infectious diseases 5:ofy073
259. Panayiotou C, Lindqvist R, Kurhade C, Vonderstein K, Pasto J, Edlund K, Upadhyay AS, Overby AK (2018) Viperin restricts Zika virus and tick-borne encephalitis virus replication by targeting NS3 for proteasomal degradation. Journal of virology
260. Payne S (2017) Family Flaviviridae. Viruses - from understanding to investigation, pp 129 - 139
261. Paz-Bailey G, Rosenberg ES, Doyle K, Munoz-Jordan J, Santiago GA, Klein L, Perez-Padilla J, Medina FA, Waterman SH, Gubern CG, Alvarado LI, Sharp TM (2018) Persistence of Zika Virus in Body Fluids - Final Report. The New England journal of medicine 379:1234-1243
262. Peng FW, Duan ZJ, Zheng LS, Xie ZP, Gao HC, Zhang H, Li WP, Hou YD (2007) Purification of recombinant human interferon-epsilon and oligonucleotide

microarray analysis of interferon-epsilon-regulated genes. Protein expression and purification 53:356-362
263. Peregrine J, Gurung S, Lindgren MC, Husain S, Zavy MT, Myers DA, Papin JF (2019) Zika Virus Infection, Reproductive Organ Targeting, and Semen Transmission in the Male Olive Baboon. Journal of virology 94
264. Perera-Lecoin M, Meertens L, Carnec X, Amara A (2014) Flavivirus Entry Receptors: An Update. Viruses 6:69-88
265. Perera R, Kuhn RJ (2008) Structural proteomics of dengue virus. Curr Opin Microbiol 11:369-377
266. Perng Y-C, Lenschow DJ (2018) ISG15 in antiviral immunity and beyond. Nature reviews Microbiology 16:423-439
267. Pettersson JH, Eldholm V, Seligman SJ, Lundkvist A, Falconar AK, Gaunt MW, Musso D, Nougairede A, Charrel R, Gould EA, de Lamballerie X (2016) How Did Zika Virus Emerge in the Pacific Islands and Latin America? mBio 7
268. Phipps-Yonas H, Seto J, Sealfon SC, Moran TM, Fernandez-Sesma A (2008) Interferon-beta pretreatment of conventional and plasmacytoid human dendritic cells enhances their activation by influenza virus. PLoS pathogens 4:e1000193-e1000193
269. Piganis RA, De Weerd NA, Gould JA, Schindler CW, Mansell A, Nicholson SE, Hertzog PJ (2011) Suppressor of cytokine signaling (SOCS) 1 inhibits type I interferon (IFN) signaling via the interferon alpha receptor (IFNAR1)-associated tyrosine kinase Tyk2. The Journal of biological chemistry 286:33811-33818
270. Pomar L, Lambert V, Madec Y, Vouga M, Pomar C, Matheus S, Fontanet A, Panchaud A, Carles G, Baud D (2019) Placental infection by Zika virus in French Guiana. Ultrasound in obstetrics & gynecology : the official journal of the International Society of Ultrasound in Obstetrics and Gynecology
271. Prisant N, Bujan L, Benichou H, Hayot PH, Pavili L, Lurel S, Herrmann C, Janky E, Joguet G (2016) Zika virus in the female genital tract. The Lancet Infectious diseases 16:1000-1001
272. Prisant N, Joguet G, Herrmann-Stock C, Moriniere C, Pavili L, Lurel S, Bujan L (2019) Upper and lower genital tract Zika virus screening in a large cohort of reproductive-age women during the Americas epidemic. Reproductive biomedicine online
273. Pu S-Y, Wu R-H, Yang C-C, Jao T-M, Tsai M-H, Wang J-C, Lin H-M, Chao Y-S, Yueh A (2011) Successful propagation of flavivirus infectious cDNAs by a novel method to reduce the cryptic bacterial promoter activity of virus genomes. Journal of virology 85:2927-2941
274. Qi H, Chu V, Wu NC, Chen Z, Truong S, Brar G, Su SY, Du Y, Arumugaswami V, Olson CA, Chen SH, Lin CY, Wu TT, Sun R (2017) Systematic identification of anti-interferon function on hepatitis C virus genome reveals p7 as an immune evasion protein. Proceedings of the National Academy of Sciences of the United States of America 114:2018-2023
275. Qi Y, Li Y, Zhang Y, Zhang L, Wang Z, Zhang X, Gui L, Huang J (2015) IFI6 Inhibits Apoptosis via Mitochondrial-Dependent Pathway in Dengue Virus 2 Infected Vascular Endothelial Cells. PloS one 10:e0132743-e0132743
276. Racicot K, Aldo P, El-Guindy A, Kwon JY, Romero R, Mor G (2017) Cutting Edge: Fetal/Placental Type I IFN Can Affect Maternal Survival and Fetal Viral Load during Viral Infection. Journal of immunology (Baltimore, Md : 1950) 198:3029-3032

277. Radukic MT, Brandt D, Haak M, Müller KM, Kalinowski J (2019) Nanopore sequencing of native adeno-associated virus single-stranded DNA using a transposase-based rapid protocol. bioRxiv:2019.2012.2027.885319
278. Raftery N, Stevenson NJ (2017) Advances in anti-viral immune defence: revealing the importance of the IFN JAK/STAT pathway. Cellular and Molecular Life Sciences 74:2525-2535
279. Rasmussen SA, Jamieson DJ, Honein MA, Petersen LR (2016) Zika Virus and Birth Defects--Reviewing the Evidence for Causality. The New England journal of medicine 374:1981-1987
280. Rastogi M, Sharma N, Singh SK (2016) Flavivirus NS1: a multifaceted enigmatic viral protein. Virology journal 13:131
281. Reder AT, Feng X (2014) How type I interferons work in multiple sclerosis and other diseases: some unexpected mechanisms. Journal of interferon & cytokine research : the official journal of the International Society for Interferon and Cytokine Research 34:589-599
282. Reiser J, Hurst J, Voges M, Krauss P, Munch P, Iftner T, Stubenrauch F (2011) High-risk human papillomaviruses repress constitutive kappa interferon transcription via E6 to prevent pathogen recognition receptor and antiviral-gene expression. Journal of virology 85:11372-11380
283. Remenyi R, Qi H, Su SY, Chen Z, Wu NC, Arumugaswami V, Truong S, Chu V, Stokelman T, Lo HH, Olson CA, Wu TT, Chen SH, Lin CY, Sun R (2014) A comprehensive functional map of the hepatitis C virus genome provides a resource for probing viral proteins. mBio 5:e01469-01414
284. Rice ME, Galang RR, Roth NM, Ellington SR, Moore CA, Valencia-Prado M, Ellis EM, Tufa AJ, Taulung LA, Alfred JM, Perez-Padilla J, Delgado-Lopez CA, Zaki SR, Reagan-Steiner S, Bhatnagar J, Nahabedian JF, 3rd, Reynolds MR, Yeargin-Allsopp M, Viens LJ, Olson SM, Jones AM, Baez-Santiago MA, Oppong-Twene P, VanMaldeghem K, Simon EL, Moore JT, Polen KD, Hillman B, Ropeti R, Nieves-Ferrer L, Marcano-Huertas M, Masao CA, Anzures EJ, Hansen RL, Jr., Perez-Gonzalez SI, Espinet-Crespo CP, Luciano-Roman M, Shapiro-Mendoza CK, Gilboa SM, Honein MA (2018) Vital Signs: Zika-Associated Birth Defects and Neurodevelopmental Abnormalities Possibly Associated with Congenital Zika Virus Infection - U.S. Territories and Freely Associated States, 2018. MMWR Morbidity and mortality weekly report 67:858-867
285. Richardson RB, Ohlson MB, Eitson JL, Kumar A, McDougal MB, Boys IN, Mar KB, De La Cruz-Rivera PC, Douglas C, Konopka G, Xing C, Schoggins JW (2018) A CRISPR screen identifies IFI6 as an ER-resident interferon effector that blocks flavivirus replication. Nature microbiology 3:1214-1223
286. Riedl W, Acharya D, Lee JH, Liu G, Serman T, Chiang C, Chan YK, Diamond MS, Gack MU (2019) Zika Virus NS3 Mimics a Cellular 14-3-3-Binding Motif to Antagonize RIG-I- and MDA5-Mediated Innate Immunity. Cell host & microbe 26:493-503.e496
287. Rivera-Correa J, de Siqueira IC, Mota S, do Rosario MS, Pereira de Jesus PA, Alcantara LCJ, Ernst JD, Rodriguez A (2019) Anti-ganglioside antibodies in patients with Zika virus infection-associated Guillain-Barre Syndrome in Brazil. PLoS neglected tropical diseases 13:e0007695
288. Robinson N, Mayorquin Galvan EE, Zavala Trujillo IG, Zavala-Cerna MG (2018) Congenital Zika syndrome: Pitfalls in the placental barrier. Reviews in medical virology:e1985

289. Roby JA, Funk A, Khromykh AA (2012) Flavivirus replication and assembly. Molecular Virology and Control of Flaviviruses. Caister Academic Press, Norfolk, UK
290. Rossi SL, Tesh RB, Azar SR, Muruato AE, Hanley KA, Auguste AJ, Langsjoen RM, Paessler S, Vasilakis N, Weaver SC (2016) Characterization of a Novel Murine Model to Study Zika Virus. The American journal of tropical medicine and hygiene 94:1362-1369
291. Rothman AL (2011) Immunity to dengue virus: a tale of original antigenic sin and tropical cytokine storms. Nature reviews Immunology 11:532-543
292. Ruggli N, Rice CM (1999) Functional cDNA clones of the Flaviviridae: strategies and applications. Advances in virus research 53:183-207
293. Rusinova IF, S.; Yu, S.; Kannan, A.; Masse, M.; Cumming, H.; Chapman, R.; Hertzog, P.J. (2013) INTERFEROME v2. 0: an updated database of annotated interferon-regulated genes. Nucleic acids research:D1040-D1046.
294. Russo FB, Jungmann P, Beltrao-Braga PCB (2017) Zika infection and the development of neurological defects. Cellular microbiology 19
295. Saeedi BJ, Geiss BJ (2013) Regulation of flavivirus RNA synthesis and capping. Wiley Interdiscip Rev RNA 4:723-735
296. Sakkas H, Bozidis P, Giannakopoulos X, Sofikitis N, Papadopoulou C (2018) An Update on Sexual Transmission of Zika Virus. Pathogens (Basel, Switzerland) 7
297. Sam SS, Omar SF, Teoh BT, Abd-Jamil J, AbuBakar S (2013) Review of Dengue hemorrhagic fever fatal cases seen among adults: a retrospective study. PLoS neglected tropical diseases 7:e2194
298. Sanjuán R, Nebot MR, Chirico N, Mansky LM, Belshaw R (2010) Viral mutation rates. Journal of virology 84:9733-9748
299. Sarasin-Filipowicz M, Wang X, Yan M, Duong FH, Poli V, Hilton DJ, Zhang DE, Heim MH (2009) Alpha interferon induces long-lasting refractoriness of JAK-STAT signaling in the mouse liver through induction of USP18/UBP43. Molecular and cellular biology 29:4841-4851
300. Savidis G, Perreira JM, Portmann JM, Meraner P, Guo Z, Green S, Brass AL (2016) The IFITMs Inhibit Zika Virus Replication. Cell reports 15:2323-2330
301. Scherer WF, Syverton JT, Gey GO (1953) Studies on the propagation in vitro of poliomyelitis viruses. IV. Viral multiplication in a stable strain of human malignant epithelial cells (strain HeLa) derived from an epidermoid carcinoma of the cervix. J Exp Med 97:695-710
302. Schilling M, Bridgeman A, Gray N, Hertzog J, Hublitz P, Kohl A, Rehwinkel J (2020) RIG-I Plays a Dominant Role in the Induction of Transcriptional Changes in Zika Virus-Infected Cells, which Protect from Virus-Induced Cell Death. Cells 9
303. Schlee M, Roth A, Hornung V, Hagmann CA, Wimmenauer V, Barchet W, Coch C, Janke M, Mihailovic A, Wardle G, Juranek S, Kato H, Kawai T, Poeck H, Fitzgerald KA, Takeuchi O, Akira S, Tuschl T, Latz E, Ludwig J, Hartmann G (2009) Recognition of 5' triphosphate by RIG-I helicase requires short blunt double-stranded RNA as contained in panhandle of negative-strand virus. Immunity 31:25-34
304. Schneider WM, Chevillotte MD, Rice CM (2014) Interferon-stimulated genes: a complex web of host defenses. Annual review of immunology 32:513-545
305. Schneider WM, Chevillotte MD, Rice CM (2014) Interferon-stimulated genes: a complex web of host defenses. Annual review of immunology 32:513-545

306. Schoenborn JR, Wilson CB (2007) Regulation of interferon-gamma during innate and adaptive immune responses. Advances in immunology 96:41-101
307. Schuessler A, Funk A, Lazear HM, Cooper DA, Torres S, Daffis S, Jha BK, Kumagai Y, Takeuchi O, Hertzog P, Silverman R, Akira S, Barton DJ, Diamond MS, Khromykh AA (2012) West Nile virus noncoding subgenomic RNA contributes to viral evasion of the type I interferon-mediated antiviral response. Journal of virology 86:5708-5718
308. Schuler-Faccini L, Ribeiro EM, Feitosa IM, Horovitz DD, Cavalcanti DP, Pessoa A, Doriqui MJ, Neri JI, Neto JM, Wanderley HY, Cernach M, El-Husny AS, Pone MV, Serao CL, Sanseverino MT (2016) Possible Association Between Zika Virus Infection and Microcephaly - Brazil, 2015. MMWR Morbidity and mortality weekly report 65:59-62
309. Schwarz MC, Sourisseau M, Espino MM, Gray ES, Chambers MT, Tortorella D, Evans MJ (2016) Rescue of the 1947 Zika Virus Prototype Strain with a Cytomegalovirus Promoter-Driven cDNA Clone. mSphere 1
310. Scutigliani EM, Kikkert M (2017) Interaction of the innate immune system with positive-strand RNA virus replication organelles. Cytokine Growth Factor Rev 37:17-27
311. Setoh YX, Prow NA, Peng N, Hugo LE, Devine G, Hazlewood JE, Suhrbier A, Khromykh AA (2017) De Novo Generation and Characterization of New Zika Virus Isolate Using Sequence Data from a Microcephaly Case. mSphere 2:e00190-00117
312. Setoh YX, Amarilla AA, Peng NYG, Griffiths RE, Carrera J, Freney ME, Nakayama E, Ogawa S, Watterson D, Modhiran N, Nanyonga FE, Torres FJ, Slonchak A, Periasamy P, Prow NA, Tang B, Harrison J, Hobson-Peters J, Cuddihy T, Cooper-White J, Hall RA, Young PR, Mackenzie JM, Wolvetang E, Bloom JD, Suhrbier A, Khromykh AA (2019) Determinants of Zika virus host tropism uncovered by deep mutational scanning. Nature microbiology 4:876-887
313. Sever R, Brugge JS (2015) Signal transduction in cancer. Cold Spring Harb Perspect Med 5:a006098
314. Shah I, Deshpande GC, Tardeja PN (2004) Outbreak of dengue in Mumbai and predictive markers for dengue shock syndrome. Journal of tropical pediatrics 50:301-305
315. Shan C, Xia H, Haller SL, Azar SR, Liu Y, Liu J, Muruato AE, Chen R, Rossi SL, Wakamiya M, Vasilakis N, Pei R, Fontes-Garfias CR, Singh SK, Xie X, Weaver SC, Shi PY (2020) A Zika virus envelope mutation preceding the 2015 epidemic enhances virulence and fitness for transmission. Proceedings of the National Academy of Sciences of the United States of America
316. Sharkey DJ, Macpherson AM, Tremellen KP, Robertson SA (2007) Seminal plasma differentially regulates inflammatory cytokine gene expression in human cervical and vaginal epithelial cells. Molecular human reproduction 13:491-501
317. Sheldon IM, Owens SE, Turner ML (2017) Innate immunity and the sensing of infection, damage and danger in the female genital tract. J Reprod Immunol 119:67-73
318. Sheppard P, Kindsvogel W, Xu W, Henderson K, Schlutsmeyer S, Whitmore TE, Kuestner R, Garrigues U, Birks C, Roraback J, Ostrander C, Dong D, Shin J, Presnell S, Fox B, Haldeman B, Cooper E, Taft D, Gilbert T, Grant FJ, Tackett M, Krivan W, McKnight G, Clegg C, Foster D, Klucher KM (2003) IL-28, IL-29 and their class II cytokine receptor IL-28R. Nature immunology 4:63-68

319. Sheridan MA, Balaraman V, Schust DJ, Ezashi T, Roberts RM, Franz AWE (2018) African and Asian strains of Zika virus differ in their ability to infect and lyse primitive human placental trophoblast. PLoS One 13:e0200086
320. Shu Q, Lennemann NJ, Sarkar SN, Sadovsky Y, Coyne CB (2015) ADAP2 Is an Interferon Stimulated Gene That Restricts RNA Virus Entry. PLoS pathogens 11:e1005150-e1005150
321. Shukair SA, Allen SA, Cianci GC, Stieh DJ, Anderson MR, Baig SM, Gioia CJ, Spongberg EJ, Kauffman SM, McRaven MD, Lakougna HY, Hammond C, Kiser PF, Hope TJ (2013) Human cervicovaginal mucus contains an activity that hinders HIV-1 movement. Mucosal immunology 6:427-434
322. Siewert E, Muller-Esterl W, Starr R, Heinrich PC, Schaper F (1999) Different protein turnover of interleukin-6-type cytokine signalling components. European journal of biochemistry 265:251-257
323. Simon O, Billot S, Guyon D, Daures M, Descloux E, Gourinat AC, Molko N, Dupont-Rouzeyrol M (2016) Early Guillain-Barre Syndrome associated with acute dengue fever. Journal of clinical virology : the official publication of the Pan American Society for Clinical Virology 77:29-31
324. Simonin Y, Erkilic N, Damodar K, Cle M, Desmetz C, Bollore K, Taleb M, Torriano S, Barthelemy J, Dubois G, Lajoix AD, Foulongne V, Tuaillon E, Van de Perre P, Kalatzis V, Salinas S (2019) Zika virus induces strong inflammatory responses and impairs homeostasis and function of the human retinal pigment epithelium. EBioMedicine 39:315-331
325. Singh PK, Guest J-M, Kanwar M, Boss J, Gao N, Juzych MS, Abrams GW, Yu F-S, Kumar A (2017) Zika virus infects cells lining the blood-retinal barrier and causes chorioretinal atrophy in mouse eyes. JCI insight 2:e92340-e92340
326. Singh PK, Guest J-M, Kanwar M, Boss J, Gao N, Juzych MS, Abrams GW, Yu F-S, Kumar A (2017) Zika virus infects cells lining the blood-retinal barrier and causes chorioretinal atrophy in mouse eyes. JCI insight 2:e92340
327. Singh PK, Singh S, Farr D, Kumar A (2019) Interferon-stimulated gene 15 (ISG15) restricts Zika virus replication in primary human corneal epithelial cells. The ocular surface
328. Sirohi D, Chen Z, Sun L, Klose T, Pierson TC, Rossmann MG, Kuhn RJ (2016) The 3.8 Å resolution cryo-EM structure of Zika virus. Science (New York, NY) 352:467
329. Song BH, Yun SI, Woolley M, Lee YM (2017) Zika virus: History, epidemiology, transmission, and clinical presentation. Journal of neuroimmunology
330. Soo KM, Khalid B, Ching SM, Chee HY (2016) Meta-Analysis of Dengue Severity during Infection by Different Dengue Virus Serotypes in Primary and Secondary Infections. PLoS One 11:e0154760
331. Spencer JL, Lahon A, Tran LL, Arya RP, Kneubehl AR, Vogt MB, Xavier D, Rowley DR, Kimata JT, Rico-Hesse RR (2018) Replication of Zika Virus in Human Prostate Cells: A Potential Source of Sexually Transmitted Virus. J Infect Dis 217:538-547
332. Sprokholt J, Helgers LC, Geijtenbeek TB (2017) Innate immune receptors drive dengue virus immune activation and disease. Future virology 13:287-305
333. Stanifer ML, Pervolaraki K, Boulant S (2019) Differential Regulation of Type I and Type III Interferon Signaling. International journal of molecular sciences 20
334. Stassen L, Armitage CW, van der Heide DJ, Beagley KW, Frentiu FD (2018) Zika Virus in the Male Reproductive Tract. Viruses 10:198

335. Stifter SA, Matthews AY, Mangan NE, Fung KY, Drew A, Tate MD, Soares da Costa TP, Hampsey D, Mayall J, Hansbro PM, Garcia Minambres A, Eid SG, Mak J, Scoble J, Lovrecz G, de Weerd NA, Hertzog PJ (2017) Defining the distinct, intrinsic properties of the novel type I interferon, epsilon. The Journal of biological chemistry
336. Sumpter R, Jr., Loo YM, Foy E, Li K, Yoneyama M, Fujita T, Lemon SM, Gale M, Jr. (2005) Regulating intracellular antiviral defense and permissiveness to hepatitis C virus RNA replication through a cellular RNA helicase, RIG-I. Journal of virology 79:2689-2699
337. Suwanmanee S, Luplertlop N (2017) Dengue and Zika viruses: lessons learned from the similarities between these Aedes mosquito-vectored arboviruses. Journal of microbiology (Seoul, Korea) 55:81-89
338. Suy A, Sulleiro E, Rodo C, Vazquez E, Bocanegra C, Molina I, Esperalba J, Sanchez-Seco MP, Boix H, Pumarola T, Carreras E (2016) Prolonged Zika Virus Viremia during Pregnancy. The New England journal of medicine 375:2611-2613
339. Swarbrick CMD, Basavannacharya C, Chan KWK, Chan S-A, Singh D, Wei N, Phoo WW, Luo D, Lescar J, Vasudevan SG (2017) NS3 helicase from dengue virus specifically recognizes viral RNA sequence to ensure optimal replication. Nucleic acids research 45:12904-12920
340. Tabata T, Petitt M, Puerta-Guardo H, Michlmayr D, Wang C, Fang-Hoover J, Harris E, Pereira L (2016) Zika Virus Targets Different Primary Human Placental Cells Suggesting Two Routes for Vertical Transmission. Cell host & microbe 20:155-166
341. Tang WW, Young MP, Mamidi A, Regla-Nava JA, Kim K, Shresta S (2016) A Mouse Model of Zika Virus Sexual Transmission and Vaginal Viral Replication. Cell reports 17:3091-3098
342. Tang WW, Young MP, Mamidi A, Regla-Nava JA, Kim K, Shresta S (2016) A Mouse Model of Zika Virus Sexual Transmission and Vaginal Viral Replication. Cell reports 17:3091-3098
343. Taniguchi T, Ogasawara K, Takaoka A, Tanaka N (2001) IRF family of transcription factors as regulators of host defense. Annual review of immunology 19:623-655
344. Tassaneetrithep B, Burgess TH, Granelli-Piperno A, Trumpfheller C, Finke J, Sun W, Eller MA, Pattanapanyasat K, Sarasombath S, Birx DL, Steinman RM, Schlesinger S, Marovich MA (2003) DC-SIGN (CD209) mediates dengue virus infection of human dendritic cells. J Exp Med 197:823-829
345. Tesla B, Demakovsky LR, Packiam HS, Mordecai EA, Rodriguez AD, Bonds MH, Brindley MA, Murdock CC (2018) Estimating the effects of variation in viremia on mosquito susceptibility, infectiousness, and R0 of Zika in Aedes aegypti. PLoS neglected tropical diseases 12:e0006733
346. Teterina NL, Lauber C, Jensen KS, Levenson EA, Gorbalenya AE, Ehrenfeld E (2011) Identification of tolerated insertion sites in poliovirus non-structural proteins. Virology 409:1-11
347. Thanachartwet V, Oer-Areemitr N, Chamnanchanunt S, Sahassananda D, Jittmittraphap A, Suwannakudt P, Desakorn V, Wattanathum A (2015) Identification of clinical factors associated with severe dengue among Thai adults: a prospective study. BMC infectious diseases 15:420
348. ThermoFisher (2012) Mutation Generation System Kit: Technical Manual.
349. Tsai YT, Chang SY, Lee CN, Kao CL (2009) Human TLR3 recognizes dengue virus and modulates viral replication in vitro. Cellular microbiology 11:604-615

350. Tsetsarkin KA, Kenney H, Chen R, Liu G, Manukyan H, Whitehead SS, Laassri M, Chumakov K, Pletnev AG (2016) A Full-Length Infectious cDNA Clone of Zika Virus from the 2015 Epidemic in Brazil as a Genetic Platform for Studies of Virus-Host Interactions and Vaccine Development. mBio 7
351. Uchida L, Espada-Murao LA, Takamatsu Y, Okamoto K, Hayasaka D, Yu F, Nabeshima T, Buerano CC, Morita K (2014) The dengue virus conceals double-stranded RNA in the intracellular membrane to escape from an interferon response. Scientific reports 4:7395
352. Urin V, Levin D, Sharma N, Harari D, Schreiber G (2015) Fine Tuning of a Type 1 Interferon Antagonist. PLoS One 10:e0130797
353. van den Pol AN, Mao G, Yang Y, Ornaghi S, Davis JN (2017) Zika Virus Targeting in the Developing Brain. The Journal of Neuroscience 37:2161
354. Van der Hoek KH, Eyre NS, Shue B, Khantisitthiporn O, Glab-Ampi K, Carr JM, Gartner MJ, Jolly LA, Thomas PQ, Adikusuma F, Jankovic-Karasoulos T, Roberts CT, Helbig KJ, Beard MR (2017) Viperin is an important host restriction factor in control of Zika virus infection. Scientific reports 7:4475
355. Vaughn DW, Green S, Kalayanarooj S, Innis BL, Nimmannitya S, Suntayakorn S, Endy TP, Raengsakulrach B, Rothman AL, Ennis FA, Nisalak A (2000) Dengue viremia titer, antibody response pattern, and virus serotype correlate with disease severity. J Infect Dis 181:2-9
356. Voigt EA, Yin J (2015) Kinetic Differences and Synergistic Antiviral Effects Between Type I and Type III Interferon Signaling Indicate Pathway Independence. Journal of interferon & cytokine research : the official journal of the International Society for Interferon and Cytokine Research 35:734-747
357. Waggoner JJ, Gresh L, Vargas MJ, Ballesteros G, Tellez Y, Soda KJ, Sahoo MK, Nunez A, Balmaseda A, Harris E, Pinsky BA (2016) Viremia and Clinical Presentation in Nicaraguan Patients Infected With Zika Virus, Chikungunya Virus, and Dengue Virus. Clinical infectious diseases : an official publication of the Infectious Diseases Society of America 63:1584-1590
358. Wang K, Zou C, Wang X, Huang C, Feng T, Pan W, Wu Q, Wang P, Dai J (2018) Interferon-stimulated TRIM69 interrupts dengue virus replication by ubiquitinating viral nonstructural protein 3. PLoS pathogens 14:e1007287-e1007287
359. Weisblum Y, Oiknine-Djian E, Vorontsov OM, Haimov-Kochman R, Zakay-Rones Z, Meir K, Shveiky D, Elgavish S, Nevo Y, Roseman M, Bronstein M, Stockheim D, From I, Eisenberg I, Lewkowicz AA, Yagel S, Panet A, Wolf DG (2017) Zika Virus Infects Early- and Midgestation Human Maternal Decidual Tissues, Inducing Distinct Innate Tissue Responses in the Maternal-Fetal Interface. Journal of virology 91
360. Wells MF, Salick MR, Wiskow O, Ho DJ, Worringer KA, Ihry RJ, Kommineni S, Bilican B, Klim JR, Hill EJ, Kane LT, Ye C, Kaykas A, Eggan K (2016) Genetic Ablation of AXL Does Not Protect Human Neural Progenitor Cells and Cerebral Organoids from Zika Virus Infection. Cell stem cell 19:703-708
361. Westcott MM, Liu J, Rajani K, D'Agostino R, Jr., Lyles DS, Porosnicu M (2015) Interferon Beta and Interferon Alpha 2a Differentially Protect Head and Neck Cancer Cells from Vesicular Stomatitis Virus-Induced Oncolysis. Journal of virology 89:7944-7954
362. WHO (2009) Dengue Guidelines for Diagnosis, Treatment, Prevention and Control. Neglected Tropical Diseases

363. WHO (2016) WHO Director-General summarizes the outcome of the Emergency Committee regarding clusters of microcephaly and Guillain-Barré syndrome.
364. WHO (2018) Revised SAGE recommendation on use of dengue vaccine.
365. WHO (2019) WHO Vaccine Pipeline Tracker.
366. WHO (2019) WHO guidelines for the prevention of sexual transmission of Zika virus: executive summary.
367. WHO (2019) Dengue and Severe Dengue.
368. Wichit S, Hamel R, Yainoy S, Gumpangseth N, Panich S, Phuadraksa T, Saetear P, Monteil A, Morales Vargas R, Misse D (2019) Interferon-inducible protein (IFI) 16 regulates Chikungunya and Zika virus infection in human skin fibroblasts. EXCLI journal 18:467-476
369. Wilmes S, Beutel O, Li Z, Francois-Newton V, Richter CP, Janning D, Kroll C, Hanhart P, Hotte K, You C, Uze G, Pellegrini S, Piehler J (2015) Receptor dimerization dynamics as a regulatory valve for plasticity of type I interferon signaling. The Journal of cell biology 209:579-593
370. Wira CR, Rodriguez-Garcia M, Patel MV (2015) The role of sex hormones in immune protection of the female reproductive tract. Nature reviews Immunology 15:217-230
371. Wu NC, Young AP, Al-Mawsawi LQ, Olson CA, Feng J, Qi H, Luan HH, Li X, Wu TT, Sun R (2014) High-throughput identification of loss-of-function mutations for anti-interferon activity in the influenza A virus NS segment. Journal of virology 88:10157-10164
372. Wu RH, Tsai MH, Chao DY, Yueh A (2015) Scanning mutagenesis studies reveal a potential intramolecular interaction within the C-terminal half of dengue virus NS2A involved in viral RNA replication and virus assembly and secretion. Journal of virology 89:4281-4295
373. Wu RH, Tsai MH, Tsai KN, Tian JN, Wu JS, Wu SY, Chern JH, Chen CH, Yueh A (2017) Mutagenesis of Dengue Virus Protein NS2A Revealed a Novel Domain Responsible for Virus-Induced Cytopathic Effect and Interactions between NS2A and NS2B Transmembrane Segments. Journal of virology 91
374. Wu Y, Liu Q, Zhou J, Xie W, Chen C, Wang Z, Yang H, Cui J (2017) Zika virus evades interferon-mediated antiviral response through the co-operation of multiple nonstructural proteins in vitro. Cell discovery 3:17006
375. Xia H, Luo H, Shan C, Muruato AE, Nunes BTD, Medeiros DBA, Zou J, Xie X, Giraldo MI, Vasconcelos PFC, Weaver SC, Wang T, Rajsbaum R, Shi PY (2018) An evolutionary NS1 mutation enhances Zika virus evasion of host interferon induction. Nature communications 9:414
376. Xu S, Ci Y, Wang L, Yang Y, Zhang L, Xu C, Qin C, Shi L (2019) Zika virus NS3 is a canonical RNA helicase stimulated by NS5 RNA polymerase. Nucleic acids research 47:8693-8707
377. Yan H, Krishnan K, Lim JT, Contillo LG, Krolewski JJ (1996) Molecular characterization of an alpha interferon receptor 1 subunit (IFNaR1) domain required for TYK2 binding and signal transduction. Molecular and cellular biology 16:2074-2082
378. Yazdani Brojeni P, Matok I, Garcia Bournissen F, Koren G (2012) A systematic review of the fetal safety of interferon alpha. Reproductive Toxicology 33:265-268
379. Ye J, Zhu B, Fu ZF, Chen H, Cao S (2013) Immune evasion strategies of flaviviruses. Vaccine 31:461-471

380. Ye Q, Liu ZY, Han JF, Jiang T, Li XF, Qin CF (2016) Genomic characterization and phylogenetic analysis of Zika virus circulating in the Americas. Infection, genetics and evolution : journal of molecular epidemiology and evolutionary genetics in infectious diseases 43:43-49
381. Yockey LJ, Varela L, Rakib T, Khoury-Hanold W, Fink SL, Stutz B, Szigeti-Buck K, Van den Pol A, Lindenbach BD, Horvath TL, Iwasaki A (2016) Vaginal Exposure to Zika Virus during Pregnancy Leads to Fetal Brain Infection. Cell 166:1247-1256.e1244
382. Yockey LJ, Iwasaki A (2018) Interferons and Proinflammatory Cytokines in Pregnancy and Fetal Development. Immunity 49:397-412
383. Yockey LJ, Jurado KA, Arora N, Millet A, Rakib T, Milano KM, Hastings AK, Fikrig E, Kong Y, Horvath TL, Weatherbee S, Kliman HJ, Coyne CB, Iwasaki A (2018) Type I interferons instigate fetal demise after Zika virus infection. Science immunology 3
384. Yoneyama M, Kikuchi M, Natsukawa T, Shinobu N, Imaizumi T, Miyagishi M, Taira K, Akira S, Fujita T (2004) The RNA helicase RIG-I has an essential function in double-stranded RNA-induced innate antiviral responses. Nature immunology 5:730-737
385. Yoshimura A, Nishinakamura H, Matsumura Y, Hanada T (2005) Negative regulation of cytokine signaling and immune responses by SOCS proteins. Arthritis Res Ther 7:100-110
386. Yu CY, Liang JJ, Li JK, Lee YL, Chang BL, Su CI, Huang WJ, Lai MM, Lin YL (2015) Dengue Virus Impairs Mitochondrial Fusion by Cleaving Mitofusins. PLoS Pathog 11:e1005350
387. Yu IM, Zhang W, Holdaway HA, Li L, Kostyuchenko VA, Chipman PR, Kuhn RJ, Rossmann MG, Chen J (2008) Structure of the immature dengue virus at low pH primes proteolytic maturation. Science (New York, NY) 319:1834-1837
388. Yun SI, Lee YM (2017) Zika virus: An emerging flavivirus. Journal of microbiology (Seoul, Korea) 55:204-219
389. Yun SI, Song BH, Frank JC, Julander JG, Olsen AL, Polejaeva IA, Davies CJ, White KL, Lee YM (2018) Functional Genomics and Immunologic Tools: The Impact of Viral and Host Genetic Variations on the Outcome of Zika Virus Infection. Viruses 10
390. Zanluca C, Melo VC, Mosimann AL, Santos GI, Santos CN, Luz K (2015) First report of autochthonous transmission of Zika virus in Brazil. Memorias do Instituto Oswaldo Cruz 110:569-572
391. Zhao B, Yi G, Du F, Chuang YC, Vaughan RC, Sankaran B, Kao CC, Li P (2017) Structure and function of the Zika virus full-length NS5 protein. Nature communications 8:14762
392. Zhao Y, Soh TS, Zheng J, Chan KWK, Phoo WW, Lee CC, Tay MYF, Swaminathan K, Cornvik TC, Lim SP, Shi P-Y, Lescar J, Vasudevan SG, Luo D (2015) A crystal structure of the Dengue virus NS5 protein reveals a novel inter-domain interface essential for protein flexibility and virus replication. PLoS pathogens 11:e1004682-e1004682
393. Zhao Z, Tao M, Han W, Fan Z, Imran M, Cao S, Ye J (2019) Nuclear localization of Zika virus NS5 contributes to suppression of type I interferon production and response. The Journal of general virology
394. Zheng H, Qian J, Varghese B, Baker DP, Fuchs S (2011) Ligand-stimulated downregulation of the alpha interferon receptor: role of protein kinase D2. Molecular and cellular biology 31:710-720

395. Zheng Y, Liu Q, Wu Y, Ma L, Zhang Z, Liu T, Jin S, She Y, Li YP, Cui J (2018) Zika virus elicits inflammation to evade antiviral response by cleaving cGAS via NS1-caspase-1 axis. The EMBO journal 37
396. ZhongLi J, HongminLi (2017) Flavivirus NS2B/NS3 Protease: Structure, Function, and Inhibition. Viral Proteases and Their Inhibitors, pp 163 - 188
397. Zhou Z, Hamming OJ, Ank N, Paludan SR, Nielsen AL, Hartmann R (2007) Type III interferon (IFN) induces a type I IFN-like response in a restricted subset of cells through signaling pathways involving both the Jak-STAT pathway and the mitogen-activated protein kinases. Journal of virology 81:7749-7758
398. Zmurko J, Neyts J, Dallmeier K (2015) Flaviviral NS4b, chameleon and jack-in-the-box roles in viral replication and pathogenesis, and a molecular target for antiviral intervention. Reviews in medical virology 25:205-223
399. Zust R, Cervantes-Barragan L, Habjan M, Maier R, Neuman BW, Ziebuhr J, Szretter KJ, Baker SC, Barchet W, Diamond MS, Siddell SG, Ludewig B, Thiel V (2011) Ribose 2'-O-methylation provides a molecular signature for the distinction of self and non-self mRNA dependent on the RNA sensor Mda5. Nature immunology 12:137-143
400. WHO (2019) Countries and territories with current or previous Zika virus transmission, accessed: 01/11/2019, https://www.who.int/ith/Zika_map.pdf?ua=1
401. CDC (2019) Dengue Around the World, accessed: 01/11/2019, https://www.cdc.gov/dengue/areaswithrisk/around-the-world.html